Evaluation of the Leachate Chemistry and Contaminants Attenuation in Acid Mine Drainage by Fly Ash and its derivatives.

Wilson Mugera Gitari

B.ed (sc) Honours (Kenyatta University); MSc Chemistry (University of Nairobi)

UNIVERSITY of the
WESTERN CAPE

Submitted in partial fulfillment of the requirements for degree of Doctor of Philosophy in Chemistry

In the Department of Chemistry

University of the Western Cape

August 2006

Supervisors: Prof David Key (Chemistry Department)

: Prof Charles Okujeni (Earth Sciences)

ABSTRACT

The mining industry in South Africa has a huge potential to impact negatively on the environment. Negative impacts include generation of reactive tailings and acid mine drainage (AMD). AMD is highly acidic (pH 2-4), sulphate-rich and frequently carries a heavy metal burden. South Africa uses more than 100 million tonnes of low grade bituminous coal annually to produce cheap electricity. The associated mining operations result in millions of tonnes of polluted water and in turn coal burning power stations produce vast amounts of waste ash such as fly ash. The highly soluble CaO occurring as sub-micron fragments on the fly ash particles is highly reactive and can be utilized in the neutralization of acid mine drainage.

Acid mine drainage (AMD) was reacted with two different South African fly ashes in a batch set-up in an attempt to evaluate their neutralization and inorganic contaminants removal capacity. The concentrations of major constituents in the AMD were found to determine the final pH attained in the reaction mixture and the reaction time of breakthrough to circum-neutral and alkaline pH. Efficiency of elemental removal in the AMD by the FA was directly linked to the amount of FA in the reaction mixture and to the final pH attained. Most elements attained ≈ 100 % removal only when the pH of minimum solubility of their hydroxides was achieved.

In the second part of the study, Acid mine drainage (AMD) was reacted with coal fly ash in a 24 hour equilibration time using 1:3 and 1:1.5 FA: AMD ratios by weight to produce neutral and alkaline process waters. The capacity of the fly ash to remove the major inorganic contaminants from AMD was examined with time. The geochemical computer software PHREEQC and WATEQ4 database were used for geochemical modeling of the process water chemistry at selected reaction times. The collected solid residues were analyzed by X-ray diffraction, scanning electron microscopy (SEM) and scanning electron microscopy-energy dispersive X-ray spectroscopy (SEM-EDX). At both ratios the reaction mixture was at saturation or oversaturated with alunite, basaluminite, jurbanite, boehmite, gibbsite, diaspore, gypsum, barite, K, Na-jarosites, ettringite, amorphous Fe $(OH)_3$ and goethite at specific contact times. The precipitation of the many inorganic contaminants was established in terms of the mineral phases at saturation or over-saturation. Sequential extraction revealed the amorphous fraction to be the most important in retention of the major and minor inorganic contaminants at pH > 6.32 which implies that the concentration of total Fe and Al in the AMD being treated has a direct effect on the clean-up efficiency of the process.

In the third part of the study, a column leaching of the solid residues (SR) blended with varying amounts of fly ash (5 %, 25 %, 40 %) and 6 % Ordinary Portland Cement (OPC) was carried out to

UNIVERSITY of the
WESTERN CAPE

assess the contaminant attenuation with time. The columns were drained with synthetic acid mine drainage (SAMD) over a period of 165 days. In addition the solid residues were modified with 1-6 % OPC and their strength development monitored over a period of 365 days. The column solid cores were observed to acidify in a stepwise fashion, exhibiting three buffer zones. The SR alone and SR blended with fly ash exhibited strong buffering capacity at pH (7.5-9) for an extended period of time (97-110 days). Encapsulation of solid residue particles by the calcium silicate hydrate gels (CSH) in OPC blended solid residues obscured the appearance of the sustained buffering at pH 7-9.5. The fly ash and OPC blend solid residues exhibited decontamination efficiencies of (82-99 %) for Al, Fe, Mn and SO_4^{2-} over the study period. However the OPC blend SR exhibited high attenuation efficiency even as the pH dropped to below 4. SR + 6 % OPC core was observed to be the most efficient interms of retention of highly mobile elements such as B and Mo. pH was observed to be the main determining factor in contaminants attenuation. Geochemical modeling results revealed that pH and SO_4^{2-} concentrations in the leachate had a significant impact on the mineral phases controlling Fe and Al concentration in the leachates. In the SR + 6 % OPC solid cores, EDX analysis revealed that CSH gels and calcium aluminate hydrate gels were being precipitated. These gels were either incorporating Fe, Mg, Mn in their matrix or encapsulating the solid residue particles that were rich in these elements.

Sequential extractions of the leached solid cores revealed the amorphous fraction to be the most important in retention of the major contaminants and were most enhanced in the OPC blend solid residues.

The OPC blend solid residue slurries developed unconfined compressive strength (UCS) (2-3 Mpa) comparable to paste formulated from sulphidic rich mine tailings confirming that the solid residues can be used for backfilling. Therefore the solid residues (SR) can successively be applied for a dual purpose in mined out areas namely, to remediate acid mine drainage waters and also provide support for the overburden.

UNIVERSITY of the
WESTERN CAPE

Keywords: Acid Mine Drainage; Fly Ash; Neutralization; Sulphates; Metal ions; Solid Residues (SR); Column Leaching; Geochemical Modeling; Sequential Extraction; Buffering.

DECLARATION

I declare that *Evaluation of the Leachate Chemistry and Contaminants Attenuation in Acid Mine Drainage by Fly Ash and its derivatives* is my own work, that it has not been submitted for any degree or examination in any other university, and that all the sources I have used or quoted have been indicated and acknowledged by complete references.

Wlison Mugera Gitari August 2006:

Signed……..:

ACKNOWLEDGEMENTS

I would like to thank the following for funding this project:

Water Research Commission (WRC)
CoalTech 2020 Consortium
National Research Foundation (NRF)
ESKOM

The following Institutions for collaboration work and the people that we worked with that led to achieving most of the deliverables:

Dhamini Surrender and Kelley Reynolds at ESKOM for assistance in Fly Ash sample collection and Hartmut Ilgner at MiningTek CSIR for assisting in slurry formulation and strength development testing.

Project Leader Leslie Petrik for the Support and provision of conference attendance funding where this work was presented.

My supervisors Prof D. L. Key (Chemistry Department) and C. O Okujeni (Earth Sciences) for their advice and support

UNIVERSITY of the
WESTERN CAPE

Prof Emmanuel Iwuoha (Chemistry department) for his strong encouraging advice and comments on this work.

Dr Olivier Etchebers for reading through my thesis work, introducing me to Geochemical Modeling, helping me prepare manuscripts for conferences and reviewing them before submission to referred journals.

To my colleagues Vernon Somerset, Michael Klink, Nicollette Hendricks and Thandi for good company and suggestions made during the entire duration of my study.

Not to forget my Family members back in Kenya who gave me all the support and encouragement to move on.

DEDICATION

This work is dedicated to my twin daughters ***Vivian Wambui*** and ***Ashley Nyakio*** who kept me strong and moving by their smiles and sweet giggles during some of the difficult times of my research work

LIST OF ACRONYMS AND ABBREVIATIONS USED

AMD	Acid Mine drainage
ASTM	American Society for Testing and Materials
FA	Fly Ash
ANRT	Association Nationale de la Recherche Technique, Paris
CCRMP	Canadian certified Reference Materials Project
CRPG	Centre de Recherches Pétrographiques et Géochimiques
MINTEK	Council for Mineral Technology, South Africa
GSJ	Geological Survey of Japan
NIM	National Institute of Metallurgy, South Africa
USGS	United States Geological Survey, Reston
SR	Solid Residues
OPC	Ordinary Portland Cement
DWAF	Department of Water Affairs and Forestry
JCPDS-ICD	Joint Committee on Powder Diffraction Standards-International Centre for Diffraction
LOI	Loss on Ignition.
CSH	Calcium Silicate Hydrate gels
SAMD	Synthetic Acid Mine Drainage

UNIVERSITY of the
WESTERN CAPE

TABLE OF CONTENTS

ABSTRACT ..... **ii**

DECLARATION ..... **iv**

ACKNOWLEDGEMENTS ..... **v**

DEDICATION ..... **vi**

LIST OF ACRONYMS AND ABBREVIATIONS USED ..... **vii**

TABLE OF CONTENTS ..... **viii**

Chapter One **1**

Introduction **1**

1 Introduction **1**

Chapter Two **6**

Generation, characteristics and environmental impacts of fly ash and acid mine drainage (AMD): Chemistry and mineralogy of the precipitates formed on increasing the pH of the AMD. A literature Review. **6**

2 Introduction **6**

2.1 Coal and coal combustion by-products **6**

2.1.1 Fly ash: Physical, Chemical and Mineralogical characteristics 8

2.1.2 Chemistry of fly ash Leachate and Geochemical factors Controlling the Mobilisation of Inorganic constituents in Fly Ash Leachate. 13

2.1.3 Major Elements in Fossil Fuel waste. 16

2.1.4 Reactions controlling major elements chemistry in waste leachate 17

2.1.5 Minor elements in fossil fuel waste leachate 19

2.1.6 Effects of redox state and reactions affecting minor element leachate chemistry 21

2.1.7 Application of thermochemical principles to process water chemistry for acid mine drainage neutralized with fly ash. 22

2.1.8 Disposal and Environmental Impacts of Fly Ash 23

2.1.9 Utilization of coal fly ash 24

2.1.10 Reclamation of wastelands 26

2.1.10.1 Infiltration barrier and underground void filling 27

2.1.11 Cement and concrete products 29

UNIVERSITY of the WESTERN CAPE

2.2 Acid Mine Drainage 30
2.2.1 Introduction 30
2.2.2 Generation of Acid Mine Drainage 31
2.2.3 Dissolution of pyrite 31
2.2.4 Role of Ferric iron in oxidation of pyrite and contribution to acidity 31
2.2.5 Microbial oxidation: role of bacteria 33
2.2.6 Effect of temperature 34
2.2.7 Deleterious Effects of Acid Mine Drainage: Impacts of Mine Drainage on Aquatic Life, Water uses, and Man-Made structures. 34
2.2.8 Durability of concrete structures 36
2.2.9 Treatment of AMD 36
2.2.9.1 Active chemical treatment methods 37
2.2.9.2 Passive treatment methods 39
2.2.9.2.1 Constructed wetlands 40
2.2.9.2.2 Anoxic limestone drains 41
2.2.9.2.3 Successive alkalinity producing systems (SAPS) 41
2.2.9.3 Treatment of acid mine drainage with fly ash 42

2.3 Leaching Studies and Backfilling of Mine voids 46
2.3.1 Introduction 46
2.3.2 Column leaching 47
2.3.3 Column set-up 51
2.3.4 Mine backfilling 54
2.3.5 Application of Binders in Waste Stabilization and their relevance in Backfilling. 56

2.4 Mineralogy of Precipitates formed on increasing the pH of the Acid Mine Drainage. 57
2.4.1 Introduction 57
2.4.2 Saturation Indices (SI) and Mineral Solubilities 58
2.4.3 Secondary Mineral Phases 59
2.4.4 Ferrous, Ferric oxides, hydroxides and hydroxy-sulfates 61
2.4.5 Aluminium oxides, hydroxides and hydroxysulfate minerals. 63
2.4.6 Hydroxides of trace metals 63
2.4.7 Carbonates 64
2.4.8 Sequential Extractions 64

2.5 Conclusions ..... ….66

2.6 Aims of the study 67

Chapter Three 69

Utilization of fly ash for remediation of coal mine waste waters: Removal of major inorganic contaminants and trace elements. 69

Abstract 69

Academic Output 69

UNIVERSITY of the WESTERN CAPE

3 Introduction 70

3.1 Experimental Procedures 70
3.1.1 Chemical characterization of fly ash, AMD and solid residues samples 70

3.2 Results and Discussion 71
3.2.1 Composition of Fly Ash Samples 71
3.2.2 Composition of Acid Mine Drainage Samples 72
3.2.3 Neutralization Reactions using different FA and AMD samples 74
3.2.4 Neutralizations reactions using different FA: AMD ratios 76
3.2.5 Major and Trace elements removal in the acid mine waters 79
3.2.5.1 Matla fly ash and Brugspruit AMD reactions 80
3.2.5.2 Matla fly ash and Navigation AMD reaction 83
3.2.6 Water quality comparisons 84
3.2.7 Sulphate removal in the acid mine waters 84
3.2.8 Leaching of elements from fly ash 85

3.3 Conclusions 88

Chapter Four 90

Utilization of fly ash for remediation of coal mine waste waters: Solubility controls on major inorganic contaminants and their partitioning in the resulting solid residues (SR) 90

Abstract 90

Academic Output 91

4 Introduction 91

4.1 Materials and Methods 93
4.1.1 Sample Description 93
4.1.2 Neutralization Reactions 93
4.1.3 XRD and Scanning electron microscope investigations 94
4.1.4 Calculation of Saturation States 94
4.1.5 Sequential Chemical Extractions of the Solid Residues (SR) 95
4.1.5.1 Water soluble fraction 95
4.1.5.2 Exchangeable fraction 95
4.1.5.3 Carbonate fraction 96
4.1.5.4 Crystalline Mn-oxides 96
4.1.5.5 Amorphous Fe, Mn, Al- oxides, (oxy) hydroxides 96
4.1.5.6 Crystalline Fe oxides 97

4.2 Results AND Discussions 97
4.2.1 Composition of fly ash and Navigation Acid mine Water 97
4.2.2 Composition of Solid Residues (SR) 99
4.2.3 Neutralization Reactions 99

UNIVERSITY of the
WESTERN CAPE

4.2.4 X-ray diffraction (XRD) and Scanning electron microscopy-Energy dispersive (SEM-EDX) Analysis of the Solid Residues 101
4.2.5 Trends of Major Elements in the Process Water for 1:3 and 1:1.5 FA: AMD Reactions with time. 110
4.2.5.1 Sulphate trends 110
4.2.5.2 Major cations and anionic species 115
4.2.5.2.1 Total Fe, Fe^{3+} and Fe^{2+} 116
4.2.5.2.2 Aluminum 117
4.2.5.2.3 Boron and molydenum 118
4.2.5.2.4 Silicon 120
4.2.5.2.5 Calcium, sodium, magnesium 123
4.2.5.2.6 Manganese, zinc and copper 126
4.2.6 Sequential Extractions 130
4.2.6.1 B and Mo concentration profiles 135
4.2.6.2 Ca and Na concentration profile 135
4.2.6.3 Al, Fe, Mn and Si concentration profiles 136
4.2.6.4 Cu and Zn concentration profile 138

4.3 Conclusions 139

Chapter Five 141

Contaminants attenuation by Fly ash and its derivatives: A column leaching study. 141

Abstract 141

Academic Output 142

5 Introduction 143

5.1 Materials and Methods 145
5.1.1 Sample Collection, preparation of Solid Residues and Column Assembly set-up 145
5.1.2 Simulated AMD preparation and Drainage 146
5.1.3 Analysis of the Leached Solid Residue Cores. 149
5.1.4 pH profile of the Leached Column Solid Cores 149
5.1.5 X-ray diffraction, Scanning Electron microscopy, Scanning Electron microscopy-energy dispersive spectroscopy (SEM-EDX) and infra-red analysis of column solid cores. 150
5.1.6 Sequential Chemical Extractions 150
5.1.7 Geochemical Modeling 151
5.1.8 Strength Development of Acid Mine Drainage and Fly Ash Solid Residues blended with Ordinary Portland Cement (OPC) 153
5.1.8.1 Preparation of the solid residues 153
5.1.8.2 Moisture content determination 153
5.1.8.3 Marsh cone test 153
5.1.8.4 Particle size determination 154
5.1.8.5 Preparation of the cylinders and curing 154

UNIVERSITY of the
WESTERN CAPE

5.2 Results and Discussion 155
5.2.1 Composition of Fly Ash, Solid residues (SR) and Ordinary Portland Cement (OPC) 155
5.2.2 Kinetics of the Simulated Acid mine Water (SAMD) 156
5.2.3 Drainage Quality 158
5.2.3.1 Evolution of pH in the column leachates 158
5.2.4 Conclusions 164

5.3 Acidity Attenuation by the Column Cores 165
5.3.1 Fly ash and solid residue (SR), solid residue (SR) + FA column cores 165
5.3.2 Solid residues (SR) + 6 % Ordinary Portland Cement (OPC) column cores 184
5.3.3 Conclusions 189

5.4 Contaminants Attenuation by Fly Ash (FA), Solid Residues (SR), Solid Residues (SR) + 25 % FA and Solid Residues (SR) + 6 % Ordinary Portland Cement (OPC) column blends. 190
5.4.1 Fly ash column cores 190
5.4.1.1 Sulphate and calcium 192
5.4.1.2 Total iron, manganese and aluminum 192
5.4.2 Solid residue (SR) column cores 193
5.4.2.1 Sulphate and calcium 194
5.4.2.2 Total iron, manganese and aluminum 195
5.4.3 Solid residues (SR) + 25 % FA 196
5.4.3.1 Sulphate and calcium 196
5.4.3.2 Total iron, manganese and aluminum 198
5.4.4 Solid residues (SR) + 6 % Ordinary Portland Cement (OPC) 199
5.4.4.1 Sulphate and calcium 200
5.4.4.2 Total iron, manganese and aluminum 201
5.4.5 Decontamination Efficiency of each Column Solid Core 202

5.5 Contaminants Attenuation Mechanisms and Solubility Controls 203
5.5.1 Sulphate and calcium 204
5.5.2 Sulphate, Aluminum and Iron 213
5.5.3 Fe (oxy) hydroxides and Al (oxy) hydroxides 215
5.5.4 Manganese 232

5.6 Mineralogical and elemental analysis of leached solid cores. 235
5.6.1 Visualization of the sectioned leached solid cores 236
5.6.2 X-ray diffraction (XRD) analysis of the leached solid cores 239
5.6.3 Fourier Transform infra-red analysis (FTIR) of the leached solid residue cores 239
5.6.4 Conclusions 244
5.6.5 Scanning electron microscopy (SEM) and Scanning Electron microscopy-Energy dispersive X-ray spectroscopy (SEM-EDX) analysis of the leached column solid cores. 244
5.6.6 pH profile of the column residue cores 252
5.6.7 Sequential chemical extraction (SSE) of the leached solid residue (SR) cores 255
5.6.7.1 Water soluble fraction 256
5.6.7.1.1 Fly Ash (FA) leached solid core 256
5.6.7.1.2 Solid residue (SR) leached solid core 262
5.6.7.1.3 Solid residue + 6 % Ordinary Portland Cement (SR + 6 % OPC) leached solid core 262
5.6.7.2 Amorphous fraction 262
5.6.7.2.1 Fly Ash (FA) leached solid core 263

UNIVERSITY of the
WESTERN CAPE

5.6.7.2.2 Solid residue (SR) leached solid core 264
5.6.7.2.3 Solid residue + 6 % Ordinary Portland Cement (SR + 6 % OPC) leached solid core 264
5.6.7.3 Reducible Fraction 266
5.6.7.3.1 Fly ash (FA) leached solid core 266
5.6.7.3.2 Solid residue (SR) leached solid core 266
5.6.8 Strength development of Ordinary Portland Cement (OPC) blend Solid Residues (SR) and implication for backfilling application. 267
5.6.8.1 Particle size analysis 268
5.6.8.2 Strength development testing 269
5.6.9 Conclusions 272

5.7 Discussion and Conclusions 272

Chapter Six 276

Conclusions and Recommendations 276

6 Introduction 276

6.1 Neutralization of AMD with fly ash 276

6.2 Contaminants removal in AMDs 277

6.3 Solubility controls on major contaminants 278

6.4 Contaminant attenuation by the fly ash and Ordinary Portland Cement blended solid residue (SR) cores. 280

References 283

Appendices 310

Appendix A 310

Analytical Techniques 310

A Introduction 310

A.1 Inductively coupled plasma mass spectrometry (ICP-MS) 311
A.1.1 Introduction 311
A.1.2 Instrument Description and Theory 311
A.1.3 Sample Introduction 312
A.1.4 Argon Plasma/Sample Ionization 312
A.1.5 ICP-MS Interface 313
A.1.6 Mass Spectrometer (MS) 313
A.1.7 Detector 314

UNIVERSITY of the WESTERN CAPE

A.1.8 Instrument Calibration 314
A.1.9 Sources of interference 315
A.1.10 Accuracy of the method and detection Limits 315

A.2 Ion chromatography 317
A.2.1 Procedure 319

A.3 Determination of Ferrous iron by colorimetry 319
A.3.1 Principle 319

A.4 pH measurements 320

A.5 Electrical conductivity (EC). 321

A.6 Alkalinity Measurement 321

A.7 Acidity Measurements 322

A.8 X-ray diffractometry 323
A.8.1 Procedure 323

A.9 Fourier-Transform Infrared Spectrometry 324

A.10 Scanning Electron Microscopy Analysis (SEM). 324
A.10.1 Introduction 324
A.10.2 Electron beam-specimen interaction 325

A.11 Scanning electron microscopy-Energy dispersive spectroscopy X-ray analysis (SEM-EDX). 325

A.12 Total elemental analysis by X-ray fluorescence spectroscopy (XRFS) 327
A.12.1 Procedure 328

A.13 Geochemical modeling of the Fly Ash and Acid Mine Drainage Interactions 329
A.13.1 Saturation Indices (SI) and Solubility Equilibria 329

Appendix B: Analytical , saturation indices and XRD analysis data. . 330

UNIVERSITY of the
WESTERN CAPE

LIST OF TABLES

Table 1.1: The production of FA by pulverized coal fired power stations in South Africa (Krüger, 2003). 2
Table 2.1: Physical properties of fly ash (Summers *et al.,* 1983). 10
Table 2.2: Major element composition (weight %) of Arnot and Sasol fly ash. (Willis, 1987) 10
Table 2.4: Geochemical grouping, dominant redox states and types of solubility-controlling solids in weathering environments for the minor elements in fossil fuel 22
Wastes (Eary *et al*., 1990). 22
Table 3.1: Chemical characteristics of fly ashes used in these experiments 72
Table 3.2: Chemical and physical characteristics of AMD samples used in the experiments 74
Table 3.3. Major and trace element removal as a function of pH for Matla fly ash, Brugspruit and Navigation AMD reactions. 81
Table 3.4: % removal of Cr with increasing FA: AMD ratio and pH in process water**.** 83
Table 4.1: Total Fe (µg/g) dry weight extracted from the coarse and fine size fractions 97
Table 4.2: Composition of Arnot fly ash and solid residues (SR) collected at pH 9.2 for 1:3: fly ash (FA): acid mine drainage (AMD) ratio. 98
Table 4.4: SEM-EDX spot % elemental analysis of solid residue collected at pH 9.2 for 1:3 FA: AMD ratio 106
Table 4.5: Calculated saturation indices for selected mineral phases at selected reaction times for FA: AMD ratio 1:3 114
Table 4.6: Calculated saturation indices for selected mineral phases at selected reaction times for FA: AMD ratio 1:1.5 115
Table 4.7. Sequential extraction for Arnot fly ash (mg/kg dry weight), % contribution of each fraction is presented in the 132
parenthesis, results presented as mean ± standard deviation (SD) for n=3 132
Table 4.8. Sequential extraction for solid residues collected at pH 4 (mg/kg dry weight), % contribution of each fraction is presented 132
in the parenthesis, results presented as mean ± (SD) for n=3 132
Table 4.10: Sequential extraction for solid residues collected at pH 6.32 (mg/kg dry weight), % contribution of each fraction is presented in the parenthesis, results presented as mean ± (SD) for n=3 133
Table 4.12: Detection limits (mg/kg dry weight) calculated for each fraction 134
Table 5.1: Column compositions and total mass (kg, dry weight basis), drainage volumes (L) and liquid to solid ratios for each column 146
Table 5.2: Composition of the Simulated Acid mine Water used in the drainage experiments (mg/L) 148
Table 5.3: Test conditions for the fly ash, solid residues, fly ash and Ordinary Portland Cement blended solid residues 148
The alternate wetting and drying regimes were done to simulate conditions when AMD is percolating and not percolating through the backfilled material. 148
Table 5.4: The number of times SAMD was drained through the columns, and the corresponding time in days and cumulative volume of SAMD (L/kg). 149
Table 5.5: Elemental content of solid residues, Arnot fly ash and Ordinary Portland cement. 155
Table 5.6: Rate of change of pH with time over the pH range 4.5-8.5 for the two model solutions. 158
Table 5.7: Total amount in mmol of ions drained through each column and calculated % contaminant removed by each column solid core 202
Table 5.8: Drainage time (days) and pH range over which the regression was calculated. 211

UNIVERSITY of the
WESTERN CAPE

Table 5.9: Characteristic absorption bands observed for FA, SR, SR + 25 % FA and SR + 6 % OPC leached solid residue cores. 239
Table 5.10: EDX elemental analysis results (weight %) for the solid residue cores 247
Table 5.11: EDX elemental analysis results (weight %) for the SR + 6 % OPC solid cores. 250
Table 5.12: pH profile of the column solid residue cores with depth**.** 253
Table 5.13: Sequential extraction results for the FA leached solid core (results presented as mean±SD for n=3 extractions, DL-detection limits) 257
Table 5.14: Sequential extraction results for the solid residue (SR) leached solid core (results presented as mean±SD for n=3 extractions) 258
Table 5.15: Sequential extraction results for the SR + 25 % FA leached solid core (results presented as mean±SD for n=3 259
extractions) 259
Table 5.16: Sequential extraction results for the SR + 6 % OPC leached solid core (results presented as mean±SD for n=3 260
extractions). 260
Table 5.17: Water/solid ratios of solid residue slurries and cured samples for batch one. 269
Table A1: Calculated lower limits of detection for elements analysed. 316
Table A2: ICP-MS analysis of NIST-1640 certified reference material (n=10) 317
Table B1: Concentration of contaminants at different FA: AMD ratio for Matla fly ash and Brugspruit AMD reactions 331
Table B2: Concentration of contaminants at different FA: AMD ratio for Matla fly ash and Navigation AMD reactions 332
Table B3: Concentration of contaminants at different FA: AMD ratio for Matla fly ash and Bank AMD reactions 333
Table B4: Concentration (mg/L) with reaction time for 1:3 FA: AMD ratio (n=3) 334
Table B5: Concentration (mg/L) with reaction time for 1:1.5 FA: AMD ratio (n=3) 336
Table B6: Concentration in mol/L and Mol_c/L for FA: AMD ratio of 1:3 for Matla fly ash and Navigation AMD. 338
Table B7: Concentration in mol/L and Mol_c/L for FA: AMD ratio of 1:1.5 for Matla fly ash and Navigation AMD**.** 339
Table B8. Analytical results for fly ash solid core 340
Table B9. Analytical results for solid residue core 342
Table B10: Analytical results for solid residue (SR) + 5 % FA core 344
Table B11: Analytical results for solid residue (SR) + 25 % FA core 346
Table B12: Analytical results for solid residue (SR) + 40 % FA core 348
Table B13: Analytical results for solid residue (SR) + 6 % FA core 350
Table B14: Summary of saturation indices (SI) for mineral phases controlling element concentration in leachates for fly ash (FA) solid core. 352
Table B15: Summary of saturation indices (SI) for mineral phases controlling element concentration in leachates for solid residue (SR) core. 353
Table B16: Summary of saturation indices (SI) for mineral phases controlling element concentration in leachates for SR + 5 % FA core. 354
Table B17: Summary of saturation indices (SI) for mineral phases controlling element concentration in leachates for SR + 25 % FA core. 355
Table B18: Summary of saturation indices (SI) for mineral phases controlling element concentration in leachates for SR + 40 % FA core. 356
Table B19: Summary of saturation indices (SI) for mineral phases controlling element concentration in leachates for SR + 6 % OPC core. 357

LIST OF FIGURES

Figure 1.1: A Map showing the collieries (marked in red) and Eskom power stations (marked in pink) where Acid Mine Drainage and Fly Ash samples were taken from. Other Eskom power stations are marked in blue (Eskom 2000; Bullock and Bell., 1997), Navigation AMD was sampled at Landau, Brugspruit AMD at Brugspruit. 5
Figure 2:1: Flow diagram of coal combustion and related processes leading to the formation of the various coal combustion products. 8
Figure 2.2: Reaction types dictating the leachate composition of fossil fuel wastes (adapted from Eary *et al*., 1990) 17
Figure 2.3: Model for the oxidation of pyrite (Stumm and Morgan, 1981). 32
Figure 2.4: Summary of biological and abiotic technologies for remediating acid mine drainage (Johnson and Hallberg, 2005). 37
Figure 2.5: Schematic arrangements of humidity cell and sub-aerial and sub-aqueous columns (Lawrence, 1995). 49
Figure 3.1. pH and EC for the reactions at a FA:AMD ratio of 1:3 between Matla, Arnot FA and Bank AMD; and Arnot FA and Navigation AMD. Values reported as mean ± SD (n=4), Error bars reflect 1 SD above and below the mean. 75
Figure 3.2. pH and EC during neutralization reactions for different Matla FA: Brugspruit AMD ratios. Values reported as mean ± SD (n=4), Error bars reflect 1 sample SD above and below the mean. 77
Figure 3.3:. pH and EC for various FA:AMD ratios for reaction between Matla FA and Navigation AMD. Values reported as mean ± SD (n=4), Error bars reflect 1 SD above and below the mean. 78
Figure 3 4:. pH and EC for various FA:AMD ratios for reaction between Matla FA and Bank AMD. Values reported as mean ± SD (n=4), Error bars reflect 1 SD above and below the mean. 78
Figure 3.5:. Variation of Ba, B, Mo and Sr concentrations as a function of FA:AMD ratios for Matla fly ash and Brugspruit AMD reactions. Values reported as mean ± SD (n=3), Error bars reflect 1 SD above and below the mean. 86
Figure 3.6:. Variation of B, Mo and Sr concentrations as a function of FA:AMD ratios for Matla fly ash and Navigation AMD reactions. Values reported as mean ± SD (n=3), Error bars reflect 1 SD above and below the mean. 86
Figure 3.7: Variation of As and Se concentrations as a function of FA:AMD ratios for Matla fly ash and Brugspruit; Navigation AMD reactions. 87
Figure 4.1: pH change with contact time for the 1:3 and 1:1.5 FA: AMD reactions. Error bar represents 1 SD above and below the mean. 100
Figure 4.2: XRD spectra of solid residues collected at increasing contact time (minutes) (G-gypsum, Q-quartz, M-mullite, AN-Arnot fly ash + Navigation AMD, 13-FA: AMD ratio, -time (minutes), AFA-Arnot fly ash). 101
Figure 4.3: SEM micrographs of Arnot fly ash (1A)(magnification=2000) and solid residues (1B, 1C and 1D) collected at pH 9.2 for 1:3 FA: AMD reaction (Magnification = 500) 103
Three main features are observed in the solid residues by SEM technique 104
Figure 4.4: SEM micrographs of solid residues (2A-mg=1000, 2B-mg=1000, 2C-mg=500 and 2D-mg=1000) collected at pH 9.2 for 1:3 FA: AMD reaction (Mg=magnification) 105
Figure 4.5: SEM micrograph of solid residues collected at pH 9.2 for 1:3 FA: AMD ratio (1A and 1B) showing the spots where EDX analysis was done (magnification=2000), 1C for solid residues collected at pH 9.88 for 1:1.5 FA: AMD ratio showing needle like crystals similar to spot G in 1B. 107

UNIVERSITY of the
WESTERN CAPE

Figure 4.6: SO_4 concentration in process water for 1:3 and 1:1.5 FA: AMD reactions. Error bar represents 1 SD above and below the mean. 111
Figure 4.7: Ph/ mineral phase diagrams for basaluminte and jurbanite for 1:3 and 1:1.5 FA: AMD ratios. 111
Figure 4.8: A plot of ($3\log\alpha Fe3+ + 2\log^{\alpha}SO_4^{2-} + \log^{\alpha} Na^{+}$) versus pH for 1:3 and 1:1.5 ratios respectively. Line represents the equilibrium with natro-jarosite [$NaFe_3(SO_4)_2(OH)_6$]. 112
Figure 4.9: Attenuation of Fe^{2+}, Fe^{3+} and total Fe with change in pH in process waters for 1:3 and 1:1.5 FA: AMD ratio. Error bar represents 1 SD above and below the mean, n=3. 117
Figure 4.10: Al concentration in process water for 1:3 and 1:1.5 FA: AMD reactions. Error bar represents 1 SD above and below the mean, n=3. 118
Figure 4.11: B concentration in process water for 1:3 and 1:1.5 FA: AMD reactions. Error bar represents 1 SD above and below the mean, n=3. 119
Figure 4.12: % $H_2BO_3^-$ in process water for 1:1.5 and 1:3 FA: AMD reactions as a function of pH. 119
Figure 4.13: Mo concentration in process water for 1:3 and 1:1.5 FA: AMD reactions. Error bar represents 1 SD above and below the mean, n=3. 120
Figure 4.14: Si concentration in process water for 1:3 and 1:1.5 FA: AMD reactions. Error bar represents 1 SD above and below the mean, n=3. 121
Figure 4.15: A plot of log H_4SiO_4 activity versus pH showing control of dissolved silica by amorphous $SiO_{2(amorphous)}$ in process water for 1:3 and 1:1.5 FA: AMD reactions. 121
Figure 4.16: A plot of 2 log H_4SiO_4 + 6 log Al^{3+} activity versus pH showing control of dissolved silica by mullite in process water for 1:3 and 1:1.5 FA: AMD reactions at pH>8. 123
Figure 4.17: Ca and Na concentration in process water for 1:3 and 1:1.5 FA: AMD reactions. Error bar represents 1 SD above and below the mean, n=3. 123
Figure 4.18: XRD spectra of gypsum that precipitated in un-acidified filtered process waters for contact times of 1-30 minutes, reference spectra for pure gypsum superimposed for comparison 124
Figure 4.19: Activity-solubiltiy diagrams for anhydrite and gypsum for 1:3 and 1:1.5 FA: AMD ratios. 125
Figure 4.20: Mg concentration in process water for 1:3 and 1:1.5 FA: AMD reactions. Error bar represents 1 SD above and below the mean, n=3. 126
Figure 4.21: Mn concentration in process water for 1:3 and 1:1.5 FA: AMD reactions. Error bar represents 1 SD above and below the mean, n=3. 127
Figure 4.22: Cu and Zn concentration in process water for 1:3 and 1:1.5 FA: AMD reactions. Error bar represents 1 SD above and below the mean, n=3. 128
Figure 4.23: Activity diagrams for the variation of ferric ion and Cu^{2+}, Zn^{2+}, and Mn^{2+} with pH in process waters for 1:3 and 1:1.5 FA: AMD ratios. 129
Figure 4.24: Activity diagrams for the variation of aluminum ion and Cu^{2+}, Zn^{2+}, and Mn^{2+} with pH in process waters for 1:3 and 1:1.5 FA: AMD ratios. 129
Figure 5.1: The 150 litre capacity agitator used to generate the solid residues used for the drainage experiments. 146
Figure 5.2: A photo and schematic drawing of the column assembly used for the leaching experiments (all columns used were PVC pipes of diameter 101 mm) 147
Figure 5.3: Cement blended Solid residue slurry cured in plastic cylinders for strength development testing at Miningtek laboratory. 154
Figure 5.4: Change in pH and EC with time for SAMD (Fe^{2+}/Fe^{3+}) ratio of 2:3 156
Figure 5.5: Change in pH and EC with time for SAMD (Fe^{2+}/Fe^{3+}) ratio of 1:1 157
Figure 5.6: Evolution of pH in the leachate with cumulative volume for the unreacted FA 160
Figure 5.7: Column leachate EC values as a function of cumulative volume for the unreacted FA. 160

UNIVERSITY of the
WESTERN CAPE

Figure 5.8: Evolution of pH in the leachate with cumulative volume for solid residues (SR). 160
Figure 5.9: Column leachate EC values as a function of cumulative volume for solid residues (SR). 160
Figure 5.10: Evolution of pH in the leachate with cumulative volume for the solid residues (SR) + 5 % FA. 161
Figure 5.11: Column leachate EC values as a function of cumulative volume for the solid residues (SR) + 5 % FA. 161
Figure 5.12: Evolution of pH in the leachate with cumulative volume for the solid residues (SR) + 25 % FA. 161
Figure 5.13: Column leachate EC values as a function of cumulative volume for the solid residues (SR) + 25 % FA. 161
Figure 5.14: Evolution of pH in the leachate with cumulative volume for the solid residues (SR) + 40 % FA. 162
Figure 5.15: Column leachate EC values as a function of cumulative volume for the solid residues (SR) + 40 % FA. 162
Figure 5.16: Evolution of pH in the leachate with cumulative volume for the solid residues (SR) + 6 % Ordinary Portland Cement. 162
Figure 5.17: Column leachate EC values as a function of cumulative volume for the solid residues (SR) + 6 % Ordinary Portland Cement 162
Figure 5.18: SEM-backscattered micrograph of gypsum crystals in FA column cores with the EDX pattern superimposed. 167
Figure 5.19: SEM-backscattered micrograph of gypsum crystals in solid residue (SR) column cores with the EDX pattern superimposed. 167
Figure 5.20: Plot of pH versus 2Log $^{\alpha}Al^{3+}$ + Log $^{\alpha}H_4SiO_4$ over the pH range 6.5-9.0 for solid residue (SR) core leachates (SR column core) 169
Figure 5.21: Plot of pH versus 2 Log $^{\alpha}Al^{3+}$ + Log $^{\alpha}H_4SiO_4$ over the pH range 6.5-9.0 for solid residue (SR) + 25 % FA core leachates (column 5) 170
Figure 5.22: Sillimanite solubility equilibria for solid residue (SR) core leachates 171
Figure 5.23: Mullite solubility equilibria for solid residue (SR) core leachate 171
Figure 5.24: Sillimanite solubility equilibria for solid residue (SR) + 25 % FA core leachates. .. 172
Figure 5.25: Mullite solubility equilibria for solid residue (SR) + 25 % FA core leachates. 172
Figure 5.26: Sillimanite solubility equilibria for FA column core leachates. 173
Figure 5.27: Mullite solubility equilibria for FA column core leachates. 173
Figure 5.28: Amorphous silica solubility equilibria for solid residue (SR) column core leachates. (solid line represents $SiO2_{(amorphous)}$ equilibria) 175
Figure 5.29: Amorphous silica solubility equilibria for solid residue (SR) + 25 % FA column core leachates. 175
Figure 5.30: Amorphous silica solubility equilibria for FA column core leachates. 176
Figure 5.31: XRD spectra of the FA column solid cores showing the change in the mullite: quartz peak ratio from top to bottom. 177
Figure 5.32: XRD spectra of the solid residue cores showing the change in the mullite: quartz peak ratio from top to bottom of core. 178
Figure 5.33: XRD spectra of the solid residue (SR) + 40 % FA cores showing the change in the mullite: quartz peak ratio from top to bottom. 178
Figure 5.34: Equilibrium pH for precipitating basic aluminum hydroxy sulphates for the SR solid cores compared to measured pH of leachate (error bars represent 1 SD above and below the mean, n=4) 182
Figure 5.35: Equilibrium pH for precipitating basic aluminum hydroxy sulphates for the FA solid cores compared to measured pH of leachate (error bars represent 1 SD above and below the mean, n=4). 182

Figure 5.36: Equilibrium pH for the dissolution of jarosite-K for the SR and FA solid cores compared to measured pH of leachate (error bars represent 1 SD above and below the mean, n=4). 183
Figure 5.37: SEM micrograph showing ettringite crystals embedded in CSH gel matrix, the EDX pattern is superimposed showing the Ca/Al ratio which approximates that of ettringite. Strong Si signal is observed, a contribution from underlying CSH gel. 185
Figure 5.38: Saturation indices for ettringite with pH change as the drainage progressed for the SR + 6 % OPC solid cores. 185
Figure 5.39: SEM micrograph showing the C-S-H gel that embedded the ettringite crystals, the EDS pattern superimposed showing Ca/Si ratio which approximates that of C-S-H gel (Taylor, 1997). 186
Figure 5.40: SEM micrograph showing extensive aggregation of the solid residue particles in the SR + 6 % OPC column cores. 187
Figure 5.41: SEM micrograph showing encapsulation of the solid residue particles in the SR + 6 % OPC column cores by a Si-rich gel. The gel could not be conclusively identified by SEM-EDX. 188
Figure 5.42: Equilibrium pH for the precipitation of jurbanite in SR + 6 % OPC solid cores compared to measured pH of leachate (error bars represent 1 SD above and below the mean, n=4). 189
Figure 5.43: Fe, Mn and Al concentration in leachates versus cumulative volume (L/kg) of SAMD for FA solid cores (error bars represent 1 SD above and below the mean, n=4). 191
Figure 5.44: Ca and SO_4^{2-} concentration in leachates versus cumulative volume (L/kg) of SAMD for FA solid cores (error bars represent 1 SD above and below the mean, n=4). 191
Figure 5.45: Fe, Mn and Al concentration in leachates versus cumulative volume (L/kg) of SAMD for SR solid cores (error bars represent 1 SD above and below the mean, n=4). 194
Figure 5.46: Ca and SO_4^{2-} concentration in leachates versus cumulative volume (L/kg) of SAMD for SR solid cores (error bars represent 1 SD above and below the mean, n=4). 194
Figure 5.47: Fe, Mn and Al concentration in leachates versus cumulative volume (L/kg) of SAMD for SR + 25 % FA solid cores (error bars represent 1 SD above and below the mean, n=4). 197
Figure 5.48: Ca and SO_4^{2-} concentration in leachates versus cumulative volume (L/kg) of SAMD for SR + 25 % FA solid cores (error bars represent 1 SD above and below the mean, n=4). 197
Figure 5.49: Fe, Mn and Al concentration in leachates versus cumulative volume (L/kg) of SAMD for SR + 6 % OPC solid cores (error bars represent 1 SD above and below the mean, n=4). 199
Figure 5.50: Ca and SO_4^{2-} concentration in leachates versus cumulative volume (L/kg) of SAMD for SR + 6 % OPC solid cores (error bars represent 1 SD above and below the mean, n=4). 200
Figure 5.51: Plots of log SO_4^{2-} activity versus log Ca activity showing control of SO_4^{2-} and Ca by gypsum solubility in the leachates for FA and SR solid cores. 205
Figure 5.52: Plots of log SO_4^{2-} activity versus log Ca activity showing control of SO_4^{2-} and Ca by gypsum solubility in the leachates for SR + 25 % FA column solid cores. 205
Figure 5.53: SEM micrographs of leached solid residues from column 1(FA) and column 5 (SR + 25 % FA) showing gypsum crystals, C1, C5bottom-Backscattered signal, C5top-secondary electron signal, with accompanying EDX pattern of the spots analyzed (enclosed in a box). 207
Figure 5.54: SEM micrographs of leached solid residues from column 2(SR) showing gypsum crystals. C2Top –Backscattered signal, magnification=500. C2middle-backscattered electron signal, magnification=3000, with accompanying EDX pattern of the spots analyzed (enclosed in a box). 208
Figure 5.55: Regressional analysis of log Fe activity versus log SO_4^{2-} activity for the FA, SR and SR + FA solid cores leachates. (R^2 reported at 95 % confidence limits). 210
Figure 5.56: SEM micrographs of leached solid residues from column 8(SR + 6 % OPC) showing gypsum crystals. C8Top–Backscattered signal, magnification=14000. C8bottom-backscattered

electron signal, magnification=1000, with accompanying EDS pattern of the spots analyzed (enclosed in a box). 212
Figure 5.57: Plots of log SO_4^{2-} activity versus log Ca activity showing control of SO_4^{2-} and Ca by gypsum solubility in the leachates for SR + 6 % OPC column solid cores. 213
Figure 5.58: Plots of saturation indices for precipitating Fe-bearing mineral phases during the leaching study period for FA and SR solid core leachates. 216
Figure 5.59: Plots of saturation indices for precipitating Fe-bearing mineral phases during the leaching study period for SR + 25 % FA and SR + 6 % OPC solid core leachates..... 216
Figure 5.60: Logarithmic activity plot of the dissolved Fe^{3+} versus pH in the leachates for FA, SR, SR + 25 % FA and SR + 6 % OPC solid cores. 218
Figure 5.61: Plot of log Fe^{3+} activity against pH for the FA solid core leachates with solubility lines for, Ⅰ-Fe(OH)3(a) ($\log^{\alpha} Fe^{3+}$= -3-3pH), Ⅱ-K-jarosite ($\log^{\alpha}Fe^{3+}$= -2.8-2pH), Ⅲ-FeOHSO4 ($\log^{\alpha}Fe^{3+}$= -7.94-pH), Ⅳ-Ferrihydrite ($\log^{\alpha}Fe^{3+}$= 4.89-3pH), Ⅴ-Schwertmannite ($\log^{\alpha}Fe^{3+}$= 2.52-2.75pH) added. Solubiltiy lines calculated using an average $\log^{\alpha} K^{+}$= -2.15 and $\log^{\alpha} SO_4$= -2.12 (calculated values from measured data) and log *Ks* values for Fe(OH)3(a), K-jarosite, FeOHSO4, Ferrihydrite, Schwertmannite are –3, -14.8, -10.06, 4.891 and 18.0 respectively (Jae Young yu, 1996; Bigham *et al*., 1996). 219
Figure 5.62: Plot of log Fe^{3+} activity against pH for the SR solid core leachates with solubility lines for, Ⅰ-Fe(OH)3(a) ($\log^{\alpha} Fe^{3+}$= -3-3pH), Ⅱ-K-jarosite ($\log^{\alpha}Fe^{3+}$= -2.16-2pH), Ⅲ-FeOHSO4 ($\log^{\alpha}Fe^{3+}$= -8.03-pH), Ⅳ-Ferrihydrite ($\log^{\alpha}Fe^{3+}$= 4.89-3pH), added. Solubiltiy lines calculated using an average $\log^{\alpha} K^{+}$= -3.25 and $\log^{\alpha} SO_4$= -2.03 (calculated values from measured data) and log Ks values for Fe(OH)3(a), K-jarosite, FeOHSO4, Ferrihydrite, are –3, -14.8, -10.06 and 4.891 respectively (Jae Young yu, 1996; Bigham *et al*., 1996a and 1996b). 220
Figure 5.63: Plot of log Fe3+ activity against pH for the SR + 25 % FA solid core leachates with solubility lines for, Ⅰ-Fe(OH)3(a) ($\log^{\alpha} Fe^{3+}$= -3-3pH), Ⅱ-K-jarosite ($\log^{\alpha}Fe^{3+}$= -2.46-2pH), Ⅲ-FeOHSO4 ($\log^{\alpha}Fe^{3+}$= -7.07-pH), Ⅳ-Ferrihydrite ($\log^{\alpha}Fe^{3+}$= 4.89-3pH), Ⅴ-Schwertmannite ($\log^{\alpha}Fe^{3+}$= 2.51-2.75pH) added. Solubiltiy lines calculated using an average $\log^{\alpha} K^{+}$= -3.23 and $\log^{\alpha} SO_4$= -2.09 (calculated values from measured data) and log Ks values for Fe(OH)3(a), K-jarosite, FeOHSO4, Ferrihydrite, Schwertmannite are –3, -14.8, -10.06, 4.891 and 18.0 respectively (Jae Young yu, 1996; Bigham *et al*., 1996a and 1996b). 221
. 221
Figure 5.64: Plot of log Fe3+ activity against pH for the SR + 6 % OPC solid core leachates with solubility lines for, Ⅰ-Fe(OH)3(a) ($\log^{\alpha} Fe^{3+}$= -3-3pH), Ⅱ-K-jarosite ($\log^{\alpha}Fe^{3+}$= -2.55-2pH), Ⅲ-FeOHSO4 ($\log^{\alpha}Fe^{3+}$= -7.83-pH), Ⅳ-Ferrihydrite ($\log^{\alpha}Fe^{3+}$= 4.89-3pH), Ⅴ-Schwertmannite ($\log^{\alpha}Fe^{3+}$= 2.52-2.75pH), α-goethite ($\log^{\alpha}Fe^{3+}$= 0.5-3pH) added. Solubiltiy lines calculated using an average $\log^{\alpha} K^{+}$= -2.90 and $\log^{\alpha} SO_4$= -2.12 (calculated values from measured data) and log *K*s values for Fe(OH)3(a), K-jarosite, FeOHSO4, Ferrihydrite, Schwertmannite, α-goethite are –3, -14.8, -10.06, 4.891, 18.0 and 0.5 respectively (Jae Young yu, 1996; Bigham *et al*., 1996a and 1996b). 222
Figure 5.65: Plots of saturation indices for precipitating Al-(oxy) hydroxide and Al-hydroxysulphates mineral phases during the leaching study period for FA solid core leachates. 225
Figure 5.66: Plots of saturation indices for precipitating Al-(oxy) hydroxide and Al-hydroxysulphates mineral phases during the leaching study period for SR solid core leachates. 226
Figure 5.67: Plots of saturation indices for precipitating Al-(oxy) hydroxide and Al-hydroxysulphates mineral phases during the leaching study period for SR + 25 % FA solid core leachates. 226

Figure 5.68: Plots of saturation indices for precipitating Al-(oxy) hydroxide and Al-hydroxysulphates mineral phases during the leaching study period for SR + 6 % OPC solid core leachates. 227
Figure 5.69: Plot of log Al^{3+} activity against pH for the FA, SR, SR + 25 % FA and SR + 6 % OPC solid core leachates with solubility lines for Al(OH)3(a) ($\log^{\alpha} Al^{3+}$= 10.8-3pH), gibbsite ($\log^{\alpha}Al^{3+}$ = 7.74-3pH), boehmite ($\log^{\alpha}Al^{3+}$= 8.58-3pH), Solubiltiy lines calculated using log K_s values for Al(OH)3(a), gibbsite, boehmite are 10.8, 7.74, and 8.58 respectively (Jae Young yu, 1996). 228
Figure 5.70: Leachate ion activities relative to stability lines for Al-hydroxysulphate minerals, gibbsite and amorphous $Al(OH)_{3(a)}$. Stability line of alunite was fixed using average value of pK and pOH calculated using PHREEQC (FA: pOH=7.21, pK^{+}=2.15; SR: pOH=7.31, pK^{+}=3.25; SR + 25 % FA: pOH=6.70, pK^{+}=3.25; SR + 6 % OPC: pOH=8.23; pK^{+}=2.90) (average values derived from the data generated using PHREEQC)..... 231
Figure 5.71: Saturation indices versus pH for selected Mn-bearing mineral phases for FA, SR, SR + 25 % FA and SR + 6 % OPC solid residue cores. 232
Figure 5.72: Leachate Mn^{2+} activities versus CO_3^{2-} activities for FA, SR, SR + 25 % FA and SR + 6 % OPC showing the pH ranges at which rhodochrosite controls Mn^{2+} activity. Log K= -10.39 (WATEQ4 database)(Ball and Nordstrom, 1991). 234
Figure 5.73: Logarithm of the activity of Mn^{2+} ion plotted against pH with equilibrium solubility lines for pyrolusite and manganite for FA, SR, SR + 25 % FA and SR + 6 % OPC solid cores. The default $\rho\varepsilon$ = 4.0 in PHREEQC was assumed in calculating the Mn^{2+} activity in equilibrium with pyrolusite and manganite. 235
Figure 5.74: Digital photos of the sectioned FA and SR leached solid cores..... 237
Figure 5.75: Digital photos of the SR + 25 % FA and SR + 6 % OPC leached solid cores..... 238
Figure 5.76: Infra-red spectra for the top, middle and bottom slices of the fly ash (FA) leached solid residues cores with the spectra of a pure unhydrous ferric sulphate imposed for comparison. 240
Figure 5.77: Infra-red spectra for the top, middle and bottom slices of the leached solid residues (SR) cores with the spectra of ammonium oxalate extracted (ES)top slice imposed for comparison. 240
Figure 5.78: Infra-red spectra for the top, lower top, upper bottom and bottom slices of the leached solid residue (SR) + 25 % FA cores..... 241
Figure 5.79: Infra-red spectra for the top, middle and bottom slices of the leached solid residue (SR) + 6 % OPC cores. 241
Figure 5.80: SEM backscattered micrographs showing spots where EDX analysis was done for the solid residue (SR) cores. 246
Figure 5.81: SEM backscattered micrographs showing spots where EDX analysis was done for the SR + 6 % OPC solid cores. 249
Figure 5.82: Graphical pH profile of the pore waters of the leached FA and solid residue (SR) cores. Error bars represent 1 standard deviation above and below the mean. 253
Figure 5.83: SEM micrograph showing numerous gypsum crystals in the top section of the leached solid residue (SR) cores. 261
Figure 5.84: Backscattered SEM micrograph showing Fe, Mn, S rich Ca-Al-Si-O gel with accompanying EDS analysis. 265
Figure 5.85: SEM micrograph showing Ca-Si-Al-O rich gel encapsulating precipitates and solid residue particles (CSO-Ca-Si-O gel was identified earlier on by SEM-EDX). 265
Figure 5.86: Particle size distribution for unreacted and AMD reacted Matla fly ash 268
Figure 5.87: Unconfined compressive strength of batch one solid residue slurries. 270
Figure 5.88: Unconfined compressive strength of batch two solid residue slurries. 270
Figure 5.89: Unconfined compressive strength of batch three solid residue slurries. 271

UNIVERSITY of the
WESTERN CAPE

FigureA1: Flow diagram of the experimental sequence, analytical techniques used, type of data generated and application 310
Figure A2: Schematic diagram of ICP-MS main processes 312
Figure A3: Calibration graph of Fe^{2+} standard solutions 320
Figure B20: XRD spectra of FA solid core sections with spectra for precipitates washed down the solid core (G-gypsum). 358
Figure B21: XRD spectra of solid residue core sections (G-gypsum) 359
Figure B22: XRD spectra of solid residue (SR) + 40 % FA core sections (G-gypsum) 360
Figure B23: XRD spectra of solid residue (SR) + 6 % OPC core sections (G-gypsum) 361
Figure B24: Summarized leachate pH trends versus evolving L/S ratios for FA, SR, SR + 5 % FA, SR + 25 % FA, SR + 40 % FA and SR + 6 % OPC solid cores (error bar represents one SD below and above the mean)..... 362

UNIVERSITY of the
WESTERN CAPE

Chapter One

Introduction

1 Introduction

The mining industry in South Africa has a huge potential to impact negatively on the environment. Negative impacts include generation of reactive dam tailings and acid mine drainage (AMD). Sources of water related pollution are underground and opencast mining, metallurgical plants, mining infrastructure and mine residual deposits. On infiltration by rainwater, mine spoil heaps leach highly acidic mine drainage to groundwater as a result of pyrite oxidation that form sulphuric acid, which in turn mobilizes toxic metal species.

South Africa uses more than 100 million tonnes of low grade bituminous coal to produce cheap electricity (Willis, 1987). The associated mining operations result in millions of tonnes of polluted water and inturn vast amounts of waste ash created by the power plants that burn coal to produce electricity. Coal combustion activities generate a total of 27.7 MT of fly ash annually (Table 1.1). These two pollutants cause major environmental problems and are expensive to dispose safely. Pulverized fly ash (PFA) is the non-combustible material (ash) leaving the furnaces when pulverized coal is combusted to power the steam turbines that make electricity. It is the sum of bottom ash and fly ash (FA).

UNIVERSITY of the
WESTERN CAPE

Table 1.1: The production of FA by pulverized coal fired power stations in South Africa (Krüger, 2003).

Power station	Locality	Production (tons)
Arnot	Middleburg (Mpumalanga)	550 000
Duhva	Witbank	400 000
Hendrina	Hendrina	1575 000
Kendal	Witbank	3500 000
Kriel	Bethal	2000 000
Matla	Bethal	2700 000
Lethabo	Sasolburg	5300 000
Matimba	Ellisras	4950 000
Tutuka	Standerton	1765 000
Majuba	Amersfoort	213 000
SASOL1	Sasolburg	750 000
SASOL1 and 2	Secunda	4000 000
Total		27 703 000

UNIVERSITY of the
WESTERN CAPE

Fly ash is the fraction of waste that enters the flue gas stream and is usually collected by means of electrostatic precipitators, bughouses or mechanical collection devices such as cyclones. It is a fine-grained powdery particulate material which is predominantly spherical in shape, either solid or hollow. It is a ferro-alumino silicate material made up of particles with sizes ranging from 20 to 80 μm with elements Si, Al, Fe, Ca, K and Na being predominant within the matrix (Adriano *at al*., 1980; Mattigod, 1990). The mineralogy of fly ash is greatly influenced by the parent coal from which it was derived. The principal components of bituminous coal fly ash prevalent in South Africa are silica, alumina, iron oxides and calcium oxide with varying amounts of unburned carbon. Fly ash has a high degree of alkalinity due to the presence of a lime fraction. It has been shown that many inorganic contaminants are also present (Mattigod *et al*, 1990; Eary *et al.*, 1990).

Fly ash is normally pumped in slurry form to ash heaps and hardens to a rock like consistency over time. Dry ash disposal is also currently being carried out at several South

Africa's power stations. The wastewater in the disposal slurry as well as rainfall leaches out toxic metals, anions and cations from the ash heaps, which pose an environmental hazard.

Acid mine drainage (AMD) is an unavoidable by-product of the mining and mineral industry. It is produced when water and oxygen come into contact with sulphide minerals. This occurs primarily in coal and gold mines and their tailings. It may also occur in soils that are close to the sea or contained in drained marshlands. Acid mine waters typically contain high concentrations of dissolved heavy metals and sulphate. They can have pH as low as 2 (Bigham *et al* 1990). Azzie (2002) carried out a large scale chemical classification of waters draining collieries on the South African Highveld. The dominant anion was SO_4^{2-} with no obvious dominant cation. A bimodal distribution of the pH of the mine waters was observed with the waters being either acidic or near-neutral. These conditions prohibit discharge of untreated acid mine waters into public streams, as they have a detrimental effect on aquatic plant and animal life. Groundwater pollution caused by the drainage of acid mine water is an equally serious problem. Coal mining in South Africa is estimated to produce 175 ML of AMD per day in the Pretoria-Witwatersrand-Vereening (PWV) area alone (Van Niekerk, 2001) and a further 120 000 ML is stored. Due the extremely low pH of AMD, metals such Fe, Al and Mn are present in high concentrations. Sulphate is also present at unacceptably high concentrations (Petrik *et al*., 2005). The current legislation requires the mines to carry out neutralization and clarification of all AMDs before allowing it to rejoin natural water streams.

Usually acid mine water is neutralized by treatment with lime, limestone, or sodium hydroxide. This results in precipitation of metal hydroxides (Cravotta *et al.,* 1999) and sulphides in the case of biological treatment using sulphate reducing bacteria (SRBs). Since the minimum solubility for the sulphide precipitates made with the different metals found in the polluted water occur at different pH values, and the hydroxide precipitates are amphoteric in nature, maximum removal efficiency of mixed metals cannot be achieved at a single pH level. For this reason acid mine water has to be treated in multiple stages. For example the Savmin process (Smit and Sibilski, 2003) involves five stages of heavy metal and magnesium precipitation, gypsum desupersaturation, ettringite precipitation for the removal of calcium and sulphate, carbonation and recycling of aluminium hydroxide.

The main advantages of using calcium carbonate for neutralizing acid mine waters over lime or sodium hydroxide are its lower price, sustained generation of alkalinity and production of smaller sludge volumes (Maree *et al*., 1996). However compared with hydrated lime Ca $(OH)_2$, limestone requires a longer reaction time to treat acid mine water. Sulphide precipitation with Na_2S, NaHS or CaS is a more effective process for the treatment of industrial waste containing highly toxic metals. Its main advantages are the attainment of a high degree of metal removal over a broad pH range, an effective precipitation of certain metals even at low pH levels and a short reaction time (Van *et al.*, 2004). However sulphide precipitation has a tendency to form toxic H_2S at low pH values. Another important disadvantage of these chemical treatments of acid mine water is the high cost of treatment chemicals. The precipitated poorly crystallized minerals (Murad *et al.,* 1994) called ochres, are classified as hazardous waste and must be disposed of in dump sites.

In South Africa most of the power stations are built in close proximity to the mines that supply them with coal. Figure 1 shows the collieries and Eskom power stations where Acid Mine drainage and Fly Ash samples for this work were collected. These results in two major environmental pollutants being produced adjacent to each other. The proximity of these wastes suggests that the problem of effective remediation may be solved through co-disposal. The highly soluble CaO occurring as sub-micron fragments on the fly ash particles is highly reactive and can be utilized in the neutralization of the acid mine drainage. This has prompted studies of the possible co-disposal of the two pollutants with the benefits of neutralizing the acid mine water and producing less polluted process waters. The neutralization of AMD using various methods and various uses of fly ash has been studied extensively (Cravotta *et al*., 1999; Hodgson *et al.,* 1982; Jenke *et al*., 1983; Maree and Todder, 2000; Thomson, 1980). The application of fly ash to control acid generation from sulphidic wastes such as mine tailings and coal spoils has also been studied (Xenidis *et al.,* 2002). Karapanagioti and Atalay (2001) carried out a laboratory evaluation of ash materials as acid-disturbed land amendments.

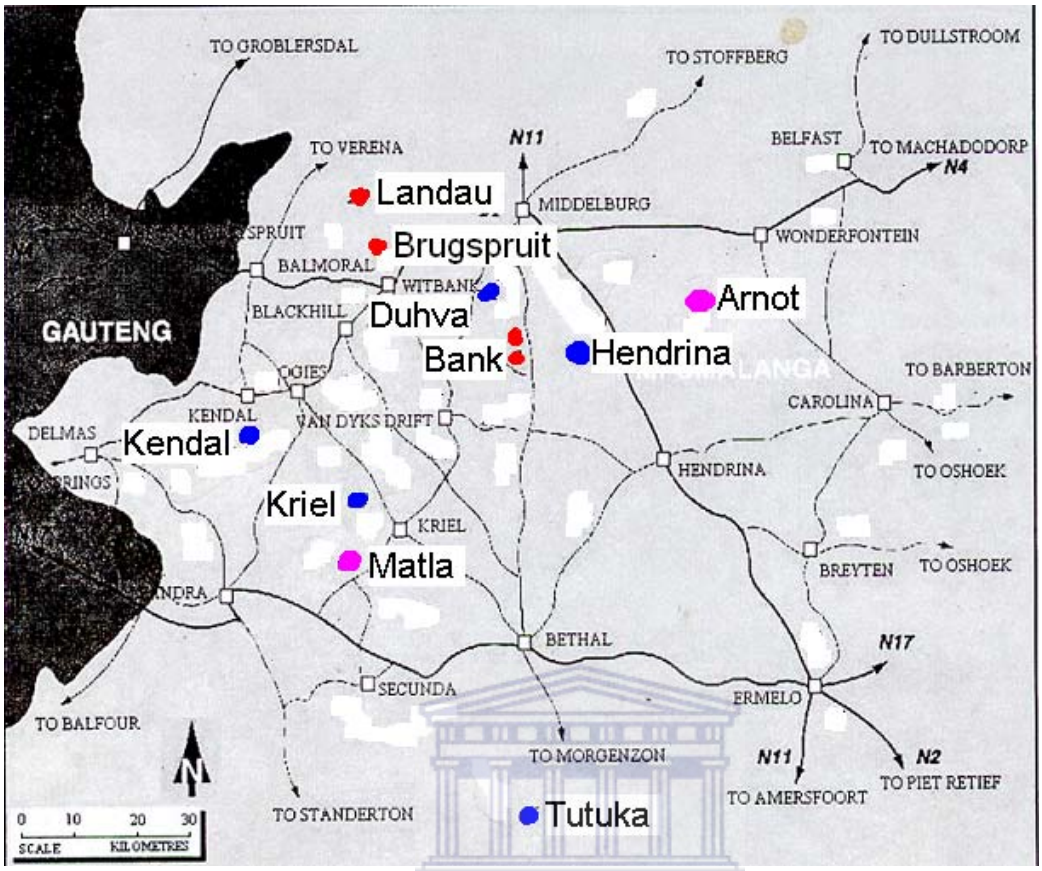

Figure 1.1: A Map showing the collieries (marked in red) and Eskom power stations (marked in pink) where Acid Mine Drainage and Fly Ash samples were taken from. Other Eskom power stations are marked in blue (Eskom 2000; Bullock and Bell., 1997), Navigation AMD was sampled at Landau, Brugspruit AMD at Brugspruit.

The alkalinity of the fly ash may not be as high as that of lime or limestone (Klink, 2004; Maree and De. Beer, 2000) but the availability of large quantities at no extra cost offers a cost effective method of neutralizing acid mine drainage. Moreover the possible formation of stable mineral phases with trace metal co-precipitation and adsorption could result in solid residues that are suitable for disposal than the unreacted fly ash. A method of utilizing the reactivity of the fly ash and modifying the solid residues to be suitable for coal mine backfilling is sought.

UNIVERSITY of the
WESTERN CAPE

Chapter Two

Generation, characteristics and environmental impacts of fly ash and acid mine drainage (AMD): Chemistry and mineralogy of the precipitates formed on increasing the pH of the AMD. A literature Review.

2 Introduction

This chapter describes the generation, properties and environmental impacts of fly ash disposal and the various application of fly ash. The chemistry of acid mine drainage and the environmental impacts and the methods that have been employed for the ameroliation of this waste water will also be discussed. The chapter also introduces the reader to the various studies that have tried to use fly ash to ameroliate acid mine drainage and the chemistry involved in these processes. A description of the mineral precipitates identified on raising the pH of the AMD is presented. The chemistry of the Portland cement as a stabilizer of fly ash with respect to fixation of heavy metals and SO_4^{2-} is discussed.

2.1 Coal and coal combustion by-products

UNIVERSITY of the
WESTERN CAPE

Coal is an easily combustible rock that contains 50 % or more by weight and 70 % by volume of carbonaceous material (Schopf, 1956). It is formed in environments that promote plant growth and under depositional conditions that favor preservation of the dead plants. Two mechanisms are involved in the conversion of organic debris into peat, allochthonous and autochonous deposition. Allochthonous deposition occurs when the vegetation is transported and redeposited by means such as moving water or wind while autochonous formations occur when the vegetative material is deposited where it grows and dies without any transportation. Autochonous formations are the most common in coal beds. Allochthonous formations contain a much greater amount of mineral matter that gets deposited along with the plant material when it is transported (Teichmuller and Teichmuller, 1975).

The mineralogy of the constituents of coal is dependent on the geology of the surrounding environment of the coal formation. The most common mineral constituents are the clay minerals, illite ($[OH]_4K_2[Si_6Al_2]Al_4O_{20}$) and kaolinite ($[OH]_8Si_4Al_4O_{10}$); sulfides such as pyrite (FeS_2) and marcasite (FeS_2); carbonates like dolomite [$CaMg(CO_3)_2$], ankerite

[$CaMg_xFe_{(1-x)}(CO_3)_2$], calcite ($CaCO_3$) and siderite ($FeCO_3$) and quartz (SiO_2). Clay minerals make up 60-90 % of the total mineral matter and quartz is found in almost all coal and can comprise from 1 to 20 % of the inorganic compounds present in the coals (Rao and Gluskoter, 1973). Many trace elements are present within coal deposits, ranging from a few percent of the total composition to a fraction of a part per million (ppm).

There are several types of inorganic residues arising from coal combustion processes: these include fly ash, bottom ash and boiler slag (Fig 2.1). They are generated from the combustion of pulverized coal in thermal power plants. Bottom ash and boiler slag settle to the bottom of the combustion chamber and consist of coarse particles (19-75 mm). Fly ash is a fine residue composed principally of spherical micron-sized particles collected from dust collection systems (Table 2.1). It is normally transported from the boilers by the flue gas streams where it is trapped by means of electrostatic precipitators. Another byproduct of coal combustion are the flue–gas–desulfurization (FGD) products which consists mainly of calcium sulfate ($CaSO_4$) or gypsum ($CaSO_4.2H_2O$). These products arise due to the need for the power plants using high sulfur (2-3.5 %) bituminous coal to reduce their SO_2 gas emissions. FGD products result from a chemical process which involves chemically combining the sulfur gases released in coal combustion by reacting them with a sorbent, such as limestone, lime or ammonia which is normally in slurry form. As the flue gas comes into contact with the slurry of calcium salts, sulfur dioxide (SO_2) reacts with the calcium to form hydrous calcium sulphate (Kalyoncu, 1999).

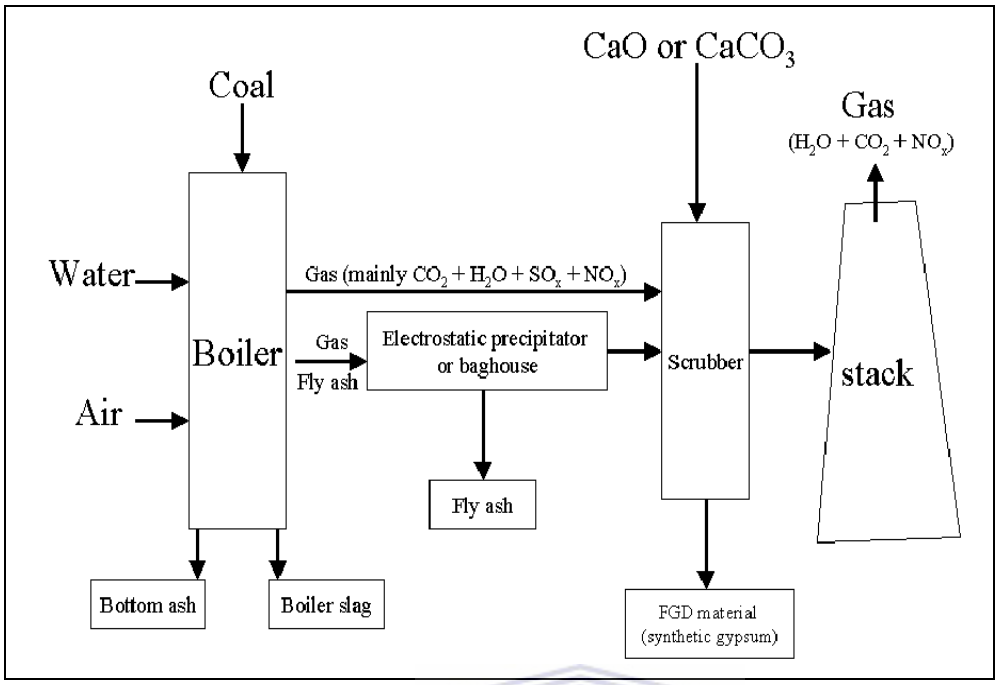

Figure 2:1: Flow diagram of coal combustion and related processes leading to the formation of the various coal combustion products.

2.1.1 Fly ash: Physical, Chemical and Mineralogical characteristics

UNIVERSITY of the
WESTERN CAPE

The physical, chemical and mineralogical properties of fly ash depend on the composition of the parent coal, the conditions during coal combustion (temperature, air/fuel ratio, coal pulverization size and rate of combustion) efficiency of emission control devices, the storage and handling of the by-products and the climate (Eary *et al.,* 1990; Xenidis *et al*., 2002)

South African Bureau of standards (SABS) (2002) defines fly ash as the powdery residue obtained by separation of the solids from the flue gases of furnaces fired with pulverized coal.

Fly ash consists of many small (0.01-100 μm diameter) glass-like particles of a generally spherical character. The fineness of fly ash particles depends largely on the combustion temperature, the grinding size of introduced coal and whether the resultant particle is spherical or irregular. Watt and Thorne, (1965) produced synthetic fly ashes and compared them to 14 industrial ashes. They were able to show that each primary fly ash particle is produced by the burning out of a single coal particle containing at least two mineral species. The spheres that make fly ash include solid glass spheres, hollow glass spheres (cenospheres) and hollow glass spheres containing other glass spheres (plerospheres). The spherical, glassy,

and transparent appearance of fly ashes indicates the melting of silicate minerals during coal combustion. The Fe-oxide content of the spheres can influence their color which ranges from water-white to yellow, orange to deep red, or brown to opaque (Fisher *et al.,* 1978). These spheres are believed to be formed as a result of the high temperature reached during the instantaneous burning of coal, where most of the mineral components in the coal melt and form small fused drops. The ash particles generally vary in size from 1.0 to 300 microns and are frequently finer than 74 microns (Helmuth, 1987).

Mehta (1994) found that fly ash particles containing high amounts of CaO are finer than those containing low quantities. A higher CaO content in the parent coal results in a higher degree of melting and subsequently an increase in concentration of smooth glass spheres. Some of the physical properties of fly ash are shown in Table 2.1. Fly ash has a high specific surface area and small particle size which offer a high potential reactivity. The specific gravity varies depending on the rank of coal from which it was derived. Measurement of specific gravity of 18 fly ashes from the United Kingdom established that they lie in the range of 1.97-2.58 g/cm^3 (Cabrera *et al*., 1986). Natusch *et al.,* (1975) reported a mean particle density of a midwestern U.S. fly ash of 2.7 g/cm^3 for non-magnetic and 3.4 g/cm^3 for magnetic particles. The great surface area ensures that the elements volatilized during combustion condense on the surface of fly ash particles in high concentrations. These elements can be mobilized under disposal conditions (Mattigod *et al*., 1990; Phung *et al*., 1979)

Table 2.1: Physical properties of fly ash (Summers *et al.,* 1983).

Physical property	Fly ash
Specific gravity (no units)	1.59-3.1
Dry bulk density (g/m^3)	1.01-1.43
Specific surface area (m^2/kg)	200-3060
Mean particle diameter (μm)	20-80

Willis (1987) found significant variations in the composition of South African fly ash (Table 2.2). These variations reflect the differences in the parent coal composition from different coal fields and coal seams. Bituminous coal comprises 98 % of South African fly ash production (Morris, 1997) and gives the ashes produced in South Africa their physical, mineralogical and chemical properties.

Table 2.2: Major element composition (weight %) of Arnot and Sasol fly ash. (Willis, 1987)

Fly ash/element	Arnot	Sasol
SiO_2	53-63	61-67
TiO_2	1.3-1.5	1.2-1.4
Al_2O_3	25-27	23-27
Fe_2O_3	4.8-5.4	3.1-4.8
MnO	0.4-0.5	0.30
MgO	1.7-2.0	1.4-1.7
CaO	6.3-7.0	6.1-7.1
Na_2O	0.16-0.21	0.76-1.3
K_2O	0.48-0.51	0.31-0.48
P_2O_3	0.38-0.89	0.22-0.51
SO_3	0.15-0.34	0.11-0.26

UNIVERSITY of the
WESTERN CAPE

Fly ash is a ferro-alumino-silicate compound containing considerable quantities of Ca, K, and Na with traces or none of C and N (Carlson and Andriano, 1993). The most common minerals found in fly ash are quartz and mullite ($Al_6Si_2O_{13}$) with lesser amounts of magnetite, maghemite, anhydrite and lime (Bezuidenhout, 1995). Mullite is formed by the decomposition of aluminosilicate phases of coal such as kaolinite. A number of studies (Mattigod *et al.*, 1990; Reardon *et al*., 1995) confirm that the three compounds reported most

frequently, quartz, glass, and mullite constitute the principal matrix of the majority of fly ashes. The principal Fe-bearing compounds are hematite (Fe_2O_3), magnetite (Fe_3O_4) anhydrite ($CaSO_4$) and lime (CaO) are the main Ca compounds and periclase (MgO) is the principal crystalline compound of Mg (Mattigod *et al.,* 1990). Lime occurs as particles on the surface of the glass spherules and is thought to originate from the decarbonation of limestone or dolomite impurities in the coal (Warren and Dudas, 1984).

Depending on the coal sources, iron may also be a major component, occurring both as a separate matrix of magnetic spinels (variations of Fe_3O_4) and other oxides, and as an element incorporated in the aluminosilicate matrix. In addition to the elements present at high concentration, which constitute the matrices, there are numerous trace elements which are considered detrimental to the environment.

The presence of major elements in fly ashes can be explained on the basis of thermal transformations of minerals present in the source coals (Mattigod *et al*, 1990). For silicate minerals, phyllosilicates such as mica, kaolinite, chorite, and montmorillonites are the most common forms in coals. Fe-bearing sulphides, carbonates, sulfates and oxides also occur in coals. Quartz and feldspars are the main framework silicates present in the inorganic fractions of coals. The transformations these minerals undergo during coal combustion are indicated in Table 2.3. The reported frequency of various inorganic phases in coals corresponds with the reported frequency of the resulting combustion products in fly ashes. The dominance of phyllosilicates and quartz in coals is reflected in the observed predominance of glass, mullite and quartz in fly ashes. The Fe-sulphides, carbonates, sulphates and oxides in coals account for the Fe-oxides in fly ashes. The presence of alkaline earth carbonates in coals account for the presence of Ca- and Mg-oxides in fly ashes.

Table 2.3: Thermal transformation of major inorganic phases during coal combustion **(**Mattigod *et al.,* 1990).

Minerals in coal	Transformation products in fly ashes
Phyllosilicates	Glass, mullite ($Al_6Si_2O_{13}$), quartz (SiO_2)
Quartz	Glass, quartz (SiO_2)
Pyrite (FeS_2), siderite ($FeCO_3$), iron sulfates	Hematite (Fe_2O_3), magnetite (Fe_3O_4)
Calcite ($CaCO_3$)	Lime (CaO)
Dolomite [$CaMg(CO_3)_2$]	Lime (CaO), periclase (MgO)
Gypsum ($CaSO_4.2H_2O$)	Anhydrite ($CaSO_4$)
Ankerite[$CaMg_xFe_{(1-x)}(CO_3)_2$]	Calcium ferrite ($CaFe_2O_4$), periclase (MgO)

Two major classes of fly ash are specified in American Society for Testing and Materials (ASTM C618) on the basis of their chemical composition resulting from the type of coal burned. These are designated Class F and Class C. Class F fly ash is normally produced from the burning of anthracite or bituminous coal [(SiO_2 +Al_2O_3 +Fe_2O_3) ≥ 70 %]. Class C is normally produced from the burning of sub-bituminous coal and lignite [(SiO_2 +Al_2O_3 +Fe_2O_3) ≥ 50 %]. Class C fly ash has cementitious properties in addition to pozzolanic properties due to free lime, whereas Class F is rarely cementitious when mixed with water.

Most existing chemical elements can be found in fly ash (Kaakinen *et al*., 1975; Klein *et al*., 1975). In their review of utilization and disposal trends of fly ash and other coal residues (Adriano *et al.,* 1980) noted that although the elemental composition of fly ash vary widely, it usually contains higher concentrations of essential plant nutrients, except N, than do common cropland soils. C and N are likely to be oxidized into gaseous constituents during the combustion of coal, thus they are usually present in fly ashes in negligible quantities.
Several research workers have noted that the most salient features of fly ash are the gradation effects of particle size on elemental concentration. Davison *et al.* (1974); Kaakinen *et al.* (1975); Klein *et al*. (1975), observed that As, Cd, Cu, Ga, Mo, Pb, S, Sb, Se, Tl and Zn tend

to increase in concentration with decreasing fly ash particle size. Bosch (1990) investigated some fly ashes from South African coal-burning power stations and noted that there was a tendency for higher concentrations of trace elements in fly ash to be associated with smaller particle sizes. It has been hypothesized that this is as a result of volatilization of elements upon combustion, followed by surface condensation and deposition as the ambient temperature drops and greater surface area in the smaller particles. These elements are preferentially enriched in a thin layer (~ 1.000 Å) at the particle surface and are readily extractable (5 to 40 %) in water (Linton *et al.,* 1975; Smith, 1980). The most volatile elements, which are the last to condense, are partitioned to the smaller particles. Eary *et al.* (1990) observed that chalcophillic elements (As, Cd, Cu, Pb, Hg, Se, V and Zn), which tend to be present as sulphide minerals or associated with organic fraction in coal, are generally more strongly volatilized during combustion and tend to become more enriched on particle surfaces than elements associated with silicate and oxide minerals in colas. The less volatile elements (Al, Ba, Ca, Ce, Co, Eu, Fe, Hf, La, Mg, Mn, Rb, Sc, Si, Sm, Sr, Ta, Th and Ti) show little tendency to partition according to particle size. There are also elements such as Be, Cr, K, Na, Ni, Sc, U, and V that would exhibit an intermediate behavior. Other research workers such as Campbell *et al*. (1978); Lee *et al*. (1975) reported similar effects of particle size on elemental concentrations.

UNIVERSITY of the
WESTERN CAPE

Fly ash from bituminous and sub-bituminous coals are characterized by high S contents and hence produce low pH when dissolved while those from lignitic coals are low in S but higher in Ca and Mg and produce high pH when dissolved (Furr *et al*., 1977; Page *et al*., 1979).

2.1.2 Chemistry of fly ash Leachate and Geochemical factors Controlling the Mobilization of Inorganic constituents in Fly Ash Leachate.

Most of the fossil fuel wastes, including fly ash, are currently being disposed of in landfills and surface impoundments (Mattigod *et al.,* 1990). Since these wastes are being introduced into an aqueous environment they can be a major source of water pollution (Rohrman, 1971). The geochemical factors here refer to the thermodynamics of specific dissolution/precipitation, adsorption/desorption, and redox reactions that occur during weathering of the fly ash and can be applied in understanding the leachate chemistry.

Several studies have been carried out to assess the possible effects of fly ash disposal on water quality, these studies involved characterizing the chemical composition of the waste solids and involved short-term batch-leaching tests (Alberts *et al*., 1985; Mattigod *et al*., 1990; Van der Sloot *et al.*, 1985). The extractability of various elements is influenced by a number of factors, such as the type and concentration of extractant, the solid-solution ratio, the duration and temperature of extraction, and the intensity of agitation during extraction (Soltanpour *et al.,* 1976). As a result, elemental concentrations in laboratory extracts of fossil fuel ashes are not reliable indicators of leachability under field conditions hence most researchers use the chemistry of equilibrium extracts as an indicator of the solubility-controlling solid phases in weathering wastes (Mattigod, 1983; Roy and Griffin, 1984).

The most common extraction procedures involving fossil fuel wastes can be grouped into two general types (i) water extractions and (ii) acid extractions (Eary *et al.,* 1990). Water extractions provide a qualitative estimate of the most readily leachable components in the waste. Acid extractions provide a rough estimate of the total quantity of an element that could eventually be leached from a waste. Acid extractions mobilize greater fractions of both major and minor constituents in the waste than water extractions. Ca, Na and S are mobilized from these wastes in concentrations ranging from tens to thousands of mg L^{-1}. K and Mg concentration may reach several hundred mg L^{-1}. Al^{3+} and Si are generally less than 70 mg L^{-1}, and dissolved Fe concentration is < 3mg L^{-1}. These trends suggest that significant fractions of Ca, K, Mg and Na in fossil fuel combustion wastes exist in highly soluble oxide and sulfate forms (Mattigod *et al*., 1990). Eary *et al*. (1990) observed that elements reported to be enriched on particle surfaces and predicted to exist as soluble oxides and salts in unweathered wastes, such as B, Cd, Cu, Mo, Se and Zn, appear to be dissolved more readily than other minor elements. The rates and amounts of the minor elements released during leaching of fossil fuel wastes are influenced by (i) the total concentrations of the minor elements in the wastes, (ii) the distributions of those elements in the waste solids, and (iii) the in-corporation of the minor elements into secondary solids as a result of weathering reactions.

Mattigod *et al*. (1990) have shown that leachates derived from various fossil fuel wastes have a wide range of pH values. The pH of waste solutions depends on the waste composition and may change over time as a function of weathering. The pH is a master variable that controls

the solubility's of many solids and hence the leaching characteristics of fossil fuel wastes. Fly ash water extracts tends to have alkaline pH values (pH 11-12). Theis and Wirth (1977) have suggested that the initial pH of water extracts of fly ashes may be related to the ratio of oxalate-extractable Fe to soluble Ca. Based on studies of 10 fly ash samples, they observed that fly ashes with Fe/Ca ratios over 3 produced acid extracts, whereas those with Fe/Ca ratios less than 3 generated alkaline extracts. Ainsworth and Rai (1987), in their study of bituminous, subbituminous and lignitic fly ashes concluded that Ca/S ratios of less than about 2.5 generated acid extracts, whereas fly ashes with Ca/S ratios higher than 2.5 produced alkaline extracts. Roy *et al.* (1984) observes that the initial pH values of water extracts of fly ashes have been known to change over time in response to the changing chemistry of the weathering wastes. They observed that over time the acidic extracts increased in pH, whereas the alkaline extracts decreased in pH. Bezuidenhout (1995) investigated the dissolution characteristics of fly ash particles and the changes associated with leachate produced at the Kriel power station ash dam in South Africa. The leachate composition was found to have a lower pH than fresh ash and decreased concentrations of Ca and SO_4^{2-}. Calcium concentrations were controlled by exposure to atmospheric CO_2 and the formation of calcite. Sulphate was postulated to be controlled by the formation of ettringite. Metal concentrations were high in leachates having a low pH. Elements such as Mn, Mo, Cu, Mg, Fe and Ba were associated with the formation of ferrihydrite. It is evident from these studies that the Ca content of a fly ash determines the equilibrium pH of the ash water extracts.

Several column leaching studies have been conducted to evaluate the leaching chemistry of fly ash samples. Different leachants have been used which include water (Dudas, 1981; Humenick *et al*., 1983), dilute acid (Warren and Dudas, 1984). These studies indicate that the leaching patterns of major elements fall into two categories. In the first category, initial leachates have high concentrations of the element, with subsequent leachates showing rapidly declining concentrations that tend to reach steady-state concentrations. In the second category, the element is below detectable concentrations in initial leachates but is subsequently being mobilised, as shown by increasing concentrations. The concentration may decline during prolonged leaching. The studies also indicate that among major elements, Ca, Na, K and S follow the first pattern. Al exhibits delayed leaching, hence follows the second pattern. Warren and Dudas (1984) observed delayed leaching of Mg and Fe which

corresponded with the pH of the leachate becoming more acidic. These studies further indicate that great fractions of Ca and S (as SO_4^{2-}) are mobilized from fly ashes during leaching, while negligible fractions of Si, Al, Fe and Mg are released. These authors further observed that, in fly ashes, Ca and S are associated with more soluble solid phases and Si, Al, Fe, and Mg are mainly recalcitrant phases. Studies of leachates and effluents from fly ash ponds indicate that they contain Ca and SO_4^{2-} as their principal cationic and anionic constituents and concentrations of other major elements are orders of magnitude smaller (Theis *et al.,* 1979).

2.1.3 Major Elements in Fossil Fuel waste.

Past studies of the environmental aspects of fossil fuel waste disposal have focused on determining elemental concentrations, elemental distributions, and empirical rates of extraction. Studies have provided empirical information on short term leaching behavior that is relevant to a specific waste but do not provide information on the dominant weathering reactions that will control the long term distribution of these elements. Eary *et al*. (1990) argue that understanding the leachate chemistry involves the consideration of the thermodynamics of specific dissolution/precipitation, adsorption/desorption, and redox speciation reactions that occur during weathering in addition to empirical data (Fig 2.2). This approach can be used to describe the reaction paths governing the alteration of the high-temperature solids to assemblages of secondary solids and aqueous species that are stable in weathering environments. In addition Rai *et al.* (1988) have shown that an approach based on thermochemical data and principles can be applied in predicting the upper limits of elemental concentrations in pore waters and leachates generated from the waste. This approach determines the chemical behavior of an element based on its total concentration in the solid waste and its accessibility to solution, the different types of solid phases and their solubility's, the kinetics of precipitation/dissolution reactions, the chemical parameters such as pH, Eh, the ionic strengths and concentration of other elements. If a solubility-controlling phase of an element that has rapid dissolution/precipitation kinetics is present in the waste, or if a secondary phase forms that dissolves and precipitates quite rapidly, then the solid phases will be in equilibrium and adsorption needs not be considered in predicting solution concentrations. The aqueous element concentrations of the element can be predicted from precipitation/dissolution reactions defined by thermo chemical data. A few studies

(Ainsworth and Rai, 1987; Mattigod, 1983; Talbot *et al.,* 1978) have evaluated leaching and extraction data as a reflection of precipitation/dissolution reactions in wastes and the presence of solid phases in weathering wastes was noted. These studies also illustrated the application of these principles to predicting the upper concentration limits of various elements leached during the weathering of these wastes. For instance data presented by Ainsworth and Rai (1987) and Fruchter *et al.* (1988) showed that dissolution/precipitation phenomena could explain the observed dissolved concentrations of a number of major and minor elements. Available laboratory data from the same authors indicate that the aqueous concentrations of Al, Ca, Fe, S and Si may be explained by solubility equilibria, whereas concentrations of alkali cations K and Na appear to be due to kinetically controlled dissolution phenomena. However, this approach may be limited by the absence of solid phases with rapid dissolution/precipitation kinetics in the waste matrix or by lack of thermo chemical data for potential secondary solid phases.

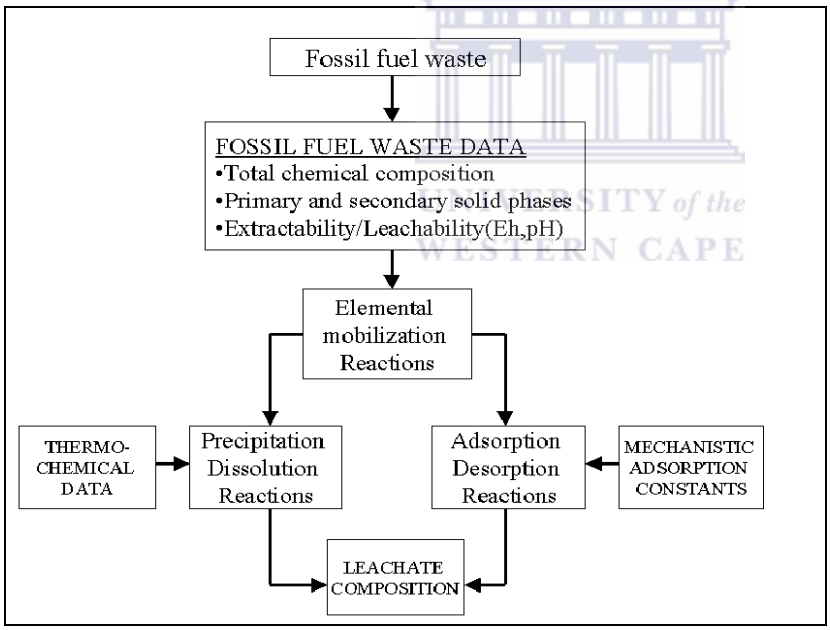

Figure 2.2: Reaction types dictating the leachate composition of fossil fuel wastes (adapted from Eary *et al*., 1990)

2.1.4 Reactions controlling major elements chemistry in waste leachate

Ainsworth and Rai 1997; Rai *et al*. (1998) have demonstrated the application of thermo chemical principles in predicting the upper concentration limits of various elements leached during the weathering of fossil fuel wastes. This is achieved by evaluating the equilibrium

solubility's of all potential secondary minerals that may form during weathering by using the solubility product data. A number of solids have been predicted to exist, such as ettringite, calcite, gypsum, portlandite, amorphous silica, imogolite, amorphous oxyhydroxide and Ca-aluminate in weathering fly ashes. These calculations give a limiting set of the most stable or metastable minerals which are then used to delineate the solubility constraints for each element as a function of selected variables, such as pH, partial pressure of gases and ligand activities. These computations are then used to indicate the upper limits of elemental concentrations attainable in leachates. Mattigod *et al.* (1990) used the ligand activities typically found in weathering fossil fuel combustion wastes at 25^{o}C and 1 atm, to show which free and complex species of major elements are expected to be dominant in the aqueous phase. These authors observed that free ionic species of alkali and alkaline earth cations are predicted to predominate at lower pH values and carbanato complexes at high pH. Sulphato complexes of alkaline earth elements predominate up to pH 9.0, beyond which carbanato complexes become the dominant species. Neutral silicic acid was predicted to be dominant up to pH 9.5. At high pH values, silicate ion would be the significant species. For Al and Fe, hydrolytic species dominate at high pH values. At low pH values dominant Al and Fe species are $AlSO_4^+$ and $FeSO_4^+$ complexes.

UNIVERSITY of the
WESTERN CAPE

Gypsum, calcite, Al-hydroxide and Fe-hydroxide have been observed in weathered fly ashes and have rapid dissolution/precipitation kinetics. Mattigod *et al.,* (1990) found it appropriate to use these minerals in setting the upper limits on aqueous concentrations of Ca, S, Al, and Fe. Calculation of Ca^{2+} activities from data points derived from laboratory experiments (Ainsworth and Rai, 1987) and pore waters from fly ash lysimeters at a field site (Fruchter *et al*., 1988) were in agreement with the predicted equilibrium dissolution of gypsum and calcite. These data also suggested that Al^{3+} activities are controlled by $AlOHSO_4$ at low pH values, by amorphous Al $(OH)_3$ at pH values of 6-9, and by gibbsite at higher pH values. Other studies by Roy and Griffin (1984) suggest that the concentrations of major elements (Al, Ca, Fe, and Si) in fly ash leachates were controlled by anhydrite, mullite, aluminum, and iron hydroxides. These studies further conclude that the aqueous concentrations of Al, Ca, Fe, S and Si may be explained by solubility equilibria, whereas concentrations of alkali cations K and Na appear to be kinetically controlled by dissolution.

However equilibrium between major elements solid phases and pore water may not exist in certain fossil fuel combustion waste disposal environments as a result of factors such as differing leaching rates and elemental distribution in the matrix. In such situations, the kinetically controlled reactions will result in pore-water concentrations that are lower than predicted equilibrium concentrations. It can be concluded that total concentrations of major elements in pore waters, as predicted from thermo-chemical principles, are affected by factors such as the kinds of solid phases, the types and concentrations of ligands and the strengths of complexation.

2.1.5 Minor elements in fossil fuel waste leachate

The rates and amounts of the minor elements released to solution during the leaching of fossil fuel wastes are influenced by (i) the total concentrations of the minor elements in the wastes, (ii) the distributions of those elements in the waste solids, (iii) the incorporation of the major elements into secondary solids as a result of weathering reactions (iv) the presence of ligands and ionic strength of the solution (Eary *et al*., 1990). The distribution of a specific element in solid phases can be important for controlling its initial rate of leaching. Elements that are enriched on particle surfaces will be more accessible to solution. Consequently, they will be more leached initially than elements that are uniformly distributed within the waste matrix. Several studies have reported that many minor elements are not uniformly distributed throughout fossil fuel wastes but are enriched in the smaller particle sizes and on the particle surfaces (Hansen and Fisher, 1980; Smith, 1980; Wadge *et al.*, 1986). The rates at which minor elements are leached from unweathered fossil fuel wastes such as fly ash are dependent on the abundances, surface morphologies, accessibility to solution, and dissolution kinetics of the primary solids containing those elements. Fly ash suspension in water can have varying pH depending on source. Various studies of fly ash leaching behavior show that pH is the principal control on trace element leachability (Eary *et al*., 1990; Hjelmar, 1990; Theis *et al.,* 1979). Eary *et al*. (1990) further observes that the rates and amounts of the minor elements released to solution during the leaching of fly ashes are also influenced by their incorporation into secondary solids as a result of precipitation reactions following the addition of water. Depending on their rate of formation, secondary solids will also affect long-term leaching rates. Adriano *et al*. (1980) observes that stockpiled fly ash undergoes weathering and leaching processes that stabilize the pH and precipitate soluble minerals.

UNIVERSITY of the
WESTERN CAPE

The dominant primary phases containing the major elements in coal ashes include various refractory solids, such as silica-rich glass, mullite, iron oxides, and in lesser amounts, alkali and alkaline earth oxides and carbonates (Mattigod *et al.,* 1990). Due to the low concentrations of minor elements in fossil fuel wastes, it is difficult to identify discrete primary solid phases or solid solutions that contain specific minor elements. The volatilization-condensation mechanism of elemental partitioning during combustion, which has been used to account for the enrichment of many minor elements onto the surfaces of fly ash particles (Smith, 1980), has resulted in the prediction that portions of most minor elements are present as oxides or ionic salts on the surfaces of the major refractory phases formed during the cooling of combustion gases.

Minor elements may also be incorporated into the structures of the major phases comprising fossil fuel wastes. For example, most of the first row transition elements (Cr, Cu, Mn, Ni, V, and Zn) have been reported by Hullet *et al.* (1980) to be distributed preferentially to the magnetic fraction of fly ashes. The magnetic fraction consists of spinel-type solids such as magnetite and ferrite and iron oxides such as hematite. These minor elements are probably present as solid solution substitutes in the spinel structure with the formula $Fe_{3-x}\ M_xO_4$ where M is the transition metal (Hullet *et al*., 1980). The more volatile chalcophilic elements such as As, Hg, Pb and Se and alkaline earth elements such as Ba and Sr were reported to be associated most strongly with the glassy fraction of fly ash (Hullet *et al*., 1980).

Phases such as magnetite, hematite and silica-glass are sparingly soluble and minor elements incorporated in them will be released to solution only as fast as those solids dissolve, assuming congruent dissolution. Alkali and alkaline earth elements that are enriched on particle surfaces as salts and oxides are likely to dissolve rapidly upon exposure to water or acidic media. These released elements can be reprecipitated as secondary solids or adsorbed to solid substrates, depending on the solubility limits of the secondary solids and solution conditions (Eary *et al*., 1990).

The low concentrations of many of the minor elements in wastes and possible solid-solution formation involving the pairing of minor elements with major constituents make detection of

secondary solids difficult. These solids will control the long-term leaching behaviors of the minor elements in disposal environment. These secondary solids can be identified by inference from comparisons of equilibrated solutions with the solubility products of specific solids (Ainsworth and Rai, 1987). Ainsworth and Rai (1987) and Rai *et al*. (1988a) in their solubility studies, demonstrated that most of the Cu, Mo, Se, Sr and V contained in fly ashes is readily accessible to solution. The concentrations of these elements remaining in solution were equal to or significantly less than the concentrations that could theoretically be leached if the ash had dissolved completely. The consistency of the pH dependent relationships for the concentrations remaining in solution with the solubility's expected for various secondary solids implied the formation of those secondary solids.

2.1.6 Effects of redox state and reactions affecting minor element leachate chemistry

In a waste-leachate environment in a state of chemical equilibrium, many secondary solids do precipitate rapidly upon reaching saturation, including hydroxides, carbonates, sulfates and sulfides. For conditions under which solubility-controlling secondary solids are absent or are slow to precipitate because of kinetic factors, dissolution rates and adsorption/desorption reactions of the primary solids will be the major processes affecting concentrations.

If the element is stable in more than one oxidation state in the environment, then the redox conditions or causes of redox transformations must also be known because the secondary solids that could form and the adsorption/desorption reactions that could occur are dependent on the oxidation state. Table 2.3 shows the geochemical grouping, dominant redox states and types of solubility-controlling solids in weathering environments for minor elements. The possible redox and precipitation/dissolution reactions involving the minor elements are complicated by the diverse chemical behaviors of the minor elements. Solution properties such as pH, ionic composition, gas fugacity and types of waste solids affect the geochemical behaviors of the minor elements. Thermodynamic calculations of solubility relationships and knowledge of kinetic factors can be used to determine the most probable set of precipitation/dissolution and redox speciation reactions affecting the concentrations of the minor elements in waste leachates (Eary *et al*., 1990). The redox state of a system affects both the types of solubility-controlling solids that can form and the adsorption/desorption

possibilities of the minor elements. Eh-pH diagrams provide excellent depictions of the stability relationships for various redox species but are only varied for equilibrium conditions.

Table 2.4: Geochemical grouping, dominant redox states and types of solubility-controlling solids in weathering environments for the minor elements in fossil fuel Wastes (Eary *et al*., 1990).

	Dominant oxidation state										Ionic character		Solubility-controlling solids				
Element	-3	-2	-1	0	1	2	3	4	5	6	Cation	Anion	Oxide	Sulfide	Sulfate	Carbonate	Other
Calcophile																	
Cu					Cu	Cu					$Cu^{1+/2+}$		$Cu^{1+/2+}$	$Cu^{1+/2+}$	Cu^{+2}	Cu^{+2}	
Pb						Pb					Pb^{2+}			Pb	Pb	Pb	
Se	Se	Se		Se				Se		Se		Se		Se-2			$Se^{(+4,+6)\ a}$
Zn						Zn					Zn^{2+}			Zn		Zn	
Lithophile																	
Ba						Ba					Ba^{2+}				Ba	Ba	
B							B					B	B				B (b)
Cr							Cr			Cr	Cr^{+3}	Cr^{+6}	Cr^{+3}				Cr^{+6} (c)
Mn						Mn		Mn			Mn^{+2}		Mn^{+4}			Mn^{+2}	
Sr						Sr					Sr^{2+}				Sr	Sr	
Siderophile																	
Mo							Mo	Mo		Mo	Mo^{+3}	Mo^{+6}	Mo^{+6}	Mo^{+4}			Mo^{+6} (d)
Ni						Ni					Ni^{+2}		Ni	Ni			

UNIVERSITY of the WESTERN CAPE

(a)-Se, Metal selenites, metal selenates, and in solid-solution with sulfur

(b)-Borates and possible incorporation into calcite and aluminium hydroxides

(c)-$Ba(Cr,S)O_4$

(d)- Metal molybdates

2.1.7 Application of thermo chemical principles to process water chemistry for acid mine drainage neutralized with fly ash.

In the fly ash/AMD neutralization reactions the highly soluble CaO from the fly ash is expected to increase the pH of the AMD. As pH increases, Fe^{3+}, Al^{3+} and Mn concentrations are expected to decrease primarily due to precipitation of hydrous oxides such as amorphous $Fe(OH)_3$, ferrihydrite, schwertmannite, or goethite and amorphous $Al(OH)_3$ or poorly crystalline gibbsite. Most of these solid phases incorporating major elements have not been positively identified but have been predicted to form in the solutions (Burgers, 2002; O'

Brien, 2000). Predicted equilibrium concentrations of these solid phases combined with the process water concentrations at a given contact time can be used to determine the most probable precipitation/dissolution reactions involved in this process. A parallel can be drawn from the reactions and chemistry of interaction between fly ash and water with that of neutralization of acid mine drainage with fly ash except that in the reactions of AMD with fly ash, reactive components in AMD are present in high concentrations unlike in the water.

2.1.8 Disposal and Environmental Impacts of Fly Ash

Fly ash produced in most coal combustion power plants is mainly disposed off in holding ponds, lagoons, landfills, stockpilling and slag heaps (Adriano *et al*., 1980; Iyer, 2002). Sluicing to holding ponds, where most solids settle and accumulate until they are removed for land filling or stockpiling, is by far the most common method. High-rate land application of fly ash is also a potential disposal method (Adriano *et al*., 1980). The fly ash produced in South Africa's coal fired power plants is disposed off mainly by two methods: in ash dams and tailing ponds. The disposal in ash dams is gaining popularity due to strict disposal regulation in most industrialized countries, coupled with the increased costs for liners associated with wet disposal (Campbell, 1998). The disposal in ash dams involves mixing the fly ash with effluent water in the ash conditioners to attain 20 % moisture content and thus produce a consistency suitable for discharge onto conveyors. With the 20 % moisture content, the ash is still in a dry lump state and is normally suitable for dumping in the mined-out open cast workings which are then rehabilitated and restored for agricultural use (Eskom, 2002). The main disadvantage of this method is the possible dispersion of the fine particles by wind hence the ash dams have to be constantly conditioned by spraying with water before they are finally compacted. Several authors have noted that when inhaled, particles <1μm in diameter may be deposited in the pulmonary tissue of the respiratory tract and gain entry into the bloodstream (Davison *et al.,* 1974). The disposal of fly ash in tailing ponds involves transporting it in slurry form to holding ponds where the solids are allowed to settle and the water is recycled for more slurry formulation. The fly ash is then stockpiled.

Fly ash disposal presents an environmental problem due to the concentration of trace elements and the increased mobility of these elements in weathering environments (Adriano *et al*., 1980; Eary *et al*., 1990; Mattigod *et al.,* 1990). Environmental impacts of fly ash are

UNIVERSITY of the
WESTERN CAPE

best exemplified in its application in soils and its effects on plants. Field and greenhouse studies have indicated many chemical constituents of fly ash may benefit plant growth and improve agronomic properties of soil (Chang *et al.,* 1977). The effects on plants are primarily due to a shifted chemical equilibrium induced by the fly ash added to soils. The concentrations of S, Mo, and B in plant tissues have been shown to increase consistently with ash application to soil. Al, Se and Sr were also consistently increased (Adriano *et al.,* 1980). Fly ash applied on acidic strip mine soils in several states increased the yields of many crops. This was attributed to increased plant nutrient availability (Ca^{2+}, Mg^{2+}). The increase in soil pH caused by ash application led to the deficiencies of Mn, Zn, Cu and Fe. Mo and Se form anionic species in fly ash amended soils and their uptake by plants is increased tremendously. Boron is considered a major limiting factor for successful cropland utilization of ashes due to its phytotoxic effects. Selenium concentrations in plant tissues consistently increased with fly ash treatment and the rate of increase was found to be proportional to either the rates of application or Se content of fly ash (Furr *et al.,* 1978).

Fly ash application to soil was found to reduce its bulk density and increased the water holding capacity. Soil hydraulic conductivity was also improved but only with fly ash input of below 20 % by volume in calcareous soils and 10 % in acidic soils (Chang *et al*., 1977). The reduction of hydraulic conductivity at high application rates was thought to be caused by the pozzolanic reaction of fly ash which tends to cement soil particles when wetted. Fly ash was also found to reduce the modulus of rapture (cohesiveness of soil particles).

2.1.9 Utilization of coal fly ash

When coal is combusted, mineral matter transforms into fly ash and is thermally altered into different forms, many of which are by themselves chemically very reactive or can be chemically activated. Fly ash has found many uses based upon both its bulk chemical and mineralogical make-up and upon the physical size distribution and shape of its particles (Barry and Russell, 1998). Some of the processes and applications of fly ash include addition to cement and concrete products, structural fill and cover material, waste stabilization/solidification, roadway and pavement utilization, addition to construction materials as a light-weight aggregate, infiltration barrier and underground void filling, and

soil, water and environmental improvement. A brief description of the uses most relevant to this study will be presented.

2.1.10 Reclamation of wastelands

Other disposal methods of fly ash include reclamation of wastelands resulting from strip mining of coal. These acidic spoils are infertile and support only sparse vegetation, subjecting them to severe erosion (Fail and Wochok, 1977). Application of fly ash has demonstrated its effectiveness in reclaiming these areas. The quantities of fly ash required to reclaim spoil areas depend upon the pH of the fly ash, the degree to which it's weathered, and the pH of the soil and spoil heaps to be reclaimed (Fail and Wochok, 1977). Fly ash has been added as an alkaline amendment to coal mine spoils and refuse banks to permit their reclamation for plant growth (Bhumbla *et al*., 1998). Amendment of acid soils with fly ash at rates of 0.05, 0.1, 0.5 and 1 % by weight, containing 30 – 40 % Ca, increased pH and reduced the water solubility and diethylene-triamine-pentacetic acid (DTPA) extractability of Fe, Mn, Ni, Co and Pb (Phung *et al*., 1979). It was demonstrated that the alkalinity of fly ash plays a significant role in regulating the availability of trace elements in the amended soils.

UNIVERSITY of the
WESTERN CAPE

2.1.10.1 Infiltration barrier and underground void filling

This process involves dry fly ash injection or slurry injection. Dry fly ash injection involves drilling boreholes into the mine void. The slurry injection is done at a higher pressure than the dry injection (Ziemkiewicz and Skousen, 2000).

Several case studies of underground void filling have been carried out in the United States of America with the main aim of recycling the coal combustion by-products in mines. Many of the initiatives have been developed to find an environmentally sound alternative to the current practice of disposing of (coal combustion by-pyroducts) CCBs in landfills and to demonstrate the beneficial and economical use of alkaline CCBs to abate AMD from underground coal mines (co-disposal insitu). CCBs includes fly ash, bottom ash, boiler slag and flue-gas-desulphurization (FGD) products. The keystone of these initiatives is that alkaline CCBs generated by clean coal technologies can be mixed with water to form a grout, which will harden into a cement-like material when pumped into an underground mine (backfilling). Once this material hardens, it seals the mine from oxygen and water, preventing the formation of acid mine drainage (AMD). Any acid that does form will be neutralized by the alkaline material. Other objectives of these case studies included reduction of subsidence problems, finding economical CCB disposal methods, and exploring methods to increase the amount of coal extracted from working mines. In the PPRP (1997), project the behavior of grouts made with combinations of CCBs were investigated to find how they flowed, hardened and strength developed on setting up. The mine was then monitored to assess the impact on groundwater and on the acid drainage. Ziemkiewicz and Skousen (2000) noted that filling of mine voids has the potential to dispose of substantial quantities of CCBs, and beneficial uses include acid drainage control, subsidence control, and soil reconstruction. CCBs are typically used in the following beneficial applications at coal mines:

Barriers to acid mine drainage formation/transport

Alkaline amendment to neutralize acidic leachates producing rock and mine wastes.

Subsidence control in underground mines

Filling underground mine voids to control acid drainage

Pit filling to reach approximate original contour in surface mines

UNIVERSITY of the
WESTERN CAPE

Rafalko *et al.* (1999) demonstrated the use of CCBs for acid mine drainage abatement in an underground mine in Maryland (USA). The strategy was to completely fill the mine voids and replace mine water with CCBs grout. The grout was placed with the intention of minimizing contact between groundwater and pyrite remaining in the mine. They developed a grout consisting of solid phase CCBs with acid mine water for slurry makeup. The grout was formulated from flue gas desulphurization (FGD) material, class F fly ash and fluidized bed combustion (FBC) ash. They used the FGD consisting mostly of calcium sulfite and calcium sulfate with no free lime as inert filler. The class F fly ash was used as the pozzolan, while the FBC was used as the cementing agent. The final mix consisting of 60% FBC, 20% FGD and 20% class F fly ash yielded 8 inches of spread using ASTM PS28-95 and a 28-day unconfined compressive strength of 520 pounds per square inch (psi) as determined by American Standards and Testing Materials Society (ASTM) C39-94. The grout did not exceed the Toxicity characteristic leaching procedure (TCLP) limits for a hazardous waste. The mine discharge pH remained around 3.0 during and after grouting. Ca, Na and K concentrations increased by an order of magnitude while SO_4^{2-}, Cu, Ni, Zn and Cl nearly doubled. However after two years, concentration of Ni and Zn were at or nearly above pre-injection levels. Grout samples drilled from the grouted mine showed little sign of insitu weathering. The grout cores yielded permeabilities between 1.89×10^{-6} and 6.02×10^{-8} cm/sec. However the project was unable to occlude all the mine voids and the grout was subjected to a high flow, chemically aggressive mine water leading to some grout dissolution.

Metikki Coal Corporation (1996) injected a mixture of non-hardening and low lime content FGD solids, acid mine drainage metal precipitates and fine coal refuse into an underground mine in slurry form. The slurry was injected into the mine at about 15 % solids content. Post injection analysis of water samples indicated below limits concentrations of Cl (Maryland limit of 860 mg/L), 30 % increase in sulphate while Al and Fe dropped substantially. The pH of the mine water increased from 3 to 4.5 (Ziemkiewicz and Skousen, 2000).

Ray D *et al.* (1995) used fly ash grout as a flowable fill into a groundwater-saturated haul tunnel beneath a state highway. The flowable fill consisting of fly ash and 16 % water was gravity fed. The initial impact was elevation of pH, dissolved solids and sulphate. Analysis of water samples six months after injection indicated sulphate and dissolved solids were several

hundred mg/L above background concentrations. Drilled cores of the grout had permeabilities of 10^{-5} cm/sec and average compressive strengths ranging from 96 to 485 psi which was evidence of lack of cementitious reactions in some parts. This was attributed to possible pH buffering and interference of the cementitious reactions by sulphate. Benzaazoua *et al*. (2002) observed that sulphate-rich water slows hydration reactions of cementitious materials.

The above case studies illustrate that flowable mixtures of fly ash can be pumped into underground mine voids to control acid mine drainage while helping to dispose of large volumes of fly ash but there seems to be a mix of success. The studies do not indicate the benefits in terms of trace metals and SO_4^{2-} levels. Ca, Na, Cl, SO_4^{2-}, Cu, increased by an order of magnitude in the post process waters. Comprehensive data on the trends for release of major and trace elements, anions like SO_4^{2-} and mineralogical transformations of the fly ash under the disposal conditions is lacking once the placement of the slurries was done.

2.1.11 Cement and concrete products

UNIVERSITY of the
WESTERN CAPE

Research has indicated that fly ash as an additive to Portland cement has a number of positive effects on the resulting concrete. It decreases the water demand of the concrete. An improvement of the particle size packing (due to the smaller size of the fly ash particles, in comparison to the aggregate) thus decreases the air entrainment in the concrete. Fly ash further increases resistance to corrosion and ingress of corrosive liquids by reacting with calcium hydroxide in the cement to form a stable, cementitious compound of calcium silicate hydrate. The less soluble calcium silicate hydrate reduces the possibility of calcium hydroxide leaching from the concrete. The reaction products also lead to the filling of capillary voids in the concrete mixture, thereby reducing the permeability of the concrete (Halstead, 1986). The fly ash acts as tiny ball bearings and improves the workability of the concrete. Addition of fly ash, when used in the correct proportions, ultimately results in a greater strength concrete than straight Portland cement (Halstead, 1986).

The beneficial blending of fly ash with Portland cement arises from the fact that hydration reactions of the cement generate portlandite, $Ca(OH)_2$ and other hydrates (Taylor, 1998). The fly ash reacts with the $Ca(OH)_2$ to produce more of the cementitious hydrates and contributes to higher strength concrete. Portland cement consists of four main compounds

which react with water, to form products involved in cementation reactions. The four reactants are tricalcium silicate (alite, Ca_3SiO_5), dicalcium silicate (belite, Ca_2SiO_4), tricalcium aluminate ($Ca_3Al_2O_6$), and tetracalcium aluminoferrite ($Ca_4Al_2Fe_2O_{10}$). The hydration reactions of Portland cement generate portlandite according to the following reactions (Taylor, 1998):

$$2Ca_3SiO_5 + 6H_2O \rightarrow Ca_3Si_2O_7.3H_2O + 3Ca(OH)_2 \quad \text{(2.1)}$$

$$2Ca_2SiO_4 + 4H_2O \rightarrow Ca_3Si_2O_7.3H_2O + Ca(OH)_2 \quad \text{(2.2)}$$

It is this portlandite from reactions 1 and 2 that reacts with fly ash to produce more of calcium silicate hydrate, that adds more strength to the concrete.

2.2 Acid Mine Drainage

2.2.1 Introduction

Acid mine drainage (AMD) is generally regarded as the principal environmental problem caused by the mining of the sulphide ore deposits. AMD is extremely acidic (as low as pH 2.0) and enriched with iron, manganese, aluminium, sulfate, and heavy metals such as lead, mercury, cadmium, zinc. When sulphide minerals such as pyrite (FeS_2), its dimorph marcasite and pyrrhotite ($Fe_{1-x}S$) are exposed to oxygen and water, an oxidation process leads to the formation of acidic waters. The geochemical processes of weathering leading to mine related acid water may be similar in terms of mineral oxidation and dissolution but the rates of reaction and environmental consequences can be quite different. Geochemical reactions in mined areas are more rapid because of: 1)-greater accessibility of air through mine workings, wastes, and tailings. 2)-greater surface areas for sulphides in mine workings wastes, especially tailings. 3)-different composition of tailings as a result of mineral processing.

In South Africa coal mining is the main source of AMD and an estimated 200 ML of AMD are produced per day in the Pretoria-Witwatersrand-Vereeniging (PWV) area (Maree *et al.,* 1996). This water requires treatment before disposal. In this section the generation of AMD, available treatment methods and environmental effects will be discussed

2.2.2 Generation of Acid Mine Drainage

Acid mine drainage results from the reaction of pyritic material with oxygen and water. The overall reaction is often written as:

$$FeS_2(s) + 3.75O_2 + 3.5H_2O \rightarrow Fe(OH)_3(s) + 2SO_4^{2-} + 4H^+ \quad \text{.....(2.3)}$$

However reaction (2.3) is an oversimplification. The reaction does not explain geochemical mechanisms; it also doesn't reflect the slow oxidation of aqueous ferrous iron in acid solutions that often results in high ferrous iron concentrations in acid mine waters (Nordstrom, 1982). Factors such as microbial catalysis, neutralization reactions, sorption reactions, and climatic effects have an important influence on pyrite weathering.

2.2.3 Dissolution of pyrite

When pyrite oxidizes there are two species that can be oxidized: the ferrous iron and the sulfidic sulphur. When pyrite is exposed to large quantities of oxygenated waters, ferrous iron easily leaches out of the pyrite but tends to stay in solution (equation 2.4).

$$FeS_2(s) + 3.5O_2 + H_2O \rightarrow Fe^{2+} + 2SO_4^{2-} + 2H^+ \quad \text{.....(2.4)}$$

UNIVERSITY of the WESTERN CAPE

The sulphide is oxidized to elemental sulphur which thereafter dissolves in the oxygenated waters to form sulphate and acidity (equation 2.5). The sulphidic sulphur in pyrite oxidizes more quickly than iron but due to the large number of electrons (14) involved there are several possible side reactions and sulfur intermediates may occur during oxidation.

$$2S + 3O_2 + 2H_2O \rightarrow 2SO_4^{2-} + 4H^+ \quad \text{.....(2.5)}$$

2.2.4 Role of Ferric iron in oxidation of pyrite and contribution to acidity

On forming SO_4^{2-} from elemental sulphur (equation 2.5) the pH drops. This reaction known as the initiator reaction leads to the development of acidic conditions. When the pH is initially >4.5 the ferrous iron formed in equation 2.4 is spontaneously oxidized in air to ferric iron and then precipitated to a ferric hydroxide [Fe $(OH)_3$] (equations 2.6 and 2.7) (Evangelou and Zhang, 1995).

$$Fe^{2+} + 0.25O_2 + H^+ \rightarrow Fe^{3+} + 0.5H_2O \quad \text{.....(2.6)}$$

$$Fe^{3+} + 3H_2O \rightarrow Fe(OH)_3(s) + 3H^+ \quad \text{.....(2.7)}$$

$$FeS_2 + 14Fe^{3+} + 8H_2O \rightarrow 15Fe^{2+} + 2SO_4^{2-} + 16H^+ \quad \text{.....(2.8)}$$

The oxidation of pyrite by ferric iron accounts for the greatest production of acidity (equation 2.8). This reaction drives the pH to < 4.5. Consequently the ferrous iron becomes more stable, with an inorganic oxidation rate of 3 x 10^{-12} mol/L/s. Ferric iron also becomes more soluble at low pH and as its concentration increases with increased acidity, and its role becomes more important as an oxidizing agent. At pH < 3 ferric iron oxidizes pyrite much more rapidly than oxygen and more rapidly than dissolved ferrous iron can be oxidized by dissolved oxygen. At neutral pH values, the rate of ferrous iron oxidation rises rapidly, but the dissolved ferric iron concentration decreases rapidly due to the precipitation of ferric iron. This implies that pyrite oxidation is initiated by oxygen at circum-neutral pH (equation 2.4) but as pH values reduces to < 4, the rate of oxidation becomes governed by equation 2.8, but oxygen is still required to replenish the supply of ferric iron (equation 2.6). The figure 2.3 below shows the model summarizing the reactions for the oxidation of pyrite.

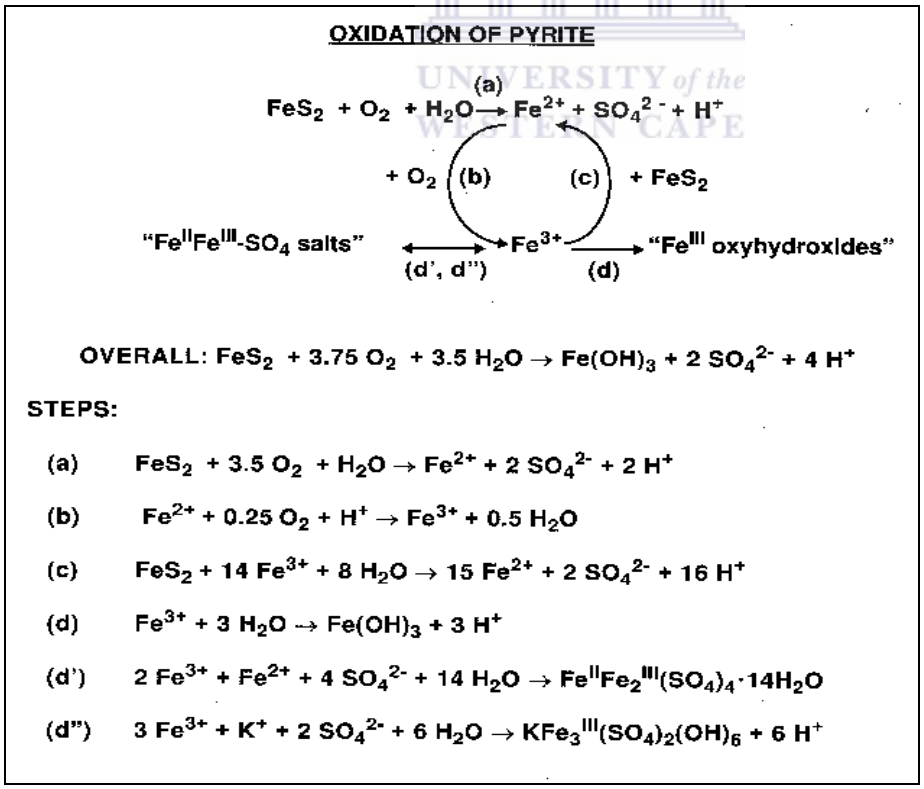

Figure 2.3: Model for the oxidation of pyrite (Stumm and Morgan, 1981).

Steps a through d correspond with reactions 2.4, 2.6, 2.8 and 2.7, respectively, in the text. Steps d' and d" represent the formation of iron-sulfate minerals, which can be stores of acidity, ferric ions, and sulfate.

2.2.5 Microbial oxidation: role of bacteria

Under acidic conditions, the ferrous iron oxidation rate becomes very slow and independent of pH (Nordstrom and Alpers, 1999). Singer and Stumm (1968) reported an abiotic rate of 2.7×10^{-12} mol/L/s at pH values below 4. Such a rate is considerably slower than the rate of oxidation of pyrite by ferric iron. Hence equation 2.6 would be the rate-limiting step were it not for the catalytic effect of bacteria.

It has been known for sometime that microorganisms are involved in the formation of acid mine drainage (Carpentor and Herndon (1933); Chapelle, 1993.) suggested that pyrite oxidation and the consequent acid mine drainage from coal deposits may be catalyzed by bacteria. Colmer and Hinkle (1947) isolated a chemoautotropic and acidophilic bacterium, Thiobacillus ferrooxidans and showed that microbial degradation of pyrite was an important factor in the production of acid mine waters.

UNIVERSITY of the
WESTERN CAPE

The catalytic effect of Thiobacillus ferrooxidans on the aqueous oxidation of ferrous to ferric iron is well established. Singer and Stumm (1968, 1970) found that bacteria increased the ferrous iron oxidation rate by a factor of 10^5 over the abiotic rate, from about 3×10^{-12} mol/L/s to about 3×10^{-7} mol/L/s. Being soluble the ferric iron formed under these conditions, can readily react with more pyrite to form soluble ferrous iron. The ferrous iron formed this way is again oxidized to ferric iron by the bacteria with consumption of oxygen and the process goes on. Thus there is a progressive, rapidly increasing rate at which pyrite is oxidized.

2.2.6 Effect of temperature

Rates of reactions that form AMD increase with increasing temperature, so that AMD is formed faster if the pyritic material is warm. An exception to this trend is the rate of Fe oxidation by *Thiobacillus ferrooxidans* above 35^{o}C. These bacteria thrive at optimum temperatures of 25 to 35^{o}C, but they become inactive or die as temperatures increase to about 55^{o}C (Cathles, 1979). Measurements indicate that oxidizing sulfide-rich materials can warm internally to temperatures at least as high as 60^{o}C because of the heat released by the oxidation reactions (Cathles and Apps, 1975). Some sulfide-rich material actually undergoes spontaneous combustion.

2.2.7 Deleterious Effects of Acid Mine Drainage: Impacts of Mine Drainage on Aquatic Life, Water uses, and Man-Made structures.

UNIVERSITY of the
WESTERN CAPE

The influx of untreated acid mine drainage (AMD) into streams can severely degrade both habitat and water quality, often producing an environment devoid of most aquatic life. The severity and extent of damage depends on a variety of factors including the frequency of influx, volume, and chemistry of the drainage, and the buffering capacity of the receiving stream (Kimmel, 1983). Drainage from underground mines, surface mines and refuse piles is the oldest and most chronic industrial pollution associated with coal mining.

Ferric iron, when discharged to surface water, is hydrolyzed to produce hydrated iron oxide and more acidity (equation 2.7). As a result the pH of the water is lowered, making it corrosive and unable to support many forms of aquatic life. Acid formation is most serious in areas of moderate rainfall, where rapid oxidation and dissolution of exposed minerals occur. Various impacts range in severity from isolated nuisance type problems to severe water quality impacts affecting large volumes of groundwater and miles of watercourse. Impacted uses include agricultural, industrial and portable water supplies, along with recreational uses, scenic resource appreciation, and aquatic organism habitat. The aggressive nature of mine drainage may also result in corrosion and incrustation problems with respect to such manmade structures as pipes, well screens, dams, bridges, water intakes, and pumps. Acid

mine drainage can also be toxic to vegetation when recharging to the shallow groundwater system.

Acid mine drainage is a complex mixture of compounds that interact to cause a variety of effects on aquatic life that are difficult to separate into individual components. Toxicity is dependent on discharge volume, pH, total acidity, and concentration of dissolved metals. The pH is the most critical component since the lower the pH, the more severe the potential effects on aquatic life. The effect of AMD is also dependent on the alkalinity or buffering capacity of the receiving stream. The higher the concentration of bicarbonate and carbonate ions in the receiving stream the higher the buffering capacity and the greater is the protection of aquatic life from adverse effects of acid mine drainage (Kimmel, 1993). In addition to chemical effects of AMD, physical effects such as increased turbidity from soil erosion, accumulation of coal fines, and smothering of the stream substrate from precipitated metal compounds may also occur (Parsons, 1968; Warner, 1971). AMD can also cause a reduction in the diversity and total numbers of macro invertebrates and changes in community structure.

Heavy metals are generally less toxic at circum-neutral pH since this represents the range of minimum solubility of most metal hydroxides. Trace metals such as zinc, cadmium, and copper present in AMD are toxic at extremely low concentrations and may act synergistically to suppress algal growth and affect fish and benthos (Hoehn and Sizemore, 1977). Precipitated iron or aluminum hydroxide may form in streams receiving mine discharges with elevated metal concentrations. These hydroxides decrease oxygen availability as they form.

2.2.8 Durability of concrete structures

Sulfates and acidity are two principal aggressive factors that affect the durability of concrete. Problems resulting from acid attack on concrete are dependent on the following variables: (1)-total acidity and pH of water and (2)-groundwater replenishment rate. When in contact with Portland cement concrete, acid will attack the exposed surface and be neutralized by the alkalinity of the concrete. Sulfates in AMD effluents or groundwater combine with certain constituents of the concrete, principally tricalcium aluminate ($Ca_3Al_2O_6$), to form calcium sulfoaluminate. This reaction is accompanied by expansion and eventual disruption of the concrete. The higher the sulfate concentration, the more active is the corrosion (Bealy, 1980).

2.2.9 Treatment of AMD

UNIVERSITY of the
WESTERN CAPE

Treatment techniques of AMD are usually reactive rather than pro-active, and are generally designed to:

(i) raise pH,

(ii) lower toxic metal concentrations (example by precipitation, adsorption)

(iii) lower aqueous sulphate concentrations,

(iv) lower the toxicity / bioavailability of metals in solution (example by oxidation, reduction)

(v) oxidize the elements in solution (example Fe (II)-Fe (III), Mn (II)-Mn (IV), As (III)-As (V),

(vi) reduce the species in solution (example SO_4-H_2S)

(vii) collect / dispose / isolate the metallic sludge generated.

Acid drainage control and treatment techniques can be broadly classified into physical, chemical and biological, and those using combinations of these processes. Within these two major groups (chemical and biological) there are processes that may be described as either active or passive.

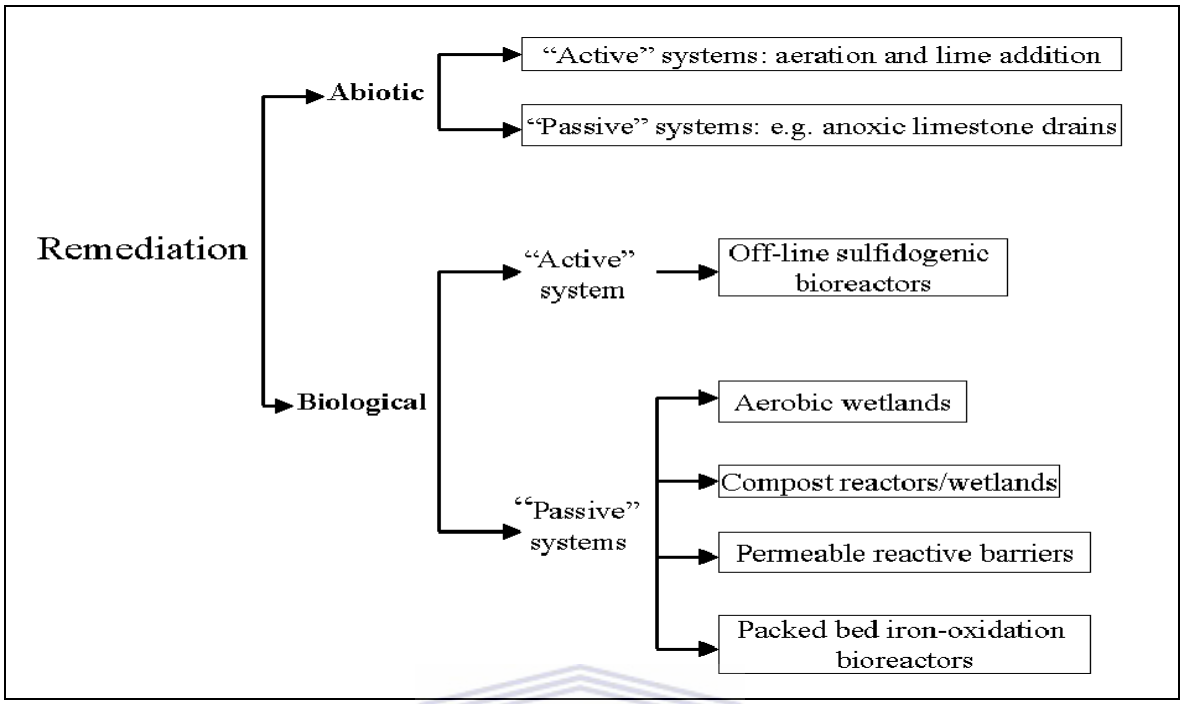

Figure 2.4: Summary of biological and abiotic technologies for remediating acid mine drainage (Johnson and Hallberg, 2005).

UNIVERSITY of the
WESTERN CAPE

2.2.9.1 Active chemical treatment methods

Active treatment methods incorporate the use of mechanized procedures for the addition of alkaline materials and require constant monitoring and maintenance. Basic chemicals are used as additives to increase the pH and cause the precipitation of metals, such as Fe, Mn, and Al. The chemicals commonly used are Ca $(OH)_2$ (hydrated lime), NaOH (caustic soda), NH_3 (ammonia), CaO (pebble quicklime) and Na_2CO_3 (soda ash) (Robb and Robinson, 1995). The chemicals used on a particular site are dependent on mine drainage characteristics and site accessibility. Other active treatment methods include dissolved air flotation and ion exchange devices, flocculants, coagulants, and oxidants (Skousen and Ziemkiewicz, 1995). Skousen *et al*. (1996) provided a detailed discussion of the benefits and disadvantages of the neutralizing chemicals commonly in use. The active treatment of AMD generally involves several basic steps: (1) aeration, (2) addition of alkalinity, (3) oxidation and precipitation, (4) clarification and sludge disposal. The most cost effective, and therefore the most commonly used reagents are the lime based reagents which include quicklime (CaO), hydrated lime (CaOH), and limestone ($CaCO_3$). Hydrated lime is the most widely used of the three lime based reagents in the treatment of acid drainage. It is easily handled and suitable in high flow

and acidity conditions. However extensive mechanical mixing of hydrated lime in water is required because it is hydrophobic. Limestone or calcium carbonate can also be used in certain circumstances. It has the lowest material cost and is safe and easy to handle. However, its use is limited due to its low solubility and its tendency to develop an external coating (armoring). Armoring is the strong adhesion or encrustation of limestone particles with hydrous Fe^{3+} and Al^{3+} compounds as the pH increases. This phenomenon has the consequence of decreasing the neutralization efficiency of limestone.

The acid mine drainage is aerated by stirring or by other mechanical agitation procedures. This promotes oxidation of ferrous iron. It is followed by addition of neutralizing agents that raise the pH and metal hydroxides precipitate out. The next step involves the separation of the neutralized process water and the sludge. Sludge consists of material removed from physical, biological and chemical treatment of wastewater. In case of chemical treatment the sludge is mainly composed of heavy metal precipitates. The separation of process water and sludge is done in a clarification tank where the sludge is allowed to settle at the bottom and then pumped to the disposal site or recirculated to the neutralization tank. The recirculation of the sludge is important in case of limestone since dissolution of limestone is slow hence the sludge has residue alkalinity (Maree *et al.,* 1996). Chemical coagulants and flocculants are added at the clarification stage to remove suspended material (Gazea *et al.,* 1996; Geldenhuys *et al*., 2003).

Addition of lime consumes acidity according to the following reactions, where water and insoluble calcium sulphate are produced.

$$Ca(OH)_2 + H_2SO_4 \rightarrow Ca^{2+} + SO_4^{2-} + H_2O \quad \text{.....(2.9)}$$

Iron, aluminium, manganese and other metals precipitate as hydroxides or basic sulphates (Jenke *et al.,* 1983).

$$Ca(OH)_2 + Fe_2(SO_4)_3 \Leftrightarrow 2Fe(OH)_3 + 3Ca^{2+} + 3SO_4^{2-} \quad \text{.....(2.10)}$$

The benefits associated with lime treatment of AMD are its ability to remove metal and its lower transport cost. Its disadvantage is the need for accurate dosing and lack of any residual alkalinity (Maree *et al.,* 1996). Metals like manganese and magnesium can be removed with lime due to its ability to raise pH of water to 12. A pH of 9.3 is needed for manganese

removal and 11.2 for magnesium removal. Lime treatment can also remove sulphate to low levels of 1200 mg/L due to the removal of magnesium and the high calcium concentration generated. Presence of Mg^{2+} ions increases the solubility of gypsum ($CaSO_4$. $2H_2O_{(s)}$) by forming magnesium sulphate ($MgSO_4$) pairs hence its removal promotes gypsum precipitation (Evangelou, 1998). The high calcium concentration leads to precipitation of gypsum hence low levels of sulphate are attained.

The treatment of AMD by limestone involves the dissolution of calcite, which is the principal component of limestone. Dissolved calcite can neutralize acidity, increase pH, increase concentrations of HCO_3^-, OH^- and Ca^{2+} in mine water by the following reactions:

$$CaCO_3(s) + 2H^+ \leftrightarrow Ca^{2+} + H_2CO_3 \quad \text{.....(2.11)}$$

$$CaCO_3(s) + H_2CO_3 \leftrightarrow Ca^{2+} + 2HCO_3^- \quad \text{.....(2.12)}$$

$$CaCO_3(s) + H_2O \leftrightarrow Ca^{2+} + HCO_3^- + OH^- \quad \text{.....(2.13)}$$

The overall rate of calcite dissolution depends on the pH, the partial pressure of CO_2 (Pco_2) and activities of Ca^{2+} and HCO_3^- near the calcite surface (Arakaki and Mucci, 1995; Morse, 1983). The use of limestone for neutralization of AMD in surficial environments has been limited because of its low solubility and slow dissolution rate relative to other alkaline reagents.

The major advantages of active treatment of AMD are the small area occupied by the plants and the large quantities of AMD that can be treated. The major setbacks are that the reagents are expensive, and the process generates an iron-rich sludge that need to be disposed of and has the potential to cause environmental damage.

2.2.9.2 Passive treatment methods

Passive treatment systems do not require continuous chemical inputs and take advantage of naturally occurring chemical and biological processes to cleanse contaminated mine waters. The treatment depends on the dynamic biogeochemical interactions as contaminated water travels through the system. In addition the systems have lower operation and maintenance cost. The disadvantages include long retention time and large treatment areas (Hedin *et al*., 1994).

UNIVERSITY of the WESTERN CAPE

The first passive systems described were natural *Sphagnum* wetlands that were improving AMD as discharges flowed through them. The primary passive technologies include constructed wetlands; anoxic limestone drains (ALD), successive alkalinity producing systems (SAPS), limestone ponds, and open limestone channels (OLC)

2.2.9.2.1 Constructed wetlands

Constructed wetlands are designed to encourage oxidation processes to precipitate unwanted metals and in turn increase the pH (Robb and Robinson, 1995). Constructed wetlands function by precipitating metal hydroxides, forming metal sulfides, and adsorbing small amounts of metals to the plant community (Skousen and Ziemkiewicz, 1995). There are two types of wetlands that are constructed, aerobic and anaerobic.

Aerobic wetland systems are designed to encourage metal precipitation through oxidation processes and are therefore normally shallow, vegetated, and have surface flow predominating (Robb and Robinson, 1995). They are used to collect water and provide sufficient residence time and aeration so that metals in the water can precipitate. The water in this case usually has net alkalinity. Fe and Mn precipitate as they are oxidized, and the precipitates are retained in the wetland or downstream.

UNIVERSITY of the
WESTERN CAPE

The extent of metal removal depends on dissolved metal concentrations, dissolved oxygen content, pH and net alkalinity of the mine water, presence of active microbial biomass, and retention time of the water in the wetland. The pH and net acidity/alkalinity of the water are particularly important because they influence both the solubility of metal hydroxide precipitates and the kinetics of metal oxidation and hydrolysis. Metal hydrolysis produces H^+, but alkalinity in the water buffers the pH and allows metal precipitation to continue. Aerobic wetlands are best used with water that contains net alkalinity to neutralize metal acidity.

Anaerobic wetland systems require that the mine water flow through an organic layer under anaerobic conditions. The organic material most commonly used is spent mushroom compost. This organic material must contain sulfate-reducing bacteria for metal sulfide precipitates to form (Robb and Robinson, 1995). These systems are used when the water has net acidity, so alkalinity must be generated in the wetland and introduced to the water before dissolved metals can precipitate. The wetland substrate may contain a layer of limestone in

the bottom or limestone may be mixed among the organic matter. Wetland plants are then transplanted into the organic substrate.

Insoluble precipitates such as hydroxides, carbonates, and sulfides represent a major sink for metal in wetlands. About 50 to 70 % of the total Fe removed from AMD by wetlands is found as ferric hydroxides (Calabrese *et al*. 1991; Henrot and Wieder 1990; Wieder 1992). Ferric hydroxide formation depends both on the availability of dissolved oxygen and on the initial oxidation state of Fe in the AMD. Wieder (1993) reported significant retention of ferric hydroxides in surface sediments of anaerobic wetlands.

2.2.9.2.2 Anoxic limestone drains

Anoxic limestone drains (ALD) are buried cells or trenches of limestone into which anoxic water is introduced before its exposure to atmospheric O_2. The limestone dissolves in acid water, raises pH, and adds alkalinity. Under anoxic conditions, the limestone does not coat or armor since Fe^{2+} is not oxidized and cannot precipitate as $Fe(OH)_2$ at pH <6.0. Once the water containing excess alkalinity reaches aerobic conditions at the ground surface, Fe^{2+} is oxidized and precipitated together with Mn^{2+} and Al^{3+} while the water remains near pH 6 (equation 2.16) (Brodie *et al*., 1990). Solid Fe $(OH)_3$ is produced by the oxidation of Fe^{2+} and consequent hydrolysis (equation 2.6):

$$Fe^{3+} + 3HCO_3^- \rightarrow Fe(OH)_3(s) + 3CO_2 \quad \text{.....(2.16)}$$

It has been observed that, if appreciable dissolved Fe^{3+} and Al^{3+} are present, clogging of limestone pores with precipitated Al and Fe hydroxides occurs (Faulkner and Skousen 1994; Watzlaf *et al.,* 1994). For waters with high sulfate concentration (>1,500 mg/L), gypsum ($CaSO_4.2H_2O_s$) may also precipitate (Nairn *et al.,* 1991).

2.2.9.2.3 Successive alkalinity producing systems (SAPS)

Successive alkalinity producing systems (SAPS) combine the use of an ALD and an organic substrate into one system (Kepler and McCleary, 1994). Oxygen concentrations in AMD are often a design limitation for ALDs. In situations where dissolved oxygen (DO)

concentrations are >1 mg/L, the acidic water has to be de-oxygenated before it is introduction into the anoxic limestone bed. In SAPS, acid water is ponded from 1 to 3 m over 0.2 to 0.3 m of organic compost, which is underlain by 0.5 to 1 m of limestone. Below the limestone is a series of drainage pipes that convey the water into an aerobic pond where metals are precipitated. The hydraulic head drives ponded water through the anaerobic organic compost, where oxygen is consumed and ferric iron is reduced to ferrous iron. Sulfate reduction and Fe sulfide precipitation can also occur in the compost. Water with high metal loads can be passed through additional SAPS to reduce high acidity generated from oxidation.

Wieder (1992) documents that the mechanism and efficiency of AMD treatment varies seasonally and with wetland age. Aerobic and anaerobic wetlands are most successful when used to treat small AMD flows of moderate water quality.

2.2.9.3 Treatment of acid mine drainage with fly ash

Fly ash has been investigated for a number of years for its ability to remove metals from solution (Erol *et al.*, 2005; Panday *et al*., 1985). This property of fly ash has also been investigated by several researchers (Hequet *et al.*, 1999; Ricoh *et al*., 1999). The fly ash has also been investigated for heavy metal removal from contaminated water with a view to developing unconventional sorbents (Apak *et al*., 1998). Several case studies have been undertaken on using fly ash to control AMD generation within abandoned coal mines. This involves injection of fly ash slurries, pure or blended with ordinary Portland cement (PPRP, 1997).

Earlier fly ash reactivity studies evaluated the neutralization potential of fly ash using dilute mineral acids such as sulphuric acid or hydrochloric acid (Doye and Duchesne, 2003; Hodgson *et al*., 1982). A major objective of these studies was to establish the neutralization characteristics and the effect of acid weathering on cation dissolution from fly ash and secondary mineral formation. The studies involved drainage of the dilute acid leachants through columns filled with ash or agitation of a FA/AMD mixture in a shaker. Column leaching experiments by Warren and Dudas (1984) used a weak sulphuric acid eluant to simulate fly ash weathering by acid rain. This study showed two buffering reactions associated with the fly ash, one at pH 12, and another one at between pH 10 and pH 8.5. A

major aspect of this study involved characterization of elements release from the fly ash. Hodgson *et al.* (1982) used hydrochloric acid as a leaching medium and obtained similar results: the neutralization reaction exhibited three distinct buffer zones: a high pH region (pH 12.0-10.5) accompanied by release of Ca, a second region (pH 9.2-8.5) accompanied by release of Mg and a third region (below pH 4.2) in which Al was released from the fly ash matrix. Stewart *et al*. (1997) took a different approach and looked at the co-disposal of fly ash with coal mining spoil. Their study involved column leaching experiments of the mine spoil blended with varying percent of fly ash over a four year period. The study established that the fly ash mixed with the mine spoil, successfully maintained the pH of the leachate at between 7.0 and 8.0, preventing the mobilization of the majority of toxic metals.

Karapangioti and Atalay (2001) titrated fly ash with different volumes of sulphuric acid solutions at pH 1 and 4.0. Ph changes were monitored with time and volume added. The experiments indicated a pattern whereby Ca and Na were released at high pH and Fe and Cr at low pH. They also established that limestone had twice as much buffering capacity but a lower initial pH, than ash materials.

UNIVERSITY of the

Warren and Dudas (1985) leached an alkaline fly ash with 0.005 mol L^{-1} H_2SO_4 in a series of leaching columns for a period of 90 days and evaluated the chemical, mineralogical and morphological nature of the precipitation products. Three types of precipitation products were identified. Calcite was formed through dissolution of Ca from the ash and subsequent reaction with CO_2 absorbed by the initial alkaline leachate. Iron dissolved from the ash under acidic conditions, precipitated as amorphous coatings on fly ash particles. Al and Si, dissolved from the glass of the ash were translocated and precipitated as an amorphous alumino-silicate material. The results suggested that the weathering of fly ash disposed in a terrestrial environment would likely occur by processes and sequences similar to those documented for alkali soils of volcanic origin.

These studies successively evaluated the leaching characteristics of fly ash in acidic media. Patterns of toxic elements release were established and the acid buffering characteristics revealed.

Other studies have used synthetic AMD to investigate the potential of fly ash as a liming agent. O'Brien (2000) reacted Sasol and Arnot fly ash and their leachates with SAMD. The

neutralization curves were characterized by four distinct regions. He observed the formation of ettringite at pH 10.0-12.0 and gypsum at pH 5.6. Ettringite was converted to gypsum as the pH was lowered. Geochemical modeling confirmed the formation of ettringite and gypsum. Kinetic studies showed that the reaction of SAMD with fly ash continued for at least 72 hours. However, the major pH and EC changes were observed within 30 minutes, due to the hydration of free lime.

Cornell and Schwertmann (1996), using synthetic Fe (II) solutions observed formation of ferrihydrite which transformed readily into hematite with some goethite at neutral pH and principally to goethite at pH>12. Two-line ferrihydrite was observed to form rapidly in solutions of Fe (II) on oxidation in laboratory controlled conditions or during treatment of ash from municipal waste incinerators, (Stipp *et al.,* 2002).

Burgers (2002) reacted synthetic AMD with Fe: Al ratios of 7.3, 0.8 and 2.5 and fly ash leachate. The upscale titration showed a near complete metal removal and substantial SO_4^{2-} removal from solution. The characterization of the precipitates revealed poorly crystalline, highly Al-substituted goethite, and ferrihydrite with large amounts of SO_4^{2-} included in the structure. Calcite was observed in precipitates made by adding synthetic acid mine drainage (SAMD) to fly ash leachate in downscale titrations. Campell (1999) noted an accumulation of calcite in weathered Kriel fly ash, South Africa. Warren and Dudas (1985) also reported an accumulation of calcite in the alkaline sections of their leaching columns.

Van den Berg *et al*. (2001) carried out a site specific study of use of fly ash to control water quality in opencast coal mines on the Highveld region (South Africa). The study investigated Matla, Hendrina and Duvha fly ash and water from Rietspruit, Optimum and Middleburg South collieries. The study involved column leaching tests, samples from the ash dams, groundwater samples and historical records. A major finding was that the safe application of fly ash depended on the relationship between the acid generating capacity of the mine spoil and the base potential of the fly ash. If the pH of the combined leachate from the fly ash and mine spoil was sufficiently high, then elements contained within the fly ash were not mobilized. The report also indicated that ash should be placed above the final decant level of the mine. Otherwise, heavy metal mobilization would occur. The report contained a review of overseas experience which indicates possibility of using fly ash to remediate AMD

underground, or as a barrier to control AMD at reclaimed surface sites, or as an ameliorant mixed with mine spoil and deposited above the decant point.

Most of the cited studies were undertaken in the USA. For example Canty (2003), carried out a test which involved the injection of 418 tons of fluidized bed ash (FBA) into an acidic (pH=4.4), flooded mine void. After injection alkalinity from the FBA was imparted to the system and neutralized the existing acid.With elevated pH levels, metal species precipitated within the mine as hydroxides and carbonates. Consequently, the AMD had an elevated pH, increased alkalinity, and a reduced metal load. Aluminum levels were reduced to below 1mg/L. Alkalinity levels were increased greatly (>138 mg/L). Some iron precipitation was observed (15-20 %), and the H^+ concentration increased by almost 100 times (pH change from 4.4 to 6.3). Gurdeep and Bradley (2001) characterized fluidized bed combustion (FBC) products, bed ash and lime-based scrubber sludge that were to be placed in an underground mine to control subsidence and found low concentration of heavy metals in the leachates. The leachates were however found to be high in dissolved solids and sulphates.

The main significant feature of these studies is that they considered in situ mixing of fly ash with AMD, and did not investigate the use of fly ash as a chemical treatment for AMD in near conventional 'liming' type plant.

Klink (2004) carried out a series of neutralization reactions of AMD with fly ash, lime and limestone. He compared the neutralization potential of fly ash, lime and limestone. He found that a given amount of lime or limestone had a higher neutralization potential than the same amount of fly ash. However this study did not clearly show the mechanisms involved in the removal or release of major and minor elements during the neutralization process. A better understanding of the interaction of the fly ash and the AMD in the neutralization process would greatly aid in optimizing this treatment. Moreover, the fate of trace metals removed from the AMD as precipitates in the solid residues will probably dictate their long term behavior on disposal.

2.3 Leaching Studies and Backfilling of Mine voids

2.3.1 Introduction

Both acid mine drainage and fly ash pose substantial environmental and economic problems for South Africa. The reaction of fly ash and acid mine drainage produces neutral or alkaline process waters with heavy metals being immobilized in the resulting solid residues by precipitation, complexation, adsorption. A desired method of disposal of fly ash has been to return it to the mined out areas, but the concern has been the probable impact on the groundwater quality.

Backfilling of mine workings with ore wastes is a current practice. Tailings or mill waste are generated after processing the mineral rock to extract the precious mineral, this involves crushing, grinding followed by physical or chemical processing. Benzaazoua *et al.* (2004) explained that backfilling with mill waste; in mines that produce considerable quantities of sulphidic waste in their milling process is a current practice for most underground mine operators. The backfill of underground openings reduces the amount of problematic tailings that have to be stored in surface impoundments. Chugh *et al.* (1998) noted that backfilling has the potential to increase mine productivity, reduce mining costs and promote beneficial use of large volumes of coal combustion by-products. Depending on the actual and perceived environmental risks of fly ash and other coal processing products disposal, different groups are promoting disposal, either on surface or underground (Chugh *et al*., 1998; PPRP, 1997; Ziemkiewizc *et al*., 2000). The keystone of these initiatives is that the alkaline coal combustion by-products (CCB) can be mixed with water to form a grout, which will harden into a cement-like material when pumped into an underground mine. Once this material hardens it seals the mine from oxygen and water, thus preventing the formation of acid mine drainage. This explains the tendency to blend mine tailings or CCB with lean amounts (1-7 %) of ordinary Portland cement (OPC) (Benzaazoua *et al.,* 2004). In addition to alkalinity the OPC also serves to increase the final compressive strength of the backfilled material. The main shortcoming of these initiatives is the reactivity of fly ash under the aggressive conditions presented by acidic mine drainage which eventually leads to the leaching of toxic elements such as Mo, Cu, Ni, Zn, Cl^- and SO_4^{2-} (Rafalko *et al*., 1999).

UNIVERSITY of the
WESTERN CAPE

In all these CCBs applications for underground placement, emphasis is on the flowability and hardening characteristics of the resulting formulations without due consideration for the chemical and mineralogical transformations that will result after placement. The literature lacks of studies looking at the leaching characteristics of fly ash/cement mixtures on a long - term basis to evaluate their possible impact on groundwater quality.

By reacting fly ash with acid mine drainage, it is believed that most of the soluble salts are dissolved by the initial "acid shock" of the AMD and thereafter precipitated again as stable phases as the pH increases with contact time. Reardon *et al.* (1995) observed that when fly ash is brought into contact with water, most of the unstable phases dissolve. The more stable and less soluble secondary phases precipitate. Some of the primary phases of fly ash, especially the glass and crystalline aluminosilicate particles, dissolve very slowly. In addition, secondary hydrous aluminosilicate products are very insoluble and build up as alteration rinds on the surfaces of the primary phases. This further impedes the dissolution of the primary phases as the flux of ions and water between these phases and the porewater becomes diffusion controlled.

UNIVERSITY of the
WESTERN CAPE

2.3.2 Column leaching

Column leaching procedure (sometimes referred to as trickle leaching) is used to study the weathering of coal combustion by-products, waste rock, ore or tailings or to determine the kinetic behavior of such materials (Mills, 1998). In either case the objective is to monitor water (leachate) quality with time by periodic sampling. The experiment consists of the following aspects:

- Subjection of sample to periodic leaching
- Collection of drainage for analysis
- Calculation of acid generation and neutralization capability depletion
- Calculation of rates of metal release
- Identification of mineral phases dictating metal release
- Prediction of water quality

The procedure helps in monitoring the weathering of a solid material sample such that the weathering products can be collected and quantified. Soluble products are mobilized by a

fixed-volume of an aqueous leachant. Prior to the commencement of the procedure, the material to be tested must be weighed, characterized chemically and mineralogically. Some materials are known to undergo complex mineralogical changes during the extended period of leaching.

Of major concern in the leaching procedure is the possible presence of particles whose size is less than 2 μm because samples containing significant quantities of such particles will produce a leachate that will require filtration before dissolved metals can be analyzed. In the column set-up, the test material is normally supported by a grid, which is covered with a filtering medium, to prevent loss of fine particles during the leaching cycles. This filtering medium must be chemically inert and non-retentive to water. It must also be porous enough for easy flow of leachate while retaining the test material. Stewart *et al*. (1997) used filter paper (Whatman no 42) for the leaching of either coal refuse or coals refuse blended with fly ash. Warren and Dudas (1984), used plexglass columns lined at the bottom with glass wool to hold back the fine particles during their fly ash leaching experiments. Stewart *et al.* (2001) used a combination of a 60-mesh (0.25mm) nylon sieve cloth and Whatman no. 42 filter paper to retain the fine material.

UNIVERSITY of the
WESTERN CAPE

Columns may be of laboratory, pilot plant or site scale with sample size ranging from a few kilograms to hundreds of kilograms. There are generally two types of column set-ups, for sub-aerial and sub-aqueous testwork procedures. They are typically 76, 102 or 152 mm in diameter, and from about 1 m to more than 3 m in height. There is little if any standardization of column test work procedure, thus allowing considerable flexibility in size and material for fabrication of columns (Mills, 1998).

Price (1997) argued that leaching column tests have some disadvantages over other leaching methods such as humidity cells. These include the retention of the primary weathering products. Therefore leachate chemistry cannot be used as a measure of the relative rates of acid generation and neutralization and of times to mineral depletion. Humidity cells are designed to accelerate the natural weathering rate of a solid material. They are not intended to provide leachates that are identical to the actual leachate produced from a solid material in the field.

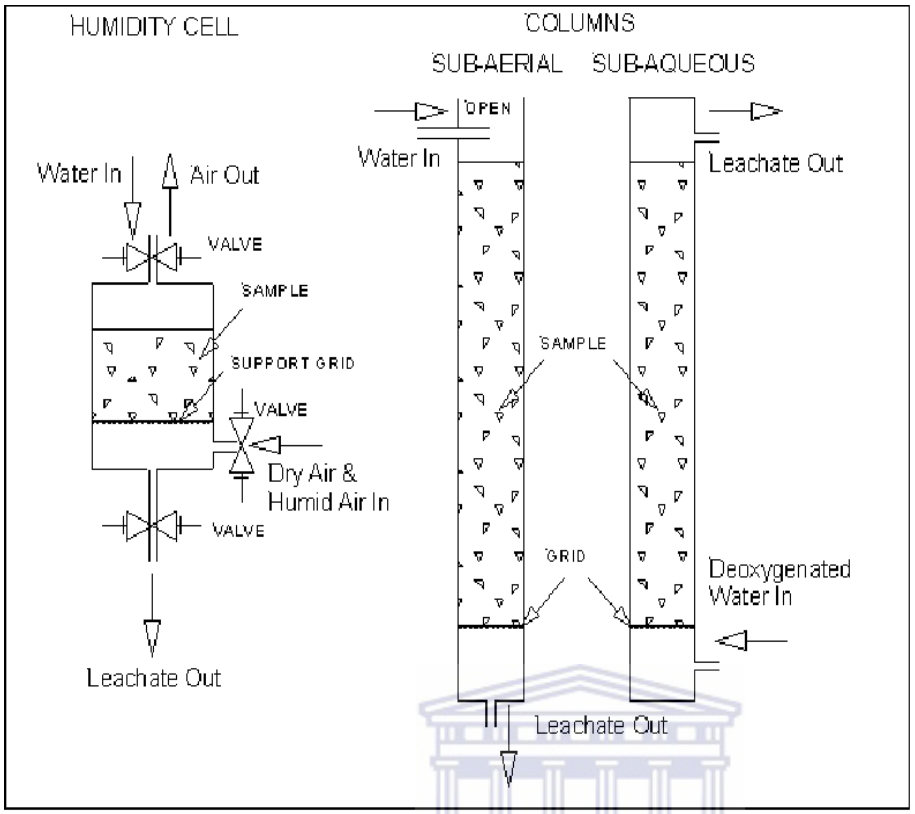

Figure 2.5: Schematic arrangements of humidity cell and sub-aerial and sub-aqueous columns (Lawrence, 1995).

UNIVERSITY of the
WESTERN CAPE

Sub-aqueous column network is conducted to simulate the leaching effects of water infiltration to and ex-filtration from material stored under water cover with no physical exposure to the atmosphere. In case of tailings or waste rock stored under water where water flow or displacement is not influenced by seepage, but by thermal or density gradients, the simulation of flow /leaching may be achieved by slow upward movement of de-oxygenated water through the column, so that anoxic conditions are maintained within the rock sample and its environment. In the case of tailings or waste rock stored under water in a natural or man made impoundment, infiltration of oxygenated water from the supernatant replaces any water lost by seepage to groundwater. In a column set-up this is simulated by the slow downward displacement of pore water by freshwater from above (Figure 2.5). Column set-ups are formulated and conditions adjusted to approximate those of the site as much as possible.

Sub-aerial column (trickle leaching) test work is conducted to simulate the leaching effects of precipitation infiltration to, and drainage from, material stored at the surface and exposed to

the atmosphere. Water addition to the column may be either fixed (certain volume per cycle) or varied to simulate the seasonal variations on site. Stewart *et al.* (1997) stopped leaching the columns for a given period of time to simulate drought conditions. The column is open to the atmosphere, so that there is no oxygen barrier, but there is usually no forced oxygenation, unlike with humidity cells (Figure 2.5). The column is operated without aggressive flushing, so that oxidation products may accumulate at particle surfaces in addition to being removed in the leachate. This behavior resembles field conditions and, as a result, leachate analyses are a better indicator of expected water quality than in humidity cells. Sample characterization before and after the test is important for the interpretation of the results. Many column studies encountered in the literature involve the determination of oxidation of sulphide materials. For example Elberling *et al*. (1994) and Nicholson *et al.* (1988) performed experiments of sulphide oxidation in an unsaturated medium. Nicholson *et al.* (1988) used a 0.08m length column and 0.057m in diameter filled with a mixture of a finely crushed quartz (80 wt %) and pyrite (20 wt %). Elberling *et al*. (1994) used columns of 1m in length and 0.11m in diameter to determine the oxidation rates of pyrrolite. The columns were irrigated with water every 1 or 2 weeks. Stromberg and Banwart (1999) performed long-term column experiments with complex sulphide waste rock to study sulphide oxidation. They used several columns of 2 m in height and 0.8 m in diameter, under a continuous flow of water.

From these studies it emerges that column leaching can be used to accelerate weathering of solid waste disposed of in the environment. However it will be difficult to simulate all the factors that are in play in real disposal scenario such as variation in gas fugacity, complex mineralogical changes that can take long to attain equilibrium and also the role of microorganism in the weathering processes.

The thrust of the current work is that the fly ash is first used to treat AMD to produce less reactive solid residues which can be disposed alone or blended with unreacted fly ash or OPC. The unreacted fly ash is expected to balance/modify the alkalinity of the solid residues and thereby maintain a circumneutral pH, so as to precipitate any metals that would be released during leaching. The unreacted fly ash is expected to lower the hydraulic conductivity of the co-disposal solids at the advanced stage of leaching.

2.3.3 Column set-up

Leaching columns have been used by many researchers (Dudas, 1981; Kanungo and Mohapatra, 2000; Simonton *et al*., 2000; Stewart *et al*., 1997; Warren and Dudas, 1984) to study acid mine drainage generation, weathering of fly ash, stability of contaminants immobilized by microbial reduction in an inert substrate, performance of reactive barriers (Komnitsas *et al*., 2004) and environmental stability assessment of OPC stabilized industrial waste (Catalan *et al*., 2002). Price (1997) argues that if the column infiltration rate is varied to simulate site conditions, then leachate analysis from a column testwork gives a better indication of the expected water quality. Dudas (1981) observes that although a number of short-term leaching, extraction, and equilibrium studies have demonstrated many of the initial dissolution characteristics of fly ash, the information obtained may not accurately represent the long-term dissolution behavior and concomitant environmental hazards or benefits of fly ash. Bradham and Carrucio (1990) and Perry (1985) agree that leaching column tests give the best approximation of field weathering conditions.

UNIVERSITY of the
WESTERN CAPE

Column set-up, design, diameter and length differ for different researchers and for different tested materials. Simonton *et al*. (2000) used large columns (10 cm diameter by 1m length) constructed of PVC to immobilize metals on kg quantities of sand. They subsequently used small polycarbonate columns (1cm diameter by 10cm length) to test the stability of the immobilized metal by leaching over a 6 month period. They leached the sand by passing simulated ground water through the columns and measuring the concentration of contaminants in the leachate. They intended to simulate the passage of uncontaminated groundwater through the contaminated sand in a sub-surface environment. Stewart *et al*. (1997) used plastic pipe (18 cm diameter by 60 cm length) to leach coal refuse, alone or blended with fly ash. The columns were hand packed with the test material. To maintain mix uniformity they used small batches of test material which were mixed frequently by tumbling during packing. The columns were packed with small increments with packing density being monitored during packing. The packing was made in triplicate for each mix tested. Xenidis *et al*. (2002) used plexi-glass columns with a diameter of 160 mm and a height of 100 cm to evaluate the potential use of lignite fly ash for the control of acid generation from sulphidic wastes. Wazlaf (1992) run a study using 5.1 cm diameter columns in triplicate. Dudas (1981)

used small lysimeters of 6.9 cm internal diameter prepared in triplicate and gently packed with 250 g of fly ash for his leaching experiments. He continuously leached the fly ash with distilled water over a 2 year period at a flow rate governed by the hydraulic conductivity of the fly ash cores.

Warren and Dudas (1985) packed fly ash into a series of five leaching columns (lysimeters), prepared in triplicate and leached for 90 days. The columns were packed with increasing quantities of fly ash (50, 75, 100, 125, and 150 g of fly ash respectively). They used a leaching solution of 0.005 mol L^{-1} H_2SO_4 with an initial pH of 2.1. The leaching solution was passed sequentially through the columns beginning with the one containing 50 g of fly ash. The leaching solution was chosen to simulate natural anthropogenically affected rain waters. A solution similar to most rain waters was used to accelerate the weathering process (Cogbill and Likens, 1974). Kanungo and Mohapatra (2000) used glass columns of 57 and 38 mm internal diameter packed with 500 g and 350 g of fly ash, with a total length of 25 and 35 cm occupied by the fly ash samples respectively for their leaching studies. They used deionised water adjusted to the initial pH 4.85 with 0.1M HNO_3, to simulate rainwater. The leachant was circulated through the columns repeatedly at the flow rate of 12.6 mL h^{-1}. They observed that the pH of the leachate was controlled by the cyclic release of elements and Fe and Al hydrolysis. Bilski and Aiva (1995) used plexiglass columns (30 cm long, 7 cm inner diameter) packed in triplicates to study the transport and leaching of cations and heavy metals from a fly ash amended soil.

Domenech *et al.,* 2002 used a column of 85 mm in diameter filled with 652 g of soil and sludge mixture to evaluate the sludge weathering and mobility of contaminants in soils affected by tailing dam spill. They observed that the pH of the leachate dropped to values around 2 after 260 days. No efficient processes existed for retaining Zn, Cd and Co which formed soluble salts. When pH of the leachate was higher than 4.5, the concentrations of Fe and Al was very low. Saturation indices showed the solution was in equilibrium with amorphous Fe $(OH)_3$ and $Al(OH)_3$. Xenidis *et al*. (2002) used plexi-glass columns with a diameter of 160 mm and a height of 100 cm to investigate the potential use of lignite fly ash for the control of acid generation from sulphidic wastes, they set up five columns. This study involved the application of wet-dry cycles on a weekly basis and each cycle involved the

addition of 2 L of deionised water. They observed that addition of fly ash at 10-63 % w/w increased the pH of the leachate to values of 8.6-10.0. Decreased concentrations of Zn and Mn were observed. Addition of fly ash at amounts of 31 and 63 % w/w reduced the water permeability of the material from 1.2 x 10^{-5} m/sec to 3 x10^{-7} m/sec and 2.5x10^{-8} m/sec respectively. Catalan *et al*. (2002) used acrylic columns measuring 5.1cm internal diameter and 20.2 cm in height for a flow through leaching of crushed stabilized/solidified natrojarosite waste. They used a buffered acetic acid/sodium acetate solution at pH 4.93. They observed that evolution of pH was consistent with the movement of a pH front that broke through the outlet face of the sample. PH was observed to decrease from values 10.5-9 to below 7.0 on breakthrough. They concluded that advancement of the pH front was controlled by the progressive depletion of alkalinity in the treated waste. Overall permeability of the material was observed to increase after pH front breakthrough. Geochemical modeling results showed that C-S-H gel coating on natrojarosite crystals provided an effective shield against direct contact with the leachant downstream of the pH front. Elevated concentrations of Cu, Pb and Zn were observed in the initial leachates but decreased as the leaching progressed. Heavy metal concentrations were observed to be oversaturated with respect to metal hydroxides.

UNIVERSITY of the
WESTERN CAPE

Komnitsas *et al*. (2004) used two 5cm inner diameter and 40cm long plexiglass columns set-up in series to study the efficiency of limestone and red mud barriers to remove inorganic contaminants Fe, Zn, Mn, Al, Ni, Cu, Co and Cd from synthetic sulphate solutions simulating AMD. Tests were conducted under dynamic flow conditions. Both reactive barriers caused the development of conditions that favored removal of heavy metal ions mainly by precipitation, co-precipitation and adsorption. Fe was mainly removed as goethite and ferrihydrite, Al as boehmite and gibbsite, Cu, Mn, Zn, Co and Ni as metal hydroxides and Cd by sorption and co-precipitation.

There doesn't seem to be a standard way of setting a column assembly. The basic principles utilized in setting up the columns are similar but the main underlying factors are that the drainage regime and the leachant is chosen so as to approximate the field conditions where the waste is to be disposed or placed in case of reactive barriers.

2.3.4 Mine backfilling

Mine backfill refers to materials, such as waste development rock, deslimed and whole mill tailings, quarried and crushed aggregate, and alluvial or eolian sand, which are placed in underground mined voids for the purposes of either disposal and/or to perform some engineering function. The disposal of mine tailings underground as opposed to surface dumps reduces their environmental impact and provides a material that can be used to improve both ground conditions and economics of mining (Weaver and Luka, 1970; Stromberg and Banwart, 1999). The waste materials are often mixed with very lean cement or other pozzolanic binders to improve their strength properties (Benzaazoua, *et al.*, 2002; Benzaazoua *et al*., 2004). There are three types of backfill: hydraulic fill, rock fill and paste fill. The most common hydraulic binder added to backfill is Ordinary Portland Cement (OPC). Research around the world has looked into alternative binders and the most common solution has been to use pozzolanic products such as fly ash and blast furnace slags (BFS). Typical binder proportions are normally 3 % to 7 % by weight. Several research works have pointed out that the presence of soluble sulphates in the backfill material has a deleterious effects on the strength of the paste fill or hydraulic fill (Benzaazoua, *et al.*, 2002; Van der Sloot, 1996). Sulphates can be derived from groundwater, contamination on site, natural sulphate minerals in the contaminated soil (example, gypsum), oxidation of pyrite or contaminated aggregates. Sulphate in solution has the ability to attack concrete causing its expansion, deterioration and disintegration. Sulphates react with calcium hydroxide and calcium aluminate hydrate in the cement paste. The products of the reactions, gypsum and (ettringite) calcium sulphoaluminate, have a considerably greater volume than the compounds they replace. This leads to expansion and disruption of the cementitious matrix (BRE, 2001) and hence loss of strength of the backfill. For a given concentration of sulphate, the rate and the amount of deterioration increases with the amount of C_3A (tricalcium aluminate) in the cementitious matrix, concentrations of calcium hydroxide and under acid conditions. A temperature of around 6^{o}C and under conditions of high humidity, sulphate solutions can attack concrete to produce thaumasite, which has more serious consequences than the formation of ettringite. Thaumasite formation decomposes CSH (calcium silicate hydrate) in the cement and thereby completely destroys the binding capacity of the cement paste (Taylor, 1998). Benzaazoua *et al*. (2002) observed that the chemical composition of the binder and backfilling material, grain size distribution, density, percent of solids of the

UNIVERSITY of the WESTERN CAPE

backfill material and the mixing water chemistry play an important role in the final strength acquisition. They observed that the presence of sulphate inhibits the precipitation of hydrates, when using slag-based binders. In Portland based binders the formation of gypsum contributed to the strength acquisition of the backfill material. This is in contrast to the deleterious effects observed with other binders (Van der Sloot, 1996). Benzaazoua *et al*. (2002) further established that the water chemistry interferes with the cement chemistry and alters the hydration processes. Of the binders they used, they observed that the OPC and fly ash based binders had fast hydration reactions and were less affected by soluble sulphate in the mixing water.

Significant gaps/questions exist regarding the use of fly ash for backfilling of coal mined out areas to reduce acid generation and to provide support for the overburden. The underground placement of fly ash reduces the amount that has to be disposed in surface dumps. Of particular concern is the long-term impact on groundwater quality if large amounts of fly ash are used for backfilling. Hence the chemical stabilization of contaminants in the fly ash is important.

UNIVERSITY of the

Campbell (1999) looked at the mineralogical properties associated with the hardening of fly ash in disposal dumps. He identified two minerals calcite and ettringite, which he associated with the hardening of ash in dumps. He also speculated the presence of thaumasite alongside ettringite. He attributed the hardening of fly ash in dumps to some of these minerals. Phung *et al.* (1979) amended soil using fly ash. They established that the application of fly ash increased the pH. DTPA (diethylenetriamine-pentaacetic acid)-extractable Fe, Mn, Ni, Co and Pb also decreased. Boron increased significantly with fly ash application. The data demonstrated that the alkalinity of fly ash plays a significant role in regulating the availability of trace elements in amended soils. Xenidis *et al.* (2002) blended sulphidic tailings with various amounts of fly ash ranging from 10 to 63 % w/w and monitored the drainage quality of the water over a test period of 600 days. This study established that the addition of fly ash to tailings at a low amount (10 % w/w) increased the pH of leachates to values of 8.6-10.0 and effectively inhibited the dissolution of Zn and Mn. Ca and SO_4^{2-} were the major ions reported in the drainage of fly ash amended columns. Higher fly ash addition rates (31 and 63 % w/w) resulted in the production of monolithic solid materials with

reduced hydraulic conductivity, however higher reduction was observed for the higher fly ash addition. The mineralogical analysis of the column solid residues indicated that higher fly ash addition favored the formation of ettringite, which was associated with the volume expansion of material. Mylona *et al*. (2000) conducted long term column tests on partially oxidized pyrite amended with limestone.

The performance of the pyrite-limestone mixtures was evaluated by monitoring the drainage quality of the columns. They observed dissolution of previously formed oxidation products in the control column, resulting in the release of significant amount of Fe, Zn, Mn, Cd, As and SO_4^{2-} and Pb. At a period of 20 days 87.8 % Zn, 46.1 % Cd, 90.7 % Mn and 2.9 % SO_4^{2-} of the cumulative metal load at 270 days had been leached. However, alkaline conditions prevailing in the limestone amended columns led to the precipitation of ferric hydroxides and gypsum. They observed reduction in permeability of the pyrite-limestone mixtures as compared to the pyrite. They attributed this to the filling of the pores by the secondary neutralization products (gypsum and ferric hydroxides).

These studies underline the potential of fly ash and limestone to remediate sulphidic waste over a given period of time. Benefits include removal of inorganic contaminants from the acidic leachates and reduction of hydraulic conductivity of the blends. However leaching of previous neutralization and precipitation products may lead to release of a significant load of toxic elements if the pH is not maintained at alkaline values.

2.3.5 Application of Binders in Waste Stabilization and their relevance in Backfilling.

There are three existing backfill types: hydraulic fill, rock fill and paste fill. However, Benzaazoua *et al*. (2002) notes that the use of paste fill is becoming an increasingly important component of underground mining. Paste fill consists of total mill tailings (full size fraction of the tailings) thickened and filtered to around 80 % dry weight to which binder and water are then added. Several workers have proposed the use of paste fill for managing acid generating tailings (Cincilla *et al.,* 1997; Grabinsky *et al.,* 2002). Their rationale is that the addition of binding agents to the paste mixture assures the retention of leachable elements such as As, Pb, Mn, Sr, B, Mo and other metals due to the calcium silicate hydrate gels

generated. Common binder used is ordinary Portland cement but alternative binders such as fly ash and blast furnace slags have also been used (Xenidis *et al*., 2002). The cohesive strength, density and solid percentage are the determining factors in the use of paste fill. The backfill cohesion is dependent on binder quality and its potential to resist harmful chemical reactions such as hydration inhibition and sulphate attack that can occur within sulphide and sulphate rich backfill. Benzaazoua *et al*, (2002) investigated the effect of mixing-water chemistry on the unconfined compressive strength (UCS) of paste fills using various binders (fly ash, blast furnace slag and ordinary Portland cement). They used three different mixing water samples: mine water, lake water and municipal water. They concluded that the binder chemistry combined with the mixing-water chemistry affects the formation of primary and secondary hydrates during paste fill strengthening. The cohesion of the paste fill matrix was found to be directly dependent on the nature of the precipitated hydrates.

It can be concluded that the binders have a dual purpose in paste fill formulations, insitu treatment of acidic leachates generated within the backfill and incorporation of toxic elements in the cementation matrix generated and strength development for mechanical support.

UNIVERSITY of the
WESTERN CAPE

2.4 Mineralogy of Precipitates formed on increasing the pH of the Acid Mine Drainage.

2.4.1 Introduction

Acid mine waters are highly reactive solutions that can dissolve most primary mineral phases when they are in contact with a solid material such as fly ash, with a consequent formation of a variety of secondary mineral phases. Treatment of AMD with alkaline material such as fly ash triggers processes such as neutralization, oxidation and metal hydrolysis which are frequently accompanied by the precipitation of metal-bearing hydroxide and hydroxyl-sulphate minerals. The understanding of secondary mineral formation has important consequences for environmental management of wastes. Secondary mineral phases with large surface areas can effectively immobilize many of the minor contaminants in acid mine waters and fly ash leachate, providing an important attenuation and detoxifying mechanism.

The type of secondary mineral phases that form depends on the composition of the AMD, pH, type and composition of the fly ash leachate or any other solid material. The initial mineral phases that precipitate tend to be poorly crystalline, metastable and may transform to more stable phases over time. The mineral phases resulting from the neutralization of AMD with fly ash are expected to be of poor crystallinity since neutralization forces rapid precipitation (Murad *et al.,* 1994).

2.4.2 Saturation Indices (SI) and Mineral Solubilities

When water analysis for major ions is available, a speciation computation can be done to determine the state of saturation with respect to any particular mineral for which thermodynamic data is available. One way of doing this is by calculation of saturation indices (SI). For a dissolution reaction SI is used as log (IAP/K_{eq}) where (IAP) represents ion activity product and K_{eq} the equilibrium constant for the reaction. This is done to achieve quantitative interpretations on the control of metal concentrations by mineral solubility. Computer codes such as MINTEQA2 (Allison *et al.,* 1991) and PHREEQC (Parkhurst, 1995) are used to calculate the SI once a comprehensive water analysis is done.

UNIVERSITY of the
WESTERN CAPE

If solubility equilibrium is achieved and if it exerts the dominant control on the concentration of one or more elements, the SI values should show a linear and horizontal trend close to zero. Such a pattern signifies that the water chemistry reflects the stoichiometry of the given mineral. The values tend to plateau with the appropriate stoichiometry of the mineral but generally on the side of super saturation. This effect might be explained by the particle size effect on solubility. The solubility products reported in literature usually refers to coarse-grained, well crystallized materials hence the variation. It could also be due to solid solution substitution of trace components. The stoichiometry of a phase controlling the solubility of an aqueous constituent can be derived from an appropriately selected ion-activity plot. For example, if pure ferric hydroxide were controlling the solubility of ferric iron, the reaction (equation 2.16) and its log equilibrium constant expression (equation 2.17) would indicate that a plot of Fe^{3+} activity versus pH should have a slope of -3 showing solubility control by a pure ferric hydroxide having a molar Fe: OH ratio of 1:3.

$$Fe(OH)_3 + 3H^+ \Leftrightarrow Fe^{3+} + 3H_2O \quad \text{.....(2.16)}$$

$$\log K = \log a_{Fe^{3+}} - 3\log a_{H^+} + 3\log a_{H_2O} \quad \text{.....(2.17)}$$

Natural waters and acid mine waters, are generally in equilibrium with respect to dissolved species in the aqueous phase but may be in varying stages of disequilibrium with respect to solid phases (Nordstrom *et al.,* 1979). Nevertheless, thermodynamic equilibrium calculations have been applied to describe the water chemistries corresponding to the aqueous-solid phase interactions and the precipitation of certain compounds from the waters with encouraging results.

2.4.3 Secondary Mineral Phases

There are several processes that may lead to the formation of secondary mineral phases from acid mine waters. They include the mixing of acid mine waters with more dilute waters and reaction with alkalinity releasing materials. The secondary mineral phases discussed here are the ones likely to form in the acid mine waters and fly ash neutralization reactions. These include (a)-metal oxides, hydroxides, hydroxysulphates, (b)-soluble sulphates and less soluble sulphates and (c)-carbonates.

UNIVERSITY of the
WESTERN CAPE

Most divalent and trivalent metals exhibit amphoterism (have properties of both an acid and a base). They produce a solubility minimum at circumneutral pH values with enhanced solubilities under both acidic and alkaline conditions. The pH-specific solubility minimum varies for each metal. This behavior provides the basis for the removal of metals during rapid neutralization of acid mine drainage by alkaline treatment. This phenomenon also leads to a difference in the efficiency of metal removal for neutralization to a given pH (Barton, 1978).

At metal concentrations greater than 10^{-6} mol L^{-1}, metal hydroxides should precipitate in the following sequence with increasing pH: Fe^{3+}, Pb, Al, Cu, Zn, Fe^{2+} and Cd. This sequence is closely followed by the pH-dependent sequence of adsorption of metals on hydrated ferric oxide surfaces (Nordstrom and Alpers 1994a).

The order of the precipitation of the hydroxides by the gradual addition of alkali has been investigated by Britton and Robinson (1932) and Hildebrand (1913). They observed that a definitive H^+ concentration within narrow limits has to be attained before the precipitation of any particular hydroxide can take place. From a solubility product point of view, an insoluble hydroxide, MOH, attains equilibrium with undissociated molecules and ions in solution (equation 2.18)

$$MOH_{solid} \Leftrightarrow MOH_{undissociated} \Leftrightarrow M^+ + OH^- \quad \text{.....(2.18)}$$

The solubility product is given by (equation 2.19)

$[M][OH^-]=[M]K_w/[H^+]$.....(2.19)

where $K_w=[H]\,[OH]$ is the ion activity product for water.

The precipitation of the hydroxide thus depends on the concentration of both metal and H^+ ions. The H^+ ions concentration necessary for the precipitation of a large number of hydroxides have been determined and constitutes a suitable basis for the classification of the hydroxides (Table 2.5). The order is parallel with increasing magnitude of the solubility products.

UNIVERSITY of the
WESTERN CAPE

Table 2.5: Ph of metal hydroxide precipitation from dilute solutions (Britton, 1956)

Element	pH range	Element	pH range
Mg	10.5	Ni	6.7
Mn^{2+}	8.5-8.8	Pb	6.0
Zn	7.0	Fe^{2+}	5.5
Co	6.8	Cu^{2+}	5.3
Cd	6.7	Cr^{3+}	5.3
Fe^{3+}	3.0	Al^{3+}	4.1

In alkali precipitations the pure hydroxide of the metal is not precipitated, instead basic salt containing some unreacted metal salt is formed. The composition of such a basic precipitate depends on the rate at which the alkali is added. Calculations of solubility products for minerals prevailing during the course of titrations justify the belief that the separation of hydroxides is the chief-determining factor in causing precipitation. The solubility product should remain constant during the course of precipitation (Britton, 1956). However Britton (1956) further states that with exception of Ni, Cu and Pb the solubility products increase as the alkali is added.

UNIVERSITY of the
WESTERN CAPE

2.4.4 Ferrous, Ferric oxides, hydroxides and hydroxy-sulphates

Ferrous hydroxide ($Fe(OH)_2$) is considerably more soluble than its ferric equivalent at a given pH and it rarely appears in nature. When slightly oxidized, it takes on a green appearance and is also known as green rust. It occurs when a Fe (II) rich solution is mixed with a highly alkaline solution and allowed to oxidize slightly. It is not credited as a mineral because it is unstable and poorly characterized.

Ferrihydrite is a poorly crystalline form of hydrous ferric iron oxide that seems to be the first phase to form upon neutralization of Fe (III)-bearing solutions at low temperature. This phase was first considered to be amorphous $Fe(OH)_3$ but careful examination by X-ray diffraction (XRD) and Mossbauer spectroscopy has revealed that this material is commonly a poorly crystalline substance with a range of structural order, yielding an XRD pattern with two to six peaks (Carlson and Schwertmann, 1981). The nominal formula of ferrihydrite is given as $Fe_5HO_8.4H_2O$ although the composition may vary as a function of particle size (Murad *et al.,* 1994).

Hematite (Fe_2O_3) and goethite [α-FeO (OH)] are the most common and most stable forms of ferric iron oxide and oxyhydroxide respectively. The solubility and stability of hematite and goethite are sufficiently close that grain size and Gibbs free energy have important influence on the phase relations. Goethite occurs in a wide range of environments (Murad *et al.,* 1994). It is much more stable than ferrihydrite, jarosite and schwertmannite (Bigham *et al*, 1996b; Nordstrom, 1982). Both goethite and hematite have slow growth kinetics at low temperatures, so the initial solid products from the hydrolysis of ferric iron are poorly crystalline metastable phases such as microcrystalline goethite or ferrihydrite. Ferrihydrite is known to convert to hematite if pH conditions are maintained between 5 and 9. Other factors that may influence the formation of these phases include humidity, Al content and presence of trace elements. Al has been observed to substitute Fe in goethite and hematite in certain soils (Nordstrom and Alpers, 1994a).

Adsorption and precipitation of a given hydrolyzable metal ion tend to take place at pH values near the first hydrolysis pK for that metal. The first pK of hydrolysis for Fe^{3+} is 2.2 and for Al is 5.0. The co-precipitation of Al in hydrous Fe^{3+} oxides formed at pH values less than 4.5 is unlikely. This fundamental difference between iron and aluminium chemistry leads to spatial and temporal separation of precipitating phases of hydrolyzed iron and aluminium during oxidation of mine waters.

Schwertmannite ($Fe_8O_8(OH)_6SO_4$) (Bigham *et al.,* 1996a) is a poorly crystalline iron-hydroxysulphate mineral that is fairly common in mine drainage environments (Bigham *et al*., 1990; Murad *et al.,* 1994). The tunnel structure of schwertmannite appears to be related to that of akaganeite (β-FeOOH), an iron oxyhydroxide with essential chloride (Murad *et al.,* 1994). The sulphate is believed to be located in the tunnels taking over the role of chloride in akaganeite. Schwertmannite or other sulphate-substituted hydrous ferric oxides are most likely to control ferric iron solubility in acid mine drainage.

The jarosite-alunite group of minerals shares a common crystal structure and stoichiometry with many possible compositional substitutions. General jarosite-alunite formula is $AB_3(SO_4)_2(OH)_6$ where the B sites are occupied by Fe (III) to form jarosites and by Al to

form alunites. The site A is occupied either by a monovalent cation or by a divalent cation alternating with a vacancy to maintain charge balance. In natural alunites and jarosites the most common occupants of site A in order of abundance are $K^+ > Na^+ > H_3O^+$. The pure potassium endmember is jarosite and the pure potassium-aluminium endmember is alunite.

2.4.5 Aluminium oxides, hydroxides and hydroxysulfate minerals.

Common Al minerals include boehmite [(γ-AlO(OH)], gibbsite [(γ-$Al(OH)_3$], bayerite α-$Al(OH)_3$, alunite $KAl_3(SO4)_2(OH)_6$, natroalunite $NaAl_3(SO4)_2(OH)_6$, ammonium alunite $(NH_4)Al_3(SO_4)_2(OH)_6$, jurbanite $Al(SO_4)(OH).5H_2O$ and basaluminite $(Al_4(SO_4)(OH)_{10}.5H_2O)$

In acid mine waters, aluminium-sulphate and –hydroxysulphate minerals become more stable than common soil minerals such as gibbsite and kaolinite. At pH values lower than about 5.5 (depending on sulfate and potassium activities) gibbsite becomes unstable relative to alunite (Nordstrom, 1982).

UNIVERSITY of the
WESTERN CAPE

Below pH values of about 4.0, jurbanite becomes more stable. Jurbanite has not been commonly found as a mineral precipitate from acid mine waters. It is suspected to have little significance as a solubility control towards Al despite the near-zero SI values commonly found. For waters with pH values lower than 4.5 to 5.0, dissolved aluminium tend to behave as a conservative ion (stays in solution). For pH values above 5.0 the solubility control of dissolved aluminium is mainly due to microcrystalline or amorphous Al $(OH)_3$. When the pH in acid mine water increases to 5.0 or higher, because of rapid mixing with circumneutral, dilute waters or an alkaline releasing material, aluminium-hydroxysulphate compound precipitate. Precipitation rates for some of these aluminous minerals may be sluggish so that equilibrium conditions are not always reached in surface waters.

2.4.6 Hydroxides of trace metals

The absence of discreet trace-metal bearing hydroxides in most oxidized mine waste suggests that other mechanisms, such as adsorption or co-precipitation with hydrous iron oxides, limit the concentrations of dissolved trace metals in mining environments (Nordstrom,1982). The

behavior of nickel in tailings impoundments and acid mine drainage precipitates illustrates the fate of trace metals in mine drainage settings, being generally tied to the one of the major elements, particularly iron. Mineralogical analysis and microanalysis by Jambor and Owens (1993), as a part of a study on the copper cliff tailings area at Sudbury, Ontario, has indicated that nickel tends to be dispersed in hydrous iron oxides rather than as discreet nickel oxide or hydroxide phases. The behavior of copper in tailings impoundments and waste rock piles is similar to the one of nickel. Ribet *et al*. (1995) observed a strong association between Ni, Cr, Co, and Pb and ferric iron (oxy) hydroxides in Nickel Rim mine-tailings impoundment. They attributed this strong association to either co-precipitation with or adsorption to ferric iron oxy(hydroxides). Discrete secondary copper oxides are rarely formed, and the copper is rather transported away from the oxidized zone in solution or fixed in other secondary phases such as sulfates, carbonates and silicates, or is co-precipitated with, or adsorbed to hydrous iron oxides.

UNIVERSITY of the
WESTERN CAPE

2.4.7 Carbonates

Many carbonates minerals occur as either primary or secondary mineral phases in mine wastes. Hydroxyl-bearing carbonates include mineral phases such as malachite $Cu_2(CO_3)(OH)_2$, azurite $Cu(CO_3)_2(OH)_2$, hydrocerussite $Pb_3(CO_3)_2(OH)_2$, hydrozincite, $Zn_5(CO_3)_2(OH)_6$ and aurichalcite $(Zn, Cu)_5(CO_3)_2(OH)_6$. Metal carbonate bearing mineral phases include rhodochrosite ($MnCO_3$).

2.4.8 Sequential Extractions

Metals in soils and sediments may be present in several different physicochemical phases that act as reservoirs or sinks of trace elements in the environments (Becket, 1988; Jenne, 1977; Sposito, 1993). These phases include broad categories such as: exchangeable; specifically adsorbed; carbonate; secondary Fe and Mn oxides; organic matter; sulphides and silicates. All of these may occur in a variety of structural forms. One of the approachs to understand the distribution of metals in the fractions is done by phase-selective chemical extractions involving multiple extracting agents (Shuman, 1985; Tessier *et al.,* 1979; Ure *et al*., 1993). Selective sequential extractions have been used on contaminated lake sediments (Tessier *et al*., 1985) and mine waste contaminated areas, soil contaminated with pyrite

sludge (Domenech *et al.*, 2002; Kuo *et al.*,1983). The reagents utilized in sequential extraction are chosen such that they are selective and specific towards a particular physico-chemical form. Hence the effectiveness of extractions depends on the degree of affinity and specificity of the extracting chemical for the target phase. The selectivity of a given reagent for a specific phase may be limited or an extracted element may readsorb during the extraction sequence (Bunzl *et al.*, 1999). Redox sensitive elements may change oxidation states during an extraction sequence resulting in erroneous conclusion regarding its partitioning (Gruebel *et al*., 1988). There fore soil or sediments extractions are at best operationally defined (Kim and Fergusson, 1991; Tessier and Cambell, 1991). Despite these limitations, the sequential extraction schemes can be a very useful method, for characterizing solid phases associated trace elements in soils and sediments (Adamo *et al.*, 1996; Ma and Rao., 1997).Despite these shortcomings selective sequential extractions provide:

a) Valuable information regarding general elemental partitioning patterns (Shuman, 1979).
b) Provide semi-quantitative estimates of contaminants within soils (Lo and Yang, 1998; Shuman, 1985).
c) Are useful for monitoring relative changes in contaminant partitioning as a consequence of changing physico-chemical conditions (Arey *et al*., 1999).

The sequential extractions will be applied to semi-quantitatively identify the transformation of major and trace elements in the solid residues as the pH increases with reaction time.

2.5 Conclusions

Acid mine drainage (AMD) is the principal environmental problem caused by the mining of sulphide ore deposits. It is extremely acidic and enriched with soluble Fe, Mn, Al, $SO_4^{2-}$and trace metals such as Pb, Hg, Cd, Zn, Cu. This wastewater requires treatment before disposal.

Active treatment methods of AMD include addition of alkaline materials such as quicklime (CaO), hydrated lime [$Ca(OH)_2$] and limestone ($CaCO_3$). Alternative liming materials that would decrease the cost of neutralization are constantly being sought.

Fly ash is a ferro-alumino-silicate mineral with the elements Si, Al, Fe, Ca, K and Na being predominant within the matrix. Current surface disposal is of major environmental concern due to the dissolution of soluble salts on interaction with water during transport and after disposal. Leaching of this highly saline metal laden leachate to the groundwater is of major concern.

UNIVERSITY of the
WESTERN CAPE

Fly ash has chemically reactive mineral matter. Due to this property, it has found several applications which include rehabilitation of acidic mine spoils, soil amendments, addition to cement and concrete products, structural fill and cover material, waste stabilization/solidification, roadway and pavement base stabilization, infiltration barrier and underground void filling and soil, water improvement. All these applications utilize the alkalinity of fly ash.

Studies have been carried out to assess the neutralization capacity of fly ash (Burgers, 2002; Doye and Duchesne, 2003; Hodgson *et al*., 1982; Klink, 2004; O'Brien 2000). A major observation of these studies is that fly ash has the capacity to neutralize acid mine water with removal of the major elements.

All these studies have not shown clearly the mechanisms involved in the removal or release of the major and minor elements during the neutralization process and mineral phases controlling their concentration. Moreover no study has shown how the major and trace elements partition themselves in the solid residues resulting from the treatment process.

A desired disposal method of fly ash has been to return it to the mine voids but the concern has been the probable impact on the groundwater quality. In all the coal combustion by-products (CCBs) application for underground placement, emphasis is on the rheological properties and strength development characteristics. The literature lacks of studies looking at the leaching characteristics of neutralized fly ash (referred to here as solid residues) alone or blended with binding materials. The leaching chemistry of the neutralized fly ash alone or blended with binders could provide a basis for utilization of the solid residues for backfilling of mine voids to provide strength and for insitu AMD treatment over time

2.6 Aims of the study

This study aims at understanding the chemistry of the neutralization of the acid mine drainage (AMD) with fly ash by considering the AMD: fly ash ratios that produce neutral and alkaline process waters. This will eventually provide details on the suitability of the fly ash as a suitable liming material for treatment of AMD. As the pH of the AMD is gradually increased due to alkalinity released from fly ash the Fe^{3+} and Al^{3+} concentrations are expected to decrease due to in situ precipitation of hydrous oxides such as amorphous $Fe(OH)_3$, ferrihydrite, schwertmannite, or goethite and amorphous $Al(OH)_3$ or poorly crystalline gibbsite. The fly ash is also expected to leach toxic elements during the initial acidic conditions and also as the pH increases. The interaction of these released elements and the species in AMD will be of importance in determining the quality of the process water. In addition the accumulation of the hydrous oxides will promote sorption and coprecipitation of dissolved elements like Mn, Cu, Co, Ni, Pb and Zn. It is hypothesized that the resulting solid residues (SR) are inert and can be used for backfilling of mined voids. However the stability of the mineral precipitates is of great concern if the solid residues were to be subjected to aggressive acidic conditions such as acidic mine drainage. An attempt will be made to modify the solid residues with unreacted fly ash and Ordinary Portland Cement (OPC) to monitor the effect on the leachate chemistry and heavy metal mobility.

This study attempts to answer the following questions:

Is fly ash a suitable liming material for AMD and at what FA: AMD ratios and reaction times will neutral and alkaline water be produced?

Which elements are effectively scrubbed from AMD and which ones are released from the fly ash and what mechanisms are involved?

What associations if any exist between the trace elements and mineral phases precipitating in the neutralization process?

Can amendment of the solid residues with unreacted fly ash or Ordinary Portland Cement (OPC) reduce the leachability of the precipitated or immobilized elements?

Can FA and its derivatives (solid residues, FA and OPC blend solid residues) attenuate contaminants in AMD over an extended period of time?

Can the OPC blended solid residues (SR) develop strength essential for the support of the overburden and passively remediate acid mine drainage over time?

The chemistry of the neutralization reactions will be investigated by use of fly ash and AMD collected from the field. Removal or addition of elements in solution will be ascertained. Mineral precipitation processes responsible for removal of the major and minor elements will be investigated. Column leaching experiments will be used to study the stability of the mineral precipitates in the solid residues either alone or blended with unreacted fly ash or Ordinary Portland Cement.

UNIVERSITY of the
WESTERN CAPE

Chapter Three

Utilization of fly ash for remediation of coal mine waste waters: Removal of major inorganic contaminants and trace elements.

Abstract

Acid mine drainage (AMD) has been reacted with two South African fly ashes in a batch set-up in an attempt to evaluate their neutralization and major, minor elements removal capacity. Different fly ash: acid mine drainage ratios (FA: AMD) were stirred in a beaker for a set time and the process water analyzed for major, minor elements and sulphate content.

The chemistry of the AMD was found to determine the final pH attained in the final reaction mixture and the reaction time of breakthrough to circum-neutral and alkaline pH. Efficiency of the elements removal was directly linked to the amount of FA in the reaction mixture and to the final pH attained. Most elements attained ≈ 100 % removal only when the pH of minimum solubility of their hydroxides was achieved (i.e. Mg=10.49-11.0, Cu^{2+}=6, Pb^{2+}=6-7). Significant leaching of B, Sr, Ba and Mo was observed as the reaction progressed and was observed to increase with quantity of fly ash in the reaction mixture. However B was observed to decrease at high FA: AMD ratios probably as result of increased co-precipitation with carbonate fraction.

Keywords: Fly ash, Acid mine drainage, Sulphates, Metal ions, Neutralisation.

Academic Output

M.W. Gitari, L.F. Petrik, O. Etchebers, D.L Key, E. Iwuoha and C. Okujeni. 2006. Treatment of acid mine drainage with fly ash: Removal of major contaminants and trace elements. Journal of Environmental Science and Health-Part A., A41 (8): 1729-47.

M.W. Gitari, V.S. Somerset, LF Petrik, DL Key, E. Iwuoha and C. Okujeni. Treatment of acid mine drainage with fly ash: Removal of major, minor elements, SO4 and utilization of the solid residues for wastewater treatment. 2005. A **poster** presented at the *World of Coal Ash symposium*, April 11-15 2005, Lexington, Kentucky, USA.

M.W. Gitari, L.F Petrik, D.L Key, C. Okujeni. 2004. Neutralization of acid mine drainage with fly ash: A laboratory investigation of metal and SO4 removal in the process waters. A **poster** presented at the 37*th National Convention of the South African Chemical Institute* (SACI) congress, July 2004, CSIR international conference centre.

3 Introduction

The principles and methods behind the passive and active treatment of AMD are well researched but alternative liming materials that would decrease the costs of treatment are constantly being sought. Electricity generating companies utilizing pulverized coal are in constant search of better and beneficial fly ash disposal methods.

The aim of this part of the study is to evaluate the neutralization potential of fly ash, establish at what ratios and contact time maximum removal of contaminants is achieved. This study is employing an overhead stirrer reminiscent of liming type treatment of AMD by limestone or lime in most mining houses to agitate the reaction mixtures.

UNIVERSITY of the
WESTERN CAPE

3.1 Experimental Procedures

3.1.1 Chemical characterization of fly ash, AMD and solid residues samples

Coal fly ashes used in these experiments were obtained from two South African power plants (Matla and Arnot) which combust pulverized coal to generate electricity. The AMD samples used were collected from Navigation colliery, Bank colliery and Brugspruit liming plant in Highveld. The Brugspruit AMD samples were seepage from an old abandoned mine and were scooped from the seepage point while Navigation AMD samples consisted of acidic water pumped from underground old mine workings to a collection dam. Bank AMD was collected from underground mine voids.

Raw AMD samples were filtered by using 0.45μm cellulose nitrate membrane to remove suspended particles and diluted with MilliQ (ultrapure) water to EC < 1.5 mS/cm and then stabilized with HNO_3 for elemental analysis. Samples for anion/cation analysis were filtered by using 0.45 μm cellulose nitrate membrane and kept at 4^oC until analysis.

Neutralization experiments were designed to develop neutralization curves that would indicate buffer characteristics and show the contact time required for the breakthrough to

alkaline pH. The batch neutralization experiments were conducted by stirring a mixture of fly ash and AMD which was pre-determined to give a specific fly ash/AMD ratio (FA: AMD). All the experiments were done in triplicate. The AMD was stirred for 30 minutes for equilibration before the fly ash was added. An overhead stirrer was used for all the experiments. The progress of the reaction was monitored by measuring the pH and EC with a Hanna HI 991301 portable pH/EC/TDS/Temperature meter.

A second batch of experiments were repeated at selected FA: AMD ratios to determine the major, trace elements removal efficiency of the fly ash with increasing pH of the process water. The reaction time varied from 120-360 minutes. The solid residues were separated by filtration and the process water samples prepared for major, trace elements and sulphate analysis.

Elemental analysis of the water samples was done by ICP-MS (ELAN 6000). The accuracy of the analysis was monitored by analysis of NIST water standards. Fe^{2+}/Fe^{3+} analysis was done by the colorimetric method using 2,2-bipyridal as the complexing reagent. Sulphate analysis was done turbidimetrically by a portable datalogging spectrophotometer (Hach DR/2010) and ion chromatography.

UNIVERSITY of the
WESTERN CAPE

Chemical characteristics of the fly ash samples were ascertained by X-ray fluorescence spectroscopy (XRF) by fusing with lithium metaborate.

3.2 Results and Discussion

3.2.1 Composition of Fly Ash Samples

The chemical characteristics of the fly ash samples used in these experiments are presented in Table 3.1 below.

The three major phases Al_2O_3, Fe_2O_3 and SiO_2 do not vary to a great extent (Table 4.1). Matla fly ash has higher Al_2O_3 content while Arnot fly ash shows higher Fe_2O_3 content. The American Society for Testing and Materials (ASTM, 1988) uses these three major phases to classify fly ashes based on source coal. From the analysis ($SiO_2 + Al_2O_3 + Fe_2O_3 \geq 70\%$) the

South African fly ashes are class F. The CaO content shows slight variation with Matla fly ash showing a slightly higher value. The total CaO content detected by XRF does not distinguish the free lime from that trapped within the glass matrix. The free CaO content of FA is important because of its availability for rapid dissolution, which has implications on the pH of the solution.

Among the minor elements both fly ashes shows high concentrations of Sr, Ba, Cr, Zr and Ni (Table 3.1). Trace elements of Mo are also present. These concentrations are within the concentration ranges reported for fly ashes (Eary *et al.,* 1990) which indicates that they are higher than values generally found in coals and soils indicating that the combustion process tends to enrich the fly ash with the minor elements.

Table 3.1: Chemical characteristics of fly ashes used in these experiments

Arnot fly ash				Matla fly ash			
element	% (w/w)	element	ppm	element	% (w/w)	element	ppm
SiO2	53.4 ± 2.4	Cu	47.3 ± 6.6	SiO2	53.8 ± 0.29	Cu	57.9 ± 9.9
TiO2	1.34 ± 0.05	Mo	5.22 ± 0.14	TiO2	1.44 ± 0.11	Mo	6.56 ± 0.15
Al2O3	23.4 ± 1.1	Ni	93.4 ± 6.5	Al2O3	26.2 ± 2.52	Ni	58.2 ± 1.2
Fe2O3	4.72 ± 0.96	Pb	56.4 ± 13.6	Fe2O3	3.40 ± 0.24	Pb	29.1 ± 7.18
MnO	0.06 ± 0.002	Sr	1463.9± 111.8	MnO	0.05 ± 0.02	Sr	2056.0 ± 205
MgO	2.69 ± 0.05	Zn	57.3 ± 4.71	MgO	2.48 ± 0.58	Zn	25.4 ± 1.35
CaO	8.43 ± 0.57	Zr	488.1± 125.7	CaO	8.50 ± 1.75	Zr	536.1 ± 131.3
Na2O	0.35 ± 0.25	Co	18.3 ± 13.08	Na2O	0.49 ± 0.05	Co	10.4 ± 3.3
K2O	0.49 ± 0.03	Cr	179.2 ± 1.14	K2O	0.86 ± 0.07	Cr	122.7 ± 27.8
P2O5	0.35 ± 0.22	V	147.4 ± 38.9	P2O5	0.60 ± 0.22	V	145.8 ± 32.8
Cr2O3	0.03 ± 0.009	Ba	928.0 ± 91.9	Cr2O3	0.03 ± 0.006	Ba	1559.2 ± 346.7
NiO	0.011± 0.001			NiO	0.009 ± 0.002		
V2O5	0.019 ± 0.002			V2O5	0.02 ± 0.003		
ZrO2	0.052 ± 0.012			ZrO2	0.055± 0.003		
LOI	2.36 ± 0.19			LOI	1.33 ± 0.36		

Concentration reported as mean ± SD (n=3), LOI-loss on ignition

3.2.2 Composition of Acid Mine Drainage Samples

The characteristics of the AMDs used in the experiments are presented in Table 3.2 below.

The pH values of the samples ranged from 2.39 for Navigation to 2.92 for Brugspruit indicating strongly acidic waters (Table 3.2). The pH of mine water can be driven towards acidic or alkaline mode depending on the relative abundance and extent of weathering of pyrite and calcite neutralization. PH values in the acidic mode imply a deficiency of calcareous minerals and absence of carbonate buffering in these AMD samples. All the samples exhibit high electrical conductivity (10.02-11.36) mS/cm). Azzie, (2002) observed electrical conductivities ranging from (4.0-13.7) mS/cm in some South African coal mine waters, the sulphate correlated positively with the EC measurements for most of the acidic coal mine waters investigated. The sulphate recorded in these samples ranged from 6155 to 14950 mg/L making this anion dominant in the wastewater samples. Major cations included Na, Ca, Mg, Al, Mn and Fe. Dissolution of silicate minerals such as feldspar, kaolinite, chlorite accounts for most or all of the dissolved K, Na, Mg, Al and Ca (Crouse and Rose, 1976).

The ferrous iron in these samples represented half or greater proportion of the total iron (Table 3.2). In most samples of coal mine waste water, an abundance of dissolved ferrous iron (Fe^{2+}) indicates that the chemical reactions are at an intermediate stage in the series of reactions where pyrite is being directly oxidized by the Fe^{3+} (Equation 3.1) (Stumm and Morgan, 1981).

$$FeS_2 + 14Fe^{3+} 8H_2O \Rightarrow 15Fe^{2+} + 2SO_4^{2-} + 16H^+ \quad \text{.....(3.1)}$$

Table 3.2: Chemical and physical characteristics of AMD samples used in the experiments

Parameter	Navigation	Bank	Brugspruit
pH	2.39 ± 0.05	2.46 ± 0.03	2.91 ± 0.02
EC(mS/cm)	10.83 ± 0.13	10.78 ± 0.15	10.02 ± 0.06
Acidity(mg/l $CaCO_3$)	6950 ± 70.7	7000 ± 70.7	500 ± 0.0
TDS(mg/L)	16765 ± 50.5	19410 ± 76.8	8975 ± 60.5
B	1.37 ± 0.163	1.51 ± 0.08	2.29 ± 0.221
Na	358.7 ± 2.95	399.9 ± 21.3	4137.9 ± 233.0
Mg	2661.7 ± 35.0	2844.2 ± 148.1	388.7 ± 19.7
Al	1068.1 ± 11.28	1140.1 ± 61.58	60.0 ± 2.9
Si	82.01 ± 1.24	87.8 ± 5.87	69.7 ± 3.5
K	23.03 ± 2.86	19.3 ± 4.21	52.6 ± 3.6
Ca	653.3 ± 10.6	1012.3 ± 75.9	842.1 ± 117.4
Mn	226.3 ± 4.7	242.3 ± 12.9	31.6 ± 1.50
Fe	5599.9 ± 80.9	6115.9 ± 327.5	250.8 ± 11.2
Fe2+	3725.1 ± 30.5	2886.3 ± 20.7	153.1 ± 9.5
Fe3+	1451.9 ± 45.2	3344.6 ± 50.5	126.1 ± 6.5
Ni	6.95 ± 0.02	7.96 ± 1.16	2.35 ± 0.13
Cu	0.355 ± 0.007	0.345 ± 0.018	0.116 ± 0.012
Co	4.3 ± 0.11	4.57 ± 0.32	1.15 ± 0.063
Zn	48.99 ± 30.63	17.7 ± 0.65	9.52 ± 0.49
Sr	7.69 ± 0.226	8.39 ± 0.45	1.05 ± 0.058
Mo	0.04 ± 0.002	0.044 ± 0.003	0.036 ± 0.004
Ba	0.209 ± 0.002	0.189 ± 0.01	0.148 ± 0.018
SO_4^{2-}	11888.1 ± 20.6	14949.7 ± 28.3	6155 ± 54.3
Cl^-	729.3 ± 15.3	265.9 ± 10.6	720 ± 11.5
NO_3^-	163.2 ± 21.6	41.6 ± 5.7	BDL

Elements concentration in mg/L except pH, EC and acidity (mg/L as $CaCO_3$), BDL-below detection limits (0.1mg/L for anions), concentration reported as mean ±SD (n=3).

UNIVERSITY of the
WESTERN CAPE

3.2.3 Neutralization Reactions using different FA and AMD samples

The pH and EC trends of the neutralization reactions at a FA to AMD ratio of 1:3 are shown in Figure 4.1. FA from Arnot and Matla both have the capacity to neutralize AMD at FA: AMD ratios of 1:3. A strong buffering region was observed at pH 6 in the neutralization of both Bank and Navigation AMD. It is associated with oxidation and hydrolysis of Fe^{2+} which releases H^+ ions and delays the rise in pH. The buffering capacity is the result of high concentrations of Fe^{2+} in the AMD (≈ 3000 – 4000 mg/L). As Navigation AMD contains more Fe^{2+} than Bank AMD (Table 3.2), the time needed for Arnot FA to overstep the acidic buffering capacity is longer in the reaction with Navigation AMD than with Bank AMD. Eventually, both solutions were taken to a pH of ≈ 9, but it took more than 200 minutes for Navigation and only 150 minutes for Bank AMD. Matla FA appeared to have less free alkalinity than Arnot FA, judging by the pH curves during the reactions between both FA

sources and Bank AMD. To reach a given circum neutral or alkaline pH value, the time required with Matla FA was longer than with Arnot FA. The alkalinity is mainly provided by CaO in FA and the delay observed with Matla FA is due to a smaller CaO content than in Arnot FA (Table 3.1).

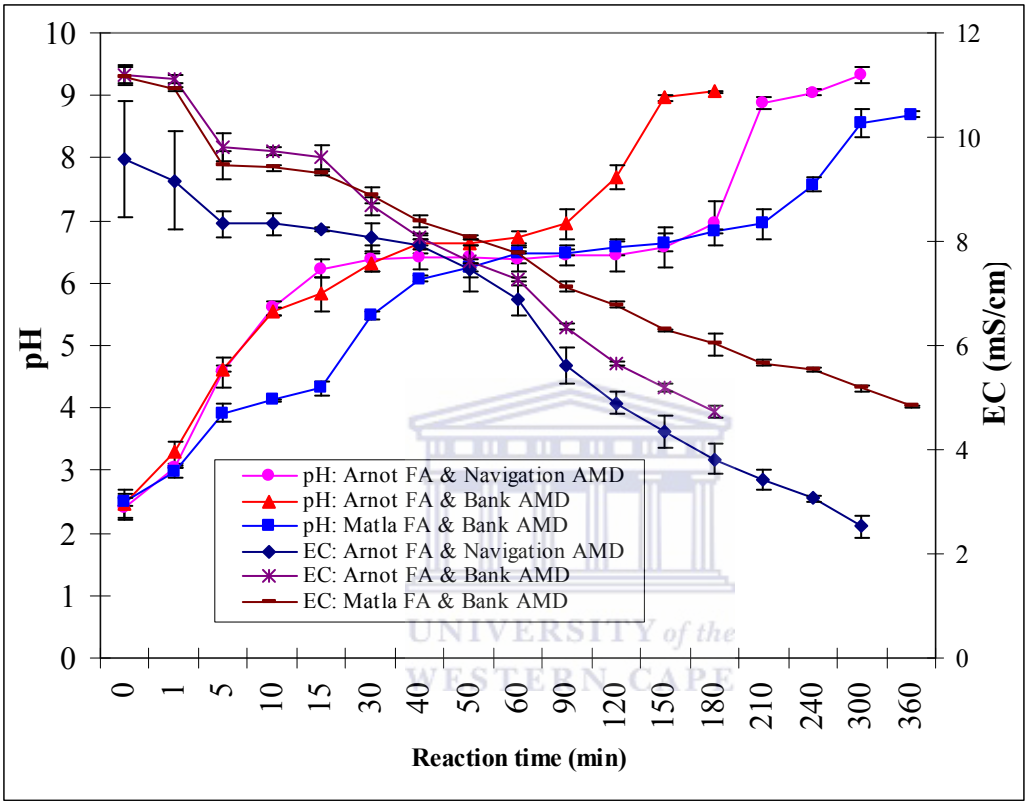

Figure 3.1. PH and EC for the reactions at a FA: AMD ratio of 1:3 between Matla, Arnot FA and Bank AMD; and Arnot FA and Navigation AMD. Values reported as mean ± SD (n=4), Error bars reflect 1 SD above and below the mean.

The EC of Navigation and Bank AMD followed the same trend during the treatment with Arnot FA. While pH neutralization was faster in Bank AMD, EC was kept at higher levels in Bank than in Navigation AMD. This may be a consequence of the sulphate, which were initially high in Bank AMD (Table 3.2). As mentioned previously, this element is the most important contributor to conductivity in mine waters. During the first 60 minutes of the neutralization reaction, the EC of Bank AMD followed the same trend, whether Arnot or Matla FA was used. Then, as the buffering capacity of Bank acidic water was first

UNIVERSITY of the WESTERN CAPE

overstepped by Arnot FA, EC started to decrease in the corresponding solution earlier than in the Bank AMD: Matla FA reaction.

These results indicate that the neutralization capacity of FA is combination specific and depends on the initial characteristics of the solution to be treated.

3.2.4 Neutralizations reactions using different FA: AMD ratios

The treatment of Brugspruit AMD with low ratios of Matla FA led to neutral pH values in the residual solution, after less than one hour of reaction time (Figure 3.2). This indicates that even low amounts of FA could be used to achieve neutralization in some cases. The reactions with ratios of FA: AMD between 1:3.5 and 1:8 allowed highly alkaline values of pH (pH >12) to be obtained. Only a few minutes were necessary for FA to neutralize Brugspruit AMD. The more FA was used, the lower EC was obtained (Figure 3.2). EC only reached a minimum of 8.5 – 9 mS/cm though. After 120 minutes the increase in EC observed in the reaction having the highest ratios of FA could be result of the presence of OH^- ions. This pH increase stopped after 90-120 minutes in the case of the 1:3.5 and 1:5 ratios, when the pH was stabilized to ≈ 12.5 in the solution. For the 1:8 ratios, pH only reached and stabilized at 12 after 150 minutes. The EC stabilized at around 9 mS/cm simultaneously.

UNIVERSITY of the
WESTERN CAPE

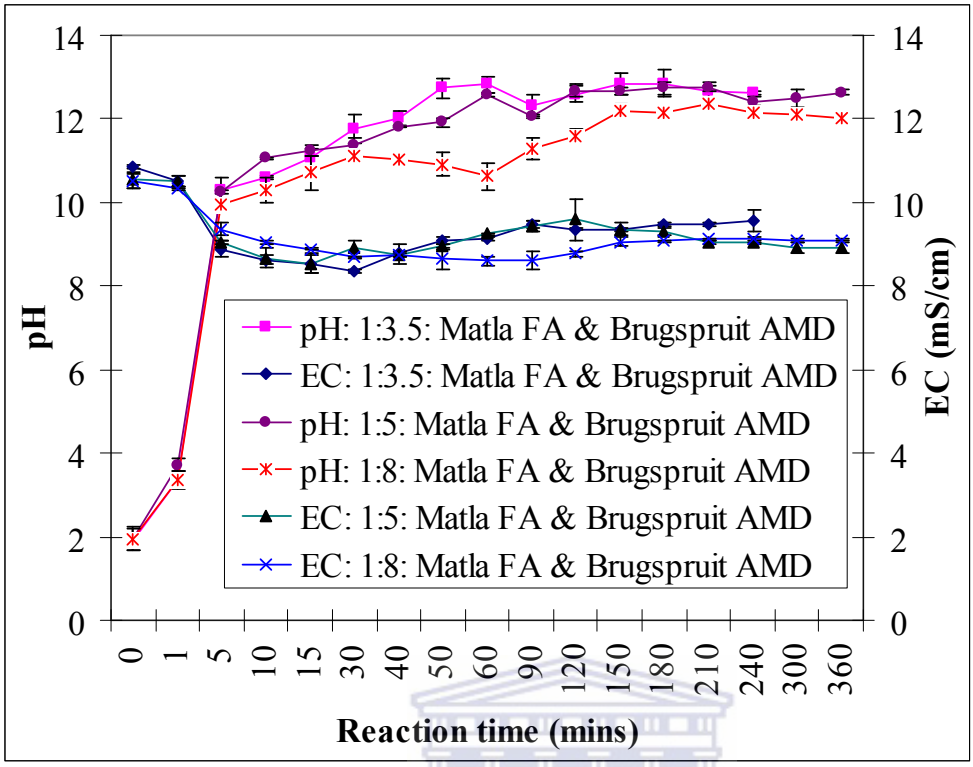

Figure 3.2. pH and EC during neutralization reactions for different Matla FA: Brugspruit AMD ratios. Values reported as mean ± SD (n=4), Error bars reflect 1 sample SD above and below the mean.

UNIVERSITY of the
WESTERN CAPE

The treatment of Navigation AMD and Bank AMD at different ratios of FA: AMD revealed different pH and EC trends (Figs 3.3 and 3.4) from those of Brugspruit AMD. Despite the high ratios employed here the breakthrough to pH >10 was only observed after 210 minutes (Figs 3.3 and 3.4). The stepwise increase in pH with time is also lacking for the Brugspruit AMD. Stepwise and gradual decrease in EC is noted for the Navigation and Bank AMD (Figs 3.3 and 3.4). The initial decrease in EC for the Brugspruit treatment is not sustained. Uhlmann *et al.* (2004) observed that the buffering observed at pH 3.5-4 is due to hydrolysis of Fe^{3+} while oxidation and hydrolysis of Fe^{2+} contributes greatly to buffering at pH 5.5-6.5 (Jenke *et al*., 1983). Comparing the duration of the buffering at pH 5.5-6.5, it's longer for Navigation AMD reactions which corresponds to its higher Fe^{2+} concentration (Figure 4.3 and 4.4 and Table 4.2). Al^{3+} could also contribute to buffering at pH 4.3-5.5 (Uhlmann *et al,*. 2004). The Brugspruit AMD had very low concentration of Fe^{3+}/Fe^{2+} and Al^{3+} as compared to Navigation and Bank AMDs (Table 3.2). This could account for the lack of stepwise decrease in pH and buffering during the treatment process.

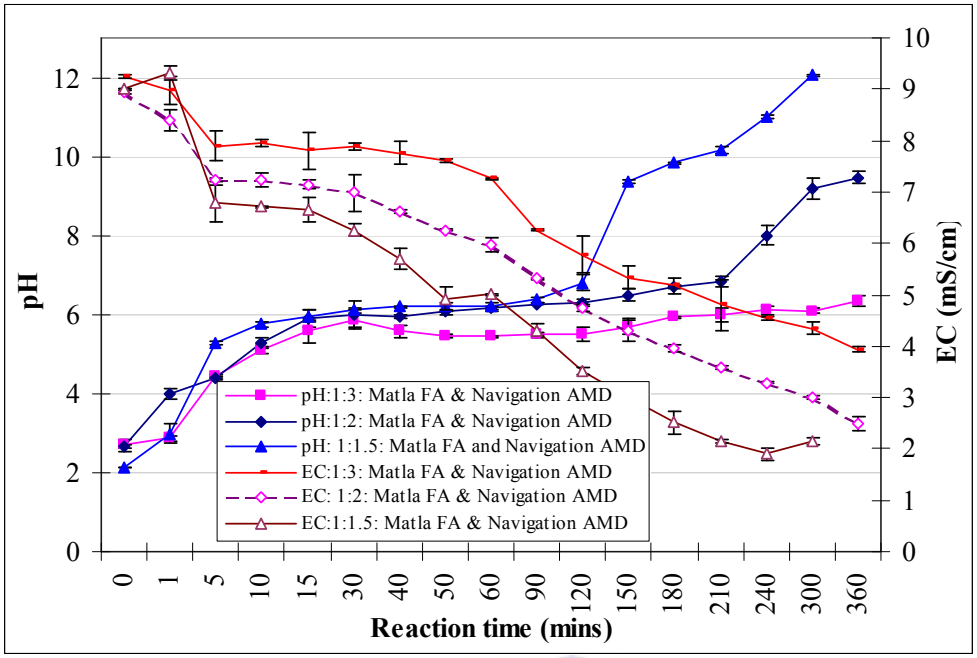

Figure 3.3:. pH and EC for various FA:AMD ratios for reaction between Matla FA and Navigation AMD. Values reported as mean ± SD (n=4), Error bars reflect 1 SD above and below the mean.

UNIVERSITY of the
WESTERN CAPE

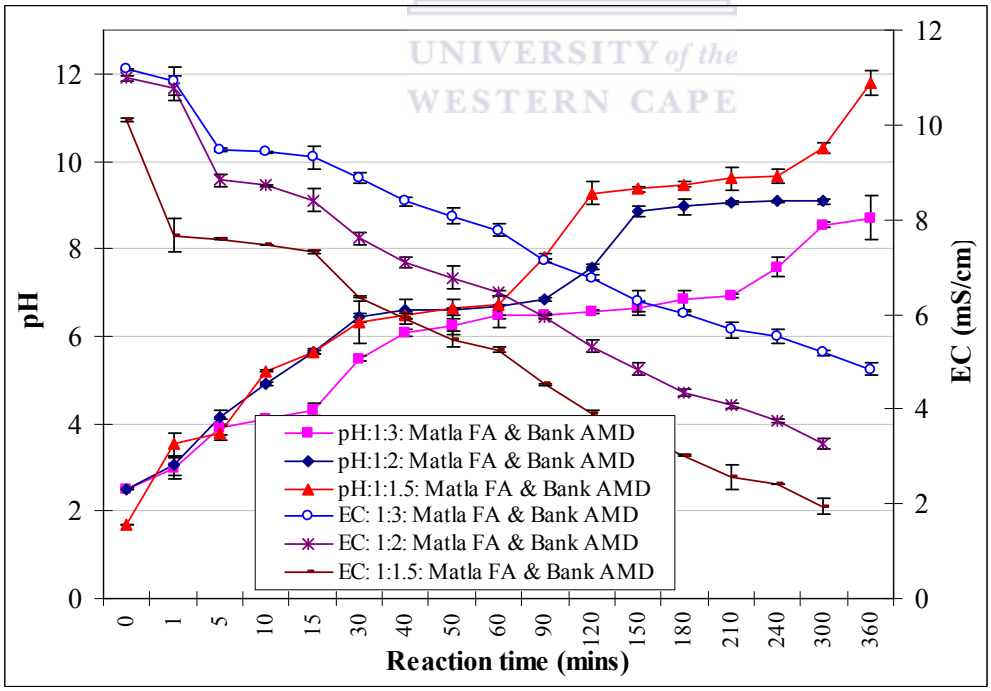

Figure 3 4:. pH and EC for various FA:AMD ratios for reaction between Matla FA and Bank AMD. Values reported as mean ± SD (n=4), Error bars reflect 1 SD above and below the mean.

The hydrolysis of AMD constituents such as Fe^{3+}, Al^{3+}, Fe^{2+} releases protons and offsets the pH increase attributed to the dissolution of the oxide components (equation 3.2).

$$Fe^{3+} + 3H_2O \Rightarrow Fe(OH)_3(s) + 3H^+$$
$$Al^{3+} + 3H_2O \Rightarrow Al(OH)_3(s) + 3H^+ \quad \text{.....(3.2)}$$

The relative quantities of soluble bases (oxides) in FA and hydrolysable constituents in AMD dictate whether the final solution at a given contact time will have a dominant acidic or basic character. The three factors that dictate the nature of the final solution in these neutralization reactions are the FA: AMD ratio, the contact time of the reaction and the chemistry of the AMD. Depending on the concentration of the major hydrolysable constituents in the AMD, FA: AMD ratios of 1:1.5, 1:2 and 1:3 would give final solution mixture of circum-neutral to alkaline pH after 360 minutes of contact. Navigation and Bank AMD had total Fe concentration > 5000 mg/L and this is probably reflected in the strong buffering exhibited at 4.5-7. Al which is also a major hydrolyzable constituent was observed to be > 1000 mg/L for both Navigation and Bank AMD and could have similarly contributed to the strong buffering observed in this pH range. Al^{3+} hydrolysis at pH 4 (equivalent to first hydrolysis constant of Al^{3+}, $pK_1 = 4$) (Fillipek *et al*., 1987). This study did not go into the details of the specific contribution of each of the constituents in the buffering of the reaction mixture at this pH range.

UNIVERSITY of the
WESTERN CAPE

3.2.5 Major and Trace elements removal in the acid mine waters

Acid mine waters are highly reactive solutions that can dissolve most primary minerals when reacted with an alkaline solid waste material such as fly ash with a consequent formation of a variety of secondary minerals. Dissolution of fly ash as it contacts AMD triggers several processes among them the increase in pH. Several authors observe that pH is the most important parameter in fly ash solutions and determines the predominant toxic elements removal mechanism (Cravotta and Trahan, 1999; M. Erol *et al*., 2005). Table 3.3 below shows the toxic elements removal efficiency as a function of solution pH for Brugspruit and Navigation AMD reacted with Matla fly ash at various FA: AMD ratios. The results are discussed with respect to pH of precipitation of the various metal species as determined from thermodynamic calculations and experimental observations from titration of solutions containing the stated species (Britton, 1956).

3.2.5.1 Matla fly ash and Brugspruit AMD reactions

Major elements Fe, Mn, Al and Mg are significantly reduced in all the ratios investigated (Table 3.3). Fe and Al shows close to 100 % removal at pH 9.16 attained by the FA: AMD ratio of 1:30. Mn removal increases from an initial of 80 % at 1:30 ratio approaching 100 % at 1:20 ratio as the pH increases to 9.73. Jenke *et al.* (1983) observed that at the pH of minimum solubility of the hydroxides of Fe^{3+} (pH 3.0), of Fe^{2+} (pH 6.0-8.0), of Mn (pH 8.41-9.0) and of Zn^{2+}(pH 6.0-6.5) a significant proportion of the initial concentration should be precipitated out of solution. At pH 12.0-12.5 attained for ratios 1:8 and 1:5 the formation of hydroxy complexes probably explains the decreased removal. Al^{3+} hydroxide exhibits minimum solubility at pH 6-6.5 (Drever, 1997). at pH > 6.5 the hydroxy complexes become more important (Shum and Lavkulich, 1999). The high removal efficiency observed as pH increases suggests another mechanism of Al^{3+} removal apart from hydroxide precipitation could be involved.

UNIVERSITY of the
WESTERN CAPE

Table 3.3. Major and trace element removal as a function of pH for Matla fly ash, Brugspruit and Navigation AMD reactions.

	Ratios		Mn	Fe	Al	Mg	Zn	Ni	Cu	Pb	SO_4^{2-}
Matla FA and Brugspruit AMD		Final	Final	Final	Final	Final	Final	Final	Final	Final	Final
	FA:AMD	pH	conc	conc	conc	conc	conc	conc	conc	conc	conc
	AMD	2.55 ±0.12	31.6 ±1.48	250.8 ±11.2	60.05 ±2.89	388.7 ±19.7	9.53 ±0.49	2.36 ±0.13	0.116 ±0.012	0.178 ±0.021	6155 ± 54.3
	1:30	9.16 ±0.04	0.028 ±0.002	2.62 ±0.42	0.15 ±0.003	0.24 ±0.021	1.13 ±0.05	0.031±0.002	0.031±0.001	0.015 ±0.002	6137 ±7.0
	1:20	9.73 ±0.13	0.066 ±0.013	3.5 ±0.42	0.99 ±0.06	1.46 ±0.21	9.19 ±1.19	0.051±0.002	0.04 ±0.002	0.017 ±0.002	5668 ±47.5
	1:8	12.04 ±0.05	0.026 ±0.002	0.85 ±0.04	2.44 ±0.25	0.83 ±0.021	16.4 ±3.45	0.194 ±0.022	0.049 ±0.003	0.018 ±0.003	4601.8 ±3.37
	1:5	12.64 ±0.14	0.339 ±0.004	4.23 ±0.15	0.15 ±0.01	297 ±21.4	1.21 ±0.05	0.332 ±0.002	0.044 ±0.002	0.011 ±0.005	NA
	1:3.5	12.62 ±0.12	6.24 ±0.65	3.52 ±0.15	0.32 ±0.02	236.9±25.3	5.06 ±0.04	0.602 ±0.021	0.045 ±0.002	0.013 ±0.001	3709.8 ±59.0
Matla FA and Navigation AMD	Ratios		Mn	Fe	Al	Mg	Zn	Ni	Cu	Pb	SO_4^{2-}
		Final	Final	Final	Final	Final	Final	Final	Final	Final	Final
	FA:AMD	pH	conc	conc	conc	conc	conc	conc	conc	conc	conc
	AMD	2.69 ±021	226.3 ±4.7	5599.9 ±80.9	1068.1±11.3	2661.7±35.0	49.0 ±30.62	6.95 ±0.018	0.355 ±0.007	0.314 ±0.107	11888.1 ± 20.6
	1:3	6.33 ±0.15	56.65 ±5.68	293.3 ±19.6	2.85 ±0.05	636.9 ±80.4	1.30 ±0.012	0.58 ±0.04	0.045 ±0.003	0.019 ±0.002	5483.3 ±14.9
	1:2.5	8.72 ±0.62	5.15 ±0.45	52.3 ±6.8	3.26 ±0.35	618.1 ±70.8	1.20 ±0.05	0.134 ±0.002	0.055 ±0.011	0.041±0.004	2414.3 ±28.1
	1:2	9.47 ±0.43	1.11 ±0.005	43.2 ±4.6	2.35 ±0.56	200.0 ±34.5	1.26 ±0.02	0.088 ±0.004	0.073 ±0.005	0.03 ±0.005	2508.1 ±247.6
	1:1.5	12.05 ±0.18	0.13 ±0.005	4.7 ±0.67	9.41 ±1.97	1.5 ±0.02	0.737 ±0.012	0.051 ±0.001	0.034 ±0.006	0.015 ±0.002	4570.7 ±110.3

Concentration in mg/L reported as mean ±SD (n=3), AMD- stands for the initial concentration before treatment, NA-not analyzed.

UNIVERSITY of the WESTERN CAPE

Among the trace ions Ni, Cu, Pb show removal from solution in % ranging from 70 - 95 % as follows: 70-95 % for Ni, 55 –75 % for Cu and 85-90 % for Pb as the pH increases (Table 3.3). The % removal for Ni increased with increase in pH reaching a maximum of 95 % at pH 12.62. The Cu and Pb removal efficiency was observed to decrease at FA: AMD ratio of 1:8 which attained a pH of 12.04. The decrease in removal of these elements could be related to the formation of soluble hydroxo species at pH > 12.0. The tendency of metal species in solution to form hydro-complexes as pH increases can be depicted in the following equations (eq 3.3- 3.7):

$$M(OH)_2(s) \Leftrightarrow M^{2+} + 2OH^- \quad \text{.....(3.3)}$$

$$M^{2+} + OH^- \Leftrightarrow M(OH)^+ \quad \text{.....(3.4)}$$

$$M^{2+} + 2OH^- \Leftrightarrow M(OH)_2 \quad \text{.....(3.5)}$$

$$M^{2+} + 3OH^- \Leftrightarrow M(OH)_3^- \quad \text{.....(3.6)}$$

$$M^{2+} + 4OH^- \Leftrightarrow M(OH)_4^{2-} \quad \text{.....(3.7)}$$

As long as the solubility product of the metal hydroxide is constant, the metal solubility decreases as the pH increases and increases with complex formation. As a result of this the metal species concentration in solution decreases until a certain pH value is reached and increases thereafter as the complex formation becomes important. Erol *et al*. (2005) observed that if the final pH of a mixture (fly ash- copper aqueous solution) exceeded 6 a sharp decrease in the Cu^{2+} was observed and at pH 8-9 the Cu^{2+} approached 100 %. Another reason for the increase could be reduced adsorption due to reduced formation of amorphous $Fe(OH)_3$, MnOOH and $Al(OH)_3$ due to the low concentration of Fe^{3+}, Mn and Al^{3+} in brugspruit AMD

Cr has maximum removal (80 %) at pH 9.16 attained for the ratio 1:30 followed by a decrease ranging from 30-50 % at pH> 9.16 (Table 3.4). Recent laboratory studies indicate that Cr is normally present in fly ash as Cr^{3+} and at pH 9.16 observed for FA: AMD ratio of 1:30 Cr will precipitate as $Cr(OH)_3$ but as pH increases the $Cr(OH)_4^-$ species become important.The presence of $Cr(OH)_4^-$ explains the decreased removal at 1:20 FA : AMD ratio.

Mg^{2+} removal efficiency approaches 100 % at pH 9.16 decreasing as the pH increased at high FA: AMD ratios. At pH 12.62 attained with FA: AMD ratio of 1:3.5, Mg^{2+} removal

decreased to less than 40 % probably due to formation of soluble hydroxo species at the high pH.

Table 3.4: % removal of Cr with increasing FA: AMD ratio and pH in process water**.**

	Matla fly ash and Brugspruit AMD					
Ratios (FA: AMD)	AMD	1:30	1:20	1:08	1:05	1:3.5
Final pH	2.55	9.16	9.73	12.04	12.64	12.62
Final conc(mg/L)	0.775	0.176	0.525	0.375	0.526	0.502
% removal	0.0	77.2	32.2	51.6	32.1	35.2
	Matla fly ash and Navigation AMD					
Ratios(FA: AMD)	AMD	1:3	1:2.5	1:2	1:1.5	
Final pH	2.69	6.33	8.72	9.47	12.05	
Final conc (mg/L)	1.114	0.069	0.163	0.141	0.083	
% removal	0.0	93.8	85.4	87.3	92.5	

3.2.5.2 Matla fly ash and Navigation AMD reaction

The pH increase as the FA: AMD ratio decreases is gradual for Navigation AMD reactions than for Brugspruit AMD (Figs 3.2 and 3.3). Consequently several metal removal trends are evident as the pH increases with increase of the FA: AMD ratio.

At the initial pH 6.33 achieved for the FA: AMD ratio of 1:3 a sharp decrease in concentration is achieved for Fe, Ni, and Zn. With subsequent FA: AMD ratios the removal efficiency of a 100 % is attained.

According to Britton, (1956) the pH of minimum solubility of the hydroxides of Fe^{3+}, Fe^{2+}, Zn^{2+} and Ni^{2+} are 3.0, 6.0-8.0, 6.0-6.5 and 6.66 respectively. Observation of the pH attained for FA: AMD ratio of 1:3 covers the optimum precipitation pH range of Fe^{3+} and Zn^{2+} and this explains the 100 % removal attained for Zn at this ratio (Table 3.3). The final pH of 6.3 attained by this ratio means that a portion of the Fe^{2+} would still be in solution and this accounts for the 94 % removal of total Fe achieved. At FA: AMD ratio of 1:2.5 the removal of total Fe is achieved as the optimum precipitation pH of Fe^{2+} is achieved. Ni^{2+} removal is also observed to approach 100 % removal at this ratio.

A sharp decrease in concentration for Cu and Pb was observed at FA: AMD ratio of 1:3. The pH attained for FA: AMD ratio of 3:1 covers the optimum hydroxide precipitation pH range

for both elements (Cu^{2+} pH 5.3, Pb^{2+} pH 6.0) as reported by Britton (1956).This explains the high % (87-94) removal attained. Erol *et al,* (2005) reported a sharp decrease in Cu^{2+} concentration when the solution pH of 6 was achieved and pH 6-7 for Pb^{2+} in aqueous solutions/fly ash mixtures. These two elements also show an increase in concentration at FA: AMD ratio 1:2 for Cu and 1:2.5 for Pb when pH is in the range 8.7-9.5 (Table 3.3). This has been extensively explained in the sub-section 3.*2.5.1* that formation of hydroxo complexes for both elements at this pH range could account for decreased removal.

Mg decreases in concentration gradually as the pH increases with a increase in FA: AMD ratios. At FA: AMD ratio of 1:3 a pH of 6.3 is attained and Mg removal is 75 %, the removal approaches 100 % at FA: AMD ratio of 1:1.5 when a pH of 12.05 was attained in the solution. This corresponds to the optimum precipitation pH of $Mg(OH)_2$ reported in literature (10.49-11.0) (Britton, 1956).

Cr removal is highest at (93 %) for 1:3 and 1:1.5 FA: AMD ratios when a pH of 6.33 and 12.05 was attained respectively (Table 3.4). Removal at pH 6.33 is attributed to precipitation of $Cr(OH)_3$, this corresponds to the pH region of minimum solubility of Cr^{3+} (Britton, 1956). Minimum removal efficiency occurs at intermediate FA: AMD ratios of 1:2.5 and 1:2 corresponding to pH of 8.72 and 9.47 respectively.

UNIVERSITY of the
WESTERN CAPE

3.2.6 Water quality comparisons

Compared to the department of water affairs and forestry (DWAF, 1996) water quality limits, treatments of Navigation AMD with Matla fly ash resulted in much cleaner water with Cu, K, Mo, Na, Zn being within the domestic water use limits for 1:3 FA: AMD ratio and Co, Cu, K, Na and Zn being within the domestic water limits for 1: 2.5 FA: AMD ratio. Treatment of Brugspruit AMD with Matla fly ash produced less cleaner water although breakthrough to alkaline pH was established within less than an hour. Only Cu, K were within the domestic limits for 1:30 FA: AMD ratio. This comparison includes only the FA: AMD ratios that resulted in process water in the pH range 6-9(Table B1-B3).

3.2.7 Sulphate removal in the acid mine waters

The % removal of sulphate as the pH increases for different FA:AMD ratios is shown in Table 3.3.

Both reactions exhibit an increased sulpate removal with increasing FA: AMD ratios. For Navigation reactions maximum removal is achieved at 1:2.5 thereafter lower removal rates are observed. The direct relationship of % sulphate removal and FA content in the reaction mixture suggests that dissolution of CaO and subsequent formation of gypsum accounts for the sulphate removal in both reactions. Increase in pH as the FA: AMD ratios increased was attributed to dissolution of CaO from fly ash.

Although the lower FA: AMD ratios for Brugspruit AMD reactions achieve alkaline pH within a short contact time, they are not accompanied by high sulphate removal. On the contrary, high FA: AMD ratios used for Navigation AMD reactions result in circum neutral and alkaline pH after a longer contact time (Fig 3.3) and are accompanied by high sulphate removal. These reactions exhibit a large buffering at pH 5.5-6.5, oxidation and hydrolysis of Fe^{2+}, formation of Al, Fe oxyhydroxysulphates, and Fe hydroxides with subsequent adsorption of sulphate accounts for the high removal rates. Uhlmann *et al*, (2004) observed strong buffering by Fe^{3+} with bound sulphate at pH 2.9 - 4.3 and buffering by Al with bound sulphate at pH 4.3 – 5.5 on titrating acidic mine water with NaOH. Moreover iron oxyhydroxides are known to sorb large quantities of sulphate (Seth and Ghazi, 1997). The chemistry of sulphate and its removal mechanisms is covered more fully in *Chapter Four*.

3.2.8 Leaching of elements from fly ash

Interaction of fly ash and acid mine drainage leads to dissolution of soluble salts on the surfaces of the fly ash and mineral precipitation may occur depending on the concentration achieved in solution. A stable solution composition is thereby achieved especially for elements whose hydroxides are highly soluble or exist as anions. Figure 3.5 below shows the concentration trends of Ba, B, Mo and Sr as function of FA: AMD ratios for Matla fly ash and Brugspruit AMD reactions while figure 3.6 shows the release of B, Sr and Mo as function of FA: AMD ratios for Matla fly ash and Navigation AMD reactions while figure3.7 shows the variation of As and Se as a function of FA: AMD ratios for Matla fly ash, Brugspruit and Navigation AMD reactions.

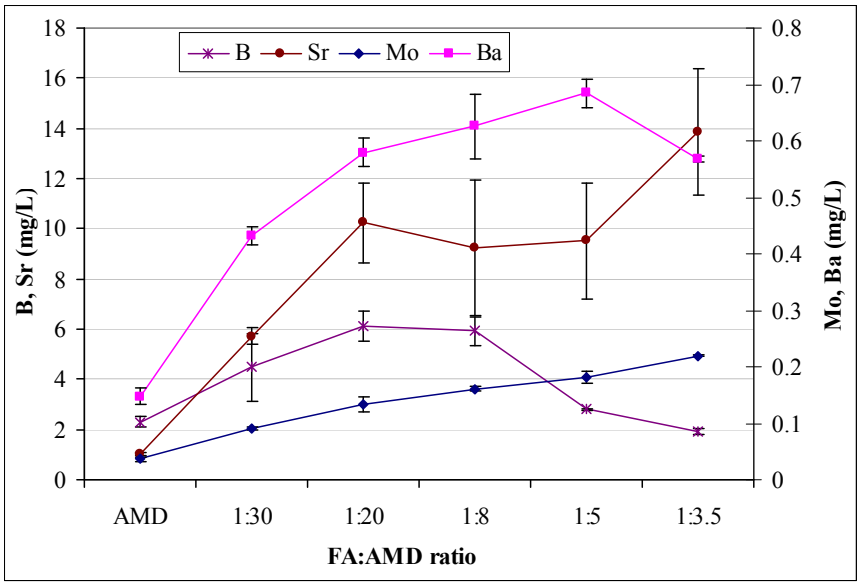

Figure 3.5:. Variation of Ba, B, Mo and Sr concentrations as a function of FA:AMD ratios for Matla fly ash and Brugspruit AMD reactions. Values reported as mean ± SD (n=3), Error bars reflect 1 SD above and below the mean.

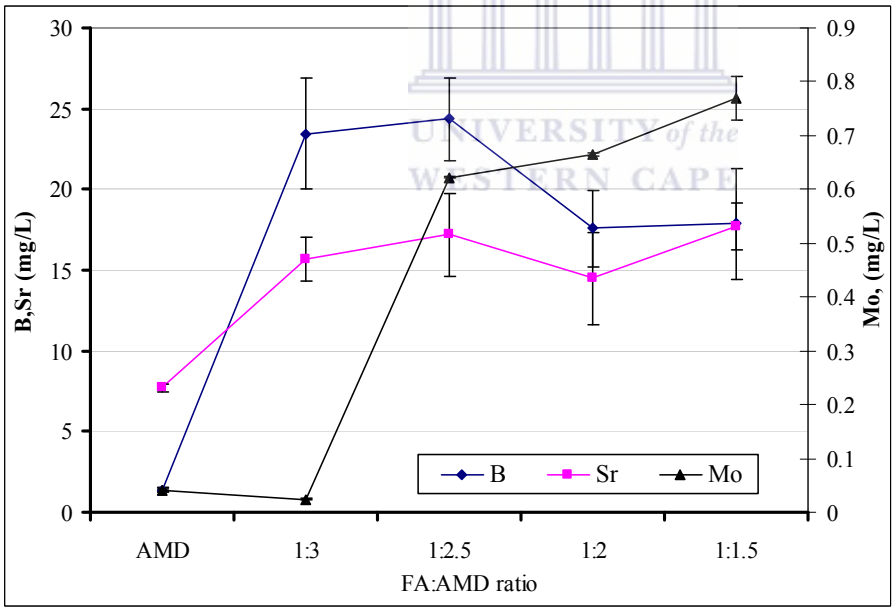

Figure 3.6:. Variation of B, Mo and Sr concentrations as a function of FA:AMD ratios for Matla fly ash and Navigation AMD reactions. Values reported as mean ± SD (n=3), Error bars reflect 1 SD above and below the mean.

In both AMDs treatments similar trends are observed registering a peak in concentration at intermediate FA: AMD ratios. Ba, Mo and Sr are observed to increase steadily with

UNIVERSITY of the WESTERN CAPE

increasing fly ash in the reaction mixture (Fig 3.5 and 3.6). This suggests that dissolution of soluble salts of these elements from fly ash accounts for the increasing concentrations. High concentrations of Ba and Sr were observed in the Matla fly ash (Table 3.1) and its increase in solution with increasing fly ash in the mixture is expected. Trends for Mo also suggest dissolution of its soluble salt from fly ash particles. Eary *et al*. (1990) observes that the rates at which minor elements are leached from unweathered fossil fuel wastes are dependent on the abundances and dissolution kinetics. B increases steadily to a maximum at 1:20 FA: AMD ratio followed by a decrease with increasing fly ash. As the reaction mixture attained pH 9.47-9.73 for both ratios (Fig 3.5 and Table 3.3) B concentrations were observed to decrease. Hollis *et al*, (1988) observed that B concentrations are likely to be lowest in alkaline leachates that are actively precipitating $CaCO_{3\,(s)}$. These reactions were carried out in open beakers and ingress of CO_2 occurred and formation of $CaCO_{3(s)}$ was expected (more evidence for possible incorporation of B in carbonate fractions is presented from selective dissolution experiments in *Chapter Four*).

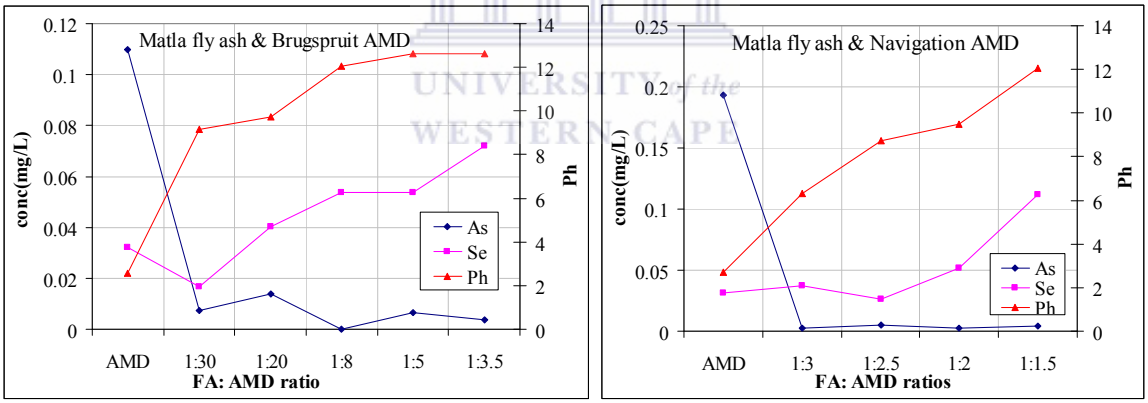

Figure 3.7: Variation of As and Se concentrations as a function of FA:AMD ratios for Matla fly ash and Brugspruit; Navigation AMD reactions.

The As trends depict a near 100 % removal as the Ph increases in the process waters for both Brugspruit and Navigation AMD (Fig 3.7). Eary *et al.* (1990) points out that As (iii) and As (v) have been reported in fly ash and that in presence of ferric ions As(iii) is oxidized to As (v). These anions may combine with metal cations to form metal arsenites or metal arsenates depending on the oxidation state. It is predicted that the increased removal is due to increased formation of metal arsenites or arsenates as dissolution of the fly ash takes place. Juillot *et al.,* 1999 observed formation of 1:1 Ca arsenates (weilite $CaHAsO_4$, haidingerite

$CaHAsO_4.H_2O$ and pharmacolite $CaHAsO_4.2H_2O$) when acidic waters with arsenate species (0.961-3.149. 10-3 mol/l) interacted with Ca^{2+} rich limestone substratum. These Ca arsenates are known to form at ph (3-6). This could probably explain the low levels of As observed as the FA: AMD ratio increased (Fig 3.7). The fly ash acted as a rich source of Ca^{2+}.

Se shows a different trend from that of As, decreasing to a minimum at 1:30 FA: AMD ratio for Brugspruit AMD and 1: 2.5 FA: AMD for Navigation AMD respectively. Thereafter an increase corresponding to the increasing amount of fly ash in the mixture is observed. This implies that FA is the source of Se. Eary *et al*. (1990) observed that Se can exist as Se(iv) or Se (vi) depending on the oxidation conditions and will be removed as metal selenites or selenates. However if the removal mechanism was via metal selenites or selenates then the trends should be similar to As. As the amount of fly ash increase in the mixture the removal mechanism for Se seems to be exhausted.

3.3 Conclusions

The hydrolysis of AMD constituents such as Fe^{3+}, Al^{3+}, Fe^{2+} offsets the pH increase attributed to the dissolution of the oxide components of the fly ash. The three factors that finally dictate the nature of the final solution in these neutralization reactions are the FA: AMD ratio, the contact time of the reaction and the chemistry of the AMD. Depending on the concentration of the major contaminants in AMD FA: AMD ratios of 1:3,1:2.5 and 1:2 resulted in neutral to circum-neutral waters after ≈ 360 minutes of reaction as a result of strong buffering at pH 4.5-6. FA: AMD ratios of 1:1.5 resulted in alkaline waters after the same time of contact (360 minutes). The fact that the concentration of the major contaminants contributed to the time of breakthrough to alkaline pH was evident with Brugspruit AMD reactions. Breakthrough occurred within 15 minutes of contact despite the low FA: AMD ratios used.

Removal of major and trace elements was observed to be high (>75 %) for both Brugspruit and Navigation AMD reactions. Efficiency of the elements removal was directly linked to amount of FA in the reaction mixture and to the final pH attained. Most elements attained ≈ 100 % removal only when the pH of minimum solubility of their hydroxides was achieved (i.e Mg=10.49-11.0, Cu^{2+}=6, Pb^{2+}=6-7). Elements such as Cu^{2+}, Pb^{2+}, Cr^{3+} and Mg were

observed to increase in solution at high pH; this was attributed to the formation of soluble hydroxo species.

A direct relationship of % sulphate removal and FA content in the reaction mixture was observed suggesting that dissolution of CaO and subsequent formation of gypsum accounts for some of the sulphate removal in both reactions.

The chemistry of the AMD was found to play a role in the removal of sulphate. Although Navigation AMD reactions resulted in circum neutral and alkaline pH after a longer contact time, this was accompanied by high sulphate removal. Formation of Fe oxyhydroxysulphates, Fe oxyhydroxides with subsequent adsorption of sulphate could have contributed to the high removal rates.

Elements whose hydroxides are highly soluble or exist as anions in solution were highly leached and would be the limitation in using fly ash for treating acid mine drainage. B and Sr were found to increase by a factor of more than 10 as the fly ash increased in the reaction mixture.

UNIVERSITY of the
WESTERN CAPE

Chapter Four

Utilization of fly ash for remediation of coal mine waste waters: Solubility controls on major inorganic contaminants and their partitioning in the resulting solid residues (SR).

Abstract

Acid mine drainage (AMD) has been reacted with coal fly ash in a 24 hour equilibration time using 1:3 and 1:1.5 FA: AMD ratios by weight to produce neutral and alkaline process waters. The capacities of the fly ash to remove the major inorganic contaminants with reaction time were examined. The elemental concentration trends with time for the two ratios were used to discern which elements have solubility control in the neutralization process. The geochemical computer code PHREEQC and WATEQ4 database was used for geochemical modeling of the process water. The resulting solid residues were analyzed by X-ray Diffraction, scanning electron microscopy (SEM) and scanning electron microscopy-energy dispersive X-ray spectroscopy (SEM-EDX) in an attempt to detect the minerals phases controlling the inorganic contaminants concentration in solution. The relative quantities of soluble bases (oxides) in fly ash and hydrolysable constituents in AMD dictated whether the final solution at a given contact time will have a dominant acidic or basic character. Fe, Al, B were observed to have solubility control for the entire contact time while Ca, Na, Mg, Si and Mn developed solubility control after the initial rapid dissolution. Increase of pH in solution with contact time caused the removal of the metal ions mainly by precipitation, co-precipitation and adsorption. Fe was mainly removed as $Fe(OH)_{3(a)}$, goethite, Al as basaluminite, boehmite and alunite at pH 5.28-6.95, $Al(OH)_{3(a)}$ at pH 6.45-6.95, and as gibbsite and diaspore at pH 5.53-9.12. Cu and Zn by adsorption onto the precipitating iron (oxy)-hydroxides and aluminum (oxy)-hydroxides. Si by dissolution of $SiO_{2(a)}$ at pH<5 and equilibrium with mullite at pH >8. Na was removed as Na-jarosite at pH 3.96-6.95 and Ca as gypsum. Sulphate was initially removed as gypsum, but at pH 5.49-6.95 SO_4^{2-} bearing Al hydroxy sulphate minerals, barite and K, Na-jarosites seemed to play a significant role in sulphate reduction.

Sequential extraction revealed that all the elements exhibited a significant retention in the carbonate and amorphous fractions which implies their non-lability unless in contact with aggressive acidic leachates. Amorphous fraction was observed to be the most important in

UNIVERSITY of the WESTERN CAPE

retention of the major and minor contaminants at pH > 6.32 which implies that the concentration of total Fe and Al in the AMD being treated will have a direct effect on the clean-up efficiency of the process.

Academic Output

Gitari M.W**,** L. F Petrik**,** O. Etchebers**,** D. L Key, E.Iwuoha and C. Okujeni. Utilization of Fly Ash for Remediation of Coal Mines Wastewater: Solubility Controls on Major Inorganic Contaminants. A **paper** submitted to *Journal of Environmental Quality.* 2006

M.W. Gitari, L.F. Petrik, O. Etchebers, D. Key, E.I. Iwuoha and C. Okujeni. 2005. Mineralogy and trace element partitioning in coal fly ash/acid mine drainage co-disposed solid residues. A **paper** presented at, *The World of Coal Ash 2005*, incorporating International Ash Utilization Symposium of the UK CAER, the ACAA's 16th International Symposium and meeting of the U.S. Office of Surface Mining, Lexington, Kentucky, USA, 11-15 April 2005.

UNIVERSITY of the
WESTERN CAPE

4 Introduction

Several authors point out that the dominant chemical characteristics of a fly ash leachate (pH, EC) are usually established within minutes of addition of water (Reardon *et al.,* 1995; Campbell, 1999; Kopsick and Angino, 1981). This results from the flush of ions to the solution from readily soluble minerals present in the ash. Secondary minerals may then precipitate out immediately depending on the ion concentration in solution after the initial rapid dissolution or after a prolonged dissolution. However the quantities of secondary mineral precipitates may be too low to be detected by X-ray diffraction or due to their amorphous nature. Reardon *et al.* (1995) argued that if an element concentration does not double when the water: solid (W: S) ratio is halved, then there must be a solid phase control on the element concentration in solution. Unlike equilibration with water, the AMD contains high concentration of SO_4^{2-}, Ca, Mg, Al, K, Mn, Si and Fe which are existence in FA and will leach out on interaction with the AMD. A decrease in concentration when the FA: AMD ratio is doubled will therefore signify existence of solubility control for that element or ion. A simple increase in concentration when FA: AMD ratio is doubled for the entire contact time

will signify lack of solubility control. The concentration trends with reaction time for these elements can therefore be used to discern whether any mineral solubility control exists in these neutralization reactions. This data in combination with direct physical methods, XRD and SEM-EDX can form a strong basis for the evaluation of the mineralogy of the resulting solid residues.

The theory and application of sequential extraction has been presented in section 2.4.9. In this study the sequential extraction procedure was intended to evaluate the mass transfer of major and trace elements from AMD and FA to the resulting precipitates admixed with residue matrix of the fly ash. It is intended to elucidate the transformation of labile toxic elements to less labile phases. The extraction sequence procedure seeks to partition the contaminants for both FA and solid residues into: double deionized water (soluble fraction), magnesium chloride (exchangeable fraction), sodium acetate-acetic acid (carbonate fraction), hydroxylamine –hydrochloride-nitric acid (Mn-oxides), ammonium oxalate in the dark (amorphous fraction) and ammonium oxalate-oxalic acid-ascorbic acid in the dark (crystalline iron oxides). The extraction scheme adopted is a combination of the methods developed by Chao (1972), Muller and Seiller (1999), and Tessier *et al*. (1979).

UNIVERSITY of the
WESTERN CAPE

Understanding the interaction between the toxic elements in both FA, AMD and mineral phases being formed or likely to control their concentration in the neutralization process will be important in designing a treatment process for AMD with fly ash as the liming agent. In addition understanding the partitioning of trace and major elements in the resulting solid residues is essential in deciding their environmental disposal or application.

The objectives of this part of the study therefore were: 1] to evaluate the evolving process water chemistry with time for the FA: AMD ratios 1:3 and 1:1.5. 2] determine the possible solubility controls for the major inorganic contaminants. 3] assess the partitioning of the major and trace elements in the resulting solid residues (SR).

4.1 Materials and Methods

4.1.1 Sample Description

The fly ash used was obtained directly from the Arnot power station in South Africa and kept in tightly locked PVC buckets to prevent ingress of CO_2 which leads to loss of alkalinity (Campbell, 1999). AMD samples here referred to as Navigation were obtained at Navigation colliery in Witbank, South Africa. Total elemental analysis of FA and SR was done on powder briquettes by XRF and reported in weight % oxide for major and ppm for minor elements. The results of the chemical characterization of the samples used are presented in Table 4.2 and 4.3.

4.1.2 Neutralization Reactions

The fly ash/AMD neutralization experiments were conducted by stirring a mixture of fly ash and AMD in which the fly ash and AMD were weighed to give a specific FA: AMD ratio. The AMD was stirred for 30 minutes for equilibration before the fly ash was added. An overhead stirrer was used for all the experiments. For the 1:3 FA: AMD ratio 133 grams of Arnot fly ash were added to 400 ml of Navigation AMD in a 800 ml beaker. For 1:1.5 FA: AMD ratio 100 grams of Arnot fly ash were added to 150 ml of Navigation AMD in a 400 ml beaker. The experiments were done in triplicate. The progress of the reaction was monitored by measuring the pH and EC with a Hanna HI 991301 portable pH/EC/TDS/Temperature probe. The reactions were stopped at designated time intervals (1, 3, 10, 15, 30, 60, 90, 150, 210, 270, 300, 360, 420, 480, 720 and 1440 minutes). The mixture was filtered through 0.45μm nucleopore membrane and the filtrate analyzed for the major elements, trace elements and the anion SO_4^{2-}. Elemental analysis of the water samples was done by ICP-MS (ELAN 6000). The accuracy of the analysis was monitored by analysis of NIST water standards. Fe^{2+}/Fe^{3+} analysis was done by the colorimetric method using 2, 2-bipyridal as the complexing reagent. SO_4^{2-} analysis was done by Ion Chromatography (Dionex DX-120).

4.1.3 XRD and Scanning electron microscope investigations

XRD spectra of the powder mounts of the solid residues were obtained by step-scanning at intervals of 0.02^0 2θ from 5^0 to 85^0 and counted for 0.5 seconds per step. A Phillips PANalytical instrument was used with a pw3830 x-ray generator operated at 40 kV and 25 mA. The X'pert graphics and identify program was used to identify the mineral phases using the JCPDF database. Samples for scanning electron microscope investigation were disaggregated in ethanol in a ultra-sonic bath. Drops were dispersed on a carbon tape using a Pasteur pipette and then air dried. A scanning electron microscope (Hitachi X-650 micron analyzer) was used to characterize the morphology of the solid residues. Analysis by scanning electron microscope coupled to energy dispersive analysis of X-rays spectrometer (SEM-EDX) of the solid residues and unreacted fly ash was done to qualitatively identify probable mineral phases that formed in the process and eluded detection by XRD.

4.1.4 Calculation of Saturation States

UNIVERSITY of the
WESTERN CAPE

Precipitation of solid phases may be the most important chemical process influencing on the fate of major (SO_4^{2-}, Fe^{3+}, Fe^{2+}, Al, Mn, Ca) and minor elements (Zn, Cu, Mo, Ni, B, Sr) in acid mine waters in this process. Activities of aqueous species and mineral saturation indices of selected mineral phases were calculated using PHREEQC software (Parkhurst, 1995) and the WATEQ4F database. Analysis data of the process water for each time interval were input and used to estimate the activities of the various species. The activities of the dissolved species were calculated with Davies equation (Davies, 1962). Fe was input as Fe^{2+}/Fe^{3+} and was utilized in calculation of the redox potential. At detection limits or below detection limits of Fe^{2+}/Fe^{3+} the default pe in WATEQ4 database was used. The data used for the ion activity calculations were pH, alkalinity, solute concentrations for Al, Ca, Cu, Fe^{2+}, Fe^{3+}, Zn, SO_4^{2-}, Na, K, Si, Mn, Pb, B, Sr, Ba, and Mo. Saturation index (SI) is used when large deviations from equilibrium are observed. For SI=0, there is equilibrium between the mineral and the solution; SI<0 reflects sub saturation, and SI>0 super saturation. For a state of sub saturation dissolution of the solid phase is expected and super saturation suggests precipitation. The calculated ion activity data was used in plotting equilibrium solubility diagrams for selected mineral phases.

4.1.5 Sequential Chemical Extractions of the Solid Residues (SR)

Sequential extractions were performed on the equivalent masses ranging from 1-10 g solid residues dry matter for the six extractions. The % moisture content of the solid residues were determined on separate portion of the wet solid residues by drying at 105^{o}C for 12 hours for each extraction and this value was used to calculate the mass of dry solid residues used. The extraction was carried out by agitating the samples in a table shaker.

After each extraction samples were centrifuged at 1000 rpm for 10 minutes and the supernatant filtered through a 0.45 μm nucleopore membrane. The extracted sample was then washed with MilliQ water, centrifuged, decanted and discarded. The extraction was done in triplicate. For each extraction a blank sample was prepared using the extraction reagents and analyzed to account for any background contribution. In addition NIST-1640 water standard reference material was analyzed after a 20 batch of samples for quality control. The extraction was done for Arnot FA and solid residues (SR) collected at pH 4, 4.92, 6.32 and 9.12 for FA: AMD ratio of 1:3.

UNIVERSITY of the
WESTERN CAPE

4.1.5.1 Water soluble fraction

The extraction was done by agitating 10 g of the wet sediment solids in 100 ml MilliQ water for 1 hour. After each extraction the samples were centrifuged at 1000 rpm for 10 minutes and the supernatant filtered through 0.45μm nucleopore membrane (Shuman, 1982). Samples were then prepared for cations and SO_4^{2-} analysis. The extracted solid samples were then rinsed in 100 ml of MilliQ water, centrifuged, decanted and discarded. The solids were finally recovered for the subsequent extraction by filtration again on a 0.45 μm nucleopore membrane. A sub-sample was kept a side for the moisture content determination.

4.1.5.2 Exchangeable fraction

7 g of wet solid residues from the water soluble fraction was extracted with 70 ml of $MgCl_2$ solution (1 M $MgCl_2$ solution) at pH 7, by continuous agitation for I hour at room

temperature (Tessier *et al.,* 1979). The $MgCl_2$ solution was prepared by dissolving 47.7 g of analytical grade $MgCl_2$ salt in 500 ml of MilliQ water.

4.1.5.3 Carbonate fraction

6 g of the wet sediments from the exchangeable fraction were extracted with 60 ml of 1 M sodium acetate/acetic acid buffer solution at pH 5 by agitating continuously for 5 hours (Tessier *at al.*, 1979). The 1 M buffer solution was prepared by dissolving 41.4 g of analytical grade sodium acetate in 500 ml and adjusting the pH with 0.5 M acetic acid solution.

4.1.5.4 Crystalline Mn-oxides

5 g of the wet solid residues from the carbonate fraction were extracted with 125 ml of 0.1 M hydroxylamine hydrochloride prepared in 0.01 M HNO_3 at pH 2 for 30 minutes by continuous agitation (Chao, 1972; Shuman, 1982). This procedure is expected to extract contaminants that are bound to crystalline Mn oxides and is estimated to be 85 % efficient at selective solubilization of crystalline Mn oxides (Chao, 1972). A few percent of total amorphous iron may also be extracted (Chao, 1972, 1984).

UNIVERSITY of the
WESTERN CAPE

4.1.5.5 Amorphous Fe, Mn, Al- oxides, (oxy) hydroxides

4 g of the wet solid residues from the crystalline Mn-oxide fraction was extracted with 800 ml of the 0.2 M ammonium oxalate/oxalic acid buffer at pH 3 for 4 hours (Cornell and Schwertmann, 1996; Schwertmann, 1973). The 200:1 W/S ratio was adopted on optimization done on the solid residues (Table 4.1) which indicated maximum dissolution after four hours of reaction time. The optimization was carried out by dissolution at two Water/Solid ratios and reaction times. Two size fractions designated as coarse and fine were used for the dissolution experiments; these were obtained by disaggregating the solid residues collected at pH 9.2 in a ultra-sonic bath using MilliQ water. The mixture was allowed to stand for 10 minutes and the solution filtered to collect the fine particles, this procedure was repeated several times by shaking the mixture gently and letting it settle before filtration to collect more of the fine solids. The remaining mixture was then filtered to collect the coarse

particles. For the main experiments however no separation was attempted, the solid residues were used as collected at different reaction times. The table below shows the total Fe collected at W/S ratios and reaction times employed.

Table 4.1: Total Fe (μg/g) dry weight extracted from the coarse and fine size fractions

Water/Solid ratio	200:1		100:1	
Dissolution time(hrs)	2	4	2	4
Coarse fraction	3458	3875	2029	2477
Fine fraction	4226	4475	2247	2584

4.1.5.6 Crystalline Fe oxides

2-2.5 g of the wet solid residues were extracted with 60-75 ml of ammonium oxalate monohydrate 0.2 M + oxalic acid 0.2 M + 0.1 M ascorbic acid mixture at pH 3.25 by agitating for 30 minutes in a water bath maintained at 95 ± 5oC (Muller and Seiller, 1999). The working solution was prepared by dissolving 17.613 g ascorbic acid in 0.2 M ammonium oxalate/oxalic acid buffer.

UNIVERSITY of the
WESTERN CAPE

4.2 Results AND Discussions

4.2.1 Composition of fly ash and Navigation Acid mine Water

The X-ray fluorescence (XRF) results (Table 4.2) show that the fly ash consists of three major phases: Al_2O_3, Fe_2O_3 and SiO_2. The American Society for Testing and Materials (ASTM, 1988) uses these three major phases to classify fly ashes based on coal source. From the analysis (SiO_2 +Al_2O_3+Fe_2O_3≥ 70%) the Arnot fly ash can be categorized as class F, which is either derived from anthracitic or bituminous coals (Mattigod *et al.,* 1990). Among the minor elements Arnot fly ash shows high concentrations of Sr, Ba, Cr, Zr and Ni. Traces of Mo are also present. These concentrations are within the concentration ranges reported by Early *et al.* (1990) and are higher than values generally found in coals and soils indicating that the combustion process tends to enrich the fly ash with minor elements.

The Navigation AMD is strongly acidic (pH 2.19). The pH of mine water depends on the relative abundance and extent of weathering of pyrite and calcite neutralization. Low pH

values of the AMD imply a deficiency of calcareous minerals and absence of carbonate buffering in mine tailings or boulders through which the groundwater flows. Major elements include Na, Ca, Mg, Al, Mn and Fe. Dissolution of silicate minerals such as feldspar, kaolinite and chlorite accounts for most or all of the dissolved K, Na, Mg, Al and Ca (Crouse and Rose, 1976). The Navigation AMD has high SO_4^{2-} content (Table 5.3) typical of leachate from sulphide rich coal mine tailings and underground mine lakes (Uhlmann et al., 2004).

Table 4.2: Composition of Arnot fly ash and solid residues (SR) collected at pH 9.2 for 1:3: fly ash (FA): acid mine drainage (AMD) ratio.

	Fly ash (FA)				Solid residues (SR)
Elements	Concentration (% w/w)	Elements	Concentration (ppm)	Elements	Concentration (% w/w)
SiO2	52.4 ± 2.36	Cu	45.3 ± 6.6	SiO2	45.81 ± 3.6
TiO2	1.34 ± 0.05	Mo	5.5 ± 1.23	TiO2	1.29 ± 0.06
Al2O3	23.4 ± 1.08	Ni	92.4 ± 6.5	Al2O3	22.57 ± 2.1
Fe2O3	4.72 ± 0.96	Pb	57.4 ± 13.6	Fe2O3	6.31± 1.29
MnO	0.06 ± 0.001	Sr	1465.9 ± 113.8	MnO	0.10 ± 0.01
MgO	2.67 ± 0.035	Zn	54.3 ± 4.71	MgO	2.33 ± 0.65
CaO	8.41 ± 0.574	Zr	478.1 ± 125.7	CaO	7.18 ± 2.62
Na2O	0.35 ± 0.253	Co	16.2 ± 13.08	Na2O	0.40 ± 0.014
K2O	0.48 ± 0.032	Cr	181.2 ± 1.14	K2O	0.53 ± 0.13
P2O5	0.34 ± 0.212	V	147.4 ± 39	P2O5	0.63 ± 0.04
Cr2O3	0.03 ± 0.009	Ba	931.0 ± 95.2	Cr2O3	NA
SO3	NA			SO3	3.52 ± 0.21

Results presented as mean ± SD for n=3

UNIVERSITY of WESTERN CAPE

Table 4.3: Chemical and physical characteristics of Navigation AMD (concentration in mg/L except for pH, EC and acidity).

Parameter	Navigation AMD	Parameter	Navigation AMD
pH	2.19 ± 0.02	Ni	6.16 ±1.23
EC (mS/cm)	15.77 ± 0.01	Cu	7.10 ± 2.14
Acidity (mg/l $CaCO_3$)	14450 ± 50.6	Zn	15.71 ± 3.46
B	10.3 ± 1.26	Se	10.39 ± 0.023
Na	102.9 ± 10.6	Sr	1.95 ± 0.021
Mg	399.4 ± 30.7	Mo	0.014 ± 0.002
Al	453.4 ± 17.9	Ba	0.108 ± 0.003
Si	99.2 ± 9.43	Pb	0.455 ± 0.022
Ca	146.9 ± 12.5	SO_4^{2-}	24880 ± 96.7
Mn	95.8 ± 7.89	Cl^-	370 ± 55.6
Fe2+	4444.9 ± 59.8	NO^{3-}	90 ± 20.3
Fe3+	2065.6 ± 10.3		

Results presented as mean ± SD for n=3

UNIVERSITY of the WESTERN CAPE

4.2.2 Composition of Solid Residues (SR)

The results of XRF analysis of the solid residue samples collected at pH 9.2 for 1:3, FA: AMD ratio are shown in Table 4.2. A comparison of the composition of FA and the SR indicates a decrease in SiO_2, CaO and MgO. The decrease in SiO_2 reflects the dissolution of amorphous SiO_2 at low pH while the decrease in CaO and MgO content in the solid residues reflects the dissolution of free lime and MgO which is responsible for the neutralizing capacity of the fly ash. An increase in Fe_2O_3, Al_2O_3 and MnO in the solid residues indicates the removal of these elements from AMD as insoluble precipitates as the pH increases.

4.2.3 Neutralization Reactions

The evolution of pH values with time for the 1:3 and 1:1.5 FA: AMD ratios are presented in Figure 4.1. The pH values for the 1:3 ratio are characterized by two buffer regions, at pH 4 - 4.5 and pH 6.0. The 1:1.5 ratio shows two buffer regions, at pH 4.5 - 5.0 and at pH 9.0. The

buffering exhibited by the AMD at the 1:1.5 ratio is stronger. This is evidenced by the lower gradient of the curves at these buffer regions.

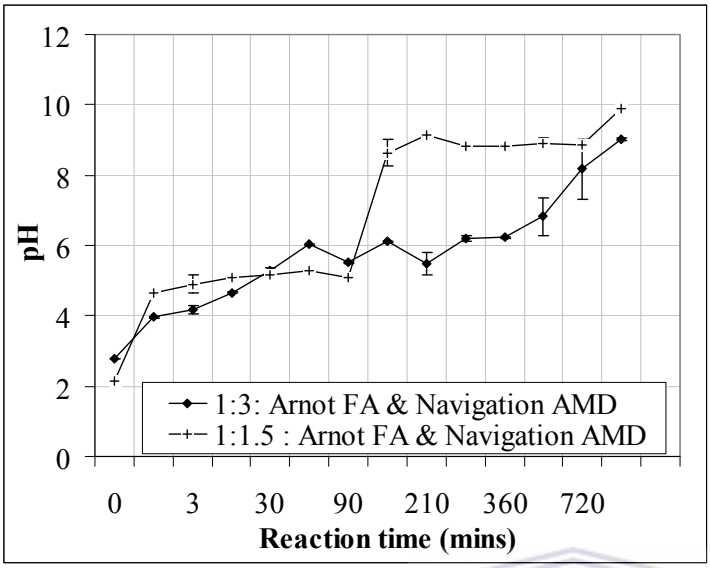

Figure 4.1: pH change with contact time for the 1:3 and 1:1.5 FA: AMD reactions. Error bar represents 1 SD above and below the mean.

The buffering region at pH 9.0 is absent in the 1:3 ratio since the system attained pH 9.0 at the last contact time investigated. The buffering region at pH 9.0 for 1:1.5 ratio could be attributed to the formation of soluble hydrous complexes by cations such as $Al(OH)_4^-$ at high pH (Ricoh *et al.*, 1999).There are two opposing processes which establish the pH value for the solution in this neutralization process. The dissolution and hydrolysis of oxide components such as CaO and MgO (equations 4.1 and 4.3) (Table 4.2) from fly ash which contributes to an increase in solution pH.

$$CaO + H_2O \rightarrow Ca^{2+} + 2OH^- \quad \text{.....(4.1)}$$

$$MgO + H_2O \rightarrow Mg^{2+} + 2OH^- \quad \text{.....(4.2)}$$

Offsetting the pH increase contributed by the dissolution of the oxide components is the hydrolysis of AMD constituents such as Fe^{3+}, Al^{3+}, Fe^{2+} and Mn^{2+} (Table 4.2 and 4.3). The relative quantities of soluble bases (oxides) in fly ash and hydrolysable constituents in AMD dictate whether the final solution at a given contact time will have a dominant acid or basic character. There are two factors that will finally dictate the nature of the final solution in these neutralization reactions:

a) FA: AMD ratio
b) Contact time

While the 1:1.5 FA: AMD ratio achieves a breakthrough to alkaline pH (8.0 to 9.0) after only 120 minutes, the 1:3 FA: AMD ratio achieves the same breakthrough after1440 minutes. This confirms the importance of the amounts of available soluble oxides and contact time in controlling the pH of the process waters.

These results indicate that by varying the FA: AMD ratio or the contact time of the reaction different pH values of the final solution can be achieved. It has also been established that the hydrolysis of the AMD constituents contributes to the buffering of pH and breakthrough to alkaline pH will depend on the alkalinity generated from the available fly ash. The higher the FA: AMD ratio the higher the pH of the final process water achieved.

4.2.4 X-ray diffraction (XRD) and Scanning electron microscopy-Energy dispersive (SEM-EDX) Analysis of the Solid Residues

The XRD of the solid residues revealed gypsum as the only new mineral phase formed at all contact times (Fig 4.2) despite the evidence of iron (oxy) hydroxide precipitation which could mean that the precipitates formed were largely amorphous. Another reason for non-detectability by XRD could be due to the masking effect by the fly ash alumino-silicate matrix and the crystalline mullite and quartz phases that are abundant in fly ash (Fig 4.2).

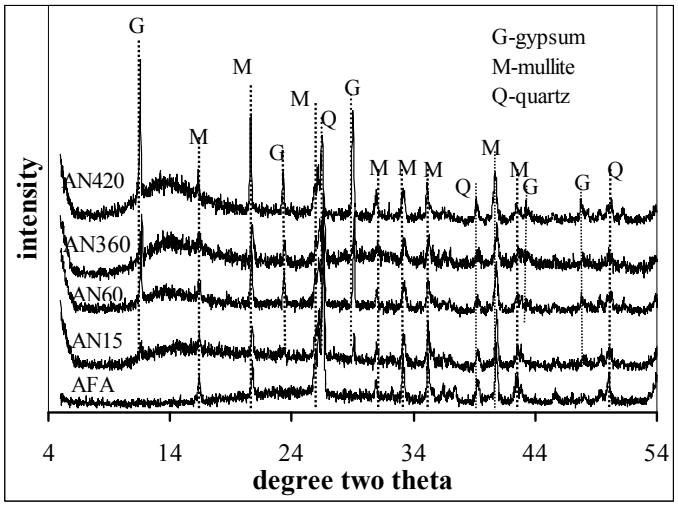

Figure 4.2: XRD spectra of solid residues collected at increasing contact time (minutes) (G-gypsum, Q-quartz, M-mullite, AN-Arnot fly ash + Navigation AMD, 13-FA: AMD ratio, -time (minutes), AFA-Arnot fly ash).

In order to better understand the mode of interaction of AMD and fly ash and the formation of mineral phases, SEM was utilized to appreciate the change in morphology of the resulting solid residues as compared with fly ash while SEM-EDX was utilized to semi-quantitatively identify the mineral phases resulting from the neutralization reactions. Spot analysis was done on selected solid residue samples.

Figures 4.3 and 4.4 shows the morphological changes taking place after interaction of the fly ash with AMD. The smooth round spheres of the fly ash (Fig 4.3-1A) are largely replaced by rough angular shaped particles which are characterized by aggregation with crystals dispersed all over (Fig 4.3-1B, 1C and 1D). The uneven rough blocky shapes observed is evidence of mineral phases/precipitates coating the sphere surfaces or removal of soluble salts that covered the fly ash surface. The small spheres are seen to be aggregating and filling in the spaces between the large spheres forming a dense mass (Fig 4.3-1C and 4.5-2A). Bulky solution precipitation could be responsible for the formation of mineral phases which are deposited in-between the fly ash spheres, thereby acting as a binding link between the fly ash particles hence the dense packing observed in the SEM micrographs.

UNIVERSITY of the
WESTERN CAPE

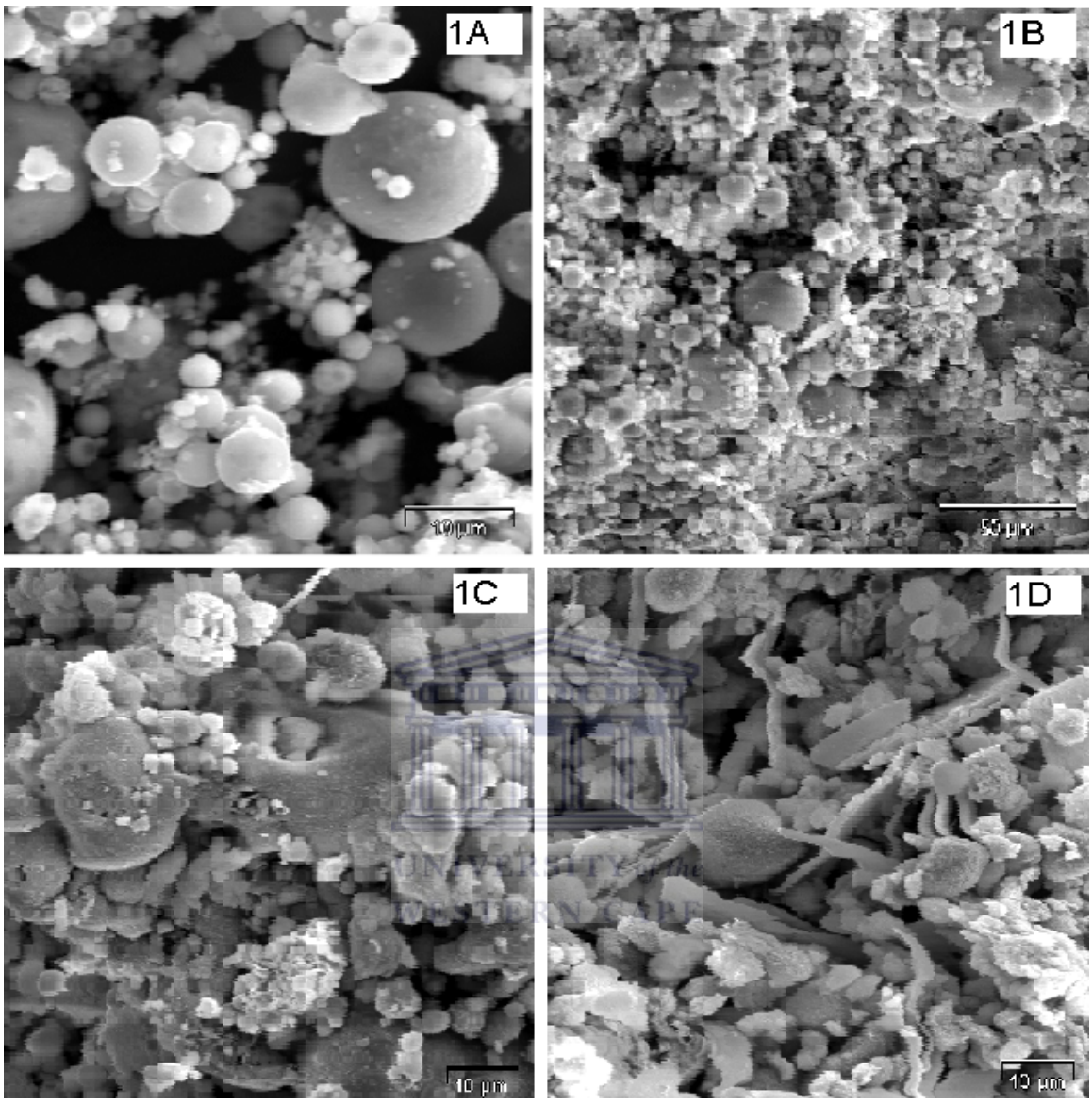

Figure 4.3: SEM micrographs of Arnot fly ash (1A) (magnification=2000) and solid residues (1B, 1C and 1D) collected at pH 9.2 for 1:3 FA: AMD reaction (Magnification = 500)

Three main features are observed in the solid residues by SEM technique.

- Smooth coating on top of the fly ash spheres sometimes with small fly ash spheres embedded in-between. This feature is more clearly observed at higher magnification (Fig 4.3-1C)
- Rods-like structures of varying length and thickness/some are flat shaped and are observed over the whole solid residue samples (Fig 4.3-1D and Fig 4.4-2A).
- Aggregation of the small fly ash particles to form lumps which fill in spaces between the large spheres creating a dense mass (Fig 4.3 1B) better observed at the bottom left corner and top right hand corner.

UNIVERSITY of the
WESTERN CAPE

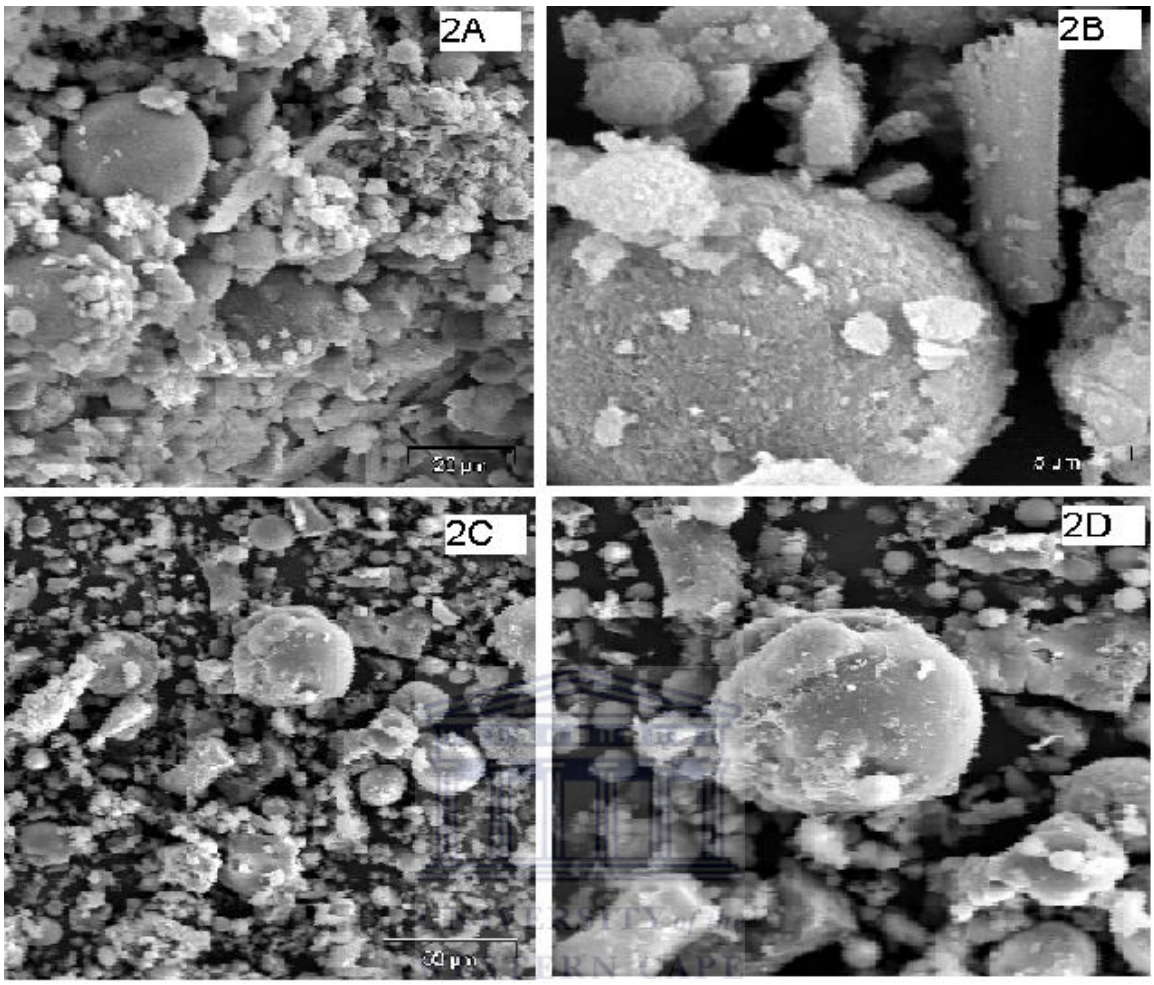

Figure 4.4: SEM micrographs of solid residues (2A-mg=1000, 2B-mg=1000, 2C-mg=500 and 2D-mg=1000) collected at pH 9.2 for 1:3 FA: AMD reaction (Mg=magnification)

- Smooth large spheres are often observed in the solid residues, they appear to have a coating, with smaller particles adhering to the surfaces (F 4.4-2B).

The figures 4.4-2C and 4.4–2D shows leached solid residue particles, they exhibit a relatively smooth etched surface of a large sphere and small spheres. Particles appear dispersed, with loss of coatings on particle surfaces. The precipitates/mineral phases that resisted the leaching are observed either on the surface of the sphere or detached from the sphere. This probably represents the initial stages of contact between fly ash and AMD before precipitation and deposition of precipitates occurs.

The SEM and SEM-EDX spot analysis were done on solid residues collected at pH 8.0-9.2 for 1:3 and at pH 9.8 for 1:1.5 FA: AMD ratio. A spot analysis of the unreacted fly ash was also done for comparison. The data trends are then used to tentatively identify the mineral

phases that could be forming in the treatment process. The spots and areas analyzed are shown in Figure 4.5 below. The accompanying SEM-EDX analyses are results expressed as weight % presented in Table 4.4 below

Table 4.4: SEM-EDX spot % elemental analysis of solid residue collected at pH 9.2 for 1:3 FA: AMD ratio

Element	Arnot fly ash	AN31-A	AN31-B	AN31-C	AN31-D	AN31-E	AN31-F	AN31-G
O	32.72	15.17	33.26	30.42	36.02	19.47	27.45	34.05
Al	20.80	19.59	15.60	14.59	11.15	28.74	32.84	10.19
Si	33.57	39.15	20.06	24.08	23.89	27.70	36.31	6.45
P	ND	ND	1.70	2.82	0.72	ND	ND	ND
S	ND	ND	1.95	1.00	8.80	0.98	ND	11.24
Mg	ND	3.14	5.07	3.13	1.26	2.05	ND	0.96
Ca	6.76	13.82	10.89	14.27	16.02	6.57	0.76	34.59
K	1.46	ND	0.43	0.61	0.45	1.60	0.78	ND
Ti	3.08	5.56	1.01	2.69	0.30	2.84	0.21	0.45
V	ND	0.34	ND	0.15	ND	1.08	ND	ND
Fe	1.60	3.23	10.04	6.24	1.38	8.97	1.64	2.08

UNIVERSITY of the WESTERN CAPE

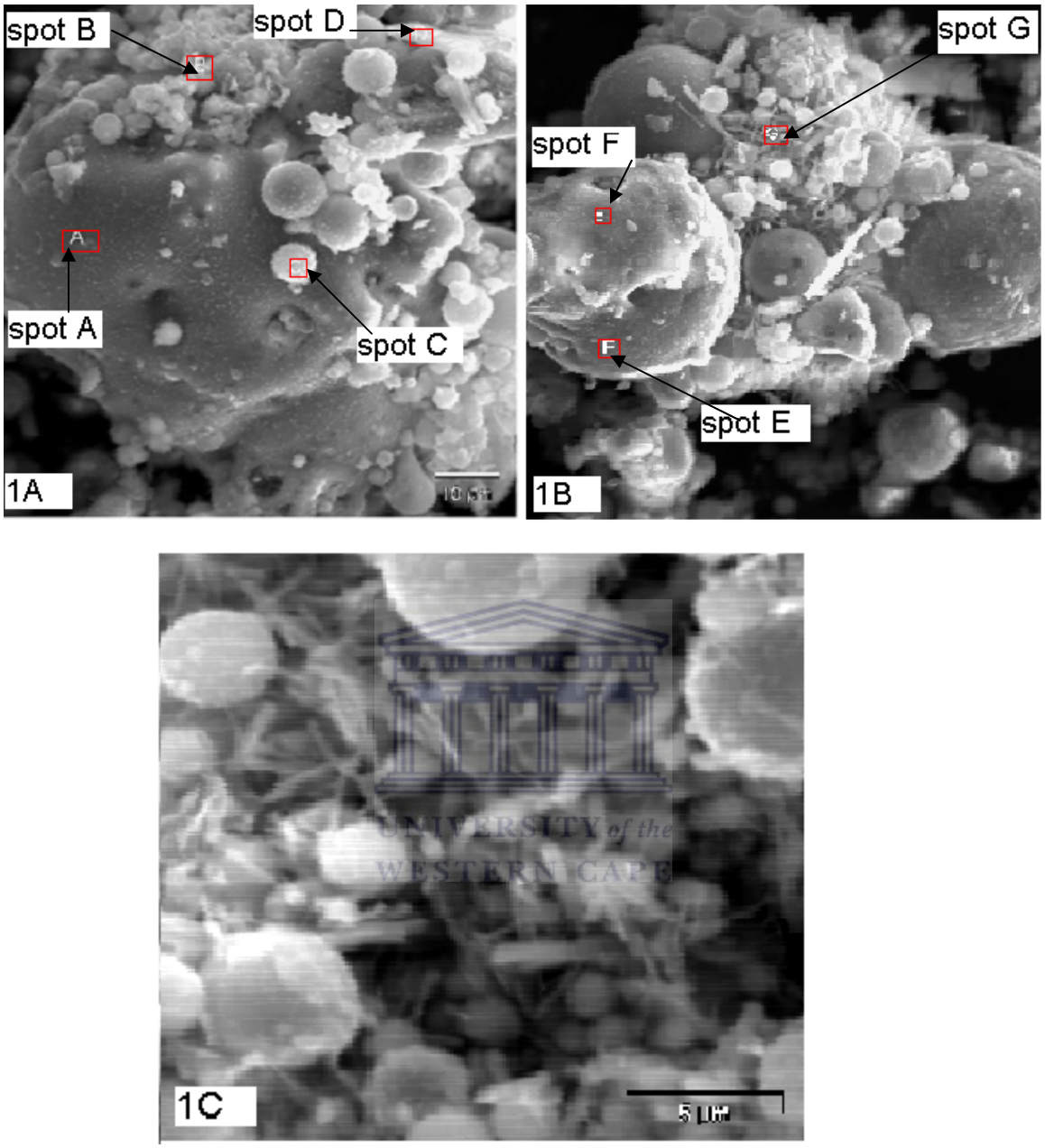

Figure 4.5: SEM micrograph of solid residues collected at pH 9.2 for 1:3 FA: AMD ratio (1A and 1B) showing the spots where EDX analysis was done (magnification=2000), 1C for solid residues collected at pH 9.88 for 1:1.5 FA: AMD ratio showing needle like crystals similar to spot G in 1B.

Spot A (Fig 4.5-1A) represents a gel like coating on a large sphere, compared to the spot analysis of the un-reacted fly ash there is increased % content of Si, Ca, Mg, Ti and a decreased O, the Al/Si ratio is 0.5. The increasing Ca, Mg and Si coupled with a decrease in

O suggest a Ca-Mg rich glass phase. The high Ti could be a result of the contribution from the underlying layers.

Spot B (Fig 4.5-1A) represents an aggregation of small fly ash spheres which are joined together by a new phase that seems to be filling in. This spot shows a significant increase in Fe (ten fold) strongly suggesting an iron-rich phase is being formed. An increase in Ca, Mg and Si similar to spot-A is observed strongly pointing to a Ca-Mg-Si rich glass phase formation.

Spot-C (Fig 4.5-1A) represents small fly ash sphere with minute point-like coatings on the surface. Spot analysis of this sphere shows increased Ca, Mg, Fe, P, S. The Fe content is double compared to the unreacted fly ash. The increase in Fe content could point to the formation of an iron-rich phase. The presence of P, S and Ca suggests a type of jarosite mineral being precipitated where K or Na is being replaced by Ca, Fe by Al, SO_4^{2-} by PO_4^{3-} and Mg probably incorporated in the jarosite. Jarosite is a hydroxysulphate of Fe and K or Na, Fe can be replaced by Al and by smaller amounts of Zn and Cu. K is usually replaced by Ca, Pb, Ba, Sr, or Ce, Sulphate can also be replaced by PO4, AsO4, CO3, SbO3, CrO4 or SiO4 (Scott, 1987)

UNIVERSITY of the
WESTERN CAPE

Spot-D (Fig 4.5-1A) represents a crystal; analysis of this crystal reveals significant increase in S and Ca. No change is observed for the Al/Si ratio compared to fly ash. An increase in O is also observed. This strongly suggests a gypsum crystal.

Spot-E (Fig 4.5-1B) represents surface of a large sphere. The spot analysis shows increase in Al and Fe and decrease in O. Al/Si =1.04. The increase in Al could be attributed to the etching action of the acidic solution on the fly ash sphere. Hullet and Weinberger (1980) observed a decrease in Si intensity in relation to Al in fly ash etched with 1 % HF. A decrease in Na, Mg Ca, and K was also observed. They attributed this to the dissolution of the relatively soluble aluminosilicate glass phase. A decrease in O content reinforces this argument. They also observed that Ti and Fe were isormorphically substituted for Al and Si in the mullite. The increase in Fe for this spot could therefore be attributed to the effect of Ca, Mg, Na, K and Si removal. This surface analysis suggest that this could be the initial

stage of the neutralization process where the strongly acidic media comes into contact with the fly ash and dissolves most of the soluble salts on the surface leaving a rough surface (Fig 4.5-1B spot E). Analysis of spot-F (Fig 4.4-1B) reveals similar elemental trends as observed for spot-E which reinforces the fact that this represents a deeply etched sphere with no secondary mineral phase formed on the surface. The Al/Si=0.94 is very close to that observed for spot-E.

Spot-G (Fig 4.5-1B) represents a mass of needle-like crystals, there is significant increase in Al, S, Ca and O compared to the unreacted fly ash suggesting an ettringite phase. O'Brien (2000) observed such a mass of needle-like crystals when he neutralized fly ash paste extracts with synthetic acid mine drainage. This precipitates were collected at circumneutral pH 9.33 while O'Brien (2000) observed ettringite formation at alkaline pH >10. A SEM micrograph for solid residues collected at pH 9.88 for 1:1.5 FA: AMD ratio showed the needle like crystals characteristic of ettringite dispersed all over (Fig 5.5-1C).

It can be concluded that the strongly acidic mine drainage on contact with the fly ash particles dissolves most of the surface soluble salts, the dissolved ions then react with the AMD components in the bulky of the solution and the minerals formed either precipitate on the surface of the large spheres or fill in between the small spheres leading to aggregation.

The SEM-EDX elemental profiles indicate a general increase in content of Ca, Mg and Si in most of the spots analyzed. Most of the spots do not show any crystallinity suggesting they are amorphous. Analysis of the crystals observed (spot-D and spot-G) (Fig 4.5-1A and 1C) suggests gypsum and ettringite are the only crystalline phases formed in this process and were probably significant in attenuation of sulphate. The observed increase in Fe content for precipitates cementing the reacted fly ash particles together and the fine coatings on the small fly ash spheres accompanied by increased O content probably indicates precipitation of iron hydroxide.

SEM and SEM-EDX analysis of the resulting solid residues has provided a semi-quantitative proof that interaction of fly ash and AMD components leads to the clean-up of the AMD through precipitation of largely amorphous Fe and Al-bearing mineral phases as the pH

increases to alkaline levels. Interaction of Ca, Mg, Al and Si has been observed to be taking place leading to the formation Ca, Mg, Al, Si and O rich gels. XRD has provided proof that gypsum is playing a significant role in contributing to the attenuation of sulphate in AMD.

4.2.5 Trends of Major Elements in the Process Water for 1:3 and 1:1.5 FA: AMD Reactions with time.

The trends of major elements, solid residue analysis by XRD, SEM-EDX and saturation indices (SI) calculated using PHREEQC geochemical model are used to deduce the mechanisms responsible for the metal removal and solubility controls involved. The SI indices calculated at selected contact times as the pH increases are presented at the end of this section in tables 4.5 and 4.6

4.2.5.1 Sulphate trends

Figure 4.6 below shows the SO_4^{2-} trends for the 1:3 and 1:1.5 FA: AMD reactions for a 24 hour contact time. Navigation AMD samples were characterized by high SO_4^{2-} levels (24880 mg/L) (Fig 5.6 and Table 5.3). A decreasing SO_4^{2-} concentration to a minimum was observed with time for both FA: AMD ratios. A sharp decrease was observed when the mixture attained pH >5.5 (Fig 4.1and 4.6) for ratio 1:1.5. At pH >6.0 Fe^{2+}oxidation is optimum and iron hydroxides that precipitate out are known to adsorb high concentrations of SO_4^{2-} (Seth and Crawford, 2000). It's also observed that the SO_4^{2-} bearing Al-hydroxysulphate mineral phases, (alunite, basaluminite and jurbanite), barite, and K, Na-jarosites are highly saturated within this pH range (5.49-6.95) for both ratios (Table 4.5 and 4.6). SEM-EDX detected S-rich precipitates in the solid residues collected at pH 9.2 for 1:3 FA: AMD ratio (Fig 4.5).This indicates that SO_4^2 bearing mineral phases are contributing to reduction of SO_4^{2-} once the reaction mixture attains pH 5.3. This would be reinforced by the fact that hydrolysis of Al^{3+} occurs at pH 4.9. It's also at this pH that a peak in Ca concentration is achieved for both ratios (Fig 4.15).

UNIVERSITY of the WESTERN CAPE

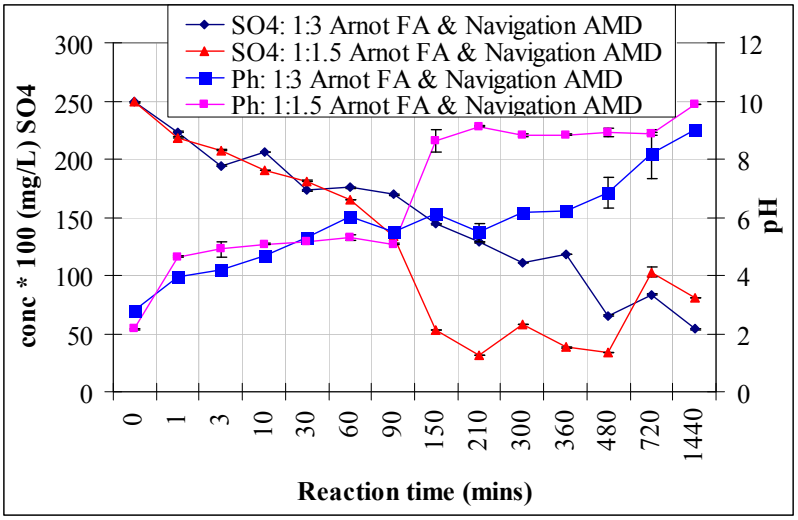

Figure 4.6: SO_4 concentration in process water for 1:3 and 1:1.5 FA: AMD reactions. Error bar represents 1 SD above and below the mean.

To reinforce this hypothesis pH/mineral phases diagrams were constructed for selected SO_4^{2} bearing phases that were predicted by PHREEQC to be precipitating (Fig 4.7)

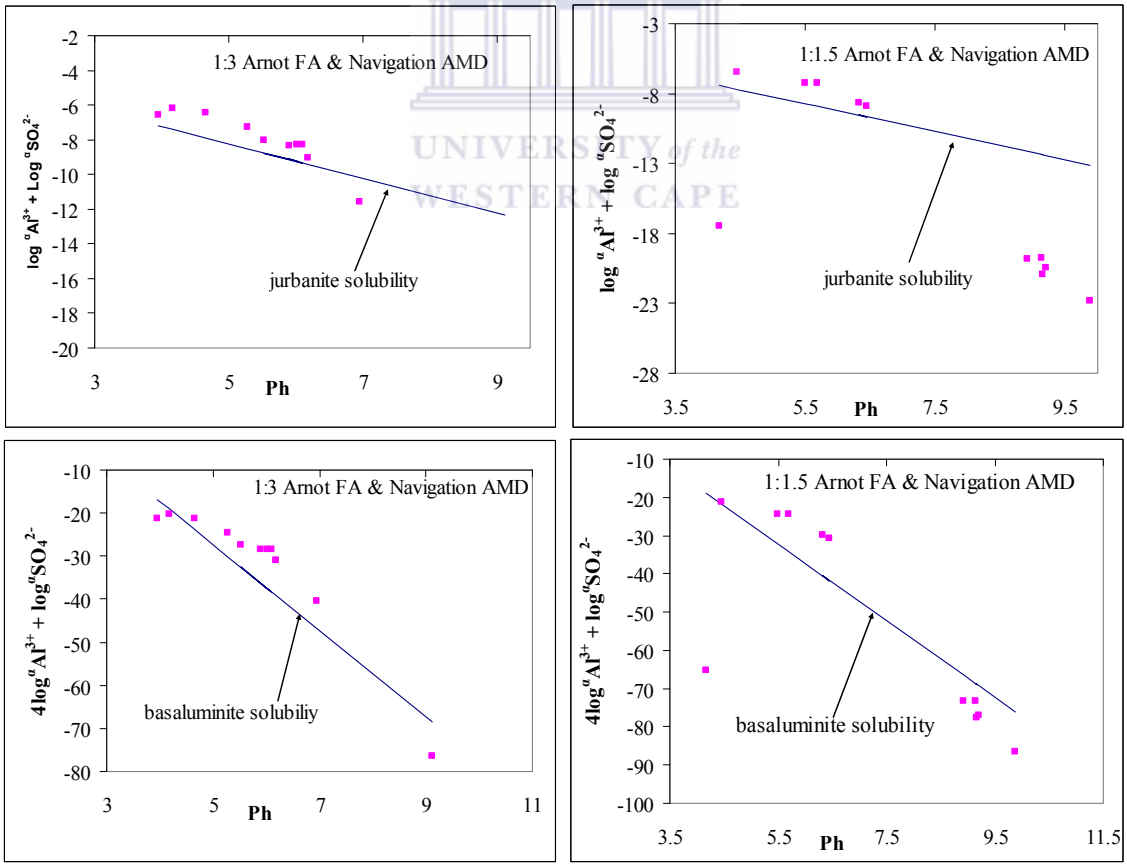

Figure 4.7: Ph/ mineral phase diagrams for basaluminte and jurbanite for 1:3 and 1:1.5 FA: AMD ratios.

UNIVERSITY of the WESTERN CAPE

An observation of figure 4.7 indicates that at pH < 6.5 jurbanite and basaluminite were controlling SO_4^{2-} activities for both ratios. The activities of Al^{3+} and SO_4^{2-} are higher than those predicted by jurbanite and basaluminite solubility which would mean that these mineral phases were in a state of disequilibrium or that other mineral phases were also controlling SO_4^{2-}concentration.The contribution of jarosite was assessed by plotting of experimental activity values ($3\log\alpha Fe3+ + 2\log^{\alpha}SO_4^{2-} + \log^{\alpha} Na^{+}$) versus pH. Equilibrium of Na-jarosite dissolution (equation 4.3) yields to the law of mass action (equation 4.4),

where log K_{eq} = -5.28.

$$NaFe_3(SO_4)_2(OH)_6 + 6H^+ \Rightarrow Na^+ + 3Fe^{3+} + 2SO_4^{2-} + 6H_2O \quad \text{.....(4.3)}$$

$$3\log(\alpha_{Fe^{3+}}) + 2\log(\alpha_{SO_4^{2-}}) + \log(\alpha_{Na^+}) = -5.28 - 6pH \quad \text{.....(4.4)}$$

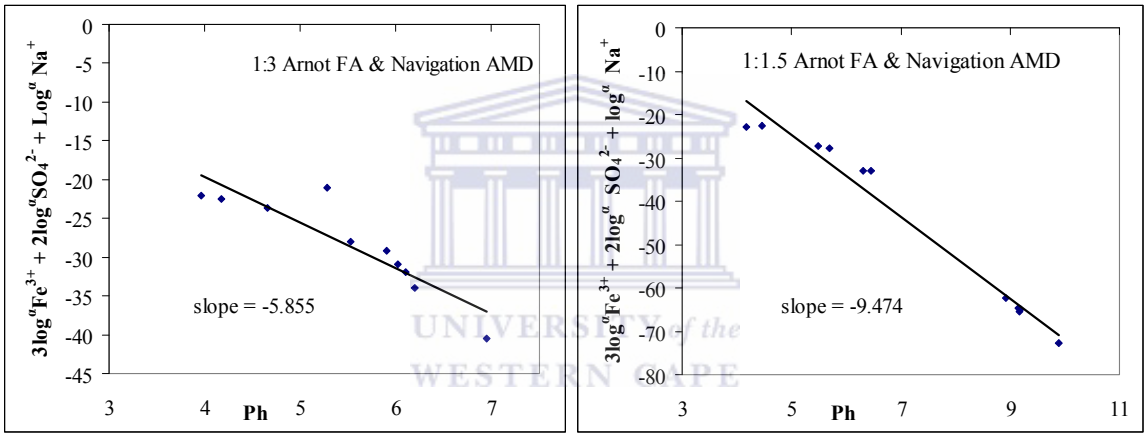

Figure 4.8: A plot of ($3\log\alpha Fe3+ + 2\log^{\alpha}SO_4^{2-} + \log^{\alpha} Na^{+}$) versus pH for 1:3 and 1:1.5 ratios respectively. Line represents the equilibrium with natro-jarosite [$NaFe_3(SO_4)_2(OH)_6$].

For the 1:3 FA: AMD ratio a slope close -6 was observed at pH 4.5-6.5 suggesting control of SO42- by natro-jarosite. A slope of -9.474 was observed for the 1:1.5 FA: AMD ratio suggesting either disequilibrium or control of sulphate by other mineral phases. The process water however showed variable supersaturation with K-, Na- and H-jarosite(Table 4.5 and 4.6). This probably explains the disequilibrium observed at certain pH conditions. However no thermodynamic data are available for intermediate jarosite members.

Analysis of the solid residues cementing the reacted fly ash particles by SEM-EDX indicated an increase in Fe, suggesting that an iron-rich phase was being formed that was amorphous to XRD (Fig 4.2 and 4.5). Doubling the mass of fly ash relative to volume of AMD did not result in an increase of final SO_4^{2-} levels, which confirms presence of solubility control (Fig

UNIVERSITY of the WESTERN CAPE

4.6). XRD and SEM-EDX detected gypsum (Fig 4.2 and 4.5) in the solid residues collected for all the contact times indicating that it had control on SO_4^{2-} levels. Calculated saturation indices (SI) indicate that gypsum was at saturation at all contact times for both FA: AMD ratios (Table 4.5 and 4.6). At pH 8 for 1:3 FA: AMD and 9.2 for 1:1.5 FA: AMD ratio SO_4^{2-} levels were observed to increase and then decrease between 720-1440 minutes. As the pH of the solution increases to (>8) the OH^- ions compete with SO_4^{2-} for adsorption sites on the amorphous iron phases leading to desorption of SO_4^{2-}. The decrease thereafter is attributed to the formation of ettringite ($CaO.Al_2O_3.3CaSO_4.32H_2O$). Ettringite was identified by SEM-EDX in the solid residues collected at pH>8.0 (Fig 4.5-1B spot G and 5.5-1C). PHREEQC predicted barite ($BaSO_4$) and celestite ($SrSO_4$) to be precipitating at most of the contact times for both FA: AMD ratios and would also contribute to the control of SO_4^{2-} in this process.

UNIVERSITY of the
WESTERN CAPE

Table 4.5: Calculated saturation indices for selected mineral phases at selected reaction times for FA: AMD ratio 1:3.

Reaction time (mins)	1 min	3 mins	30 mins	90 mins	210 mins	480 mins	1440 mins
pH	3.96	4.17	5.28	5.53	5.9	6.95	9.12
$Al(OH)_{3(a)}$	-4.11	-3.19	-0.86	-0.86	-1.16	0.02	-2.44
$Alunite(KAl_3(SO_4)_2(OH)_6)$				7.99	7.15	6.1	-7.87
$Barite(BaSO_4)$	1.03	0.79	7.99	1.36	1.29	1.11	1.03
$Basaluminite(Al_4(OH)_{10}SO_4)$	-4.41	-1.34	1.36	4.99	3.58	5.27	-8.96
Boehmite(AlOOH)	-1.91	-0.98	4.99	1.35	1.05	2.23	-0.22
$Brucite(Mg(OH)_2)$	-11.73	-11.24	-11.58	-8.33	-8.24	-5.2	-0.96
$Celestite(SrSO_4)$	-0.07	0.2	0.23	0.3	0.27	0.22	0.2
$Cu(OH)_2$	-6.15	-5.83	-6.33	-3.86	-3.87	-3.14	-1.99
Diaspore(AlOOH)	-0.17	0.74	-0.99	3.08	2.76	3.95	1.49
$Fe(OH)_{3(a)}$	1.53	-6.79	1.82	4.16	3.73	4.23	2.68
$Gibbsite(Al(OH)_3)$	-1.39	-0.48	-2.2	1.85	1.54	2.72	0.26
Goethite(FeOOH)	4.88	5.32	5.16	7.59	7.18	7.68	6.14
$Gypsum(CaSO_4{:}2H_2O)$	-0.29	0.04	0.18	0.17	0.14	-0.12	-0.15
$Jarosite\text{-}K(KFe_3(SO_4)_2(OH)_6)$				12.85	11.72	8.62	-2.58
$Jarosite\text{-}Na(NaFe_3(SO_4)_2(OH)_6)$	6.58	7.54	7.62	10.1	8.85	5.62	-5.54
$JarositeH((H_3O)Fe_3(SO_4)_2(OH)_6)$				7.13	5.93	1.36	-11.99
$Jurbanite(AlOHSO_4)$	0.64	1.21	-0.09	0.72	0.37	-1.49	-8.32
$Ni(OH)_2$	-7.48	-7.28	-7.39	-4.47	-4.89	-3.09	
$Nsutite(MnO_2)$	-11.29	-10.76	-10.43	-8.9	-9.36	-9.65	-13.72
Manganite (MnOOH)	-7.6	-7.12	-7.12	-4.81	-5.07	-3.86	-4.57
$Pb(OH)_2$	-8.12	-8.58	-9.41	-6.21	-5.81	-3.86	0.19
$Kaolinite(Al_2Si_2O_5(OH)_4)$	0.09	2.21	-1.6	5.26	4.49	5.46	-0.48
$Sepiolite(Mg_2Si_3O_{7.5}\ OH{:}3H_2O)$	-14.14	-12.81	-13.93	-9.46	-9.53	-5.57	1.38
$SiO_{2(a)}$	-0.27	-0.11	-0.3	-0.91	-0.98	-1.68	-2.19
$Wairakite(CaAl_2Si_4O_{12}{:}2H_2O)$	-12.69	-9.55	-14.06	-6.75	-6.03	-3.68	-6.3
$Zn(OH)_{2(a)}$	-9.38	-9.02	-9.49	7.99	-7.23	-4.84	-1.26

(-ve sign indicate under saturation and +ve sign super saturation, 0-saturation)

UNIVERSITY of the WESTERN CAPE

Table 4.6: Calculated saturation indices for selected mineral phases at selected reaction times for FA: AMD ratio 1:1.5.

Reaction time (mins)	1 min	10 min	60 min	150 min	360 min	720 min	1440 min
pH	3.8	5.49	6.45	8.92	9.14	9.2	9.88
$Al(OH)_{3(a)}$	-3.27	-0.29	0.96	-2.17	-1.44	-2.35	-2.62
Alunite($KAl_3(SO_4)_2(OH)_6$)		10.49	10.05	-6.49	-5.22	-7.37	-10.44
Barite($BaSO_4$)	1.72	0.8	1.16	1.17	1.3	1.07	1.37
Basaluminite($Al_4(OH)_{10}SO_4$)	-1.35	7.91	10.95	-6.86	-4.44	-7.78	-10.26
Boehmite(AlOOH)	-1.07	1.91	3.17	0.03	0.76	-0.15	-0.42
Brucite($Mg(OH)_2$)	-11.26	-8.47	-6.48	-1.43	-1.24	-1.89	-1.59
Celestite($SrSO_4$)	0.4	0.26	0.26	0.07	0.2	0.45	0.45
$Cu(OH)_2$	-5.26	-2.66	-1.74	-2	-1.83	-1.72	-1.37
Diaspore(AlOOH)	0.67	3.65	4.91	1.77	2.5	1.59	1.32
Ettringite($Ca_6Al_2(SO_4)_3(OH)$)	-36.97	-26.24	-16.96	-7.58	-5.41	-6.94	-3.26
$Fe(OH)_{3(a)}$	3.67	6.14	7.25	5.07	4.96	4.82	4.32
Ferrihydrite(FeOOH)	1.79	4.25	5.36	3.17	3.07	2.93	2.43
Gibbsite($Al(OH)_3$)	-0.55	2.44	3.69	0.56	1.29	0.38	0.11
Goethite(FeOOH)	5.13	7.6	8.71	6.52	6.42	6.27	5.77
Gypsum($CaSO_4{:}2H_2O$)	0.53	-0.01	0.13	0.09	-0.04	0.17	0.16
Jarosite-K($KFe_3(SO_4)_2(OH)_6$)		13.58	12.7	-1	-2.22	-2.05	-5.85
Jarosite-Na($NaFe_3(SO_4)_2(OH)_6$)	7	10.45	10.68	-3.95	-5.04	-4.87	-8.56
JarositeH($(H_3O)Fe_3(SO_4)_2(OH)_6$)	5.17	7.23	6.59	-10.54	-11.82	-11.61	-15.97
Jurbanite($AlOHSO_4$)	1.19	1.5	0.78	-7.64	-7.41	-8	-9.69
$Ni(OH)_2$	-7.79	-4.84	-2.92	-0.05	0.51	0.11	1.19
Nsutite(MnO_2)	-11	-8.56	-7.87	-4	-3.74	-4.25	-2.73
Manganite (MnOOH)	-7.24	-4.65	-3.35	0.3	0.35	-0.23	0.62
$Pb(OH)_2$	-7.68	-4.81	-3.93	-0.03	0.69	0.16	1.43
Kaolinite($Al_2Si_2O_5(OH)_4$)	2.24	8.07	9.05	0.41	2.67	-0.13	-1
Sepiolite($Mg_2Si_3O_{7.5}OH{:}3H_2O$)	-12.51	-7.13	-5.45	1.09	2.67	-0.09	0.02
$SiO_{2(a)}$	-0.04	-0.1	-0.87	-2.06	-1.66	-2.14	-2.31
Wairakite($CaAl_2Si_4O1_2$)	-8.96	-1.13	0.44	-5.33	-1.92	-5.79	-5.58
$Zn(OH)2_{(a)}$		-6.41	-5.33	-1.32	-1.32	-1.53	-1.43

(-ve sign indicate under saturation, +ve sign super saturation and 0-saturation

4.2.5.2 Major cations and anionic species

The trends of major cations and anionic species in the process waters with time are shown in Figures 4.9-5.14, 4.17, 4.19, 4.20 and 4.21 below

Two groups of elements are evident from the concentration profiles obtained for the two ratios. Fe, Al, B do not show increase of the concentration in solution with doubling of fly ash for the entire contact time (Figs 4.9-4.11). This is evidence for solubility control on their concentration for the entire contact time investigated (Reardon *et al.,* 1995). The second group of elements Ca, Na, Mg, Si, Mo and Mn show increase of concentration in solution at the higher FA: AMD ratio at certain contact times (Figs 4.11, 4.13, 4.14, 4.17, 4.19, 4.20 and

UNIVERSITY of the WESTERN CAPE

4.21). This indicates development of solubility controls through dissolution kinetics or equilibrium precipitation (Doye and Duchesne, 2003). The main feature prevalent in this group of elements is the increase of concentration in the first 3 minutes of contact with AMD for the 1:1.5 FA: AMD as compared to 1:3 FA: AMD ratio. This observation indicates that these elements could be present initially as readily soluble mineral phases or salts. As the dissolution increases and their concentration builds up in the reaction mixture, their interaction with species in AMD results in precipitation of new mineral phases that control their concentration in solution thereafter.

4.2.5.2.1 Total Fe, Fe^{3+} and Fe^{2+}

The removal of total iron follows a similar trend for both ratios, with > 90 % being removed on the mixture attaining pH>7.0 (Fig 4.9). The initial decrease in concentration indicates removal of Fe^{3+} probably as amorphous Fe $(OH)_3$. According to Britton (1956), Fe^{3+} hydroxide precipitates out at pH 3.0. PHREEQC simulation indicates that the solution was over-saturated with amorphous $Fe(OH)_3$ and goethite (FeOOH) for the entire contact time for both FA: AMD ratios (Table 4.5 and 4.6).The increase thereafter could be attributed to leaching from fly ash. Significant quantities of Fe_2O_3 were identified by XRF (Table 4.2) in the fly ash. The H^+ from the AMD reacted with the iron oxide, releasing Fe^{3+}which subsequently hydrolyzed (William and Griffin, 1984). On the mixture attaining pH > 5.5, a significant drop in total Fe concentration was observed for both ratios (Fig 4.9). The sharp drop on total iron at this pH is accounted for by the optimum oxidation of Fe^{2+} (Stumm and Lee, 1961) followed by hydrolysis. Observation of figure 4.9 indicates that the removal pattern at pH>6.0 of total Fe follows that of Fe^{2+} for the ratio 1:3 and 1:1.5. The Fe^{2+} is completely removed from solution at pH 8.0. The observed pattern indicates that Fe^{2+} is removed from solution by precipitation, probably as amorphous Fe $(OH)_3$ after oxidation and subsequent hydrolysis. Calculation of saturation indices shows that amorphous amorphous Fe $(OH)_3$ and goethite are at over-saturation for the entire duration of the experiment (Table 4.6). SEM-EDX detected Fe rich mineral phases coating fly ash particles in the solid residues (Fig 4.5). This indicates that the iron rich mineral phases are too amorphous to be detected by XRD or the concentration is below the detection limits.

UNIVERSITY of the
WESTERN CAPE

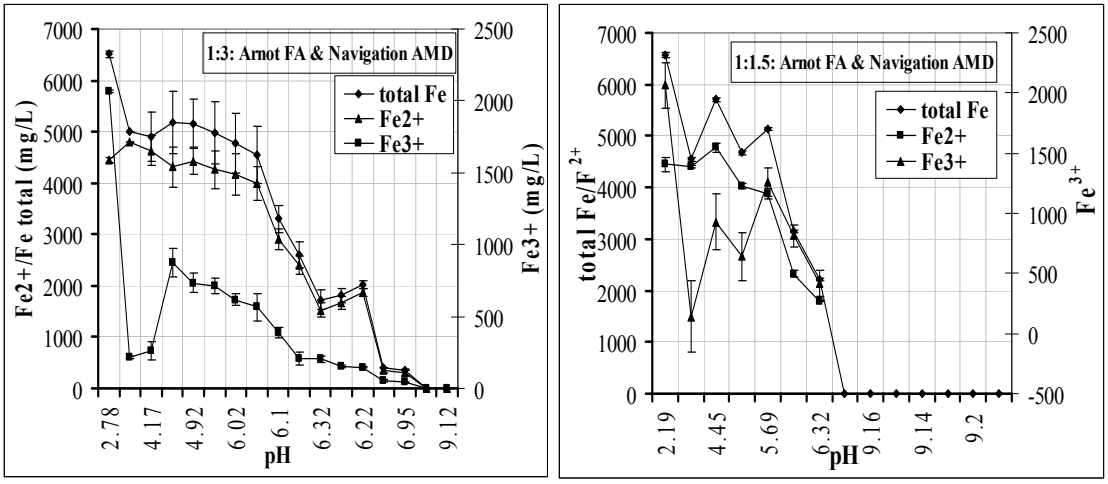

Figure 4.9: Attenuation of Fe^{2+}, Fe^{3+} and total Fe with change in pH in process waters for 1:3 and 1:1.5 FA: AMD ratio. Error bar represents 1 SD above and below the mean, n=3.

4.2.5.2.2 Aluminum

At both FA: AMD ratios, Al decreased with increasing pH (Figs 4.10). The concentration decreased significantly when the reaction mixture attained a pH 5.0 (Fig 4.1). At pH 3.96-5.9, jurbanite is slightly oversaturated, suggesting control on Al concentration at the initial stages of the neutralization process. At pH of about 5.0 (first hydrolysis constant for Al, pK_1=5.0) some form of hydrolyzed aluminum will precipitate. Calculation of saturation indices for 1:3 FA: AMD ratio shows that, amorphous $Al(OH)_3$ remains under-saturated for the entire contact time, basaluminite, boehmite and alunite were oversaturated between 30 and 480 minutes of contact when pH of the solution ranged from 5.28-6.95 (Table 4.6). Gibbsite and diaspore remains oversaturated at pH 5.53-9.12. At the pH range of 5.28-6.95 and SO_4^{2-} concentration >10,000 mg/L (Fig 4.6 and Table 4.5 and 4.6) SO_4^{2-} bearing Al-mineral phases appear to control Al concentration in the process waters. As the SO_4^{2-} concentration drops to below 10,000 mg/L gibbsite and diaspore appear to take over the control of Al as the pH increases. Gibbsite is not stable in acid sulphate waters (Nordstrom, 1982); this explains the predicted precipitation as SO_4^{2-} concentration decreases. At near-neutral waters Al concentrations are generally controlled by gibbsite (Hem and Robertson, 1970). At 1:1.5 FA: AMD ratio the SO_4^{2-} bearing Al-mineral phases alunite, basaluminite appear to control Al concentration over the pH range 5.49-6.45 (Table 4.5 and 4.6). Jurbanite over-saturation pH range is lower than alunite and basaluminite confirming its importance in

UNIVERSITY of the WESTERN CAPE

controlling Al at low pH. The process water appear to be over-saturated with respect to gibbsite and boehmite at pH range 5.49-9.88 (Table 4.5 and 4.6) confirming the importance of these mineral phases in controlling Al concentration once the solution achieves pH >5.0 and SO_4^{2-} concentration <10,000 mg/L (Fig 4.6).

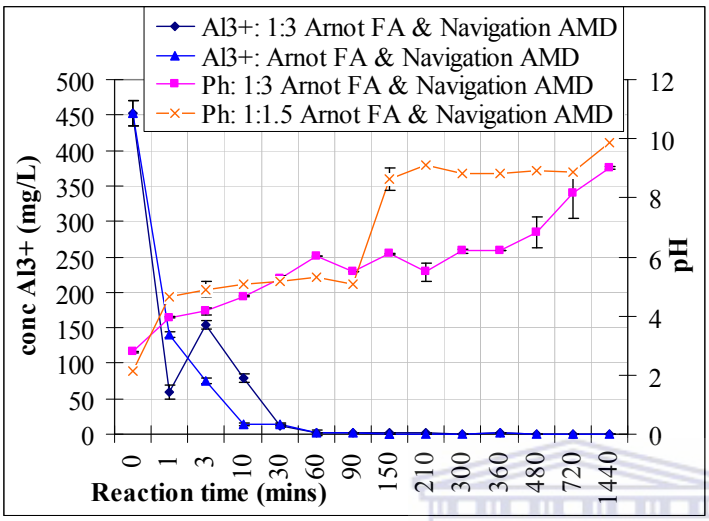

Figure 4.10: Al concentration in process water for 1:3 and 1:1.5 FA: AMD reactions. Error bar represents 1 SD above and below the mean, n=3.

UNIVERSITY of the WESTERN CAPE

At both 1:3 and 1:1.5 FA: AMD ratios boehmite and gibbsite appear to control Al concentration at pH>5.0. The SO_4^{2-} bearing Al-mineral phases appear to control Al within the pH window of 5.49-6.45 overlapping to some extent the pH window in which the Al (oxy)-hydroxides appear to control Al concentration. This clearly indicates that control of Al concentration cannot be resolved to a particular mineral phase at any pH.

4.2.5.2.3 Boron and molydenum

B concentration show pH dependence (Fig 4.11) for both 1:3 and 1:1.5 FA: AMD ratios. An initial increase is observed for both ratios to a maximum. The peak in concentration for both ratios occurs at pH 4.5-7 (10-480 minutes) for 1:3 FA: AMD ratio and pH 6.32 (90 minutes) for 1:1.5 FA: AMD ratio. This is followed by a decrease as the pH increases. For both ratios the decrease is observed when the reaction mixture attains pH > 8.5 (Fig 4.1 and 4.11). The initial increase is due to dissolution of soluble surface oxide precipitates (Hullet and Weinbeger, 1980). The higher concentration observed for 1:3 (FA: AMD) ratio could indicate that B concentration is limited by the dissolution rates of its soluble oxides for the

first 60 minutes of contact with AMD. Several authors (Akira *et al.*, 2005; Kitano *et al.,* 1978) have reported interaction of borate-boron with Ca at high pH and this could explain the decrease in concentration as the pH increases for both ratios. The carbonate fraction was observed to be the most important in retention of B in this process (Table 4.7-4.11). Precipitating ettringite is also reported to incorporate oxyanions such as borate in alkaline solutions and could account for the decreasing B concentrations at high pH. Ettringite was identified by SEM-EDX for the 1:3 and 1:1.5 FA: AMD ratio solid residues collected at pH > 9 (Fig 4.5). Speciation of B by PHREEQC indicates a significant increase in % of borate ions in the reaction mixture as the pH increases to > 8 (Fig 4.12) reaffirming the hypothesis that borate-boron is being incorporated in a precipitating solid phase.

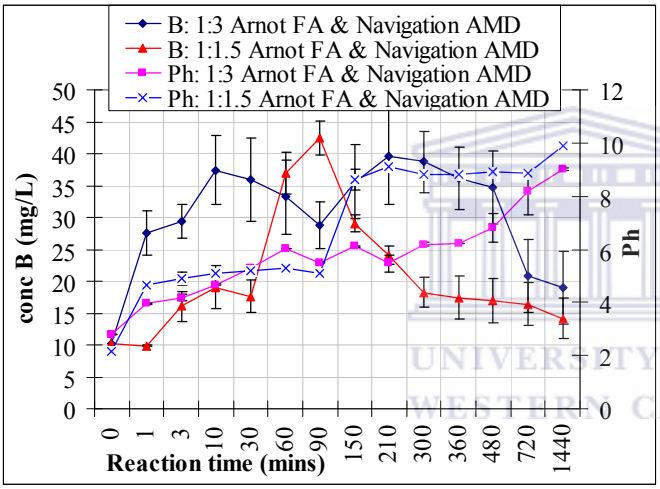

Figure 4.11: B concentration in process water for 1:3 and 1:1.5 FA: AMD reactions. Error bar represents 1 SD above and below the mean, n=3.

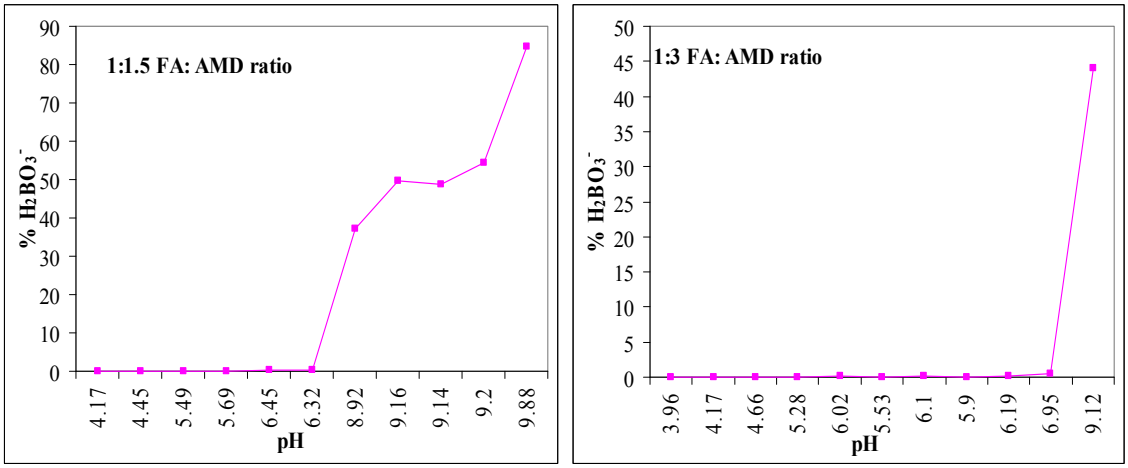

Figure 4.12: % $H_2BO_3^-$ in process water for 1:1.5 and 1:3 FA: AMD reactions as a function of pH.

The concentration trends for Mo show existence of solubility control for the first 30 minutes of reaction. (Fig 4.13). Thereafter the concentration for the 1:1.5 FA: AMD ratio remains higher than 1:3 FA: AMD ratio. The Mo trends also exhibit pH dependence. The concentration remained below 0.2 mg/L at pH < 6.83 for 1:3 FA: AMD ratio. For the 1:1.5 FA: AMD ratio the concentration remained below 0.4 mg/L at pH < 5.1. Mo exists as the MoO_4^{2-} ion at pH > 3 (Eary *et al.*, 1990) and it's likely that it's being removed as metal molybdates at pH< 6.83. This becomes evident as the pH increases to above 8 when Fe and Al are out of solution for both ratios. Mo concentration thereafter increases to values > 0.8 mg/L.

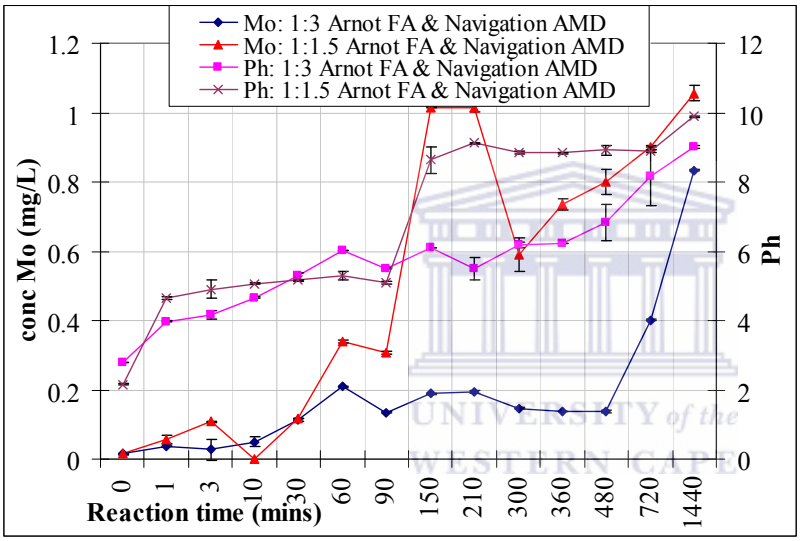

Figure 4.13: Mo concentration in process water for 1:3 and 1:1.5 FA: AMD reactions. Error bar represents 1 SD above and below the mean, n=3.

4.2.5.2.4 Silicon

For Si, the concentration for the 1:1.5 FA: AMD ratio remained slightly higher than the 1:3 FA: AMD ratio for the first 30 minutes of the experiment (Fig 4.14). This signified lack of solubility control and that fly ash was releasing Si. A sharp decline in Si concentration was observed when the mixture attained pH > 5.0 for both ratios, eventually the 1:3 FA: AMD ratio shows a slight increase than 1:1.5 FA: AMD ratio at between 150-360 minutes. This signified development of solubility control for Si. Dissolved Si may be controlled by dissolution of minerals such as SiO_2 (a) at low pH. The highest concentration of Si

corresponds to low pH where SiO_2 (a) is under-saturated (Fig 4.1, Table 4.5 and 4.6.). The equilibrium reaction of $SiO_{2\,(amorphous)}$ can be represented as (equation 4.5):

$$SiO_{2(amorphous)} + 2H_2O \Rightarrow H_4SiO_4$$
$$\log K_{25} = -2.71 \quad \ldots\ldots (4.5)$$

A plot of log activities of H_4SiO_4 versus pH shows control by $SiO_{2\,(amorphous)}$ at pH < 5 for both ratios (Fig 4.15). An observation of the saturation indices for kaolinite indicates super-saturation at 90 minutes of contact when the solution attained pH >5.0 (Fig 4.1, Table 4.5 and 4.6). However a plot of log activities of H_4SiO_4 versus pH for kaolinite equilibria (data not shown) did not reveal control of H_4SiO_4 activity by kaolinite.

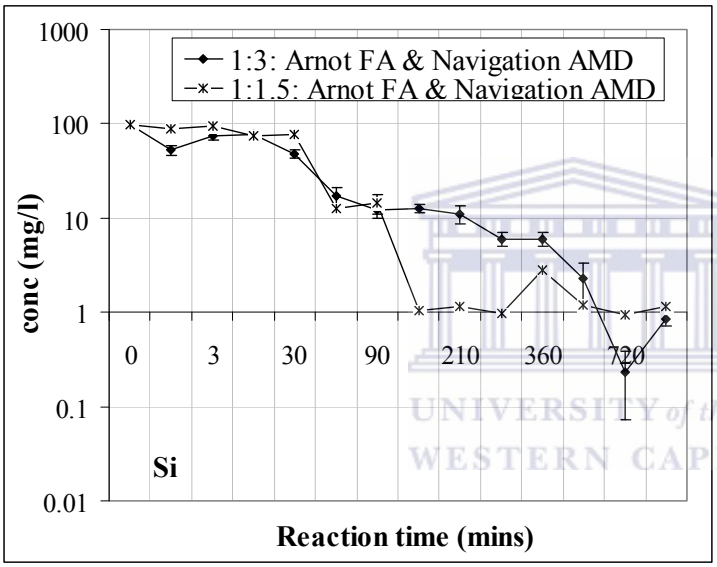

Figure 4.14: Si concentration in process water for 1:3 and 1:1.5 FA: AMD reactions. Error bar represents 1 SD above and below the mean, n=3.

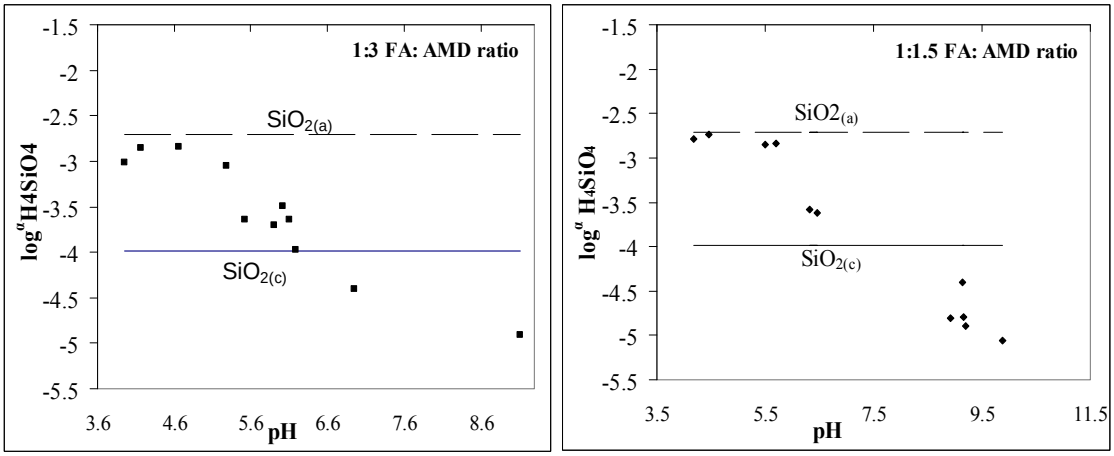

Figure 4.15: A plot of log H_4SiO_4 activity versus pH showing control of dissolved silica by amorphous $SiO_{2(amorphous)}$ in process water for 1:3 and 1:1.5 FA: AMD reactions.

UNIVERSITY of the WESTERN CAPE

Mullite an aluminosilicate crystalline phase present in fly ash was tested for its possible control of dissolved silica in this process. The theoretical activities Al^{3+} and H_4SiO_4 for mullite were calculated by using the equilibrium expression derived from the following equations (4.6, 4.7 and 4.8).

$$Al_6Si_2O_{13(mullite)} + 18H^+ \Leftrightarrow 6Al^{3+} + 2H_4SiO_4 + 5H_2O \quad \text{.....(4.6)}$$
$$Log\ K = 45.41$$

From equation 4.8 the equilibrium for the dissolution of mullite can be written as

$$K = \frac{[H_4SiO_4]^2[Al^{3+}]^6}{[H]^{18}} = 10^{45.41} \quad \text{.....(4.7)}$$

Taking logarithm to base 10 results in the following expression

$$45.41 = 2\,Log\,H_4SiO_4 + 6Log\,Al^{3+} + 18pH \quad \text{.....(4.8)}$$

Using the solubility constant for mullite and measured pH the activities of Al^{3+} and H_4SiO_4 at equilibrium with mullite for the process water were calculated over the measured pH range. A plot of mullite equilibria over the entire pH range reveals control of H_4SiO_4 by mullite at pH > 8 (Fig 4.16).

UNIVERSITY of the
WESTERN CAPE

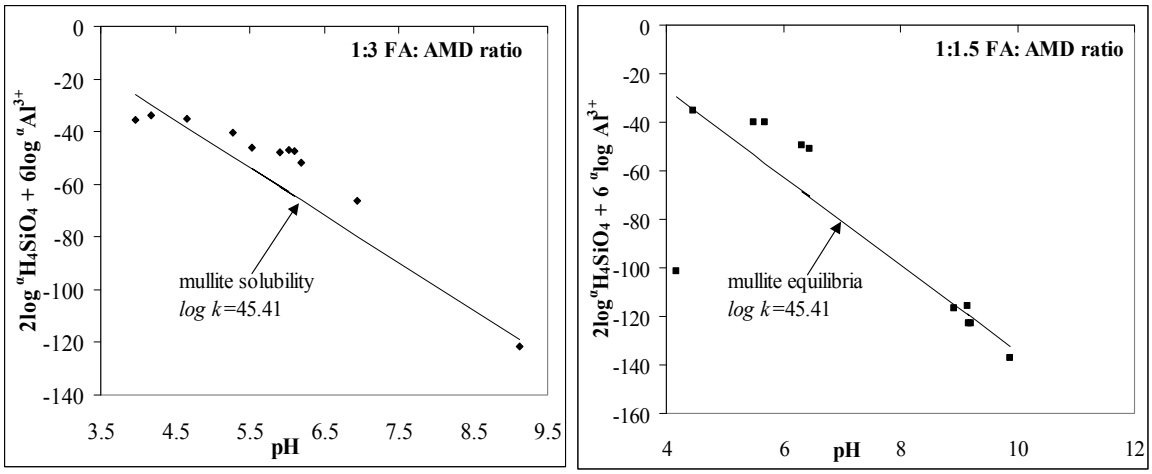

Figure 4.16: A plot of 2 log H_4SiO_4 + 6 log Al^{3+} activity versus pH showing control of dissolved silica by mullite in process water for 1:3 and 1:1.5 FA: AMD reactions at pH>8.

4.2.5.2.5 Calcium, sodium, magnesium

The concentration of Ca and Na exhibited a similar trend (Figs 4.17), initially showing an increase within 3-10 minutes of contact for both ratios. The FA: AMD ratio 1:1.5 initially gives higher concentration than the 1:3 ratio which indicates that fly ash releases these elements on contacting AMD and that their initial concentration will be dictated by the FA: AMD ratio used. This also indicates that these elements exist as highly soluble salts probably on the surfaces of the fly ash. The values for the 1:1.5 ratio, after the initial increase drops to levels slightly lower than the 1:3 ratio for both elements suggesting development of solubility control.

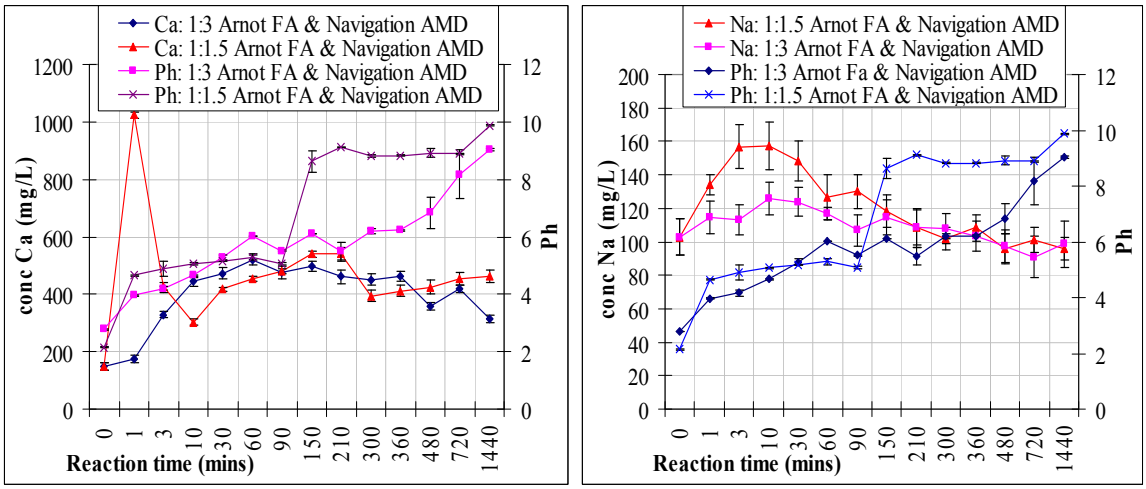

Figure 4.17: Ca and Na concentration in process water for 1:3 and 1:1.5 FA: AMD reactions. Error bar represents 1 SD above and below the mean, n=3.

The solution was highly over-saturated with Na-jarosite (Table 4.5 and 4.6, Fig 4.17), which could account for the decreasing levels of Na. Gypsum was detected by XRD in all the solid residues collected at different contact times (Fig 4.2). The importance of gypsum in the control of Ca and SO_4^{2-} in the early stages of the neutralization process is further confirmed by the immediate precipitation of gypsum in un-acidified process water samples collected within 30 minutes of contact on standing (Fig 4.18). Saturation indices (Table 4.5 and 4.6) show that the solution was slightly over-saturated with gypsum from 3 to 210 minutes of contact indicating that gypsum controlled Ca concentration in process waters.

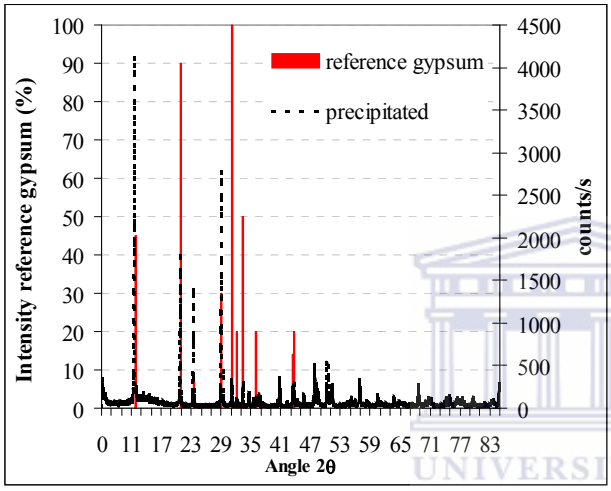

UNIVERSITY of the
WESTERN CAPE

Figure 4.18: XRD spectra of gypsum that precipitated in un-acidified filtered process waters for contact times of 1-30 minutes, reference spectra for pure gypsum superimposed for comparison

However activity-solubility diagrams for both anhydrite and gypsum revealed they were both important in control of Ca^{2+} and SO_4^{2-} at certain pH ranges (Fig 4.19). Contrally to positive identification of gypsum by XRD the solubility diagrams shows that anhydrite was important at pH ranges of 4.17- 5.9 for 1:3 FA: AMD ratio and pH 8.92-9.88 for 1:1.5 FA: AMD ratio. On the other hand gypsum was important as a control at pH 3.96 or there about for 1:3 FA: AMD ratio and pH 6.19-9.12 for 1:1.5 FA: AMD ratio. It seems anhydrite was a stronger control of Ca_{2+} and SO_4^{2-} at high pH while was only important at low pH. But the fact that anhydrite was not detected by XRD could indicate that it was aging to gypsum with time.

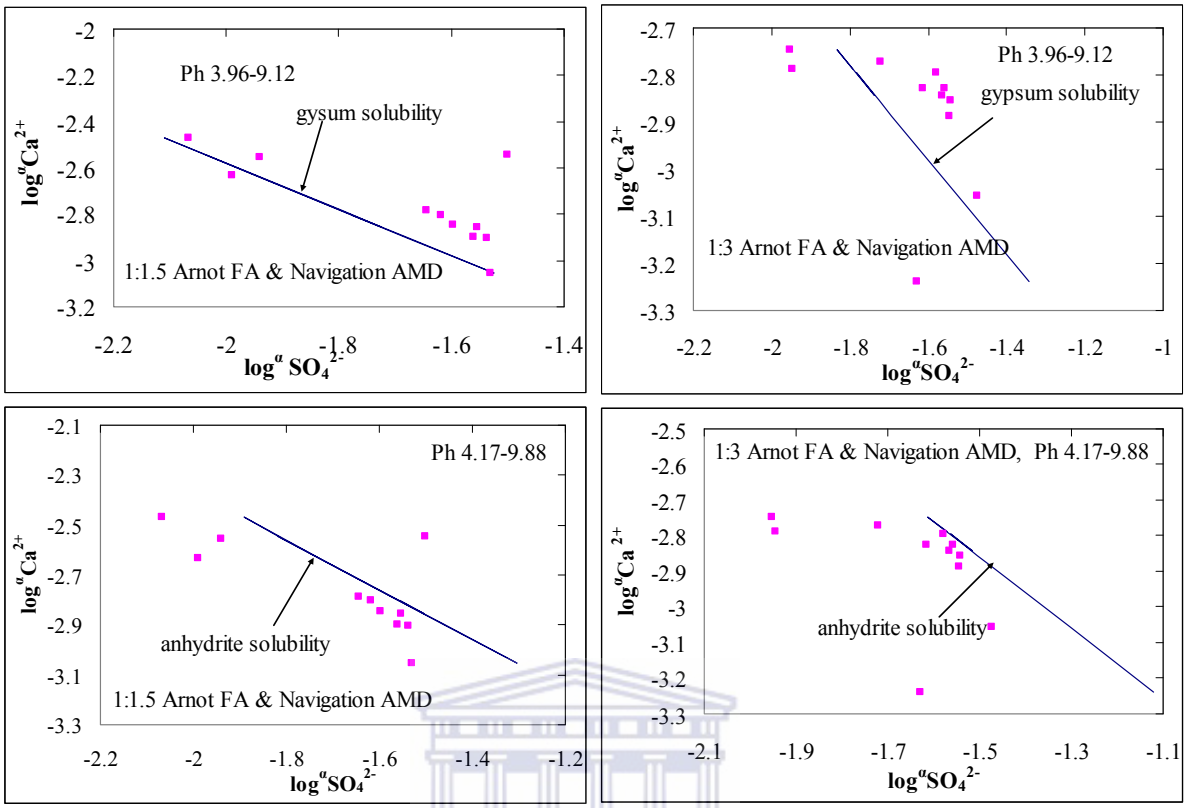

Figure 4.19: Activity-solubiltiy diagrams for anhydrite and gypsum for 1:3 and 1:1.5 FA: AMD ratios.

UNIVERSITY of the
WESTERN CAPE

For both ratios, Mg concentration was observed to increase with contact time, until the mixture attained pH > 7 for 1:3 FA: AMD ratio and pH > 8 for 1:1.5 FA: AMD ratio (Fig 4.20). The fact that the 1:1.5 FA: AMD ratio exhibited higher concentration than the 1:3 FA: AMD ratio indicates that fly ash was the source of Mg and no solubility control existed at pH < 7. Then a significant drop in concentration was observed and a solubility control seems to have developed at pH > 7 (Fig 4.1 and 4.20). The fact that a significant amount of Mg is lost from solution at a lower pH than predicted by thermodynamic calculations (pH=9.8) (Britton, 1956) especially for the 1:1.5 FA: AMD ratio indicates that another Mg-bearing mineral phase and not brucite is controlling Mg concentration. At pH >8.0, saturation index calculations indicate over-saturation with sepiolite (Table 4.5 and 4.6) which could be a control for Mg. Stoessell (1988) observed formation of sepiolite at similar pH conditions. Analysis of the solid residues (SR) by SEM-EDX (Fig 4.5-1A, spot A and B) revealed formation of a Ca, Mg and Si rich gel.

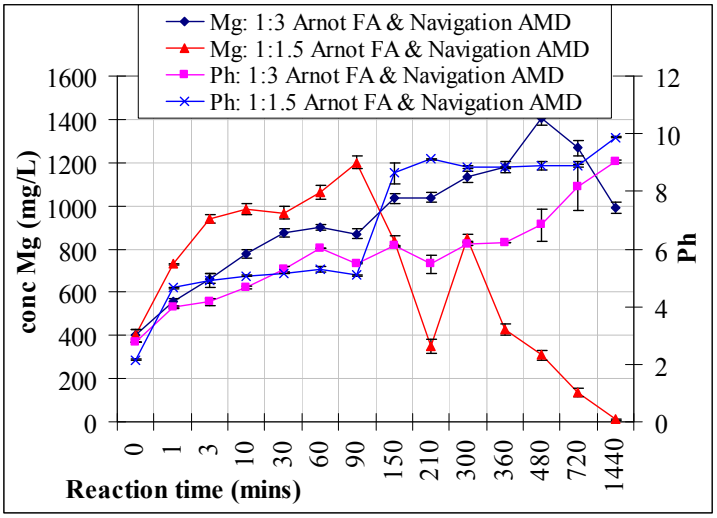

Figure 4.20: Mg concentration in process water for 1:3 and 1:1.5 FA: AMD reactions. Error bar represents 1 SD above and below the mean, n=3.

4.2.5.2.6 Manganese, zinc and copper

Mn concentration was slightly higher for the 1:1.5 FA: AMD ratio upto to 30 minutes of reaction. This was an indication of lack of solubility control and that fly ash was leaching Mn into the reaction mixture. XRF identified Mn in the fly ash samples. However after 30 minutes Mn developed a solubility control which was pH dependent, a slight reduction in Mn concentration for both ratios was observed at pH 5-5.5 (Fig 4.1 and 4.21). This probably indicates possible adsorption of Mn^{2+} on the precipitating amorphous aluminum (oxy)-hydroxides and iron (oxy)-hydroxides at this pH range. Large amounts of Fe can efficiently co-precipitate Mn^{2+} for solutions having Fe: Mn ratios of 2 or greater (Raymond, 2005). According to thermodynamic calculations Mn^{2+} would be expected to be out of solution at pH ≈ 9.0 (Britton, 1956) as $Mn(OH)_2$. The fact that this removal occurs at pH ≈ 5-5.5 indicates that the product cannot be $Mn(OH)_2$. PHREEQC simulation indicated the solution to be under-saturated with pyrochroite ($Mn(OH)_{2(a)}$) for the entire contact time for both ratios. Near complete removal of Mn^{2+} was thereafter observed for both ratios as the reaction mixture attained pH (7-9). According to Hem and Robertson (1990) Mn oxidation rate increases dramatically even under abiotic conditions at pH > 9-9.5 and this is enhanced by the complete removal of Fe in the reaction mixture. An observation of figure 4.9 shows that at pH>8 Fe was precipitated out of solution. Faulkner and Richardson, (1989) observes that Manganese auto-oxidizes at pH values of 8.5 or greater. This observation indicates that Mn^{2+}

UNIVERSITY of the WESTERN CAPE

is being oxidized into an insoluble oxide such as birnessite (MnO_2), todorokite ($Mn^{II}Mn^{IV}{}_3O_7$) and bixbyite (Mn_2O_3) and possibly converting to manganite (MnOOH) over time (Hem, 1964). PHREEQC simulation indicated the solution to be at saturation or over-saturation with manganite at pH > 8.5 for 1:1.5 FA: AMD ratio (Fig 4.2 and Table 4.6).

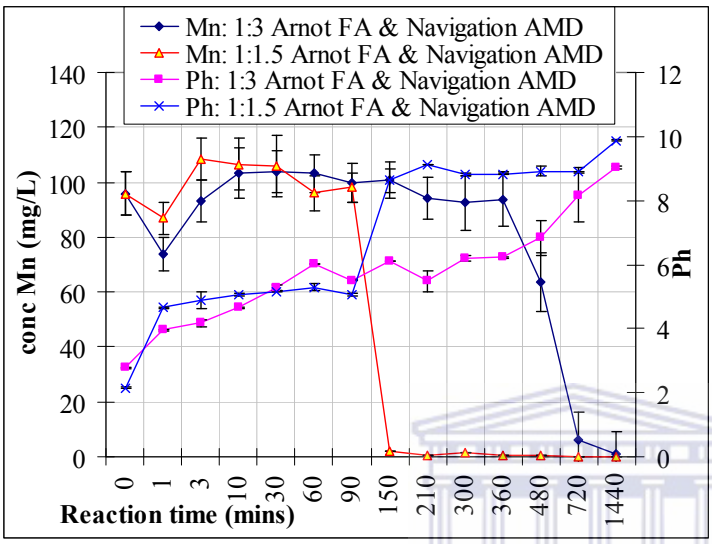

Figure 4.21: Mn concentration in process water for 1:3 and 1:1.5 FA: AMD reactions. Error bar represents 1 SD above and below the mean, n=3.

UNIVERSITY of the
WESTERN CAPE

Cu and Zn show evidence of solubility control when the mixture attains pH (5.5-6) and 5 respectively. According to Britton (1956) Cu hydroxide precipitates at pH ≈5.3, Zn hydroxide at pH ≈ 7.0. Observation of the removal trends for Cu for both ratios indicates that greater than 75 % of the total concentration is out of solution when the mixture attained pH>5.5 (Fig 4.1 and 4.22). At ratio 1:3 a significant drop in concentration is observed at lower pH than 5.5 which indicates another process apart from hydroxide precipitation is responsible for Cu removal. PHREEQC simulation indicates the solution to be under-saturated with Cu $(OH)_2$ for the entire contact time for both FA: AMD ratios (Table 4.5 and 4.6). At pH >5.0 optimum oxidation of Fe^{2+} is achieved and co-precipitation and adsorption by the iron oxy-hydroxides being precipitated could partly account for the removal of Cu (Cravotta and Trahan, 1999). Moreover pK_1= 4.9 for Al hydrolysis and co-precipitation and adsorption of Cu^{2+} and Zn^{2+} with the Al (oxy)-hydroxides is possible. Similarly it can be observed that Zn concentration significantly reduced on the mixture attaining pH > 5.5 (Fig

4.22) which is lower than that predicted by thermodynamic calculations for precipitation of $Zn(OH)_2$ (pH ≈7) (Britton, 1956).

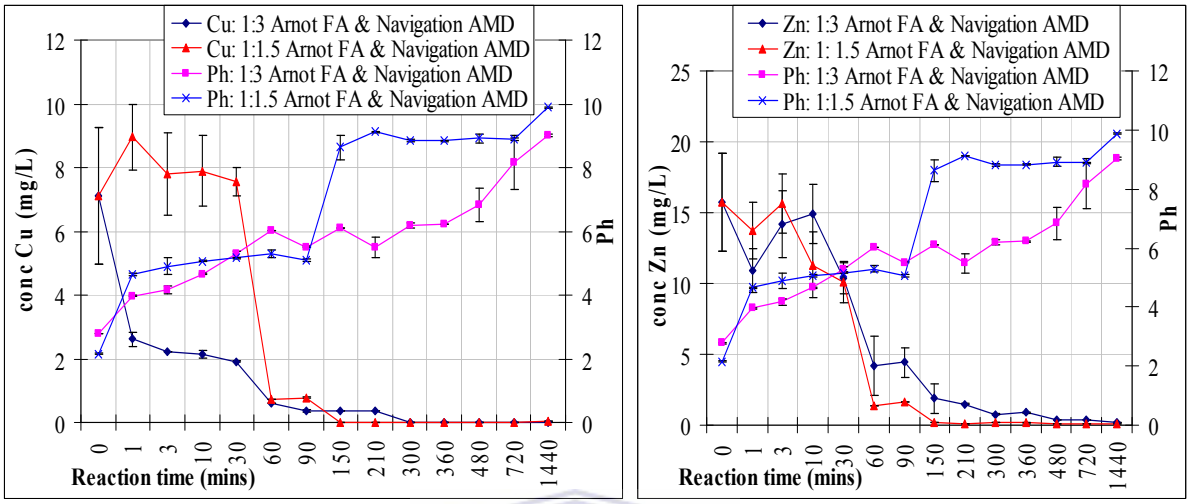

Figure 4.22: Cu and Zn concentration in process water for 1:3 and 1:1.5 FA: AMD reactions. Error bar represents 1 SD above and below the mean, n=3.

PHREEQC simulation indicates the solution to be under-saturated with amorphous $Zn(OH)_2$ for the entire contact time for the two FA: AMD ratios (Table 4.5 and 4.6). PHREEQC simulation indicates the solution to be over-saturated with amorphous $Al(OH)_3$, amorphous $Fe(OH)_3$ and goethite for the entire contact time for the two FA: AMD ratios (Table 4.5 and 4.6). Regression of the log activity data for Al^{3+} and Fe^{3+} suggests control of the reaction mixture chemistry by precipitation of amorphous $Al(OH)_3$ (Fig 4.24) and amorphous $Fe(OH)_3$ (Fig 4.23) for FA: AMD ratios. This indicates that a significant proportion of Cu and Zn could have been removed through adsorption onto the iron oxy-hydroxides or aluminum oxy-hydroxides that formed during the neutralization process. A plot of log activities of Cu^{2+}, Zn^{2+}, Mn^{2+} and Al^{3+} suggests co precipitation or adsorption of Cu^{2+} and Zn^{2+} with Al (oxy)-hydroxides at pH 5.3-6.5 but not for Mn^{2+} (Fig 4.24). Sequential extraction revealed the amorphous fraction to be the most important in retention of Cu and Zn at pH> 5. A similar plot with Fe^{3+} activity explains the trends for Cu^{2+} and Zn^{2+} at pH ≈5 (Fig 4.23).

UNIVERSITY of the WESTERN CAPE

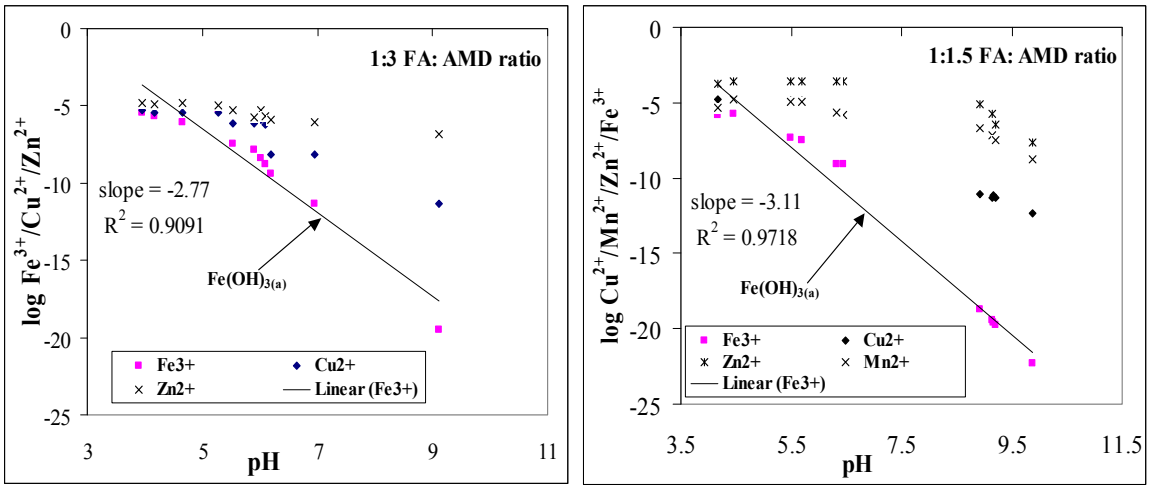

Figure 4.23: Activity diagrams for the variation of ferric ion and Cu^{2+}, Zn^{2+}, and Mn^{2+} with pH in process waters for 1:3 and 1:1.5 FA: AMD ratios.

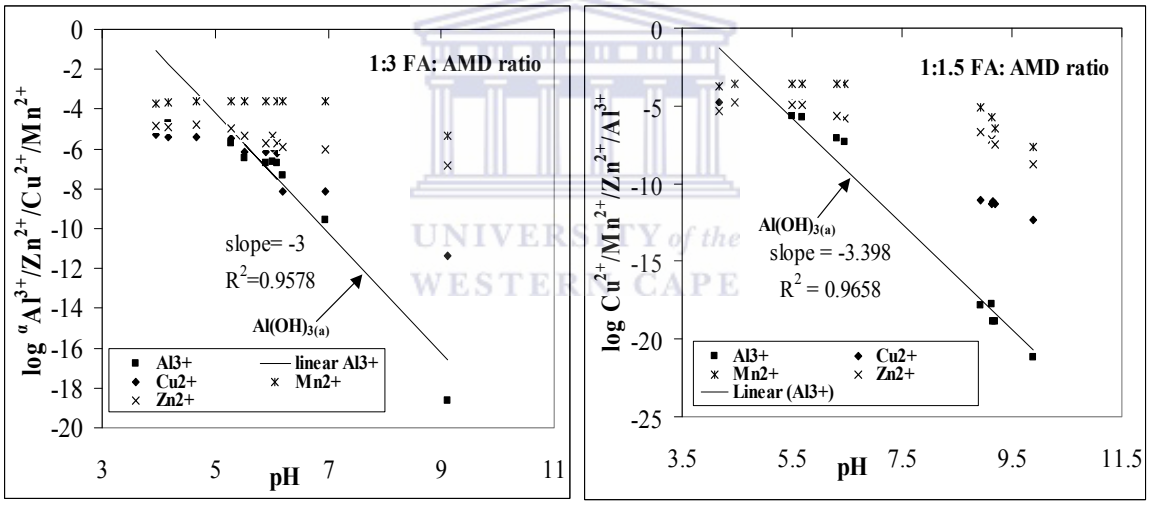

Figure 4.24: Activity diagrams for the variation of aluminum ion and Cu^{2+}, Zn^{2+}, and Mn^{2+} with pH in process waters for 1:3 and 1:1.5 FA: AMD ratios.

The FA: AMD neutralization reactions at the two ratios has aided in showing that solubility controls exist for most of the inorganic contaminants. An important feature is that two groups of contaminant were identified depending on their mode of reaction. Fe, Al and B were observed to have solubility control for the entire reaction time. A second group of elements Ca, Na, Mg, Si, Zn, Cu and Mn were observed to develop solubility controls after initial dissolution from fly ash. PHREEQC modeling suggested co-precipitation or adsorption of Cu and Zn with the precipitating amorphous Fe and Al (oxy) hydroxides.

UNIVERSITY of the WESTERN CAPE

4.2.6 Sequential Extractions

The hypothesis that the toxic trace elements from fly ash and AMD are transformed into into non-labile mineral phases was tested. Six operational defined fractions were chosen based on the work done by Chao (1972), Muller and Seiller (1999), Tessier *et al*. (1979). The residue fraction was ignored since it contains non-labile elements locked up in the residue aluminosilicate matrix of the fly ash and was assumed to be of less significance in dictating the redistribution of the elements in the resulting mineral phases. The results are discussed with respect to the increase in pH and precipitation of Fe, Mn and Al, the main contaminants in AMD. The total extracted concentration in mg/kg dry weight for the six fractions is used to derive the % contribution of each extracted fraction for the solid residues collected at pH 4, 4.92, 6.32 and 9.12. The results of the sequential extraction are presented in Tables 4.9-4.11 below together with the detection limits for each fraction.

UNIVERSITY of the
WESTERN CAPE

The trends of the operational defined totals of the six fractions depict the dissolution and attenuation characteristics of the trace and major elements observed in the treatment process. The operational defined totals of B, Ca and Mo decrease as the pH increases compared to the fly ash. This reflects the initial dissolution of their soluble salts and release into solution. At pH 9.12 B and Ca registered increase in concentration reflecting the removal of the borate-boron and Ca probably as gypsum. The decrease in Mo probably reflects its release into solution as the molybdate ion at circum-neutral to alkaline pH. Mo remained below 0.2 mg/L at pH<6.83 however a significant increase to a maximum of 0.85 mg/L was observed as the pH increased to 9.12. Mo is known to exist as molybdate ion at circum-neutral to alkaline pH (Eary *et al.*, 1990)

Na exhibits increasing content in the solid residues for pH ≤ 4.92 compared to the fly ash (Table 4.7 and 4.8). At pH ≥ 6.32 it remains almost constant. This observation reaffirms the conclusions from the concentration profiles observed in the treatment process and the PHREEQC modeling which showed that at pH ≤ 4.92 Na was removed as Na-jarosite (Table 4.5). Al, Mn and Fe show continuous increase with pH in the solid residues collected reaffirming their continuous removal through precipitation. At pH > 4 the Al concentrations

remains almost constant indicating significant portion of the total Al is removed once the solution attains pH 4. However at pH 9.12 a decrease in content is observed indicating dissolution of the Al (oxy) hydroxides could be occurring at alkaline pH. A significant feature for Fe is observed as the pH increases. At pH 4 the Fe content of the solid residues doubles compared to the fly ash (Table 4.7 and 4.8). This reflects the precipitation of Fe^{3+} from AMD. At pH 6.32 concentration triples compared to the fly ash, which reflects the oxidation, hydrolysis and precipitation of Fe^{2+} once the solution attains pH 6. Si content shows a continuous increase as compared to fly ash and does not vary much as the pH enters the circum-neutral range. PHREEQC modeling predicted Si rich Ca, Mg, Fe gels to be precipitating in the solid residues collected at pH 9.12.

UNIVERSITY of the
WESTERN CAPE

Table 4.7. Sequential extraction for Arnot fly ash (mg/kg dry weight), % contribution of each fraction is presented in the Parenthesis, results presented as mean ± standard deviation (SD) for n=3

Arnot fly ash										
mg/kg dry weight	B	Na	Ca	Si	Al	Mn	Fe	Cu	Zn	Mo
Water soluble fraction	<0.085 (0.05)	29.08±1.45 (0.01)	7138.5±230 (32.0)	10.09±1.21 (0.11)	2.88±0.11 (0.02)	0.04±0.01 (0.02)	15.9±3.45 (0.14)	0.072±0.02 (0.09)	0.115±0.01 (1.4)	0.829±0.03 (3.8)
Exchangeable fraction	35.8±5.5 (19.6)	10.6±1.13 (0.004)	2230.6±120 (10.0)	20.49±3.67 (0.2)	0.209±0.02 (0.001)	0.021±0.005 (0.008)	14.8±4.52 (0.13)	0.095±0.02 (0.11)	1.58±0.01 (2.0)	0.693±0.03 (3.2)
Carbonate fraction	113.7±20.1 (62.1)	258924.2±1500 (98.6)	11774.5±460 (52.8)	1296.6±35.7 13.6)	23.8±2.92 (0.16)	57.6±5.78 (22.3)	<0.559 (0.005)	4.8±1.72 (5.7)	11.2±1.39 (14.0)	2.3±0.13 (10.6)
Mn-oxides	2.2±0.12 (1.2)	192.8±15.7 (0.07)	1073.8±101 (4.8)	273±35.8 (2.9)	274.7±13.7 (1.9)	58.9±7.85 (22.8)	<1.385 (0.01)	1.72±0.32 (2.1)	2.71±0.21 (3.4)	0.147±0.11 (0.7)
Amorphous fraction	31.1±3.6 (16.9)	2875.6±125.6 (1.1)	<60.2 (0.3)	4624.7±234 (48.5)	8537.8±321 (58.6)	91.7±15.4 (35.5)	3159.5±156 (27.6)	63.1±20.4 (75.2)	41.3±12.3 (51.6)	16.8±4.57 (77.6)
Fe-oxides(crystalline)	<0.22 (0.12)	419.7±23.5 (0.2)	<8.76 (0.04)	3319±163 (34.8)	5738.1±238 (39.4)	49.8±12.4 (19.3)	8272.1±360 (72.2)	14.1±2.45 (16.8)	23.2±5.31 (29.0)	0.879±0.05 (4.1)
Operational defined totals	183.11	262451.98	22286.36	9543.88	14577.49	258.06	11464.24	83.89	80.11	21.65

Table 4.8. Sequential extraction for solid residues collected at pH 4 (mg/kg dry weight), % contribution of each fraction is presented in the parenthesis, results presented as mean ± (SD) for n=3

UNIVERSITY of the WESTERN CAPE

Solid residues at 3 minutes reaction time, pH 4										
mg/kg dry weight	B	Na	Ca	Si	Al	Mn	Fe	Cu	Zn	Mo
Water soluble fraction	9.7±2.1 (6.3)	531.1±20.7 (0.2)	3321.2±600.9 (16.2)	9.04±1.56 (0.09)	14.8±2.2 (0.09)	0.014±0.005 (0.005)	<0.586 (0.003)	48±6.75 (37.4)	22.2±3.7 (19.1)	2.17±0.13 (11.6)
Exchangeabe fraction	52.7±3.9 (43.1)	28.6±1.7 (0.01)	6594.1±350 (32.2)	19.3±2.91 (0.2)	1.44±0.06 (0.008)	0.266±0.02 (0.1)	80.9±10.5 (0.37)	2.12±0.3 (1.65)	4.15±0.05 (3.6)	0.738±0.02 (3.94)
Carbonate fraction	51.4±7.9 (33.3)	283561.1±1900 (98.5)	9384.8±207 (45.9)	2162.8±60.9 (20.6)	5568.4±145.6 (32.2)	86±15.5 (32.5)	1379.3±30.7 (6.3)	5.11±0.32 (4.0)	7.8±1.52 (6.7)	0.763±0.04 (4.1)
Mn-oxides	<0.201 (1.3)	183.1±21.2 (0.06)	1082.4±70.2 (5.3)	477±13.4 (4.5)	709.9±30.5 (4.1)	63.1±12.2 (23.9)	<1.385 (0.006)	0.457±0.03 (0.36)	2.6±1.2 (2.3)	0.096±0.015 (0.5)
Amorphous fraction	40.1±4.3 (26.0)	3210.9±138 (1.11)	<60.2 (0.3)	6337.1±189 (60.4)	7450.4±280 (43.1)	77.1±20.5 (29.2)	9576.7±254 (44.0)	61.7±13.4 (48.0)	66.1±5.1 (57.2)	14.4±3.8 (76.8)
Fe-oxides (crystalline)	<0.22 (0.1)	397.1±10.6 (0.13)	<8.76 (0.04)	1489.3±103 (14.2)	3557.7±145 (20.6)	38±3.54 (14.4)	10746.9±432 (49.3)	11.1±1.4 (8.6)	12.8±2.6 (11.1)	0.576±0.06 (3.0)
Operational defined totals	154.32	287911.96	20451.46	10494.54	17302.64	264.48	21785.77	128.49	115.65	18.74

Table 4.9:. Sequential extraction for solid residues collected at pH 4.92 (mg/kg dry weight), % contribution of each fraction is presented in the parenthesis, results presented as mean ± (SD) for n=3

Solid residues at 30 minutes reaction time, pH 4.92										
mg/kg dry weight	B	Na	Ca	Si	Al	Mn	Fe	Cu	Zn	Mo
Water soluble fraction	17.3±3.2 (15.3)	99.8±18.7 (0.03)	7126.9±900 (28.1)	3.8±0.95 (0.04)	24.7±3.5 (0.1)	0.032±0.01 (0.01)	11.7±2.34 (0.06)	0.132±0.02 (0.2)	0.724±0.01 (0.65)	3.8±0.41 (22.9)
Exchangeable fraction	32±2.89 (28.3)	23±1.87 (0.007)	6928±101 (27.3)	12.3±2.11 (0.1)	1.1±0.12 (0.006)	0.369±0.03 (0.1)	73.6±9.7 (0.36)	0.051±0.01 (0.08)	3.09±0.11 (2.8)	0.598±0.03 (3.6)
Carbonate fraction	62±4.9 (54.8)	308666.8±1300 (98.8)	9897.7±308 (39.0)	2408±87 (24.4)	5820.8±180 (33.0)	96±21 (36.1)	992.9±66 (4.8)	4.08±0.32 (6.2)	9.5±0.21 (8.5)	0.487±0.002 (2.94)
Mn-oxides	<0.201 (0.2)	187±30.7 (0.06)	1372.1±80.4 (5.4)	524.8±25.6 (5.3)	858.6±20.4 (4.9)	60.1±5.8 (22.6)	<1.385 (0.007)	1.2±0.13 (1.8)	8.25±1.45 (7.4)	0.115±0.021 (0.7)
Amorphous fraction	<1.51 (1.3)	3004.4±209 (0.96)	<60.2 (0.2)	5303.7±302 (53.8)	7615.5±411 (43.1)	71.2±15.8 (26.8)	8025.8±312 (38.9)	47.7±10.2 (72.5)	70.2±7.8 (62.9)	11.02±3.12 (66.5)
Fe-oxides(crystalline)	<0.22 (0.2)	374.1±54.2 (0.1)	8.76 (0.03)	1608.8±120 (16.3)	3341.6±235 (18.9)	38.3±5.4 (14.4)	11529.2±560 (55.9)	12.6±2.2 (19.2)	19.8±3.5 (17.7)	0.562±0.021 (3.4)
Operational defined totals	113.2	312355.1	25393.7	9861.4	17662.3	266	20634.6	65.8	111.6	16.6

Table 4.10: Sequential extraction for solid residues collected at pH 6.32 (mg/kg dry weight), % contribution of each fraction is presented in the parenthesis, results presented as mean ± (SD) for n=3

UNIVERSITY of the WESTERN CAPE

Solid residues at 360 minutes reaction time, pH 6.32										
mg/kg dry weight	B	Na	Ca	Si	Al	Mn	Fe	Cu	Zn	Mo
Water soluble fraction	16.4±2.6 (18.8)	100.1±10.6 (0.04)	8377.2±210 (46.3)	6.5±1.21 (0.06)	8.5±2.1 (0.05)	0.006±0 (0.002)	<0.586 (0.002)	0.04±0.001 (0.03)	0.778±0.04 (0.6)	2.33±0.05 (12.9)
Exchangeable fraction	0.031±0.002 (0.04)	0.022±0.002 ….	6.57±0.13 (0.04)	0.012±0 (0.001)	0.001±0 …….	0.0003±0 …….	0.07±0.013 (0.0002)	<0.001 (0.002)	0.003±0 (0.003)	0.0006±0 (0.003)
Carbonate fraction	66.2±7.7 (75.9)	263508.8±1400 (98.6)	8302.8±369 (45.9)	2287.3±80.3 (21.1)	5028.6±156 (28.3)	108.7±10.6 (33.5)	2248.8±39.2 (6.83)	5.85±0.05 (5.3)	8.09±1.4 (6.7)	0.268±0.02 (1.5)
Mn-oxides	<0.201 (0.2)	129.2±15.8 (0.05)	1331±101 (7.4)	524.2±38.2 (4.8)	803.9±90.8 (4.52)	84.6±34.5 (26.1)	<1.385 (0.004)	8.25±1.21 (7.5)	9±1.3 (7.5)	0.018±0.002 (0.1)
Amorphous fraction	4.12±0.14 (4.72)	3080.7±231.2 (1.2)	<60.2 (0.33)	7085.9±122 (65.5)	9835.6±270 (55.3)	116.6±20.1 (35.0)	28830.2±463 (87.6)	84.9±9.3 (77.1)	87.7±10.6 (73.0)	15.2±2.7 (84.4)
Fe-oxide(crystalline)	<0.22 (0.2)	449.3±37.4 (0.2)	<8.76 (0.05)	917±35.7 (8.5)	2095±20.2 (11.8)	14.3±1.5 (4.41)	1844.8±115 (5.6)	11.08±0.98 (10.1)	14.5±2.4 (12.1)	0.187±0.021 (1)
Operational defined totals	87.2	267268.1	18086.5	10820.9	17771.6	324.2	32925.8	110.1	120.1	18

Table 4.11. Sequential extraction for solid residues collected at pH 9.12 (mg/kg dry weight), % contribution of each fraction is presented in the parenthesis, results presented as mean ± (SD) for n=3

Solid residues at 1440 minutes reaction time, pH 9.12										
mg/kg dry weight	B	Na	Ca	Si	Al	Mn	Fe	Cu	Zn	Mo
Water soluble fraction	33±3.6 (20.1)	112.3±16.8 (0.04)	8052.4±190 (29.2)	5.3±0.5 (0.05)	7.3±1.1 (0.04)	0.028±0.001 (0.005)	15.4±2.4 (0.04)	0.08±0.002 (0.08)	0.821±0.020 (0.7)	1.45±0.05 (11.1)
Exchangeable fraction	19.8±3.1 (12.1)	29.2±1.5 (0.01)	10730.5±400 (38.8)	23.8±2.3 (0.2)	0.452±0.04 (0.003)	0.23±0.024 (0.04)	<0.586 (0.002)	0.06±0.012 (0.06)	3.23±0.06 (2.63)	0.217±0.014 (1.7)
Carbonate fraction	86.3±9.2 (52.7)	261869.9±2300 (98.6)	6424.4±401 (23.3)	2070.5±79.4 (20.4)	5071.9±122 (30.1)	147.2±31.2 (26.9)	1325.6±37.3 (3.8)	3.67±0.04 (3.6)	11.03±2.34 (9.0)	0.145±0.004 (1.1)
Mn-oxides	2.33±0.4 (1.4)	142.9±23.5 (0.1)	1422.3±90.3 (5.1)	538±23.4 (5.3)	824.6±40.5 (4.9)	234.4±12.5 (42.8)	<1.385 (0.004)	1.72±0.14 (1.7)	11.2±2.14 (9.1)	0.192±0.012 (1.5)
Amorphous fraction	<1.51 (0.9)	2865.9±1.38 (1.1)	<60.2 (0.2)	6260.8±188 (61.5)	8452.5±267 (50.1)	149.1±23.5 (27.2)	31467.8±503 (89.9)	85.5±15.1 (84.1)	82.7±11.2 (67.5)	10.8±1.2 (82.4)
Fe-oxides (crystalline)	21±4.1 (12.8)	544.4±54.2 (0.2)	933.2±13.8 (3.4)	1275.5±94.1 (12.5)	2509.9±236 (14.9)	16.8±1.1 (3.1)	2197.6±223.6 (6.3)	10.7±1.2 (10.5)	13.5±0.78 11.0	0.304±0.002 (2.32)
Operational defined totals	163.94	265564.6	27623	10173.9	16866.7	547.8	35008.4	101.7	122.5	13.1

Table 4.12: Detection limits (mg/kg dry weight) calculated for each fraction

UNIVERSITY of the WESTERN CAPE

Detection limits for each fraction										
mg/kg dry weight	B	Na	Ca	Si	Al	Mn	Fe	Cu	Zn	Mo
Water soluble fraction	0.0851	9.2761	3.3926	0.7170	0.0179	0.0047	0.5864	0.0010	0.0069	0.0002
Exchangeable fraction	0.0851	9.2761	3.3926	0.7170	0.0179	0.0047	0.5864	0.0010	0.0069	0.0002
Carbonate fraction	0.0812	8.8438	3.2345	0.6836	0.0171	0.0045	0.5591	0.0009	0.0066	0.0002
Mn-oxides	0.2010	21.9081	8.0126	1.6935	0.0423	0.0112	1.3849	0.0023	0.0164	0.0004
Amorphous fraction	1.5102	164.5670	60.1880	12.7209	0.3179	0.0841	10.4033	0.0175	0.1230	0.0031
Fe-oxides(crystalline)	0.2199	23.9597	8.7629	1.8521	0.0463	0.0122	1.5146	0.0025	0.0179	0.0004

4.2.6.1 B and Mo concentration profiles

In the fly ash 62.1% of the B is present in the carbonate fraction and a significant fraction is present in the exchangeable (19.6 %) and amorphous fraction (16.9 %) (Table 4.7) Several authors have observed association of borate-boron with calcite (Akira *et al*., 2005; Kitano *et al*., 1978) and this probably explains the high concentration observed in the carbonate fraction. An observation of Ca trends indicate occurrence of 52.8 % in the carbonate fraction which collaborates the borate-boron-calcite association. A significant (77.6 %) of Mo is present in the amorphous fraction probably locked up in the amorphous aluminosilicate glass matrix and also in the carbonate fraction (10.6 %).

An observation of the sequential extraction results (Tables 4.7-4.11) indicates that B is being re-distributed among three fractions: exchangeable, carbonate and amorphous oxides as the pH increases. The increase in B concentration in the exchangeable fraction probably reflects the adsorption of released B $(OH)_3$. As the pH increases to > 5 most of the B gets partitioned to the water soluble fraction with a significant portion being retained by the crystalline Fe-oxide fraction.

UNIVERSITY of the
WESTERN CAPE

Mo seems to be redistributed within two main fractions: water soluble and the amorphous oxide (Table 4.7-4.11). As the pH increases and dissolution of the amorphous glass phase in the fly ash occurs, Mo is translocated to the water soluble fraction. This could be a limitation in the application of the fly ash in this process. However at pH 6.32 a significant portion (84.4 %) of the total Mo is retained in the amorphous precipitates (Table 4.10). This indicates that hydrolysis and precipitation of Fe^{2+} has an impact in the attenuation of Mo and tends to confirm that Mo was indeed removed formation of metal molybdates...

4.2.6.2 Ca and Na concentration profile

Ca sequence in the extracted fractions represents redistribution between three phases: water soluble, exchangeable and carbonate (Table 4.7-4.11). In the fly ash Ca is highest in carbonate fraction (52.8 %) indicating its presence as $CaCO_3$ and water soluble fraction (32 %) as CaO. As dissolution occurs on contact with AMD redistribution occurs in the three fractions, water soluble and the carbonate fractions still retain a significant proportion of the

total Ca. Retention of Ca in the carbonate fraction despite dissolution at acidic pH indicates that formation of calcite due to ingress of CO_2 was taking place. Formation of soluble $CaSO_4$ at acidic pH and high SO_4^{2-} content could also account for the increased retention in the water soluble fraction (Table 4.8). Anhydrite was predicted to be controlling Ca2+ and SO42- concentrations at pH 4.17 for 1:3 and 8.92-9.88 for 1:1.5 FA: AMD ratios (Fig 4.19). At pH 9.12 the exchangeable fraction becomes significant in retention of Ca as water soluble and carbonates fractions (Table 4.11).

Na shows redistribution amongst three fractions: water soluble, amorphous oxides and crystalline Fe-oxide. In the fly ash Na is mainly present in the carbonate fraction (98. 6 %) which suggests its occurrence as a carbonate. Na remains retained in the carbonate fraction as the pH increases to 9.12, but the % retained in the amorphous fraction is observed to increase to 1.1 % (Table 4.11). However it should be noted that there is release of Na into the reaction mixture judging by the decreasing operational defined totals (Tables 4.7-4.11). The high retention of both elements in the carbonate fraction at pH 4 (Table 4.8) suggests that at 3 minutes of reaction time due to inadequate mixing local pockets of high alkalinity existed especially at the particle surfaces and ingress of CO_2 accompanied by the formation of CO_3^{2-} could have led to the precipitation $CaCO_3$ and Na_2CO_3.

4.2.6.3 Al, Fe, Mn and Si concentration profiles

The distribution of Al, Fe and Mn in the fly ash indicates their occurrence in the amorphous aluminosilicate matrix and in crystalline Fe and Mn-bearing phases. On contact with AMD these solid phases release Fe, Mn and Al into solution which on elevation of pH precipitates to form amorphous (oxy) hydroxides and probably crystalline oxides. The trends for the three elements represent relocation to the amorphous fraction as the pH of the reaction mixture increases (Table 4.7-4.11).

The high proportion of Al (39.4 %) in Fe-oxide fraction in fly ash represents its occurrence as $Ca_6Al_4Fe_2O_{15}$ crystalline phases (Mattigod *et al*., 1990) and the decrease in content in this fraction as the pH increases probably represents its dissolution and relocation to the amorphous Fe-Al hydroxide phases. At pH 4 a significant portion (32.2 %) is retained in the carbonate fraction. The solid residues at pH 4 were collected after only 3 minutes of reaction time which means pockets of high alkalinity accompanied by ingress of CO_2 existed

especially at the surface of fly ash particles that could have led to local precipitation of metal carbonates (Table 4.8).The presence of Al in the this fraction probably represents an admixture with an Al-mineral phase. At pH > 6.32 the amorphous fraction became the dominant phase retaining Al, indicating a significant proportion of Al from AMD was hydrolyzing to form amorphous Al-(oxy) hydroxides. However the carbonate fraction still retains a significant proportion at this pH range (28.3-30 %) (Table 4.10-4.11).

The high % (22.3) of Mn in the carbonate and Mn-oxide fraction (22.8 %) (Table 4.7) indicates the presence of Mn in the fly ash as $MnCO_3$, MnO or Mn_3O_4 respectively (Eary *et al*., 1990). The 19.3 % present in Fe-oxide fraction represents Mn present in the spinel type solids which include magnetite, ferrite and hematite (Eary *et al*., 1990). A significant portion (35.5 %) is locked up in the amorphous aluminosilicate matrix (Table 4.7). At pH 4-5 there is increased content in the carbonate fraction for reasons explained in sections for Na and Ca. At pH 6.32 the amorphous and carbonate fractions (Table 4.10) become significant in the retention of Mn. However as the solution attains pH 9.12 the Mn-oxide and amorphous fractions become important (Table 4.11). At pH > 7 Mn^{2+} oxidation is fast (Eary *et al.*, 1990) and PHREEQC modeling predicted precipitation of manganite (MnOOH) (Table 4.6). However the author is cautioned that PHREEQC predicts over saturation of manganite due to the thermodynamics at assumed equilibrium of this phase.

Fe is present in fly ash mainly as crystalline Fe-oxides (72.2 %) and in amorphous form probably as Ca, Al ferric phases (Mattigod *et al*., 1990). These phases on contact with highly acidic AMD undergo dissolution releasing Fe^{3+} into the reaction mixture. This is observed in the decreased content in the Fe-oxide and amorphous fraction at pH 4 (Table 4.7). However a significant proportion is relocated to the carbonate fraction at this pH reaffirming the existence of local pockets of high alkalinity and ingress of CO_2 leading to the precipitation of metal carbonates. As the solution attains pH 6.32 the amorphous fraction becomes significant in retention of Fe (87.6-89.9 %) (Table 4.10-4.11). This coincides with the pH of optimum oxidation and hydrolysis of Fe^{2+} which indicates that it's hydrolyzing mainly to amorphous Fe (oxy) hydroxides.

The Si trend shows a redistribution amongst three fractions as the fly ash interacts with AMD: amorphous, Fe-oxide and carbonate fractions. At pH > 4 the amorphous fraction becomes most important in retention of Si.

4.2.6.4 Cu and Zn concentration profile

Cu profile shows redistribution within three fractions: amorphous, water soluble and Mn-Fe-oxide fraction as the pH increases (Table 4.7-4.11). The high (75.2 %) in the amorphous fraction in fly ash indicates the presence of Cu in the amorphous aluminosilicate glass matrix (Hullet *et al*., 1980) and 16.8 % in Fe-oxide fraction shows the incorporation in the magnetic fraction consisting of spinel type solids such as magnetite, ferrite and hematite (Hullet *et al.*, 1980). At pH 4 dissolution of the Cu bearing mineral phases is observed to occur with relocation to the carbonate fraction due to the local development of high concentrations of CO_3^{2-} due to ingress of CO_2. At pH > 5 the amorphous and Fe-Mn-oxide fraction become significant in retention of Cu indicating the importance of adsorption processes in controlling the attenuation of Cu. Zn is observed to be undergoing redistribution in amorphous, Fe, Mn-oxides fractions. Carbonate fraction seems to be important at pH 4 and as the solution attains pH > 5 (Table 4.9-4.11). The significance of the three fractions: amorphous, Mn Fe-oxide indicates the importance of the adsorption processes in controlling the attenuation of Zn as the pH increases.

UNIVERSITY of the
WESTERN CAPE

In conclusion it can be ascertained that the alkali metals Na, and Ca after the initial dissolution are mainly retained in the carbonate and amorphous fractions with a significant fraction also retained in water soluble fraction. Mo was retained in the water soluble fraction at pH > 4. The retention in the water soluble fraction presents a risk in the disposal of these solid residues due to possible re-solubilization on contact with water or acidic leachates. All the elements indicated a significant retention in the carbonate and amorphous fractions which implies their non-lability unless in contact with aggressive acidic leachates. Amorphous fraction was observed to be the most important in retention of the major and minor contaminants at pH > 6.32 which implies that the concentration of total Fe and Al in the AMD being treated will have a direct effect on the efficiency of the process.

4.3 Conclusions

The objective of this study was to evaluate the chemistry of the resulting process water as the sulphate and metal rich AMD interacts with fly ash, and to relate the solution chemistry to the formation of mineral phases. Understanding the behavior and ultimate fate of the SO_4^{2-}, and major elements in AMD and fly ash during the treatment process is a major determinant in usage of fly ash as a neutralization agent.

The dissolution and hydrolysis of oxide components such as CaO and MgO from fly ash on contact with AMD contributes to an increase in solution pH. As a consequence an increase in dissolved concentration of Ca and Mg is observed as the reaction progresses. There are two factors that finally dictate the final pH of the process waters, the FA: AMD ratio, and contact time.

Increased removal of elements such as Mg, Mn, Al, Si, total Fe, Zn, Cr and Cu was observed at 1:1.5 (FA: AMD) ratio indicating the importance of precipitation reactions in this process.

UNIVERSITY of the
WESTERN CAPE

The elements Fe, Al and SO_4^{2-} appear to have solubility control for the entire contact time investigated. Calculated SI values and mineralogical analysis indicate that SO_4^{2-}, Fe and Al were indeed controlled by mineral solubility. Al concentrations were controlled by secondary phases such as boehmite, basaluminite and gibbsite, Fe by amorphous $Fe(OH)_3$ and goethite, Ca and SO_4^{2-} by both anhydrite and gypsum. The elements Na, Ca, Mg, B, Mo, Si, Mn, Zn and Cu concentration showed development of solubility control at certain contact times after the initial dissolution. It is probable that they were present as soluble salts and, on dissolution, interact with components in AMD to form new stable mineral phases which control their concentrations. Na was controlled by precipitation Na-jarosite at pH < 6.45. B probably by adsorption on to the precipitating Al and Fe-(oxy) hydroxides at pH <4 and incorporation in carbonates at pH > 8. Mo and As were probably mainly attenuated by precipitation of metal molybdates and metal arsenites/arsenates respectively...

Mn, Zn and Cu were removed from solution at a lower pH (5.5-7.0) than predicted by thermodynamic calculations indicating that other processes such as adsorption and co-

precipitation were responsible for increased metal removal. PHREEQC simulation however indicated the solution to be at saturation or at over-saturation with manganite at pH > 8.5 for 1:1.5 FA: AMD ratio indicating increased oxidation of Mn^{2+} and formation of insoluble oxides.

Fe^{2+} was removed through oxidation and subsequent hydrolysis and this was evident when the mixture attained pH.5.5. A corresponding decrease in SO_4^{2-} concentration was observed indicating the relevance of the iron-(oxy)-hydroxides in SO_4^{2-} removal in this process. This was clearly evident at 1:1.5 FA: AMD ratio with levels dropping to minimum of 3178 mg/L on the mixture attaining pH>5.5 as compared to 1:3 ratio.

Sequential extraction revealed that all the elements exhibited a significant retention in the carbonate and amorphous fractions which implies their non-lability unless in contact with aggressive acidic leachates. Amorphous fraction was observed to be the most important in retention of the major and minor contaminants at pH > 6.32 which implies that the concentration of total Fe and Al in the AMD being treated will have a direct effect on the efficiency of the process.

UNIVERSITY of the
WESTERN CAPE

Chapter Five

Contaminants attenuation by Fly ash and its derivatives: A column leaching study.

Abstract

A treatment model was developed in which Fly Ash (FA) is used to neutralize Acid Mine Drainage (AMD) from coal mines. This treatment option promises to be a substitute for the currently used lime or limestone based AMD treatment. This study also looked at the suitability of using solid residues (SR) recovered from the process as a backfill material. A column leaching study of the solid residues blended with varying amounts of fly ash (5 %, 25 %, 40 %) and 6 % Ordinary Portland Cement (OPC) has been carried out to assess the contaminant attenuation with time. The column solid cores acidified in a stepwise fashion, exhibiting three buffer zones. Initial leachate pHs were as follows: FA>SR +6 % OPC>SR+40 % > SR+25 %>SR ≈ SR+5 %. The SR alone and SR blended with fly ash appeared to have a significant buffering capacity, maintaining neutral to alkaline pH for an extended period of time (97-110 days) as opposed to OPC blended SR. Dissolution of CaO in fly ash and solid residues blended with fly ash impacted high pH in the initial leachates while hydrations reactions in OPC blend solid residues contributed to high initial pH. Dissolution of $SiO_{2(amorphous)}$ and mullite in the solid residues contributed to sustained buffering at pH 7-9.5 for solid residues and fly ash blended solid residues. Encapsulation of solid residue particles by the calcium silicate hydrate gels (CSH) in OPC blended solid residues reduced interaction of particles with SAMD hence the buffering at pH 7-9.5 was not observed.

The fly ash and OPC blend solid residues exhibited decontamination efficiencies of (82-99 %) for Al, Fe, Mn and SO_4 over the study period. However the OPC blend SR exhibited high attenuation efficiency even as the pH dropped to below 4. Contaminants attenuation of the solid cores depended on four factors: a] increasing the pH to alkaline or circum-neutral values, b] sustainability of the pH at circum-neutral values for FA blend solid residues, c] capacity to induce precipitation of amorphous Al, Fe, Mn (oxy) hydroxides, Ca-Si-Al-O, Ca-Al-O rich gels, d] capacity to release Ca which was dependent on % FA in the blend.

The pH was observed to be the main determining factor in contaminants attenuation, concentration increased in the leachates once the leachate pH dropped to below 4. Ion activity diagrams revealed that pH and SO_4^{2-} concentration in the leachates had an impact on

the mineral phases controlling Fe and Al. Mn^{2+} chemistry was controlled by pyrolusite (MnO_2) at pH > 7.5 and manganite (MnOOH) at pH 5.94-8.62.

Crystalline phases enriched in Al, Fe, S and O were observed to have precipitated in the leached solid residue cores (SR). Their elemental contents suggests them to be Al, Fe-hydroxysulphates or Al, Fe, Mn-(hydr) oxides. In the SR + 6 % OPC solid cores, EDX analysis revealed that CSH gels and calcium aluminate hydrate gels were being precipitated. These gels were either incorporating Fe, Mg, Mn in their matrix or encapsulating the solid residue particles that were rich in these elements.

Sequential extractions revealed that the amorphous fraction was the most important in retention of the major contaminants and was most enhanced in the OPC blend solid residues due to formation of amorphous CSH gels.

The OPC blend solid residue slurries developed unconfined compressive strength (UCS) (2-3 Mpa) comparable to paste formulated from sulphidic rich mine tailings. The study confirms that the solid residues can be used for backfilling.

If placed in a mining area generating AMD, these solid residue blends could provide a passive method of treatment of polluted mine water and also provide support for the overburden.

UNIVERSITY of the
WESTERN CAPE

Academic Output

M.W. Gitari; L.F. Petrik; O. Etchebers; V.R. Kumar Vadapalli; D.L. Key, and E. Iwuoha. Utilization of fly ash for remediation of coal mines waste water: Reaction on AMD and possible backfilling with residual solids. A **paper** *presented at The South African Institute of mining and Metallurgy. Colloquim:* Sustainable development in the life of coal mining in South Africa, 13th July 2005, Carnival city, Boksburg.

M.W. Gitari L.F. Petrik; O.Etchebers; D.L, Key; C. Okujeni and E. Iwuoha.Contaminant mobility in fly ash amended Acid mine drainage/fly ash co-disposal solid residues: A column leaching Study. A **paper** *presented in the East and Southern Africa Environmental chemistry Workshop (ESAECW) and the Sixth Theoritical Chemistry Workshop in Africa (TCWA)* on 5th –9th Dec 2005, Windhoek, Namibia

5 Introduction

Backfilling in addition to providing support to pillars, reducing subsidence, reducing void volume, also plays a role in mitigating the environmental concerns of underground fires and the future production of AMD as well as neutralizing existing AMD (USEPA, 1999). South African FA was already investigated as a backfill material and successfully applied on a few occasions (Ilgner, 2000; Ilgner, 2002). However no studies were found relating to the possible use of solid residues (SR) resulting from FA, obtained after reaction with AMD, for backfill.

In addition to passively treating the AMD percolating through, a potential backfill material should also develop strength to support overburden in backfill areas.

Benzaazoua *et al*. (2002) points out that waste materials used for backfilling are often mixed with very lean (1-7 %) cement or other pozzolanic binders to improve their strength properties. In this context the solid residues were also modified with 6 % Ordinary Portland Cement (OPC) in an attempt to understand the binder matrix effect on the treatment of SAMD. A preliminary investigation of the strength development of the solid residues was also carried out over a one year period.

Significant questions exist regarding the use of fly ash as a backfill material either alone or blended with binders such as OPC in coal-mined areas, particularly the long-term effects on water quality if large quantities of this material was placed underground. In that context the main objectives of this part of the study were:

i. to determine the effects of blending fly ash/acid mine drainage solid residues(SR) with unreacted fly ash and Ordinary Portland cement on the quality of acid mine drainage (AMD) leachates.

ii. understand the mechanisms of acidity attenuation by the solid residues, contaminant attenuation mechanisms and leaching characteristics as the SAMD percolated through.

iii. develop a mineralogical model for the dynamic L/S system

iv. to relate these effects to the possible environmental ramifications of this practice in coal mining areas.

v. assess the strength development of the OPC blend solid residues (SR) slurries formulated with AMD/FA process waters.

In this chapter the results of a six months study of the interaction of simulated acid mine water with the FA/AMD solid residues is presented.

5.1 Materials and Methods

5.1.1 Sample Collection, preparation of Solid Residues and Column Assembly set-up

Fly Ash samples were collected at Arnot power stations in South Africa. The chemical composition of FA and solid residues was ascertained by X-ray fluorescence spectroscopy (XRF) by fusing with lithium metaborate. The solid residues were dried for 12 hours at 105^{o}C and ground to a fine powder before analysis. AMD was sampled at Navigation plant toe seep dam (Landau colliery). The solid residues were generated by reacting Arnot fly ash and Navigation AMD in a ratio (FA: AMD) of 1:3 using a 150 litre capacity agitator at center for scientific and industrial research (CSIR) in Pretoria (South Africa) (Fig 5.1). The mixture was stirred at a rate of 1000 RPM, the EC and pH were monitored during the course of the reaction. The reaction was stopped when a pH of 9.20 was attained. The mixture was allowed to settle and the liquid phase was drained. The solids were then air dried. The solids were crushed and mixed thoroughly to attain homogeneity and thereafter placed in columns. The diameter of the columns was constant at 101 mm (10.1 cm) but the length covered by each blend varied. The solid residues were packed into columns in small portions of 500 gms. After each addition the material was then gently pressed with a 1 L PVC bottle in order to pack sediments. Each column was duplicated for each different composition of solid material (Table 5.1 and 5.3). Calculation of the loading weights in the columns was done taking into account the moisture content of the solid residues. The moisture content was determined by oven drying the wet solid residues at 105^{o}C for 12 hours. The % moisture content was 12.09 ± 0.01 %.

A whatman filter paper cut to fit the PVC pipe was inserted on the top and bottom of tube on which a plastic grid with 8 evenly spread holes were placed, this were meant to hold the fine particles and spread the leachate respectively. Height of packing was as follows: FA-13 cm, SR-11 cm, SR + 5 % FA-11.8 cm, SR + 25 % FA- 15 cm, SR + 40 % FA- 18.8 cm and SR + 6 % OPC-12.8 cm.

Figure 5.1: The 150 litre capacity agitator used to generate the solid residues used for the drainage experiments.

Table 5.1: Column compositions and total mass (kg, dry weight basis), drainage volumes (L) and liquid to solid ratios for each column.

UNIVERSITY of the
WESTERN CAPE

Column number	Column composition	Mass solids (kg)	SAMD added per drainage (L)	Total SAMD added after 16 drainages (L)	Liquid:Solid ratio per drainage (L/kg)	Total Liquid:Solid ratio (L/kg)
1	Fly ash (FA)	1.000	0.350	5.60	0.350	5.600
2	Solid residue (SR)	0.897	0.350	5.60	0.390	6.243
3	SR + 5 % FA	0.925	0.350	5.60	0.378	6.054
5	SR + 25 % FA	1.172	0.450	7.20	0.384	6.143
6	SR + 40 % FA	1.465	0.555	8.88	0.379	6.061
8	SR + 6 % OPC	0.935	0.350	5.60	0.374	5.989

5.1.2 Simulated AMD preparation and Drainage

Simulated AMD was used in the column study because of logistical constraints and to exclude variability. The model solutions simulating acid mine drainage were formulated using soluble salts of the major elements in AMD (Fe, Al, Mn and SO_4^{2-}). The simulated AMD used in the drainage experiments contained 2000 mg/L Fe^{3+}, 3000 mg/L Fe^{2+}, 1000 mg/L Al^{3+}, 200 mg/L Mn^{2+} and 14407 mg/L SO_4^{2-} (Table 5.2). It was modeled to simulate

Navigation AMD which was used in the initial experiments. It was prepared by dissolving the required amounts of Ferric sulphate unhydrous [Fe_2 $(SO_4)_3$], Ferrous sulphate heptahydrate $FeSO_4.7H_2O$, Aluminium sulphate 18-hydrate, Al_2 $(SO_4)_3.18H_2O$, Manganese （Ⅱ）nitrate tetra hydrate Mn $(NO_3)_2.4H_2O$. All chemicals used were of analytical grade. The weighed salts were dissolved in 0.005 M H_2SO_4 solution prepared using milliQ water to prevent immediate precipitation of ferric iron. The final pH of the solution ranged from 1.82 –1.84. The actual concentration of the simulated AMD was ascertained by inductively coupled-mass spectrometry (ICP-MS) for major elements and ion chromatography (IC) for SO_4^{2-}. The SAMD neutralization kinetics were developed to confirm its buffering properties as compared to the natural AMD, reactions were carried out for 24 hours and EC and pH monitored over time, this was done at two levels of Fe^{2+}/Fe^{3+}(1000:1000ppm) and (2000:3000 ppm) giving a total concentration of Fe similar to the natural AMD (Navigation AMD). The simulated AMD was prepared each time, a few minutes before the drainage experiments. The column assembly used for the drainage experiments is shown in figure 5.2 below.

UNIVERSITY of the WESTERN CAPE

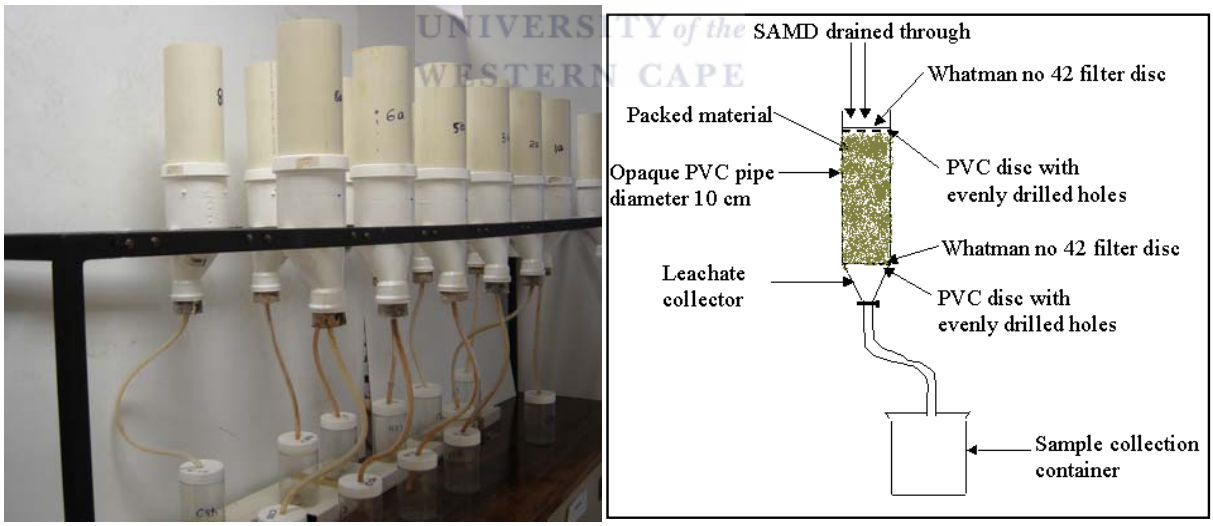

Figure 5.2: A photo and schematic drawing of the column assembly used for the leaching experiments (all columns used were PVC pipes of diameter 101 mm)

Table 5.2: Composition of the Simulated Acid mine Water used in the drainage experiments (mg/L)

Contaminant	calculated	SAMD1	SAMD2	ave	std
Al	1000	907.60	909.75	908.67	1.07
Mn	200	201.40	198.86	200.13	1.27
Fe (total)	5000	4657.01	4795.70	4726.36	69.34
SO4	14407				

Table 5.3: Test conditions for the fly ash, solid residues, fly ash and Ordinary Portland Cement blended solid residues

Column code	weight of co-disposal/fly ash (kg)	dry weight (kg)	weight of ash/OPC added(g)	fly% fly ash/OPC added (dry weight)	Height of column solids (cm)	drainage volume (L) per experiment
C1a	1.000	1.000			13	0.35
C1b	1.000	1.000			13	0.35
C2a	1.000	0.879			11	0.35
C2b	1.000	0.879			11	0.35
C3a	1.000	0.925	46	5	11.8	0.35
C3b	1.000	0.925	46	5	11.8	0.35
C5a	1.000	1.172	293	25	15	0.45
C5b	1.000	1.172	293	25	15	0.45
C6a	1.000	1.465	586	40	18.8	0.555
C6b	1.000	1.465	586	40	18.8	0.555
C8a	1.000	0.935	56.1	6	12.8	0.35
C8b	1.000	0.935	56.1	6	12.8	0.35

UNIVERSITY of the WESTERN CAPE

The simulated AMD was added to each column over a period of several minutes. Columns 1, 2, 3 and 8 were leached with batches of 350 mL SAMD. Columns 5 and 6 containing different masses of solid material were leached with 450 and 555 mL, respectively in order to maintain a consistent liquid to solid ratio between all the columns (Table 5.1). Drainage was done after 7 days for the first 53 days and thereafter after 14 days until stoppage of the experiment at 165 days (Table 5.4). Leachates from previous drainage were collected before the next drainage. Leachates were analyzed within 24 hours for pH, EC and Eh. Sub-samples were thereafter preserved with HNO_3 for analysis of metals by inductively coupled-mass spectrometry (ICP-MS) for major elements and un-acidified samples diluted accordingly for SO_4^{2-} analysis by ion chromatography (IC). Samples were refrigerated at 4^oC until analysis.
The alternate wetting and drying regimes were done to simulate conditions when AMD is percolating and not percolating through the backfilled material.

Table 5.4: The number of times SAMD was drained through the columns, and the corresponding time in days and cumulative volume of SAMD (L/kg).

		Volume (L/kg) of SAMD added per column					
Drainage No	Time (days)	Column 1	Column 2	Column 3	Column 5	Column 6	Column 8
1	1	0.35	0.40	0.38	0.38	0.38	0.37
2	7	0.70	0.79	0.76	0.77	0.76	0.74
3	15	1.05	1.18	1.13	1.15	1.14	1.11
4	22	1.40	1.57	1.51	1.54	1.52	1.48
5	29	1.75	1.95	1.89	1.92	1.90	1.85
6	36	2.10	2.34	2.27	2.30	2.27	2.22
7	44	2.45	2.73	2.65	2.69	2.65	2.59
8	53	2.80	3.12	3.02	3.07	3.03	2.96
9	67	3.15	3.51	3.40	3.46	3.41	3.33
10	81	3.50	3.90	3.78	3.84	3.79	3.70
11	97	3.85	4.29	4.16	4.22	4.17	4.07
12	110	4.20	4.68	4.54	4.61	4.55	4.44
13	124	4.55	5.07	4.91	4.99	4.93	4.81
14	138	4.90	5.46	5.29	5.38	5.31	5.18
15	152	5.25	5.84	5.67	5.76	5.69	5.55
16	165	5.60	6.23	6.05	6.14	6.06	5.92

University of the
WESTERN CAPE

5.1.3 Analysis of the Leached Solid Residue Cores.

At the end of the drainage experiment the columns were left intact for another three months without being drained. The columns were then cut lengthwise into two equal sections by using a saw. One of the sections was divided into three sections for column C1, C2, C3, C5 and C8 while for column C6 was divided into four sections. Physical, chemical and mineralogical analyses were performed on the three or four sections of the solid cores.

5.1.4 PH profile of the Leached Column Solid Cores.

The samples for pH determination were scooped across the length of the surface of the half-section and blended to create a composite sample. Samples were scooped after every 2 cm down the column solid residue cores for columns C1, C2, C3, and C8 and after every 2.5 cm for columns C5 and C6 (leached solid cores were relatively longer). Ph was determined using 1:1 solid residue: water ratio by following the method of Eckert (1988).

10 grams of the leached solid residues were weighed and put in a beaker and an equal amount (10 ml) of de-ionized water added. The mixture was then stirred thoroughly for 5

seconds, allowed to settle for 15 minutes and the pH of the supernatant recorded. The procedure was triplicated.

5.1.5 X-ray diffraction, Scanning Electron microscopy, Scanning Electron microscopy-energy dispersive spectroscopy (SEM-EDX) and infra-red analysis of column solid cores.

To evaluate the mineralogical changes resulting from the interaction of the SAMD with the various solid residue (SR) blends, samples from the sectioned solid residue cores were subjected to XRD and SEM analysis.

The solid samples were thawed from the sectioned column according to the sections starting from the top of the column to the bottom. The samples were then crushed and oven-dried for 12 hours at 105^{o}C to remove the interstitial water, and then crushed further to obtain a fine powder. The XRD spectra were obtained by a PANalytical X-ray diffractometer (XRD) using Cu $K\alpha$ radiation generated at 20 mA and 40 KV. Specimens were step scanned as random powder mounts from 5 to 85^{o} 2θ integrated at 0.02^{o} 2θ per second. X-ray diffraction analysis can detect crystalline phases present at 5 % mass. Powder samples for SEM and SEM-EDX were loaded on copper stubs coated with carbon graphite glue mixture and then carbon coated for 30 minutes. Both backscatter and secondary electron modes were used for image acquisition.

Dried powdered solid residue cores section samples were also analyzed by Fourier transformed infra-red spectroscopy (FTIR). The powder samples were mixed with 95 % dried analar grade KBr, ground with mortar and pestle and pressed into a transparent disc and thereafter scanned over the wave number range 4000 cm^{-1} to 200 cm^{-1}.

5.1.6 Sequential Chemical Extractions

To complement the data on mineralogical analysis and to be able to account for the contaminants profiles obtained in the leachates and the contaminant attenuation behavior of the FA solid residues (SR) and the tested SR blends, the solid residue core sections were subjected to sequential chemical extraction based on the work of Ribet *et al.* (1995), Schwertmann *et al.* (1982) and Tessier *et al*. (1979). All the extraction experiments were carried out with wet samples scooped from the column sections starting at the top to the

bottom of the column. These extractions were done to determine the water soluble fraction, amorphous fraction and reducible fraction. All experiments were carried out in triplicate.

a) Water soluble fraction: the distilled-water soluble fraction was determined by agitating 5 g of the wet solids in 50 ml of MilliQ water with a table shaker for 1 hour, the mixture was then centrifuged at 1000 rpm for 10 minutes, filtered through a 0.45 μM nucleopore membrane. The obtained supernatant was then prepared for metal and SO_4^{2-} analysis. A parallel sub-sample was dried for 12 hours at 105^oC to determine the moisture content so as to be able to calculate the dry weight.
b) Amorphous fraction: 1.0 gm of the wet solid residues from (a) were extracted with 200 ml of 0.2 M ammonium oxalate buffer at pH 3.0 in the dark in the dark. The buffer was prepared by adding 1100 ml of 0.2 M oxalic acid solution to 1500 ml of 0.2 M ammonium oxalate solution to obtain a final pH of 3.07. The buffer was prepared fresh during each series of extraction for a given column sections. The extraction was done by agitating the mixture in a table shaker for 4 hours. The mixture was then centrifuged at 1000 rpm for 10 minutes, filtered through a 0.45 μM nucleopore membrane and the supernatant prepared for metal and SO_4^{2-} analysis.
c) Reducible fraction: 0.5 gms of the wet solids from (b) were added to 15 ml of 1.0 M hydroxylamine hydrochloride ($NH_2OH.HCL$) solution in 25 % (v/v) acetic acid solution and then heated to 95 ± 5^oC for 6 hours to remove the crystalline Fe and Mn (hydr) oxides (Tessier *et al*., 1979). The 1.0 M hydroxylamine hydrochloride solution was made by dissolving 13.898 gms of hydroxylamine hydrochloride salt in 200 ml of 25 % acetic acid solution. The extraction was done by agitating the mixture in a table shaker with a water bath maintained at 95 ± 5^oC. The mixture was then centrifuged at 1000 rpm for 10 minutes after cooling, filtered through a 0.45 μM nucleopore membrane and the supernatant prepared for metal and SO_4^{2-} analysis.

5.1.7 Geochemical Modeling

Activities of aqueous species and mineral saturation indices of selected mineral phases were calculated using PHREEQC software (Parkhurst, 1995) and the WATEQ4F database which was modified to include ettringite. FeOOH was added to the database with Log K = 4.891 for

ferrihydrite. Sillimanite, a mineral similar to mullite (main aluminosilicate matrix in fly ash) was added since its thermodynamic data is available (Lindsay, 1979). The alkalinity reported as mg $CaCO_3$/L was recalculated to mg HCO_3^-/L as required for input by PHREEQC. Analysis data of the leachates for the various column solid cores for each drainage were input and used to estimate the activities of the various species. The activities of the dissolved species were calculated with Davies equation (Davies, 1962). All the dissolved Fe was assumed to be oxidized to Fe^{3+} thus redox reactions were eliminated from the modeling to simplify the equilibrium calculation. The data used for the calculations were pH, alkalinity, $\rho\varepsilon = 4$, solute concentrations for Al, Ca, Cu, Fe, Zn, SO_4^{2-}, Na, K, Si, Mn, Pb, B, Sr, Ba, and Mo.

UNIVERSITY of the
WESTERN CAPE

5.1.8 Strength Development of Acid Mine Drainage and Fly Ash Solid Residues blended with Ordinary Portland Cement (OPC).

5.1.8.1 Preparation of the solid residues

The solid residues were prepared by reacting Navigation AMD and Matla fly ash in a 1:3 ratio (FA: AMD) using an overhead stirrer at a speed of 450 rpm. Three batches of solid residues (SR) were prepared. The solids for batch one were prepared by using Matla FA from unit 5 and those for batch two and three by using Matla FA from unit 3. On attaining a pH of 9.0 (for batches one and two) and 11.0 (for batch three) the reaction mixture was filtered and the wet solids were pressed at 150 kPa. The pressure was increased gradually to drive out most of the water until bubbling was observed. A sample was preserved for moisture content determination. The remaining solid residues were kept in a tightly locked plastic container.

5.1.8.2 Moisture content determination

The moisture content was determined, to obtain the dry weight of the solids, by drying the wet solids at 105^0 C for 12 hours. The moisture content was in turn used for the calculation of the amount of the binder (Ordinary Portland Cement) needed for each blending rate.

5.1.8.3 Marsh cone test

To estimate the amount of water that will be needed to make the slurry suitable for pumping; a marsh cone test was performed. This was done by adding tap water to a solid residue slurry blended with 3 % binder (ordinary Portland cement) until the time for 1 L to run out had dropped to less than 10 seconds. The resulting value was taken as the required water content for make-up of pumpable slurry. Solids from batch one and two were also submitted to marsh cone test.

UNIVERSITY of the WESTERN CAPE

5.1.8.4 Particle size determination

Particle size analysis was done by FRITSCA analysette sieves for particle sizes greater than 38 μm. For particles smaller than 10 μm, a laser particle sizer FRITSCH ANALYSETTE 22 at Miningtek CSIR (Johannesburg) was used.

5.1.8.5 Preparation of the cylinders and curing

The wet solids were blended with a pozzolanic binder (Castle cement) at rates of 1 %, 3 % and 6 % dry weight basis. Several batches of cylinders were prepared, by using ordinary tap water for batch one and by using the process water obtained from the treatment of acid mine drainage with fly ash at a ratio of 1:3 (FA: AMD) for batches two and three. The wet solids were slurried with the required amount of water as determined from the marsh cone test. Then they were poured into the cylindrical tubes and placed in plastic bags, a bottle of water being placed next to them to maintain the required level of humidity for the curing process (Fig 5.3). All samples were duplicated. The prepared cylinders were cured and monitored for strength development for one year.

UNIVERSITY of the
WESTERN CAPE

Figure 5.3: Cement blended Solid residue slurry cured in plastic cylinders for strength development testing at Miningtek laboratory.

5.2 Results and Discussion

5.2.1 Composition of Fly Ash, Solid residues (SR) and Ordinary Portland Cement (OPC)

The table 5.5 below shows the chemical characteristics of the fly ash, solid residues and ordinary Portland cement used in the column studies

Table 5.5: Elemental content of solid residues, Arnot fly ash and Ordinary Portland cement.

Solid residues				Ordinary portland cement		Arnot fly ash			
Element	wt %	Element	ppm	Element	wt %	Element	wt %	Element	ppm
SiO_2	45.88	Mo	6.2	SiO_2	35.26	SiO_2	53.39	Mo	5.23
Al_2O_3	24.57	Sr	1954.4	Al_2O_3	12.83	Al_2O_3	23.40	Sr	1463.9
TiO_2	1.19	Pb	46.8	TiO_2	0.80	TiO_2	1.34	Pb	56.35
Fe_2O_3	6.31	Co	29.5	Fe_2O_3	1.44	Fe_2O_3	4.72	Co	18.25
MnO	0.10	Mn	642.9	MnO	0.36	MnO	0.06	Cr	179.2
MgO	2.39	Cr	230.6	MgO	3.55	MgO	2.70	Zn	57.33
CaO	7.14	Zn	144.3	CaO	42.82	CaO	8.43	Cu	47.34
Na_2O	0.41	Cu	52.3	Na_2O	0.05	Na_2O	0.35	Ni	93.41
K_2O	0.51	Ni	83.3	K_2O	0.59	K_2O	0.49	Ba	928
P_2O_5	0.68	Ba	136.9	P_2O_5	0.15	P_2O_5	0.35		
SO_3	3.48			Cr_2O_3	0.002	Cr_2O_3	0.03		
Cr_2O_3	0.04					NiO	0.011		
NiO	0.01								

UNIVERSITY of the WESTERN CAPE

The high weight % of Si, Al and Ca reflect the main components of Ordinary Portland Cement (OPC). OPC consists primarily of compounds of calcium and silicon with smaller amounts of iron and aluminium compounds (Taylor, 1997). Compared to fly ash and the solid residues, OPC had high amounts of Mn and Mg which could be mobilized during the leaching study. The solid residues and fly ash have high weight % of SiO_2, Al_2O_3 which reflects the main components of fly ash, aluminosilicate matrix. This has been established to be mainly quartz and mullite (Gitari *et al*., 2004). The decrease in CaO content in the solid residues compared to fly ash reflects the free lime utilized in the neutralization of AMD. A decrease in MgO is also observed which indicates its additional contribution to the neutralization capacity of the fly ash.

A decrease in SiO_2 is observed in the solid residue which is attributed to the dissolution of the alumino-silicate matrix during the neutralization process. An enrichment of Fe and Al is observed in the solid residues as a result of the removal of these elements from AMD as insoluble precipitates. Other elements observed to be enriched in the solid residues include Mo, Sr, Co, Cr and Zn.

5.2.2 Kinetics of the Simulated Acid mine Water (SAMD)

To test the performance of the formulated Acid Mine Drainage, reactions were carried out at FA: AMD ratios of 1:3 and 1:1.5 using Arnot fly ash. PH and EC were recorded over a 24 hour period. Different Fe^{2+}/Fe^{3+} ratios were used in an attempt to simulate the ratios observed in natural acid mine drainage samples. The kinetics of the reactions are shown in figures 5.4 and 5.5.

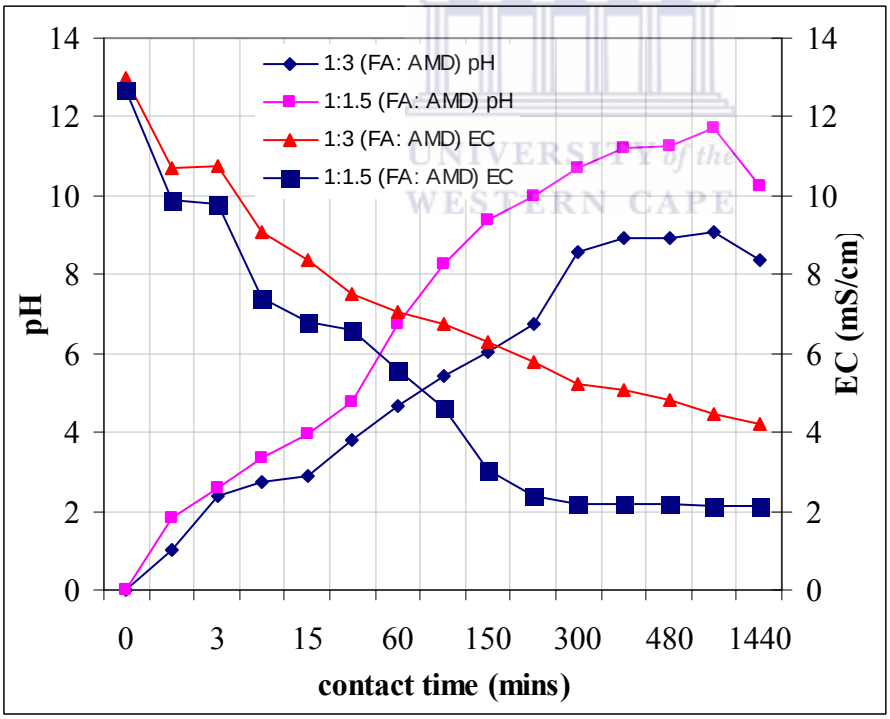

Figure 5.4: Change in pH and EC with time for SAMD (Fe^{2+}/Fe^{3+}) ratio of 2:3

UNIVERSITY of the WESTERN CAPE

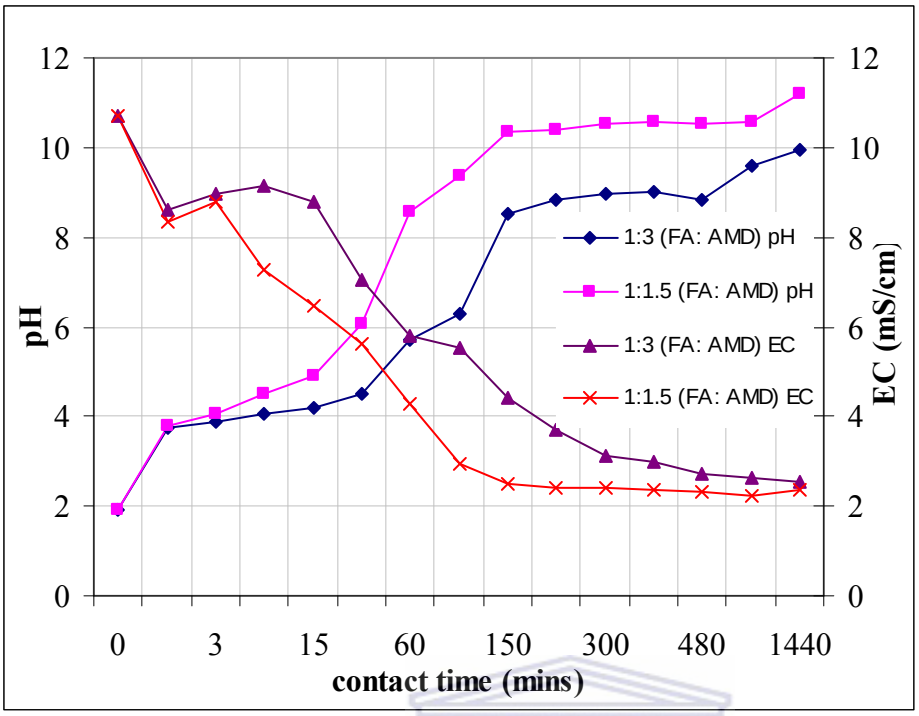

Figure 5.5: Change in pH and EC with time for SAMD (Fe^{2+}/Fe^{3+}) ratio of 1:1

The buffer regions associated with neutralization of natural AMD are observed. At pH 2.0-5.0, 5.5-6.0 and at pH 8.5-9.0. A decrease in pH is observed at longer contact times for the 2:3 (Fe^{2+}/Fe^{3+}) ratio probably due to unoxidized ferrous iron which on oxidation and hydrolysis releases acidity (H^+). Observation of the figure 5.4 and 5.5 shows that EC trends are similar for both FA: AMD ratios tested, however the 1:1.5 ratio shows a faster decrease. A significant decrease in EC is observed once the mixture attains pH 5.5. This has been observed in earlier experiments using Navigation and Brugspruit AMDs (Gitari *et al*., 2004). The control on buffering capacity of the solution by Fe^{2+} is evident at pH 4.5-8.5 range, the rate of increase in pH is steeper for 1000 ppm Fe^{2+} solution than the 2000 ppm Fe^{2+} solution (Figs 5.4, 5.5 and Table 5.6). The formulated acid mine drainage was thus observed to fit the major neutralizing characteristics of the natural acid mine drainage.

UNIVERSITY of the WESTERN CAPE

Table 5.6: Rate of change of pH with time over the pH range 4.5-8.5 for the two model solutions.

Solution	Fe2+/Fe3+ (1:1)		Fe2+/Fe3+ (2:3)	
FA: AMD	1:3	1:1.5	1:3	1:1.5
ΔpH/ΔT	0.025	0.081	0.016	0.057

5.2.3 Drainage Quality

5.2.3.1 Evolution of pH in the column leachates

Results of pH profiles are presented for FA, SR, SR + 5 % FA, SR + 25 % FA, SR + 40 % FA and SR + 6 % OPC columns. The figures 5.6- 5.17 below show the pH and EC of the leachates as a function of cumulative drainage volume (L/kg).

In chapter four and five of this work it has been established that SO_4^{2-} is the most important contributor of conductivity in the acid mine waters being investigated. Azzie (2002) observed that SO_4^{2-} was responsible for the high conductivity of a variety of mine waters and it was the major anion. In this context the EC profiles are plotted parallel to the pH profiles as an indication of the change in EC as the SO_4^{2-} is removed from the percolating SAMD and the trends are not discussed further. The description of the pH profiles of the leachates for different column cores is presented.

UNIVERSITY of the WESTERN CAPE

The pH values of leachates recovered from unreacted fly ash cores were initially alkaline (pH > 12.0). Acidification of the ash occurred in a step-wise fashion with the columns exhibiting three buffer regions. This stepwise acidification of fly ash has been observed by other researchers (Hodgson *et al*., 1982; Komnitsas *et al*., 2004; Warren and Dudas, 1984). The buffering regions were observed as the pH decreased, at pH 12.0-10.0, 8.0-7.0, 5-5.5 and 4.0 (Fig 4.6). However the pH of the buffer regions displayed variability for the duplicate columns which could have occurred due to channeling effects. However the variability decreased as the treatment systems approached the acidic buffer region. Stewart *et al.* (2001) observed variation in the pH trends for their replicates in the early phases of a column drainage study for coal refuse blended with fly ash. At 97th day of drainage both columns

show a decrease in pH to below 5.0. A buffer zone is observed at pH 4.0 and is sustained as the experiment comes to a close at 165 days (Fig 5.6 and Table 5.4).

UNIVERSITY of the
WESTERN CAPE

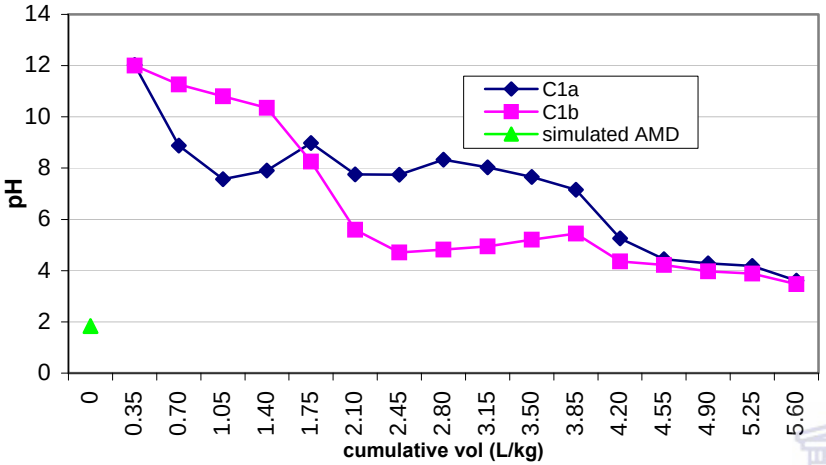

Figure 5.6: Evolution of pH in the leachate with cumulative volume for the unreacted FA

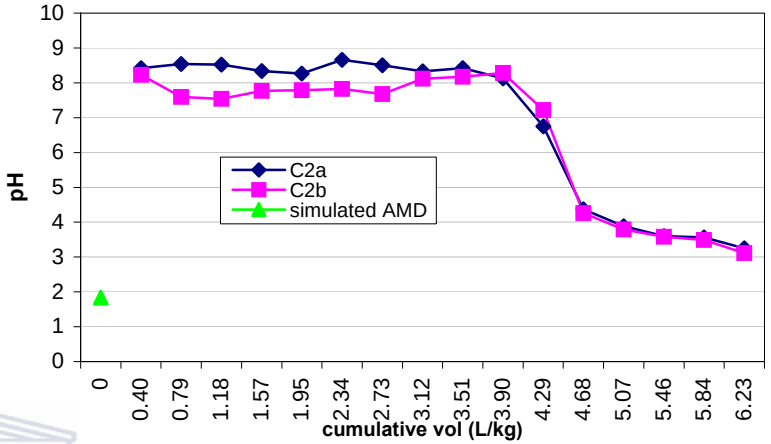

Figure 5.8: Evolution of pH in the leachate with cumulative volume for solid residues (SR).

UNIVERSITY of the
WESTERN CAPE

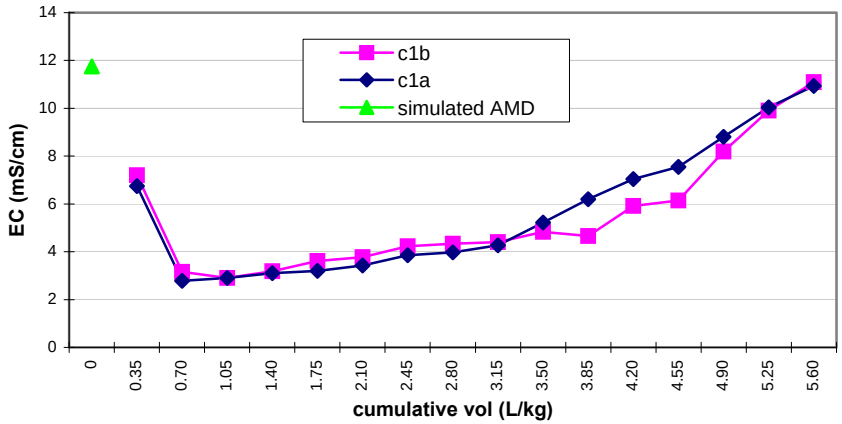

Figure 5.7: Column leachate EC values as a function of cumulative volume for the unreacted FA.

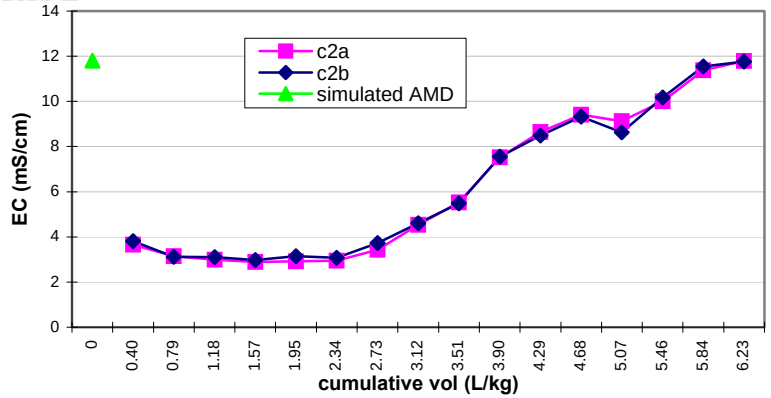

Figure 5.9: Column leachate EC values as a function of cumulative volume for solid residues (SR).

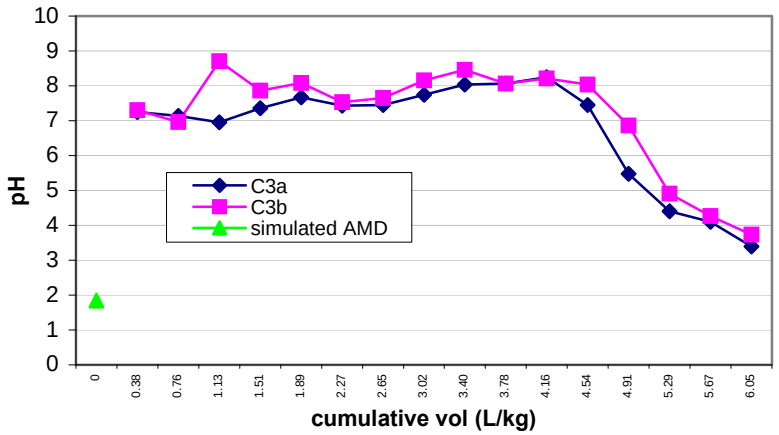

Figure 5.10: Evolution of pH in the leachate with cumulative volume for the solid residues (SR) + 5 % FA.

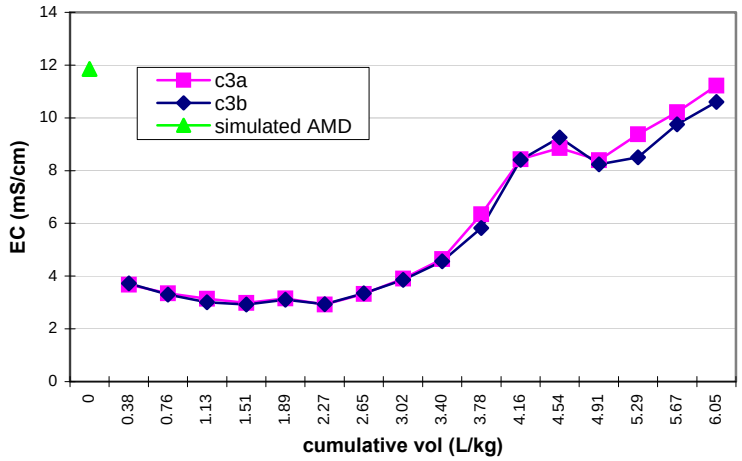

Figure 5.11: Column leachate EC values as a function of cumulative volume for the solid residues (SR) + 5 % FA.

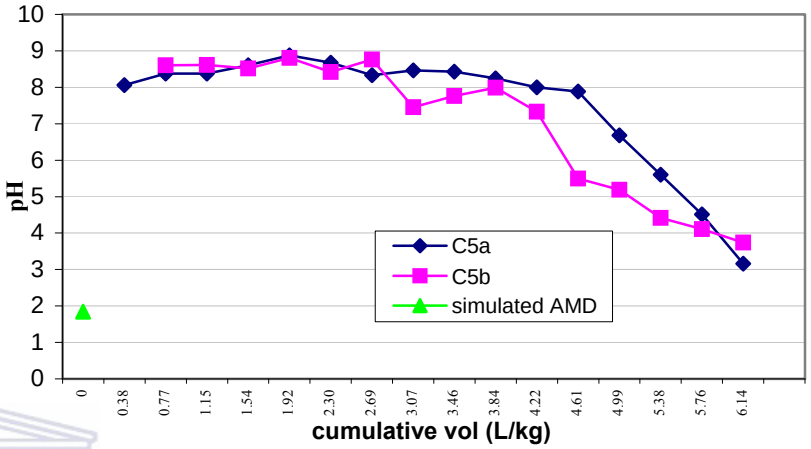

Figure 5.12: Evolution of pH in the leachate with cumulative volume for the solid residues (SR) + 25 % FA.

UNIVERSITY of the
WESTERN CAPE

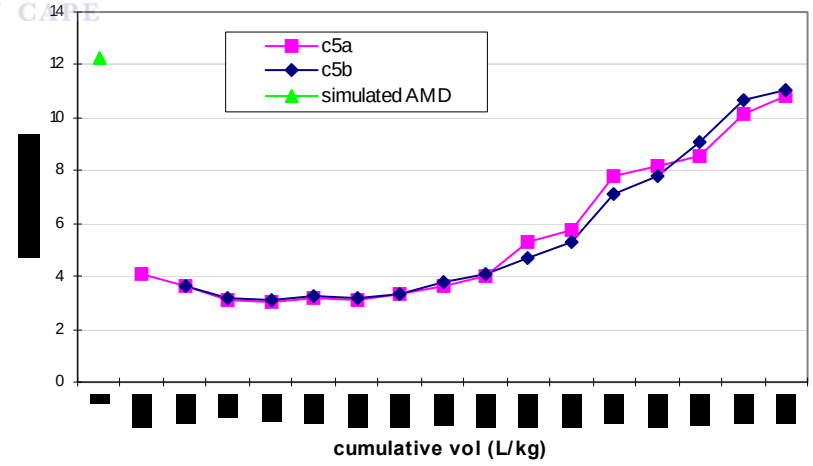

Figure 5.13: Column leachate EC values as a function of cumulative volume for the solid residues (SR) + 25 % FA.

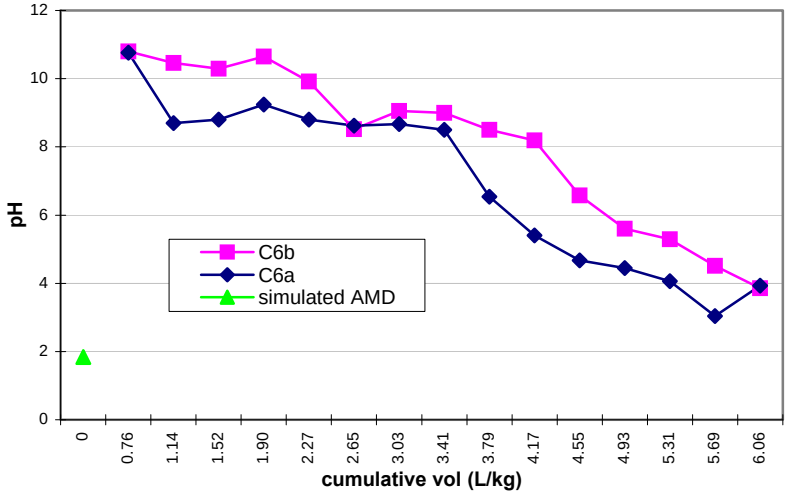

Figure 5.14: Evolution of pH in the leachate with cumulative volume for the solid residues (SR) + 40 % FA.

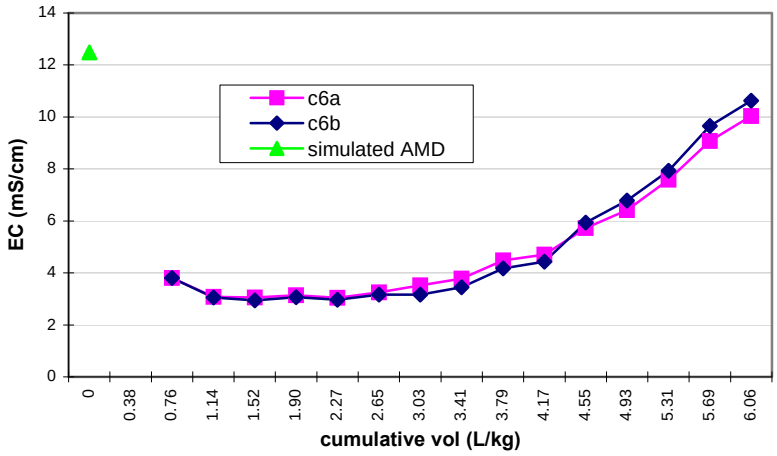

Figure 5.15: Column leachate EC values as a function of cumulative volume for the solid residues (SR) + 40 % FA.

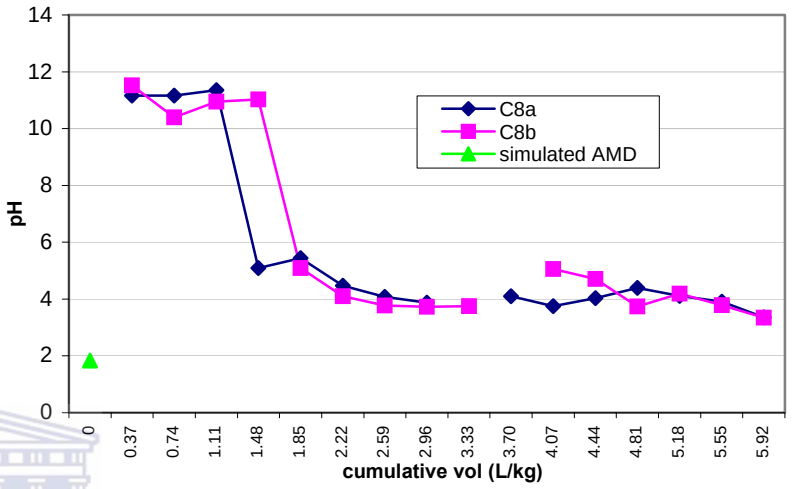

Figure 5.16: Evolution of pH in the leachate with cumulative volume for the solid residues (SR) + 6 % Ordinary Portland Cement.

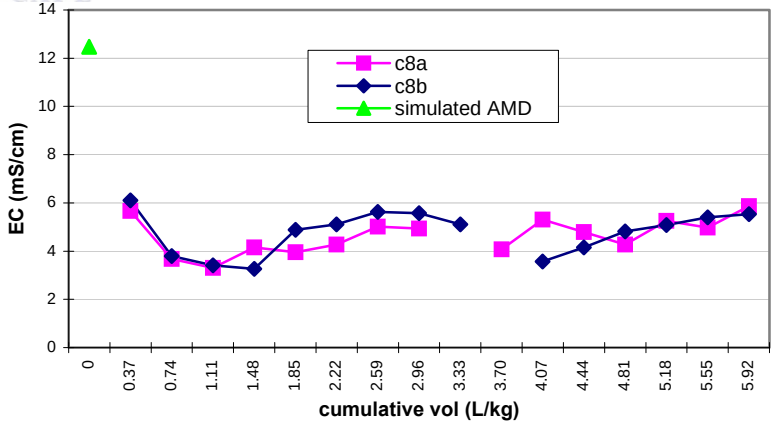

Figure 5.17: Column leachate EC values as a function of cumulative volume for the solid residues (SR) + 6 % Ordinary Portland Cement

UNIVERSITY of the WESTERN CAPE

The solid residue (SR) core leachates were initially circum-neutral (pH 8.5) upto 81 days when 3.57 L/kg of SAMD had been added (Fig 5.8 and Table 5.4), this comprised the first buffer zone, thereafter the pH dropped with subsequent leaching. Column C2a first buffer zone was observed at a slightly higher pH than for column C2b. At 110 days of drainage the acidic buffer region was observed with pH dropping to below 4.5. A gradual drop in pH was subsequently observed (pH 4.0-3.5) as the drainage came to a close at 165 days. Two acidification steps were observed for the duration of the experiment.

The pH values of leachates recovered from the solid residue (SR) + 5 % FA cores were initially neutral (Fig 5.10) (pH 7-7.5). Apart from the increase to pH 8.5 for column C3b leachates at 15 days both columns generally exhibited a gradual increase in pH as the drainage progressed to a maximum of 8-8.5 at 97-110 days of drainage. Thereafter both columns exhibited a decrease in pH to below 4.0 at the close of the experiment. The pH profile strongly mirrored that of the SR cores with the pH being slightly less than 8.0 at the first buffer region. These solid cores exhibited two acidification steps for the entire duration of the experiment.

UNIVERSITY of the

The solid residue (SR) + 25 % FA column core leachates maintained largely a pH>8.0 upto 110 days corresponding to 3.77 L /kg of SAMD added (Fig 5.12 and Table 5.4). This pH was slightly higher than for the SR and SR + 5 % FA cores. The sudden pH front breakthrough observed for SR and SR + 5 % FA was not observed in this column core. The addition of the fly ash at this rate probably delays the breakthrough to the acidic region. The pH is noted to decrease steadily with drainage after 97 and 110 days for column C5b and C5a respectively.

The solid residue (SR) + 40 % FA column core leachates were initially alkaline (pH ≈11.0) (Fig 5.14). The pH drop for the two columns occurred stepwise with three buffer zones being exhibited, the buffer zones occurred at pH 10.5-11.0, 8.0-9.0 and 4.0-6.0.
Variability in the pH of the leachates for the two column cores was observed for a large duration of the experiment (i.e, 152 days of drainage) (Fig 5.14 and Table 5.4) except at pH 8.5-9.0. Column C6a maintained a lower pH in the leachates for a significant duration of the drainage experiment. This variability was also observed in fly ash core leachates. The variability is observed to decrease to a minimum as the buffer zones are approached. The pH

profile of the leachates strongly mirrored that of the fly ash cores suggesting that at blending rates > 40 % FA the dissolution kinetics of the fly ash dominates for the duration investigated.

The leachates of the solid residue (SR) + 6 % OPC cores were initially highly alkaline (pH 10.5-11.5) (Fig 5.16). The cores exhibited two buffer regions at pH 10.5-11.5 and pH 4 –5.5. The lower pH buffer region was maintained for longer duration of the leaching study compared to the high pH buffer region (Table 5.4). The change from the high pH buffer region to the lower one was quite rapid; it required drainage of 1.52 L/kg of SAMD for the pH to drop from 11.5 to 5.5 at 29 days for column C8b. The high pH leachates generated initially were attributed to the hydration reactions of OPC which release $Ca(OH)_2$ and calcium silicate hydrate (CSH) gels according to equations (5.1) and (5.2)(Taylor, 1997).The rapid drop in pH thereafter probably indicates completion of the hydration reactions and transformation of the released $Ca(OH)_2$.

$$2Ca_3SiO_5 + 6H_2O \Rightarrow CSH + 3Ca(OH)_2 \quad \text{.....(5.1)}$$

$$2Ca_2SiO_4 + 4H_2O \Rightarrow CSH + Ca(OH)_2 \quad \text{.....(5.2)}$$

UNIVERSITY of the
WESTERN CAPE

5.2.4 Conclusions

The FA cores, the solid residue (SR) + FA and solid residue (SR) + 6 % OPC cores exhibited stepwise acidification process which indicates that several acidity attenuation mechanisms are involved as the drainage progresses. FA cores exhibited three acidification steps, SR, SR+FA and SR+ 6 % OPC cores two acidification steps. The higher pH buffer region (7.5-9) was sustained for a longer duration than the lower one (3-4) in SR and SR+FA cores. SR+OPC cores sustained the lower buffer region (3.5-4) for a longer duration of the experiment.

An observed similarity in pH profile of the SR + 40 % FA solid core with the FA column core probably indicates that at 40 % or higher blending rate, dissolution kinetics of the fly ash will dominate. The solid residue cores (SR) appeared to have a significant buffering capacity, maintaining a neutral to slightly alkaline pH in the leachates for an extended period of time (97 days). Blending of the solid residue (SR) with fly ash of upto 25 % by weight increases the pH of the leachates to circum-neutral, alkaline pH and reduces the time of

breakthrough to acidic zone. If placed in a mining area generating AMD, these SR could provide a passive method of treatment of polluted coal mine water. The alkaline properties of the original FA or of the solid residues would thus give a possibility to passively treat AMD, with a neutralization reaction taking place in situ over an extended period of time. The use of Ordinary Portland Cement as a binder reduces this neutralization capacity to 22 days (Fig 5.16 and Table 5.4). Results obtained in the case of addition of the OPC binder may indicate possible excessive aggregation of residue particles or physical encapsulation by the generated CSH gel in the Ordinary Portland Cement amendment that may have reduced the active surface area of particles available for neutralization.

5.3 Acidity Attenuation by the Column Cores

5.3.1 Fly ash and solid residue (SR), solid residue (SR) + FA column cores

Stepwise acidification of all the column residue cores was observed as the drainage progressed. This suggests that different acidity attenuation mechanisms were responsible for the buffering zones observed and eventual clean-up of the SAMD percolating through.

UNIVERSITY of the
WESTERN CAPE

An observation of pH profile for the entire drainage period indicates that FA and solid residue (SR) + 40 % FA column cores exhibited similar trends pointing to a probable similarity in the kinetics and evolving chemistry as the drainage progresses. Moreover for the period of the study the kinetics observed (pH and EC) strongly points to those of dissolution of the unreacted fly ash used to blend the solid residues. In this context more detailed discussion of the evolving chemistry are confined to the fly ash column cores only. Similarly the pH profile of the solid residue (SR), solid residue (SR) + 5 % FA and solid residue (SR) + 25 % FA column cores are similar pointing to similar dissolution kinetics and chemistry. The significant difference noted for the three solid cores is that the time the leachate pH was sustained at ≈ pH 8.0 was extended to 110 days for the solid residue (SR) + 5 % FA and solid residue (SR) + 25 % FA as compared to the solid residue (SR) column cores. Another notable difference is that the solid residue (SR) + 25 % FA cores sustained a pH > 8.0 in the leachates for 110 days as compared to the solid residue (SR) and solid residue (SR) + 5 % FA cores. Detailed discussions of the evolving chemistry are confined to solid residue (SR) and solid residue (SR) + 25 % FA column cores.

FA solid cores had the highest initial pH of the leachates (9.2- 12.0) compared with the solid residues (SR) and solid residues + FA solid cores (Figs 5.6, 5.8, 5.10, 5.12 and 5.14).

The high pH of the leachates for the FA columns was attributed to the dissolution of CaO as the acidic mine water contacted the fly ash particles (equation 5.3). The generated Ca $(OH)_2$ is highly soluble at alkaline pH and interacts with SO_4^{2-} in the SAMD to form gypsum which precipitates.

$$CaO + 2H^+ \Rightarrow Ca(OH)_{2\,(aq)} \quad \text{.....(5.3)}$$

$$Ca(OH)_2 + SO4 + 2H^+ \Rightarrow CaSO_4\,2H_2O_{\,(gypsum)} \quad \text{.....(5.4)}$$

Gypsum was identified by XRD and SEM-EDX in all the FA sectioned column solid cores (Figs 5.18 and 5.19). The pH of the initial leachates for the solid resides (SR) and solid residue (SR) + FA solid cores decreased in the order FA > SR + 25 %> SR + 5 % > SR strongly indicating that addition of fly ash to the solid residues was responsible for the initially high pH generated in the leachates. That dissolution of CaO from the fly ash particles was responsible for the initial high pH of the leachates is supported by the fact that the initial decrease in Ca is only observed for the FA solid core leachates (Figs 5.44, 5.46, 5.48 and 5.50). The decrease in Ca in the solid residue (SR) + FA solid cores leachates are not obvious (Fig 5.48). Part of the reason is, the solid residues were loaded in the columns while wet (moisture content 12.1 %) and interaction of the wet solid residues initiated CaO dissolution and formation of $Ca(OH)_2$ and on drainage with SAMD, reaction with SO_4^{2-} occurred leading to locking of Ca^{2+} as gypsum.

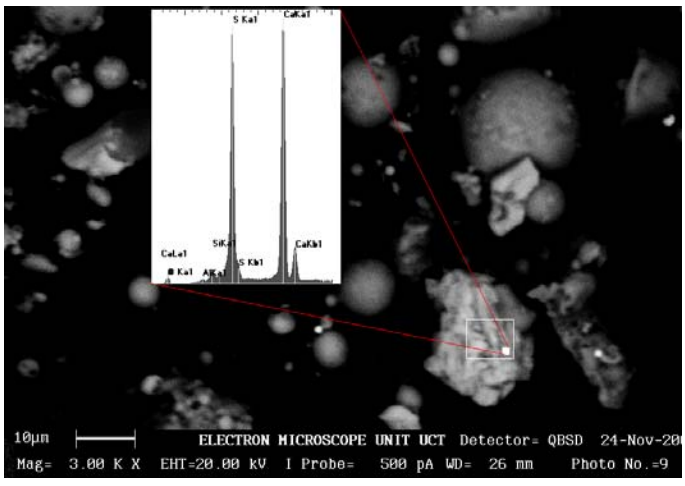

UNIVERSITY of the
WESTERN CAPE

Figure 5.18: SEM-backscattered micrograph of gypsum crystals in FA column cores with the EDX pattern superimposed.

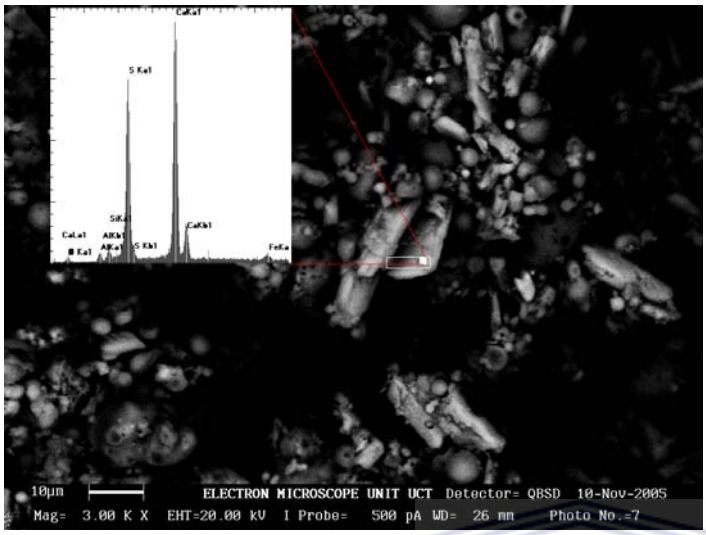

Figure 5.19: SEM-backscattered micrograph of gypsum crystals in solid residue (SR) column cores with the EDX pattern superimposed.

The solid residue (SR) cores and solid residue (SR) + FA cores exhibited strong acidity attenuation at pH 7.5-9.0. This pH buffer zone was sustained for slightly over 110 days for solid residue (SR) + 5 % FA and solid residue (SR) + 25 % FA and 97 days for solid residue (SR) cores (Figs 5.8, 5.10, 5.12, 5.14 and Table 5.14). The effect of FA addition to the solid residues (SR) is observed with the SR + 25 % FA solid cores where the pH front breakthrough to acidic zone is steady as compared to the SR cores which exhibit a sharp breakthrough. Acidity attenuation at this pH range is also observed for the FA cores from 29-97 days of drainage while for the solid residue (SR) + 40 % FA cores it was observed at 15-97 days.

Several mechanisms responsible for the acidity attenuation at this pH range in these solid cores can be proposed. After the initial rapid dissolution of CaO and other soluble salts coating the fly ash particles the aluminosilicate matrix, amorphous SiO_2 and Quartz are exposed to interact with the percolating SAMD and there is a possibility of their dissolution with time. Laboratory studies of quartz dissolution and precipitation kinetics indicate that quartz dissolution and precipitation are extremely slow at low temperatures (25^{o}C) (Rimstidt

and Barnes, 1980). The measured temperature of all the column leachates varied from 19.1-23.6^{o}C hence contribution of quartz to the dissolved silica would be insignificant. Seoanne and Leiros (2001) argued that the minerals most susceptible to weathering after the initial rapid dissolution of CaO and other soluble salts in fly ash were probably aluminosilicates. Dissolution of these minerals consumes hydrogen ions as indicated in Equation (5.5) for sillimanite (Lindsay, 1979).

$$Al_2SiO_{5(sil\,\mathrm{lim}\,anite)} + 6H^+ \Rightarrow 2Al^{3+} + H_4SiO_4 + H_2O \qquad \text{.....(5.5)}$$
$$Log\,K = 15.45$$

Sillimanite was chosen to confirm the contribution of aluminosilicate minerals in attenuation of acidity and buffering of pH at 7.5-9.0 for the solid residue (SR) and solid residue (SR) + FA solid column cores. Sillimanite is a mineral similar to mullite (Lindsay, 1979). Saturation indices (SI) were calculated over the pH range 7.5-9.0 for the solid residue (SR) and solid residue (SR) + 25 % FA solid cores. An observation of the calculated SI over this pH range for the solid residue (SR) core leachates (Table B14.) indicates that sillimanite was over-saturated upto 44 days becoming under-saturated for the rest of the drainage time. The transition from over-saturation to under-saturation is not pH dependent over the said pH range and could mean two things: (i) it,s contribution to buffering at this pH range is confined within a certain initial period of the drainage experiment. (ii) it's contribution to attenuation of acidity and hence buffering becomes indirect via conversion to a new mineral phase. For the solid residue (SR) + 25 % FA a slightly different scenario is observed where sillimanite remains near saturation for most of the drainage period (Table B17) strongly indicating it was in an equilibrium state under the acidic conditions.

UNIVERSITY of the
WESTERN CAPE

From equation (5.5) the equilibrium for the dissolution of sillimanite can be written as

$$K = \frac{[Al^{3+}]^2\,[H_4SiO_4]}{[H^+]^6} = 10^{15.45} \qquad \text{.....(5.6)}$$

Taking logarithm to base 10 results in the following expression

$$15.45 = 2Log[Al^{3+}] + Log[H_4SiO_4] + 6pH \qquad \text{.....(5.7)}$$

If sillimanite is contributing significantly to the attenuation of acidity over this pH range then a plot of pH versus 2Log ^{a}[Al] + Log ^{a}[H4SiO4] should give a straight line graph with a slope of -6 and y-intercept of 15.45 over the pH range 7.5-9.0 corresponding to the stoichiometry of equation (5.5). An observation of the plots over this pH range for solid residue (SR) and solid residue (SR) + 25 % FA core leachates indicates a stoichiometry corresponding to equation (5.5) confirming the contribution of sillimanite in buffering the pH in this range.

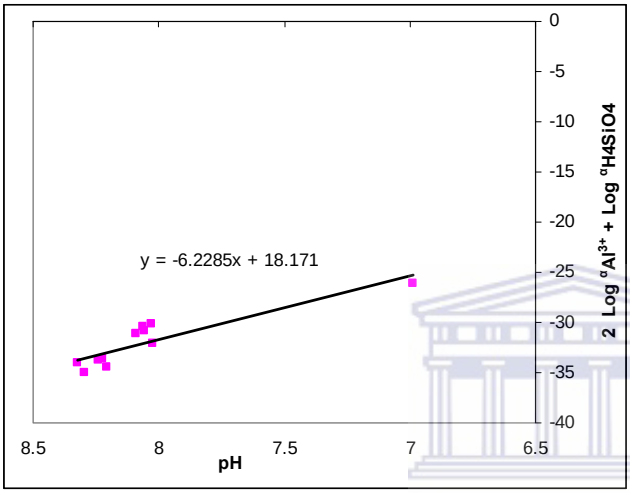

UNIVERSITY of the
WESTERN CAPE

Figure 5.20: Plot of pH versus 2Log $^{\alpha}Al^{3+}$ + Log $^{\alpha}H_4SiO_4$ over the pH range 6.5-9.0 for solid residue (SR) core leachates (SR column core).

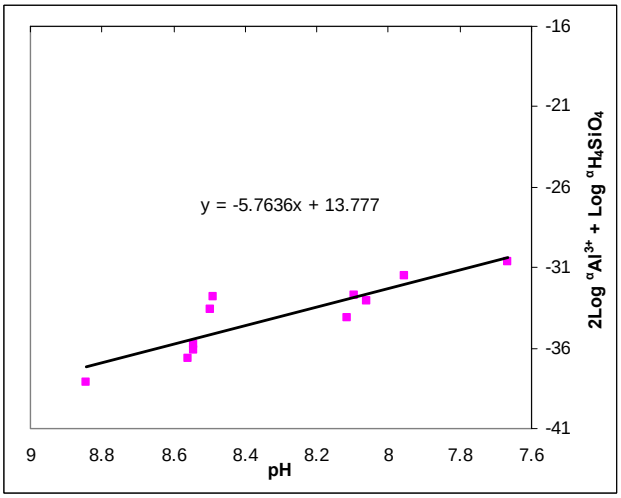

Figure 5.21: Plot of pH versus 2 Log $^{\alpha}Al^{3+}$ + Log $^{\alpha}H_4SiO_4$ over the pH range 6.5-9.0 for solid residue (SR) + 25 % FA core leachates (column 5).

Plots of solubility equilibria for mullite and sillimanite which are the main crystalline aluminosilicate phases, in the investigated fly ash were constructed and the calculated activities of Al^{3+} and H_4SiO_4 from the experimental data were used to derive the experimental solubility curves (log K = 45.41 obtained from Roy and Griffin. (1984) (Figs 5.22-5.27).

The theoretical activities Al^{3+} and H_4SiO_4 for mullite were calculated by using the equilibrium expression derived from the following equations (5.8, 5.9 and 5.10).

$$Al_6Si_2O_{13(mullite)} + 18H^+ \Leftrightarrow 6Al^{3+} + 2H_4SiO_4 + 5H_2O \quad \text{.....(5.8)}$$
$$Log\ K = 45.41$$

From equation (5.8) the equilibrium for the dissolution of mullite can be written as

UNIVERSITY of the
WESTERN CAPE

$$K = \frac{[H_4SiO_4]^2[Al^{3+}]^6}{[H]^{18}} = 10^{45.41} \quad \text{.....(5.9)}$$

Taking logarithm to base 10 results in the following expression

$$45.41 = 2\,Log\,H_4SiO_4 + 6Log\,Al^{3+} + 18\,pH \quad \text{.....(5.10)}$$

Using the solubility constant for mullite and measured pH the activities of Al^{3+} and H_4SiO_4 at equilibrium with mullite for the leachates can be calculated.

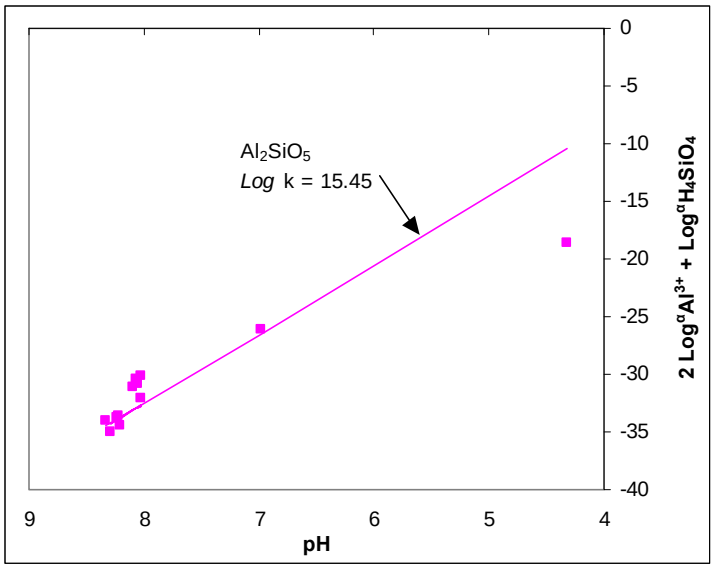

Figure 5.22: Sillimanite solubility equilibria for solid residue (SR) core leachates

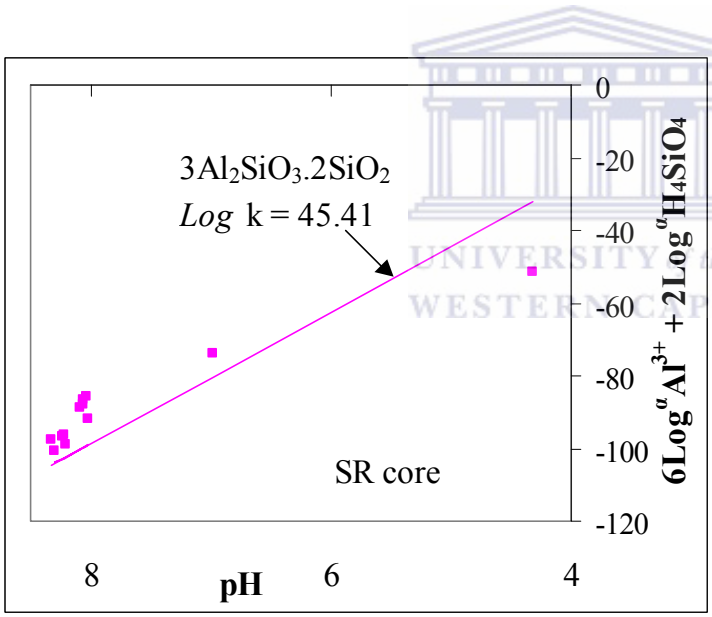

Figure 5.23: Mullite solubility equilibria for solid residue (SR) core leachate

UNIVERSITY of the
WESTERN CAPE

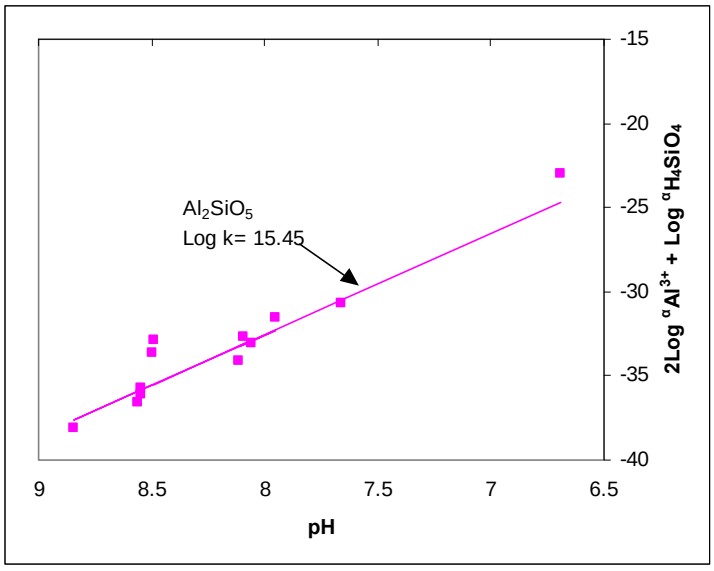

Figure 5.24: Sillimanite solubility equilibria for solid residue (SR) + 25 % FA core leachates.

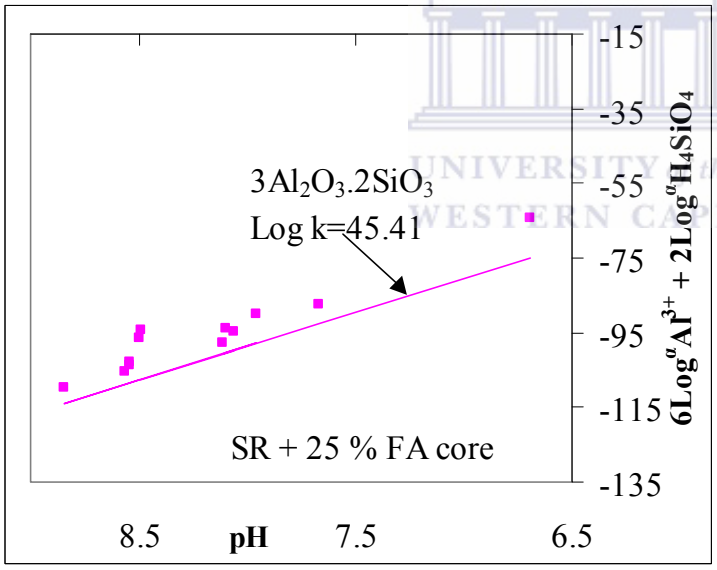

Figure 5.25: Mullite solubility equilibria for solid residue (SR) + 25 % FA core leachates.

UNIVERSITY of the WESTERN CAPE

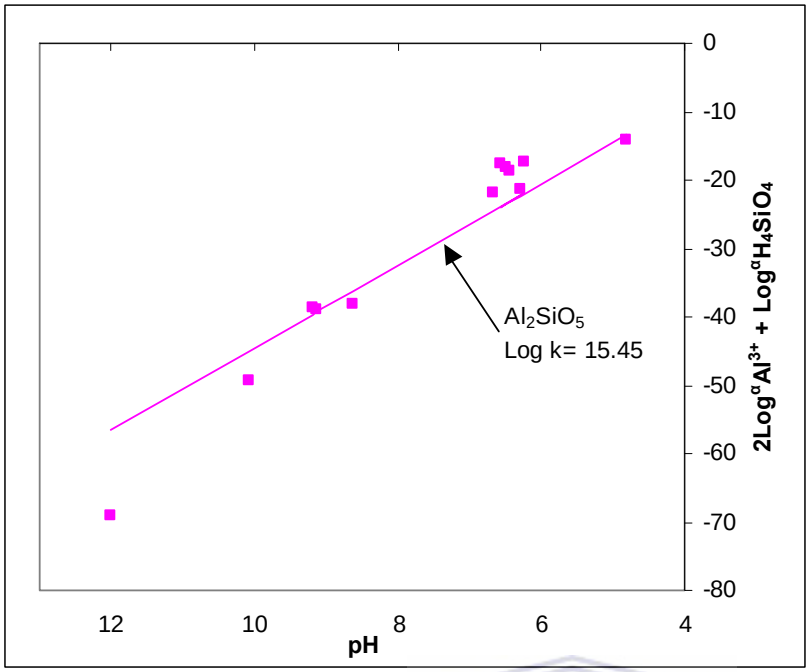

Figure 5.26: Sillimanite solubility equilibria for FA column core leachates.

UNIVERSITY of the
WESTERN CAPE

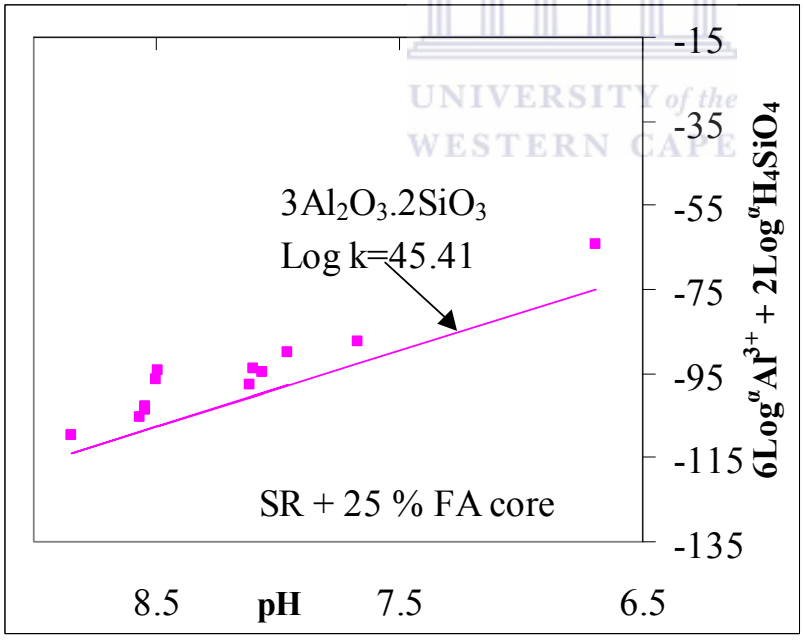

Figure 5.27: Mullite solubility equilibria for FA column core leachates.

Aqueous solution modeling indicates that the solid residue (SR), solid residue (SR)+ 25 % FA and FA core leachates were in equilibrium with sillimanite over the pH range 6.99-8.33. The FA core leachates were observed to be in equilibrium with mullite over the pH range 8.62-10.08 while the SR, SR + 25 % FA core leachates remained over-saturated over the pH

range 6.5-8.85. This could be interpreted to mean that sillimanite and mullite were controlling both Al^{3+} and H_4SiO_4 concentration in the leachates over the pH range 6.5-8.85. The strong equilibrium observed with sillimanite for the SR and SR + 25 % FA points to the importance of this amorphous aluminosilicate matrix in controlling the chemistry of the leachates over this pH range. A peculiar phenomenon is observed with FA cores leachates becoming over-saturated with both mullite and sillimanite at pH 6.22-6.68. Roy and Griffin (1984) observed equilibrium with mullite for acidic fly ash extracts at pH 4.1 after equilibration for along time with water (up to 140 days), the fly ash extracts became over-saturated with mullite as the pH approached 6.0.

Apart from the amorphous aluminosilicate minerals fly ash also consists of mineral phases such as quartz and amorphous SiO_2. Solubility of quartz is very low (Brownlow, 1979) hence would not dissolve rapidly under the acidic leaching conditions at low temperature. Langmuir (1997) points out that the most soluble form of SiO_2 is the amorphous silica. Therefore dissolution of amorphous silica is expected to contribute to the control of leachate chemistry over this pH range. To confirm this, equilibria diagrams for amorphous silica were plotted for the FA, SR, SR + 25 % solid cores which exhibited extended buffering at pH 6.5-8.9.

UNIVERSITY of the
WESTERN CAPE

Equilibrium for amorphous silica can be written as for quartz (equation 5.11)

$$SiO_{2(am)} + 2H_2O \Rightarrow H_4SiO_4 \quad \text{.....(5.11)}$$

The silicic acid being a weak acid dissociates in two steps (constants used are for 25°C).

$$H_4SiO_4 \Rightarrow H^+ + H_3SiO_4^- \qquad \beta_1 = \kappa_1 = 10^{-9.82} \quad \text{.....(5.12)}$$

$$H_3SiO_4^- \Rightarrow H^+ + H_2SiO_4^{2-} \qquad \kappa_2 = 10^{-13.10} \quad \text{.....(5.13)}$$

The cumulative constant for the reaction:

$$H_4SiO_4 \Rightarrow 2H^+ + H_2SiO_4^{2-} \qquad \beta_2 = \kappa_1 \times \kappa_2 = 10^{-22.92} \quad \text{.....(5.14)}$$

From equation 5.14 the equilibrium for equilibration of silicic acid resulting from dissolution of amorphous silica can be expressed as

$$K = \frac{[H^+][H_2SiO_4^{2-}]}{[H_4SiO_4]} = 10^{-22.92} \quad \text{.....(5.15)}$$

Taking logarithms to base 10 on both sides of equation (5.15) gives:

$$22.92 = 2pH - [Log\, H_2SiO_4^{2-} - Log\, H_4SiO_4] \ldots\ldots\ldots\ldots\ldots\ldots\ldots\ldots\ldots\ldots..\ldots\ldots\ldots..(5.16)$$

Equation (5.16) was then used to derive the plots for silicic acid equilibria over the pH range of 6.5- 8.85. The plots are shown in figures 5.28, 5.29 and 5.30.

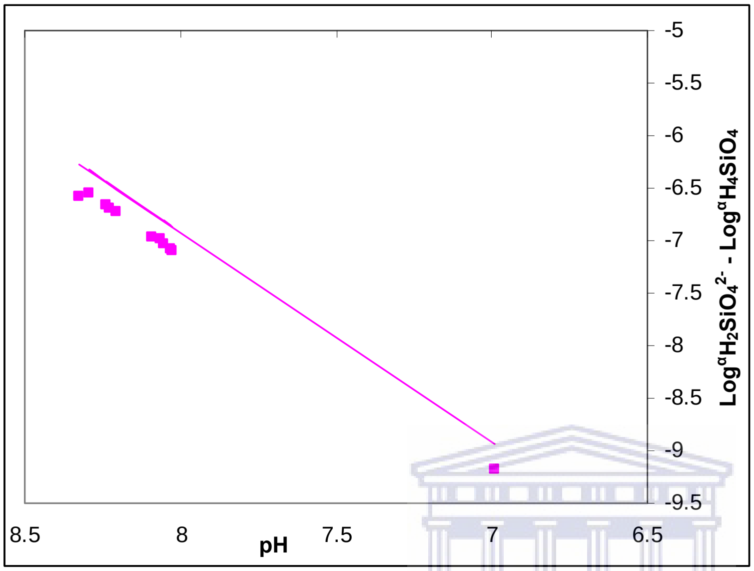

Figure 5.28: Amorphous silica solubility equilibria for solid residue (SR) column core leachates. (solid line represents SiO2$_{(amorphous)}$ equilibria)

UNIVERSITY of the
WESTERN CAPE

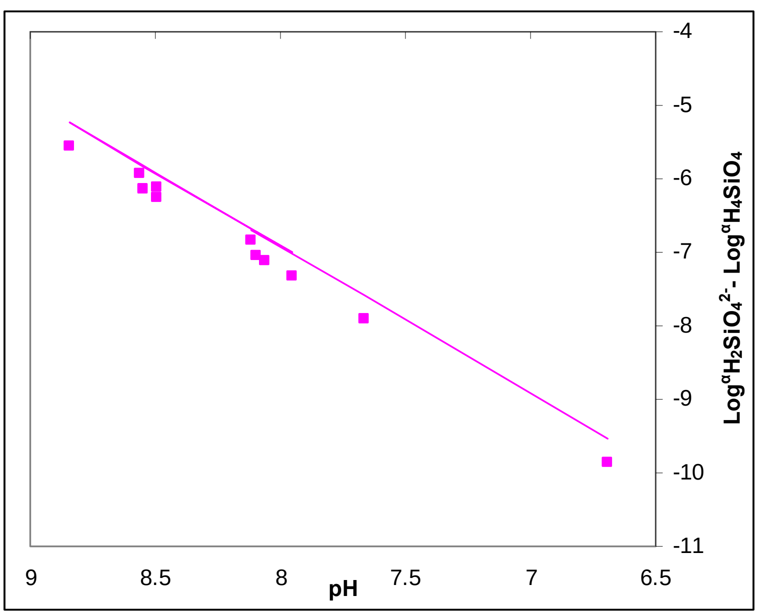

Figure 5.29: Amorphous silica solubility equilibria for solid residue (SR) + 25 % FA column core leachates.

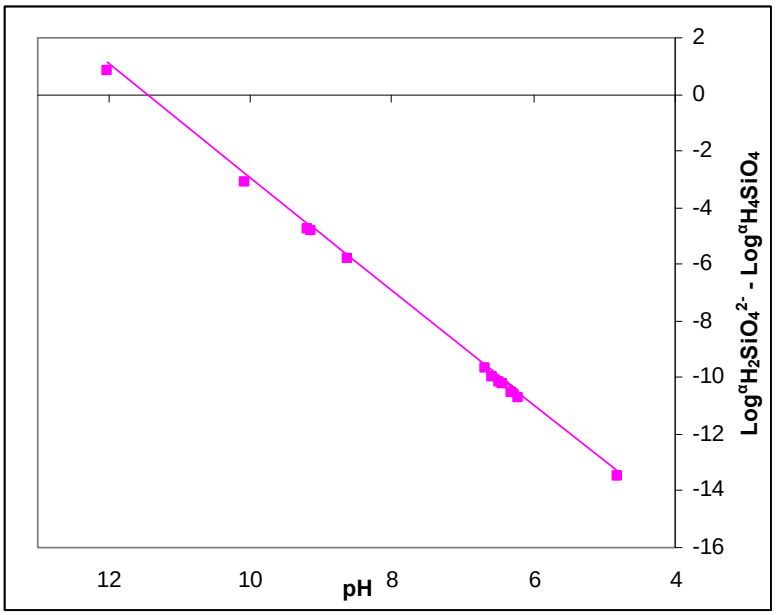

Figure 5.30: Amorphous silica solubility equilibria for FA column core leachates.

UNIVERSITY of the
WESTERN CAPE

An observation of the amorphous silica equilibria as a function of pH indicates that the leachates were near equilibrium with amorphous silica over the pH range 6.5-8.85. The equilibration is less for the solid residue (SR) core leachates than for the solid residue (SR) + 25 % FA core leachates. This is probably due to the slightly high pH generated in this column. This is confirmed further by the total equilibrium observed in the FA cores. This strongly indicates that amorphous silica largely controlled solubility of aqueous H_4SiO_4 in the leachates at this pH range. An observation of the calculated saturation indices for amorphous silica indicates that it was under-saturated for the entire drainage period confirming that it was undergoing dissolution in the FA, solid residue (SR) and solid residue (SR) + 25 % FA cores.

Evidence that part of the glassy phase was soluble and was contributing to the consumption of acidity as the drainage progressed is seen in the change in the ratio of the mullite: quartz peak in the XRD patterns for FA, SR and SR + FA column solid cores (Figs 5.31, 5.32 and 5.33). The change in the ratio of the diffraction peak intensities for mullite and quartz indicates that dissolution of the glassy material from the ash particles occurred and varied with depth. This led to increase in intensity of the mullite peak relative to quartz. This is a possible indication that the $SiO_{2(a)}$ in the solid residues (SR) or coatings on the mullite were dissolving relative to quartz. This is observed until at the bottom of the column where most

likely precipitates formed in the upper parts of the column are deposited on the lower section. Warren and Dudas.(1984) observed that Al and Si leached from the ash under acidic conditions appeared to be derived from the glassy matrix of the fly ash particles. The change in the ratio of diffraction peak intensities for mullite: quartz indicated that dissolution of the glassy material decreased with depth in the ash core according to the chemical dissolution gradient. The upper and middle parts of the solid cores in this study experienced the greatest chemical dissolution and probably this explains the increased relative intensity of mullite. Analysis of the leached solid residue cores indicated a chemical gradation with the top section of each column showing the highest load of precipitates and low pH and the last section showing the highest pH indicating least chemical reactivity (Figs 5.74, 5.75 and 5.80). Chemical extraction results indicated an increase of Al, Si and Fe in the solid cores from top section to the bottom section for the amorphous fraction (Tables 5.11, 5.12, 5.13 and 5.14). This confirms that highest degree of chemical activity was at the top decreasing to the bottom of the solid core as the SAMD percolated through the solid residues.

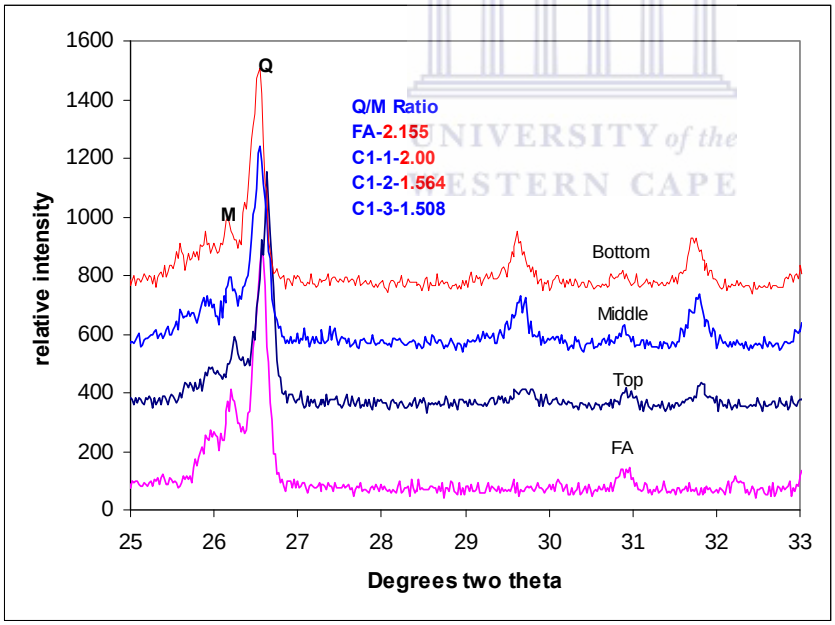

Figure 5.31: XRD spectra of the FA column solid cores showing the change in the mullite: quartz peak ratio from top to bottom.

UNIVERSITY of the WESTERN CAPE

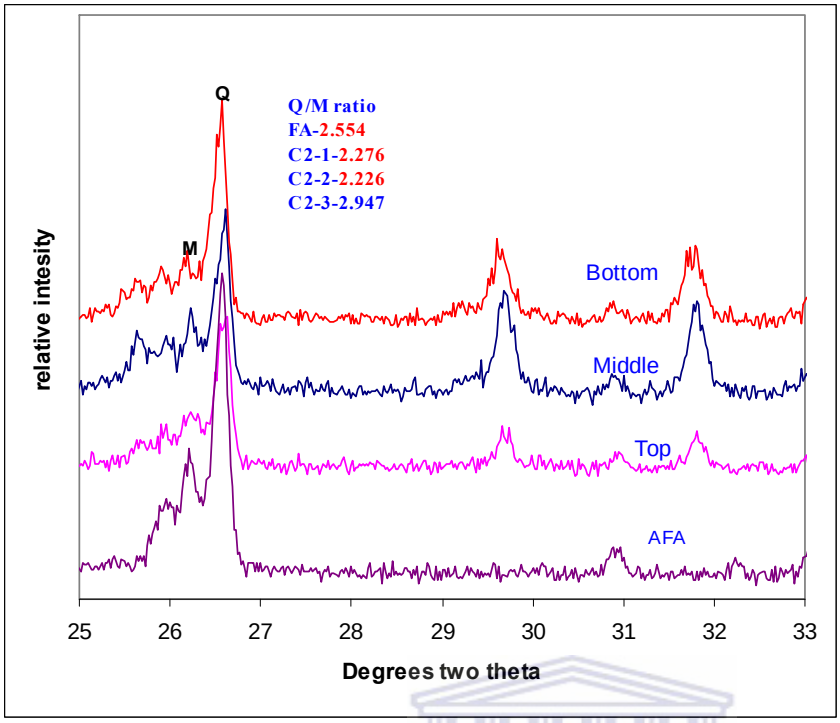

Figure 5.32: XRD spectra of the solid residue cores showing the change in the mullite: quartz peak ratio from top to bottom of core.

UNIVERSITY of the
WESTERN CAPE

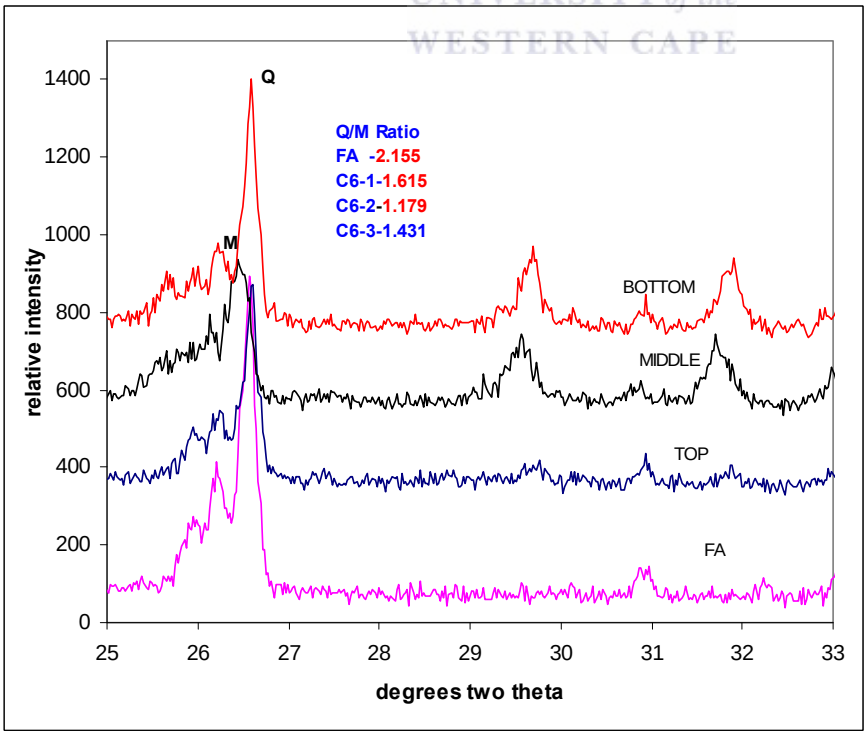

Figure 5.33: XRD spectra of the solid residue (SR) + 40 % FA cores showing the change in the mullite: quartz peak ratio from top to bottom.

At this point it can be tentatively concluded that at pH 6.5-8.5 the silicic acid system is controlling the pH in the leachate analogous to the control of pH in natural waters by the carbonate system (Drever, 1997). The buffering of the leachate pH by the silicic acid system will only hold as long as there is $SiO_{2\ (amorphous)}$ dissolution from SR, SR + FA solid cores or generation of silicic acid by the dissolution of the aluminosilicate matrix, otherwise the buffering is overwhelmed when the $SiO_{2\ (amorphous)}$ is completely dissolved from the fly ash matrix. Yong *et al*. (2001) determined heavy metal (Cu, Zn, Pb) retention capacity of some estuarine alluvia soils using column tests by draining with a landfill leachate at pH 1.5. The resulting effluent was buffered at pH 7.5-9.5.The soils mainly consisted of kaolinite, illite and chlorite. This collaborates the results obtained in this study which observed that after the initial rapid hydration of CaO resulting in alkaline pH the leachates were thereafter buffered at pH 7.5-9.5 for a greater duration of the experiment by the slow dissolution of amorphous silica and aluminosilicates.

PHREEQC simulation indicates that the leachates for the FA solid cores were oversaturated or at equilibrium with $Al(OH)_{3(amorphous)}$ at 36-97 days of drainage (pH 8-8.5) (Fig 5.65 and Table B14). An observation of the Al trends in the leachates (Fig 5.43) show a decrease in Al concentration at 29 days of drainage. Except for the peak at 53 days which was attributed to resolubilization of previously formed precipitates the concentration remained below 6 ppm until 97 days of drainage. Precipitation of $Al(OH)_{3(a)}$ can occur through the following reaction (equation 5.17) consuming acidity and contributing to buffering of pH in the region of pH 8-8.5.

$$Al(OH)_4^- + H^+ \Rightarrow Al(OH)_3 + H_2O \quad \text{.....(5.17).}$$

Calculation of equilibrium pH ($Log\ K_{eq}$= 5.6) using activities of $Al(OH)_4^-$ over the pH range did not reveal a correlation with the measured pH. The equilibrium alone could not account for the pH observed. This could partly be due to the fact that $Al(OH)_{3(a)}$ could also be generated directly from the hydrolysis of Al^{3+} from the fresh SAMD feed.

After the buffer zone at pH 7.5-9, the FA, SR and solid residue (SR) + FA solid cores were observed to enter the acidic buffer zone (pH 3-4) as the drainage progressed (Figs 5.6, 5.8, 5.10, 5.12, 5.14 and 5.16). The transition to the acidic buffer zone occurred at different drainage times for each solid core. Several researchers (Adams and Rawajifih, 1977; Bigham

and Nordstrom, 2000; and Nordstrom, 1982) have pointed out that precipitation of basic aluminum sulfate minerals occur in acid sulphate waters. They point out that basaluminite is the first to occur if the solution is sufficiently enriched in sulphate and at pH below 4.5 jurbanite becomes the most stable while alunite is stable at pH range 3.3-5.7. Their formation may follow the reactions below (equations 5.18-5.20):

$$4Al(OH)_3 + 2H^+ + SO_4^{2-} + 3H_2O \Rightarrow Al_4(OH)_{10}(SO_4).5H_2O_{(basalu\,min\,ite)} \quad \text{.....(5.18)}$$

Log K_{eq} = 17.3

$$3Al(OH)_3 + 3H^+ + K^+ + 2SO_4^{2-} \Rightarrow KAl_3(OH)_6(SO_4)_2 + 3H_2O_{(alunite)} \quad \text{.....(5.19)}$$

Log K_{eq} = 28.3

$$Al(OH)_3 + SO_4^{2-} + 2H^+ + 3H_2O \Rightarrow Al(OH)(SO_4).5H_2O_{(jurbanite)} \quad \text{.....(5.20)}$$

Log K_{eq} = 12.0

PHREEQC simulation indicates that (Figs 5.65 and 5.66; Tables B14 and B15) the leachates from the FA, SR, were under-saturated with respect to basaluminite, alunite and jurbanite at pH>8 but became saturated as the pH dropped below 6. The SR + 25 % FA solid cores had not entered the acidic buffer zone at the time of stopping the drainage experiment. Amorphous Al $(OH)_3$ and gibbsite were postulated to be precipitating at pH range 4-11 but became under-saturated in the leachates as the pH dropped to below 4. Precipitation of the basic aluminum sulphate minerals therefore could contribute to acid attenuation according to equations 6.18-6.19 and contribute to buffering of pH in the acidic zone. To test this hypothesis equilbrium pH for these reactions were calculated and compared with the measured pH. The results showed that the equilibrium pH for basaluminite and alunite was out of range of the measured pH hence could not be contributing to buffering in this range but jurbanite was within the range (pH 3.5-5) (Figs 5.34 and 5.35). Khanna *et al*, (1987) suggested that retention and release of sulphate in acidic forest soils was by the successive precipitation and dissolution of jurbanite. They suggested that jurbanite formed from the dissolution of gibbsite. In this study jurbanite could be forming from amorphous Al $(OH)_{3(a)}$ since no crystalline Al phase was identified. Equilibrium pH for alunite in the FA solid cores is within the range of the measured pH (6.5) for days 36-97 of drainage indicating that it was

UNIVERSITY of the
WESTERN CAPE

a strong pH buffer at circum-neutral values. PHREEQC simulation indicates that alunite was oversaturated over the same pH range and drainage period (Fig 5.65 and Table B14).

UNIVERSITY of the
WESTERN CAPE

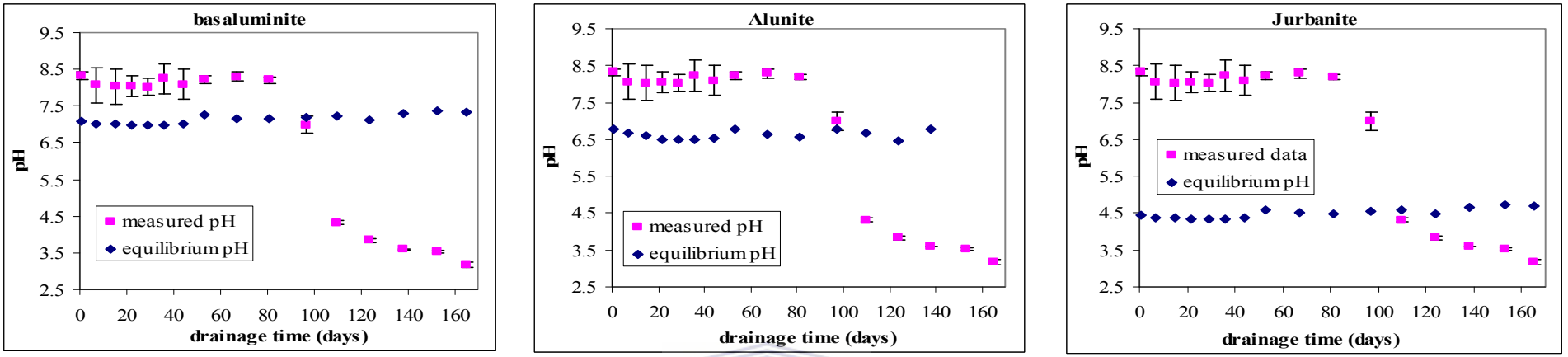

Figure 5.34: Equilibrium pH for precipitating basic aluminium hydroxy sulphates for the SR solid cores compared to measured pH of leachate (error bars represent 1 SD above and below the mean, n=4)

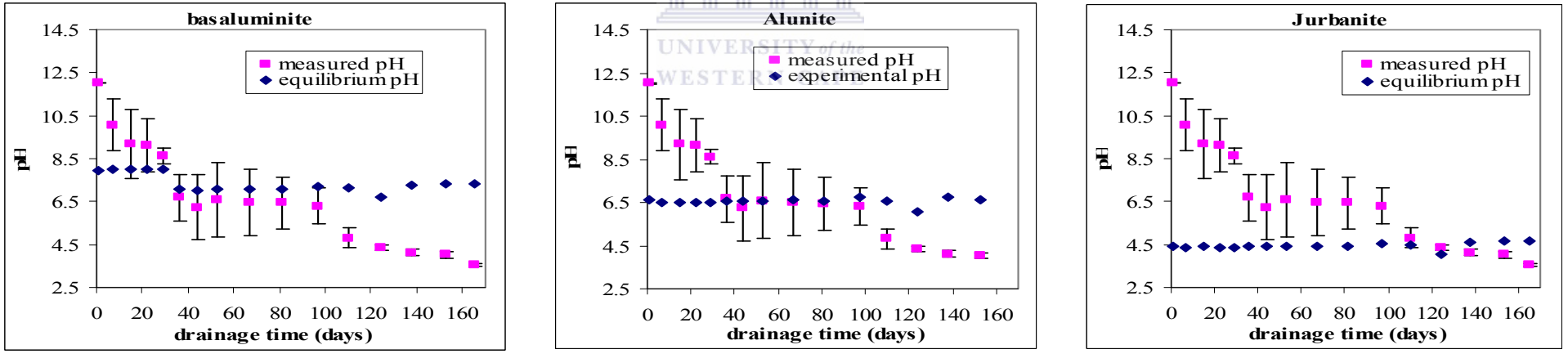

Figure 5.35: Equilibrium pH for precipitating basic aluminium hydroxy sulphates for the FA solid cores compared to measured pH of leachate (error bars represent 1 SD above and below the mean, n=4).

Langmuir (1997) observes that ferric and ferrous sulphates (e.g. coquimbite, the jarosites, melanterite and szomolnokite) are strong acid buffers that keep the pH values at or below 3 until they are dissolved. PHREEQC simulation shows that leachates collected over the pH range 6.5-7 were over-saturated with respect to jarosite-K but became under-saturated as the pH dropped to below 5. For the SR cores the leachates were over-saturated with respect to jarosite-K at the pH range of 8-8.3 becoming highly under-saturated as the pH dropped to below 5. Dissolution of jarosite-K at acidic pH can occur through the following reaction (equation 5.21)

$$KFe_3(SO_4)(OH)_6 + 3H_2O \Rightarrow K^+ + 3Fe(OH)_{3(ppt)} + 2SO_4^{2-} + 3H^+ \quad \text{..... (5.21)}$$

$Log\ K_{eq}$=$10^{-19.5}$

Calculated equilibrium pH for the dissolution of jarosite-K indicates it could be contributing to the buffering of pH at the acidic buffer zone (pH 3.5-4). The equilibrium pH is within the range of the measured pH (Fig 5.36) but it is clear that as the pH drops to below 3.5 dissolution of jarosite-K alone cannot account for the pH.

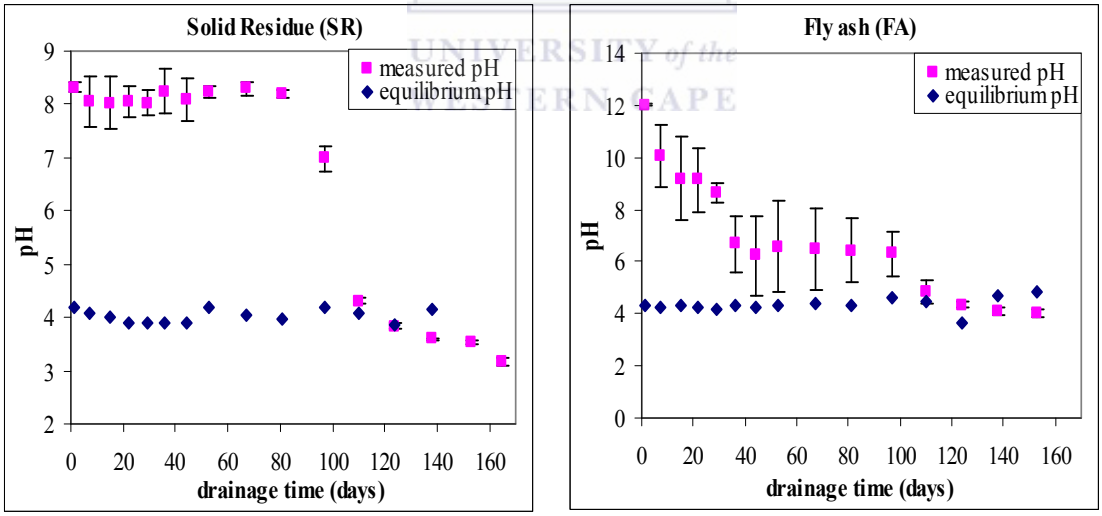

Figure 5.36: Equilibrium pH for the dissolution of jarosite-K for the SR and FA solid cores compared to measured pH of leachate (error bars represent 1 SD above and below the mean, n=4).

The disequilibrium observed could indicate that the system is a continuous dynamic process.

At 165 days of drainage all the column leachates were showing a pH drop to below 3, this drop in pH corresponded with an increase in the major contaminants concentration in the leachate (Mn^{2+}, Fe, and SO_4^{2-}). At 165 days of drainage the Mn^{2+} concentration was higher

than in the initial feed for all the columns while for SO_4^{2-}, FA, SR and SR + 5 % FA columns showed high levels. Therefore it can be said that the pH as the drainage came to a close was mainly buffered by free H^+ and formation of hydrogensulphate (HSO_4^-).

5.3.2 Solid residues (SR) + 6 % Ordinary Portland Cement (OPC) column cores

The SR + 6 % OPC cores exhibited two buffer regions at pH 10.5-11.5 and pH 4 –5.5. On contact with water OPC undergoes hydration releasing $Ca(OH)_2$ which is highly soluble and causes the high pH of the initial leachates. The rapid drop in pH thereafter probably indicates completion of the hydration reactions and transformation of the released $Ca(OH)_2$ to ettringite and gypsum (Cocke and Mollah, 1993). Calculation of saturation indices indicates that ettringite was precipitating in the initial leachates upto 15 days when pH >11.0 (Fig 5.38 and Table B19). SEM-EDX also identified ettringite crystals in the solid cores (Fig 5.37).

UNIVERSITY of the
WESTERN CAPE

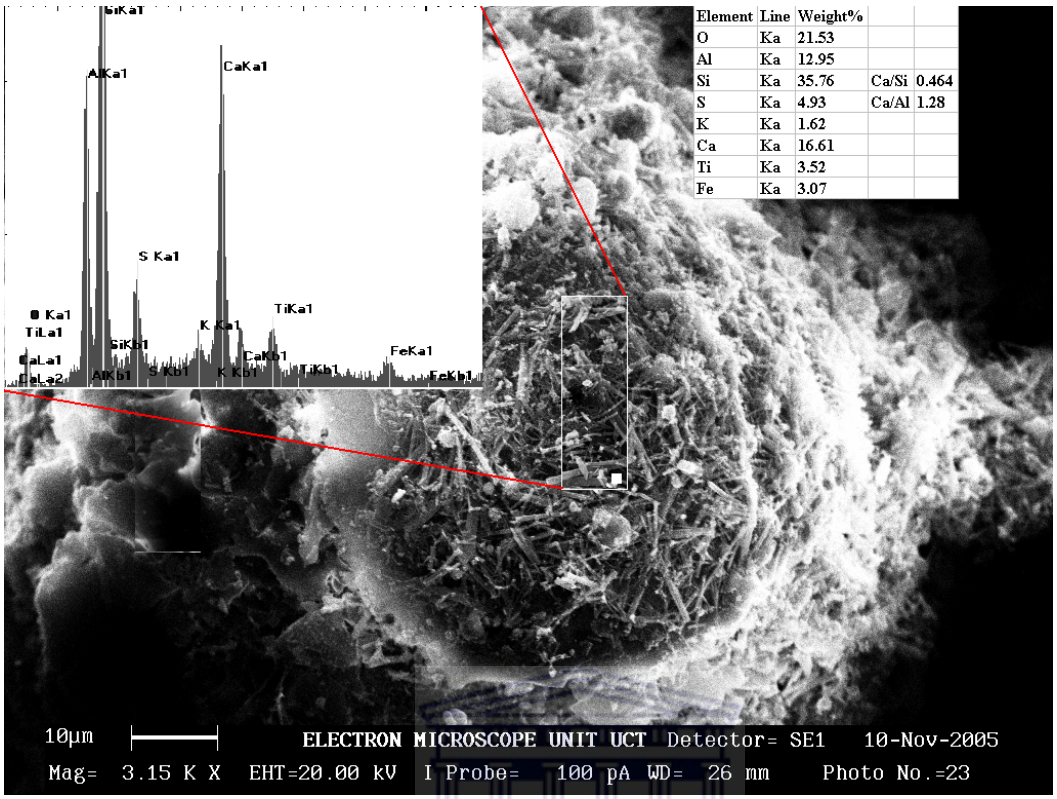

Figure 5.37: SEM micrograph showing ettringite crystals embedded in CSH gel matrix, the EDX pattern is superimposed showing the Ca/Al ratio which approximates that of ettringite. Strong Si signal is observed, a contribution from underlying CSH gel.

UNIVERSITY of the WESTERN CAPE

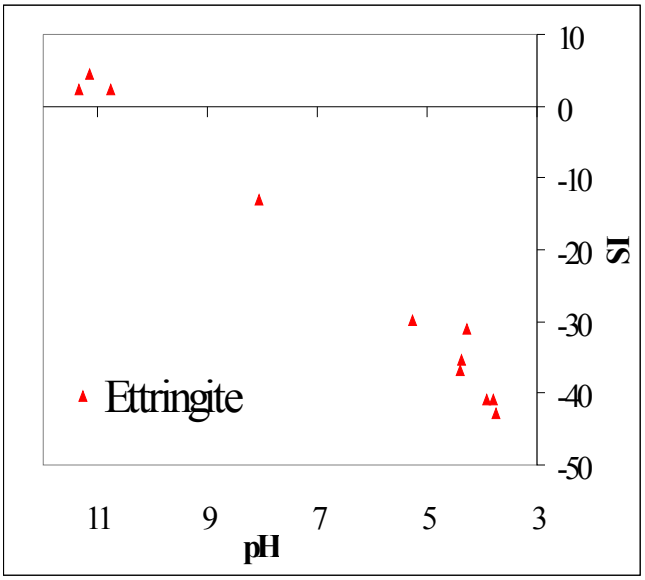

Figure 5.38: Saturation indices for ettringite with pH change as the drainage progressed for the SR + 6 % OPC solid cores.

Ettringite could be formed through two pathways during cement hydration and depending on the chemistry of the water being used. Cocke and Mollah. (1993) summarizes the hydration

reactions of cement and points out that the first stage of cement hydration involves the formation of ettringite from calcium aluminates in presence of gypsum (equation 5.22).

$$Ca_3A + 3CaSO_4 + 32H_2O \Rightarrow 3CaO.Al_2O_3.3CaSO_4.32H_2O_{(ettringite)} \quad \text{.....(5.22)}$$

NB-cement nomenclature, A=Al_2O_3

The second stage involves the formation of CSH gel and generation of portlandite (equation 5.23). SEM and SEM-EDX analysis did show extensive formation of CSH gel (Fig 5.39).

$$2C_3S + 6H_2O \Rightarrow 3CaO.2SiO_2.3H_2O_{(C-S-H)} + 3Ca(OH)_{2(portlandite)} \quad \text{.....(5.23)}$$

NB-cement nomenclature, C=CaO, S=SiO_2, C-S-H=calcium silicate hydrate gel.

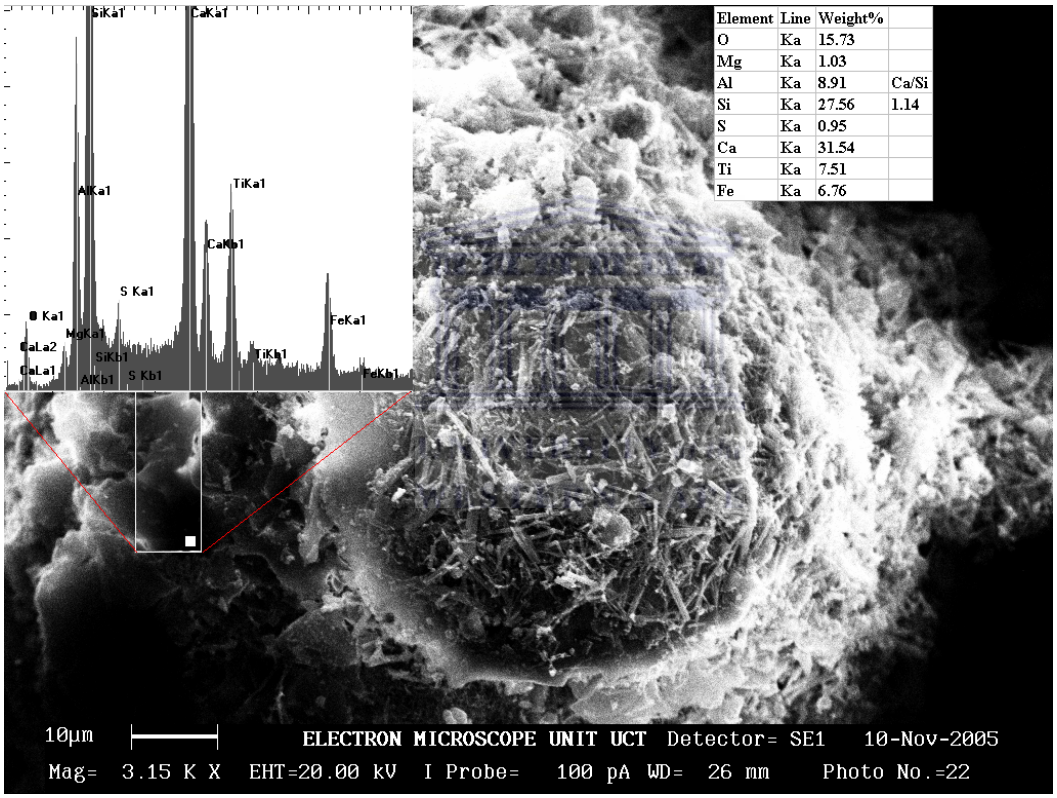

Figure 5.39: SEM micrograph showing the C-S-H gel that embedded the ettringite crystals, the EDS pattern superimposed showing Ca/Si ratio which approximates that of C-S-H gel (Taylor, 1997).

In presence of high sulphate waters ettringite can form directly during the cement hydration reactions (equationn 5.24). The simulated AMD had high sulphate concentrations (14,407 mg/L) and ettringite precipitation highly possible.

$$2Al^{3+} + 6Ca^{2+} + 3SO_4^{2-} + 12OH^- + 32H_2O \Rightarrow Ca_6Al_2(SO_4)_3(OH)_{12}.32H_2O \quad \text{.....(5.24)}$$

The SR + 6 % OPC maintained pH of the leachates above 10.5 for 22 days when 1.4 L of SAMD had been added. A sharp drop in pH was thereafter observed. The lack of the buffering at pH 6.5-9 in these solid core was attributed to the possible aggregation and physical encapsulation of the solid residues by the C-S-H gel formed (Figs 5.40 and 5.41). The interaction between the solid residues and SAMD was thereafter likely to be diffusion controlled.

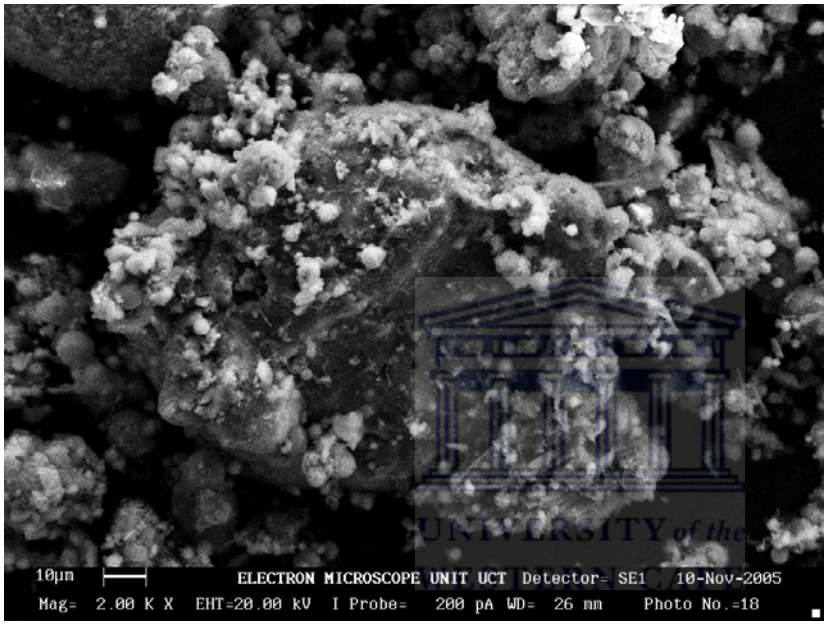

Figure 5.40: SEM micrograph showing extensive aggregation of the solid residue particles in the SR + 6 % OPC column cores.

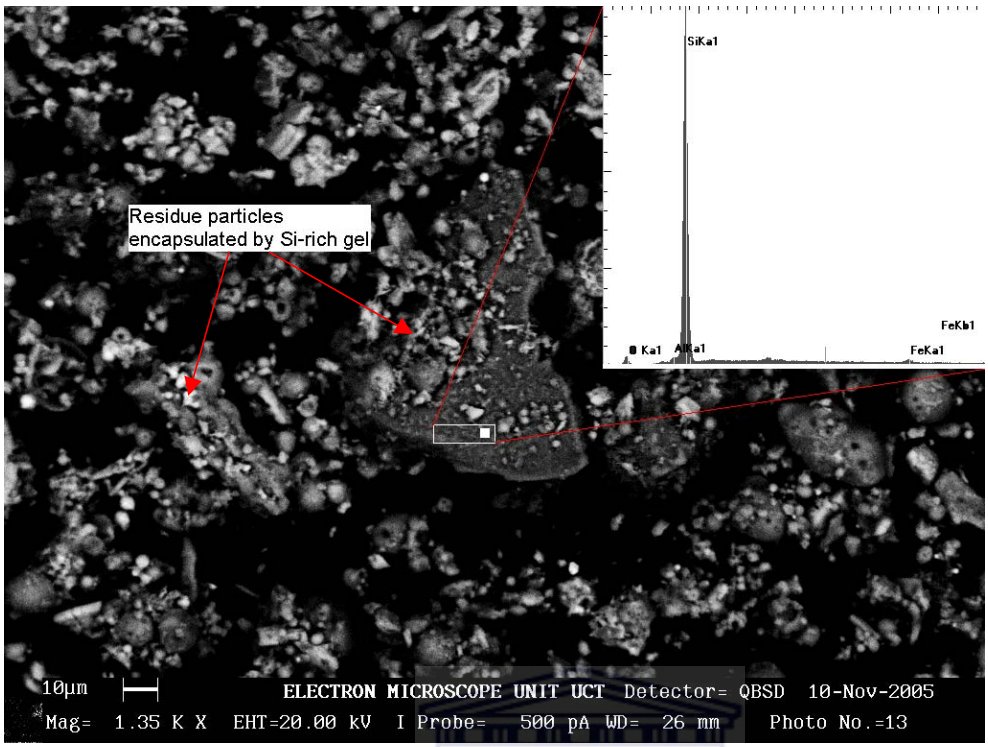

Figure 5.41: SEM micrograph showing encapsulation of the solid residue particles in the SR + 6 % OPC column cores by a Si-rich gel. The gel could not be conclusively identified by SEM-EDX.

UNIVERSITY of the
WESTERN CAPE

PHREEQC simulation indicated that as the pH dropped to below 5, the leachates were at equilibrium or slightly over-saturated with respect to jurbanite. Calculation of equilibrium pH for the formation of jurbanite over the drainage period (29-165 days) shows that jurbanite could have been contributing to the buffering of pH at the range 4-4.5 as the drainage progressed (Fig 5.42). At some point the pH differed by 0.5 indicating that formation of jurbanite could not alone account for the pH observed.

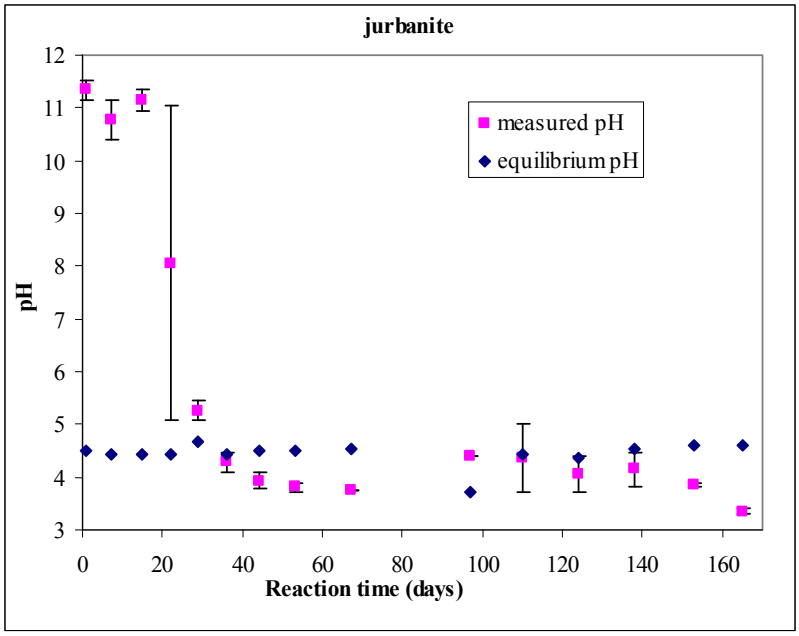

Figure 5.42: Equilibrium pH for the precipitation of jurbanite in SR + 6 % OPC solid cores compared to measured pH of leachate (error bars represent 1 SD above and below the mean, n=4).

UNIVERSITY of the
WESTERN CAPE

5.3.3 Conclusions

The FA cores, the solid residue (SR) + FA and solid residue (SR) + 6 % OPC cores were observed to undergo a stepwise acidification process with several acidity attenuation mechanisms involved as the drainage progressed. Initial leachate pH varied as follows: FA>SR +6 % OPC>SR+40 %>SR+25 %>SR≈SR+5 %. Dissolution of CaO in fly ash and solid residues blended with fly ash impacted high pH in the intial leachates while hydrations reactions in OPC blend solid residues contributed to high initial pH. Dissolution of $SiO_{2(a)}$ and mullite in the solid residues contributed to sustained buffering at pH 7-9.5 for solid residues and fly ash blended solid residues. Encapsulation of solid residue particles by the calcium silicate hydrate gels (CSH) in OPC blended solid residues reduced interaction of particles with SAMD hence the buffering at pH 7-9.5 was not observed. At pH 6.5-7 PHREEQC simulation revealed that equilibrium of alunite with amorphous Al $(OH)_3$ was contributing to the buffering of pH in this range. PHREEQC modeling showed that equilibrium with jurbanite could have contributed to the buffering of pH in the range 4-4.5 in the OPC blend solid residue cores while for SR and FA solid cores equilibrium with K-

jarosite could have contributed to the buffering of pH at the 3.5-4 however equilibrium with these minerals alone could not account for the pH observed.

5.4 Contaminants Attenuation by Fly Ash (FA), Solid Residues (SR), Solid Residues (SR) + 25 % FA and Solid Residues (SR) + 6 % Ordinary Portland Cement (OPC) column blends.

The results of the contaminants attenuation efficiency with reaction time for the FA, SR, SR + 25 % FA and SR + 6 % OPC column blends cores are presented. From the pH profiles discussion it was observed that the significant difference between the various SR + FA blends was that the duration that the leachate pH was sustained at ≈ pH 8.0 was extended to 110 days for the solid residue (SR) + 5 % FA and solid residue (SR) + 25 % FA as compared to the solid residue (SR) column cores. The FA and SR + 40 % FA column cores exhibited similar kinetics. The main mechanism in the fly ash blends is raising the pH and sustainability of the buffering capacity at circum-neutral pH for efficiency clean-up of the SAMD; this was observed to depend on the % FA in the blend. Addition of OPC to the solid residues was observed to introduce significant changes to the leachate chemistry as compared to the FA blends. On this basis the detailed discussion of the contaminants attenuation mechanisms will be confined to FA, SR, SR + 25 % FA and SR + 6 % OPC solid cores.

5.4.1 Fly ash column cores

The figures 5.43-5.44 below shows Fe, Al, Mn, SO_4^{2-} attenuation trends with cumulative volume of SAMD drained through, Ca trends are also included due to its influence in SO_4^{2-} attenuation.

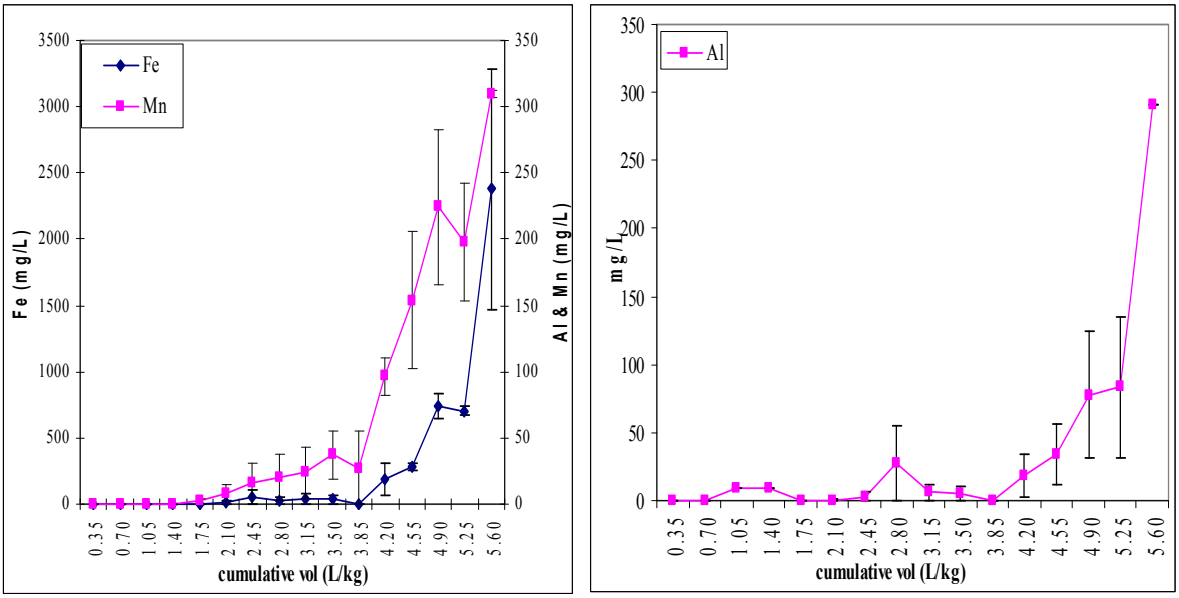

Figure 5.43: Fe, Mn and Al concentration in leachates versus cumulative volume (L/kg) of SAMD for FA solid cores (error bars represent 1 SD above and below the mean, n=4).

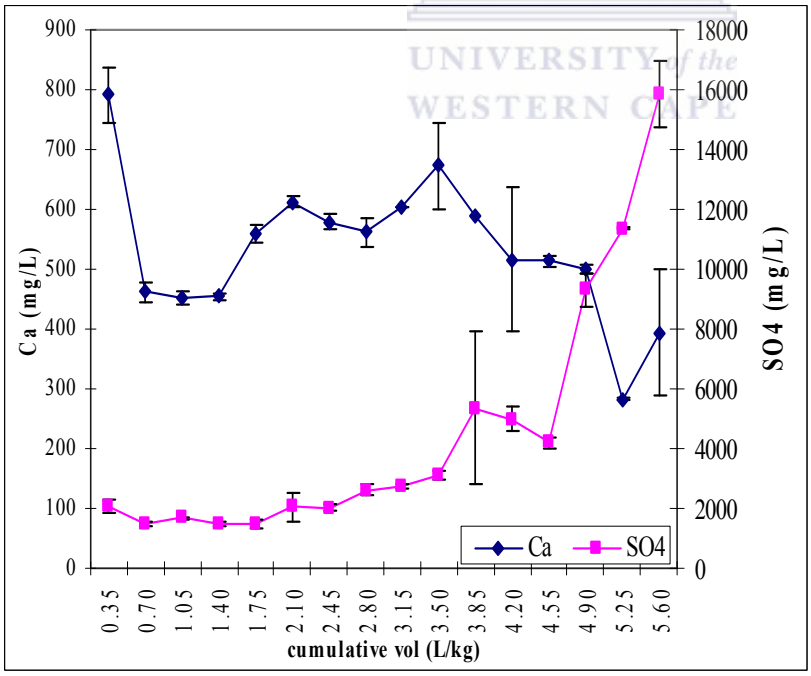

Figure 5.44: Ca and SO_4^{2-} concentration in leachates versus cumulative volume (L/kg) of SAMD for FA solid cores (error bars represent 1 SD above and below the mean, n=4).

.

5.4.1.1 Sulphate and calcium

The simulated AMD contained 14407 mg/L SO_4^{2-} in addition to release of SO_4^{2-} from the fly ash. At the onset of the drainage experiments, the pH of the leachate was highly alkaline due to dissolution of CaO in the fly ash (Fig 5.44). The removal of SO_4^{2-} from the AMD was quite efficient with SO_4^{2-} in the leachate dropping to ≈ 2000 mg/L compared to the initial feed (Fig 5.44). Dissolution of soluble Ca salts and subsequent precipitation of gypsum accounts for the low levels of SO_4^{2-} in the leachates. The parallel trends displayed by the concentrations of Ca and SO_4^{2-} in the leachate upto 81 days when 3.5 L of SAMD had drained through probably indicate that gypsum could be controlling their concentration in solution. A gradual increase in SO_4^{2-} concentration in the leachates upto 97 days when 3.85 L of SAMD had drained through was observed as the pH dropped. As the SO_4^{2-} concentration increases, Ca starts to decrease indicating that the Ca concentration has dropped below the level at which gypsum super saturation is attained and gypsum is no longer exacting any control on SO_4^{2-} concentration. The highest concentration of SO_4^{2-} observed at 97 days is still far less than the concentration of the initial feed which indicates SO_4^{2-} attenuation mechanisms are still operationally even as the pH enters the acidic buffer region.

UNIVERSITY of the
WESTERN CAPE

5.4.1.2 Total iron, manganese and aluminum

The initial simulated AMD contained 200 mg/L Mn^{2+} and 5000 mg/L total iron (Fe^{2+}/Fe^{3+}). The alkaline conditions generated due to the dissolution of CaO in the fly ash created optimum conditions for the precipitation of Mn and Fe (Fig 5.43). Concentration of Fe and Mn observed in the leachates for over 29 days when 1.75 L of SAMD had drained through were low, 0.002-2.24 mg/L Mn and 1.92-2.09 mg/L Fe. At 36 days of drainage the fly ash ability to remove Mn^{2+} weakened and a gradual increase in concentration was observed with subsequent drainages. However a sharp increase in concentration in the leachate was observed at 110 days corresponding to a pH drop to below 6.0. However the highest Mn^{2+} concentration observed in the leachates was half the initial feed concentration indicating that Mn retention mechanisms were still active. At 36 days of drainage when 2.1 L of SAMD had drained through a gradual increase in concentration of Fe was observed. This was attributed to the unprecipitated Fe^{2+} in the initial feed as Fe^{3+} is precipitated out of solution at this pH 6-8. Analysis of leachates recovered at 36 days confirmed Fe^{2+} which increased in

concentration with subsequent drainages. A sharp increase in Fe concentration is then observed at 110 days corresponding to pH drop to below 5.0. This again is attributed to unprecipitated Fe^{2+} in the initial feed.

The initial simulated AMD contained 1000 mg/L Al^{3+}. Al concentration in the leachates shows a distinct trend. Initially when the pH values are highly alkaline (Fig 5.6), the concentration in the leachate is low (0.021-0.189) mg/L for the first 7 days (Fig 5.43). This is followed by a rapid increase in concentration as the pH drops to the range of 8-11.0. This is again followed by a drop in concentration at 29 and 36 days respectively (0.092 - 0.953 mg/L). A sharp increase in concentration is again observed at 53 days corresponding to a pH drop to below 6.0. This increase was attributed to the probable partial re-solubilization of earlier formed precipitates or possible channeling in one of the duplicate columns leading to low pH (4.82) and subsequent dissolution of earlier formed precipitates.

5.4.2 Solid residue (SR) column cores

The figures 5.45-5.46 below shows Fe, Al, Mn, SO_4^{2-} attenuation trends with time, Ca trends are also included due to its influence in SO_4^{2-} attenuation.

UNIVERSITY of the
WESTERN CAPE

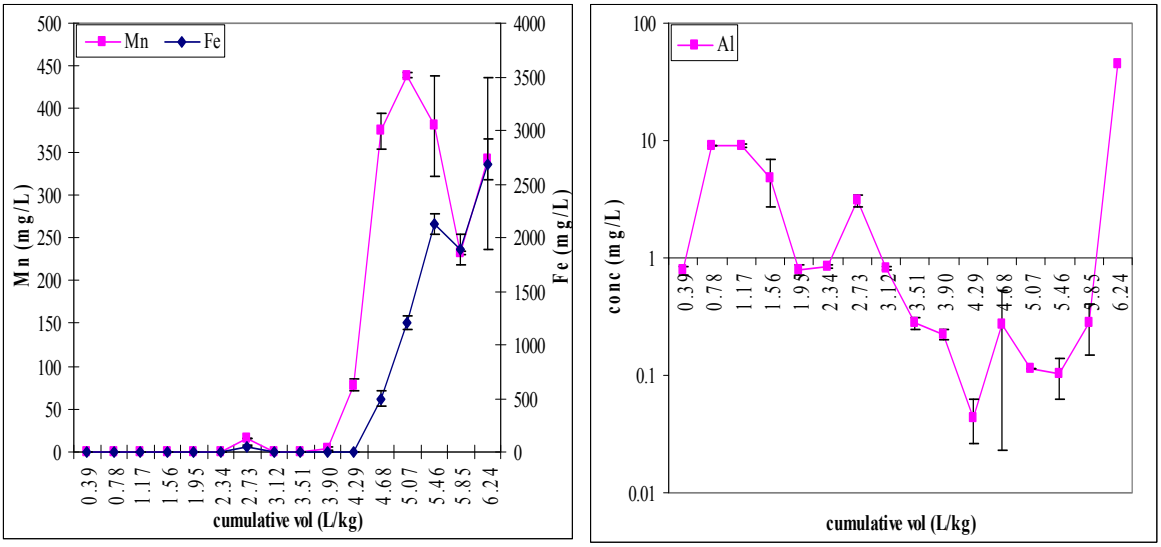

Figure 5.45: Fe, Mn and Al concentration in leachates versus cumulative volume (L/kg) of SAMD for SR solid cores (error bars represent 1 SD above and below the mean, n=4).

.

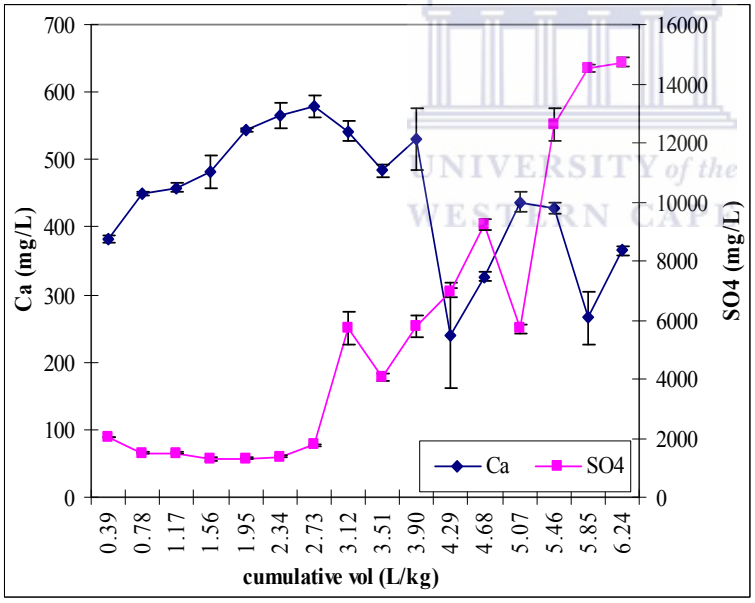

Figure 5.46: Ca and SO_4^{2-} concentration in leachates versus cumulative volume (L/kg) of SAMD for SR solid cores (error bars represent 1 SD above and below the mean, n=4).

5.4.2.1 Sulphate and calcium

The initial decrease in Ca concentration observed with FA columns is lacking in SR columns. This is attributed to dissolution during neutralization with AMD to generate the solid residues. The solid residues exhibit a slightly higher efficiency of SO_4^{2-} removal than the fly

ash solid cores, with concentrations at less than 2000 mg/L upto 44 days when 2.45 L of SAMD had drained through (Fig 5.46). A sharp increase in concentration to 6500 mg/L 53 days when 2.58 L of SAMD had drained through was observed. This phenomenon has been observed in the fly ash solid cores for elements like Al, Mn and Fe (Fig 5.43 and 5.44) and is attributed to probable re-solubilization of previous formed precipitates. The SO_4^{2-} concentrations thereafter are observed to increase sharply as the pH drops (Fig 5.46) and reach a maximum of 9500 mg/L at the acidic buffer region. This increase indicates that the SO_4^{2-} attenuation mechanism is exhausted at between 53 and 67 days on addition of 3.51 L of SAMD. At the stoppage of the drainage experiments the SO_4^{2-} concentration in the leachates was greater than in the initial feed strongly indicating re-solubilization of previously formed precipitates under the strongly acidic conditions.

5.4.2.2 Total iron, manganese and aluminum

The solid residues exhibited high efficiency in removal of Mn and Fe from SAMD. The concentrations for Fe remained below 1.8 mg/L and Mn below 0.24 mg/L upto the 10th drainage (Fig 5.45) on addition of 3.90 L/Kg of SAMD. From day 1 to 81 days the pH of the leachates was greater than 7.0 (Fig 5.8) and precipitation of these elements as insoluble hydroxides accounts for the low concentrations observed. A sudden increase in concentration for both elements is observed at 44 days when 2.45 L of SAMD had been added, the increase does not correspond to any pH drop, and this is attributed to partial re-solubilization of previously formed precipitates. A sharp increase in concentration for Mn at 97 and 110 days and Fe at 110 days coincided to a drop in pH to below 7.0.

Al concentrations remain below 9mg/L up to 110 days (Fig 5.45) when 4.2 L of SAMD had been added (Table 5.4). Considering the initial concentration in the simulated AMD of 1000 mg/L the solid residues show a high efficiency of Al attenuation. The trend for Al is similar to that of the FA solid cores, showing sharp increase within 15 to 22 days and again at 44 days (Table 5.4). These increases do not correspond to any pH drop which strongly points to re-solubilization of previously formed precipitates. Unlike for the FA solid cores where the concentration increases as the pH drops below 5.0, for the SR the concentration remains below 0.27 mg/L. The concentration of Al reaches a maximum of 45 mg/L only under highly acidic conditions (Figs 5.6 and 5.8). This indicates that a great deal of Al is adsorbed onto the surface and that the SR has a high capacity to retain Al.

UNIVERSITY of the WESTERN CAPE

5.4.3 Solid residues (SR) + 25 % FA

The figures 5.47-5.48 below shows Fe, Al, Mn, SO_4^{2-} attenuation trends with time, Ca trends are also included due to its influence in SO_4^{2-} attenuation.

5.4.3.1 Sulphate and calcium

The SO_4^{2-} concentration in the SR + 25 % FA column show a decrease from an initial value of 2472 mg/L to 909 mg/L at 7 days (Fig 5.48) when 0.7 L of SAMD had been added. The concentration remained below 1596 mg/L upto 44 days when 3.15 L of SAMD had been added (Table 5.4). A sudden peak in concentration is observed at 53 days (5647 mg/L), followed by a subsequent drop to 2321 mg/L at 67 days (Fig 5.48 and Table 5.4). This peak in concentration has been observed in SR (Fig 5.46) and SR + 5 % FA columns (Table B10) and is attributed to re-solubilization of previously formed precipitates. This peak in concentration corresponds to the change of drainage intervals from 7 to 14 days (Table 5.4). The longer 14 days interval imposed dry conditions which
led to the precipitation of soluble sulphates after evaporation which re-dissolved on resumption of drainage. Domenech *et al* (2002) observed a similar phenomenon in their column experiments.

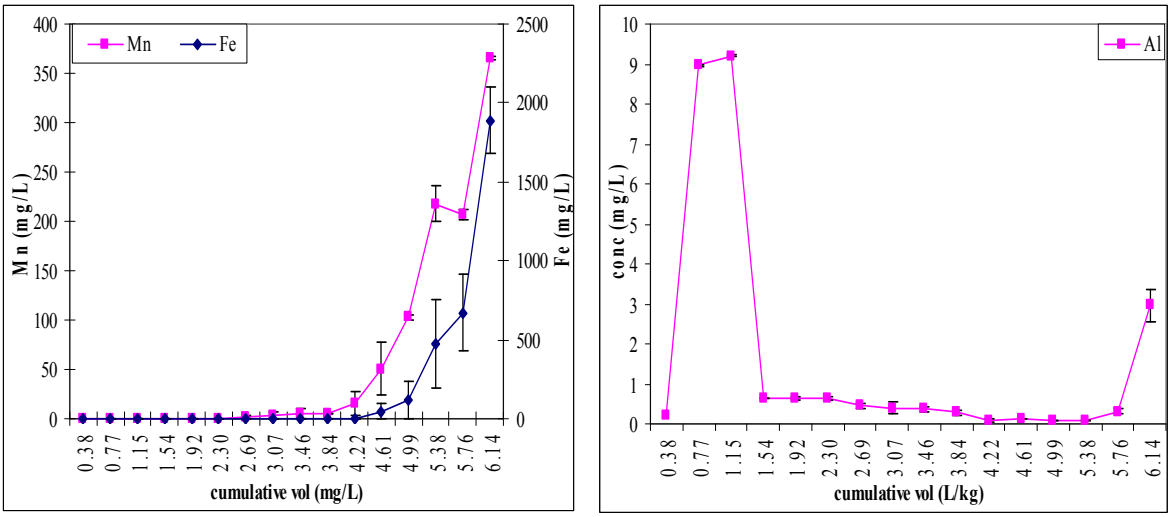

Figure 5.47: Fe, Mn and Al concentration in leachates versus cumulative volume (L/kg) of SAMD for SR + 25 % FA solid cores (error bars represent 1 SD above and below the mean, n=4).

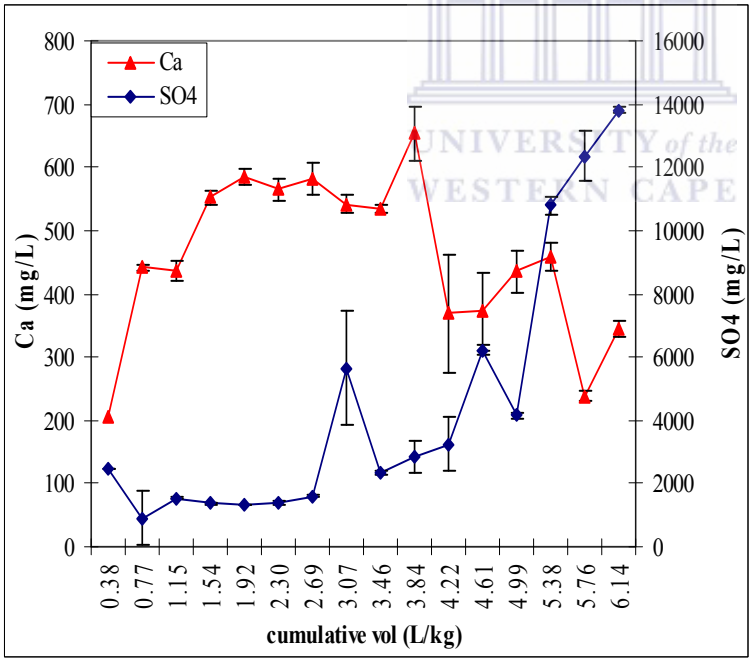

Figure 5.48: Ca and SO_4^{2-} concentration in leachates versus cumulative volume (L/kg) of SAMD for SR + 25 % FA solid cores (error bars represent 1 SD above and below the mean, n=4).

They observed an accumulation of water soluble sulphates at the top of the column which they attributed to precipitation of soluble sulphates through evaporation. At 110 days a sharp

increase in concentration was observed which coincided to a drop in pH to below 7.0 (Fig 5.12).

A similar trend for Ca is observed as for SR, SR + 5 % FA (Table B9 and B10) solid cores. The initial decrease at 7 days of drainage observed in FA columns is not observed for SR + 25 % FA columns. A peak in Ca concentration is observed at 81 days when 4.5 L of SAMD had been added, a phenomenon observed in all other solid cores. The cumulative Ca leached varied in the following order: FA > SR+ 25 % FA > SR + 5 % FA >SR + 6 % OPC which strongly indicates that Ca released in the leachate was directly linked to the % FA in the blend. A phenomenon observed for the Ca profile during the drainage experiment is that after the initial rapid release of Ca incase of FA cores, Ca attains almost a steady state between 22-81 days of drainage (Table 5.4). This clearly points to two different sources of Ca in the FA blended solid residues.

UNIVERSITY of the
WESTERN CAPE

5.4.3.2 Total iron, manganese and aluminum

The concentration of Mn in the leachates remained below 15.7 mg/L and Fe below 2.74 mg/L upto at 97 days (Fig 5.47). The pH of the leachates was maintained above 8.0 (Fig 5.12). Precipitation of metal hydroxide at the alkaline pH could account for the low concentration observed. At 110 days (Table 5.4) a steady increase in concentration is observed corresponding to the breakthrough of the pH front (Fig 5.12) with subsequent drop in pH to below 7.0. At 124 days Mn attained a concentration equivalent to the feed (SAMD) which increased with subsequent drainages. This was a strong indication that re-solubilization of previous formed precipitates was active under the acidic regime. Dissolution of the fly ash could also be contributing to the high concentration of Mn (Table 5.5). By 165 days (Fig 5.47 and Table 5.4) the Fe concentration was still below the initial feed concentration.

The concentration of Al exhibits a similar leaching pattern as observed in other column cores (FA, SR, SR + 5 % FA) except the peak at 44 days (Fig 5.47 and Table 5.4). The peak at 7-15 days corresponds to the phenomena observed in other columns. After 15 days of drainage the concentration remains below 0.64mg/L up to 153 days on addition of 3.6 L of SAMD when a sharp increase is observed. A highly efficient removal of Al is exhibited through the

165 days of leaching considering that the initial feed concentration was 1000 mg/L. This indicates that Al was being strongly adsorbed on the surfaces of the residue solids since the pH had entered the acidic zone and hydrolysis with precipitation of Al hydroxides would be minimal.

5.4.4 Solid residues (SR) + 6 % Ordinary Portland Cement (OPC)

The figures 5.49-5.50 below shows Fe, Al, Mn, SO_4^{2-} attenuation trends with time, Ca trends are also included due to its influence in SO_4^{2-} attenuation.

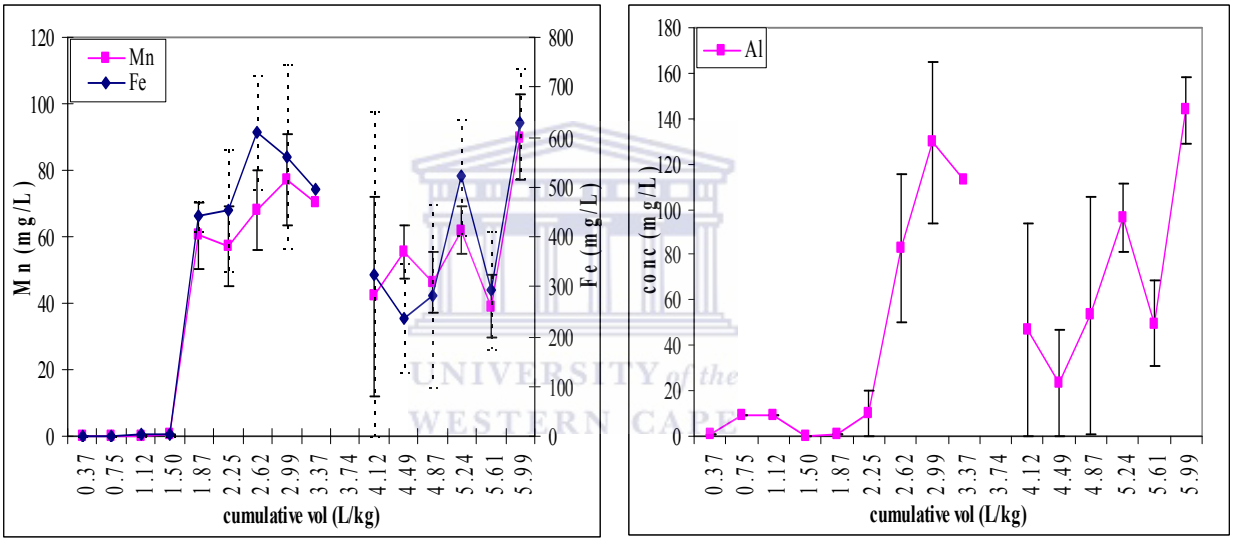

Figure 5.49: Fe, Mn and Al concentration in leachates versus cumulative volume (L/kg) of SAMD for SR + 6 % OPC solid cores (error bars represent 1 SD above and below the mean, n=4).

.

UNIVERSITY of the WESTERN CAPE

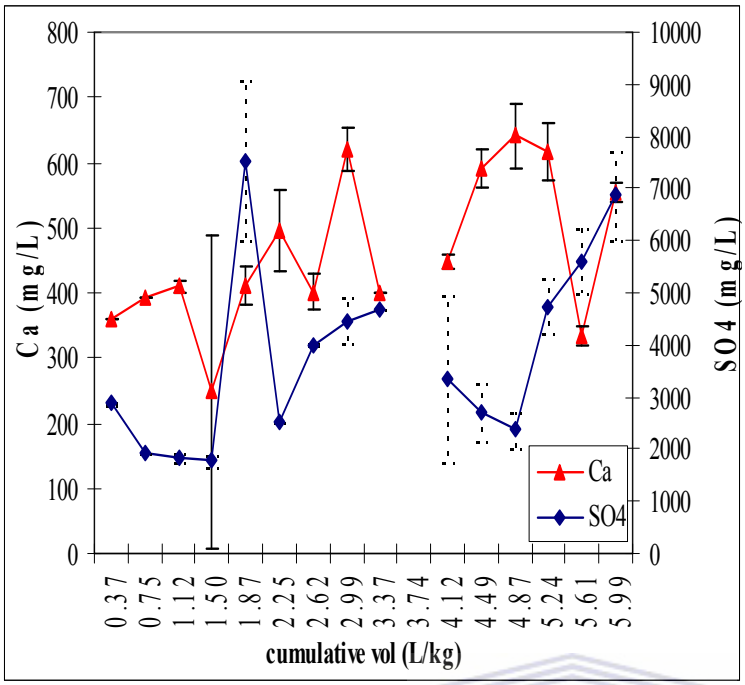

Figure 5.50: Ca and SO_4^{2-} concentration in leachates versus cumulative volume (L/kg) of SAMD for SR + 6 % OPC solid cores (error bars represent 1 SD above and below the mean, n=4).

UNIVERSITY of the WESTERN CAPE

5.4.4.1 Sulphate and calcium

The SO_4^{2-} concentration in the leachates drops from 2875.8mg/L at day 1 to a steady value at 7 - 22 days (1767-1906 mg/L) (Fig 5.50 and Table 5.4). The high pH generated in the leachates at day 1 to 22 days induces several processes that lead to the removal of SO_4^{2-} from the leachant. Hydration of OPC releases Ca^{2+} and OH-, Ca^{2+} and SO_4^{2-} precipitates out as gypsum and ettringite in presence of Al, while Fe, Al and Mn will precipitate out as metal hydroxides with corresponding adsorption of SO_4^{2-}. At 29 days of drainage a sharp increase in concentration was observed when 1.87 L of SAMD had been added (Table 5.4). This coincided to a pH drop to below 5.5 (Fig 5.16), the high concentration probably results from the re-solubilization of previously formed precipitates. This was followed by a drop in concentration at 36 days of drainage. The concentration of SO_4^{2-} at 110 days is below 3000 mg/L a low concentration compared to other columns which is a strong indication that SR + 6 % OPC solid cores has high capacity to adsorb or incorporate SO_4^{2-} at highly acidic conditions.

5.4.4.2 Total iron, manganese and aluminum

The concentration of Mn remains below 0.35 mg/L upto 22 days while Fe maintains a value below 2.07 mg /L (Fig 5.49). The pH of the leachates was maintained above 10.5 upto 22 days (Fig 5.16). The low concentration observed was attributed to precipitation of metal hydroxides at the high pH and possible incorporation in the resulting CSH gel. A sharp increase in concentration for both elements was observed at 29 days on addition of 1.87 L/kg of SAMD (Table 5.4) when the pH was observed to drop to below 6. Peaks in concentration for both elements are then observed at 44 and 53 days and again at 138 days, a phenomenon observed with other elements Zn, Ni and Cu. These peaks in concentration are attributed to re-solubilization of previously formed precipitates as the pH drops to below 6 and 4 respectively. At 165 days both elements show a sharp increase corresponding to the pH drop to below 4 (Fig 5.49). The final concentrations at the close of the leaching experiment are 89.9 mg/L and 628.5 mg/L for Mn and Fe respectively. This column solid cores show a high efficiency of Mn and Fe removal than all other SR blends even at high acidic conditions. The concentration of both elements remains well below that of the initial feed. This indicates that OPC could have induced other mechanisms for attenuation of these metals that are not prevalent in the other blends, such as encapsulation in the calcium silicate hydrate (CSH) gel.

UNIVERSITY of the
WESTERN CAPE

The concentration profile for Al is similar to that observed in SR + 25 % FA and SR + 40 % FA (data not shown) solid cores. An initial increase in concentration is observed at 7 - 15 days (9.01 - 9.33 mg/L) (Fig 5.49). This corresponds to the high pH buffer region and formation of Al $(OH)_4^-$ will dominate (Drever, 1997). From 36 days the concentration increases to a peak at 53 days of drainage (129.4 mg/L). This is a phenomena observed in other solid cores. These peaks are attributed to the re-solubilzation of previously formed precipitates, reason being they don't correspond to any pH drop. A sharp increase in concentration is observed at 165 days as the pH drops to below 4. The concentrations at the close of the leaching experiments are higher than for other solid core which indicates that the Al adsorption capacity of this OPC blend is low (Figs 5.43, 5.45, 5.47, 5.49).

5.4.5 Decontamination Efficiency of each Column Solid Core.

In order to estimate the efficiency of the column solid cores for passive decontamination of the percolating SAMD, total amounts of elements drained through the solid cores and thereafter recovered were calculated. The total amount of elements/ions in mmol drained through each column were calculated based on the total SAMD volume drained through for each column solid core and the recovery was calculated based on the leachate collected for the study period. The calculated % contaminant removed by each column is presented in Table 5.7.

Table 5.7: Total amount in mmol of ions drained through each column and calculated % contaminant removed by each column solid core

mmol/element	Al	Fe	Mn	SO4
Total input	207.56	501.34	41.51	806.79
FA(recovered)	6.42	24.38	6.22	95.94
% removed	**96.91**	**95.14**	**85.02**	**88.12**
SR (recovered)	0.90	48.52	10.88	134.84
% removed	**99.57**	**90.32**	**73.79**	**83.29**
SR + 5 % FA(recovered)	0.30	16.92	6.39	142.55
% removed	**99.86**	**96.63**	**84.61**	**82.33**
SR + 6 % OPC (recovered)	8.30	25.76	3.61	105.37
% removed	**96.00**	**94.86**	**91.31**	**86.94**
Total input	266.85	644.62	26.21	1037.30
SR + 25 % FA (recovered)	0.38	23.36	7.13	113.41
% removed	**99.82**	**95.34**	**82.83**	**89.07**
Total input	326.16	787.87	32.04	1267.82
SR + 40 % FA (recovered)	0.63	23.45	7.24	122.76
% removed	**99.70**	**95.32**	**82.55**	**90.32**

The removal of elements from solution can be seen in table 5.7 where the total amount (mmol) of each constituent drained through the columns and the total amount (mmol) of each constituent in the leachates for each column may be seen. The FA, SR + 25 % FA, SR + 40 % FA and SR + 6 % OPC have a higher capacity than SR and SR + 5 % FA column solid core to remove SO_4^{2-}. Apart from the SR + 6 % OPC solid core the SO_4^{2-} removal seems to be favored by increasing % FA in the blend. Dissolution of CaO from the added fly ash and formation of Ca $(OH)_2$ from OPC hydration in presence of SO_4^{2-} results in precipitation of

gypsum. The FA, SR + 5 % FA, SR + 25 % FA, SR + 40 % FA and SR + 6 % OPC exhibit superior capacity to attenuate Fe and Mn^{2+} than the SR solid cores. This is a result of the added alkalinity from the unreacted fly ash in each column raising the pH of the SAMD solution which results in the precipitation of those elements from solution. The SR and SR + FA solid cores however show a higher capacity than other columns in removal of Al. SR solid core was observed to have a high capacity to remove Al at low pH. The precipitated compounds are, however stable in all the columns and do not re-enter the leachate solution. The concentration of these elements only starts to increase in the leachate once the alkalinity in each column has been exhausted and the pH drops to below 4 (Figs 5.6, 5.8, 5.10, 5.12, 5.14 and 5.16). Based on the calculated decontamination efficiency the re-solubilization observed in the early stages of the drainage experiments does not seem to be significant in contributing to release of previously immobilized contaminants.

5.5 Contaminants Attenuation Mechanisms and Solubility Controls

The contaminants profiles in the leachates as discussed in sub-sections 5*.4.1, 5.4.2, 5.4.3, 5.4.4,* suggest several mechanisms that could be involved in attenuation of the contaminants as the percolating SAMD interacts with the solid residue particles, fly ash particles and solid residue + OPC particles. The high efficiency of the FA and SR + FA blends to remove Fe, Mn and SO_4^{2-} suggests that the high alkalinity generated leads to precipitation of the heavy metals and that dissolution of CaO in the fly ash and also in the aluminosilicate matrix could be playing a role in the long-term attenuation of sulphate. The high efficiency of the SR cores to remove Al could be attributed to the slow release of alkalinity and buffering of pH at 6.5-9 for a large duration of the study. This pH range is within the hydrolysis pH of Al (pK= 4.9) and precipitation of various Al hydroxides is greatly favored. The attenuation efficiency of the contaminants seems to be tied to the solid cores being able to generate sufficient alkalinity; it is observed that the contaminants concentration in the leachates starts to increase as the pH drops to below 4 signaling the depletion of the alkalinity in the solid cores. However the SR + 6 % OPC cores exhibit high attenuation efficiency even as the pH drops to below 4. The above observations indicate that as the SAMD percolates through the solid cores the contaminants are subsequently attenuated by precipitation, co-precipitation and adsorption reactions. The following section discusses the probable mechanisms responsible

for the attenuation of the contaminants and the probable secondary solid-phase controls on the concentration of each contaminant in the leachates.

5.5.1 Sulphate and calcium

The FA, SR + FA column solid cores exhibited high efficiency of SO_4^{2-} attenuation for the first 81 days of the drainage experiments (Figs 5.44, 5.46, 5.48 and Table 5.4). The efficiency of SO_4^{2-} removal was greatly dependent on the % FA in the blended SR. The SR + 40 % FA column core maintained lower levels of SO_4^{2-} than the FA core for a longer duration of the study (Figs 5.44 and Table B12) indicating that SO_4^{2-} removal was through a combination of several mechanisms. The removal of SO_4^{2-} through gypsum precipitation seems to occur through two steps:

a) Initial rapid dissolution of CaO from the fly ash and precipitation thereafter as gypsum in presence of the SO_4^{2-} rich SAMD for the FA and SR + FA column cores. This is observed in the initial rapid drop of SO_4^{2-} in these solid core leachates.
b) An almost constant level of SO_4^{2-} is maintained thereafter which is parallel to the level of Ca in the leachates. This is most noticeable in the SR leachates. Dudas (1981) observed that after the initial rapid release of Ca from fly ash, slow dissolution of the fly ash matrix with concomitant nearly constant levels of Ca is observed. The Ca levels observed for the SR and SR + FA cores after the initial dissolution can be attributed to the dissolution of the fly ash matrix and could partly account for the continuous attenuation of SO_4^{2-}.

UNIVERSITY of the
WESTERN CAPE

Calculation of saturation indices (SI) indicates that initially the leachates were slightly under saturated with respect to gypsum for the FA, SR and SR + FA solid cores attaining equilibrium at between 36-110 days of drainage (Table 5.4; Tables B14-B18). This attainment of equilibrium corresponds to the peak in Ca concentration for the mentioned column solid cores (Figs 5.44, 5.46, 5.48). This is most noticeable for SR cores where the leachates become highly oversaturated at between 53-97 days of drainage. This confirms that after the initial rapid dissolution of CaO, dissolution of CaO locked in the aluminosilicate matrix was occurring gradually as the drainage progressed and this is most evident in the SR solid cores. As the Ca concentration drops with increase in acidity the leachates become slightly under saturated again and this is paralleled by an increase in SO_4^{2-} concentration in

the leachates. Plots of *Log* $^{\alpha}$ SO4 versus *Log* $^{\alpha}$Ca strongly points ($^{\alpha}$ represents activity of the species as determined using PHREEQC) to control of Ca and SO_4^{2-} by precipitation of gypsum (Figs 5.51-5.52).

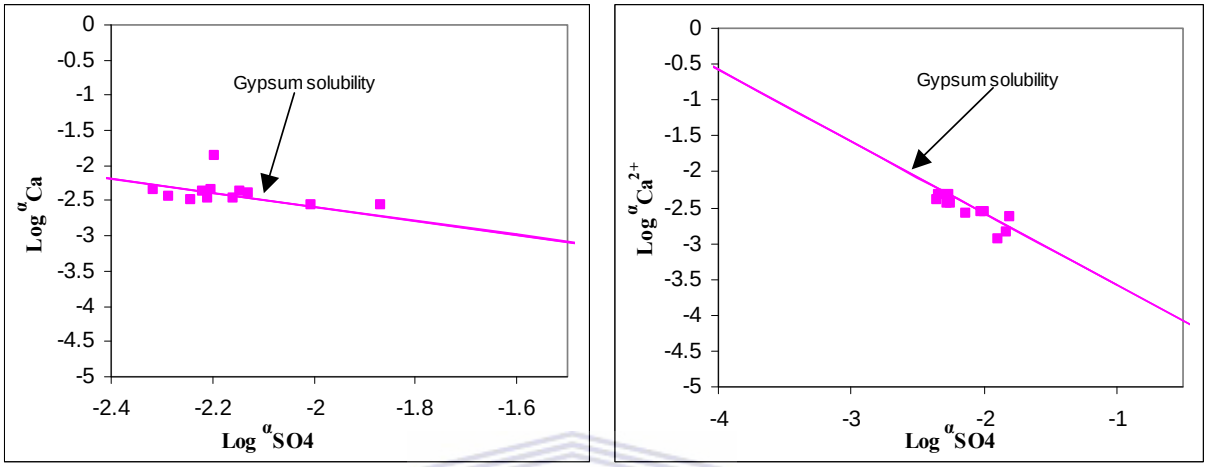

Figure 5.51: Plots of log SO_4^{2-} activity versus log Ca activity showing control of SO_4^{2-} and Ca by gypsum solubility in the leachates for FA and SR solid cores.

UNIVERSITY of the WESTERN CAPE

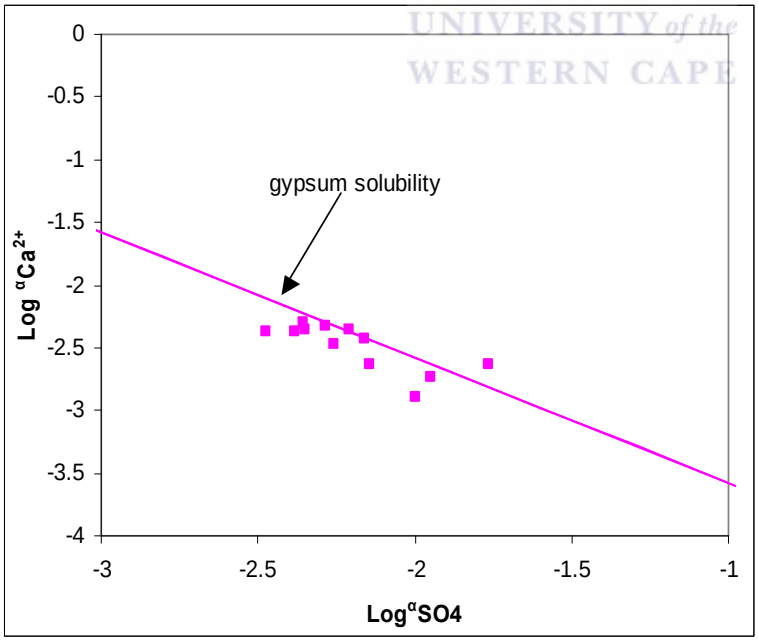

Figure 5.52: Plots of log SO_4^{2-} activity versus log Ca activity showing control of SO_4^{2-} and Ca by gypsum solubility in the leachates for SR + 25 % FA column solid cores.

Further evidence of the gypsum precipitation came from the XRD, SEM and SEM-EDX analysis of the leached solid cores. SEM and SEM-EDX analysis revealed extensive formation of gypsum crystals in the entire length of the solid core from top to bottom (Figs 5.53 and 5.54). High frequency of gypsum crystals was however observed in the top section of each column which showed the highest degree of interaction with SAMD (Figs 5.74 and 5.75). The presence of gypsum crystals on all the sections of the leached solid residue cores indicates that under the strongly acidic conditions, gypsum was not significantly re-dissolved if any. XRD identified gypsum in all sections of the leached solid cores (Figs B20-B23).

UNIVERSITY of the
WESTERN CAPE

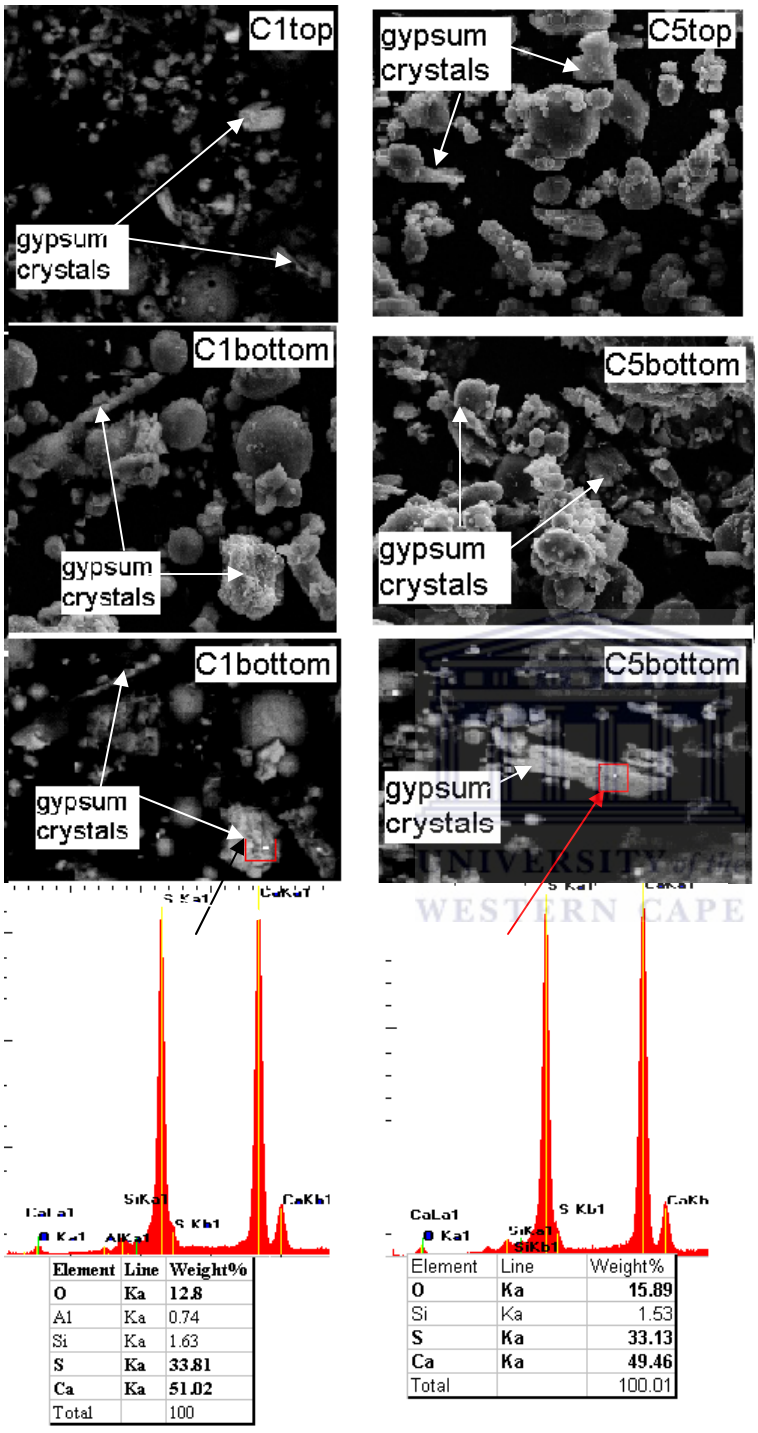

Element	Line	Weight%
O	Ka	12.8
Al	Ka	0.74
Si	Ka	1.63
S	Ka	33.81
Ca	Ka	51.02
Total		100

Element	Line	Weight%
O	Ka	15.89
Si	Ka	1.53
S	Ka	33.13
Ca	Ka	49.46
Total		100.01

Figure 5.53: SEM micrographs of leached solid residues from column 1(FA) and column 5 (SR + 25 % FA) showing gypsum crystals, C1, C5bottom-Backscattered signal, C5top-secondary electron signal, with accompanying EDX pattern of the spots analyzed (enclosed in a box).

UNIVERSITY of the WESTERN CAPE

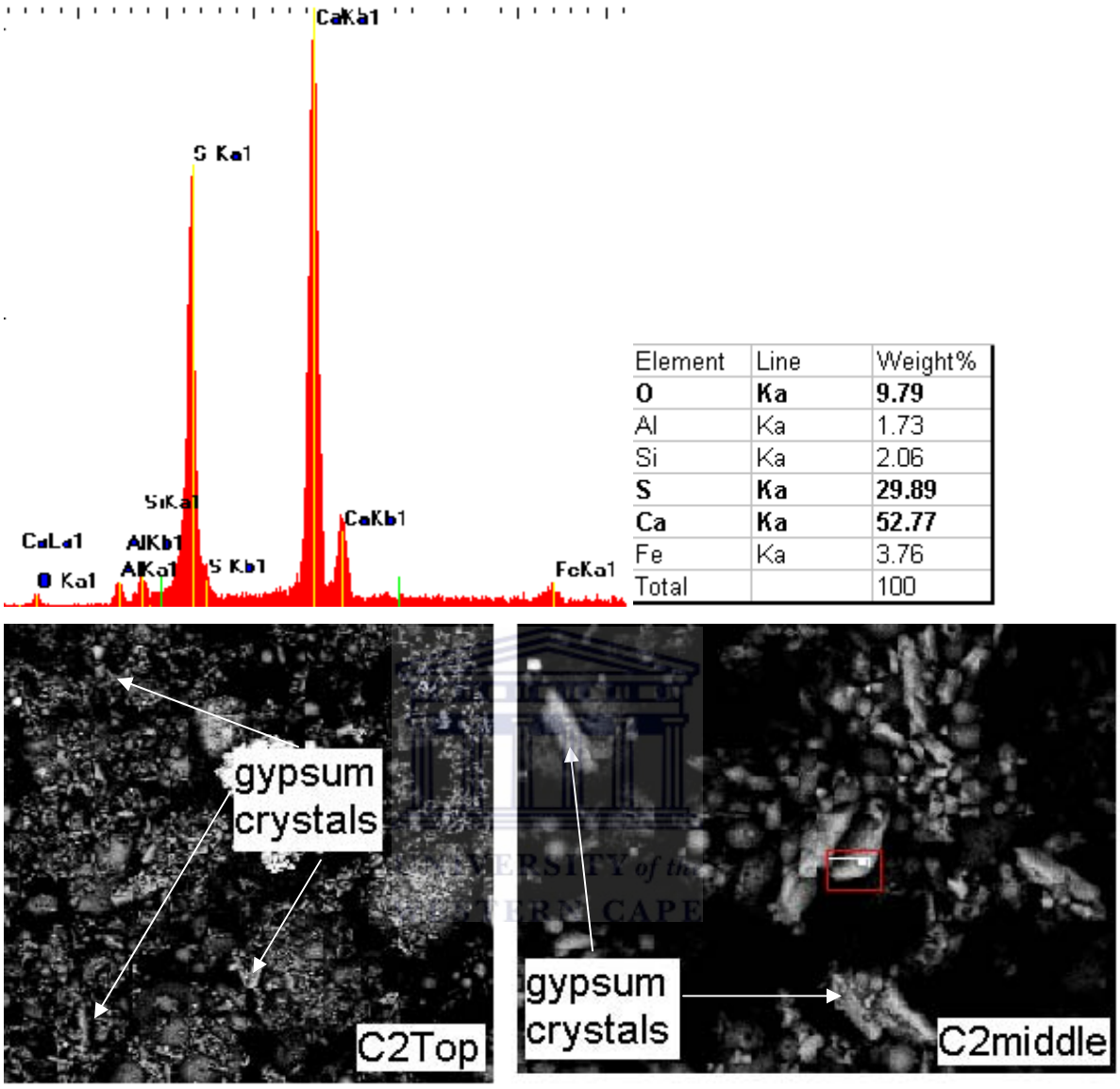

Element	Line	Weight%
O	**Ka**	**9.79**
Al	Ka	1.73
Si	Ka	2.06
S	**Ka**	**29.89**
Ca	**Ka**	**52.77**
Fe	Ka	3.76
Total		100

Figure 5.54: SEM micrographs of leached solid residues from column 2(SR) showing gypsum crystals. C2Top –Backscattered signal, magnification=500. C2middle-backscattered electron signal, magnification=3000, with accompanying EDX pattern of the spots analyzed (enclosed in a box).

An observation of the SO_4^{2-} trends for the FA and SR + FA solid cores (Figs 5.44, 5.46, 5.48) indicates that the attenuation of SO_4^{2-} is greatest when Fe and Al are low in the leachates. Attenuation of SO_4^{2-} by Fe and Al mineral phases could be through structural incorporation in phases such as jarosite, jurbanite, alunite and adsorption by amorphous ferric hydroxides. This becomes more evident as the pH drops to below 4 when precipitation of ferrous and ferric ions decreases and a corresponding increase in SO_4^{2-} is observed. PHREEQC

simulation predicted these minerals to be precipitating within the pH range 4.5-11 (Tables B14-B19). Regression of log Fe activity versus log SO_4^{2-} activity within the pH range 4.5-11 for the FA and SR + FA column cores leachates indicated a strong relationship (Fig 5.55 and Table 5.8). Although the strong regression observed is not a confirmation of any chemical interaction between SO_4^{2-} and Fe-mineral phases being formed, it's a strong indication that a form of interaction could be taking place. This interaction could be structural incorporation of SO_4^{2-} or adsorption on the precipitate surfaces. Seth and Ghazi (1997) points out that Fe precipitates formed in acid mine drainage environments consist of between 600-800 mmol/kg SO_4^{2-}. Seth and Elliot (2000) go on to confirm that 30-45 % of this SO_4^{2-} is ammonium oxalate soluble meaning it's associated with the amorphous iron oxy hydroxides. Despite the high levels of Fe and Al precipitating out within this pH range no Fe or Al mineral phase was detectable by XRD.

UNIVERSITY of the
WESTERN CAPE

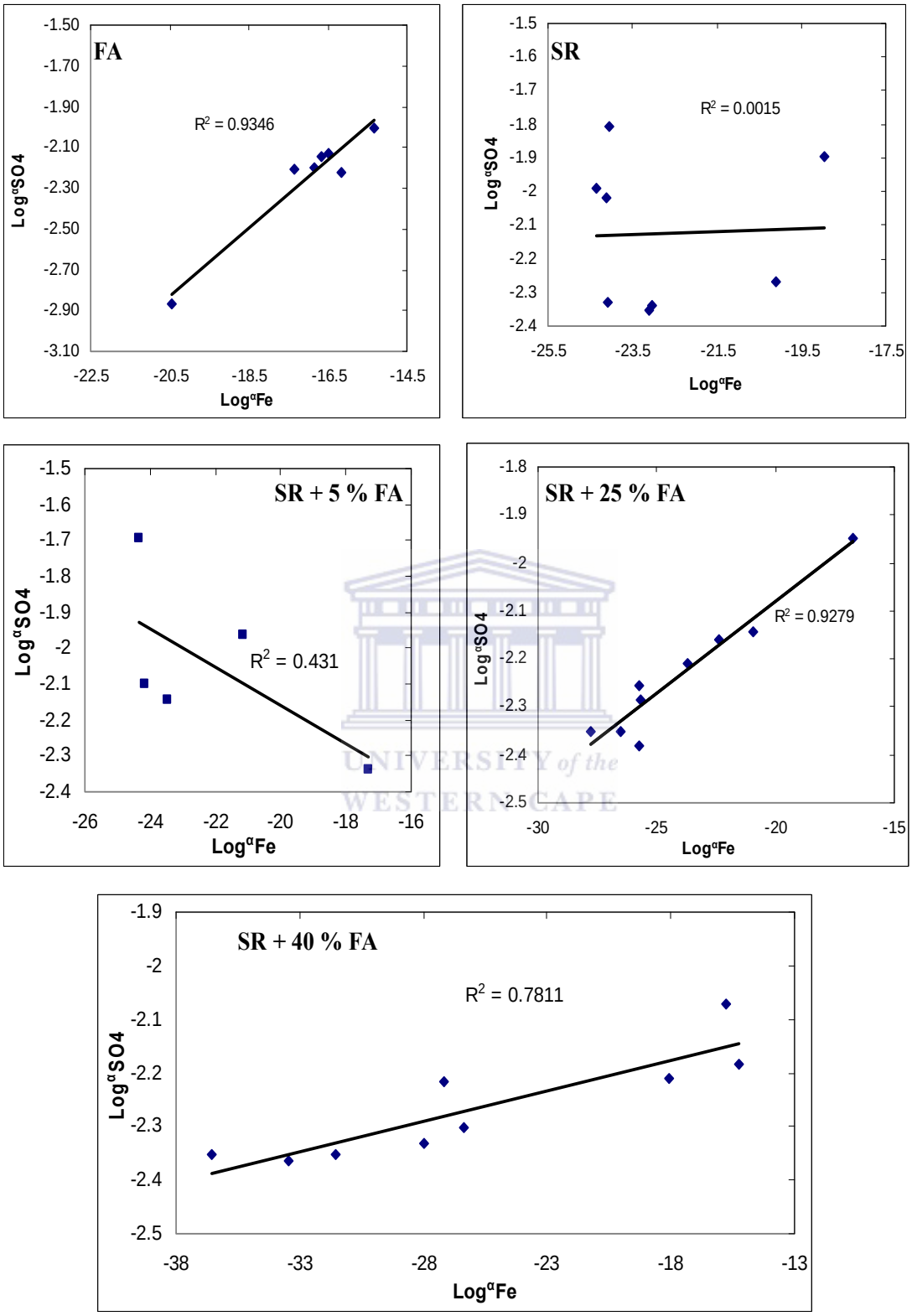

Figure 5.55: Regression analysis of log Fe activity versus log SO_4^{2-} activity for the FA, SR and SR + FA solid cores leachates. (R^2 reported at 95 % confidence limits).

Table 5.8: Drainage time (days) and pH range over which the regression was calculated.

Column core	drainage time(days)	pH range	R^2
FA	36-124	7-8	0.9346
SR	22-97	8-8.5	0.002
SR +5% FA	44-110	7.5-6.5	0.431
SR +25% FA	15-124	8-8.5	0.9279
SR +40% FA	22-124	4.5-11	0.7811

In the SR + 6 % OPC column cores two mechanisms for the attenuation of SO_4^{2-} were identified as the column core acidified.

a) Ettringite formation at the high pH generated by OPC hydration in presence of Al and SO_4^{2-} from SAMD.

Extensive formation of ettringite was observed in all sections of the column solid core, which means it did not undergo dissolution as the pH dropped to below 4. Ettringite is known to undergo incongruent dissolution to gypsum and Al-hydroxide at pH ≤ 10.7 (Myeni *et al.*, 1998). Observation of ettringite in the leached solid cores is contrary to Myeni *et al*. (1998) findings since the pH dropped to below 4 during the course of the drainage experiments. Analysis of the ettringite crystal by SEM and SEM-EDX revealed that they were coated by C-S-H gel which resisted dissolution under the acidic regime and kept the crystals intact (Fig 5.39).

UNIVERSITY of the
WESTERN CAPE

b) Gypsum formation as the leaching of CaO in the aluminosilicate matrix occurred gradually as the drainage progressed. Apart from the sharp increase in SO_4^{2-} content in the leachates at 29 days of drainage, the Ca and SO_4^{2-} trends appear to be parallel which probably indicates control by the same mineral phases over the range 29-124 days when the pH was maintained at 4-4.5. SEM and SEM-EDX, XRD identified the presence of gypsum in all the sections of the leached solid cores (Fig 6.56 and Figs B8-B11). PHREEQC simulation predicted control of Ca and SO_4^{2-} by gypsum solubility except at pH >10.5 (Fig 5.57) when ettringite was at equilibrium in the leachates (Fig 5.38).

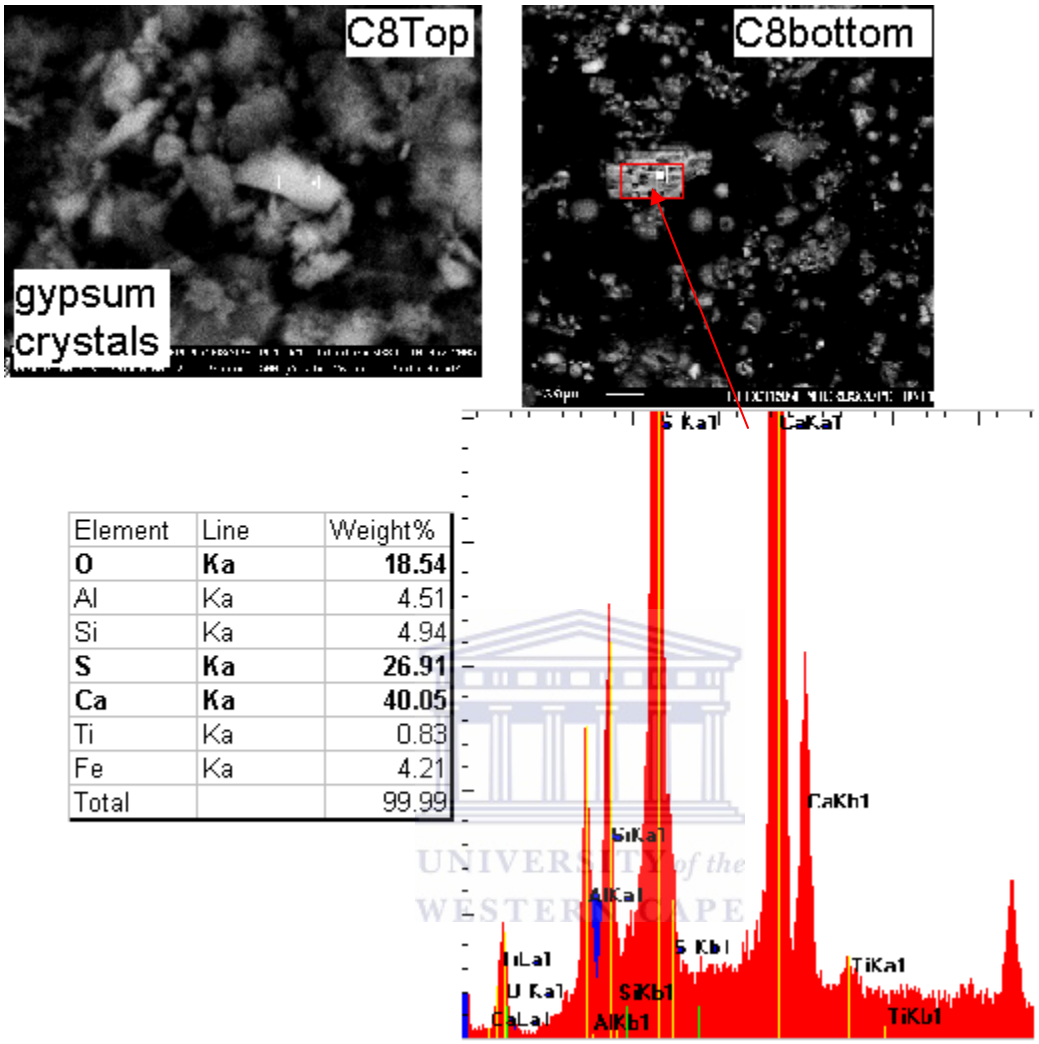

Figure 5.56: SEM micrographs of leached solid residues from column 8(SR + 6 % OPC) showing gypsum crystals. C8Top–Backscattered signal, magnification=14000. C8bottom-backscattered electron signal, magnification=1000, with accompanying EDS pattern of the spots analyzed (enclosed in a box).

UNIVERSITY of the WESTERN CAPE

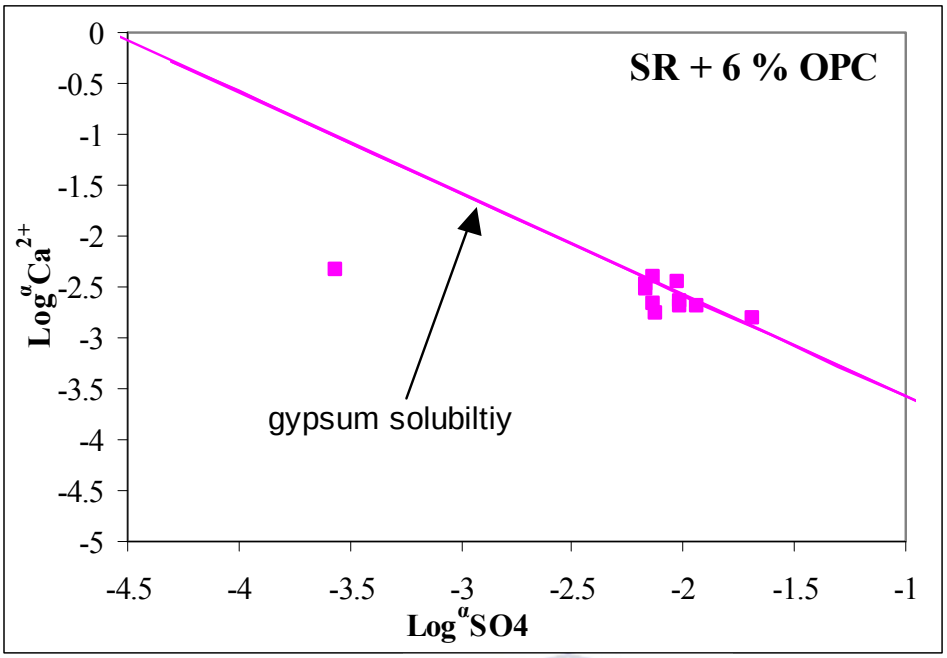

Figure 5.57: Plots of log SO_4^{2-} activity versus log Ca activity showing control of SO_4^{2-} and Ca by gypsum solubility in the leachates for SR + 6 % OPC column solid cores.

5.5.2 Sulphate, Aluminum and Iron

UNIVERSITY of the
WESTERN CAPE

Alkaline materials such as fly ash are highly reactive when exposed to natural waters and are known to modify soil element dissolution patterns and to control surface and sub-surface water quality in their vicinity (Mattigod *et al*., 1990). Reaction of these materials with acidic mine drainage produces varying pH (6-12) depending on FA: AMD ratios and the chemistry of the AMD (Gitari *et al.*, 2006). In addition the fly ash releases dissolved Ca, Al, Mg, K, Si and SO_4^{2-} which interact with species in AMD to form gypsum, amorphous Fe hydroxides, Al-hydroxides and jarosite-K type mineral phases.

It's reported that at near neutral pH Al-hydroxide phases such as gibbsite (γ-Al $(OH)_3$), boehmite (γ-AlOOH), and diaspore (α-AlOOH) are precipitated (Fillipek *et al.*, 1987; Doye and Duchesne, 2003) and control Al concentration in solution.

Several authors have observed that in a $Al_2(SO4)_3$-H_20 system basic Al-sulphates, such as basaluminite $(Al_4(OH)_{10}(SO_4).\ 5H_2O$, aluminite $(Al_2(OH)_4(SO_4).7H_2O$, jurbanite $(Al(OH)SO_4.5H_2O)$ and alunogen $(Al_2(SO4)_3.17\ H_2O$ form at acidic pHs (<7) (Adams and

Rawajfih, 1977; Khanna *et al.,* 1987, Nordstrom and Alpers,1999). Myeni *et al*, (1998) goes on to confirm that at below neutral pH Al-hydroxy sulphate phases can precipitate rapidly in natural systems and thus potentially influence major and trace elements dynamics in these environments.

Due to the high concentration of Ca from fly ash, Al and SO_4^{2-} from SAMD, the system created in the drainage experiments for the FA, SR, SR + FA and SR + OPC resembled more closely a $Ca(OH)_2$-$Al_2(SO_4)_3$-H_2O system that is open to Fe^{3+}, Fe^{2+}, K^+, Mg^{2+}, Mn^{2+}, SiO_2 and CO_3^{2-} since the drainage was done in the open hence the system was in contact with CO_2 from the atmosphere. Myeni *et al*, (1998) observed that addition of Fe^{3+}, Mg^{2+}, K^+ and Si $(OH)_4^0$ to the system formed Fe oxy-hydroxides, minerals belonging to alunite-jarosite family, clays and a zeolite leonhardite.

Langmuir and Whittemore (1971) have suggested that Fe $(OH)_3$ and poorly crystalline goethite are the first ferric phases to precipitate when AMD is neutralized, but transforms to more stable phases, crystalline goethite and lepidocrocite. At pH > 5 ferrihydite is formed from rapid oxidation and hydrolysis of Fe^{2+} (Schwertmann and Tyalor, 1989).

UNIVERSITY of the
WESTERN CAPE

Interaction of SAMD with FA, SR, SR + FA and SR + OPC solid cores generated pH in the leachates ranging from highly alkaline (> 10.7), near neutral (8-9.5) and acidic (3-6.5) as the drainage progressed. This section will discuss the precipitation of Fe-hydroxides, Al-hydroxides, Al-hydroxysulphates and jarosite-K type of minerals in the column solid cores as the acidification progressed to pH below 4 and justify their role in the control of the major contaminants and eventual clean-up of the percolating SAMD. Discussion will mainly center on the FA, SR, SR + 25 % FA and SR + 6 % OPC with an occasional mention of the other solid cores. Obtaining a positive proof that a water is in equilibrium with a mineral phase involves two steps, first a saturation-state calculation based on a complete analysis of the water should indicate that the mineral occurs under equilibrium conditions and secondly examination of the reaction mixture should reveal evidence of crystal formation. Analysis of the leached solid residues by XRD did not reveal any crystalline Al or Fe mineral phases. This could be due to the amorphous nature of the phases precipitating out or due to the diluting effect of the fly ash matrix. Therefore the SEM and SEM-EDX has been used

extensively to analyze the leached solid residue cores to help draw a conclusion on the likely mineral phases that precipitated. As stated earlier in Chapter three the SEM-EDX analysis can only provide semi-quantitative data hence the identification of the mineral phases should be taken with caution. However several authors have successively utilized SEM-EDX technique to identify and confirm the presence of mineral phases in different matrices (Catalan *et al*., 2002; Myeni *et al*., 1998; Warren and Dudas, 1985)

5.5.3 Fe (oxy) hydroxides and Al (oxy) hydroxides

PHREEQC simulation predicted several Fe (oxy) hydroxides and Fe-hydroxysulphate to be precipitating on interaction of the SAMD with the FA, SR, SR + FA and SR + OPC. Calculation of SI indices indicated the leachates to be supersaturated with respect to Fe(OH)(a), ferrihydrite, goethite and hematite (Figs 5.58, 5.59 and Table B14-B19). Precipitation of these phases during the drainage experiments explains the low concentrations observed in the leachates for 110 days (Figs 5.43, 5.45, 5.47, 5.49 and Table 5.4). An observation of figures 5.58 and 5.59 shows that goethite, hematite and magnetite were predicted to be the most stable phases for all the column solid core leachates. The leachates were at over-saturation at pH > 3.4. Goethite and hematite have similar solubility (K_{sp} hematite $\cong 10^{-43}$-10^{-42}, K_{sp} goethite $\cong 10^{-44}$-10^{-43}) and stability, but slow kinetic rates, hampered nucleation of the stable phases by contaminating metal ions and anions, this leads to the formation of poorly crystalline metastable phases such as ferrihydrite and microcrystalline goethite at surficial temperatures (Bigham, 1994; Schwertmann and Taylor, 1989). At pH > 6 the leachates appear to be over-saturated or at equilibrium with ferrihydrite, Bigham(1994) observed that ferrihydrite is likely to form in slightly acidic to alkaline solutions with high levels of dissolved Fe. At pH > 4.29 the leachates appear to become saturated with amorphous $Fe(OH)_3$.

UNIVERSITY of the
WESTERN CAPE

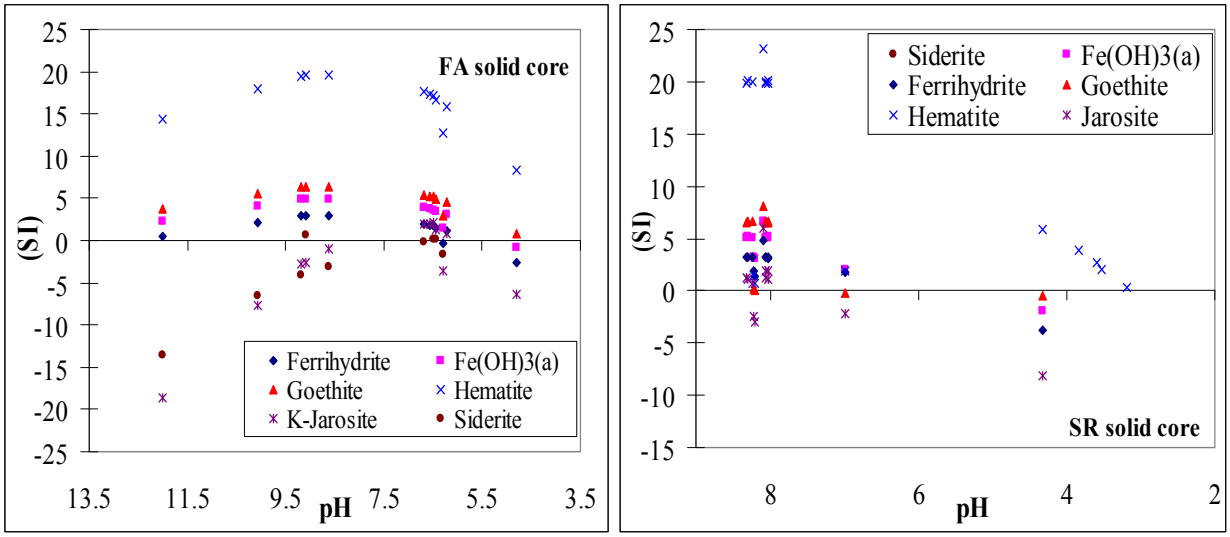

Figure 5.58: Plots of saturation indices for precipitating Fe-bearing mineral phases during the leaching study period for FA and SR solid core leachates.

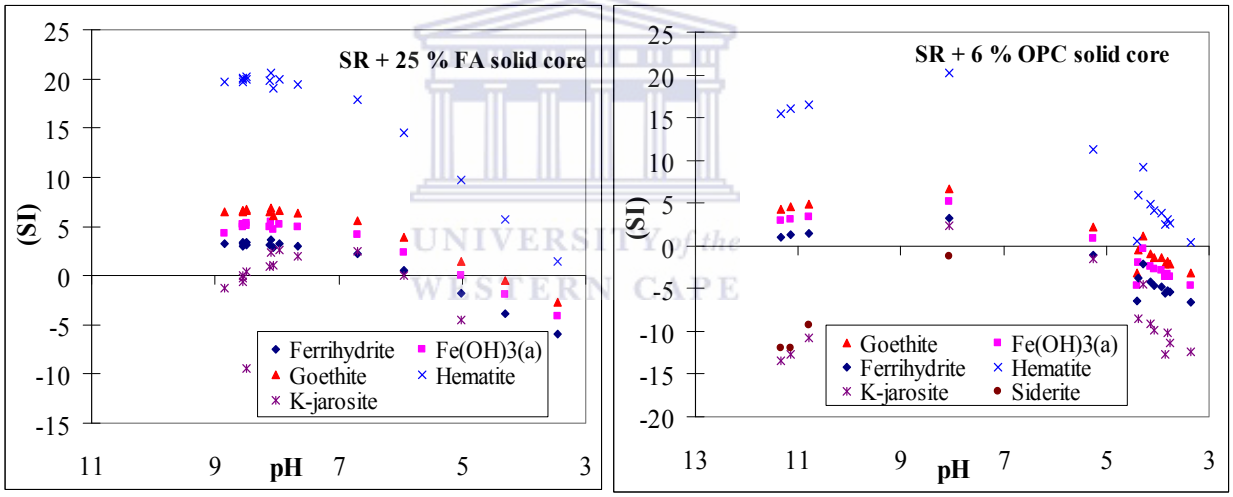

Figure 5.59: Plots of saturation indices for precipitating Fe-bearing mineral phases during the leaching study period for SR + 25 % FA and SR + 6 % OPC solid core leachates.

The leachates were observed to be saturated with respect to K-jarosite and (H, K, Na) $Fe_3(OH)_3(SO_4)_2$ over a pH range 6.43-6.68 for the FA solid core, 6.99-8.33 for the SR core and 5.94-8.52 for the SR + 25 % FA core but under-saturated over the entire pH range for the SR + 6 % OPC core (Figs 5.58 and 5.59). Azzie. (2002) observed over-saturation in a set of mine waters with respect to K-jarosite over the pH range 2.5-8 from some South African coal mines.

At this point it can be tentatively concluded that although PHREEQC predicts crystalline Fe-(oxy) hydroxides to precipitate, the precipitates are amorphous, XRD and SEM-EDX could not detect any crystalline phases in the leached solid residues. The high SO4 content and presence of interfering ions in the SAMD could have hampered the precipitation of these mineral phases. These observations strongly suggest that some kind of amorphous Fe-oxy (hydroxide) phase is being formed. A regression of log activities of Fe^{3+} versus pH over the entire pH range indicates two slopes at pH>5.5 and the second at pH<5.5 (Fig 5.60). If precipitation of a pure ferric hydroxide was controlling the chemistry of the leachates (equation 5.25) a plot of log Fe^{3+} activity versus pH should have a slope of –3. The observed 1st slope (-2.04 to -2.89) is roughly consistent with precipitation of a ferric hydroxide phase. The leachate chemistry is controlled by reactions involving Fe^{3+} at pH>5.5 while at pH <5.5 the chemistry of the leachate could not be interpreted in-terms of Fe^{3+} alone.

$$Fe(OH)_3 + 3H^+ \Rightarrow Fe^{3+} + 3H_2O$$
$$Log\ K = Log\ Fe^{3+} + 3pH \quad \text{.....(5.25)}$$

UNIVERSITY of the
WESTERN CAPE

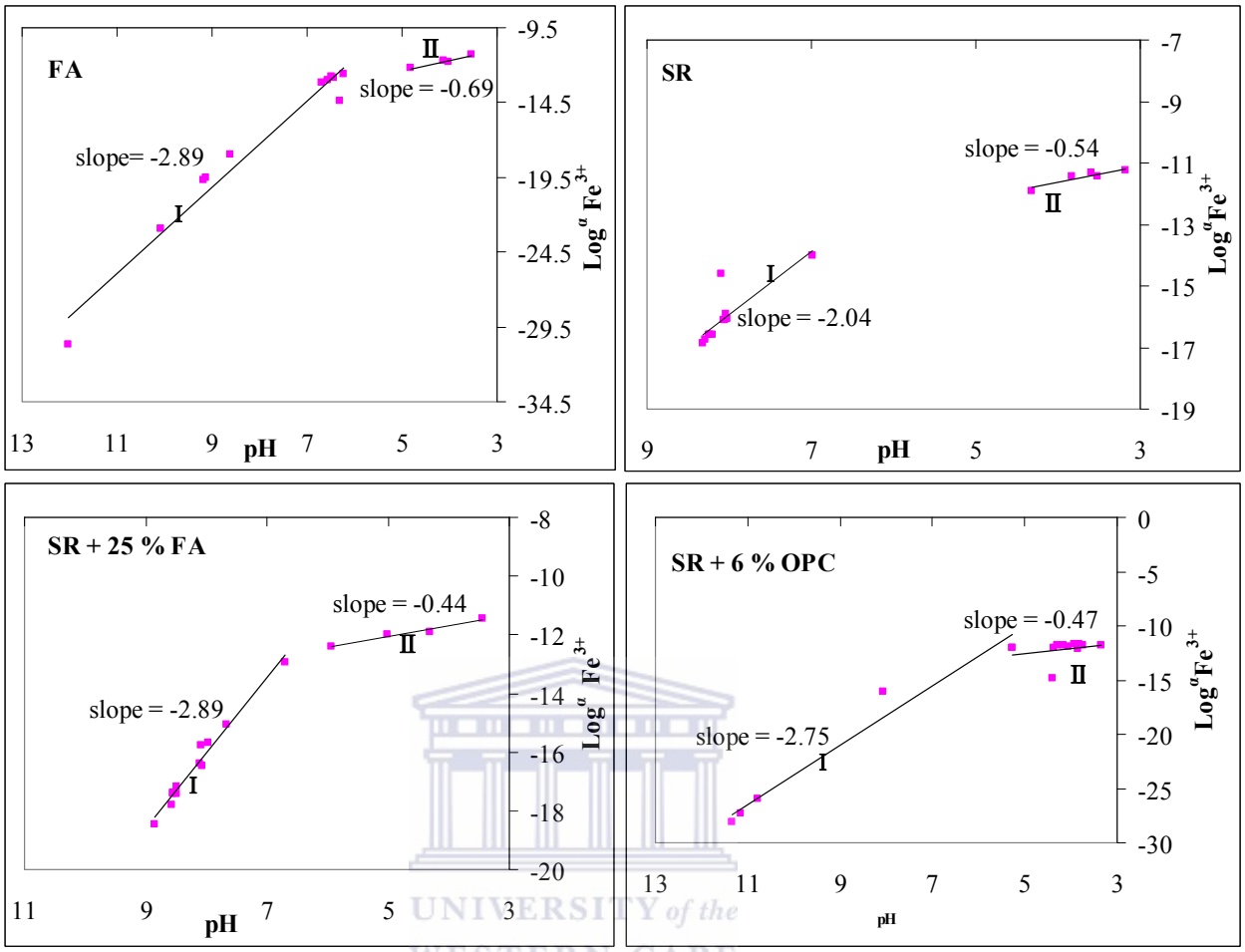

UNIVERSITY of the
WESTERN CAPE

Figure 5.60: Logarithmic activity plot of the dissolved Fe^{3+} versus pH in the leachates for FA, SR, SR + 25 % FA and SR + 6 % OPC solid cores.

For a given condition, acid mine water may precipitate not the most over-saturated solid phase but other metastable phases due to kinetic reasons. If an equilibrium state is reached among all the dissolved species in aqueous phase and the precipitating solid phases, equilibrium modeling may be successively utilized to interpret and predict the chemical compositional changes of water solutions due to precipitation. The calculated activities of the dissolved species are plotted on a solubility diagram to deduce the precipitating mineral phases, since the alignment of the plotted activities may have different slopes according to the stoichiometry of the precipitating solid phase (Nordstrom, 1982; Sullivan *et al*., 1988).

The figures 5.61-5.63 shows the constructed solubility diagrams for selected phases in the Fe_2O_3-SO_3-H_2O system at 298 K for the calculated activities of Fe^{3+} in the leachates for the FA, SR, SR + 25 % FA and SR + 6 % OPC solid cores.

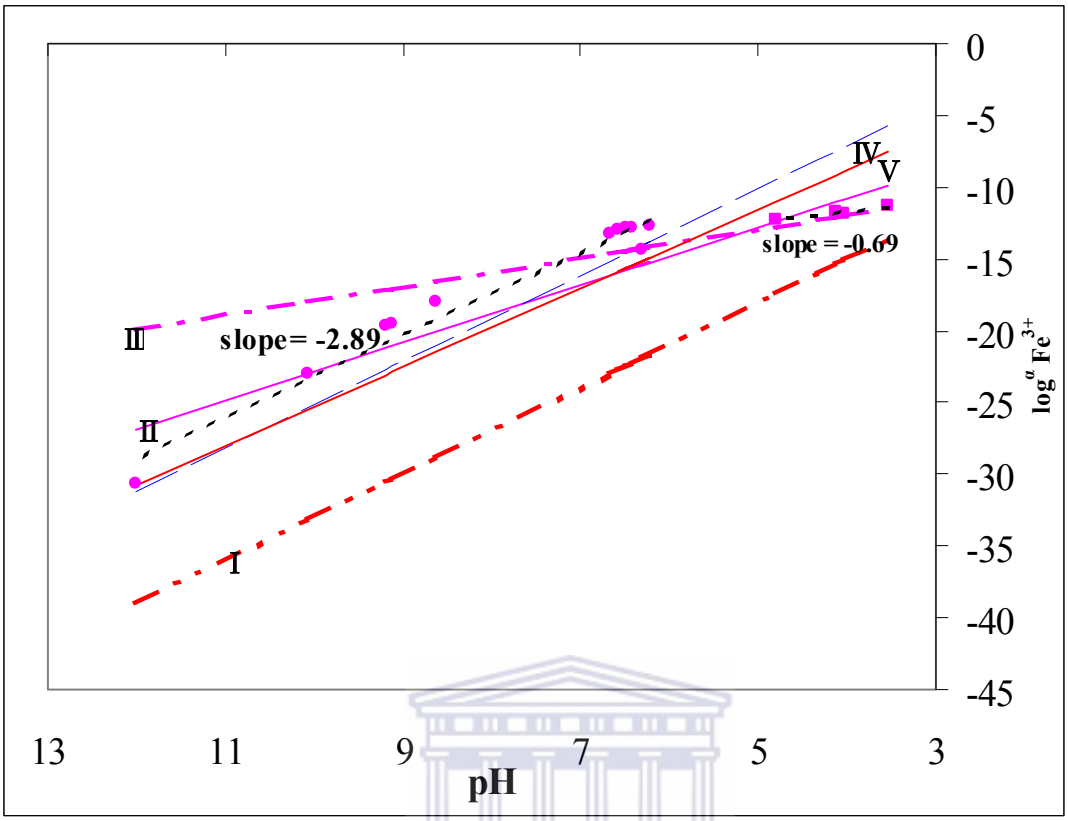

Figure 5.61: Plot of log Fe^{3+} activity against pH for the FA solid core leachates with solubility lines for, Ⅰ -Fe(OH)3(a) ($log^{\alpha} Fe^{3+}$= -3-3pH), Ⅱ -K-jarosite ($log^{\alpha}Fe^{3+}$= -2.8-2pH), Ⅲ-FeOHSO4 ($log^{\alpha}Fe^{3+}$= -7.94-pH), Ⅳ-Ferrihydrite ($log^{\alpha}Fe^{3+}$= 4.89-3pH), Ⅴ-Schwertmannite ($log^{\alpha}Fe^{3+}$= 2.52-2.75pH) added. Solubiltiy lines calculated using an average $log^{\alpha} K^{+}$= -2.15 and $log^{\alpha} SO_4$= -2.12 (calculated values from measured data) and log *Ks* values for Fe(OH)3(a), K-jarosite, FeOHSO4, Ferrihydrite, Schwertmannite are –3, -14.8, -10.06, 4.891 and 18.0 respectively (Jae Young yu, 1996; Bigham *et al*., 1996).

UNIVERSITY of the
WESTERN CAPE

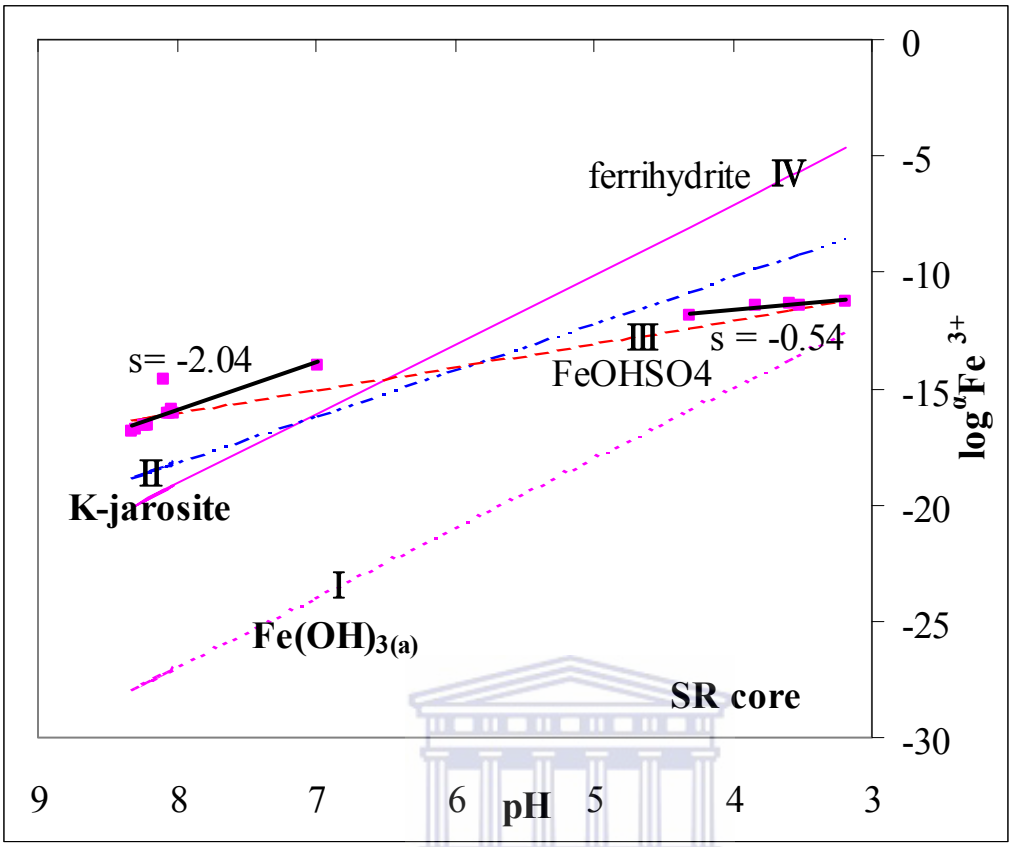

UNIVERSITY of the
WESTERN CAPE

Figure 5.62: Plot of log Fe^{3+} activity against pH for the SR solid core leachates with solubility lines for, I -Fe(OH)3(a) (log$^{\alpha}$ Fe^{3+}= -3-3pH), II -K-jarosite (log$^{\alpha}Fe^{3+}$= -2.16-2pH), III-FeOHSO4 (log$^{\alpha}Fe^{3+}$= -8.03-pH), IV-Ferrihydrite (log$^{\alpha}Fe^{3+}$= 4.89-3pH), added. Solubiltiy lines calculated using an average log$^{\alpha}$ K^{+}= -3.25 and log$^{\alpha}$ SO_4= -2.03 (calculated values from measured data) and log Ks values for Fe(OH)3(a), K-jarosite, FeOHSO4, Ferrihydrite, are –3, -14.8, -10.06 and 4.891 respectively (Jae Young yu, 1996; Bigham *et al*., 1996a and 1996b).

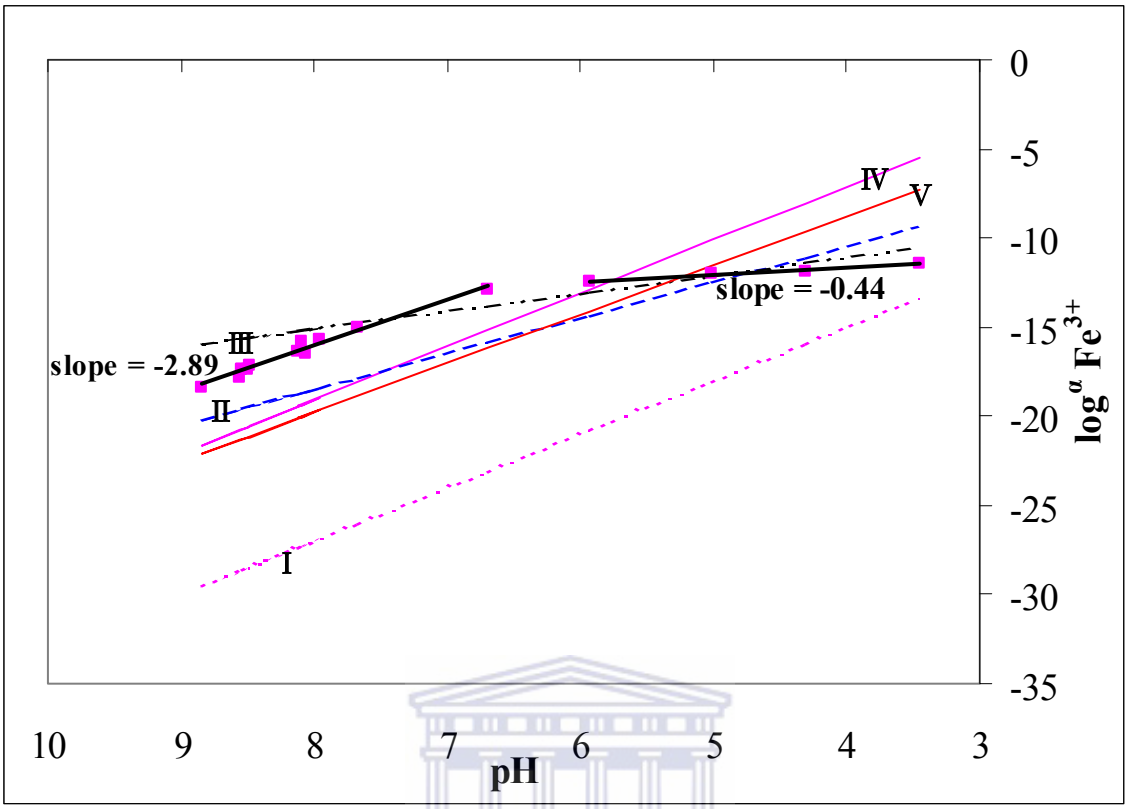

Figure 5.63: Plot of log Fe3+ activity against pH for the SR + 25 % FA solid core leachates with solubility lines for, I -Fe(OH)3(a) ($\log^{\alpha} Fe^{3+}$= -3-3pH), II -K-jarosite ($\log^{\alpha}Fe^{3+}$= -2.46-2pH), III-FeOHSO4 ($\log^{\alpha}Fe^{3+}$= -7.07-pH), IV-Ferrihydrite ($\log^{\alpha}Fe^{3+}$= 4.89-3pH), V-Schwertmannite ($\log^{\alpha}Fe^{3+}$= 2.51-2.75pH) added. Solubiltiy lines calculated using an average $\log^{\alpha} K^{+}$= -3.23 and $\log^{\alpha} SO_4$= -2.09 (calculated values from measured data) and log Ks values for Fe(OH)3(a), K-jarosite, FeOHSO4, Ferrihydrite, Schwertmannite are –3, -14.8, -10.06, 4.891 and 18.0 respectively (Jae Young yu, 1996; Bigham *et al*., 1996a and 1996b).

.

UNIVERSITY of the
WESTERN CAPE

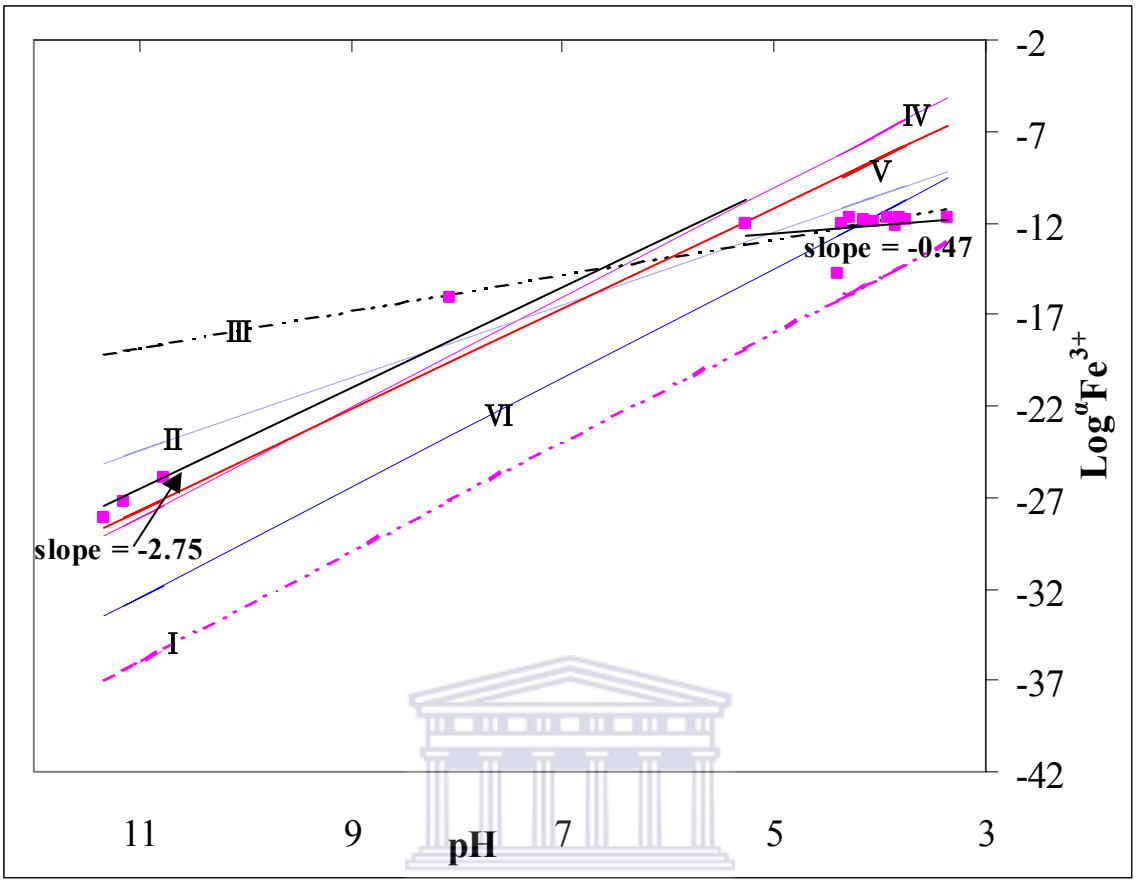

UNIVERSITY of the
WESTERN CAPE

Figure 5.64: Plot of log Fe3+ activity against pH for the SR + 6 % OPC solid core leachates with solubility lines for, I -Fe(OH)3(a) (log$^{\alpha}$ Fe^{3+}= -3-3pH), II -K-jarosite (log$^{\alpha}$Fe^{3+}= -2.55-2pH), III-FeOHSO4 (log$^{\alpha}$Fe^{3+}= -7.83-pH), IV-Ferrihydrite (log$^{\alpha}$Fe^{3+}= 4.89-3pH), V-Schwertmannite (log$^{\alpha}$Fe^{3+}= 2.52-2.75pH), α-goethite (log$^{\alpha}$Fe^{3+}= 0.5-3pH) added. Solubiltiy lines calculated using an average log$^{\alpha}$ K^{+}= -2.90 and log$^{\alpha}$ SO$_4$= -2.12 (calculated values from measured data) and log *K*s values for Fe(OH)3(a), K-jarosite, FeOHSO4, Ferrihydrite, Schwertmannite, α-goethite are –3, -14.8, -10.06, 4.891, 18.0 and 0.5 respectively (Jae Young yu, 1996; Bigham *et al*., 1996a and 1996b).

The activity diagrams reveal that the leachate water chemistry is mainly controlled by ferrihydrite at pH>5.5 for all the solid cores, precipitation of K-jarosite and schwertmannite may also control the leachate chemistry at pH 4-5.5 but its not obvious (Figs 5.61-5.64). Bigham *et al* (1996) in a study involving ochreous precipitates and associated acidic mine drainage waters observed that above pH 5.5 mineralogy of the precipitates was influenced by

ferrihydrite and those at intermediate pH values by schwertmannite. At pH <5.5 $FeOHSO_4$ seems to control the chemistry of the leachates.

If the chemistry of the leachates at pH < 4.5 was being controlled by the precipitation and dissolution of $FeOHSO_4$ (equation 5.26) then a plot of calculated logarithmic activity of Fe^{3+} versus pH at constant SO_4^{2-} activity should have a slope of -1.

$$FeOHSO_4 + H^+ \Rightarrow Fe^{3+} + SO_4^{2-} + H_2O$$
$$Log\ K_s = \log Fe^{3+} + \log SO_4^{2-} + pH = 10.06 \quad \text{.....(5.26)}$$

The observed regression slope at pH <5.5 ranged (-0.44 to –0.69) (Figs 5.60) which is fairly close to -1 and suggests control of the leachate chemistry by $FeOHSO_4$. Sullivan *et al*. (1988) performed an oxidizing equilibrium study with oil shales containing pyrite and suggested that Fe^{3+} activities were controlled by $FeOHSO_4$ solubility at a relatively low pH

The Fe^{3+} activities are several orders of magnitude higher than those predicted from control by ferrihydrite. Apparent super-saturation with ferric hydroxides or ferrihydrite occurs at high pH values above about 4. The super-saturation may be explained by substitution or adsorption of sulphate for hydroxide ions or on ferrihydrite and the formation of a more soluble schwertmannite-like phase. Apparent super-saturation with respect to ferric hydroxide might also be explained by the formation of colloidal iron particles that passed through the 0.45μm nucleopore membranes. This apparent super-saturation behavior of ferrihydrite and other ferric hydroxide is commonly seen for both surface waters and ground waters (Nordstrom and Alpers, 1999). Regression analysis of the calculated log Fe^{3+} activity of the leachates yielded slopes ranging from (-2.04 to –2.89) which is inconsistent with the precipitation of a pure ferric hydroxide phase or ferrihydrite. Kimball *et al.* (1994) found a regressed slope of -2.23 from iron data on the acid mine waters during a neutralization experiment. The observed slope (-2.04 to –2.89) could be interpreted to represent a ferric hydroxide in which SO_4^{2-} has partially substituted hydroxide, i.e., $Fe\ (OH)_{2.04\text{-}2.89}(SO4)_{0.11\text{-}0.96}$. Infra-red analysis of the leached solid residues identified structural sulphate which confirms incorporation of sulphate in the Fe-bearing mineral phases. Bigham (1994) noted that ferrihydrite is associated with mine drainage in the pH range of about 5 – 8. The slope of -2.04 to -2.89 is observed in the pH range 6.5-8.5 in this study. This suggests that the apparent stoichiometry is more likely to represent a sulphate-substituted ferrihydrite,

UNIVERSITY of the
WESTERN CAPE

schwertmannite or other hydrous ferric oxide with a molar Fe: OH of 1: (2.04-2.89). It is also possible that mixtures of different iron minerals phases are precipitating from these leachates over this pH range and the slope is not clearly resolvable into a particular reaction.

PHREEQC simulation predicted several Al (oxy) hydroxides and Al-hydroxysulphate mineral phases to be precipitating on interaction of the SAMD with the FA, SR, SR + FA and SR + OPC as the drainage progressed. Calculation of SI for Al-bearing mineral phases indicated super-saturation with respect to amorphous Al $(OH)_3$, basaluminite, gibbsite, jurbanite, alunite, boehmite, diaspore and ettringite at different stages of the drainage process (Figs 5.65-5.68 and Tables B14-B19). The saturation state of the Al-bearing mineral phases appear to follow different patterns in each of the column probably due to the different pH regimes and chemical processes generated by the FA, SR, SR + 25 % FA and SR + 6 % OPC solid cores. The saturation of the Al-hydroxides $(Al(OH)_{3(a)})$, boehmite, gibbsite and diaspore seem to occur within the same pH range (4-11.3). At pH 4 (close to 1^{st} $pK_1(Al^{3+})$ = 4.91) some form of hydrolyzed aluminum will precipitate (Fillipek *et al*., 1987). However for SR (pH 6.99) and SR + 25 % FA (pH 5) solid cores the pH at which initial saturation is predicted is higher than for FA (pH 4) and SR + 6 % OPC (pH 4). A possible reason could be that at high FA concentration and in presence of OPC large amounts of sulphate is removed even at lower pH hence formation of the (oxy)-hydroxides is more favorable.

At pH 4, FA and SR + 6 % OPC solid core leachates, sulphate concentration were in the range (2500-5000 mg /L) while SR + 25 % FA and SR leachates were in the range (6500-9000 mg /L). At pH > 7 the sulphate concentration was below 2500 mg/L for SR and SR + 25 % FA core leachates which corresponds to the saturation range of boehmite, gibbsite and diaspore. The saturation of alunite, jurbanite and basaluminite on the contrary appear to be saturated at higher pH (5-8.09) for SR and SR + 25 % FA solid cores leachates, while for FA and SR + 6 % OPC solid cores, saturation is observed at pH (3.36-6.68).

Ettringite saturation was only observed in FA and SR + 6 % OPC solid cores at pH > 11.15. Ettringite is only stable at pH>10 otherwise it undergoes incongruent dissolution to gypsum and Al-hydroxides (Myeni *et al.*, 1998).

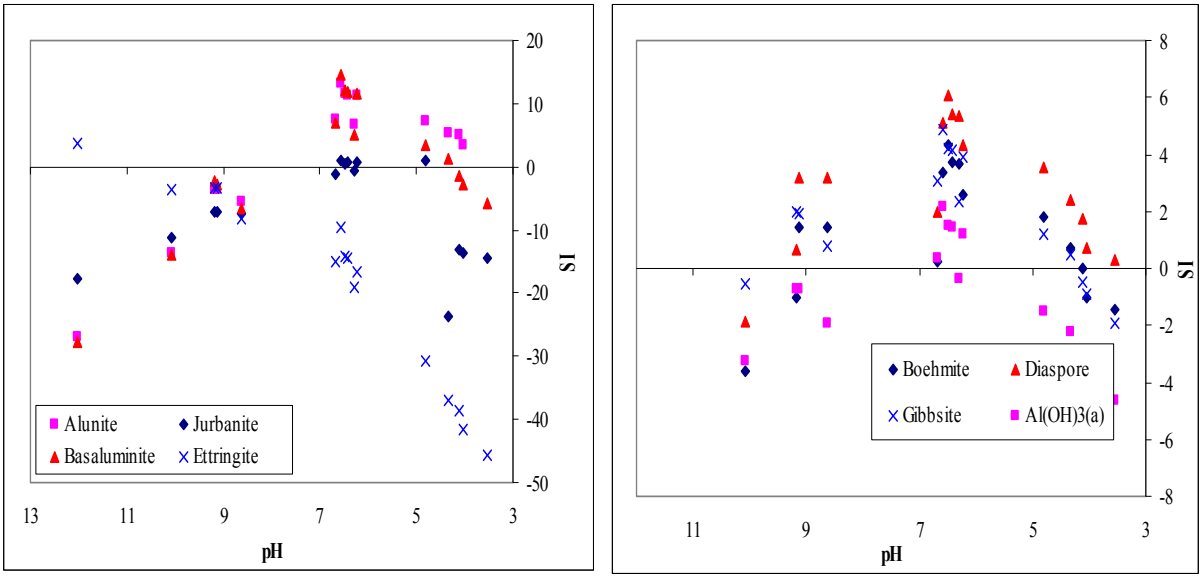

Figure 5.65: Plots of saturation indices for precipitating Al-(oxy) hydroxide and Al-hydroxysulphates mineral phases during the leaching study period for FA solid core leachates.

UNIVERSITY of the
WESTERN CAPE

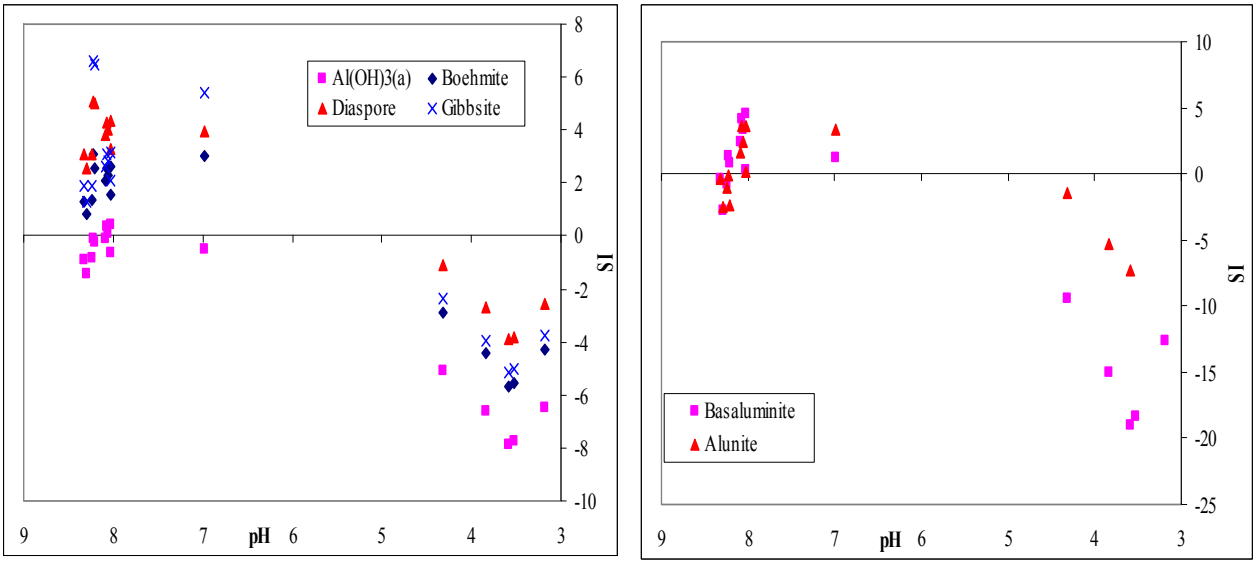

Figure 5.66: Plots of saturation indices for precipitating Al-(oxy) hydroxide and Al-hydroxysulphates mineral phases during the leaching study period for SR solid core leachates.

UNIVERSITY of the
WESTERN CAPE

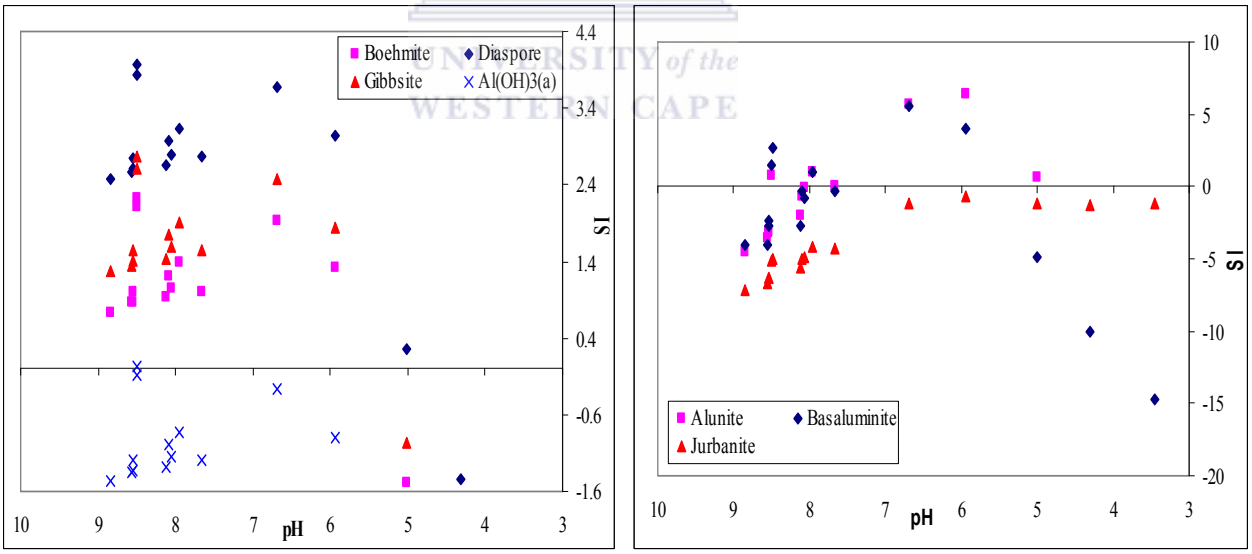

Figure 5.67: Plots of saturation indices for precipitating Al-(oxy) hydroxide and Al-hydroxysulphates mineral phases during the leaching study period for SR + 25 % FA solid core leachates.

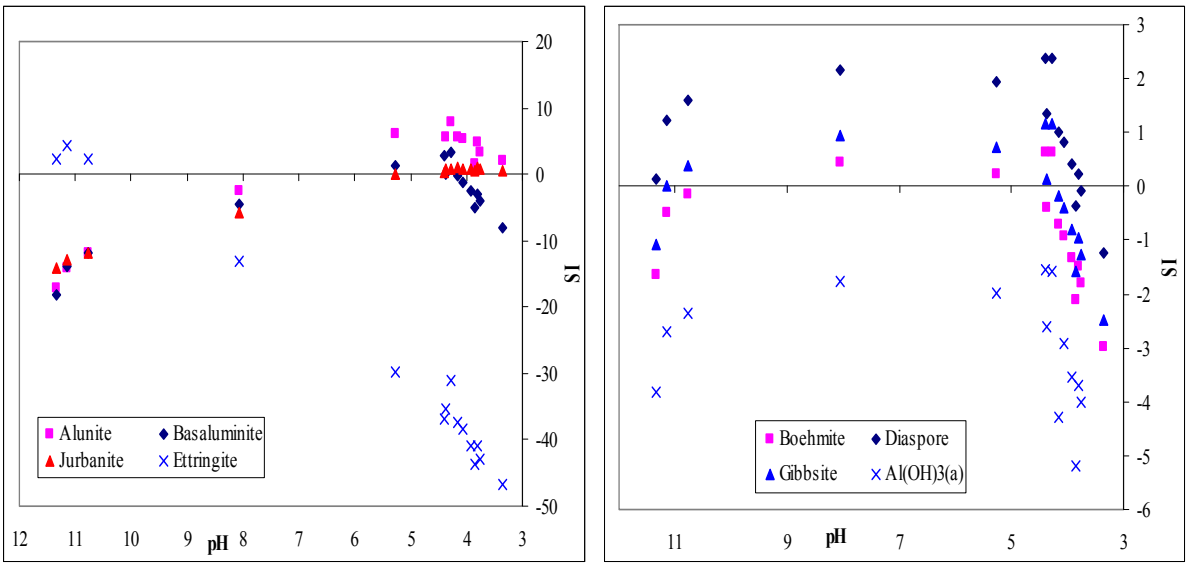

Figure 5.68: Plots of saturation indices for precipitating Al-(oxy) hydroxide and Al-hydroxysulphates mineral phases during the leaching study period for SR + 6 % OPC solid core leachates.

Similar to Fe^{3+} calculated Al^{3+} activities are plotted on a solubility diagrams to deduce the precipitating mineral phases. Figure 5.69 shows the constructed solubility diagrams for selected phases in the Al_2O_3-H_2O system at 298 K for the calculated activities of Al^{3+} in the leachates for the FA, SR, SR + 25 % FA and SR + 6 % OPC solid cores. The corresponding activities due to the precipitation of the pure aluminum hydroxide phases are also shown.

UNIVERSITY of the
WESTERN CAPE

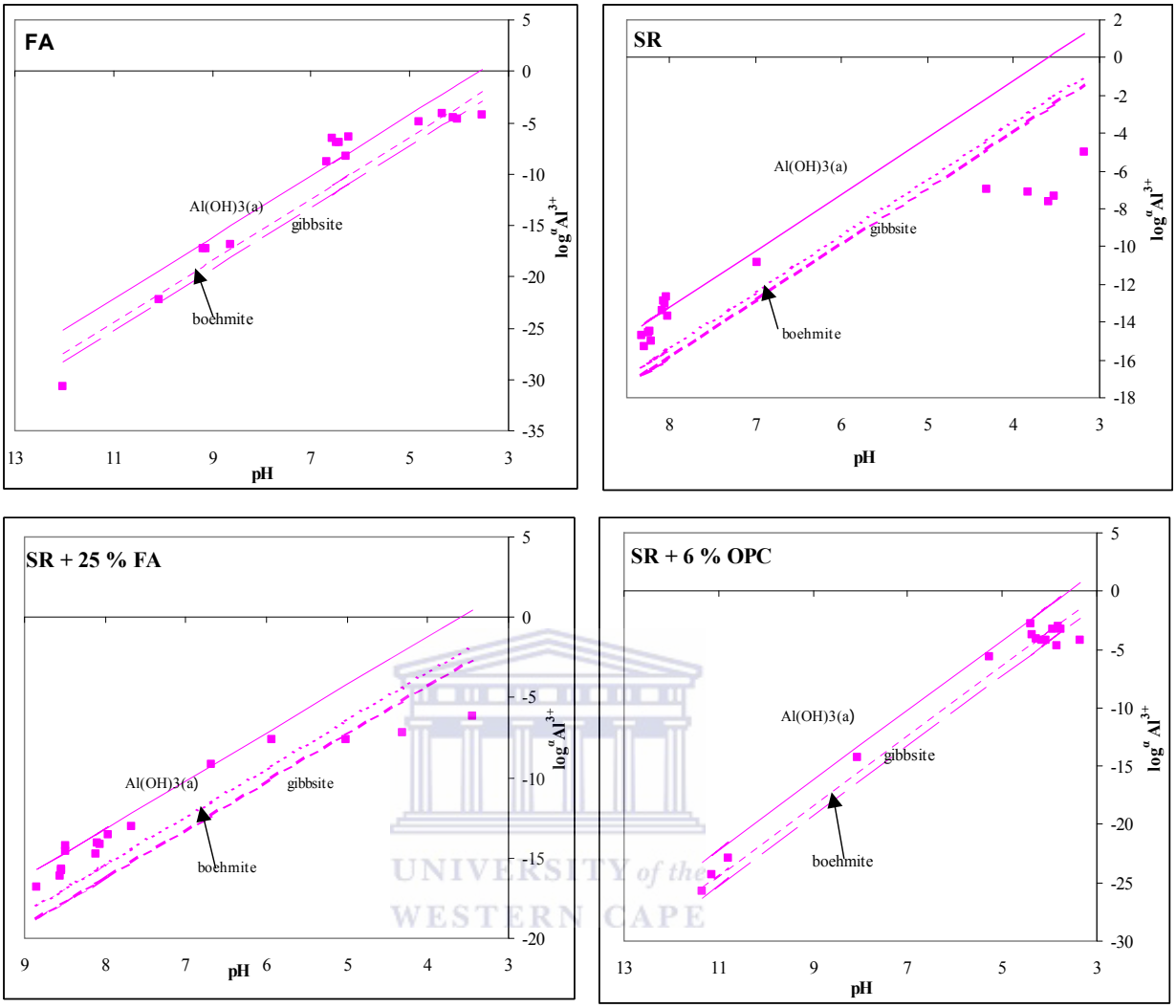

Figure 5.69: Plot of log Al^{3+} activity against pH for the FA, SR, SR + 25 % FA and SR + 6 % OPC solid core leachates with solubility lines for Al(OH)3(a) ($\log^{\alpha} Al^{3+}$= 10.8-3pH), gibbsite ($\log^{\alpha}Al^{3+}$ = 7.74-3pH), boehmite ($\log^{\alpha}Al^{3+}$= 8.58-3pH), Solubiltiy lines calculated using log K_s values for Al(OH)3(a), gibbsite, boehmite are 10.8, 7.74, and 8.58 respectively (Jae Young yu, 1996).

Figure 5.69 suggests that the chemistry of the leachates is controlled by the precipitation of amorphous $Al(OH)_3$ at between pH 5.5-9.5 for SR and SR + 25 % FA solid cores. In addition at pH 3.5-11 boehmite and gibbsite seems to be playing a role in the chemistry of the leachates for FA and SR + 6 % OPC solid cores. It can be tentatively concluded that amorphous $Al(OH)_3$ is controlling Al^{3+} activity in the leachates for SR and SR + 25 % FA solid cores while boehmite or gibbsite are controlling Al^{3+} activity in the leachates for FA

and SR + 6 % OPC solid cores. It has been discussed in this section that pH and SO_4^{2-} content in the leachates have a direct influence on whether Al-hydroxide or Al-hydroxysulphates will be kinetically favored to precipitate. A low SO_4^{2-} concentration (<2500 mg/L) seems to favor precipitation of Al-hydroxides and SO_4^{2-} > 5000 mg/L favors precipitation of Al-hydroxysulphates. To further elucidate the Al-hydroxysulphates precipitating under the pH and SO_4^{2-} regimes generated by the different solid cores, ion activity diagrams relative to stability lines for Al-hydroxysulphates minerals; jurbanite ($Al(OH)SO_4.5H_2O$), alunite ($KAl_3(SO_4)_2(OH)_6$) and basaluminite ($Al_4(OH)_{10}SO_4.17H_2O$), gibbsite and $Al(OH)_{3(a)}$ were generated following the method of Wolt *et al*.(1992).

The solubility relations of basic Al-hydroxysulphates in solution can be expressed as [2pH + pSO4] and [pAl + pOH + pSO4] (Wolt *et al.,* 1992) using appropriate pK_{sp} for jurbanite (17.8), alunite (85.6) and basaluminite (117.7) as given by Nordstrom, 1982; Allison *et al*., 1991 and the negative logarithm of the ion activity product of water, pK_w =14. The following relations (equations 5.27-5.29) derived by Wolt *et al*. (1992) were used in this study:

Jurbanite: $p(Al)(OH)(SO4) = [pAl + pOH + pSO4] = 17.8$ ……..……(5.27)

Basaluminite: $[pAl + pOH + pSO4] = 8.4 + 3/4[2pH + pSO4]$ ……..…..(5.28)

Alunite: $[pAl + pOH + pSO4] = (19.13 - 1/3[pK + pOH]) + 1/3[2pH + pSO4]$ ……..…..(5.29)

Since gibbsite and amorphous $Al(OH)_3$ were proved to be controlling Al^{3+} in the solid cores the following relations were also derived using pK_{sp}=33.9 and pK_{sp}=31.2 (Nordtsrom *et al*., 1990) for gibbsite and $Al(OH)_{3(a)}$ respectively.

Gibbsite: $[pAl + pOH + pSO4] = 5.9 + [2pH + pSO4]$ ...……..……...……..…..(5.30)

Al(OH)3(a): $[pAl + pOH + pSO4] = 3.2 + [2pH + pSO4]$ ……..….(5.31)

Figure 5.70 shows the stability lines of Al-hydroxysulphates minerals, gibbsite and amorphous $Al(OH)_3$ imposed on the leachate ion activities plotted with [pAl + pOH + pSO4] as function of [2pH +pSO4]. The data for the leachate solutions fall along the line fixed by amorphous Al(OH) from which Al^{3+} activity was calculated for SR and SR + 25 % FA solid cores and along the line fixed by gibbsite from which Al^{3+} activity was calculated for FA and SR + 6 % OPC solid cores (Fig 5.70). The leachate chemistry seems to be clearly unrelated to alunite solubility for all the solid cores. For the FA and SR + 6 % OPC solid core leachates the ion activities fall within the region circumscribed by the basaluminite, jurbanite and gibbsite solubility (Fig 5.70). For the FA solid cores basaluminite and gibbsite seem to be the

stable solid-phases controlling Al^{3+} and SO_4^{2-} activities when [2pH + pSO4] ≥ 19.56 and at [2pH + pSO4] ≤ 15.56 basaluminite, jurbanite and gibbsite control the ion activities. In the SR + 6 % OPC solid cores a similar solid-phase trend is observed, at [2pH + pSO4] ≥ 18.25 basaluminite and gibbsite control the ion activities and at [2pH + pSO4] ≤ 12.37 basaluminite, jurbanite and gibbsite seem to control the ion activities. In the SR solid cores at [2pH + pSO4] ≥ 15.87 basaluminite and amorphous Al $(OH)_3$ control the ion activities while at [2pH + pSO4] ≤ 10.46 jurbanite exerts control. For the SR + 25 % FA solid core at [2pH + pSO4] ≥ 15.33 basaluminite and amorphous Al $(OH)_3$ control the ion activities while at [2pH + pSO4] ≤ 14.06 jurbanite exerts control. There is ample evidence of solubility control of Al^{3+} activity by jurbanite under acidic and high SO_4^{2-} conditions (Wolt *et al*., 1992; Von and Stehouwer, 2003; Agbenin, 2003).

UNIVERSITY of the
WESTERN CAPE

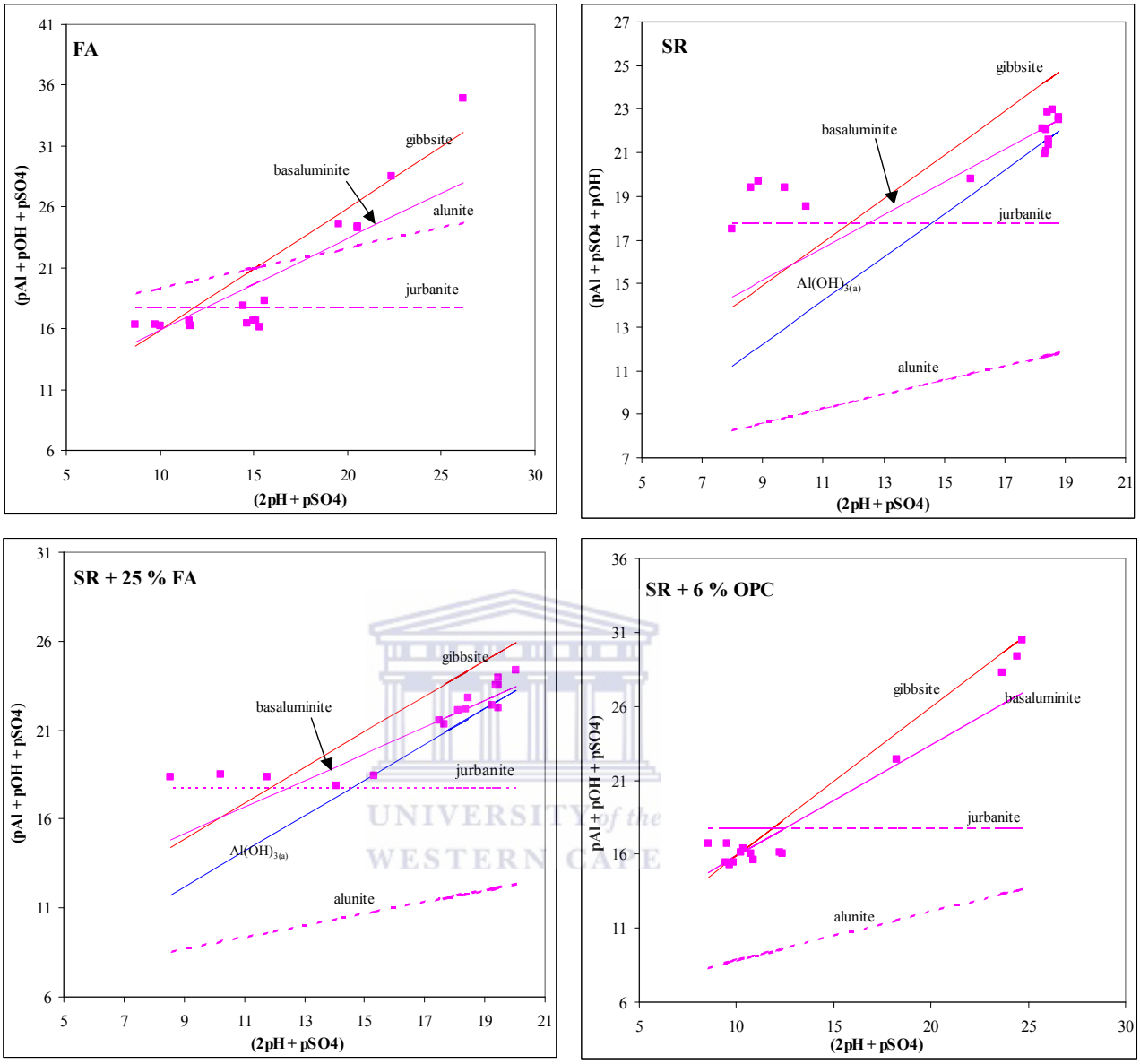

Figure 5.70: Leachate ion activities relative to stability lines for Al-hydroxysulphate minerals, gibbsite and amorphous Al $(OH)_{3(a)}$. Stability line of alunite was fixed using average value of pK and pOH calculated using PHREEQC (FA: pOH=7.21, pK^{+}=2.15; SR: pOH=7.31, pK^{+}=3.25; SR + 25 % FA: pOH=6.70, pK^{+}=3.25; SR + 6 % OPC: pOH=8.23; pK^{+}=2.90) (average values derived from the data generated using PHREEQC).

UNIVERSITY of the WESTERN CAPE

5.5.4 Manganese

PHREEQC simulation indicates that the leachates were saturated or over-saturated with respect to pyrolusite, nsutite and manganite at pH > 10.08 and rhodochrosite at pH 5.94-10.08 (Fig 5.71). Under mildly oxidizing and high pH conditions Mn^{2+} can be oxidized to Mn^{4+} /$Mn^{3+}$with formation of insoluble MnO_2 (pyrolusite), MnOOH (manganite) and nsutite (MnO_2). The oxidation/reduction potential at pH >11.0 in this study ranged (-32.1-268 mv). Manganese autooxidizes at pH values of 8.5 or > and according to Eh-pH diagrams developed by Faulkner and Richardson (1989) Mn^{2+} will be oxidized to MnO_2 at pH > 11 and Eh (mv) ≥ 250. At circumneutral to alkaline pH values carbonate minerals that form in an open system could remove Mn^{2+}. Rhodochrosite was near saturation or at saturation at pH 6.99-10.08 in this study.

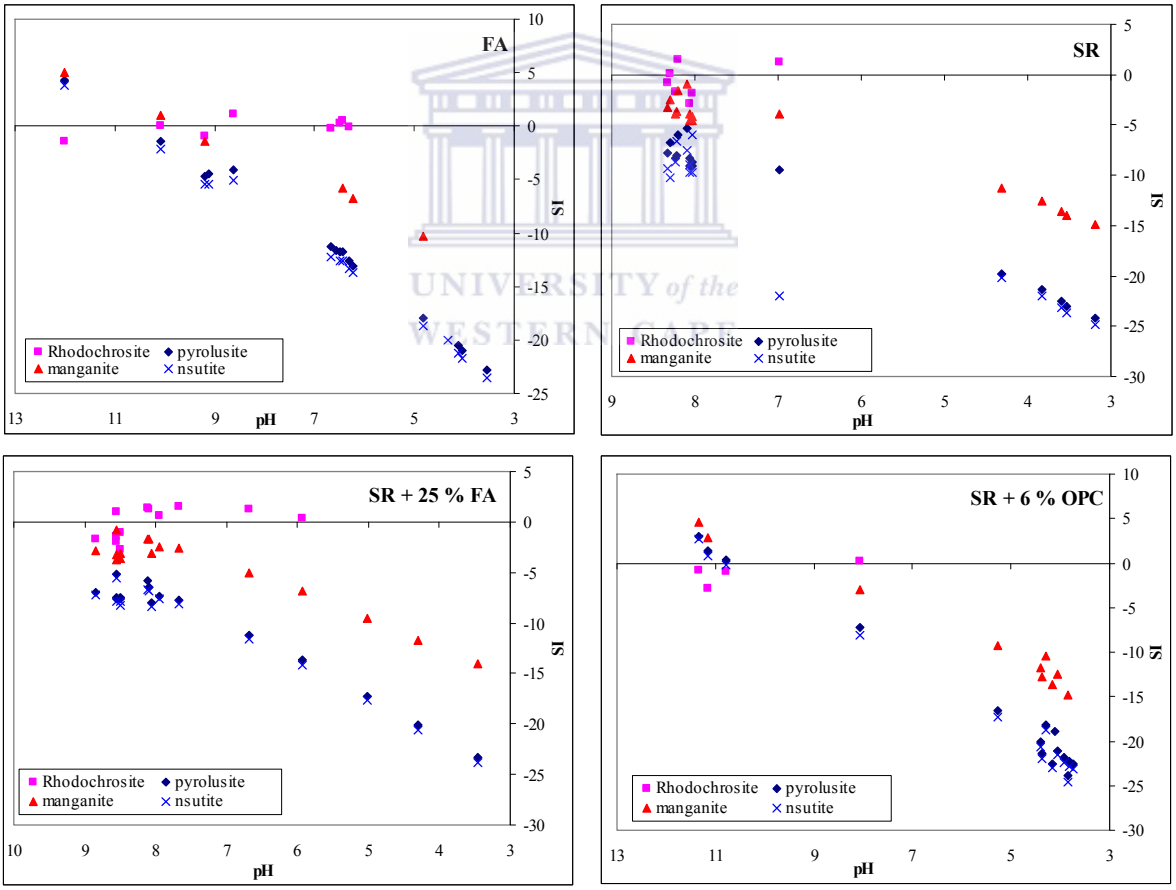

Figure 5.71: Saturation indices versus pH for selected Mn-bearing mineral phases for FA, SR, SR + 25 % FA and SR + 6 % OPC solid residue cores.

UNIVERSITY of the WESTERN CAPE

Komnitsas *et al*. (2004) treated simulated acidic leachates with limestone and red mud in a column leaching study and observed precipitation of rhodochrosite when pH was at alkaline values. Zachara *et al*. (1991) also supports the probability of rhodochrosite precipitation at alkaline pH values. To confirm the extent to which the precipitation of rhodochrosite was contributing to the attenuation of Mn^{2+}, solubility diagrams were constructed using activity of Mn^{2+} calculated using PHREEQC (Fig 5.72)(equations 5.32-5.34). The CO_3^{2-} activities fall along the line described by rhodochrosite at pH 5.94 – 8.62 confirming the control of leachate chemistry by this mineral phase.

$$MnCO_3 \Rightarrow Mn^{2+} + CO_3^{2-} \quad Log\, K = -10.39 \qquad (5.32)$$

where

$$K = [Mn^{2+}][CO_3^{2-}] \qquad (5.33)$$

Taking logarithms to base 10 on both sides

$$Log\, Mn^{2+} = -10.39 - Log\, CO_3^{2-} \qquad (5.34)$$

UNIVERSITY of the
WESTERN CAPE

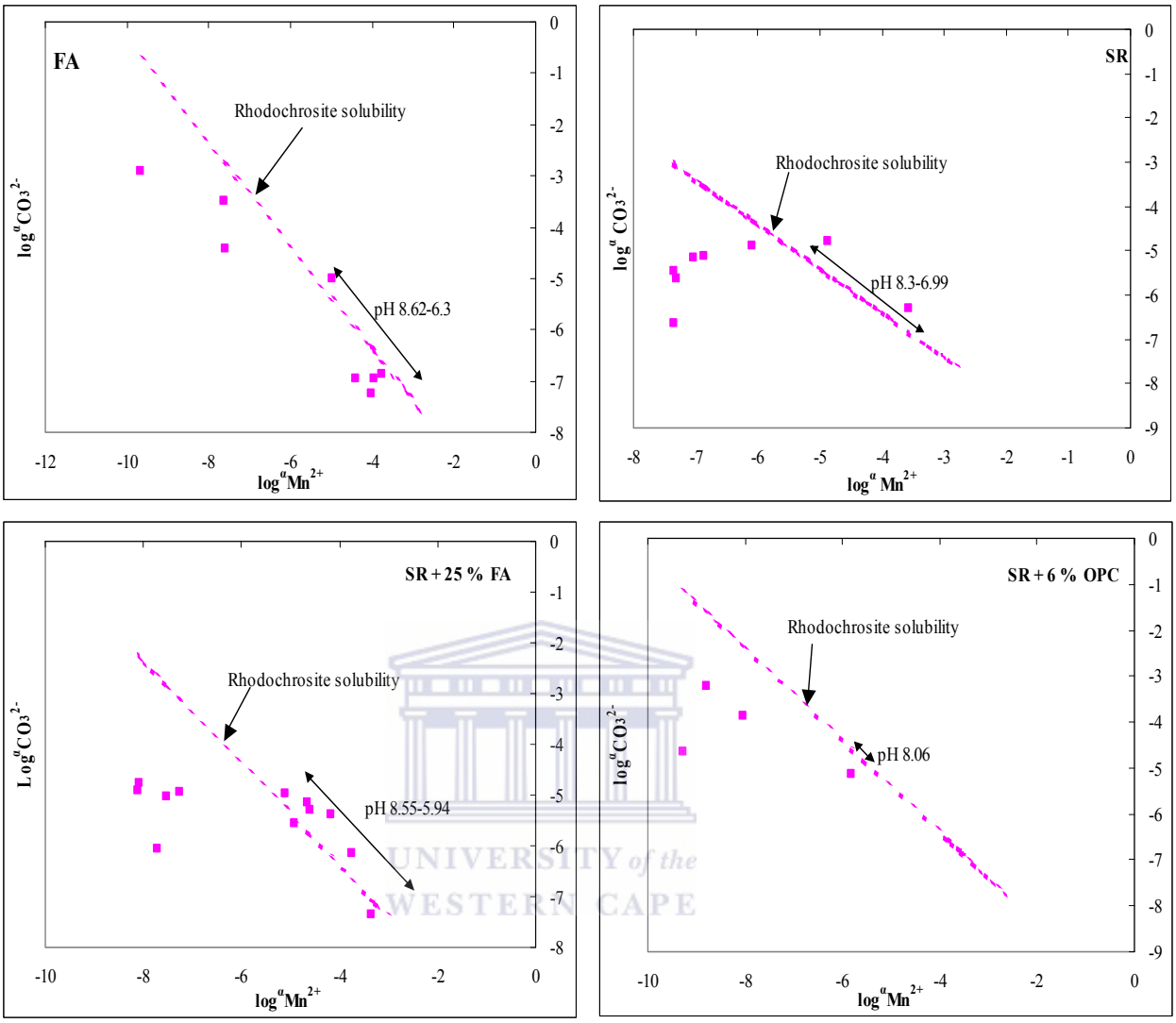

Figure 5.72: Leachate Mn^{2+} activities versus CO_3^{2-} activities for FA, SR, SR + 25 % FA and SR + 6 % OPC showing the pH ranges at which rhodochrosite controls Mn^{2+} activity. Log *K*= -10.39 (WATEQ4 database)(Ball and Nordstrom, 1991).

Plotting of solubility lines of pyrolusite (β-$MnO_{2,\ \log K=41.38}$) and manganite (γ-MnOOH $_{\log K= 25.34}$) over the pH range of the leachates revealed that both pyrolusite and manganite were controlling the chemistry of the leachate at pH >9 for FA and SR + 6 % OPC solid cores. For SR and SR + 25 % FA the ion activities data cluster along the line defined by the manganite at pH >7.5 (Fig 5.73). Hem and Lind (1993) titrated Mn-rich ground waters with 0.1 molar NaOH solution with and without CO_2 present, these experiments yielded hausmannite which aged to manganite.

UNIVERSITY of the WESTERN CAPE

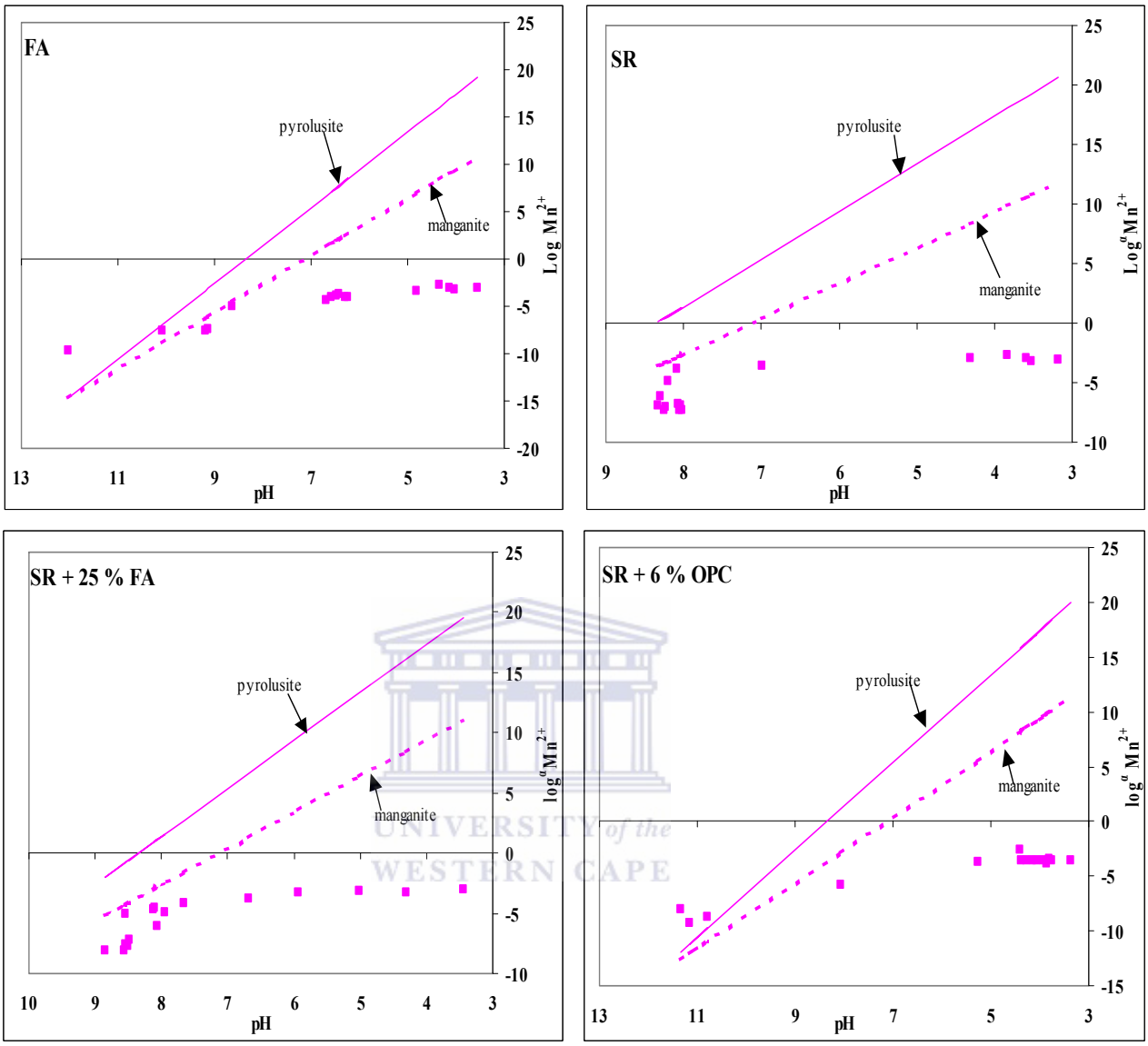

Figure 5.73: Logarithm of the activity of Mn^{2+} ion plotted against pH with equilibrium solubility lines for pyrolusite and manganite for FA, SR, SR + 25 % FA and SR + 6 % OPC solid cores. The default ρε = 4.0 in PHREEQC was assumed in calculating the Mn^{2+} activity in equilibrium with pyrolusite and manganite.

5.6 Mineralogical and elemental analysis of leached solid cores.

In view of the findings of the modeling experiments suggesting that Fe-bearing hydroxide phases, Fe-hydroxysulphate mineral phases, Al-bearing hydroxide minerals, Al – hydroxysulphates, Ca-SO4 mineral phases and Mn-bearing mineral phases were likely to control the leachate chemistry as the drainage progressed. An attempt was made to

collaborate this information with direct physical evidence of these mineral phases in the leached solid residues. This section will present a discussion with a view to drawing a conclusion on the presence or absence of these predicted mineral phases.

5.6.1 Visualization of the sectioned leached solid cores

Figures 5.74 and 5.75 below shows the surfaces of the sectioned column solid cores for FA and SR cores. After sectioning of the columns the extent of interaction of the synthetic acid mine drainage (SAMD) with FA and the solid residues (SR) was evident. Yellowish/brownish coloration was observed in all the leached solid cores. The highest intensity of the coloration was observed at the top layer of each of the leached solid cores. The least coloration was observed in the FA cores. The intensity of the yellowish/brownish coloration decreased down the length of the leached solid core. The highest intensity of the coloration was observed in the SR core.

Hard grayish cemented layers were observed in SR + 25 %, SR + 40 % FA and SR + 6 % OPC at length varying from 8.5 –13.5 cm down the length of the solid core. The appearance of these grayish layers suggested local formation of hardpan layers as a result of precipitates formed cementing the leached solid residue particles. The hardpan layer results from the migration of formed precipitates as the pH front moves down the column solid cores. The yellowish/brownish coloration is characteristic of ochreous precipitates that occur in acid mine drainage impacted environments (Jeong and Soo, 2003).

UNIVERSITY of the
WESTERN CAPE

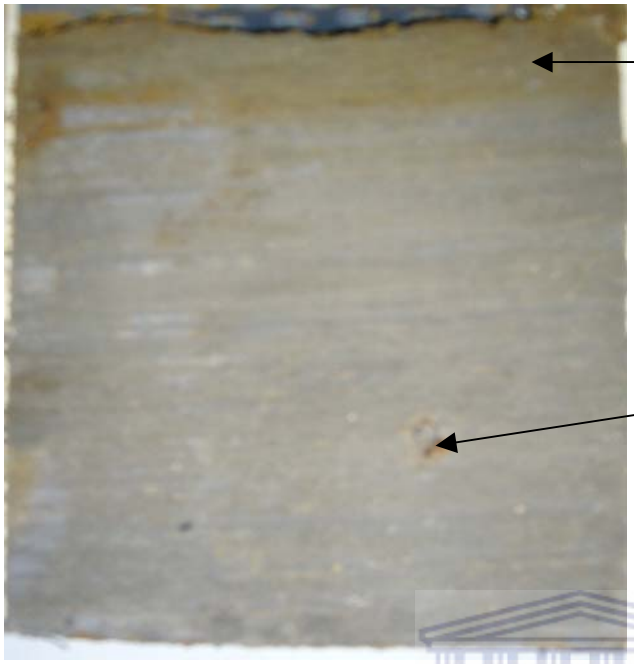

Column 1(FA)

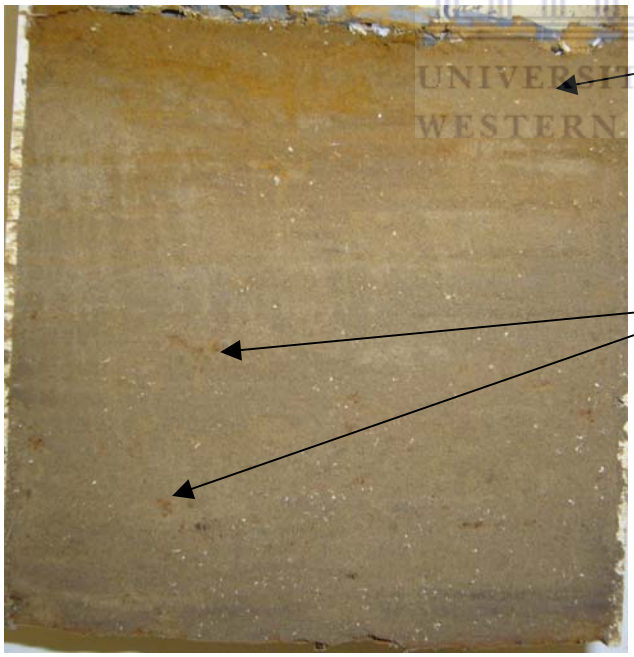

Column 2 (SR)

Figure 5.74: Digital photos of the sectioned FA and SR leached solid cores

UNIVERSITY of the
WESTERN CAPE

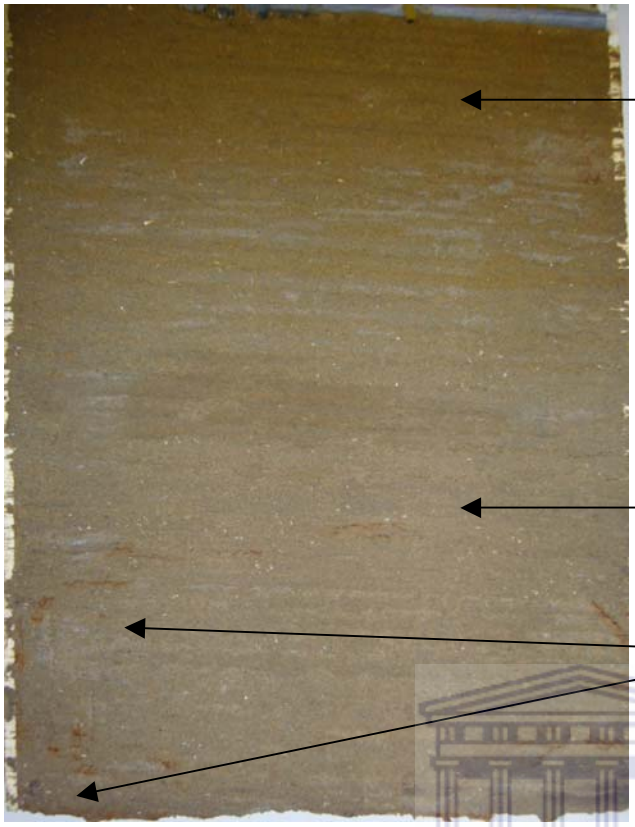

Column 5(SR + 25 % FA)

UNIVERSITY of the WESTERN CAPE

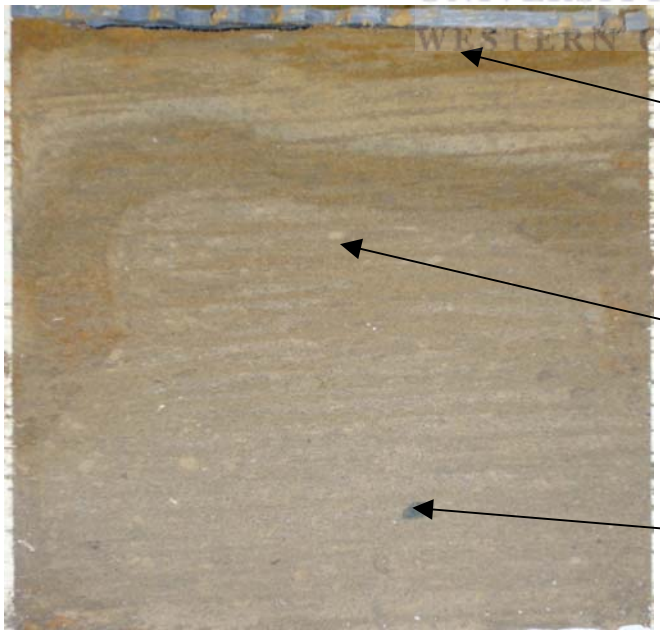

Column 8 (SR + 6 % OPC)

Figure 5.75: Digital photos of the SR + 25 % FA and SR + 6 % OPC leached solid cores

5.6.2 X-ray diffraction (XRD) analysis of the leached solid cores

Although the visualization of the sectioned solid cores revealed extensive formation of ochreous precipitates in all sections of the solid cores XRD did not reveal presence of any crystalline Al or Fe-bearing mineral phases (Figs B20-B23). This would indicate that the precipitates were too amorphous to be detected by XRD or they were below detection limits. XRD revealed the presence of gypsum ($CaSO_4$. $2H_2O$) and calcium sulphate hydrate ($CaSO_4.0.6H_2O$) as the only new crystalline mineral phases.

5.6.3 Fourier Transform infra-red analysis (FTIR) of the leached solid residue cores

The main absorption bands observed in the leached solid residue core sections are presented in the Table 5.9 and Figs 5.76-5.79.

Table 5.9: Characteristic absorption bands observed for FA, SR, SR + 25 % FA and SR + 6 % OPC leached solid residue cores.

UNIVERSITY of the
WESTERN CAPE

Absorption band/peak(cm^{-1})	Leached solid residue cores			
	FA	SR	SR + 25 % FA	SR + 6 % OPC
3200-3600	√	√	√	√
2800-2915 with peaks at 2912,2844 and 2812	√	√		√
2290, 2350	√	√	√	√
1600-1606	√	√	√	√
1360,1382-1390			√	√
1070-1134 with peaks at 1122-1134 and a shoulder at 986-996	√	√	√	√
656-658	√	√	√	√
596-600	√	√	√	√
436-454	√	√	√	√

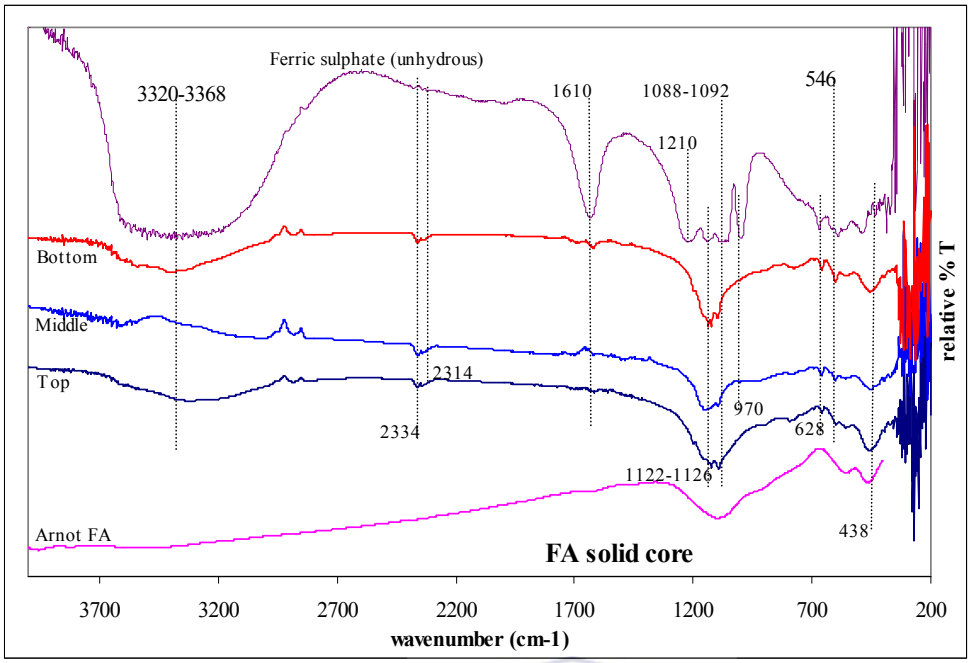

Figure 5.76: Infra-red spectra for the top, middle and bottom slices of the fly ash (FA) leached solid residues cores with the spectra of a pure unhydrous ferric sulphate imposed for comparison.

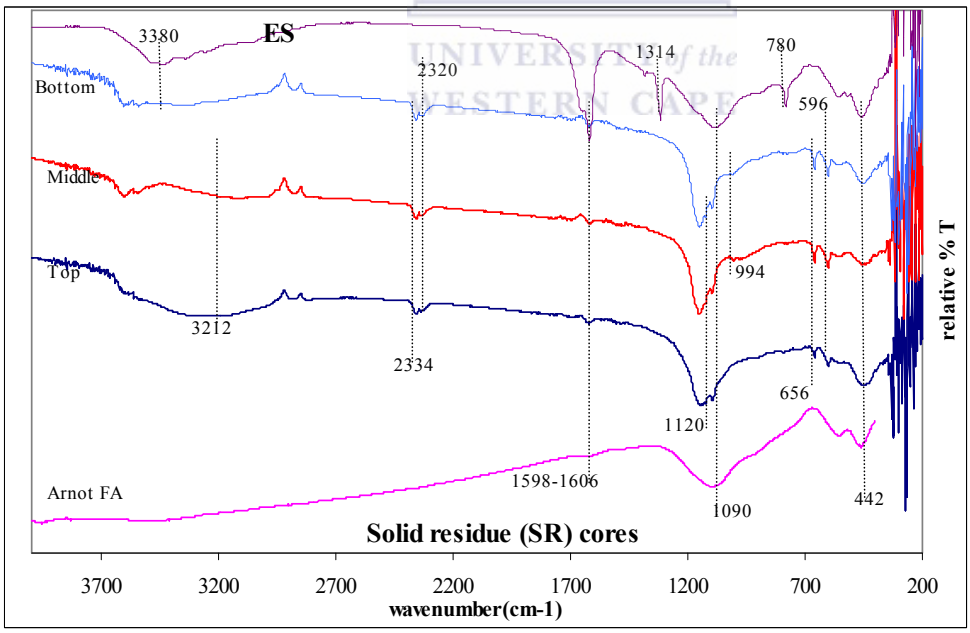

Figure 5.77: Infra-red spectra for the top, middle and bottom slices of the leached solid residues (SR) cores with the spectra of ammonium oxalate extracted (ES) top slice imposed for comparison.

UNIVERSITY of the WESTERN CAPE

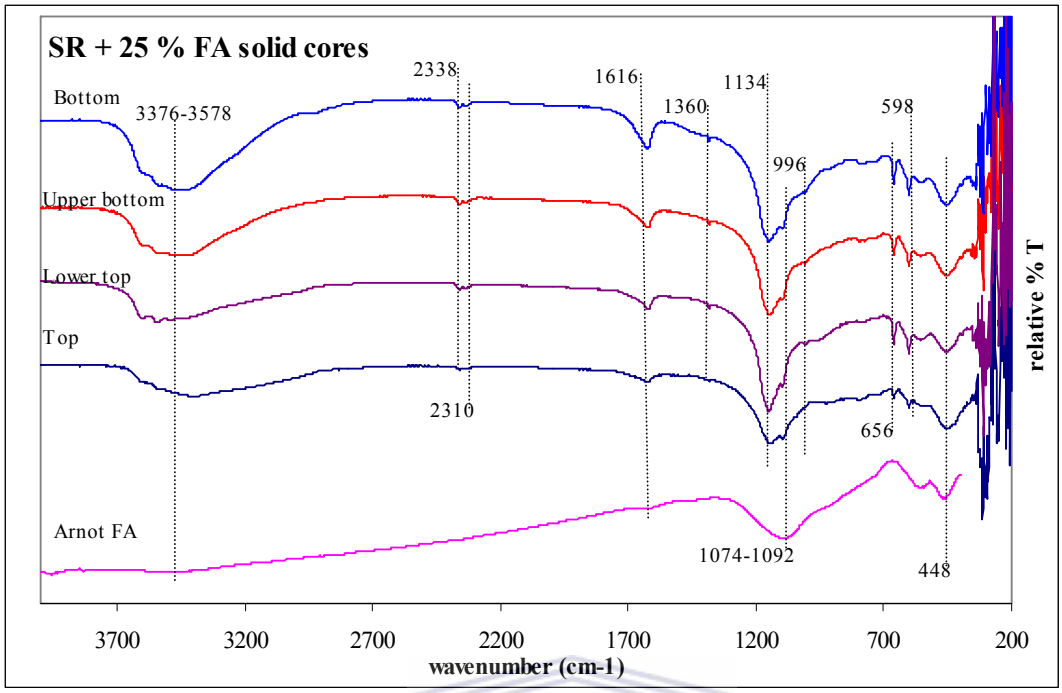

Figure 5.78: Infra-red spectra for the top, lower top, upper bottom and bottom slices of the leached solid residue (SR) + 25 % FA cores.

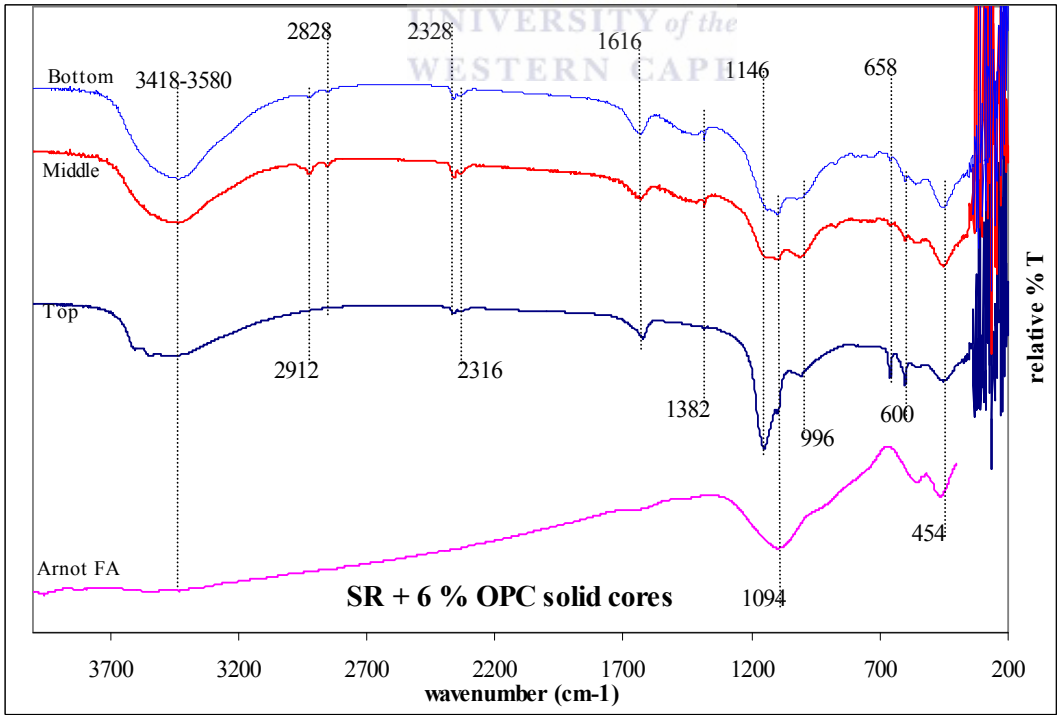

Figure 5.79: Infra-red spectra for the top, middle and bottom slices of the leached solid residue (SR) + 6 % OPC cores.

UNIVERSITY of the WESTERN CAPE

The unreacted fly ash displayed absorption bands within the region of 1594-1600, 900-1120 and 440-554 cm^{-1}. A weak broad band was observed within the region of 3300-3500 cm^{-1}. The bands within the 3300-3500 cm^{-1} region correspond to stretching vibrations for structural OH groups while bands within 1594-1600 cm^{-1} correspond to OH stretching vibrations for strongly adsorbed water (Figs 5.76-5.79). The band from 900-1120 cm^{-1} with a maximum at 1074 cm^{-1} is common for aluminosilicates and is usually well developed in spectra for glass materials (Farmer, 1974). XRD of Arnot fly ash revealed presence of quartz and mullite (Fig B20-B23). Farmer (1974) further observes that the aluminosilicate bands from 900 – 1200 cm^{-1} with a maximum at 1025cm^{-1} will partially mask the characteristic absorption bands for SO_4^{2-} containing compounds. All the leached solid residue cores displayed the bands at 3200-3600 cm^{-1} and 1600-1606 cm^{-1} due stretching vibrations for structural and strongly adsorbed water OH groups respectively (Figs 6.76-6.79).

All the leached solid residue cores displayed strong absorption bands within the region 1070-1134 with peaks at 1122-1134 and a shoulder at 986-996 cm^{-1}. Bigham *et al*. (1990) compared IR spectra of a few natural and synthetic specimens of Fe hydroxides and sulfates and found that any specimen containing SO_4^{2-} either chemically bonded or adsorbed shows absorption bands between 1100-1200 cm^{-1}. This band is attributed to the stretching vibrations of SO_4^{2-} (ν_3). The SAMD interacting with the FA and the FA blend solid residue during the drainage experiment contained SO_4^{2-} > 14000 mg/L and PHREEQC simulation predicted precipitation of iron (oxy)-hydroxides and iron hydroxysulphates.

Unlike in the unreacted fly ash the absorption band at 1100-1200 cm^{-1} in all the leached solid residue cores shows splitting into two bands with a peak at 1120-1138 cm^{-1}, second one at 1092 cm^{-1} and shoulder at 994-996 cm^{-1} for the FA and 6 % OPC blend solid residue cores. Several authors (Bigham *et al*., 1990; Lazaroff *et al*., 1982; Lazaroff *et al*., 1985) point out that if the symmetry of SO_4^{2-} decreases with coordination, a splitting of the ν_3 fundamental occurs. For unidentate complex (C_{3v} symmetry) two bands appear.

Appearance of the ν_1 (970 cm^{-1}) mode may also indicates low site symmetry for SO_4^{2-}. Thus the bands at1120-1138 cm^{-1}, second one at 1092 cm^{-1} and shoulder at 994-996 cm^{-1}most probably arise from the formation of a bidentate complex between SO_4^{2-} and Fe in leached

solid residue precipitates. Such complexes forms as a result of replacement of OH groups with SO_4^{2-} at the mineral surface through ligand exchange or within the structure during precipitation. However it would be difficult to distinguish by IR whether this SO_4^{2-} is adsorbed or structural since these two bonds could be similar in energy and geometry (Bigham *et al.,* 1990).

The leached solid residue cores exhibited sharp absorption peaks at 656 $cm^{-1}$and 600 cm^{-1} which were attributed to structural OH deformation and $\nu_4(SO_4^{2-})$ respectively (Nakamoto, 1997). Lazaroff *et al*. (1982) points out that the shoulder at 640-650 cm^{-1} could indicate presence of jarosites. K-jarosite was predicted to be precipitating by PHREEQC in the FA, SR, SR + 25 % FA and SR + 6 % OPC solid cores. The top section of the FA, SR, SR + 25 % FA leached solid cores exhibited broad absorption bands of the type usually associated with amorphous solids. Comparison with IR spectra of unhydrous ferric sulphate suggests that the solid precipitates are composed of ferric-oxide sulphates (Fig 5.76). Lazaroff *et al*. (1982) observed similar IR spectra for amorphous ferric sulphate precipitates produced by bacteria oxidation. That the absorption maxima observed at 1122-1134 cm^{-1} and a shoulder at 986-996 cm^{-1} is due to IR activity of SO_4^{2-} is confirmed by the disappearance of the absorption bands on treating the leached solid residues with ammonium oxalate for four hours in the dark (Fig 6.77) (Schwertmann *et al*., 1982). The presence of strong absorption bands at 778 cm^{-1} corresponding to OH deformation of goethite appear to suggest increased intensity of goethite after ammonium oxalate extraction (Shokarev *et al.*, 1972). The peaks observed at 436-454cm^{-1} are most likely Fe-O stretching vibrations (Kulumani and Jasobanta, 1996). Gypsum is revealed by the $2\nu_3$ (SO_4^{2-}) overtone near 2130-2220 cm^{-1} (Sutter *et al*., 2005).

5.6.4 Conclusions

The FTIR results revealed the incorporation of SO_4^{2-} in the resulting Fe and Al mineral phases either through adsorption or structural incorporation. Splitting of the ν_3 fundamental mode arises from the formation of a bidentate complex with the metal ions, however the results could not reveal whether the SO_4^{2-} is structural or adsorbed.

5.6.5 Scanning electron microscopy (SEM) and Scanning Electron microscopy-Energy dispersive X-ray spectroscopy (SEM-EDX) analysis of the leached column solid cores.

Excessive aggregation of the solid residue particles in the leached solid cores was observed confirming the extent of formation of mineral phases other than gypsum and ettringite. As observed and discussed in chapter five of this work, the precipitated mineral phases tend to fill between the particles or deposit on the surface of the leached particles. Moreover PHREEQC simulation strongly predicted precipitation of Al, Fe- (oxy) hydroxides, Al-hydroxysulphates, Fe-hydroxysulphates and it's predicted that some Ca-Al-hydroxysulphates could also have been precipitating in course of the drainage experiment. None of these phases were detected by XRD probably due to poor crystallinity or low concentration due to dilution by the residue matrix. In this section attempt is made to semi-quantitatively identify these mineral phases in the leached solid residue (SR) and solid residue (SR) + 6 % OPC solid cores. Due to the limitations of the SEM-EDX as per the analysis volume (1 μm^3) there is bound to be contribution from the underlying matrix and the results should be taken with caution. The results can only provide a general trend of enrichment of elements in the identified precipitates or crystals and hence only a general conclusion can be drawn. The un-reacted Arnot fly ash was also analyzed by SEM-EDX to provide the baseline for comparison with the solid residue samples. For all the SEM-EDX analysis the K_α line was utilized in calculations of the % elemental concentration of the areas and spots analyzed.

The figure 5.80 below shows the spots that SEM-EDX analysis were done for the leached solid residue cores and Table 5.10 shows the EDX elemental composition results. Where applicable the results are discussed and conclusions drawn in relation to the EDX analysis of the Arnot fly ash, three spots on the Arnot fly ash were analyzed to give an average

background concentration. Precipitates or crystals aggregating on the solid residue particles were selected for analysis.

The spot SR-06 concentration differs from the fly ash in that P and S are detectable and Ca increases which would suggest a Ca, S rich precipitate is being formed probably $CaSO_4$ or gypsum. The precipitates appear to project in three dimensions which means they are crystalline. The decrease in Fe, Si, O, and Ti probably represents the dilution effect due to increase in Ca and S, but Al is observed to increase. This spot would probably represent a deposition of a Ca, S rich crystalline phase on a fly ash residue that resisted dissolution and this could probably explain the strong Al-Si-O-Fe signal. Spot SR-07 appears to be amorphous precipitates cementing the residue particles together. An enrichment of Fe, Al, S is observed. This is supported by the increase in the Al/Si ratio (0.76) as compared to the fly ash (0.38) and also the decrease in O/Al ratio as compared to fly ash ($1.2 \rightarrow 0.66$) (Table 5.10). The increase in Fe, Al, and S would probably suggest some kind of Fe, Al-hydroxysulphates. A corresponding increase in Cu would probably be due to adsorption in the precipitating phases.

UNIVERSITY of the
WESTERN CAPE

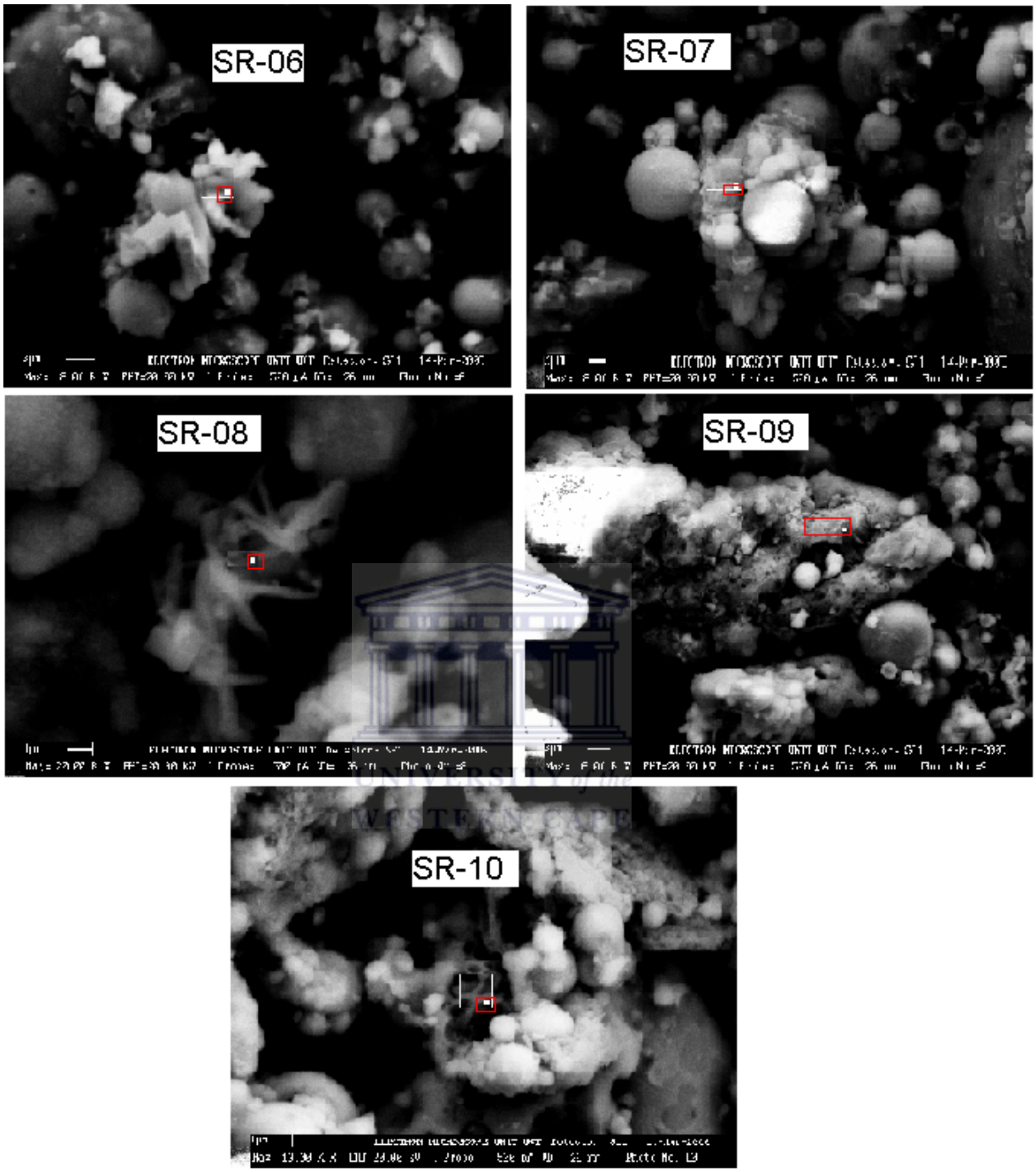

Figure 5.80: SEM backscattered micrographs showing spots where EDX analysis was done for the solid residue (SR) cores.

Table 5.10: EDX elemental analysis results (weight %) for the solid residue cores

Arnot FA		SR1-06		SR1-07		SR1-08		SR1-09		SR1-10	
Element	Weight %	Element	Weight%	Element	Weight%	Element	Weight%	Element	Weight%	Element	Weight%
O	14.52	O	13.93	O	8.3	O	5.87	O	11.73	O	12.98
Al	12.11	Al	14.66	Al	12.6	Al	4.71	Al	22.79	Al	20.74
Si	32.01	Si	26.57	Si	16.53	Si	4.46	Si	34.45	Si	37.95
P		P	1.01			P	2.8	P	0.43	P	0.47
S		S	5.11	S	6.73	S	11.02	S	3.81	S	2.39
K		K	1.06	K	0.62					K	1.78
Ca	2.57	Ca	3.16	Ca	1.12	Ti	0.91	Ca	0.71	Ca	2.13
Ti	2.53	Ti	1.67	Ti	1.2	Fe	70.22	Ti	0.58	Ti	0.93
Fe	36.66	Fe	31.58	Fe	51.55			Fe	24.3	Fe	19.63
				Cu	1.35			Ni	0.23	Ni	0
Cu	0.7	Cu	1.25					Cu	0.95	Cu	0.99
Total %	102.74	Total %	100	Total %	100	Total %	99.99	Total %	99.98	Total %	99.99

The spot SR-08 represents a crystalline material that has tentacle like structures projecting outwards and some forming circular formations resulting in hollow openings in-between. The concentration trends indicate enrichment in Fe, S and Al (note the Al/Si ratio increases to 1.6 as compared to FA (0.38) (Table 5.10) suggesting a similarity to the precipitates observed at spot SR-07. This means that SR-07 and SR-08 are both crystalline phases, it's only that the detailed crystalline nature of the SR-07 could not be revealed at the lower magnification (SR-07, magnification = 8 000: SR-08, magnification = 20 000). Area SR-09 represents an O, Al-rich amorphous phase aggregating together to form a dense mass. There is relative increase in O as compared to fly ash which strongly suggests an Al-(hydr) oxide phase. PHREEQC modeling predicted precipitation of amorphous Al $(OH)_3$. SR-10 is a crystalline material resembling in morphology the crystals observed in spot SR-08. It's enriched in Al, O, S and Ca.

In conclusion, crystalline phases enriched in Al, Fe, S and O were observed to have precipitated in the solid cores (SR). Although they cannot be conclusively resolved to a particular mineral phase from the semi-quantitative EDX elemental analysis due to limitations stated earlier, their elemental contents suggests Al, Fe-hydroxysulphates or Al, Fe-(hydr) oxides. The enrichment in Ca, Al, S and O would also suggest formation of

monosulphate type of minerals ($3CaO.\ Al_2O_3.CaSO_4.12\ H_2O$) similar to hydrating cement in SO_4^{2-} rich waters (Cocke and Mollah, 1993). Gypsum was also observed to be forming and depositing on the solid residue particles that resisted dissolution.

The figure 5.81 below shows the various spots analyzed for SR + 6 % OPC leached solid cores and Table 5.11 shows the corresponding EDX analysis results.

UNIVERSITY of the
WESTERN CAPE

Figure 5.81: SEM backscattered micrographs showing spots where EDX analysis was done for the SR + 6 % OPC solid cores.

Table 5.11: EDX elemental analysis results (weight %) for the SR + 6 % OPC solid cores.

Arnot FA		SROPC-11		SROPC-12		SROPC-13		SROPC-14		SROPC-15		SROPC-16	
Element	Weight %	Element	Weight%	Element	Weight%	Element	Weight%	Element	Weight%	Element	Weight%	Element	Weight%
O	14.52	O	19.69	O	17.71	O	15.15	O	20.23	O	12.65	O	16.63
Mg	1.64	Mg	4.28	Mg	1.94	Mg	2.94	Mg	1.33	Mg	0.38	Mg	4.55
Al	12.11	Al	8.45	Al	9.71	Al	9.15	Al	28.33	Al	4.97	Al	10.04
Si	32.01	Si	17.48	Si	24.4	Si	18.79	Si	39.19	Si	4.96	Si	19.51
P		P	3	P	1.16	S	4.86	S	0.68	S	3.59	S	10.78
S		S	3.41	S	8.89	Ca	18.5	Ca	6.3	Ca	70.93	Ca	14.68
Ca	2.57	Ca	33.31	Ca	26.13	Ti	2.06	Fe	3.94	Fe	2.51	Mn	1.82
Ti	2.53	Ti	0.99	Ti	1.43	Mn	1.82					Fe	21.98
Mn		Mn	1.92	Fe	8.62	Fe	26.73						
Fe	36.66	Fe	6.53										
Cu	0.7	Cu	0.94										
Total %	102.74	Total %	100	Total %	99.99	Total %	100	Total %	100	Total %	99.99	Total %	99.99

Spot SROPC-11 represents a tube-like crystalline material. The crystal is observed to be en-riched in Ca, Si, and O, the Ca/Si ratio = 1.9 (Table 5.11) would strongly suggest this to be calcium silicate hydrate gel. Cocke and Mollah. (1993) observes that CSH gels have Ca/Si ratio ranging from 1.5-1.7. Kindness *et al*. (1994) observed this crumbled foil morphology that is consistent with CSH gel on reacting tricalcium silicate with Cr (iii) salts. The presence of Mg, Fe, Ti, Cu and Mn, S, Al suggests incorporation or precipitation of metal-(hydr) oxides in the cement matrix. Spot SROPC-12 represents a mass of what appears to be amorphous precipitates and crystals adhering to these precipitates. The precipitates appear to be enriched in Ca, S, O and Si. The Ca/Si ratio of 1:1 would suggest a CSH gel but the presence of S and Ca/Al ratio of 3 would suggest calcium aluminate hydrate gel or Ca, Al-hydroxysulphate could also be present. These precipitates can best be described as a mixture of CSH gels, calcium aluminate hydrate gels or Ca, Al-hydroxysulphate. SROPC-13 is a crystalline phase with a structure similar to spot SR-10 and SR-08 observed in the solid residues. The elemental composition closely resembles that of SROPC-12 except the decrease in Ca and enrichment of Fe. The Ca/Si ratio of 0.98 suggests this is not CSH gel. The increase in O/Al ratio (1.7) would suggest formation of Fe-(hydr) oxide within the CSH gels. The formation of the Fe-(hydr) oxide is supported by the fact that S is observed to decrease compared to SROPC-12.

The spot SROPC-14 appears to be a mass of solid which is en-riched in O, Si and Al suggesting a strongly etched solid residue particle or a mass of solid residue particles encapsulated with CSH gel as suggested by the high Ca content. The lower Ca/Si ratio (0.16)

would suggest contribution of the Si signal from the encapsulated or underlying aluminosilicate residual matrix. Alternatively enrichment of O, Si and Al would suggest the first stage of hydrolysis of an activated aluminosilicate material similar to the process of aluminosilicate gel formation prior to the crystallization of zeolites. Van Jaarsveld *et al.,* (1997) showed that fly ash due to its large amount of amorphous aluminosilcates can easily dissolve in alkali media and promote geopolymerisation. The amount of the amorphous aluminosilicate materials can be increased by activating with alkaline solution such as NaOH (Chang and Shih, 1998). Addition of 6 % OPC to the solid residues was observed to initiate alkaline conditions that would have dissolved the amorphous aluminosilicate phases. The mass enriched in O, Si and Al would probably represent geopolymerisation of the dissolved aluminosilicate phases (Xu and Van Deventer, 2000). Van Jaarsveld *et al.,* 1999 proposed that heavy metals immobilization can occur through a combination of physical encapsulation and chemical bonding into the amorphous phase of the geopolymeric matrix and the observed encapsulation of the solid residue particles is varied.

Spot SROPC-15 represents aggregating mass of precipitates that don't appear to be crystalline. They are en-riched in Ca, Al and O, the Ca/Si ratio of 14.3 (Table 5.11) suggests this not to be a CSH gel and neither a calcium aluminate hydrate gel. The high calcium content (70.9 %) in combination with S (3.59) would suggest a gypsum or calcium sulphate phase. This is supported by the enrichment of O as indicated by the increase in the O/Al ratio (2.54) compared to FA (1.2). Spot SROPC-16 structure closely resembles crystalline material observed at spot SROPC-11, judging by the Ca/Si = 0.75, Al/Si = 0.51 and O/Al =1.66, this material seems to be enriched in Al, Ca, O and S as compared to FA, the decrease in Si is probably due to dilution effect. The high concentration of Fe, Mn, and Mg would suggest a calcium aluminate hydrate gel incorporating or encapsulating solid residue particles. The high Ca and S content would suggest phases such as gypsum or Fe, Al-hydroxysulphates.

In conclusion trends of the EDX analysis show that CSH gels and calcium aluminate hydrate gels were being precipitated. These gels were either incorporating Fe, Mg, Mn in their matrix or encapsulating the solid residue particles that were rich in these elements. The high Ca, S, O, Fe, and Al observed in some spots would strongly suggest presence of Fe, Al-(hydr)

UNIVERSITY of the WESTERN CAPE

oxides, Fe and Ca-Al hydroxysulphates either separately or being precipitated with CSH and calcium aluminate hydrate gel matrices.

5.6.6 PH profile of the column residue cores

The table 5.12 below and Figure 6.82 shows the variation of the pH of the solid cores with depth.

UNIVERSITY of the
WESTERN CAPE

Table 5.12: pH profile of the column solid residue cores with depth**.**

depth (cm)	depth (cm)	FA solid core		SR core		SR + 5 % FA		SR + 25 % FA		SR + 40 % FA		SR + 6 % OPC	
1	1	ave	SD	ave	SD	ave	SD	ave	SD	ave	SD	ave	SD
3	3.5	3.68	0.07	3.29	0	3.21	0.03	3.11	0	3.06	0.045	4.15	0.16
5	6	4.47	0.035	3.86	0.04	3.81	0.04	3.80	0.075	3.74	0.08	7.45	0.205
7	8.5	5.06	0.16	4.22	0.05	4.14	0.01	4.26	0.09	4.03	0.075	8.81	0.145
9	11	6.65	0.125	6.54	0.14	6.56	0.02	6.08	0.165	5.30	0.1	8.95	0.195
11	14	7.17	0.055	6.92	0.22	7.37	0.12	6.85	0.24	6.36	0.31	9.29	0.34
	15	7.47	0.11	6.98	0.21	7.5	0.15	7.35	0.18	6.66	0.295	9.07	0.215
										7.20	0.25		

Results presented as mean ± SD n=3

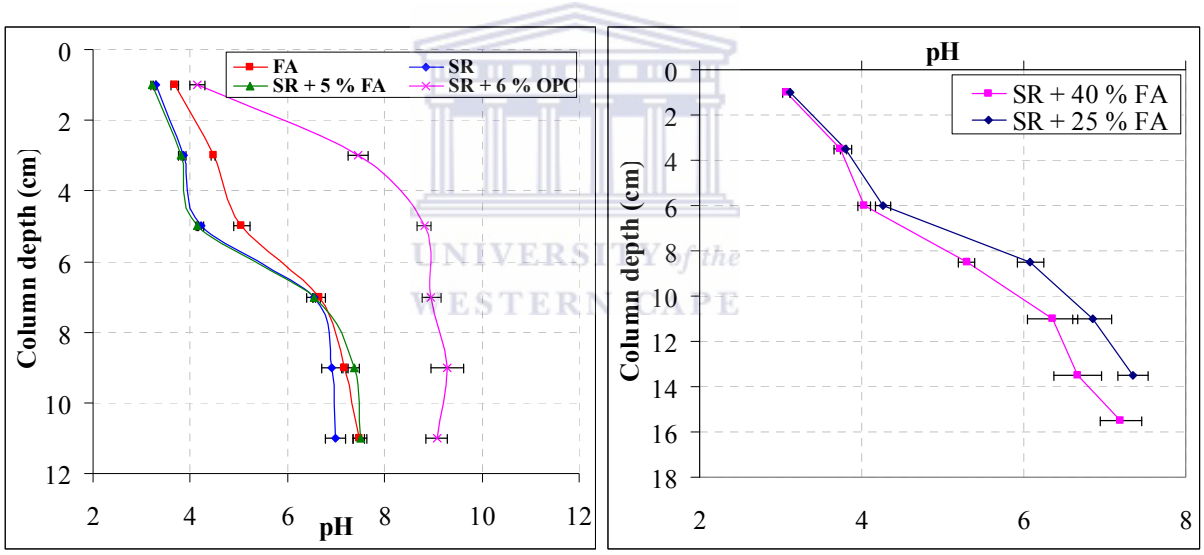

Figure 5.82: Graphical pH profile of the pore waters of the leached FA and solid residue (SR) cores. Error bars represent 1 standard deviation above and below the mean.

The pH profile down the column solid residues exhibit similar pattern for all the columns. The fly ash (FA) cores showed a higher pH up to a depth of 5 cm than SR, SR + 5 % FA, SR+ 25 % FA and SR + 40 % FA solid cores. This is attributed to the residue alkalinity present in the fly ash (FA) core. The residues at the top of the solid cores had the pH ranging from 3.0-4.0, at the middle 5.0-6.0 and at the bottom section 6.0 -7.40. The solid cores show a clear transition from being acidic at the top to circum-neutral at the bottom. The transition is gradual for FA, SR + 25 % FA and SR+ 40 % FA solid cores and sharp for SR and SR + 5

% FA solid cores. The profile of SR + 6 % OPC solid core deviates from the pattern observed, from pH 4.31 at a depth of 1 cm, the pH shoots to 7.66 at a depth of 2 cm and is maintained at pH > 8.0 up to the bottom of the solid core. The pH of solid residue cores for column SR + 6 % OPC were constantly higher than for SR, SR + 5 % FA, SR+ 25 % FA and SR + 40 % FA solid cores. The high pH of the SR + 6 % OPC solid residue cores could have been due to cementation reactions of ordinary Portland cement (OPC), where the generated calcium silicate hydrate gels (CSH) encapsulated the solid residue particles reducing the surface area of contact with the leachant. This was proofed by SEM and SEM-EDX analysis. The leachates from this column had initially high pH (Fig 5.82) which represented the onset of OPC hydration reactions followed by the release of the CSH products and portlandite. The pH thereafter dropped to below 4.0. This confirms the prediction that after formation of the CSH gel the interaction of the solid residue particles with SAMD was significantly reduced and the slow dissolution of the aluminosilicate matrix and mullite inhibited. The hydration reactions of OPC generate portlandite following reactions (equations 5.35 and 5.36) (Taylor, 1998) and will contribute to the initially high pH of the leachates.

$$2Ca_3SiO_5 + 6H_2O \Rightarrow CSH + Ca(OH)_2 \quad \text{.....(5.35)}$$

$$2Ca_2SiO_4 + 4H_2O \Rightarrow CSH + Ca(OH)_2 \quad \text{.....(5.36)}$$

UNIVERSITY of the
WESTERN CAPE

The low pH exhibited by all the solid cores at the top of the column could be due to several reasons; this represents the surface of initial contact of solid cores with the acidic leachant which is neutralized before leaching down the column hence this represents the region of maximum depletion of alkalinity. Being in contact with the atmosphere, oxidation of Fe^{2+} is bound to be maximum, precipitation of the oxidized Fe^{2+} and subsequent hydrolysis of Fe^{3+} in the leachant generates more acidity that consumes the alkalinity generated by the solid cores. Hydrous sulphate minerals are likely to have formed under these conditions. All the solid cores showed increased intensity of the yellowish coloration associated with iron hydroxides and (oxy) hydroxysulphates at the top section. At high Fe concentrations in solution, secondary sulphate phases can precipitate on the surface of the solid residue particles especially under evaporating conditions. These columns were left un-drained for 7-14 days and these precipitates could have formed at the surface of the solid residue cores due to evaporation. The hydrous sulphate minerals can be a source of acidity (Alpers *et al.,*

1994). This is could have been released on dissolution on resumption of drainage, example Halotrichite and Coquimbite (equations 6537 and 5.38 respectively).

$$FeAl_2(SO_4)_4.22H_2O + 0.2O_2 \Rightarrow Fe(OH)_3 + 2Al(OH)_3 + 4SO_4^{2-} + 8H^+ + 13.5H_2O \text{ ..(5.37)}$$

$$Fe_2(SO_4)_3.9H_2O \Rightarrow 2Fe(OH)_3 + 3SO_4^{2-} + 6H^+ + 3H_2O \text{ ……..(5.38)}$$

It can be concluded at this point that addition of fly ash to the solid residues (SR) slows down the acidification of the column solid cores. Blending with OPC reduces the interaction of the solid residues with the leachant due to encapsulation of the residue particles by the generated CSH gel. This slowed down the acidification of the solid residue core and dissolution of the aluminosilicate matrix and mullite with subsequent reduction in Ca released. This probably would explain the low SO_4^{2-} attenuation efficiency of SR + 6 % OPC solid core as compared to FA, SR + 25 % FA and SR + 40 % FA cores.

5.6.7 Sequential chemical extraction (SSE) of the leached solid residue (SR) cores

In the section of contaminant attenuation profiles it has been shown that the main mechanisms responsible for retention of the contaminants is precipitation, adsorption, oxidation and hydrolysis as the pH is buffered at alkaline (10-12) and circumneutral pH (6-9.5). Precipitates identified include gypsum, ettringite and those predicted to be precipitating by PHREEQC include Al $(OH)_{3(amorphous)}$, Fe $(OH)_{3(amorphous)}$, $FeOHSO_4$, jurbanite, manganite and rhodochrosite. The sequential extraction of the solid residue cores was done to assess the mass of trace metals associated with each of the dominant secondary mineral phases and also qualitatively collaborate the contaminant retention capacity of the FA, SR + FA and SR + OPC blends. A second objective of the sequential extraction was to confirm the mechanisms proposed for the attenuation of the contaminants. Three fractions were considered: water soluble fraction, amorphous fraction and reducible fraction. The amorphous fraction was considered to be significant based on the fact that despite the high % attenuation efficiency of the contaminants, no crystalline Al or Fe bearing mineral phases were detected by XRD. Consequently selective sequential extractions were done on FA, SR, SR + 25 % FA and SR + 6 % OPC on top, middle and bottom solid core slices. However due to the similarity of the extraction profiles of the SR and SR + 25 % FA cores the discussion of the results is

confined to FA, SR and SR + 6 % OPC solid cores. The tables 6.13-6.16 shows sequential extraction results for FA, SR, SR + 25 % FA and SR + 6 % OPC leached solid cores. Detection limits (mg kg^{-1}) for each fraction are presented together with the results in Table 5.13.

A widely used technique for understanding elemental distributions in the solid phase in soil and sediments involves the use of selective sequential extractions (SSE) (Chao, 1984; Tessier *et al*., 1985). SSE procedures have also been used on mine waste contaminated areas (Kuo *et al.,* 1983; Ma and Rao., 1997; Ramos *et al.,* 1994). The use of SSEs is based on the premise that chemical reagents can remove elements from specific fractions of the solid phase by destroying the binding agents between metals and the matrix (Tessier *et al*, 1979). However the amount of any one given element extracted from a particular phase is dependent on the reagent concentration and type, extraction sequence and solid/solution ratio hence the term operationally defined values (Miller *et al*., 1986).

UNIVERSITY of the
WESTERN CAPE

5.6.7.1 Water soluble fraction

The water fraction contains metals derived from re-dissolution of water soluble phases such as gypsum ($CaSO_4$. $2H_2O$) or calcium sulphate hydrate ($CaSO_4$.0.6 H_2O), both were identified by XRD in the leached solid cores (Figs B20-B23). These can also result from the re-dissolution of tertially phases which could have accumulated during the drying and evaporation of core surface during the drainage experiments (an interval of 7-14 days was imposed between respective drainages). It can also include metals desorbed from Mn, Al or Fe (oxy) hydroxide surfaces.

5.6.7.1.1 Fly Ash (FA) leached solid core

Fe shows an increase from 10.7 mg kg^{-1} at the top to 4446 mg kg^{-1} at the bottom, this indicates the retention profile of Fe as acidification of the FA core occurs. Least acidified part of the core (bottom) retains most of the Fe in the pore water (Figs 5.80 and Table 5.13).

Table 5.13: Sequential extraction results for the FA leached solid core (results presented as mean±SD for n=3 extractions, DL-detection limits)

Fly Ash solid core				water soluble fraction (mg kg^{-1} dry solids)							
	Al	Fe	Mn	Si	Ca	Ni	Zn	Cu	B	Sr	Mg
Top	229.3±9.4	10.7±8.4	116.0±4.0	BDL	3466.2±70.6	7.6±0.8	2.9±0.7	BDL	0.35±0	44.3±0.7	1082.3±41.9
Middle	170.4±24.2	2758.0±89.9	2.01±0.6	BDL	2698.3±493.4	BDL	BDL	BDL	BDL	4.5±0.4	21.2±11
Bottom	1790.7±73.1	4446.4±364.6	17.2±0.51	486.6±15.3	1138.3±68.9	31.5±1.5	40.7±17.1	2.1±0.9	70.3±0	75.7±3.1	253.7±10.3
DL	0.018	0.577	0.005	0.706	3.34	0.009	0.007	0.001	0.084	0,0005	1.56
				Amorphous fraction (mg kg^{-1} dry solids)							
	Al	Fe	Mn	Si	Ca	Ni	Zn	Cu	B	Sr	Mg
Top	1960.5±178.6	BDL	1786.1±21.9	BDL	84598.7±11208	BDL	48.5±7.5	BDL	BDL	1056±70.7	20570.8±1299
Middle	15484.5±669.4	18056.1±3772.4	58.1±15.7	5669.8±0	BDL	225.8±0	131.3±9.3	105.2±72.2	1410±0	68.1±3.6	1172.9±75.5
Bottom	49718.3±2533	94258.7±6998	487±45.4	12468.7±749	102398.1±12115	641.4±64.6	231.2±13.5	102.8±6.7	73.1±0	3191.1±155.9	6381.9±241.2
DL	0.332	10.86	0.088	13.3	62.83	0.164	0.128	0.018	1.58	0.010	29.42
				Reducible fraction (mg kg^{-1} dry solids)							
	Al	Fe	Mn	Si	Ca	Ni	Zn	Cu	B	Sr	Mg
Top	3.7±2.8	BDL	292.9±2	BDL	11899.4±2698	BDL	18.7±0	BDL	4.3±0	201.8±4.5	3876.2±21.2
Middle	2149.5±8.6	922.3±214	76.8±8.4	251.8±124	BDL	24.5±18.9	16.5±15.3	16.2±0	26.3±0	8.9±0.02	630.4±48.7
Bottom	7486.7±305.3	13136±344	200.6±14.5	1868.8±18.9	15786.5±178	90.4±4.1	28.9±3.7	7.3±2.4	BDL	536.7±2.1	983.2±42.5
DL	0.05	1.62	0.013	1.98	9.39	0.024	0.019	0.003	0.236	0.002	4.90

UNIVERSITY of the WESTERN CAPE

Table 5.14: Sequential extraction results for the solid residue (SR) leached solid core (results presented as mean±SD for n=3 extractions)

Solid residue core				water soluble fraction (mg kg-1 dry weight)							
	Al	Fe	Mn	Si	Ca	Ni	Zn	Cu	B	Sr	Mg
Top	744.7±13.7	BDL	158.4±3.3	BDL	3835.6±136	4.2±0	7.3±1.1	BDL	BDL	71.5±1.8	850.7±23
Middle	BDL	5184.8±297	0.71±0.7	85.6±0	852.3±0	5.7±0.4	91.5±30	BDL	49±14.6	9.5±0.5	5.9±0.2
Bottom	2385.9±130	4536.6±275	20.3±1	866.9±85.5	2487.1±180	32.6±1.2	6.3±6.3	3.2±0	BDL	173.9±5.7	350.3±20.7
				Amorphous fraction fraction (mg kg-1 dry weight)							
	Al	Fe	Mn	Si	Ca	Ni	Zn	Cu	B	Sr	Mg
Top	6969.7±21.2	BDL	1803.9±86	BDL	54358.3±2317	BDL	404.1±266	BDL	BDL	1170.7±20	14094.2±588
Middle	25056.7±635	13289±3729	7.8±7.3	5064.1±1111	BDL	BDL:	2358.5±0	BDL	BDL	189.4±134	1360.2±101
Bottom	53632.4±1811	53682.5±2302	339.7±0.97	18056.9±58	97514.9±3816	342.3±18.8	181.3±81	35.5±3.5	BDL	4772.8±126	6604.7±176
				Reducible fraction fraction (mg kg-1 dry weight)							
	Al	Fe	Mn	Si	Ca	Ni	Zn	Cu	B	Sr	Mg
Top	1.9±0	BDL	212.5±19.7	BDL	9993.4±988	BDL	71.9±63	BDL	BDL	250.1±18.5	3578.8±222
Middle	1195.1±51	2760.9±376	189.8±7.9	804.9±104	BDL	12.7±0	372.5±0	BDL	BDL	27.6±7.9	1316±56
Bottom	10433.4±1777	8460.8±59.5	371.9±12	3255.3±38.8	18507±2037	49.1±1.6	15.3±3	3.6±0	BDL	884.4±1.2	1315.6±1

UNIVERSITY of the WESTERN CAPE

Table 5.15: Sequential extraction results for the SR + 25 % FA leached solid core (results presented as mean±SD for n=3 extractions)

SR + 25 % FA solid core					Water soluble fraction (mg kg^{-1} dry weight)						
	Al	Fe	Mn	Si	Ca	Ni	Zn	Cu	B	Sr	Mg
Top	759.4±1	BDL	147.2±3.8	13.7±5.4	3880.8±380	BDL	12.9±6	DBL	BDL	72±0.5	752.1±7.4
Middle	279.4±47	3934.4±390	1.8±1	BDL	1510.5±1120	16.5±3	BDL	31.2±12.2	BDL	6.8±0.1	21.6±1.4
Bottom	2674.6±48	4599.5±65	22.6±0.1	616.9±28	3373.3±2148	9.1±0.4	BDL	6.6±0.6	BDL	206.4±13	394.7±4.5
					Amorphous fraction (mg kg^{-1} dry weight)						
	Al	Fe	Mn	Si	Ca	Ni	Zn	Cu	B	Sr	Mg
Top	7564.8±262	38.4±0	1614±123	642.7±207	66183.1±323	BDL	127.8±60.7	BDL	BDL	1135.6±32.4	11427±1070
Middle	27389±287	19341.5±681	29.9±3	5226.7±1122	46022.2±7122	219.5±17.8	BDL	319±16.4	BDL	69.3±2	1426.6±27.8
Bottom	43568.5±9322	47850.9±17577	332.3±98.3	11582.3±1448	135313.5±47718	142.5±9.2	16.2±0	102.5±3.9	BDL	4120.9±1248	5560.2±1389
					Reducible fraction (mg kg^{-1} dry weight)						
	Al	Fe	Mn	Si	Ca	Ni	Zn	Cu	B	Sr	Mg
Top	21.2±14.3	BDL	143.8±15.2	BDL	13786±609	5.6±5.6	56.6±36.3	3±0	BDL	264.3±17.8	4080.7±353
Middle	2467.7±142	2715.5±67.8	321.5±6.9	4208.1±2745	41130.3±30499	58.9±7.2	BDL	35±12.7	377±0	15.6±1.5	1936.5±56.7
Bottom	8412.9±288	9977.1±822	436.5±6.3	2446.3±133	23765.9±1175	23.1±0.3	19.7±0	16.8±1	BDL	939.3±35.1	1249.5±59

UNIVERSITY of the

Table 5.16: Sequential extraction results for the SR + 6 % OPC leached solid core (results presented as mean±SD for n=3 extractions).

SR + 6 % OPC leached solid core				Water soluble fraction (mg kg^{-1}dry weight)							
	Al	Fe	Mn	Si	Ca	Ni	Zn	Cu	B	Sr	Mg
Top	316.6±2.1	31.9±18.5	66.8±6.4	17.4±7.3	5067.2±629	3.6±0.84	0.93±0.3	3.5±1.6	7.3±0	72.8±0.3	455±38.5
Middle	918.6±97.9	3441.9±274	2.1±0	84.6±71.2	63561.3±22827	5.1±0	BDL	19.1±0.06	17.6±0	5.6±0.16	46.2±4
Bottom	2662.6±65.5	5713.4±754	22.4±0.72	714.5±29.1	10500.4±152	6.6±0.5	BDL	7.1±0.5	BDL	271.4±3.5	371.3±7.6
				Amorphous fraction (mg kg^{-1} dry weight)							
	Al	Fe	Mn	Si	Ca	Ni	Zn	Cu	B	Sr	Mg
Top	141.6±71.5	434.2±0	912.5±19	BDL	94080.9±6561	66.9±15.2	4.5±4.5	20.9±8.1	163.8±0	1785.2±47	15522.2±598.4
Middle	23705.3±353	25404.8±432	1567.6±7.2	3783.9±1	1704152.7±66180	140.6±49.2	BDL	163.7±40.9	BDL	95.1±5.7	10917.3±183
Bottom	66678±1020	117019.6±3051	4741±506	21531±1207	315495.3±22965	177.2±15.5	71.6±10.7	131.5±46.4	BDL	7535.8±71.7	17065.5±2484
				Reducible fraction (mg kg^{-1} dry weight)							
	Al	Fe	Mn	Si	Ca	Ni	Zn	Cu	B	Sr	Mg
Top	33.3±12.9	42.3±42.3	2.4±0.5	BDL	15687.2±1139.6	11.5±0.3	BDL	6.67±2	0.073±0	245.3±2.5	740.8±24.5
Middle	2286.1±153	2089.5±610	114.3±16.7	578.8±0	240551.4±13117	27.3±1	BDL	63±34.4	BDL	7.2±0.5	1380.9±70
Bottom	7867.3±274	12448.8±805.8	319.5±6.6	2944.8±8.1	35617.6±6599	17.1±0.32	5±6.3	20.7±4.7	BDL	980.7±5	2120.4±374.4

UNIVERSITY of the WESTERN CAPE

This further indicates that the Fe in this fraction is probably derived from dissolution of previously precipitated phases which moved with the pH front as the core acidified. Ca exhibited high concentration at the top decreasing at the bottom section. This indicates that the retention profile of Ca was probably dictated by precipitation of soluble phases such as gypsum which decreased as the SO_4^{2-} was attenuated with migration of the SAMD down the solid core. SEM-EDX revealed gypsum crystals to be highly concentrated at the top section of the solid cores (Fig 5.81).

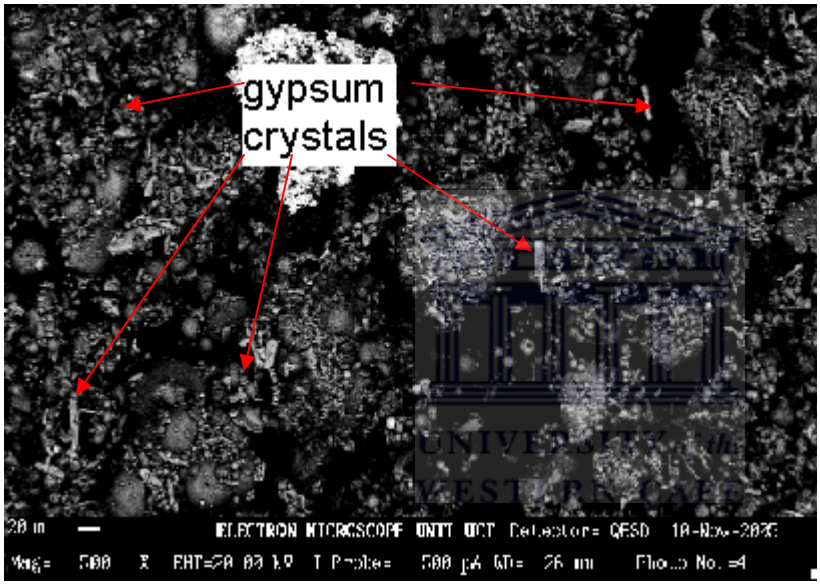

Figure 5.83: SEM micrograph showing numerous gypsum crystals in the top section of the leached solid residue (SR) cores.

Al, Mn, Ni, Zn, Cu, B, Sr and Mg show a similar retention profile with high concentration at the top and bottom section. However for Al, Ni, Zn, Cu, B and Sr the bottom section indicated higher concentration, this corresponds to the high pH of the pore water at this section (Fig 5.80). This probably indicates that the high concentrations were derived from soluble mineral phases that precipitated at alkaline pH. The high concentration at the top and bottom section could also be indicative of re-dissolution of tertially mineral phases formed as a result of evaporation and drying of the pore water at the top and bottom of the solid cores. The solid cores were in contact with the atmosphere at the top and bottom. Si, Ni, Zn, Cu and B were not detected in the middle section.

5.6.7.1.2 Solid residue (SR) leached solid core

Al, Mn, Ca, Sr and Mg show a similar profile with high concentration exhibited at the top and bottom section, with the middle section only exhibiting low or non detectable concentrations (Table 5.12). This profile is similar to that observed for FA solid cores. Fe, Zn and B exhibit a similar trend showing high concentration in the middle section. Si, Ni and Cu show a similar pattern increasing down from the surface to the bottom of the solid core. This trend mirrors the increasing pH of the pore water in the solid residue core (Fig 5.80). This probably indicates re-dissolution of previously formed precipitates under the circum-neutral pH regime.

5.6.7.1.3 Solid residue + 6 % Ordinary Portland Cement (SR + 6 % OPC) leached solid core

Al, Fe, Si, Ca and Ni show increasing trend from top to the bottom section of the solid core. This increasing trend mirrors the pH profile of the pore water (Table 5.16 and Fig 5.82) in the solid core and probably reflects the dissolution of mineral phases precipitated during the high pH initially generated on initial contact with SAMD. Mn, Sr and Mg exhibit high concentration in the top and bottom sections. For Mn this probably indicates dissolution of phases that formed as a result of oxidation at alkaline pH near surface where supply of O_2 was adequate. PHREEQC predicted manganite to be controlling Mn^{2+} activity at alkaline pH. Rhodochrosite that formed under alkaline pH (8-9) as predicted by PHREEQC would dissolve as the solid core acidifies.

UNIVERSITY of the
WESTERN CAPE

5.6.7.2 Amorphous fraction

Mineralogical analysis of the leached solid residue cores by XRD did not reveal any crystalline Fe or Al-bearing mineral phases. FTIR analysis suggested adsorption or incorporation of SO_4^{2-} in Al or Fe bearing mineral phases. However visualization of the sectioned leached solid cores revealed extensive yellowish/brownish coloration characteristic of ochreous precipitates (Jeong and Soo, 2003) (Figs 5.74-5.75). SEM and SEM-EDX

revealed amorphous precipitates, ettringite, gypsum and CSH gels in the leached solid residue cores. PHREEQC simulation predicted precipitation of amorphous Al $(OH)_{3(amorphous)}$, Fe $(OH)_{3(amorphous)}$, $FeOHSO_4$, jurbanite, ferrihydrite in the leachates of the solid residue cores. The ammonium oxalate extraction (AOD) in the dark was intended to remove the amorphous Fe, Al and Mn (oxy) hydroxides together with adsorbed or co-precipitated ions. The AOD does not specifically extract one particular phase but all non-crystalline Al, Fe and Mn all at once from the solid phase (Jackson *et al.*, 1986)

5.6.7.2.1 Fly Ash (FA) leached solid core

Al, Fe, Si, Ni, Zn, Cu, and Ca show an increase from the top to the bottom section (Table 5.13). It should be noted that the increase of Al (from 1960.5-49718.3 mg kg^{-1}), Fe (detection limit to 10.86-94258.7 mg kg^{-1}) and Si (13.3-12468 mg kg^{-1}) is significantly greater than for other elements. This suggests that the increase in AOD extracted Ni, Zn, and Cu corresponds to the amounts adsorbed on amorphous Al, Fe and Si precipitates down the solid core. Mn, Sr and Mg show a similar concentration profile with high concentration at the top and bottom section. The high concentration for Mn at the top section indicates that Mn was retained at the top section where high pH was generated initially and oxidation was likely occurring. PHREEQC simulation predicted formation of manganite at alkaline pH. For Mg this could also represent dissolution of precipitates formed under the alkaline pH regime or increased adsorption of Mg. Sr probably represents increased retention as celestite ($SrSO_4$) which was predicted to be precipitating by PHREEQC and would consequently undergo dissolution under the acidic conditions employed. Ca concentration profile indicates a trend that is not dictated by adsorption on amorphous Al or Fe phases but by a phase like gypsum. The increased concentration in this fraction is probably due to increased dissolution of gypsum under the acidic regime employed. The fact that Ni, Cu, Zn and B were detected in the middle section of this fraction while they were at detection limits in the same section for the water soluble fraction strongly indicates their adsorption onto the Al and Fe amorphous precipitates.

UNIVERSITY of WESTERN CAPE

5.6.7.2.2 Solid residue (SR) leached solid core

Al, Fe and Si show a steady increase from the top to bottom section of the solid core (Table 5.14). This points to an increase in amorphous precipitates down the solid core and relocation of precipitates formed earlier at the top of the solid core. The trend mirrors the pH profile of the pore water in the solid core with the pH increasing down the solid core (Fig 5.80). The non-detectability of Ni and Cu in the top and middle section and subsequent detection in the bottom section probably indicates translocation with the amorphous Al and Fe precipitates. Ca exhibits high concentration at the top and bottom section being undetected in the middle section. Mn, Sr and Mg were detected in all the sections with the top and bottom section exhibiting high concentrations.

5.6.7.2.3 Solid residue + 6 % Ordinary Portland Cement (SR + 6 % OPC) leached solid core

UNIVERSITY of the
WESTERN CAPE

Al, Fe, Mn and Si exhibited an increasing trend from the top to the bottom section of the solid residue core (Table 5.16). This strongly indicates importance of the amorphous precipitates in retaining the contaminants in the solid cores. A marked efficiency of the SR + 6 % OPC solid core than FA and SR in retention of the contaminants is observed. This is most noticeable with Fe, the amount retained in the bottom section is double (117019 mg kg^{-1}) compared to that retained by SR (53682 mg kg^{-1}). A similar phenomenon is observed with Mn, Mg, Cu, Sr and B. This probably indicates the role encapsulation of the precipitates and solid residue particles by the CSH gel had on the contaminants retention capacity of this solid core. SEM-EDX identified Fe, Mn rich Ca-Si-Al-O gels (Fig 5.84) in this solid core which suggests adsorption or incorporation of Mn in amorphous Fe rich precipitates or Al-Si-O rich gels.

Element	Weight%
O	16.68
Mg	5.04
Al	10.69
Si	27.42
S	6.52
Ca	6
Mn	1.95
Fe	25.69

Figure 5.84: Backscattered SEM micrograph showing Fe, Mn, S rich Ca-Al-Si-O gel with accompanying EDX analysis.

This could also represent encapsulation of Mn (oxy) hydroxides and Fe amorphous (oxy) hydroxides in Al-Si-O or Ca-Si-Al-O gels. Encapsulation was extensive in this solid core as identified by SEM (Fig 5.85).

UNIVERSITY of the
WESTERN CAPE

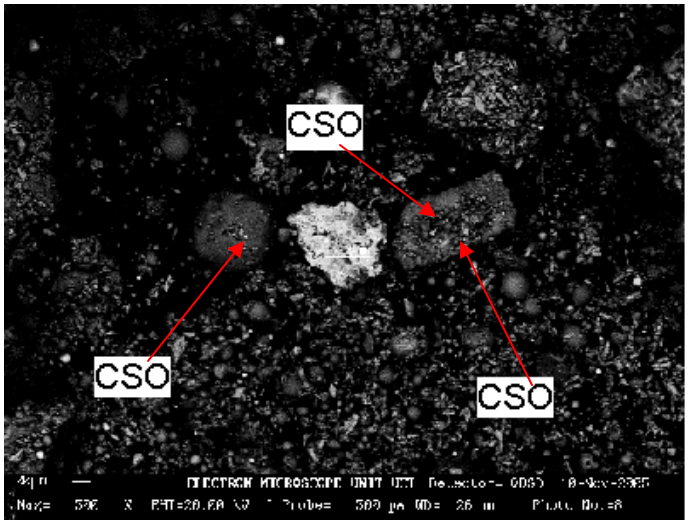

Figure 5.85: SEM micrograph showing Ca-Si-Al-O rich gel encapsulating precipitates and solid residue particles (CSO-Ca-Si-O gel was identified earlier on by SEM-EDX).

The increased Ca retention as compared to other solid cores was due to precipitation of gypsum, ettringite and the high Ca content of OPC (Table 5.5). The increased retention could

also be due to incorporation of Ca in precipitating Si-Al-O rich gels that were identified in the solid residue cores by SEM-EDX (Fig 5.84). This solid core also exhibited increased retention of B. Eary *et al*. (1990) points out that borate can be incorporated in precipitating aluminum hydroxides.

5.6.7.3 Reducible Fraction

This fraction was intended to quantitatively estimate the effect of the strongly acidic SAMD on the crystalline Fe, Mn (oxy) hydroxides in the fly ash residues.

5.6.7.3.1 Fly ash (FA) leached solid core

The Fe concentration shows an increase (from detection limits 1.62 mg kg^{-1} to13136 mg kg^{-1}), Mn registered high concentration in the top and bottom section while Al shows a smooth increase in concentration from top to bottom (3.7-7486 mg kg^{-1}). This probably indicates the degradation of the residual matrix of the fly ash which decreases down the solid core as the SAMD interacted with the fly ash. Ca, Zn and Ni show the same trend reinforcing this concept.

UNIVERSITY of the
WESTERN CAPE

5.6.7.3.2 Solid residue (SR) leached solid core

Al, Fe and Si show an increasing trend from non-detectability for Fe and Si at the top section to highest concentration at the bottom section. Again the increasing trend seems to show the gradation of the fly ash residual matrix as the SAMD percolates down the solid residue core. The concentration for the other elements observed probably represents concentration locked in the residual matrix. B was not detected indicating that it's only present as soluble salts on the surfaces of the fly ash spheres and not in the aluminosilicate matrix. Mg seems to be highly concentrated in the top section for all the extractions but shows highest concentration in the amorphous fraction.

In conclusion the importance of amorphous precipitates in the attenuation of contaminants was demonstrated in the high concentrations retained in the amorphous fraction in the sequential extractions. Gypsum precipitation was also observed to be a significant SO4 retention pathway as also evidenced by the high concentrations of Ca observed in the water soluble fraction and also in the amorphous fraction. High retention of contaminants Fe, Mn, Al, Ca and Si was observed in the amorphous fraction in the SR + 6 % OPC solid core which renders credence to the fact that formation of amorphous calcium silicate hydrate, calcium ferrite hydrate and possibly calcium aluminate hydrate gels were contributing to the increased contaminants retention in this solid core. Glasser (1970) observes that cation immobilization by CSH gels and by (hydr) oxide precipitation is the most important in cement systems.

5.6.8 Strength development of Ordinary Portland Cement (OPC) blend Solid Residues (SR) and implication for backfilling application.

UNIVERSITY of the
WESTERN CAPE

The strength development of the solid residues blended with Ordinary Portland Cement was done over one year period as a preliminary study to evaluate possibility of using the solid residues for backfilling of mined areas. The study was carried out with Matla fly ash and Navigation AMD and the solid residues (SR) were generated at circum-neutral pH 9 for batch one and two and pH 11 for batch three.

Strength measurement of the solid residues blended with varying rates of OPC (1 %, 3 %, and 6 %) on a dry weight basis was done as a function of time. The solid residues in addition to treating AMD passively, should also provide mechanical strength to support the overburden, moreover the unconfined compressive strength (UCS) are essential for the rock mechanics to model the force interaction and lateral load bearing of cemented strength. Unconfined compressive strength testing was performed according to ASTM (D2166-85) for the cured cylinders. Samples prepared from Matla fly ash/Navigation AMD were used for the strength testing. Samples were formulated using municipal tap water and process water from the FA/AMD treatment process.

5.6.8.1 Particle size analysis

Figure 6.86 shows the particle size distribution for unreacted Matla fly ash and AMD reacted fly ash (i.e., solid residues (SR) made from the reaction between Matla fly ash and Navigation AMD). After reaction with AMD, there was a slight increase in the percentage of particle size in the range of 1 to 20 μm. This is probably a consequence of the precipitates being formed during the neutralization reaction. The other size fractions (< 1 μm and > 20 μm) were not modified by the reaction with AMD. The overall pattern of size distribution is not affected when fly ash is reacted with AMD. This fly ash appears to be very fine; all its particles are smaller than 40 μm in size.

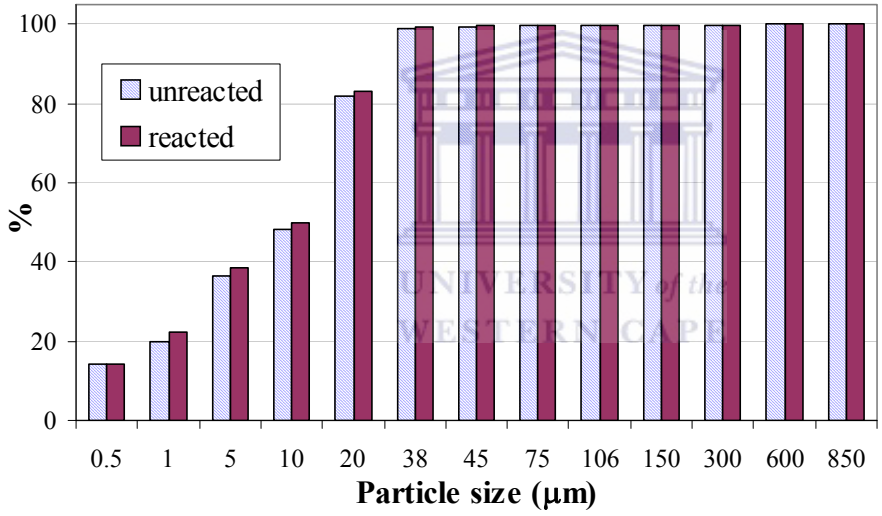

Figure 5.86: Particle size distribution for unreacted and AMD reacted Matla fly ash

UNIVERSITY of the
WESTERN CAPE

5.6.8.2 Strength development testing

The water/solid ratios of the solid residue slurries and cured samples from the three different batches are presented in Table 5.17. The initial water/solid ratios in the co-disposal material were 0.727, 0.692 and 0.700 for batch one, two and three respectively.

Table 5.17: Water/solid ratios of solid residue slurries and cured samples for batch one.

Batch number	Binder ratio (%)	Water/solid ratio in slurry	Water/solid ratio in cured sample
	1	0.589	0.533
1	3	0.577	0.510
	6	0.559	0.499
	1	0.714	0.538
2	3	0.700	0.612
	6	0.678	0.533
	1	0.860	0.600
3	3	0.850	0.555
	6	0.823	0.625

UNIVERSITY of the
WESTERN CAPE

Figures 5.87-5.89 shows the strength development profiles of the cylinders prepared from the three batches of solid residue slurries. Strength development testing was reported as unconfined compressive strength (UCS).

Strength development in the three different batches was found to be proportional to the proportion of binder used (Figs 5.87, 5.88 and 5.89). A more rapid strength development is observed in the first 28 days of curing for the solid residue slurries formulated with process waters (batch two) than the one formulated with tap water (batch one). This early accelerated strength development could be due to the formation of gypsum on hydration of the cement binder, with the process waters acting as a rich source of sulphates. The process waters had SO_4^{2-} content ranging from 5483 ±14.9 at circum-neutral pH and 4570.7 ± 110.3 (n=3) at alkaline pH. Overall the solid residue slurries formulated using the process waters had greater unconfined compressive strength at all levels than the solid residues slurries formulated using municipal tap water.

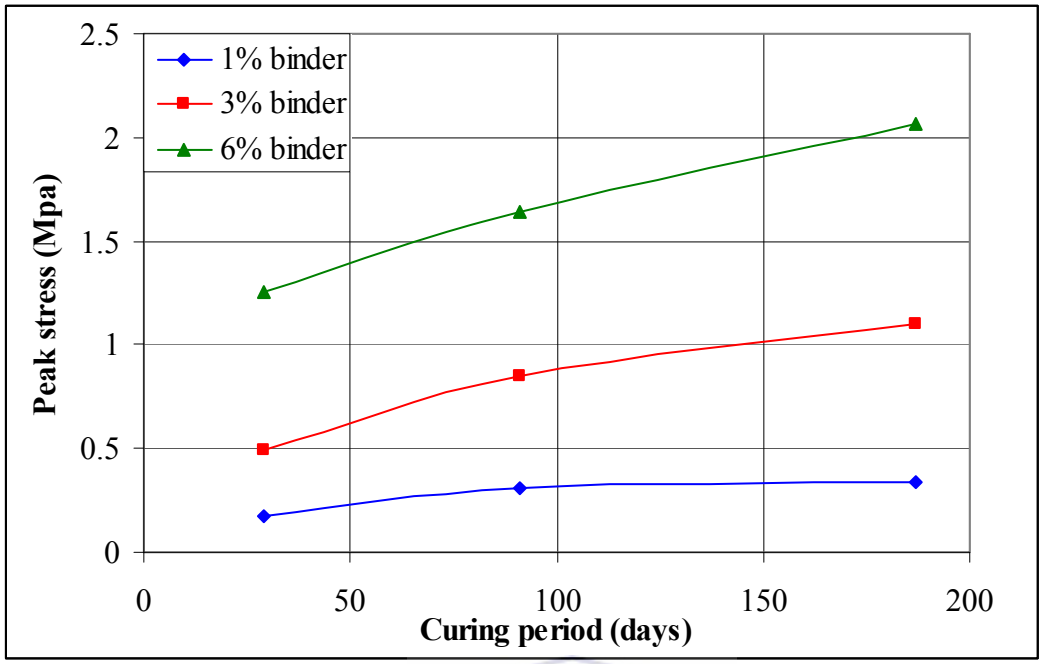

Figure 5.87: Unconfined compressive strength of batch one solid residue slurries.

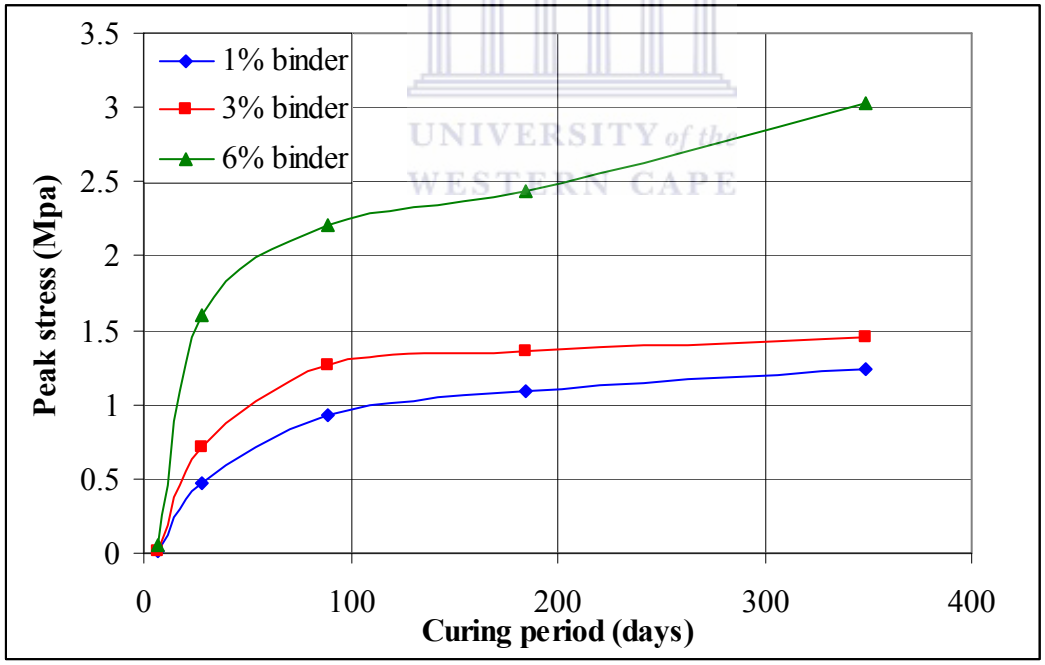

UNIVERSITY of the
WESTERN CAPE

Figure 5.88: Unconfined compressive strength of batch two solid residue slurries.

Moreover similar trends were observed in these studies compared to values obtained from the literature (Grice, 1998) that indicated addition of a binder increased compressive strength, to between 0.75-4MPa, and values obtained in this study were within this range. The UCS and EM are essential for the rock mechanics to model the force interaction and lateral load

bearing of cemented strength. Both compressive strength and elastic modulus were still increasing after one year under the experimental conditions of storage. The best result was achieved by batch two, as the UCS reached 1.23 MPa (with 1% binder mix) to 3.03 MPa (with 6 % binder) after one year. These results tend to validate the possibility of using solid residues for backfilling. The lower strength development values observed for batch three could be due to less CaO available for formation of CSH gel since it had already been consumed during the neutralization process. This system was driven to pH 11 unlike batch one and two. Another reason could be the lower SO_4^{2-} content hence less precipitation of gypsum. Benzaazoua and others (2002) observed that gypsum was significant in contributing to the final strength of sulphidic mine tailings backfill paste samples prepared with OPC binders ranging from 1-6 %.

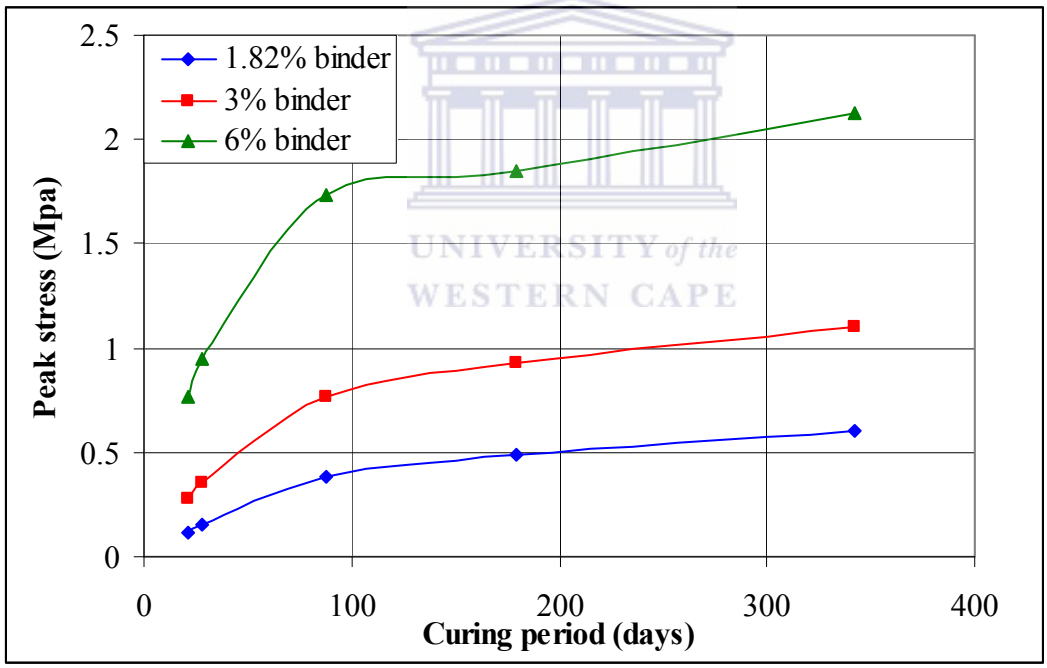

Figure 5.89: Unconfined compressive strength of batch three solid residue slurries.

UNIVERSITY of the WESTERN CAPE

5.6.9 Conclusions

In conclusion, with the addition of cement as a binder, the strength of the solid residue slurries is relatively high and it appears suitable for the purpose of confinement of mined out areas. The stability of the OPC blend solid slurries is demonstrated through its capacity to develop strength over time. Similar results were obtained in a previous study made on unreacted fly ash (Ilgner, 2000). These experiments tend to confirm that even after being submitted to reaction with AMD, fly ash remains a suitable material for backfilling. Hence, the proposed use of fly ash to first ameliorate AMD by use as a substitute liming treatment, and then apply the recovered solid residues for back fill material is herewith proved to be feasible.

5.7 Discussion and Conclusions

UNIVERSITY of the
WESTERN CAPE

The FA cores, the solid residue (SR) + FA and solid residue (SR) + 6 % OPC cores were observed to undergo a stepwise acidification process with several acidity attenuation mechanisms involved as the drainage progressed. The higher pH buffer region (7.5-9) was sustained for a longer duration than the lower one (3-4) in SR and SR+FA cores. SR+ 6 % OPC cores sustained the lower buffer region (3.5-4) for a longer duration of the experiment than the other solid cores.

An observed similarity in pH profile of the SR + 40 % FA solid core with the FA column core probably indicates that at 40 % or higher blending rate, dissolution kinetics of the fly ash will dominate and this would probably represent the highest fly ash blending rate that is practical under field conditions. The solid residue cores (SR) appeared to have a significant buffering capacity, maintaining a neutral to slightly alkaline pH in the leachates for an extended period of time (97 days). Blending of the solid residue (SR) with fly ash had the effect of increasing the pH of the initial leachates to circum-neutral, alkaline pH and increased the time of breakthrough to acidic zone. This work has proved that, if placed in a mining area generating AMD, these SR could provide a passive method of treatment of polluted coal mine water over an extended period of time. The use of Ordinary Portland Cement as a binder reduced this neutralization capacity to 22 days and release of alkalinity was slowed down. Results obtained in the case of addition of the OPC binder may indicate possible excessive aggregation of residue particles or physical encapsulation by the generated

C-S-H gel in the Ordinary Portland Cement amendment that may have reduced the active surface area of particles available for neutralization. The solid residues promise to provide a further passive treatment or prevent AMD formation underground and thereby reduce contamination caused by AMD by maintaining alkaline to circum-neutral pH over extended period.

Three main acidification steps were observed as the solid cores released alkalinity on contact with SAMD. These were pH 9.2-12, 7.5-9.5 and 4.5. The initial alkaline pH that was not sustained for long was due to the dissolution of CaO in the unreacted fly ash in FA solid core and the FA blend solid residues (SR). The pH of the initial leachates for the solid resides (SR) and solid residue (SR) + FA solid cores decreased in the order FA > SR + 25 %> SR + 5 % > SR strongly indicating that addition of fly ash to the solid residues was responsible for the initially high pH generated in the leachates. In the OPC blend solid core the cement hydration reactions generated portlandite that was immediately consumed as a result of formation of gypsum, ettringite and other cement hydration products. The SR and SR + FA column cores sustained a strong buffering capacity at pH 7.5-9.5 for a longer duration of the experiment than FA and SR + 6 % OPC. PHREEQC simulation predicted that the aluminosilicate glass and mullite were undergoing dissolution and were responsible for buffering in this pH region. XRD also confirmed the dissolution of the aluminosilicate glass matrix covering the fly ash spheres. This feature was proved to be significant in retardation of heavy metal contaminants via precipitation. This buffering will be maintained as long the dissolution of the aluminosilicate glass matrix and mullite is occurring otherwise the pH drops to below 4. A sharp drop in pH was thereafter observed. This concept is further confirmed by the lack of the buffering at pH 6.5-9 in SR + 6 % OPC solid core which was attributed to the possible aggregation and physical encapsulation of the solid residues by the C-S-H gel formed. Yong *et al*. (2001) working on heavy metal soil retention capacity of some alluvia soils mainly composed of kaolinite, illite and chlorite when drained with landfill leachate spiked with Pb, Cu and Zn observed that the pH was successively buffered at between 7.5-9.5. They further observed that this feature was significant in retardation of heavy metal contaminants via precipitation. Dissolution and formation of alunite was predicted to buffer pH at ≈6.5 indicating that it could have contributed to the overall pH buffering in this region.

Rapid dissolution of CaO from the fly ash and precipitation thereafter as gypsum in presence of the SO_4^{2-} rich SAMD for the FA and SR + FA column cores led to the initial drop of Ca and SO_4^{2-} in the leachates. An almost constant level of SO_4^{2-} was thereafter maintained which was parallel to the level of Ca in the leachates. This was attributed to the slow dissolution of the fly ash matrix with concomitant nearly constant levels of Ca released. The Ca levels attributed to the dissolution of the fly ash matrix could partly account for the continuous attenuation of SO_4^{2-}. As the acidification of the solid cores progressed the leachate pH dropped and subsequently the SO_4^{2-} levels were observed to increase steadily but the increase differed for different solid cores. SR + 6 % OPC was observed to be superior in attenuation of SO_4^{2-} even at acidic pH. At low pH basaluminite was predicted to be strongly controlling Al^{3+} and SO_4^{2-} at pH>4 in this solid core. Incorporation of SO_4^{2-} in the generated Al-Si-O rich gels could also account for the high SO_4^{2-} retention efficiency of this solid core. Extensive formation of ettringite that was eventually encapsulated by C-S-H gel which resisted dissolution under the acidic regime also contributed to the SO_4^{2-} retention efficiency in this solid core.

UNIVERSITY of the
WESTERN CAPE

The main mechanisms responsible for the eventual clean-up of AMD was observed in the fly ash blends to be increase of the pH to alkaline and circum-neutral levels and sustainability of the buffering capacity at circum-neutral pH, this was observed to depend on the % FA in the blend. Addition of % fly ash in the range (5 - 25) to the solid residues (SR) would increase the time that buffering capacity at circum-neutral pH is sustained. Addition of 40 % FA to the solid residues obscures the activity of the residue aluminosilicate glass matrix and mullite of the solid residues such that the buffering capacity at circum-neutral pH is not a significant feature. The buffering capacity exhibited at 40 % FA resembles that of unreacted fly ash core. Addition of OPC to the solid residues was observed to introduce significant changes to the leachate chemistry as compared to the FA blends.

The FA, SR + 5 % FA, SR + 25 % FA, SR + 40 % FA and SR + 6 % OPC all exhibit high capacity to attenuate Fe and Mn^{2+} than the SR solid cores. The added alkalinity from the un-reacted fly ash in each column increased the pH of the SAMD solution which resulted in the precipitation of those elements from solution. PHREEQC simulation predicted precipitation of Al, Fe and Mn (oxy) hydroxides at alkaline pH. Al and Fe-hydroxysulphates were also

predicted to be precipitating at pH 3.5-6.5. This is confirmed by the fact that a steady increase in the contaminants concentration is observed in all the solid cores as the pH drops to below 4. However the SR + 6 % OPC cores continued exhibit high attenuation efficiency even as the pH dropped to below 4. The above observations goes on to confirm that apart from precipitation, the OPC blend solid residue initiated other attenuation mechanisms such as co-precipitation and encapsulation of precipitates formed by generated CSH gels. The importance of amorphous precipitates in the attenuation of contaminants was demonstrated in the high concentrations retained in the amorphous fraction in the sequential extractions. Gypsum precipitation was also observed to be a significant SO_4^{2-} retention pathway as also evidenced by the high concentrations of Ca observed in the water soluble fraction and also in the amorphous fraction. High retention of contaminants Fe, Mn, Al, Ca and Si was observed in the amorphous fraction in the SR + 6 % OPC solid core which renders credence to the fact that formation of amorphous calcium silicate hydrate, calcium ferrite hydrate and possibly calcium aluminate hydrate gels were contributing to the increased contaminants retention in this solid core.

In addition to passively treating the AMD, the solid residues (SR) were observed to develop strength that can be crucial if they were used for backfilling applications. Addition of OPC binder to the solid residues (SR) at the rates of (1-6 %) achieved unconfined compressive strength (UCS) of 1.23 MPa (with 1 % binder mix) to 3.03 MPa (with 6 % binder) after one year.

Hence the solid residues (SR) can successively be applied for a dual purpose in mined out areas: remediate acid mine drainage waters over an extended period of time and also provide support for the overburden.

UNIVERSITY of the
WESTERN CAPE

Chapter Six

Conclusions and Recommendations

6 Introduction

This study was designed to try and answer the following questions regarding the application of fly ash for remediation of coal mines waste waters

Is fly ash a suitable remediation material for AMD and at what FA: AMD ratios and contact times will neutral and alkaline water be produced?

Which elements are effectively scrubbed from AMD and which ones are released from the fly ash and what mechanisms are involved?

What associations if any exist between the trace elements and mineral phases precipitating in the neutralization process?

Can amendment of the solid residues with unreacted fly ash or Ordinary Portland Cement (OPC) reduce the leachability of the precipitated or immobilized elements?

Can the OPC blended solid residues (SR) develop strength essential for the support of the overburden and passively remediate acid mine drainage over time?

UNIVERSITY of the
WESTERN CAPE

Therefore the following discussion will dwell on the success and limitations of the study with regard to each of the above questions and also give recommendations on the way forward.

6.1 Neutralization of AMD with fly ash

Neutralization reactions carried with different fly ash and AMD revealed that fly ash can be used effectively to neutralize AMD (question a). Several significant features were observed in these neutralization reactions.

- The pH and EC trends were observed to follow the same trends for different fly ashes which imply the same neutralization and contaminants removal mechanisms were involved regardless of type of fly ash.
- In the reactions using FA: AMD ratio of 1:3, it was observed that the time needed for Arnot FA to overstep the acidic buffering capacity is longer in the reaction with Navigation AMD than with Bank AMD. Eventually, both solutions were taken to a

pH of ≈ 9, but it took more than 200 minutes for Navigation and only 150 minutes for Bank AMD. This implies that residence time during the neutralization will depend on type of fly ash and AMD.

- The EC trends similarly indicated interesting trends for the two reactions, the EC of Navigation and Bank AMD followed the same trend during the treatment with Arnot FA. While pH neutralization was faster in Bank AMD, EC was kept at higher levels in Bank than in Navigation AMD. This may be a consequence of the sulphate, which were initially high in Bank AMD. This implies that effective remediation of a given coal mine waste water will depend on its chemistry and also on the type of fly ash.

The effect of the AMD chemistry was exhibited when different AMD samples were treated with Matla fly ash. The treatment of Brugspruit AMD with low ratios of Matla FA led to neutral pH values in the residual solution, after less than one hour of reaction time indicating that even low amounts of FA could be used to achieve neutralization in some cases. The reactions with ratios of FA: AMD between 1:3.5 and 1:8 allowed highly alkaline values of pH (pH >12) to be obtained and only a few minutes were necessary for FA to neutralize Brugspruit AMD.

These results clearly indicate that the neutralization capacity of FA is combination specific and depends on the initial characteristics of the acid mine waters to be treated. This means that each fly ash/AMD mixture has its own specific optimum ratio at which breakthrough to alkaline pH will occur. This might present a limitation to the neutralization of AMD with fly ash with regard to location of the two waste streams, for instance the best suited fly ash to treat a given AMD water might not be located close enough for the process to be the most economically a viable option.

6.2 Contaminants removal in AMDs

This section addresses question (b). Major inorganic contaminants removal was directly linked to the increase of fly ash in the reaction mixture which indicates that precipitation of metal oxides/hydroxides was the dominant removal mechanism.

- The treatment seems to have a mixture of success with the reaction between Matla fly ash and Brugspruit AMD showing relatively lower levels removal of efficiency. Selected FA: AMD ratios can be used to achieve neutral to circum-neutral pH.

Compared to the DWAF water quality limits, treatments of Navigation AMD with Matla fly ash resulted in much clean water with Cu, K, Mo, Na, Zn being within the domestic water use limits for 1:3 FA: AMD ratio and Co, Cu, K, Na and Zn being within the domestic water limits for 1: 2.5 FA: AMD ratio. Treatment of Brugspruit AMD with Matla fly ash produced less clean water although breakthrough to alkaline pH was established within less than an hour. Only Cu, K were within the domestic limits for 1:30 FA: AMD ratio. However this comparison includes only the FA: AMD ratios that resulted in process water in the pH range 6-9. (Table B1-B3).

- The poor element removal efficiency in the Brugspruit AMD can be traced to low concentration of the major hydrolysable contaminants which buffer the pH at 4.5-7 and induce several contaminants attenuation mechanisms which may include adsorption (Drever, 1997). This aspect needs to be investigated more fully with synthetic AMD containing various concentrations of the major hydrolysable contaminants to establish the baseline concentration at which these adsorption processes are induced.

From these results it appears that this treatment system will work best if the major hydrolysable contaminants are above a certain critical baseline concentration otherwise the trace elements remain above the DWAF domestic water limits.

6.3 Solubility controls on major contaminants.

Knowing the mineral phases likely to control a contaminant in a water treatment process is crucial in designing the remediation technology to employ and what optimum conditions to employ. This also contributes to assisting in the design of the treatment plant. Experiments were designed to evaluate the solubility controls on the major elements. The challenge that was experienced in achieving this objective (questions b and c) was that the solid residues collected after given reaction times were largely amorphous. This was partly due to dilution by the un-reacted residue matrix of the fly ash. The precipitating contaminant bearing mineral phases were predicted by PHREEQC modeling based on aqueous solution analysis. The only direct physical evidence of the precipitation of these mineral phases is by SEM-EDX which must be taken with caution since it cannot conclusively identify the mineral

phases due to the analysis volume limitations and contribution of signal by the underlying residual fly ash matrix.

- SEM-EDX analysis strongly suggested precipitation of Fe-O rich and Ca-S rich phases. The results indicated that the major inorganic contaminants Fe, Al, B concentrations were controlled by mineral solubility. Other contaminants concentrations such as Ca, Na, Mg, Si and Mn seemed to develop solubility control after the initial rapid dissolution.

Increase in pH seemed to play a crucial role in the removal of the major and minor inorganic contaminants. Fe was mainly removed as Fe (OH)3(a), while Al^{3+} as basaluminite, boehmite and alunite at pH 5.28-6.95, Al $(OH)_{3(a)}$ at pH 6.45-6.95, and as gibbsite and diaspore at pH 5.53-9.12. Cu and Zn removal seemed to be tied strongly to the precipitation of Al $(OH)_{3(a)}$ at pH 5.3-6.5 confirming the importance of this major inorganic contaminant in the treatment process. Gypsum was observed to be crucial in the removal of sulphate and this was the only mineral phase that was identified directly by XRD. In addition celestite and barite played a role in attenuation of sulphate. Na removal could only be accounted for at 3.96-6.95 due to precipitation of Na-jarosite.

UNIVERSITY of the

PHREEQC modeling suggested that at pH > 8.5 Mn^{2+} was being oxidized and forming insoluble manganite.

Judging by the information from the solubility controls it's evident that this treatment process has a limitation in that the contaminants will be removed from solution at different contact times and PHS. This might suggest designing a multi-stage treatment process for eventual clean-up of the AMDs. Another limitation would be retention of the alkali metal contaminants such as Na, Ca, Mg and Sr and oxyanions such as Mo in solution at pH > 9. Another step would have to be incorporated to lower the concentration of these elements after the initial treatment process.

Sequential extractions confirmed the observation that adsorption or co-precipitation on the amorphous phases was one of the contaminants removal mechanisms. The amorphous fraction was observed to be the most important in retention of the major and minor contaminants at pH > 6.32 which implies that the concentration of total Fe and Al in the AMD being treated could have a direct effect on the clean-up efficiency of the process.

6.4 Contaminant attenuation by the fly ash and Ordinary Portland Cement blended solid residue (SR) cores.

Column leaching has been used to simulate conditions of co-disposal of solid waste such as mine spoils and fly ash or sludge from different chemical processes as described in *Chapter Two*. The idea being to model the situation in the field and thereafter use the information to predict the effect on the environment probably on disposal of sludge or co-disposing two solid waste streams. In this study solid residues (SR) were modified with fly ash at varying % and 6 % Ordinary Portland Cement, fly ash was also monitored as a control. The effect of the blended solid residues on the chemistry of the synthetic AMD was evaluated with drainage time (questions d and e).

The leachate chemistry revealed interesting results.

- Acidification of all the solid cores was observed to occur in a stepwise fashion. Blending of the solid residues with fly ash had several effects on the leachate chemistry, the initial leachate pH was observed to be dependent on the % fly ash in the blend and secondly it influenced the duration of sustainability of buffering at pH 7-9.5.
- A significant feature of the solid residue and fly ash blended solid residue cores was the sustained buffering at pH 7-9.5. Another significant feature of the solid residue core drainage results is the potential of the solid residues to buffer pH at 7-9.5 and contribute to contaminants attenuation for extended periods of time. This was quite significant, since the solid residues resulted from the treatment of AMD with fly ash where the alkalinity due to CaO had been fully utilized. This important finding goes to confirm the importance of these solid residues for the purpose of mine backfilling since they will continue to passively buffer pH and clean-up percolating AMD.
- Another important finding is that blending with 6 % OPC obscured the release of this alkalinity from the solid residues but this was compensated by the inducement of other contaminants attenuation mechanisms even at pH below 5.
- By the time of stoppage of the drainage experiments at 165 days, contaminants concentration in the leachates in the SR + 40 % solid residue cores were observed to

be increasing. Since this particular core contaminants concentrations release kinetics were observed to follow closely that of the fly ash solid core, It could be argued that at 165 days the buffering capacity due to CaO was exhausted and this solid core was now entering the phase where the dissolution of $SiO_{2(amorphous)}$ and mullite were buffering the pH at 7-9.5. Therefore it's recommended for longer drainage experiments probably for one year or longer to be carried out to ascertain the final break-up of the alkalinity of this solid core and also confirm to what extent the re-dissolution of the previously formed precipitates will occur.

Alternatively the solid residues could be used as passive treatment barriers, this would require probably drainage of the solid residues with SAMD under a dynamic flow regime to quantify the amount of coal mines waste water that can be treated over a given period of time. This study considered a worst case scenario by using a highly polluted SAMD simulating Navigation Dam toe seep (5000 ppm Fe, 14407 mg/L SO_4^{2-}, 1000 mg /L Al, 250 mg/L Mn^{2+} and 4253 mg/L $CaCO_3$ acidity). As a passive treatment barrier it can possibly be effectively used to treat large quantities of moderately polluted AMD.

- Sequential extractions again revealed that the amorphous fraction was the most important in retention of the major contaminants and was most enhanced in the OPC blend solid residues due to formation of amorphous CSH gels.

- The unconfined compressive strength (UCS) (2-3 Mpa) developed by the OPC blend solid residue slurries of (2-3 Mpa) confirms that the solid residues can be used for backfilling. More extensive investigations need to be carried out by using different binders such as blast furnace slag and silica fumes which are waste products possessing pozzolanic properties.

In conclusion the study has shown to a high degree of certainty that the solid residues (SR) can successively be applied for a dual purpose in mined out areas: remediate acid mine drainage waters and also provide support for the overburden in mined out areas.

The geochemistry of the interaction of the backfilled solid residues will greatly depend on the chemistry of the percolating solutions, this study looked at the worst case scenario of a highly

acidic acid mine water. Future studies should be carried out with various polluted mine waters and models developed to be able to predict environmental benefits of this envisaged practice.

UNIVERSITY of the
WESTERN CAPE

References

Adamo, P., Dudka, S., Wilson, M.J., McHardy, W.J. 1996.Chemical and mineralogical forms of Cu and Ni in contaminated soils from the Sudbury mining and smelting

Adams, F., and Z. Rawajfih. 1997. Basaluminite and alunite: A possible cause of sulphate retention by acid soils. *Soil Sci. Soc. Am. J.* 41: 686-692.

Adriano D.C, A.L. Page, A.A. Elseewi, A.C. Chang, and I. Straughan. 1980. Utilization and Disposal of Fly Ash and Other Coal Residues in Terrestial Ecosystems: A Review. *J. Environ. Qual.,* Vol. 9, No. 3,

Agbenin, O. John. 2003. Soil saturation extract composition and sulphate solubility in a tropical semiarid soil. *Soil Sci. Soc. Am. J.* 67: 1133-1139.

Ainsworth, C.C., and D. Rai. 1987. Chemical characterization of fossil fuel wastes. EPRI EA-5321. *Electric Power Res. Inst*., Palo Alto, CA.

Akira I, Y Sakaguchi, T Nakajima, H Takanashi, A Ohki, Shinji Kambara. 2005. Leaching characteristics of boron and selenium for various coal fly ashes. *Fuel*, 84: 479-485.

Alberts, J.J., M.C. Newman and D.W. Evans. 1985. Seasonal Variation of trace elements in dissolved and suspended loads for coal ash ponds and pond effluents. *Water Air Soil Pollution* 26: 111-128.

Allison, J.D., D.S. Brown, and K.J. Novo-Gradac. 1991. MINTEQA2, *A geochemical assessment data base and test cases for environmental systems*: Vers. 3.0 users manual. Report EPA/600/3-91/-21. Athens, GA: U.S.EPA.

Alpers, C.N., D.W. Blowes, D.K. Nordstrom and J.L. Jambor. 1994. Secondary minerals and acid mine-water chemistry. *In* Environmental geochemistry of sulfide mine-wastes, ed, by D.W. Blowes, and J.L. Jambor, Shortcourse Handbook, V.22, Mineralogical Association of Canada, pp 247-270.

Andreas S. 2005. Pers Comm. University of Cape Town. South Africa.

Apak R., E. Tutem., M. Hugul and J. Hizal. 1998. Heavy metal cation retention by unconventional sorbents (Red Muds and Fly Ashes). *Water Research*. Vol. 32. No. 2, pp. 430-440.

Arakaki, T., Mucci, A., 1995. Acontinuous and mechanistic representation of calcite reaction-controlled kinetics in dilute solutions at 25^{o}C and 1 Atm total pressure. *Aquat. Geochem*. 1, 105-130.

UNIVERSITY of the WESTERN CAPE

Arey, J.S., J.C. Seaman, and P.M. Bertsch. 1999. Immobilization of uranium in contaminated sediments by hydroxyapatite addition. *Environ. Sci. Technol*. 33: 337-342.

ASTM D2166-85, ASTM PS28-95, ASTM-C39-94. American Society for Testing and Materials, 1993. American Society for Testing and Materials. *In*: Annual book of ASTM standards Soil and Rock; Building Stones Vol. 4.08. Philadelphia.

ASTM. 1988. American Society for Testing and Materials. Standard specification for fly ash and raw or calcined natural pozzolan for use as a mineral admixture in Portland cement concrete. C618-88. ASTM, Philadelphia, PA.

Azzie, B. A-M. Coal mine waters in South Africa: Their geochemistry, quality and classification. *PhD Thesis*, 2002. University of Cape Town, SA.

Azzie, B. A-M. The geochemistry and quality of waters from selected collieries on the South African Highveld. *MSc Thesis*. 1999. University of Cape Town, South Africa.

B.R.E. 2001. Concrete in Aggressive Ground, Building Research Establishment, Special Digest 1.***In* Van der Sloot** H.A. Developments in evaluating environmental impact from utilization of bulky inert wastes using laboratory leaching tests and field verification. *Waste Management.* Vol 16, issues (1-3) pgs 65-81, 1996.

Ball, J.W., and D.K. Nordstrom. 1991. User's manual for WATEQ4, with revised thermodynamic database and test cases for calculating speciation of major, trace, and redox elements in natural waters. *U.S. Geological Survey Open-File Report* 91-183. Menlo Park, CA.

Barret J.R., Coulthard M A. and Dight P.M. 1978. Determination of fill stability. Mining with backfill - 12th Canadian Rock Mechanics Symposium, Canadian Institute of Mining and Metallurgy, Quebec., 19, 85 – 91.

Barry E. Scheetz and R Earle. 1998, Utilization of fly ash. Ceramics, composites and intergrowths, *Current opinion in solid state and materials science*, 3: 510-520.

Barton, P. 1978. The acid mine drainage. *In* Nriagu, J.O. (ed), Sulfur in the Environment, part Ⅱ. Ecological Impacts: John Wiley and Sons, NewYork, pp. 313-358.

Bealy, M., 1980. Concrete pipe Handbook, American Concrete pipe Association. Chapter 6, pp 1-21 .In Impacts of mine drainage on aquatic life, water uses, and man-made structures. www.dep.state..pa.us

Beckett, P.H.T., 1988. The use of extractants in studies on the trace metals in soils, sewage sludges and sludge-treated soils.Advan. Soil Sci. 9, 144–175.

Benzaazoua M., P. Marion., I. Picquit., B. Bussiere. 2004. The use of pastefill as a solidification and stabilization process for the control of acid mine drainage. *Minerals Engineering*

Benzaazoua, M; T Belem, Bruno Bussiere. 2002. Chemical factors that influence the performance of mine sulphidic paste backfill. *Cement and Concrete Research* 32, 1133-1144

Bezuidenhout, N. Chemical and mineralogical changes associated with leachate production at Kriel power station ash dam. *Unpublished M.Sc*. 1995. Thesis. University of Cape Town.

Bhumbla D.K, Keefer R.F, Singh RN. 1998. Selenium uptake by alfalfa and wheat grown on a mine spoil reclaimed with fly ash. In:*Proceedings of mine drainage and surface mine reclamation conference,*US Department of the Interior,Bureau of MinesInformation Circular, IC 9184,Washington,DC,1988.p.15 – 21. *Cited in* Anthimos Xenidis, Evangelia

Bigham J.M. 1994. Chapter 4: Mineralogy of ochre deposits formed by sulfide oxidation. *In*: Jambor JL, Blowes DW (eds) Environmental geochemistry of sulfide Mine-wastes, short course handbook. Mineralogical Association of Canada (Vol 22), Waterloo, Ontario, pp 103-132.

Bigham J.M. Schwertmann U. and Pfab G. 1996b Influence of pH on mineral speciation in a bioreactor simulating acid mine drainage. *Applied Geochemistry*, Vol 11, pp, 845-849.

Bigham J.M., Schwertmann U., Carlson L and Murad E. 1990. A poorly crystallized oxyhydroxysulfate of iron formed by bacterial oxidation of Fe(II) in acid mine waters. *Geochim. Cosmo. Acta* 54: 2743-2758.

Bigham J.M., Schwertmann U., S.J. Traina, R.L. Winland and M. Wolf. 1996a. Schwertmannite and the chemical modeling of iron in acid sulfate waters. *Geochimica et Cosmochimica Acta.* Vol. 60, No 12: 2111-2121.

Bigham, J.M. & Nordstrom, D.K. 2000. Iron and aluminum hydroxysulfates from acid sulfate waters. In: *Sulfate Minerals: Crystallography, Geochemistry, and*

Environmental Significance (eds C.N. Alpers, J.L. Jambor & D.K. Nordstrom), pp. 351–403. Mineralogical Society of America, **Washington, DC.**

Bilski J.J. and Alva A.K. 1995. Transport of heavy metals and cations in a fly ash amended soil. *Bull. Environ. Contam. Toxicol*. 55: 502-509.

Bosch G.L. The mineralogy and chemistry of pulverized fuel ash produced by three A South African coal burning power stations. Unpublished *MSc Thesis*, 1990. University of Cape Town, SA.

Bradham, W.S. and F.T. Carrucio. 1990. A comparative study of tailings analysis using acid/base accounting, cells, columns, and soxhlets. P.19-25. *In* J. Skousen et al.(ed) Proc., 1990 Mining and Reclamation conf. and Exhibition, Charleston, WV. 23-26 April. 1990. Am. Soc. For surface Mining and Reclamation, Lexington, KY. *In* Stewart et al. Evaluation of leachates from coal refuse blended with fly ash at different rates. *Journal of Environmental quality*. 30: 1382-1391(2001).

Britton and Robinson. 1932. Trans, Faraday, Soc., 28: 531 *In* Britton Hubert T.S. Hydrogen Ions: Their determination and importance in pure and industrial Chemistry. 4th edition, vol 2, 1956. Chapman and Hall Ltd.

Britton H T.S. Hydrogen Ions: Their determination and importance in pure and industrial Chemistry. 4th edition, vol 2, 1956. Chapman and Hall Ltd.

Brodie, G.A., C.R. Britt, H. Taylor, T. Tomaszewski, and D. Turner. 1990. Passive anoxic limestone drains to increase effectiveness of wetlands acid drainage treatment systems. In: Proceedings, Twelfth National Association of Abandoned Mined Land Conference, Breckinridge, CO.

Brownlow, A. H. 1979. *Geochemistry*. Englewood Cliffs, NJ: Prentice-Hall, Inc.

Bullock, S.E.T. and Bell, F.G. 1997. Some problems associated with past mining at a mine in the Witbank Coalfield, South Africa. *Environmental Geology*, 33 (1): 61-71.

Bunzl, K., M. Trautmannsheimer, and P. Schramel. 1999. Partitioning of heavy metals in a soil contaminated by slag: A redistribution study. J. Environ. Qual. 28:1168–1173.

Burgers, C. L. Synthesis and Characterisation of sesquioxidic precipitates formed by the reaction of acid mine drainage with fly ash leachate. *MSc Thesis*. 2002 University of Stellenbosch

Cabrera, J.G., Hopkins, and C.J., Woolley, G.R. 1986. Evaluation of the properties of British pulverised fuel ashes and their influence on the strength of concrete. ***In-***

Malhotra, V.M. ed. Proceedings of the 2rd International congress of fly ash silica fume, slag, and natural pozzolans in concrete, Madrid. American Concrete Institute Special Publications 91, 1, 115-144

Calabrese, J.P., A.J. Sexstone, D.K. Bhumbla, G.K. Bissonnette, and J.C. Sencindiver. 1991. Application of constructed cattail wetlands for the removal of iron from acid mine drainage. p. 559-575. *In:* Proceedings, Second International Conference on the Abatement of Acidic Drainage, Vol. 3, MEND, September 16-18, 1991, Montreal, Canada.

Campbell A. 1999. Chemical, physical and mineralogical properties associated with the hardening of some South African fly ashes. *MSc thesis*, University of Cape Town, RSA.

Campbell, J.A., J.C. Laul, K.K. Nielson, and R.D. Smith. 1978. Separation and chemical characterization of finely-sized fly ash particles. *Anal. Chem*. 50: 1032-1040.

Canty Geofrey. 2003. The use of coal combustion by-products for insitu treatment of Acid Mine Drainage. (Oklahoma Conversion Commission), West Virginia water Research Institute.

Carlson, C.L., and D.C. Adriano. 1993. Environmental impacts of coal combustion residues. *Journal of Environmental quality.* 22: 227-247.

Carlson, L., and U. Schwertmann. 1981. Natural ferrihydrites in surface deposits from Finland and their association with silica. *Geochim. Cosmochim. Acta,* 45: 421-429.

Carpentor, L.V and Herndon, L.K. 1933. Acid mine drainage from bituminous coal mines. West Virginia University Engineering. *Exploration Station Research Bulletin* No. 19, pp38.

Catalan J.J. Lionel., E Merliere., C Chezick. 2002. Study of the physical and chemical mechanisms influencing the long-term environmental stability of natrojarosite waste treated by stabilization/solidification. *Journal of Hazardous Materials* B94 : 63-88.

Cathles, L.M. and J.A. Apps, 1975. A model of the dump leaching processing that incorporates oxygen balance, heat balance, and convection. *Metallurgical Transactions*, v. 6B, pp. 617-624.

UNIVERSITY of the
WESTERN CAPE

Cathles, L.M., 1979. Predictive capabilities of a finite difference model of copper leaching in low grade industrial sulfide waste dumps. *Mathematical Geology*, v.1, 11, no. 2, pp. 175-186.

Chang, A.C., L.J. Lund, A.L. Page, and J.E. Warneke. 1977. Physical properties of fly ash-amended soils. *J.Environ. Qual*. 6:267-270.

Chang, H.L., Shih, W.H. 1998. A general method for the conversion of fly ash into zeolites as ion exchangers for cesium, *Industrial and Engineering Chemical Research* 37, 71-78

Chao, T.T. 1972. Selective dissolution of manganese oxides from soils and sediments with acidified hydroxylamine hydrochloride. *Soil Sci. Soc. Am. J*. 36: 764-768.

Chao, T.T. 1984. Use of partial dissolution techniques in geochemical exploration. *J.Geochem. Explor*. 20: 101-135.

Chapelle F.H., Bradly P.M. and McMahon, P.B. 1993. Subsurface microbiology, chapter 8, *In* regional ground water quality, Alley, W.M. (ed), Van Nastrand Reinhold, New York.

Chavarie, C., D. Karamenev, F. Godard, A. Garnier, and G. Andre, 1993. Comparison of kinetics of ferrous iron oxidation by three different strains of Thiobacillus ferrooxidans. *Geomicrobiology Journal*, v. 11, pp. 57-63.

Chugh Y.P, D. Dutta and L. Buliang. 1998. Underground placement of coal processing waste and coal combustion by-products based paste backfill for enhanced mining economics. Interim Final Technical Report Sep 1997-Aug 1998. ICCI project Number: 97US-1.Southern Illinois University of Carbondale.

Chukhrov, F.V., B.B. Zvyagin, L.P. Ermilova, and A.I. Gorshkov, 1973. New data on iron oxides in the weathering zone. *In:* Proceedings of the International Clay Conference, 1972, Madrid, v. 1, pp. 397-404.

Cincilla, W.A., Landriault, D.A., Verburg, R. Application of paste technology to surface disposal of mineral wastes. *In: proceedings of the conference Tailings and Mine waste*, 97 Balkena, Fort Collins, pp343-356. *In* **Benzaazoua** M., P. Marion., I. Picquit., B. Bussiere. The use of pastefill as a solidification and stabilization process for the control of acid mine drainage. *Minerals Engineering* , 2004.

UNIVERSITY of the WESTERN CAPE

Cocke, D.L., Mollah, M.Y.A. The Chemistry and leaching mechanisms of hazardous substances in cemnetitious solidification/stabilization systems. In: Chemistry and microstructure of solidified waste forms; Spence, R.D., Ed; Lewis publishers, Boca Raton, FL, 1993: pp 187-241.

Cogbill, F.V., and G.E. Likens. 1974. Acid precipitation in the NorthEastern United States. *Water Resource. Res*. 10: 1133-1137. *In* Warren C. J and Dudas M.J. Weathering processes in relation to leachate properties of alkaline fly ash. *Journal of Environmental quality.,* Vol 13, 4, 1984.

Colmer, A.R and Hinkle, M.E. 1947. The role of microorganisms in acid mine drainage. *Science,* 106, pp 253-256.

Cornell, R.M., Schwertmann, U. 1996. The iron Oxides. VCH. Verlagsgesellchaft, MBC

Cravotta III, A. Charles, Mary Kay Trahan. 1999. Limestone drains to increase pH and remove dissolved metals from acidic mine drainage. *Applied Geochemistry* 14, 581-606

Crouse, H.L.; A.W. Rose. Natural beneficiation of acid mine drainage by interaction with stream water and stream sediment. *In*: 6th Symposium on Coal Mine Drainage Research, National Coal Association/Bituminous Coal Research, Inc., 1976; 237-269.

Davies C.W. 1962. Ion Association. Butterworth Publications, Washington D.C.

Davison, R.L., D.F.S. Natusch, J.R. Wallace, and C.A. Evans, Jr. 1974. Trace elements in fly ash: Dependence of concentration on particle size. *Environ. Sci. Technol*. 8: 1107-1113.

Department of Water Affairs and Forestry **(DWAF).** 1996. South African Water Quality Guidelines Volume 4: Agricultural Water Use: Irrigation, 2nd Edition.

Domenech C., C. Ayola and J. de Pablo. 2002. Sludge weathering and mobility of contaminants in soil affected by the Aznacollar tailing dam spill (SW Spain). *Chemical Geology* 190. 355-370.

Doye I and J Duschesne. 2003. Neutralization of acid mine drainage with alkaline industrial residues: Laboratory investigation using batch-leaching tests. *Applied Geochemistry* 18. 1197-1213.

Drever I. J. 1997. The geochemistry of natural waters: surface and groundwater environments. Prentice-Hall, Inc, pg 25 –37.

UNIVERSITY of the
WESTERN CAPE

Dudas, M. J. 1981. Long-term leachability of selected elements from fly ash. *Environ*. *Sci. Technol*. 15: 840-843.

Early L.E, D Rai, S.V. Mattigod, and C.C. Ainsworth. 1990. Geochemical Factors Controlling the Mobilization of Inorganic Constituents from Fossil Fuel Combustion Residues: II. Review of the Minor Elements. *J. Environ. Qual*. 19: 202-214.

Eaton, A.D., Clesceri, L.S. and Greenberg, A.E. 1995. *Standard Methods for the Examination of Water and Wastewater.* 19th Edition. American Public Health Association, Washington.

Eckert, D.J, 1988. Recommended pH and lime requirement tests. P 6-8. In W.C. Dahnke (ed), Recommended chemical soil test procedures for the North Central Region, North Dakota Agri. Expt. Sta. Bulletin No. 499 (Revised).

Elberling, B., Nicholson, R.V., Reardon, E.J., Tibble, P. E .1994. Valuation of sulphide oxidation rates: a laboratory study comparing oxygen fluxes and rates of oxidation product release. *Can. Geotech. J.* 31. 375-383

Erol M, S. Küçükbayrak, A. Ersoy-Meriçboyu, T. Ulubaş. 2005. Removal of Cu2+ and Pb2+ in aqueous solutions by fly ash. *Energy Conversion and Management* 46: 1319-1331.

Erol. M, S. Kucukbayrak, A. Ersoy-Mericboyu, T. Ulubas. 2005. Removal of Cu^{2+} and Pb^{2+} in aqueous solutions by fly ash. *Energy Conversion and Management* 46. 1319-1331.

Eskom, 2000. Environmental Report. Towards sustainability.

Eskom, 2002. Annual Report, Incorporating Lethabo-phoenix of the nineties.

Evangelou V.P. 1998. Environmental soil and water chemistry: principles and applications. John Wiley and Sons.

Evangelou, V.P and Zhang, Y.L. 1995. A Review: Pyrite oxidation mechanisms and acid mine drainage prevention. *Critical Reviews in Environmental science and Technology,* 25, 141-199

Fail, J.L., Jr., and Z.S. Wochok. 1977. Soybean growth on fly ash ash-amended strip mine spoils. *Plant Soil* 48: 472-484.

Farmer, V.C., J.D. Russell, and M.L. Berrow. 1980. Imogolite and proto-imogolite allophane in spodic horizons: evidence for a mobile aluminum silicate complex in podzol formation. *J. soil Sci*. 31: 673-684.

Faulkner, B.B., and J.G. Skousen. 1994. Treatment of acid mine drainage by passive treatment systems. p. 250-257. *In:* International Land Reclamation and Mine Drainage Conference, U.S. Bureau of Mines SP 06A-94, April 24-29, 1994, Pittsburgh, PA.

Faulkner, S.P and Richardson, C.J. 1989. Physical and chemical characteristics of freshwater wetland soils; *In* Hammer. D.A. (ed), constructed wetlands for wastewater treatment-municipal, industrial, and Agricultural: Lewis Publishers, Chelsea, Mich., pp 41-72.

Fillipek, H. L., Nordstrom, D.K. and Ficklin H. W. 1987. Interaction of acid mine drainage with waters and sediments of west squaw creek in the West Shasta Mining District, California. *Environ. Sci. Technol.*, Vol. 21, No. 4. pg 388-396.

Fisher, G.L., B.A. Prentice, D. Silberman, J.M. Ondov, A.H. Bierman, R.C. Ragaini, and A.R. McFarland. 1978. Physical and morphological studies of size-classified coal fly ash. *Environ. Sci. Technol.* 12: 447-451.

Fruchter, J.S., D. Rai, J.M. Zachara, and R.L. Schmidt. 1988. Leachate chemistry at the Montour fly ash test cell. EPRI Rep. EA-5922. *Electric Power Res. Inst.,* Palo Alto, CA.

UNIVERSITY of the
WESTERN CAPE

Furr, A.K., T.F. Parkinson, R.A. Hinrichs, D.R. Van Campen, C.A. Bache, W.H. Gutenmann, L.E. St. John, Jr., I.S. Pakkala, and D.J. Lisk. 1977. National survey of elements and radioactivity in fly ashes: absorption of elements by cabbage grown in fly ash-soil mixtures. *Environ. Sci. Technol*. 11: 1104-1112.

Furr, A.K., T.F. Parkinson, W.H. Gutenmann, I.S. Pakkala, and D.J. Lisk. 1978a. Elemental content of vegetables, grains, and forages field-grown on fly ash-amended soil. *J. Agric. Food Chem*. 26: 847-851.

Gazea, B., Adam, K. and Kontopoulos, A. 1996. A review of passive systems for the treatment of acid mine drainage. *Minerals Engineering*, 9, 1, 23-42

Geldenhuys, A.J., J.P. Maree., M. de Beer. and P. Hlabella. 2003. An integrated limestone/lime processes for partial sulphate removal. *The journal of The South African Institute of Mining and Metallurgy.*

Gitari M.W, L.F. Petrik, O. Etchebers, D.L Key, E. Iwuoha and C. Okujeni. 2006. Treatment of acid mine drainage with fly ash: Removal of major contaminants and

trace elements. *Journal of Environmental Science and Health-Part A*. Vol, A41 (8):1729-47.

Gitari M.W, LF Petrik, DL Key, C. Okujeni. 2004. Neutralisation of acid mine drainage with fly ash: A laboratory investigation of metal and SO4 removal in the process waters. 37th National Convention of the South African Chemical Institute (SACI), July 2004

Gitari M.W, LF Petrik, O Etchebers, DL Key, C. Okujeni. Mineralogy and trace element partitioning in coal fly ash/acid mine drainage co-disposed solid residues.2005. World of Coal Ash, April 11-15 2005, Lexington, Kentucky, USA.

Gitari M.W, LF Petrik, O Etchebers, VR Kumar Vadapalli, D Key, and E. Iwuoha.2005. Utilisation of fly ash for remediation of coal mines wastewater: reaction on AMD and possible backfilling with residual solids. The South African Institute of mining and metallurgy. A *colloquium*, Sustainable development in the life of coal mining in South Africa, July 2005, Carnival City, Boksburg.

Gitari M.W, V.S. Somerset, L.F Petrik, DL Key, E. Iwuoha and C. Okujeni. Treatment of acid mine drainage with fly ash: Removal of major, minor elements, SO4 and utilization of the solid residues for wastewater treatment. 2005. World of Coal Ash, April 11-15 2005, Lexington, Kentucky, USA.

Glasser, F.P. Chemistry of cement-solidified waste forms. In: chemistry and microstructure of solidified waste forms; Spence, R. D., Ed.; Lewis Publishers, Boca Raton, FL, 1993; pp

Grabinsky, M.W., Therieult, J., Welch, D., 2002. An overview of paste thickend tailings disposal on surface. In: *Proceedings of the Symposium 2002 sur 1' environnement et les mines: defis et perspectives.* Rouyn-Noranda, CIM, Papier 533. In**: Benzaazoua** M., P. Marion., I. Picquit., B. Bussiere. The use of pastefill as a solidification and stabilization process for the control of acid mine drainage. *Minerals Engineering* , 2004.

Grice, T. 1998: Underground mining with backfill. The 2nd Annual Summit – Mine Tailings Disposal Systems, Brisbane.

Gruebel, K.A., J.A. Davis, and J.O. Leckie. 1988. The feasibility of using sequential extraction techniques for arsenic and selenium in soils and sediments. *Soil. Sci. Soc. Am. J.* 52: 390-397.

UNIVERSITY of the WESTERN CAPE

Gurdeep Singh, Bradley, C. Paul. 2001. Assessment of groundwater quality impacts due to use of coal combustion by-products to control subsidence from underground mines. *Environmental International*, 26: 567-571.

Halstead W.J.1986. Use of fly ash in concrete. National Highway Research Program Synthesis of Highway Practice # 127. Washington, D.C: Transportation Research Board; In Barry E. Scheetz and Russell Earle. 1998, Utilization of fly ash. Ceramics, composites and intergrowths, *Current opinion in solid state and materials science*, 3: 510-520.

Hansen, L.D and G.L. Fisher. 1980. Elemental distribution in coal fly ash particles. *Environ Sci. Technol*, 14: 1111-1117.

Hedin, R.S., R.W. Nairn, and R.L.P. Kleinmann. 1994. Passive treatment of coal mine drainage. US, Bureau of Mines Information Circular 9388, Pittsburgh, PA.

Helmuth, R. 1987.. Fly ash in cement and concrete. Portland cement Association, Skokie, Illinois.

Hem, J. D and Robertson, C.E. 1990. Aluminum hydrolysis reactions and products in mildly acidic aqueous systems: In Melchior. D.C., and Basset, R.L. (eds). Chemical modeling of Aqueous systems, Ⅱ. ACS symposium series 416: American Chemical Society. Washington, D.C: 429-446.

Hem, J.D. and Lind, C.J. 1993. Manganese minerals and associated fine particulates in the streambed of Pinal Creek, Arizona, USA: a mining-related acid drainage problem. *Applied Geochem*, 8: 67-80.

Henrot, J., and R.K. Wieder. 1990. Processes of iron and manganese retention in laboratory peat microcosms subjected to acid mine drainage. *J. Env. Qual*. 19:312-320.

Hequet V., Ricoh P., Lecuyer I and Cloirec Le. P. Removal of Cu^{2+} and Zn^{2+} in Aqueous Solutions by Sorption onto Fly Ash and Fly Ash Mixtures. *International Ash utilization symposium*, Center for Applied Energy Research, University of Kentucky, 1999.

Hildebrand. 1913.J .American Chem, Soc 35: 847, *In* Britton Hubert T.S. Hydrogen Ions: Their determination and importance in pure and industrial Chemistry. 4th edition, vol 2, 1956. Chapman and Hall Ltd.

UNIVERSITY of the
WESTERN CAPE

Hjelmar. O. 1990. Leachate from land disposal of coal fly ash. *Waste Management and Research.*; 8:429

Hodgson L, Dan Dyer, and D.A. Brown. 1982. Neutralization and dissolution of High-Calcium fly ash. *J. Environmental Quality*., Vol. 11, no. 1, 93-98.

Hoehn, R.C. and D.R. Sizemore, 1977. Acid mine drainage (AMD) and its impact on a small Virginia stream. *Water Res. Bull.* V. 13, pp. 153-160.

Hollis, J.F.; R. Keren.; M.Gal. 1988. Boron release and sorption by fly ash as affected by pH and particle size. *J. Environ. Qual.* 7: 181-184.

Hullet L.D. and A.J. Weinbeger. 1980. Some etching studies of the microstructure and composition of large aluminosilicate particles in fly ash from coal-burning power plants. *Environmental Science and Technology*, vol 14, No 8.

Humenick, J.M., M. Lang, and K.F. Jackson. 1983. Leaching characteristics of lignite ash. *J. Water Pollut. Control Fed*. 55: 310-316.

Hurtmut Ilgner. *Personal communication*. Dec, 2003 Hydraulic Transport Backfill laboratory, CSIR-mining Technology, Johannesburg, South Africa.

Ilgner H.J. Cost-effective utilisation of fine and coarse ash to maximise underground coal extraction and to protect the environment. Coaltech 2020 Report, Secunda, Coal Indaba Conference, 2002, 19 p.

Ilgner H.J. The benefits of ashfilling in South African coal mines. Coal - the future, 12th International Conference on Coal Research, ICCR, SAIMM, 2000.

Iyer Ramasubramania. 2002. The surface chemistry of leaching coal fly ash. *Journal of Hazardous Materials* B93, 321-329.

Jackson, M.L., C.H. Lim., and L.W. Zelazny. 1986. Oxides, hydroxides and aluminosilicates, p113-119. *In* A Klute (ed). Methods of soil analysis. Part 1. 2nd ed. Agron. Monogr. 9. ASA and SSSA, Madison, WI.

Jae-Young Yu. 1996. Precipitation of Fe and Al Compounds from the Acid Mine Waters in the Dogyae Area. Korea: A Qualitative Measure of Equilibrium Modelling, Applicability and Neutralization Capacity. *Aquatic Geochemistry* 2: 81-105

UNIVERSITY of the WESTERN CAPE

Jambor J.L., Owens D.R. 1993. Mineralogy of the tailings impoudment at the former Cu-Ni deposit of Nickel Rim mines, Eastern edge of the Sudbury structure, Ontario Energy, Mines and Resources, CAN., CANMET. Div Rep. MSL 93-4 (CF)

Japie E. Krüger. 2003**.** South African coal fly ash: A cement extender. A South African coal Ash Association (SACAA) publication.

Jarvis, K. E.; A. L. Gray; and R. S. Houk. 1992. Handbook of Inductively Coupled Plasma Mass Spectrometry. Chapman and Hall: New York.

JCPDF, 1980.Joint Committee on Powder diffraction Standards database manual and mineral diffraction file.

Jenke R.D and Gordon K. Pagenkpof. 1983. Chemical changes in concentrated, acidic, metal-bearing waste waters when treated with lime. *Environmental Science and Technology*, Vol 17, No. 4, 217-223.

Jenne, E.A., 1977. Trace element sorption by sediments and soils — site and processes. In: Chappell, W., Peterson, S.K.(Eds.), Proc. Symp. Molybdenum in the Environment. MarcelDekker, New York, pp. 425–552.

Jeong, J.K and Soo, J.K. 2003. Mineralogy of ferrihydrite and schwertmannite from the acid mine drainage in the Donghae Coal Mine Area. *J. Miner. Soc. Korea*. 16: 191-198

Johnson B.D and Hallberg B. K. 2005. Acid mine drainage remediations options:a review . *Science of the Total Environment* 338, 3-14.

Juillot, F. Ildefonse, Ph., Morin, G., Calas, G., Kersabiec de, A. M., Benedetti, M. 1999. Remobilization of arsenic from buried wastes at an industrial site: mineralogical and geochemical control. *Applied Geochemistry*. 14: 1031-1048.

Kaakinen, J. W., R. M. Jorden, M. H. Lawasani, and R.E. West. 1975. Trace element behavior in coal-fired power plant. *Environ. Sci. Technol*. 9: 862-869.

Kalyoncu, R.S. Coal combustion products: U.S. Geological Survey Minerals Yearbook 1999, Vol. 1. *In* U.S. Geological Survey Fact Sheet FS-076-01, August 2001

Kanungo S.B and R. Mohapatra, 2000. Leaching behavior of various heavy metals in aqueous medium from two fly ash samples. *Journal of environmental quality,* 29: 188-196.

Karapanagioti H.K and Atalay A.S. 2001. Laboratory evaluation of ash materials as acid-disturbed land amendments. *Global Nest: J. Vol* 3, No 1, pp 11-21.

UNIVERSITY of the WESTERN CAPE

Kepler, D.A., and E.C. McCleary. 1994. Successive alkalinity-producing systems (SAPS) for the treatment of acidic mine drainage. p. 195-204. *In*: International Land Reclamation and Mine Drainage Conference, U.S. Bureau of Mines SP 06A-94, April 24-29, 1994, Pittsburgh, PA.

Khanna, P.K., Prenzel, J., Meiwes, K.J., Ulrich, B., Matzner, E., 1987. Dynamics of sulfate retention by acid forest soils in an acidic deposition environment. *Soil. Sci. Soc. Am. J.* 51, 446-452.

Kim, N.D., and J.E. Fergusson. 1991. Effectiveness of a commonly used sequential extraction technique in determining the speciation of cadmium in soils. *Sci. Tot. Environ.* 105: 191-209.

Kimball, B.A., R.E. Broshears, K.E. Bencala, and D.M. McKnight.1994. Coupling of hydrologic transport and chemical reactions in a stream affected by acid mine drainage. *Environ. Sci. Technol*. 28: 2065-2073.

Kimmel, W.G., 1983. The impact of acid mine drainage on the stream ecosystem. In Pennsylvania Coal: Resources, Technology Utilization, (S.K. Majumdar and W.W. Miller, eds), The pa. Acad. Sci. Publ., pp 424-437.

Kindness A; A Macias and F.P. Glasser. 1994. Immobilization of chromium in cement matrices. *Waste Management*, Vol. 14. No. 1. pp, 3-11.

Kitano Yasushi, Minoru Okumura and Masatoshi Idogaki. 1978. Coprecipitation of Borate-boron with calcium carbonate. *Geochemical journal,* Vol. 12: 183-189.

Klein, D.H., A. W. Andren, J.A. Carter, J.F. Emery, C. Feldman, W. Fulkerson, W.S. Lyon, J.C. Ogle, Y. Talmi, R.I. Van Hook, and N. Bolton. 1975. Pathways of thirty-seven trace elements through coal-fired power plants. *Environ. Sci. Technol*. 9: 973-979.

Klink. M**.** The potential use of South African coal fly ash as a neutralization treatment option for acid mine drainage. *MSc Thesis.* 2004. University of the Western Cape.

Komnitsas K., G. Bartzas and I. Paspaliaris. 2004. Efficiency of limestone and red mud barriers: Laboratory column studies. *Minerals Engineering*, Volume 17, Issue 2, February 2004, pg 183-194.

Kopsick, D. and Angino, E. E. 1981. Effect of leachate solutions from fly ash and bottom ash on groundwater quality. *Journal of hydrology*. 54: 341-356.

Kulumani Parida and Jasobanta Das. 1995. Studies on Ferric Oxide Hydroxides Ⅱ. Structural properties of goethite samples (α-FeOOH) prepared by Homogeneous precipitation from $Fe(NO_3)_3$ solution in the presence of sulfate ions. *Journal of colloid and interface science.* 178, 586-593.

Kuo, L., P.E. Heilman and A.S. Baker. 1983. Distribution and forms of copper, zinc, cadmium, iron and manganese in soils near a copper smelter. *Soil Sci*. 135: 101-109.

Langmuir, D and Whitemore, D. O**.** 1971. Variations in the stability of precipitated ferric oxyhydroxides. *In*: Hem, J.D. (ed) Nonequilibrium systems in natural water chemistry. Advances in chemistry series, nr 106, pp 209-234.

Langmuir, Donald. 1997. Aqueous Environmental Geochemistry. Prentice-Hall, Inc.

Lawrence, R.W. 1995. Prediction of Acid Rock Drainage-Fundamentals and Tools, notes from MEND Workshop, Montreal, PQ, December 7-8, p27 *In* Kinetic Testwork Procedures by Chris Mills, http:/Technology. Infomine.com.

Lazaroff N., Melanson L., Lewis E., Santoro N., and Pueschel C. 1985. Scanning electron microscopy and infrared spectroscopy of iron sediments formed by Thiobacillus ferrooxidans. *Geomicrobiol. J*. 4, 231-268.

Lazaroff N., Sigal W., and Wasserman A. 1982. Iron oxidation and precipitation of ferric hydroxysulfates by resting Thiobacillus ferrooxidans cells. *Appl. Environ. Microbiol.* 43, 924-938.

Lee, R.E., Jr., H.L. Crist, A.E. Riley, and K.E. Macleod. 1975. Concentration and size of trace metal emissions from a power plant, a steel plant, and a cotton gin. *Environ. Sci. Technol.* 9:643-647.

Lindsay, W.L. 1979. Chemical equilibria in soils. John Wiley and Sons, New York.

Linton, R.W., A. Loh, D.F.S. Natusch, C.A. Evans, Jr., and P. Williams. 1975. Surface predominance of trace elements in airborne particles. *Science.* 191: 852-854.

Lo, I.M.-C., and X-Y. Yang. 1998. Removal and redistribution of metals from contaminated soils by a sequential extraction method. *Waste Manage*. 18: 1-7.

Ma, L.Q., and G.N. Rao. 1997. Chemical fractionation of cadmium, copper, nickel and zinc contaminated soils. *J. Environ.Qual*. 26: 259-264

UNIVERSITY of the
WESTERN CAPE

Maree J. P and M. De Beer. 2000. Effect of power station Ash on water quality when contacted with acid mine water. COALTECH 2020, Report TASK 2.7.1: To determine and quantify the benefits of ashfilling (and slurries) in coal mining.

Maree J.P. and G.J Van Tonder. Limestone neutralization of Iron (II) rich acid water.*WISA 2000 biennial conference*, Suncity, South Africa, 28th May to 1st June 2000.

Maree J.P., Van Tonder, G.J. and Millard, P. 1996. Underground neutralization of mine water with limestone. *Water Research Commission Report No. 609/1/96*, Pretoria, South Africa.

Mattigod, S.V., 1983. Chemical composition of aqueous extracts of fly ash: Ionic speciation as a controlling factor. *Environ Technol. Lett*. 4:485-490.

Mattigod, S.V., Dhanpat Rai, Eary, L.E. and Ainsworth, C.C. 1990: Geochemical factors controlling the mobilisation of inorganic constituents from fossil fuel combustion residues: 1. Review of the major elements. *Journal of environmental quality*, 19,188-201.

Mehta, P.K. 1994. Testing and correlation of fly ash properties with respect to pozzolanic bahavior. Electric Power Research Institute, Report CS314. Palo Alto, CA.

Mettiki Coal Corporation, 1996. Underground mine Back Stowing. In Ziemkiewicz, F. Paul and Jeff Skousen, 2000. Use of coal combustion by-products for reclamation, center for Agriculture, natural resources and community development, West Virginia University Extension service. In the spring issue of "*Green lands*" magazine

Miller, W.P., D.C. Martens and L.W, Zelazny. 1986. Effect of sequence on extraction of trace metals from soils. *Soil Sci. Soc. Am, J.* 50: 598-601.

Mills Chris; 1998: Kinetic Testwork Procedures. *cited in* technology.infomine.com/enviromine.

Morris, G.K. Energy minerals; Coal. In: Metals and Minerals; Annual review, 1997. *Mining Journal LTD*., London.

Morris, R., E.W. Taylor, D.J.A. Brown and J.A. Brown, 1989. Acid toxicity and aquatic animals. *Society for Experimental Biology Seminar series*, v. 34, Cambridge University Press, pp 282.

UNIVERSITY of the WESTERN CAPE

Morse, J.W., 1983. The kinetics of calcium carbonate dissolution and precipitation. In: Reeder, R.J. (Ed), Carbonates-mineralogy and chemistry, 11, 227-264. *Mineral. Soc. Am. Reviews in Mineralogy*.

Moses, C.O. and J.S. Herman, 1991. Pyrite oxidation at circumneutral pH. *Geochimica et Cosmochimica Acta*, v. 55, pp. 471-482.

Muller, J., Seiler, K.P. 1999. Relevance of self-sealing processes in pyrite sinters for heavy metal mobility. *In*: Armanson, A.H. (Ed), 5th Symposium in Geochemistry of the Earth's Surface. Balkema, Rotterdam, pp 211-214.

Murad E, U. Schwertmann, Jerry M. Birgham, and L. Carlson. 1994. Mineralogical Characteristics of poorly crystallized precipitates formed by oxidation of Fe^{2+} in acid sulfate waters. *American Chemical Society*, pg 191-200.

Myeni, B.C.S., Triana, J.S., and Logan, T. T. 1998. Ettringite solubility and geochemistry of the $Ca(OH)_2$-$Al_2(SO_4)_3$-H_2O system at 1 atm pressure and 298 K. *Chemical Geology*,148, 1-19.

Mylona E., A. Xenidis and I. Paspaliaris**.** 2000. Inhibition of acid generation from sulphidic wastes by the addition of small amounts of limestone. *Minerals Engineering*, Vol. 13, No. 10-1, pp. 1161-1175.

Mylona, Ioannis Paspaliaris. 2002. Potential use of lignite fly ash for the control of acid generation from sulphidic wastes. *Waste Management* 22, 631 – 641

Nairn, R.W., R.S. Hedin, and G.R. Watzlaf. 1991. A preliminary review of the use of anoxic limestone drains in the passive treatment of acid mine drainage. In: Proceedings, Twelfth West Virginia Surface Mine Drainage Task Force Symposium, April 3-4, 1991, Morgantown, WV.

Nakamoto, K.**.** Infrared and Raman spectra of inorganic and coordination compounds, Part A: Theory and application in inorganic chemistry. 1997. 5th edition, John Wiley and Sons Inc., New York.

Natusch, D.F. S., C.F. Bauer, H. Matusiewicz, C.A. evans, J. Baker, A. Loh, R.W. Linton, and P.K. Hopke. 1975. Characterization of trace elements in fly ash. P. 553-575. In T.E. Hutchison(ed) Proc. of Int. Conf. On Heavy metals in Environ., Toronto, Ontario, Canada, 27-31 Oct. 1975. Vol. 2, part 2.*In*- **Adriano** D.C, A.L. Page, A.A. Elseewi, A.C. Chang, and I. Straughan. Utilization and Disposal of Fly Ash and Other

UNIVERSITY of the
WESTERN CAPE

Coal Residues in Terrestial Ecosystems: A Review. *J. Environ. Qual.,* 1980, Vol. 9, No. 3.

Nicholson, R.V., Gillham, R.W. 1998. Reardon, E.J. Pyrite oxidation in carbonate-buffered solution: 1. Experimental kinetics. *Geochim. Cosmochim. Acta* 52, 1077-1085.

Nordstrom, D.K and Alpers, C.N. 1999. Geochemistry of acid mine waters. *In:* The environmental geochemistry of mineral deposits part A: processes, techniques and health issues, Plumlee, G.S and Logsdon M.J. (Eds), *Reviews in Economic Geology* Vol 6A,133-160, SEG Inc, Michigan.

Nordstrom, D.K, Alpers, C.N., Blowes, D.W. & Jambor, J.L.1994a. Secondary minerals and acid-mine waterchemistry. *In* The Environmental Geochemistry of Sulfide Mine-Wastes (J.L. Jambor & D.W. Blowes, eds.). *Mineral. Assoc. Can., Short Course Handbook* **22**, 247-270.

Nordstrom, D.K., C.N. Alpers, and J.W. Ball, 1991. Measurement of negative pH values and high metal concentrations in extremely acidic mine waters from Iron Mountain, California (abst.). *Geol. Soc. of Amer.* Abstracts with Program, v. 23(5), p. A383.

Nordstrom, D.K., L.N. Plumber, D. Langmuir, E. Busenberg, and H. M. May. 1990. Revised chemical equilbrium data for major water-mineral reactions and their limitations. *In* chemical modeling of aqueous systems *II*, ed D.C. Melchior and R.L. Basset. Am. Chem. Soc. Ser. 416, pp. 398-413. Washington, DC: Am. Chem. Soc.

Nordstrom, S.K. 1982. The effect of sulfate on aluminum concentrations in natural waters: Some stability relations in the system Al_2O_3-SO_3-H_2O at 298^{o}K. *Cosmochim Acta* 46: 681-692

O'Brien, R.D. 2000. The Neutralisation of Acid Mine Drainage by Fly Ash. *MSc Thesis*, University of Cape Town, RSA.

Olesik, John W. 1996. "Fundamental Research in ICP-OES and ICP-MS." Analytical

Page, A.L., A.A. Elseewi, and I. Straughan. 1979. Physical and chemical properties of fly ash from coal-fired power plants with reference to environmental impacts. *Residue Rev*. 71:83-120.

Panday K.K, Gur, Prasad and V.N. Singh. 1985. Copper (ii) removal from aqueous solutions by fly ash. *Water Res,* Vol 19, No7: 869-873.

UNIVERSITY of the WESTERN CAPE

Parkhurst, D.L. 1995. User's guide to PHREEQC-A computer program for speciation, Reaction-Path, Advective-Transport, and Inverse Geochemical calculations. U.S. Geological Survey water-Resources Investigations Report 95-4227.

Parsons, J.D., 1968. The effects of acid strip-mine effluents on the ecology of a stream. *Arch. Hydrobiol.,* V. 65, pp. 25-50.

Perry, E.F. 1985. Overburden analysis: An evaluation of methods. P. 369-375. *In* D. Graves (ed) 1985 National Symp. On surface Mining, hydrology, sedimentology, and reclamation, Lexington, KY. 7-10 Dec. 1985. Office of Eng. Services, Univ. of Kentucky, Lexington, KY. *In* Stewart et al. Evaluation of leachates from coal refuse blended with fly ash at different rates. *Journal of Environmental quality.* 30: 1382-1391(2001).

Petrik L. Simultaneous water recovery and utilisation of two harmful effluents, fly ash permeate and acid mine drainage, for the production of high capacity inorganic ion exchange material useful for water beneficiation. Water Research Commission (WRC). Final report: K5/1242, 2003, 130 p.

Petrik. L, R. White, M. Klink, V. Somerset, D.L.Key, E. Iwuoha, C. Burgers and M.V. Fey. Utilization of Fly Ash for Acid Mine Drainage remediation. *WRC Report* No. 1242/1/05

Phung HT, Lund LJ, Page AL, Bradford GR. 1979. Trace elements in fly ash and their release in water and treated soils. *Journal of Environmental Quality* 8(2): 171 – 175.

PPRP. 1997. Power plant update: Recycling coal combustion by-products in mines. Vol 5, number 1 spring 1997. http://wvwri.nrcce.wvu.edu/sidebar/iwpeast.php#.

Price, W.A. (1997), *DRAFT Guidelines and Recommended Methods for the prediction of Metal Leaching and Acid Rock Drainage at Minesites in British Columbia*, British Columbia Ministry of Employment and Investment, Energy and Minerals Division, Smithers, BC, (April), 143p. *Cited in* Mills C. 1998, Kinetic Testwork Procedures in *technology.infomine.com/enviromine*.

Querol, X. N., Moreno, J.C., Umana, A., Alastuey, E., Hernandez, A., Lopez-Soler, F. Plana. 2002. Synthesis of zeolites from coal fly ash: an overview. *International journal of coal Geology* 50 : 413-423.

Rafalko, L. and P. Petzrick. 1999. The Western Maryland coal combustion by-products/acid mine drainage initiative, the winding ridge project. Pp 70-1 to 70-16. In proceedings,

UNIVERSITY of the
WESTERN CAPE

13th International symposium on use and management of coal combustion products, Volume 3(TR-111829-V3), January 1999, Orlando, Florida. In Ziemkiewicz, F. Paul and Jeff Skousen, 2000. Use of coal combustion by-products for reclamation, Center for Agriculture, natural resources and community development, West Virginia University Extension Service. In the spring issue of "*Green Lands"* magazine.

Rai, D., S.V. Mattigod, L.E. Eary, and C.C. Ainsworth. 1988a. Fundamental approach for predicting pore-water composition in fossil combustion wastes. P. 317-324. *In* G.J. McCarthy and F.P. Glasser (ed) Fly ash and coal conversion by-products characterization, and disposal III. *Materials Research Society Symposia proceedings*. Vol. 86. Materials Res. Soc., Pittsburg, PA.

Ramos, L., L.M. Hernandez and M.J. Gonzalez. 1994. Sequential fractionation of copper, lead, cadmium and zinc in soils from or near Dona National Park. J. Environ. Qual. 23: 50-57.

Rao C.P; Guskoter H.J: Occurrence and distribution of minerals in Illnois coals. In illinois State Geological Survey. Urbana, IL: US Geological survey; 1973, 476:56.*In* Barry E. Scheetz and Russell Earle. 1998, Utilization of fly ash. Ceramics, composites and intergrowths, *Current opinion in solid state and materials science*, 3: 510-520.

Raymond J. Lovett. 2005. Removal of manganese from acid mine drainage. Department of Chemistry. West Virginia University, Morgantown, WV. 26506.

Reardon, E.J., C.A. Czank., C.J. Warren., R. Dayal and H.M. Johnston., 1995. Determining controls on element concentrations in fly ash leachate. *Waste Management and Research* 13, 435-450.

region, *Canada. Environ. Pollut*. 91, 11–19.

Ribet, I., C.J. Ptacek., D.W. Blowes and J.L. Jambor. 1995. The potential for metal release by reductive dissolution of weathered mine tailings. *Journal of contaminant hydrology* 17, 239-273.

Ricoh P., Hequet V., Lecuyer I and Cloirec Le. P. Influence of operating conditions on heavy metal cation removal by fly ash in Aqueous solutions. *International Ash utilization symposium*, Center for Applied Energy Research, University of Kentucky, 1999.

Rimstidt, J.D., and H.L. Barnes. 1980. The kinetics of silica water reactions. *Geochim. Cosmochim. Acta.* 44: 1683-99.

Robb, G. A. and Robinson, J. D. F.1995. Acid drainage from mines. *The Geographical Journal,* 161: 47-54

Rohrman, F.A. 1971. Analyzing the effect of fly ash on water pollution. *Power* 115 (8): 76-77.

Roy, W. R, and Griffin, A. Robert. 1984. Illinois Basin Coal Fly Ashes. 2. Equilibria Relationships and Qualitative Modeling of Ash-Water reactions. *Environ. Sci. Technol.*, Vol. 18, No, 10.

SABS 1491-2: 2002, Portland cement extenders, Part 2: Fly ash (FA) and ultra-fine fly ash (UFFA). Pretoria: *South African Bureau of Standards,* 2002.

Schopf, J.M. 1956: A definition of coal. *Economic Geology*, 51, 521-561.

Schwertmann, U and Taylor, R.M. 1989. Iron oxides. *In*: Dixon JB, Weed SB (eds) Minerals in soil environments, 2nd edn. Society of America (SSSA Book Series nr. 1) Soil Science, Madison, WI pp 370-438.

Schwertmann, U. 1973. Use of oxalate for Fe extraction from soils. *Can. J. Soil Sci*. 53: 244-246.

Schwertmann, U., Schulze, D.G., Murad, E., 1982. Identification of ferrihydrite in soils by dissolution kinetics, differential X-ray diffraction, and Mossbauer Spectroscopy. *Soil Sci. Soc. Am. J.* 46, 869-875.

Scott, K.M., 1987. Solid solution in, and classification of gossan-derived members of the alunite-jarosite family, northwest Queensland, Australia. *Am. Mineral*. 72: 178-187.

Seoane, S and Leiros, C. M. 2001. Acidification-Neutralization processes in a lignite Mine Spoil Amended with Fly Ash or Limestone. *J. Environ. Qual.* 30: 1420-1431.

Seth. R, Elliot, C.W, 2000. The effects of pH regulation upon the release of sulfate from ferric precipitates formed in acid mine drainage. Applied Geochemistry 15, 27-34.

Seth. R, Ghazi, A.M., 1997. Release of sorbed sulfate from iron oxy hydroxides precipitated from acid drainage associated with coal mining. Environ. Sci. Technol, 31. 2136-2140.

Shokarev, M. M., E.V. Margulis, F.I. Vershinina, L.I. Beisekeeva, and L.A. Savchenko. 1972. Infrared spectra of iron (III) hydroxide sulphates and hydroxides. *Russ. J. Inorg. Chem.* 17: 1293-1296.

UNIVERSITY of the
WESTERN CAPE

Shum, M. and Lavkulich, L. 1999. Speciation and solubility relationships of Al, Cu and Fe in solutions associated with sulfuric acid leached mine waste rock. *Environmental Geology*. 38: Issue 1. 59-68.

Shuman, L.M. 1979. Zinc, manganese, and copper in soil fractions. *Soil Sci.* 127: 10-17.

Shuman, L.M. 1982. Separating soil iron and manganese oxide fractions for microelement analysis. Soil Sci. Soc. Am. J. 46:1099–1102.

Shuman, L.M. 1985. Fractionation method for soil micronutrients. *Soil Sci*. 140: 11-22.

Simonton S, M. Dimsha, B. Thomson, L.L. Barton, and G.Cathey. 2000. Long- term stability of metals immobilized by microbial reduction. *Proceedings of the 2000 conference on hazardous waste research.*

Skougstad, M.W., Fishman, M.J., Friedman, L.C., Erdmann, D.E.,Duncan, S.S. (Eds.), 1979. Methods for Determination of In-organic Substances in Water and Fluvial Sediments: Techniques of Water-Resources Investigations of the U.S. Geological

Skousen, j., Hilton, T. and Faulkner, B. 1996: Overview of acid mine drainage treatment with chemicals. Chapter 23, *In:* Acid Mine Drainage: Control and Treatment, Skousen, J.G. and Ziemkiewicz, P.F. (Eds), 2nd Edition, West Virginia University, Morgantown, West Virginia.

UNIVERSITY of the
WESTERN CAPE

Skousen, J.G. and Ziemkiewicz, P.F. (eds.) 1995. Acid Mine Drainage Control and Treatment.National Mine Land Reclamation Publication. 27 ch. 254 pp. 2nd edition.

Smit, J and U.E. Sibilski. 2003. Pilot Plant study to treat Typical Gold Mine Wastewater using the Savmin process. In proceedings Water in Mining 2003 conference held in Brisbane Australia: 13-15 October.

Smith R. D. 1980. The trace element chemistry of coal during combustion and the emissions from coal-fired plants. *Prog. Energy Combust. Sci*. 6: 53-119.

Soltanpour, P.N., A. Khan, and W.L. Lindsay. 1976. Factors affecting DTPA-extractable Zn, Fe, Mn and Cu from soils. Commun. *Soil Sci. Plant Anal.* 7:797-821.

Sposito, G. 1983. The chemical forms of trace metals in soils. *In*: Thornton. I (Ed), Applied Environmental Geochemistry. Academic press, London, pp 123-170.

Stewart B.R, W.L. Daniels, L.W. Zelazny, and M.L. Jackson. 2001. Evaluation of leachates from coal refuse blended with fly ash at different rates. *Journal of Environmental quality*. 30: 1382-1391.

Stewart R. Barry, W. Lee Daniels, and Meral L.Jackson. 1997. Evaluation of leachate quality from co-disposed coal fly ash and coal refuse. *Journal of Environmental quality*. 26:1417-1424.

Stipp S.L.S., M. Hansen, R. Kristensen, M.F. Hochella Jr, L. Bennedsen, K. Dideriksen, T. Balic-Zunic, D. Leonard, H-J Mathieu. 2002. Behaviour of Fe-oxides relevant to contaminant uptake in the environment. *Chemical Geology,* 190: 321-337.

Stoessell, R.K. 1988. 25oC and 1 atm dissolution experiments of sepiolite and kerolite. *Geochemica et Cosmochimica. Acta,* 52: 365-374.

Stromberg, B., Banwart, S. 1999. Weathering kinetics of waste rock from the Aitik copper mine, Sweden: scale dependent rate factors and pH controls in large column experiments. J. Contam. Hydrol. 39: 59-89.

Stumm, W and Lee, G.F. 1961. Oxygenation of ferrous iron. Industrial and Engineering Chemistry. 53 (2): 143-146.

Stumm, W. and J.J. Morgan, 1981. Aquatic chemistry. Wiley *Interscience*, 470 p.

Sullivan P.J. and Yelton J.L. 1988. An evaluation of trace element release associated with acid mine drainage. *Environmental Geology and Water Sciences* 12, 181-186.

Sullivan P.J., Yelton, J.L. and Reddy K.J. 1988. Solubility relationships of aluminum and iron minerals associated with acid mine drainage. *Environmental Geology and Water Sciences* 11, 283-287.

Summers, K.V., Rupp, G. L. and Gherini, S. A. 1983. Physical-chemical characteristics of utility solid wastes. EPRI EA-3236, Electrical Power Research Institute, Palo Alto, CA, USA.

Sutter. B; J.B. Dalton; S.A. Ewing; R. Amundson, and C.P. McKay. 2005. Infrared spectroscopic analyses of sulfate, nitrate, and carbonate-bearing atacama desert soils: analogs for the interpretation of infrared spectra from the martian surface. *Lunar and Planetary Science* XXXVI

Talbot, R.W., M.A. Anderson, and A.W. Andren. 1978. Qualitative model of heterogeneous equilibria in a fly ash pond. *Environ. Sci. Technol*. 12:1056-1062

Taylor, H.F.W. 1998. Cement Chemistry 2rd Edition. Thomas Telford, London.

Teichmuller T.M. and Teichmuller R. 1975. The geological basis of coal formation. *In* Stach's Textbook of coal petrology. Edited by Murchison DG, Taylor GH, Zierke F.

UNIVERSITY of the
WESTERN CAPE

Berlin-Stuttgart: Gebruder Borntrager; 5-53. *In* **Barry** E. Scheetz and Russell Earle. 1998, Utilization of fly ash. Ceramics, composites and intergrowths, *Current opinion in solid state and materials science*, 3: 510-520.

Tessier, A., and Campell, P.G.C. 1991. Comment on pitfalls of sequential extractions. *Wat. Res*. 25: 115-117.

Tessier, A., Campell, P.G.C. and Bison, M. 1979. Sequential extraction procedure for the speciation of particulate trace metals. *Anal. Chem*. 51: 844-850.

Tessier, A., F. Rapin, and R. Carigan. 1985. Trace metals in oxic lake sediments: possible adsorption onto iron (oxy) hydroxides. *Geochim. Cosmochim ACTA*. 49: 183-194.

Theis T.L, Richter R.O. 1979. Chemical speciation of heavy metals in power plant ash pond leachate. *Environ Sci Technol* . 13: 219.

Theis, T.L., and J.L. Wirth. 1977. Sorptive behavior of trace metals on fly ash in aqueous systems. *Environ. Sci. Technol*. 11: 1096-1100.

Thomson J.G. 1980. Acid mine waters in South Africa and their amelioration. *Water SA* Vol. 6. No. 3 July.

Uhlmann, W, H.; Buttcher, O. Totsche.; C. E. W. Steinberg. 2004. Buffering of Acidic Mine Lakes: The Relevance of Surface exchange and solid bound sulphate. *Mine Water and Environment.* 23, 20-27.

Ure, A., Quevaullier, P.H., Muntau, H., Griepink, B. 1993. Speciation of heavy metals in soils and sediments. Anaccount of the improvement and harmonization of extraction techniques undertaken under the auspices of the BCR of the CEC. *Int. J. Environ. Analyt. Chem. 5*1, 135–151.

USEPA (United States Environmental Protection Agency). The Class V underground injection control study: mining, sand, or other backfill wells. Office of Ground Water and Drinking Water, 1999, 10, 74 p.

Van den Berg, J.J., Cruywagen, L., De Necker, E. and Hodgson, F.D.I. 2001: Thesuitability and impact of power station fly ash for water quality control in coal opencastmine rehabilitation. Report to the Water Research Commission, WRC Report No.745/1/01.VINNICOMBE, D.A. 2000: Acid Mine Drainage: Neutralisation, Conditioning and Partial

UNIVERSITY of the
WESTERN CAPE

Van der Sloot H.A. 1996.Developments in evaluating environmental impact from utilization of bulky inert wastes using laboratory leaching tests and field verification. *Waste Management.* Vol 16, issues (1-3) pgs 65-81.

Van der Sloot, H.A., J. Wijkstra, C. A. Van Stigt and D. Hoede, 1985. Leaching of trace elements from coal ash and coal-ash products. Wastes Ocean 4: 467-497.

Van Hille, R., Foster, T., Storey, A., Duncan, J. & Lewis, A. (2004): Heavy Metal Precipitation by Sulphide and Bicarbonate: Evaluating Methods to predict anaerobic Digester Overflow Performance. – In: Jarvis, A. P., Dudgeon, B. A. & Younger, P. L.: mine water 2004 – Proceedings International Mine Water Association Symposium 2. – p. 141-150, 6 Fig., 1 Tab.; Newcastle upon Tyne (University of Newcastle).

Van Jaarsveld, J.G.S., Van Deventer, J.S.J., Lorenzen, L., 1997. The potential use of geopolymeric materials to immobilize toxic metals: Part 1. *Theory and applications. Minerals Engineering* 10 (7), 659-669.

Van Niekerk, A. Presentation at coaltech 2020 colloquium, Witbank Civic Theatre, March 2001. *Cited in* Burgers C.L 2002. Synthesis and characterisation of sesquioxidic precipitates formed by reaction of acid mine drainage with fly ash leachate. *Msc Thesis*. University of Stellenbosch.

Von Willert, J. Frank and Stehouwer C. Richard. 2003. Compost, limestone, and gypsum effects on calcium and aluminum transport in acidic mine spoil. *Soil Sci. Soc. Am. J.* 67: 778-786.

Wadge, A., M. Hutton, and P.J. Peterson. 1986. The concentrations and particle size relationships of selected trace elements in fly ashes from U.K. coal fired power plants and a refuse incinerator. *Science of the Total Environ* 54: 13-27.

Warner, R.W., 1971. Distribution of biota in a stream polluted by acid mine-drainage. *Ohio J. Sci.,* v. 71, pp. 202-215.

Warren C. J and Dudas M.J.1985. Formation of Secondary minerals in artificially weathered fly ash. *Journal of Environmental quality*., vol 14, no 3.

Warren, C.J., and M.J. Dudas. 1984. Weathering processes in relation to leachate properties of alkaline fly ash. *J. Environ. Qual.* 13: 530-538

Watt, J.D. and Thorne, D.J. 1965. Composition and pozzolanic properties of pulverized fly ashes. 1. Composition of fly ashes from some British power stations and properties of their component particles. *Journal of applied chemistry* 15: 585-594.

UNIVERSITY of the
WESTERN CAPE

Watzlaf, G.R., 1992. Pyrite oxidation in saturated and unsaturated coal waste. *In:* Proceedings of the 1992 National Meeting of the American Society for Surface Mining and Reclamation, pp. 191-203.

Watzlaf, G.R., J.W. Klemherz, J.O. Odoski, and R.S. Hedin. 1994. Performance of the Jennings Center anoxic limestone drain. U.S. Bureau of Mines Report SP 0613-94, Pittsburgh, PA.

Weaver W.S., R. Luka, Laboratory studies of cement-stabilized mine tailings, *Can. Min. Metall. Bull.* 64 (701)(1970) 988-1001 ***In*** **Benzaazoua** M., Tikou Belem, Bruno Bussiere. Chemical factors that influence the performance of mine sulphidic paste bakfill. *Cement and Concrete Research* 32 (2002) 1133-1144

Webster G. Jenny, Peter J. Swedlund and Kerry S. Webster (1998). Trace metal adsorption onto an acid mine drainage Iron (III) oxyhydroxysulfate. *Environmental Science and Technology,* Vol 32, No 10.
Weinheim, Germany.

Wieder, R.K. 1992. The Kentucky wetlands project: A field study to evaluate man-made wetlands for acid coal mine drainage treatment. Final Report to the U.S. Office of Surface Mining, Villanova University, Villanova, PA.

Wildeman, T., J. Gusek, and G. Brodie. 1991. Wetland design for mining operations. Draft handbook presented at the 1991 American Society for Surface Mining and Reclamation Conference, Durango, CO.

William, R. Roy and Robert A. Grifin. 1984. Illinois Basin Coal Fly Ashes. 2. Equilibria Relationships and Qualitative Modeling of Ash-Water Reactions. Environ. Sci. Technol, Vol 18, No 10: 739-742.

Willis, J.P. 1987.Variations in the composition of South African fly ash. Ash- a valuable resource, 2-6, *Council for Science and Industrial Research*, vol. 3.

Wolt J.D., N.V. Hue., and R.L. Fox. 1992. Solution Sulfate chemistry in three sulfur-retentive hydrandepts. *Soil Sci. Soc. Am. J.* 56: 89-95

Xenidis Anthimos, Evangelia Mylona, Ioannis Paspaliaris. 2002. Potential use of lignite fly ash for the control of acid generation from sulphidic wastes. *Waste Management* 22 : 631 – 641.

UNIVERSITY of the
WESTERN CAPE

Xu, H., Van Deventer, J.S.J., 2000. The geopolymerisation of alumino-silicate materials. *International Journal of mineral processing* 59, 247-266.

Yong, R.N., Yaacob, W.Z.W., Bentley, S.P., Harris, C and Tan, B.K. 2001. Parttitioning of heavy metals on soil samples from column tests. *Engineering geology*. Vol 60, pp 307-3222.

Zachara, J.M., Cowan, C.E. and Resch, C.T. 1991. Sorption of divalent metals on calcite. *Geochim. Cosmochim. Acta* 55, 1549-1562.

Ziemkiewicz, F. Paul and Jeff Skousen, 2000. Use of coal combustion by-products for reclamation, center for Agriculture, natural resources and community development, West Virginia University Extension service. In the spring issue of "*Green Lands*" magazine.

Appendices

Appendix A

Analytical Techniques

A Introduction

This chapter describes the analytical techniques used and the principles involved. A summary of the experimental design, execution, analytical techniques used, data generated and application is presented in figure A1 below

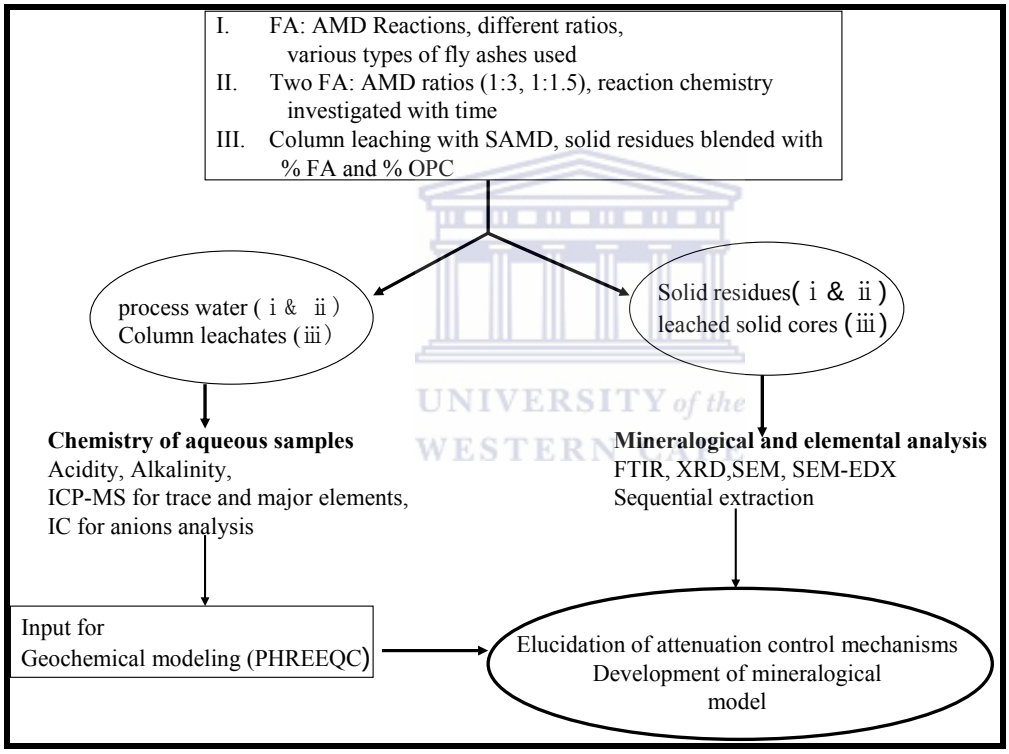

FigureA1: Flow diagram of the experimental sequence, analytical techniques used, type of data generated and application

A.1 Inductively coupled plasma mass spectrometry (ICP-MS)

A.1.1 Introduction

Inductively coupled plasma mass spectroscopy (ICP-MS) was developed in the late 1980's to combine the easy sample introduction and quick analysis of ICP technology with the accurate and low detection limits of a mass spectrometer. The resulting instrument is capable of trace multielement analysis, often at the part per trillion level. ICP-MS has been used widely over the years, finding applications in a number of different fields including drinking water, wastewater, natural water systems/hydrogeology, geology and soil science, mining/metallurgy, food sciences, and medicine.

A.1.2 Instrument Description and Theory

ICP technology was built upon the same principles used in atomic emission spectrometry. In ICP-MS, a plasma or gas consisting of ions, electrons and neutral particles, is formed from Argon gas, which is then utilized to atomize and ionize the elements in the sample matrix. These resulting ions are then passed through a series of apertures (cones) into a high vacuum mass analyzer where the isotopes of the elements are identified by their mass-to-charge ratio. The intensity of a specific peak in the mass spectrum is proportional to the amount of the elemental isotope from the original sample. An ICP-MS can be thought of as four main processes, including sample introduction and aerosol generation, ionization by an argon plasma source, mass discrimination, and the detection system. The figure A2 below illustrates this sequence of processes.

UNIVERSITY of the
WESTERN CAPE

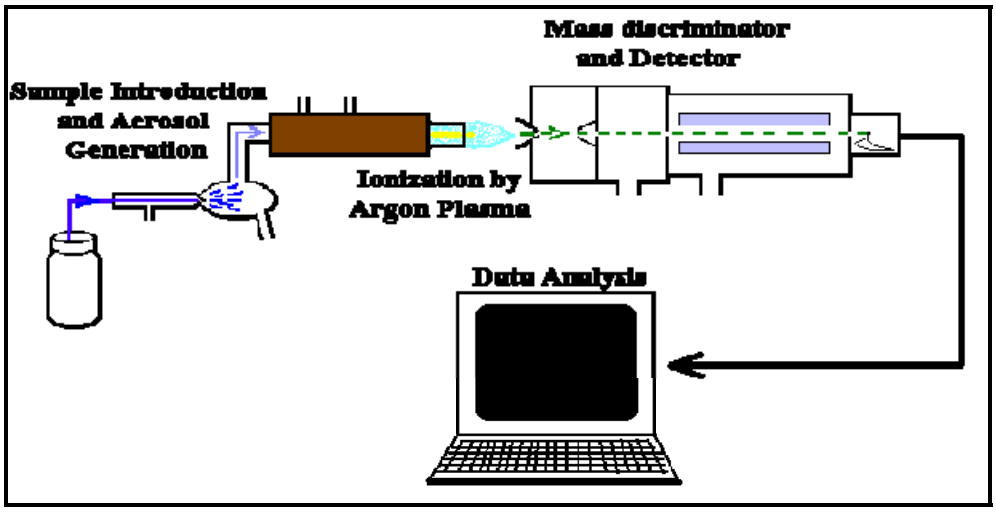

Figure A2: Schematic diagram of ICP-MS main processes

A.1.3 Sample Introduction

ICP-MS spectrometers can accept solid as well as liquid samples. Solid samples are introduced into the ICP by way of a laser ablation. Aqueous samples are introduced by way of a nebulizer which aspirates the sample with high velocity argon, forming a fine mist. The aerosol then passes into a spray chamber where larger droplets are removed via a drain (Jarvis *et al.,* 1992). Typically, only 2% of the original mist passes through the spray chamber (Olesik, 1996). This process is necessary to produce droplets small enough to be vaporized in the plasma torch.

UNIVERSITY of the
WESTERN CAPE

A.1.4 Argon Plasma/Sample Ionization

Once the sample passes through the nebulizer and is partially desolvated, the aerosol moves into the torch body and is mixed with more argon gas. A coupling coil is used to transmit radio frequency to the heated argon gas, producing an argon plasma "flame" located at the torch (Jarvis *et al.,* 1992). The hot plasma removes any remaining solvent. As this aerosol sample passes through the plasma, it collides with free electrons, argon cations, and neutral argon atoms, causing any molecules initially present in the aerosol to be quickly and completely broken down into charged atoms. Some of these charged atoms will recombine with other species in the plasma to create both stable and meta-stable molecular species, which will then be transmitted into the

mass analyzer along with the charged atoms. In addition to being ionized, sample atoms are excited in the hot plasma, a phenomenon which is used in ICP-atomic emission spectroscopy.

A.1.5 ICP-MS Interface

Because atomization/ionization occurs at atmospheric pressure, the interface between the ICP and MS components becomes crucial in creating a vacuum environment for the MS system. Ions flow through a small orifice, approximately 1 millimeter in diameter, into a pumped vacuum system. Here a supersonic jet forms and the sample ions are passed into the MS system at high speeds, expanding in the vacuum system (Jarvis *et al.,* 1992). The entire mass spectrometer must be kept in a vacuum so that the ions are free to move without collisions with air molecules. Since the ICP is maintained at atmospheric pressure, a pumping system is needed to continuously pull a vacuum inside the spectrometer. In order to most efficiently reduce the pressure several pumps are typically used to gradually reduce pressure to 10^{-5} mbar before the ion stream reaches the quadrupole.

UNIVERSITY of the
WESTERN CAPE

A.1.6 Mass Spectrometer (MS)

In the first stage of the mass spectrometer ions are removed from the plasma by a pumped extraction system. An ion beam is produced and focused further into the actual unit. There are several different types of mass analyzers which can be employed to separate isotopes based on their mass to charge ratio. Quadrupole analyzers are compact and easy to use but offer lower resolution when dealing with ions of the same mass to charge (m/z) ratio. Double focusing sector analyzers offer better resolution but are larger and have higher capital cost. The quadrupole mass filter is made up of four metal rods aligned in a parallel diamond pattern. A combined DC and AC electrical potential is applied to the rods with opposite rods having a net negative or positive potential. Ions enter into the path between all of the rods. When the DC and AC voltages are set to certain values only one particular ion is able to continue on a path between the rods and the others are forced out of this path. This ion will have a specific m/z ratio. Many combinations of voltages are chosen which allows an array of different m/z ratio ions to be detected.

A.1.7 Detector

The most common type of ion detector found in an ICP-MS system is the channeltron electron multiplier. This cone or horn shaped tube has a high voltage applied to it opposite in charge to that of the ions being detected. Ions leaving the quadrupole are attracted to the interior cone surface. When they strike the surface additional secondary electrons are emitted which move farther into the tube emitting additional secondary electrons. As the process continues even more electrons are formed, resulting in as many as 10^8 electrons at the other end of the tube after one ion strikes at the entrance of the cone (Jarvis *et al.*, 1992).

A.1.8 Instrument Calibration

Any sample entered into the mass spectrometer under similar conditions will return a count rate of events at the detector that can be converted directly to the concentration for each element from an established calibration curve. The response of the mass spectrometer in counts per second is directly proportional to the concentration of a given element in a sample; this allows the system to be calibrated by incorporating a series of external standards of differing concentrations. The challenge, therefore, is to ensure that conditions are identical for each sample, and that potential variables that can affect the analysis are recognized and compensated. Possible factors that can affect the sampling conditions of the ICP-MS are: variations in plasma ionization efficiency; possible clogging or erosion of cone apertures; differing matrix concentrations in samples that could result in matrix suppression; temperature and humidity fluctuations in the laboratory environment; and or, formation of molecular species within the sample that may interfere with another element in an unexpected manner. Any one of these variations or conditions can render the accurate analysis of the respective sample difficult or impossible unless certain methods or procedures are employed to minimize the potential for such difficulties. Some of the procedures employed to minimize these problems are:

- Incorporation of an external calibration series encompassing the elements to be analyzed. This is designed to cover a range of concentrations that will completely bracket the concentration of analyte in the sample.

UNIVERSITY of the
WESTERN CAPE

- Internal standards can be incorporated for each sample at known concentrations for the desired element(s) to compensate for any variation in the intensity of the element signal. These internal standards can then be used to correct the measured instrument response to the known concentration.

A.1.9 Sources of interference

There are two types of interferences that affect ICP-MS, these are spectral and matrix.

Spectral interference arises from ions other than the analyte ions (M^+) which form in the plasma from the plasma gas atoms or atmospheric gas. The most abundant ions are from atoms such as Ar, O, N and H. They form polyatomic ions which have the same mass as some metals. Examples of ions causing spectral interference include Ar^+, Ar_2^+, ArO^+, ArH^+, M-Ar, O^+, O_2^+, OH^+, H_2O^+, N_2^+, MO^+, M-H^+, M-OH^+ and doubly charged analyte ions.

ICP-MS is sensitive to dissolved solids (lower counts are reflected in its response). Dilution of the sample minimizes these effects. Samples were filtered through 0.45µm cellulose nitrate filter and diluted to EC < 1.5 mS/cm with Milli-Q (18 MΩ) water and stabilized with HNO_3 acid.

UNIVERSITY of the
WESTERN CAPE

A.1.10 Accuracy of the method and detection Limits

After the experiments, filtration and preservation with ultra pure HNO_3, the aqueous samples were submitted to the instrument operator for analysis.

An ELAN 6000 PE-SCIEX ICP-MS system at University of Cape Town (UCT) geology department was used to carry out the analysis of water samples reported in this work. The preserved samples were then prepared for analysis by diluting 150 µL to 15 ml with 5 % ultra pure HNO_3. 50 µL of 3 ppm internal standard consisting of In and Bi was added to correct for drift. A certified reference material (NIST 1640) diluted 10 times in 5 % ultra pure HNO_3 was analyzed under the same conditions to ascertain the accuracy of the analysis. Several blank samples prepared from MilliQ water were also analyzed along side the samples. Multi-element standards consisting of B, Na, Mg, Al, Si, K, Ca, V, Cr, Mn, Fe, Ni, Co, Cu, Zn, As, Se, Sr, Mo, Cd, Ba and Pb at concentration of 13, 45, 150 and 250 ppb prepared in 5 % HNO_3 was used for the instrument calibration.

One of the great advantages of ICP-MS is extremely low detection limits for a wide variety of elements. Some elements can be measured down to part per quadrillion range while most can be detected at part per trillion levels. The lower limits of detection (LLD) were calculated for various elements and reported as mg/L and mmol/L (Table 3.1) using equation equation A1 below.

$$LLD = 3 \times \sqrt{(2 \times wblk\ cps)} \times (concentration\ in\ std\ /(std\ cps - wblk\ cps) \quad \text{.....(A1)}$$

where wblk cps and std cps are the counts per second in the water blank and standard respectively (Andreas Spath pers comm, 2005)

Table A1: Calculated lower limits of detection for elements analysed.

Element	mg/L	mmol/L	Element	mg/L	mmol/L
B	0.00672	6.22E-07	Co	3.78E-05	6.41E-10
Na	0.73271	3.19E-05	Cu	7.77E-05	1.22E-09
Mg	0.12548	5.16E-06	Zn	0.00055	8.38E-09
Al	0.00142	5.25E-08	As	0.00012	1.6E-09
Si	0.05664	2.02E-06	Se	0.00037	4.72E-09
Ca	0.26798	6.69E-06	Sr	4.35E-05	4.96E-10
V	0.00005		Mo	1.37E-05	1.42E-10
Cr	0.00063	1.24E-08	Cd	6.32E-06	5.63E-11
Mn	0.00037	6.82E-09	Ba	8.11E-06	5.9E-11
Fe	0.04632	8.29E-07	Pb	1.93E-05	9.32E-11
Ni	0.00070	1.19E-08			

UNIVERSITY of the
WESTERN CAPE

To assess the accuracy during sample measurements, results of NIST-1640 water standard analyzed with each batch of samples was used to calculate the bias. The results are presented in table 3.2 which compares the mean measured values and certified values of the elements analyzed. Bias is calculated to show the deviation of the measured values from the certified values.

Bias= Mean measured concentration-certified concentration

% Bias=bias/certified concentration in standard*100

Most of the elements exhibited a % bias of less than 10 % except Si, Fe, Zn and Mo.

Table A2: ICP-MS analysis of NIST-1640 certified reference material (n=10)

Element	certified	ave	std dev	Bias(-/+)	% Bias
B	0.3011	0.3011	0.0053	0.0053	1.7635
Na	29.350	29.350	2.5682	2.0323	6.9243
Mg	5.8190	5.8190	0.2762	0.1210	2.0794
Al	0.0520	0.0520	0.0032	0.0031	5.9570
Si	4.7300	4.7300	0.5389	0.7074	14.956
K	0.9940	0.9940	0.0941	0.0988	9.9346
Ca	7.0450	7.0450	0.1431	0.2217	3.1466
Cr	0.0386	0.0386	0.0008	0.0014	3.6412
Mn	0.1215	0.1215	0.0021	0.0009	0.7235
Fe	0.0343	0.0301	0.0027	0.0042	12.244
Ni	0.0274	0.0274	0.0006	0.0005	1.8572
Co	0.0203	0.0203	0.0002	0.0002	0.7655
Cu	0.0852	0.0852	0.0015	0.0012	1.3577
Zn	0.0532	0.0532	0.0063	0.0074	13.981
As	0.0267	0.0267	0.0005	0.0005	1.8888
Se	0.0220	0.0220	0.0003	0.0000	0.0007
Sr	0.1242	0.1242	0.0011	0.0007	0.5670
Mo	0.0468	0.0468	0.0128	0.0084	18.021
Cd	0.0228	0.0228	0.0006	0.0006	2.5440
Ba	0.1480	0.1480	0.0028	0.0003	0.2277
Pb	0.0279	0.0279	0.0006	0.0001	0.4831

UNIVERSITY of the
WESTERN CAPE

A.2 Ion chromatography

Ion chromatography is a form of liquid chromatography that uses ion-exchange resins to separate atomic or molecular ions based on their interaction with the resin. Its greatest utility is for analysis of anions (such as fluoride, chloride, nitrite, nitrate, and sulfate) for which there are no other rapid analytical methods. It is also commonly used for cations (like lithium, sodium, ammonium, and potassium) and biochemical species such as amino acids and proteins. Most ion-exchange separations are done with pumps and metal columns using conductivity detectors.

The column packings for ion chromatography consist of ion-exchange resins bonded to inert polymeric particles (typically 10 μm diameter). For cation separation the cation-exchange resin is usually a sulfonic or carboxylic acid, and for anion separation the anion-exchange resin is usually a quaternary ammonium group. For cation-exchange with a sulfonic acid group the reaction is:

$-SO_3^- H^+(s) + M^{x+}(aq) <===> -SO_3^- M^{x+}(s) + H^+(aq)$…….……(A2)

where M^{x+} is a cation of charge x, (s) indicates the solid or stationary phase, and (aq) indicates the aqueous or mobile phase. The equilibrium constant for this reaction is:

$$K_{eq} = \frac{[-SO_3^- M^{x+}]_s [H^+]_{aq}}{[-SO_3^- H^+]_s [M^{x+}]_{aq}} \quad \text{.....(A3)}$$

Different cations have different values of K_{eq} and are therefore retained on the column for different lengths of time. The time at which a given cation elutes from the column can be controlled by adjusting the pH ($[H^+]_{aq}$).

Ions in solution are detected by measuring the conductivity of the solution. In ion chromatography, the mobile phase contains ions that create a background conductivity, making it difficult to measure the conductivity due only to the analyte ions as they exit the column. This problem is reduced by selectively removing the mobile phase ions after the analytical column and before the detector. This is done by converting the mobile phase ions to a neutral form or removing them with an eluent suppressor, which consists of an ion-exchange column or membrane. For cation analysis, the mobile phase is often HCl or HNO_3, which can be neutralized by an eluent suppressor that supplies OH^-. The Cl^- or NO_3^- is either retained or removed by the suppressor column or membrane. The same principle holds for anion analysis. The mobile phase is often NaOH or $NaHCO_3$, and the eluent suppressor supplies H^+ to neutralize the anion and retain or remove the Na^+.

UNIVERSITY of the
WESTERN CAPE

Any ionic substance that produces a detector response and has a retention time coinciding with that of an analyte, or near enough to cause peak overlap, may interfere with the determination. Low molecular weight organic acids, such as formic acid, may interfere with the determination of fluoride and chloride. A high concentration of any one ion may interfere with the resolution, and sometimes the retention, of others (Eaton *et al*., 1995). Most samples require dilution for determination of major ions by ion chromatography, which can introduce additional errors.

Generally the minimum detectable concentrations for anions by this method are near 0.1 mg/L for Br^{-1}, Cl^{-1}, NO_3^-, NO_2^-, PO_4^{3-} and SO_4^{2-} (Eaton *et al*., 1995).

A.2.1 Procedure

The samples were filtered through 0.22 μm Millipore filter membranes to remove suspended solids and then diluted with MilliQ water to obtain EC values of between 50 and 100 μS/cm. Samples were then submitted to the operator for analysis. SO_4^{2-}, Cl^-, NO_3^- and PO_4^{3-} anions were analyzed using a Dionex DX-120 ion chromatograph with an Ion Pac AS14A column and AG14-4 mm guard column at Soil Science department in Stellenbosch University. The eluent was Na_2CO_3 and $NaHCO_3$.

A.3 Determination of Ferrous iron by colorimetry

A.3.1 Principle

Ferrous iron in the raw AMD samples, co-disposal process waters and the column leachates were determined by the bipyridal complex method. The method is applicable to filtered samples containing between 10 and 4000 mg/L Fe^{2+} or total iron. It consists of adding 1 ml of 2,2'.bipyridine solution (0.5 g/L) to a 25-ml sample. The Fe^{2+} reacts immediately to form a red complex. The complex forms when the pH of the test solution is between 3 and 10 (Skougstad *et al.,* 1979). If the pH is not within this range it's adjusted with a sodium acetate/acetic acid buffer. The absorbance of the colored solution at 540 nm wavelength obeys Beer's law. A Double beam GBC UV/VIS 920 spectrophotometer at the department of chemistry in the University of the Western Cape was utilized by the author for absorbance measurement.
The buffer giving the pH range for maximum formation of the Fe^{2+} complex was prepared as follows:

70 g sodium acetate and 0.2 g 2,2-bipyridyl reagent was made up to 500 ml using MQ water. The Fe^{2+} complex was produced by adding 2 ml of the buffered 2,2-bipyridyl solution to 2 ml of the sample solution and then adding 1.6 ml MQ water. The sample solutions were diluted so that the Fe^{2+} concentration was in the range of 1-15 mg/L. The absorbance of the samples at 540 nm wavelength was measured by UV spectrophotometer. Standard Fe^{2+} solutions ranging in

concentration from, 0, 1, 2, 3, 4, 5, 7, 10, and 15 mg/L were used for instrument calibration. The figure 3.2 shows a calibration graph obtained with the prepared standards.

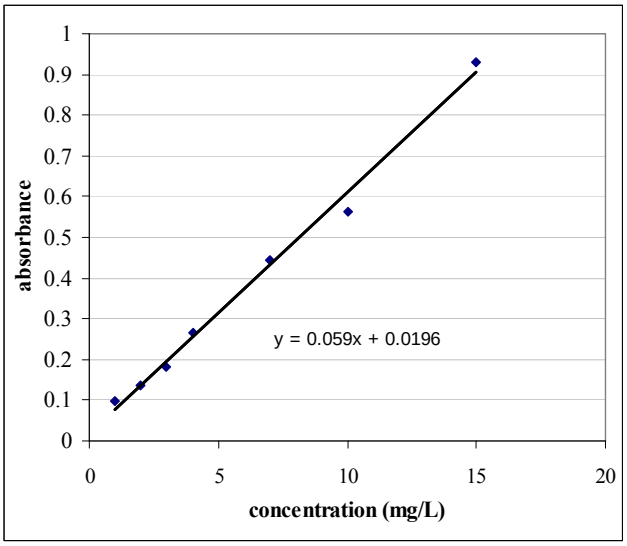

Figure A3: Calibration graph of Fe^{2+} standard solutions

A.4 PH measurements

The pH of a solution is a measure of the hydrogen ion activity (α_{H^+}) in solution:
PH= -log α_{H^+}

The glass membrane electrode used to measure pH generates an electrical potential in response to the H+ activity in solution. When combined with a reference electrode of known constant potential, the potential difference between the two electrodes can be measured by a potentiometer (pH meter) to determine the solution pH. Combination electrodes have a glass electrode and reference electrode combined in one probe. PH is measured relative to the known H^+ activity of one or more pH buffer solutions which are used to calibrate the pH meter.

All pH measurements were done using a Hanna HI 991301 portable pH/EC/TDS/Temperature probe. The pH probe was calibrated using two buffer solutions of pH 4.01 and 7.01.

UNIVERSITY of the
WESTERN CAPE

A.5 Electrical conductivity (EC).

Conductivity is a measure of the ability of an aqueous solution to carry an electric current. This ability depends on the presence of ions, on their total concentration, mobility, and valence, and on the temperature of measurements. Solutions of most inorganic compounds are relatively good conductors. Molecules that do not ionize significantly in aqueous solutions do not conduct a current or if they do, its very low.

The electrical conductivity measurements were done using a Hanna HI 991301 portable pH/EC/TDS/Temperature probe. Prior to measurements the probe was calibrated by using a standard of 12.88 mS/cm at room temperature.

A.6 Alkalinity Measurement

Alkalinity is defined as the capacity of the water to neutralize a strong acid to a designated pH. Alkalinity in most natural waters is due to bicarbonate, but other salts of weak acids and hydroxide may also contribute to alkalinity. Water samples with pH between 4.5 and about 8.5 will most likely have only bicarbonate alkalinity. Alkalinity is determined by titration with an acid. The method of Eaton *et al*. (1995) in determining alkalinity.

The method involved titrating 20 ml of the sample solution with 0.01 N HCl to an end point of 4.5. The alkalinity was then calculated using the formula shown below (equation A4) and reported in mg/L $CaCO_3$. The pH during titration was monitored by use of a Metrohm pH meter equipped with a combined LL pH glass electrode.

$$Alkalinity\,(mgCaCO_3 / L = \left[A \times N \times 50 \times 1000\right] / ml\ sample \quad \text{.....(A4)}$$

where:

A=ml standard acid used

N=normality/molarity of acid used.

The alkalinity reported as mg /L $CaCO_3$ was recalculated to mg/L HCO_3^- (equations A5 and A6) and this data was used for input during solution modeling by PHREEQC software.

$$mg\ HCO_3^- / L = mol\ HCO_3^- / L \times 61.0171 \times 1000 \quad \text{.....(A5)}$$

where

$$mol\ HCO_3^- / L = \frac{mg\ CaCO_3 / L}{50\,000} \quad \text{.....(A6)}$$

A.7 Acidity Measurements

The acidity of water is defined as its quantitative capacity to neutralize a strong base to a designated pH and is generally considered with alkalinity because of their interrelationship. The measured value may vary significantly with the end-point pH used in the determination, hydrolyzing salts such as iron or aluminium sulphates may contribute to the measured acidity according to the method of determination. There are three general reasons for determining acidity:

- To check the pH
- To estimate the amount of liming agent that is required for neutralization
- To obtain a parameter to relatively compare water samples. Acidity is quantitatively used in modeling.

UNIVERSITY of the
WESTERN CAPE

Acidity is dependent on the pH value and the buffering capacity of the water body and is also expressed interms of an equivalent concentration of $CaCO_3$ in mg/L at the designated pH.

The procedure involved titrating 20 ml sample with 0.1M NaOH to an end point of 8.3. Samples in this study had high concentration of hydrolysable ions (Gitari *et al*., 2005) and were pretreated with hot hydrogen peroxide. The peroxide treatment involved adding 5 drops of the hydrogen peroxide and heating for five minutes. The solution after cooling was titrated with 0.1 M NaOH to pH 8.3. The acidity was then calculated using the formula shown below (equation A7) (Eaton *et al.*, 1995) and reported in mg/L $CaCO_3$. The pH during titration was monitored by use of a Metrohm pH meter equipped with a combined LL pH glass electrode.

$$Acidity\,(mgCaCO_3 / L = \left[B \times N \times 50 \times 1000\right] / ml\ sample \quad \text{.....(A7)}$$

where:

B= volume of 0.1 M NaOH used

N= Normality/Molarity of NaOH used.

Titration to pH 8.3 endpoint represents a measure of total acidity

A.8 X-ray diffractometry

Fresh fly ash samples, co-disposal solid samples collected at neutral and alkaline pH ranges and column solid residue core samples were analysed by XRD. Powder XRD is a standard analytical technique in mineralogy. XRD has been widely used in study of mineral assemblage resulting from acid mine environments and for synthesized acid mine drainage oxides (Bigham *et al* 1990; Murad *et al*., 1994; Webster *et al*., 1998). Slow step scanning in combination with other techniques such as FTIR can allow identification of poorly crystalline iron oxide minerals (Murad *et al*., 1994).

XRD utilizes the fact that X-rays of similar wavelength (λ) to the distance between lattice planes in a crystal (d) are diffracted by the nuclei of atoms. At certain angles of incidence of the X-rays to the lattice planes (θ), the diffracted X-rays positively interfere, creating a peak in the detected signal. The angles at which this occurs are defined by the Braggs'law (equation A8):

$n\lambda=2d\sin\theta$……..……..……(A8)

If the angle of incidence θ and the wavelength λ are known, the spacing d of the reflecting atomic planes can be determined from the above equation. The lattice spacing is characteristic of the mineral, thus, the X-ray diffraction method can be used for the identification of minerals and for the analysis of mixtures of minerals. Tables of d-spacing have been compiled for most minerals.

XRD instruments produce charts of 2θ (abscissa) vs intensity (ordinate), i.e. peaks are shown against double the incident angle (i.e, incident +diffracted). Samples are powdered to ensure that the grains are randomly orientated.

The identification of minerals in this work was done by comparison with published d –spacing data and relative intensities for the major peaks (Joint Committee on Powder Diffraction Standards) manual (JCPDS, 1980) and X'pert Graphics and identify software.

A.8.1 Procedure

The solid residue samples were dried for 12 hours at 105^{o}C to remove the adsorbed water and ground to a fine powder. The fine powdered samples were then pressed into rectangular

aluminum sample holders using the back of an alcohol wiped spatula and then clipped into the instrument sample holder. The powder mounts were step-scanned at intervals of 0.02^{o} 2θ from 5^{o} to 85^{o} and counted for 0.5 seconds per step. A Phillips PANalytical instrument was used with a pw3830 x-ray generator operated at 40 kV and 25 mA University of Cape Town, Geology Department.

A.9 Fourier-Transform Infrared Spectrometry

Infrared spectrometry is a standard analytical tool that utilizes the fact that chemical bonds between unlike atoms can absorb IR light and cause vibrations of the bonds. The IR wavelength absorbed is characteristic of a particular bond in a particular molecule or mineral and can be measured by an FT-IR spectrometer. The different functional groups (SO_4^{2-}, OH^-, NO_3^-, O-Si-O) can be identified in unknown material by comparison with published charts.

Bond vibrations are of two main types; stretching vibrations in which the bond-length changes and bending (deformation) vibrations in which bond angles change. Most modern FT-IR instruments produce plots with wave number (units: cm^{-1}) on the abscissa and percent transmission (or absorbance) on the ordinate.

UNIVERSITY of the
WESTERN CAPE

The FT-IR analysis of all samples in this work were carried out on a Perkin Elmer 1600 series spectrophotometer in the range 4000 cm^{-1} and 200 cm^{-1}. The results were compared with published data for the purpose of identification of the functional groups.

A.10 Scanning Electron Microscopy Analysis (SEM).

A.10.1 Introduction

Fresh fly ash samples, fly ash/acid mine drainage and column solid residues were analysed with scanning electron microscopy in an attempt to understand the mineralogical changes occurring. Three signals were used during the analysis: secondary electrons, backscattered electrons and X-rays.

A.10.2 Electron beam-specimen interaction

Solid specimens subjected to electron beam excitation in a scanning electron microscope exhibit complex interaction with primary beam electrons which result in a variety of signals. To analyze a specimen visually one might choose to see the "picture" by collecting and displaying secondary or backscattered electrons among other signals. The interactions of the electron beam and the specimen may be classified in two groups elastic and inelastic. The elastic interaction results when the primary electron beam comes into close proximity with a specimen atom nucleus and bounds with negligible energy loss, the electrons so scattered are referred to as backscattered electrons. Inelastic interaction results when a primary electron beam collides with an electron from the specimen atom and loses significant energy to that atom, this causes the atom to ionize and electrons may be emitted as a result of that ionization, these electrons are referred to as the secondary electrons. The backscattered mode is useful for several applications. One is atomic number contrast, topographic contrast which maximizes the effect of straight line paths of these electrons. This results in shadowing effects unlike secondary electron mode where imaging is done around corners.

UNIVERSITY of the
WESTERN CAPE

A.11 Scanning electron microscopy-Energy dispersive spectroscopy X-ray analysis (SEM-EDX).

Characteristic x-ray emission is one process by which an atom may stabilize itself following ionization by the electron beam. It follows that their energy difference, emitted as x-radiation, is also a discrete quantity and is characteristic of the atom from which it is released. SEM-EDX analysis is based on the identification of radiation of a specific wavelength or energy for elemental analysis of the specimen since each element in the specimen has its characteristic wavelength and energy. EDX is useful in obtaining rapid quantitative analysis of an unknown sample.

Qualitative and quantitative analytical information obtained by SEM can be presented in several ways.

a) Analysis of a selected region of chemically homogeneous region such as a phase

b) Analysis of a part of a sample.

c) An analysis to determine the variation of composition within a region of the sample

This is normally accomplished by a spot analysis in which the electron beam is stopped and positioned on the point to be analyzed (considered a sampling volume of $1\mu m^3$). Alternatively this can be done by scanning an area (area analysis) within a chemically homogeneous region. Variation of chemical composition within a sample can be carried out by use of backscattered electron compositional imaging to identify regions of chemical homogeneity and then carry out spot analysis of these areas.

The volume analyzed is that region for which the x-rays which reach the detector are emitted and this depends on where the x-rays are generated (i.e., how far the electron beam penetrates the sample) and how strongly the x-rays are absorbed by the specimen on the way out. The volume therefore is going to depend on the electron beam energy, the average atomic weight of the sampling volume, the wavelength of the characteristic x-rays being studied, and the absorption coefficient of the specimen for these x-rays and the angle of incidence of the electrons on the surface. Of the x-rays emitted, more will probably come from near the surface than will be able to escape from deeper inside the specimen. The analysis is therefore not a uniformly representative of the whole sampling volume. Therefore the analysis of a bulk specimen is likely to come from a volume of about 1μm x 1μm x 1μm hence the likelihood of contribution from the bulky matrix in the specimen.

Further the quantitative energy dispersive analysis involves the determination of the actual elemental composition of a sample as a percent of the total detectable sample composition. This type of analysis would be very simple if the relative intensities of the spectral peaks obtained were equal to the relative abundance of the atoms of the corresponding elements in the specimen, in such a case the ratio of a peak's intensity to the sum of intensities of all peaks would equal that element's composition as a percent of the whole specimen. In reality this is not the case, peak intensity is not a direct measure of specimen composition. Several factors other than elemental abundance affect relative peak intensities. For example rate of x-ray production varies with atomic number such that heavy elements produce more x-rays than light elements and x-ray yield varies from one element to another because of differences in absorption and secondary fluorescence

The results are thus at best regarded as semi-quantitative and the results are used to better understand the complex mineralogical changes taking place on interaction of acid mine drainage with fly ash, interaction of solid residues with simulated acid mine water in presence of unreacted fly ash or ordinary Portland cement (OPC) over an extended period of time.

In this work backscattered electron imaging was used to identify regions of relative homogeneity and thereafter spot or area analysis done. The results were reported as percent content of the total per the volume analyzed.

Analysis was done on powder samples that had been oven dried at 105^{o}C for 12 hours and crushed to fine particles. The powder samples were sprinkled on a special glue mixed with carbon graphite and subsequently coated with carbon to produce sample conductance. The morphology of the samples was established by both the backscattered and secondary electron mode. Both the secondary and backscattered electron detector were operated at the following settings:

EHT: 2.93 A

Beam current: 20 kV which was enough to excite X-rays.

UNIVERSITY of the
WESTERN CAPE

A.12 Total elemental analysis by X-ray fluorescence spectroscopy (XRFS)

XRF utilizes the characterization of X-ray spectral information to determine the elemental composition of solid samples. X-ray spectra are created by the interaction of an X-ray source with the electrons of the sample atoms. The excitation source causes ejection of an inner shell electron from a sample atom, creating a vacancy in the electron shell and leaving the atom in an excited state. During de-excitation, an electron transition occurs from an outer shell to fill this vacancy. The change in energy associated with the transition takes the form of X-ray radiation, which is detected and analyzed. The electronic configuration for each element is unique and thus the atoms of an element produce a characteristic set of X-ray spectral lines for the elements in the portion of the sample undergoing excitation.

Wavelength dispersive XRF uses the rotation through a measured angle (2θ) of a crystal known interplanar spacing (d) to separate the X-ray energy of different wavelengths (λ) from the sample, in accordance with the Bragg equation: $n\lambda=2d\sin\theta$

where n is an integer denoting the spectral order. A proportional detector then measures the intensity of radiation at each wavelength as the analyzing crystal is rotated. The intensity is plotted against wavelength (or rotation angle) to produce a spectrum of peaks from which the elements in the sample are determined qualitatively, or quantitatively if the instrument is calibrated for each element.

Major elements, Fe, Mn, Ti, Ca, K, S, P, Si, Al, Mg and Na were determined using powder briquettes and reported in weight % oxide. All analysis were done at Stellenbosch University at the central analytical facility.

A.12.1 Procedure

Chemical analyses were done by XRFS on a Philips 1404 Wavelength Dispersive spectrometer, at the University of Stellenbosch. The spectrometer is fitted with a Rh tube, six analyzing crystals, namely: LIF200, LIF220, LIF420, PE, TLAP and PX1 and the detectors are a gas-flow proportional counter, scintillation detector or a combination of the two. The gas-flow proportional counter uses P10 gas, which is a mixture of 90% Argon and 10% Methane. Major elements were analysed on a fused glass bead at 50 kV and 50 am tube operating conditions and trace elements were analyzed on a powder briquette at 60 kV and 40 mA tube operating conditions. Matrix effects in the samples were corrected for by applying theoretical apha factors and measured line overlap factors to the raw intensities measured with the SuperQ Philips software. Standards that were used in the calibration procedures for both major and trace element analyses are as follows: AGV-1 (Andesite from USGS), BHVO-1 (Basalt from USGS), JG-1 (Granodiorite from GSJ), JB-1 (Granodiorite from GSJ), GSP-1 (Granodiorite from USGS), SY-2 (Syenite from CCRMP), SY-3 (Syenite from CCRMP), STM-1 (Syenite from USGS), NIM-G (Granite from MINTEK), NIM-S (Syenite from MINTEK), NIM-N (Norite from MINTEK), NIM-P (Pyroxenite from MINTEK), NIM-D (Dunite from MINTEK), BCR (Basalt from USGS), GA (Granite from CRPG), GH (Granite from CRPG), DRN (Diorite from A NRT), and BR (Basalt from CRPG).

UNIVERSITY of the WESTERN CAPE

A.13 Geochemical modeling of the Fly Ash and Acid Mine Drainage Interactions

Geochemical modeling is a powerful tool for evaluating geochemical processes. When properly applied modeling can provide valuable insights into processes controlling the release, transport and fate of contaminants in surface water environments. Several computer codes are available for modeling, these include WATEQ4F (Ball and Nordstrom, 1991), MINTEQA2 (Allison *et al*., 1991) and PHREEQC (Parkhurst, 1995). All these computer codes perform the following type of calculations using chemical analysis of aqueous samples as input, temperature and pH. The geochemical code PHREEQC was used in this work. PHREEQC simulates chemical reactions and transport processes in natural as well as polluted waters. The WATEQ4F database supplied with the PHREEQC computer code was used for the calculations.

A.13.1 Saturation Indices (SI) and Solubility Equilibria

The saturation index (SI) is used to describe the extent to which a particular solution is supersaturated or under saturated with respect to a particular solid phase. Saturation index only indicates what would happen thermodynamically; it does not indicate the rate at which the process will proceed. A mineral having a saturation index less than zero may dissolve very slowly or not at all depending on the kinetics of the reaction (Drever, 1997). If the saturation index is greater than zero, the mineral might precipitate but cannot dissolve. If the saturation index is close to zero, the mineral may not be reacting at all or may be reacting reversibly, which means the mineral could be dissolving or precipitating. Hence the SI is an important tool in the geochemical interpretation of water chemistry. The saturation indices and activities utilized in this work were calculated using PHREEQC computer code using the formula:

$$SI = \log\left[\frac{IAP}{K_{eq}}\right] \quad \text{.....(A9)}$$

where *IAP* is the ion activity product calculated from measured solution concentrations after activity and speciation calculations were performed, K_{eq} is the equilibrium constant.

UNIVERSITY of the WESTERN CAPE

Appendix B: Analytical, saturation indices and XRD analysis data.

This section presents the data generated from analysis of aqueous samples by the analytical techniques presented in Appendix A, the saturation indices data generated using PHREEQC, the XRD graphics and summarized graphic trends of leachate pH with drainage, of the leached column solid cores.

Concentration of final process water at different FA: AMD ratios for reactions using Matla fly Ash (mg/L) (n=3)

Tables B1-B3 presents the clean-up efficiency of Matla fly ash for different acid mine drainage samples at different FA: AMD ratios and pH

Table B1: Concentration of contaminants at different FA: AMD ratio for Matla flies ash and Brugspruit AMD reactions

												DWAF Lmits	
FA: AMD	AMD		1:3.5		1:5		1:8		1:20		1:30		Irrigation	Domestic use
elements	ave	SD	ave	SD	ave	SD	ave	SD	ave	SD	ave	SD		
B	2.29	0.221	1.92	0.123	2.79	0.004	5.93	0.57	6.12	0.59	4.48	1.35	0.5	0-0.5
Na	4137.99	233.007	1482.34	50.64	1561.34	55.04	1580.24	45.5	3034.67	80.84	2394.18	100.4	70	100
Mg	388.65	19.707	0.24	0.021	1.46	0.21	0.833	0.021	297.04	21.4	236.86	25.3		30
Al	60.04	2.886	0.15	0.003	0.99	0.06	2.44	0.25	0.153	0.011	0.32	0.015		
Si	69.73	3.495	0.82	0.013	2.65	0.28	3.29	0.201	13.99	2.91	16.72	1.25		
K	52.59	3.634	20.21	3.74	21.26	1.34	15.54	2.5	45.33	5.69	37.53	5.43		50
Ca	842.11	117.44	546.89	60.34	478.65	20.56	793.38	30.58	877.22	20.56	635.68	30.98		32
Cr	0.77	0.067	0.5	0.034	0.526	0.023	0.375	0.028	0.525	0.021	0.176	0.022		
Mn	31.58	1.481	0.028	0.002	0.066	0.013	0.026	0.002	0.339	0.004	6.24	0.65		
Fe	250.84	11.203	2.62	0.421	3.497	0.251	0.853	0.037	4.23	0.15	3.52	0.15		
Ni	2.35	0.127	0.031	0.002	0.051	0.002	0.194	0.022	0.332	0.002	0.602	0.021	0.2	0-0.02
Co	1.15	0.063	0.001	0.0005	0.002	0.0005	0.004	0.00057	0.017	0.001	0.115	0.002	0.05	0-0.05
Cu	0.11	0.011	0.031	0.001	0.04	0.002	0.049	0.003	0.044	0.002	0.045	0.0015	0.2	1
Zn	9.52	0.491	1.13	0.052	9.19	1.19	16.44	3.45	1.21	0.05	5.047	0.035	1	3
As	0.11	0.004	0.004	0.001	0.006	0.001	BDL		0.014	0.002	0.007	0.002		
Se	0.032	0.006	0.072	0.003	0.054	0.003	0.054	0.018	0.04	0.015	0.017	0.001		
Sr	1.046	0.057	13.86	2.54	9.539	2.31	9.23	2.68	10.23	1.58	5.71	0.32		
Mo	0.036	0.0037	0.219	0.002	0.181	0.011	0.16	0.004	0.134	0.013	0.092	0.003	0.01	0-0.05
Cd	0.012	0.0007	0.002	0.0004	0.002	0.001	0.003	0.00035	0.001	0.0005	0.002	0.0005		
Ba	0.148	0.0147	0.569	0.005	0.684	0.026	0.626	0.058	0.579	0.026	0.432	0.015		
Pb	0.178	0.02	0.015	0.002	0.017	0.002	0.018	0.003	0.011	0.005	0.013	0.001		
SO4	6165	10	6137	7	5668.03	47.53	4601.77	3.37	7182.96	7.46	3709.80	58.99		
Cl	720	22.3	385.28	19.5	285.52	6.8	276.15	20.3	449.73	15.8	326.12	19.2		
pH	2.55	0.12	9.16	0.04	9.73	0.13	12.04	0.05	12.64	0.14	12.62	0.12		6-9

Ave=average, SD=standard deviation

UNIVERSITY of the WESTERN CAPE

Table B2: Concentration of contaminants at different FA: AMD ratio for Matla flies ash and Navigation AMD reactions

FA: AMD	AMD		1:3		1:2.5		1:2		1:1.5		DWAF Limits	
elements	ave	SD	ave	SD	ave	SD	ave	SD	ave	SD	Irrigation	Domestic use
B	1.37	0.163	23.44	3.44	24.38	2.56	17.57	2.356	17.86	3.456	0.5	0-0.5
Na	358.72	2.946	71.76	10.23	72.53	9.87	68.21	10.12	62.02	21.8	70	100
Mg	2661.67	35.008	636.85	80.45	618.06	70.8	200.04	34.5	1.5	0.02		30
Al	1068.09	11.279	2.85	0.05	3.26	0.35	2.35	0.56	9.41	1.97		
Si	82.01	1.238	4.39	0.52	2.05	0.003	2.3	0.16	1.09	0.03		
K	23.03	2.856	16.27	2.45	19.45	1.56	14.87	2.35	10.33	2.45		50
Ca	653.33	10.626	368.19	23.8	495.11	20.45	448.53	19.67	477.92	35.63		32
Cr	1.11	0.009	0.069	0.003	0.163	0.013	0.141	0.001	0.083	0.015		
Mn	226.25	4.742	56.65	5.68	5.15	0.456	1.11	0.005	0.133	0.005		
Fe	5599.92	80.862	293.3	19.57	52.25	6.78	43.23	4.578	4.7	0.67		
Ni	6.95	0.018	0.58	0.04	0.134	0.002	0.088	0.004	0.051	0.001	0.2	0-0.02
Co	4.3	0.105	0.312	0.012	0.014	0.001	0.019	0.003	0.002	0.0015	0.05	0-0.05
Cu	0.355	0.007	0.045	0.003	0.055	0.011	0.073	0.005	0.034	0.006	0.2	1
Zn	48.99	30.624	1.3	0.012	1.2	0.05	1.26	0.02	0.736	0.012	1	3
As	0.193	0.012	0.003	0.0005	0.005	0.0015	0.003	0.0005	0.004	0.001		
Se	0.032	0.002	0.037	0.002	0.026	0.003	0.052	0.001	0.112	0.003		
Sr	7.69	0.226	15.71	1.34	17.18	2.543	14.48	2.87	17.72	1.48		
Mo	0.04	0.002	0.025	0.002	0.622	0.002	0.665	0.002	0.77	0.04	0.01	0-0.05
Cd	0.032	0.001	0.003	0.0015	0.004	0.001	0.003	0.0015	0.002	0.0004		
Ba	0.209	0.002	0.369	0.003	0.347	0.032	0.336	0.034	0.319	0.013		
Pb	0.314	0.107	0.019	0.002	0.041	0.004	0.0301	0.005	0.0154	0.0021		
SO4	11949.6	61.5	5483.3	14.9	2414.3	28.1	2508.1	247.6	4570.7	110.3		
NO3	163.17	10.01	68.43	7.82	23.69	5.34	<0.1	0	93.44	10.21		
Cl	729.27	100.1	65.8	3.21	63.168	6.21	44.744	3.03	88.172	9.65		
pH	2.69	0.21	6.33	0.15	8.72	0.62	9.47	0.43	12.1	0.18		6-9

UNIVERSITY of the WESTERN CAPE

Table B3: Concentration of contaminants at different FA: AMD ratio for Matla flies ash and Bank AMD reactions

											DWAF Limits	
FA: AMD	AMD		1:3		1:2		1:1.5		1:1		Irrigation	Domestic use
elements	ave	SD	ave	SD	ave	SD	ave	SD	ave	SD		
B	1.51	0.081	15.02	2.23	24.58	4.23	18.22	3.65	3.19	0.05	0.5	0-0.5
Na	399.96	21.304	116.02	10.61	127.98	15.68	127.36	12.56	133.98	20.65	70	100
Mg	2844.17	148.053	891.27	50.78	434	20.45	2.29	0.22	0.382	0.001		30
Al	1140.06	61.582	0.476	0.025	0.587	0.006	7.79	0.36	0.559	0.021		
Si	87.77	5.866	1.32	0.015	2.53	0.15	1.14	0.021	0.824	0.032		
K	19.34	4.205	11.26	3.521	2.98	0.23	8.37	0.534	8.19	0.121		50
Ca	1012.25	75.883	289.06	30.63	464.15	36.75	409.45	25.56	439.38	20.65		32
Cr	1.15	0.106	0.186	0.016	0.05	0.004	0.063	0.002	0.107	0.002		
Mn	242.33	12.973	2.66	0.05	0.297	0.003	0.049	0.003	0.052	0.002		
Fe	6115.87	327.503	2.249	0.013	0.41	0.06	2.08	0.02	1.89	0.04		
Ni	7.96	1.155	0.118	0.003	0.215	0.002	0.032	0.001	0.075	0.003	0.2	0-0.02
Co	4.57	0.322	0.003	0.0005	0.002	0.0001	0.002	0.0004	0.002	0.0004	0.05	0-0.05
Cu	0.344	0.018	0.031	0.001	0.03	0.002	0.019	0.003	0.022	0.001	0.2	1
Zn	17.66	0.651	0.469	0.016	0.412	0.006	2.18	0.02	0.689	0.006	1	3
As	0.074	0.008	0.017	0.001	0.003	0.0005	0.005	0.0003	0.003	0.0002		
Se	0.033	0.006	0.029	0.004	0.101	0.001	0.129	0.005	0.111	0.001		
Sr	8.39	0.435	11.28	3.61	12.87	2.13	15.69	1.29	29.23	3.57		
Mo	0.044	0.003	0.472	0.025	0.76	0.04	0.859	0.006	0.86	0.015	0.01	0-0.05
Cd	0.03	0.002	0.001	0.0002	0.002	0.0002	0.003	0.0003	0.003	0.0004		
Ba	0.189	0.010	0.225	0.004	0.253	0.001	0.436	0.001	0.96	0.005		
Pb	0.175	0.0003	0.023	0.001	0.027	0.003	0.012	0.0004	0.019	0.002		
SO4	14949.69	100.100	3737.6	60.8	7275.5	120.5	1813.48	30.5	1774.22	20.3		
NO3	41.55	5.700	17.92	4.5	46.08	3.7	14.058	2.3	30.558	6.1		
Cl	265.92	10.600	35.84	3.9	119.04	3.21	40.612	7.3	77.784	11.6		
pH	2.5	0.3	8.7	0.42	9.08	0.23	11.78	0.46	12.32	0.25		6-9

UNIVERSITY of the WESTERN CAPE

Analytical Data for FA: AMD reactions 1:3, 1:1.5 for Matla fly ash and Navigation AMD reactions.

Table B4: Concentration (mg/L) with reaction time for 1:3 FA: AMD ratio (n=3)

reaction time	AMD		1 mins		3 mins		10 mins		15 mins		30 mins		60 mins		90 mins		150 mins	
Elements	ave	SD	ave	SD	ave	SD	ave	SD	ave	SD	ave	SD	ave	SD	ave	SD	ave	SD
B	10.3	1.26	27.48	3.45	29.46	2.65	37.41	5.4	34.31	6.54	35.93	5.87	33.20	3.68	28.76	5.79	35.59	7.52
Na	102.93	10.56	114.31	9.78	113.29	8.97	125.50	9.76	128.32	8.75	123.75	3.78	117.17	9.72	106.74	10.56	114.67	11.65
Mg	399.35	30.67	554.17	17.6	662.88	21.6	777.39	21.6	819.66	18.67	874.16	13.79	899.87	21.78	870.34	20.67	1034.16	23.45
Al	453.38	17.85	58.44	9.8	154.78	5.78	79.18	6.7	45.17	2.34	11.54	4.56	2.04	0.41	2.28	0.078	2.46	0.546
Si	99.16	9.43	52.18	6.7	74.64	6.4	77.19	3.9	65.26	4.58	47.64	3.78	17.22	2.57	12.38	1.28	12.54	2.35
K	BDL		BDL		BDL		76.07	7.91	BDL		BDL		12.35	4.73	12.68	3.47	19.96	3.68
Ca	146.91	12.45	174.21	13.5	328.40	10.6	443.75	15.67	458.06	19.68	472.63	19.07	519.82	20.75	476.31	17.56	498.67	23.45
Cr	BDL		BDL		BDL		0.639	0.031	BDL		BDL		BDL		BDL		BDL	
Mn	95.8	7.89	73.79	6.2	93.02	7.6	103.41	9.01	100.53	7.75	103.98	6.78	103.23	7.34	99.78	6.78	100.80	7.67
Fe	6576.97	56.89	5014.94	56.7	5378.24	38.9	5798.30	43.78	5623.35	38.9	5573.33	45.78	5362.42	50.67	5112.65	54.35	3572.18	34.57
Ni	6.16	1.23	5.44	0.86	4.99	0.78	10.85	2.17	6.91	1.1	7.32	0.69	6.95	0.387	7.01	0.254	4.53	0.546
Co	2.49	0.567	1.95	0.34	2.48	0.21	2.75	0.345	2.69	0.067	2.68	0.023	2.55	0.056	2.50	0.021	2.00	0.022
Cu	7.10	2.135	2.61	0.213	2.24	0.004	2.14	0.12	2.09	0.034	1.91	0.012	0.605	0.025	0.362	0.002	0.351	0.001
Zn	15.71	3.456	10.91	1.56	14.18	2.35	14.92	2.113	13.37	1.07	10.35	2.104	4.20	1.05	4.42	1.03	1.87	0.035
As*	BDL		0.021	0.001	0.024	0.002	0.006	0.002	BDL		0.001	0.0005	0.005	0.001	0.005	0.001	0.001	0.0003
Se	0.390	0.023	0.178	0.002	0.119	0.004	0.022	0.001	0.027	0.002	BDL		BDL		0.038	0.002	0.035	0.001
Sr	1.95	0.021	5.55	0.55	9.02	1.06	9.88	2.11	9.47	2.19	10.25	0.14	11.12	2.57	12.34	2.14	11.99	1.112
Mo	0.014	0.002	0.037	0.002	0.027	0.03	0.049	0.014	0.057	0.003	0.112	0.001	0.208	0.002	0.134	0.002	0.190	0.005
Ba	0.108	0.003	0.081	0.02	0.044	0.001	0.133	0.001	0.128	0.002	0.118	0.002	0.154	0.003	0.179	0.005	0.181	0.001
Pb	0.455	0.022	0.080	0.001	0.014	0.002	0.012	0.001	0.059	0.005	0.005	0.001	0.008	0.001	0.005	0.002	0.005	0.002
Cl	370	55.6	304		226.68		145		155		135		2240		280		175	
NO3	90	20.3	270		160.01		85		BDL		BDL		45		85		BDL	
SO4	24880	96.7	15390	100.5	22347.784	65.4	19445	103.2	20605	68.4	19490	19.8	17305	150.3	17535	200.5	16940	100.6
pH	2.78	0.01	3.96	0.02	4.17	0.01	4.66	0.03	4.92	0.1	5.28	0.2	6.02	0.01	5.53	0.01	6.1	0.01
Acidity	14450	50.6	11200	33.5	10850	60.8	11600	90.2	10725	22.5	10100	33.4	9725	20.6	9250	70.4	7350	60.5
EC(mS/cm)	15.5	0.01	13.87	0.2	13.96	0.12	13.16	0.05	11.95	0.41	11.44	0.03	10.94	0.06	10.79	0.01	9.52	0.02
Fe2+	4444.91	59.8	4801.94	10.6	4636.89	300.6	4309.5	400.2	4429.86	250.4	4260.79	360.5	4162.37	399.2	3987.95	321.5	2917.3	201.7

UNIVERSITY of the WESTERN CAPE

Table B4: continued…..

	210 mins		270 mins		300mins		360 mins		420mins		480 mins		720 mins		1440 mins	
Elements	ave	SD	ave	SD	ave	SD	ave	SD	ave	SD	ave	SD	ave	SD	ave	SD
B	39.62	3.79	38.42	4.87	38.674	5.67	36.100	5.73	41.040	5.73	34.677	2.356	20.819	3.14	18.912	4.31
Na	108.40	10.66	105.21	8.98	107.623	10.11	103.666	12.34	105.701	13.74	97.280	11.45	90.726	7.89	98.626	9.35
Mg	1038.85	30.12	1125.31	25.68	1131.572	32.17	1177.101	34.76	1459.809	25.65	1406.134	27.84	1268.123	26.79	991.905	21.54
Al	1.08	0.05	1.69	0.06	0.646	0.005	1.206	0.003	0.593	0.002	0.356	0.001	0.358	0.002	0.166	0.015
Si	11.01	1.04	6.71	0.98	6.041	1.06	5.976	0.16	3.061	0.14	2.276	0.055	0.233	0.001	0.853	0.003
K	17.00	2.65	21.93	1.76	22.803	1.56	23.026	3.56	22.000	2.88	19.837	1.3	16.986	3.58	18.017	1.98
Ca	461.59	21.6	447.02	18.97	450.200	14.57	461.894	12.78	364.162	14.57	357.255	16.77	418.519	10.99	314.418	13.76
Cr	BDL		BDL		BDL		BDL		BDL		BDL		0.005	0.001	0.007	0.002
Mn	94.22	8.79	88.04	9.87	92.459	10.65	93.875	9.98	66.313	7.83	63.625	6.34	6.341	0.041	1.179	0.023
Fe	2859.90	35.67	1912.14	37.89	1958.057	37.28	2091.935	27.57	262.551	13.77	358.840	11.13	3.035	0.002	2.628	0.013
Ni	3.27	0.254	2.31	0.15	2.693	0.128	1.736	0.201	0.217	0.005	0.275	0.004	BDL		BDL	
Co	1.68	0.023	1.25	0.041	1.396	0.046	1.381	0.001	0.345	0.002	0.384	0.002	0.010	0.001	0.003	0.001
Cu	0.359	0.005	0.023	0.013	0.003	0.001	0.006	0.001	0.012	0.001	0.003	0.001	0.019	0.002	0.008	0.002
Zn	1.48	0.015	0.783	0.023	0.769	0.004	0.877	0.023	0.407	0.003	0.360	0.51	0.348	0.003	0.192	0.001
As*	0.004	0.001	0.001	0.0003	0.001	0.0003	0.001	0.0005	0.001	0.0003	BDL		0.001	0.0005	0.002	0.001
Se	0.036	0.002	0.032	0.002	0.048	0.002	0.031	0.001	0.020	0.002	0.037	0.003	0.075	0.002	0.146	0.003
Sr	11.87	1.254	12.80	1.45	13.314	2.16	13.569	3.15	14.569	0.61	14.816	1.47	12.376	1.59	13.535	2.135
Mo	0.195	0.003	0.163	0.001	0.147	0.004	0.138	0.002	0.190	0.001	0.136	0.002	0.400	0.002	0.834	0.003
Ba	0.163	0.001	0.142	0.002	0.135	0.001	0.136	0.004	0.140	0.002	0.135	0.001	0.100	0.013	0.112	0.001
Pb	0.012	0.001	0.002	0.001	BDL		0.001	0.0003	0.002	0.001	0.001	0.0005	0.004	0.001	0.002	0.001
Cl	125		86.25		92.5	11.1	65	6.4	73.33	9.8	75	3.2	60	5.6	65	7.3
NO3	25		BDL		25		BDL		BDL		57.5		BDL		BDL	
SO4	14400	80.5	12858.75	60.2	11037.5	85.4	11812.5	20.6	8755.79	101.2	6565	65.5	8355	45.6	5365	30.2
pH	5.9	0.05	6.32	0.03	6.19	0.08	6.22	0.01	6.86	0.05	6.95	0.54	8.49	0.85	9.12	0.05
Acidity	4900	70.1	2925	26.5	2825	22.3	3325	100.4	575	28.6	600	13.4	75	7.4	150	11.8
EC(mS/cm)	8.79	0.04	6.26	0.01	6.1	0.11	7.92	0.22	7.43	0.13	7.22	0.02	6.85	0.01	4.8	0.05
Fe2+	2400.87	165.7	1522	139.8	1663.57	120.4	1865.86	68.7	349.39	54.7	315.05	68.2	0.904	0.189	0.91	0.126

Ave=average, SD=standard deviation

Table B5: Concentration (mg/L) with reaction time for 1:1.5 FA: AMD ratio (n=3)

reaction time	AMD		1min		3mins		10mins		30mins		60mins		90mins	
Elements	ave	SD	Ave	SD	Ave	SD	Ave	SD	Ave	SD	Ave	SD	Ave	SD
B	10.295	1.26	9.882	0.021	16.073	2.31	19.077	3.330	17.567	2.540	36.977	3.21	42.511	2.63
Na	102.932	10.56	134.141	5.76	156.692	13.05	157.300	14.52	148.542	12.01	126.487	13.46	130.090	10.12
Mg	399.352	30.67	729.934	1.91	940.568	20.56	986.698	25.02	968.065	30.61	1064.221	31.46	1200.941	27.81
Al	453.377	17.85	140.102	4.578	75.024	3.87	14.155	2.560	13.434	1.970	1.905	0.102	1.665	0.013
Si	99.159	9.43	87.010	4.53	95.600	6.54	75.508	5.79	77.641	3.98	12.459	1.46	14.501	3.41
K	ND		ND		93.729	3.54	42.061	2.34	115.430	5.32	2.617	0.21	9.231	0.650
Ca	146.907	12.45	1023.433	12.67	427.116	14.56	302.537	10.89	417.009	7.65	453.378	10.31	481.261	7.89
Cr	ND		ND		ND		0.191	0.001	ND		ND		ND	
Mn	95.797	7.89	86.846	5.76	108.274	7.56	106.641	9.45	105.908	11.14	96.112	6.32	98.118	5.48
Fe	6576.965	56.89	4547.307	30.51	5706.496	40.45	4673.637	28.96	5134.391	30.67	3141.926	21.63	2218.271	20.65
Ni	6.157	1.23	1.178	0.011	3.103	0.002	2.288	0.007	2.721	0.001	2.099	0.012	1.439	0.032
Co	2.487	0.567	2.393	0.012	2.970	0.003	2.962	0.002	2.750	0.002	1.772	0.015	1.359	0.023
Cu	7.103	2.135	8.969	1.03	7.793	1.302	7.893	1.101	7.550	0.431	0.729	0.013	0.782	0.017
Zn	15.712	3.456	13.744	2.02	15.630	2.103	11.291	2.301	10.054	1.461	1.368	0.004	1.606	0.014
As	ND		0.030	0.002	0.091	0.002	0.057	0.002	0.077	0.002	0.028	0.002	0.014	0.011
Se	0.390	0.023	1.658	0.013	ND		0.603	0.002	0.694	0.003	0.050	0.001	0.162	0.002
Sr	1.945	0.021	14.532	1.48	12.117	1.11	10.845	2.103	11.415	2.102	11.633	2.103	11.912	1.11
Mo	0.014	0.002	0.056	0.013	0.107	0.002	ND		0.118	0.001	0.339	0.003	0.307	0.003
Ba	0.108	0.003	0.368	0.004	0.530	0.005	0.045	0.001	1.140	0.005	0.104	0.002	0.159	0.004
Pb	0.455	0.022	0.114	0.001	0.255	0.002	0.181	0.001	0.164	0.002	0.016	0.001	0.013	0.001
Cl	370	20.1	125	13.900	55	3.200	75	6.700	135	11.400	120	12.600	85	7.700
NO3	90	10.3	30	11.700	65	4.810	20	2.540	ND		385	30.500	220	20.300
PO4	ND		130	20.700	ND		ND		ND		ND		95	6.200
SO4	24880		21840		20780		19035		18095		16520		13360	
pH	2.19	0.02	4.17	0.03	4.45	0.26	5.49	0.03	5.69	0.02	6.45	0.11	6.32	0.04
Acidity	14450		12175		11525		11175		10525		6475		5325	
EC(mS/cm)	15.77	1.21	11.36	0.05	10.63	0.02	9.16	0.11	8.81	0.02	7.6	0.05	7.67	0.03
Fe2+	4444.91	187.9	4405.3	300.6	4777.2	235.6	4030.96	200.1	3876	120.6	2327	90.8	1800	110.2

UNIVERSITY of WESTERN CAPE

Table B5: continued……

reaction time	150mins		210mins		300mins		360mins		480mins		720mins		1440mins	
Elements	Ave	SD	Ave	SD	Ave	SD	Ave	SD	Ave	SD	Ave	SD	Ave	SD
B	29.037	1.38	24.118	1.42	18.234	2.34	17.420	3.42	17.015	3.45	16.393	3.42	14.167	3.21
Na	118.402	9.86	108.608	10.24	102.082	6.89	108.250	7.89	96.171	8.45	101.279	7.68	95.908	6.78
Mg	836.357	23.45	349.595	30.42	849.643	21.36	427.468	23.67	308.518	22.31	137.295	21.35	10.873	1.21
Al	0.185	0.00	0.162	0.002	0.400	0.005	1.612	0.012	0.384	0.004	0.236	0.002	0.608	0.002
Si	1.038	0.00	1.165	0.004	0.971	0.023	2.841	0.001	1.188	0.011	0.937	0.007	1.173	0.003
K	19.790	2.31	16.595	3.45	12.198	2.51	13.152	2.311	11.717	1.37	12.658	1.31	9.365	0.98
Ca	539.498	10.75	540.952	20.75	394.706	19.71	412.243	20.123	425.376	24.16	454.476	21.05	462.773	20.13
Cr	ND		ND		ND		ND		ND		ND		0.011	0.001
Mn	1.948	0.005	0.358	0.003	1.721	0.021	0.435	0.003	0.276	0.004	0.136	0.003	0.008	0.002
Fe	1.801	0.001	1.550	0.003	2.194	0.014	1.845	0.012	1.434	0.013	1.458	0.006	1.542	0.012
Ni	0.012	0.001	0.011	0.001	0.018	0.003	0.015	0.002	0.009	0.002	0.008	0.002	0.007	0.002
Co	0.006	0.002	0.001	0.001	0.002	0.001	0.002	0.001	ND		ND		ND	
Cu	0.008	0.001	0.018	0.002	0.013	0.002	0.012	0.002	0.009	0.003	0.015	0.001	0.034	0.003
Zn	0.195	0.002	0.111	0.001	0.203	0.001	0.140	0.004	0.131	0.001	0.100	0.005	0.087	0.013
As	0.002	0.001	0.003	0.001	0.003	0.001	0.003	0.001	0.002	0.001	0.003	0.001	0.004	0.001
Se	0.140	0.003	0.210	0.005	0.114	0.011	0.285	0.015	0.250	0.006	0.357	0.021	0.539	0.013
Sr	10.181	1.006	10.555	1.503	11.952	2.150	13.763	2.540	14.628	2.301	16.799	3.211	17.303	2.301
Mo	1.015	0.001	1.014	0.011	0.590	0.050	0.736	0.016	0.800	0.035	0.901	0.006	1.055	0.023
Ba	0.137	0.003	0.162	0.002	0.140	0.020	0.187	0.012	0.152	0.002	0.087	0.001	0.177	0.015
Pb	0.002	0.001	0.002	0.001	0.005	0.002	0.006	0.002	0.005	0.002	0.002	0.001	0.013	0.001
Cl	40	10.600	20	11.300	23	2.100	23	3.400	17	1.200	81	13.100	78	15.400
NO3	97.5	10.300	39	5.800	12	4.200	148	16.400	82	12.800	15	1.870	75	16.400
PO4	ND		16	3.800	ND		ND		ND		190		151	
SO4	5320		3178		5789	35.800	3796	80.200	3385	120.300	10272	60.500	8104	250.200
pH	8.92	0.38	9.16	0.02	8.7	0.04	9.14	0.03	9.15	0.15	9.2	0.04	9.88	0.02
Acidity	ND		ND		ND		ND		ND		ND		ND	
EC(mS/cm)	4.52	0.02	3.16	0.03	4.5	0.01	4.12	0.2	3.7	0.02	3.12	0.03	1.95	0.03
Fe^{2+}	ND	ND	ND	ND	ND	ND	ND	ND	ND	ND	ND	ND	ND	ND

UNIVERSITY of the WESTERN CAPE

Table B6: Concentration in mol/L and Mol_c/L for FA: AMD ratios of 1:3 for Matla fly ash and Navigation AMD.

reaction time	1 mins		3 mins		10 mins		30 mins		60 mins		90 mins		150 mins		210 mins		300 mins		480 mins		1440 mins	
Elements	mol/L	mol_c/L	mol/L	mol_c/L	mol/L	mol_c/L	mol/L	mol_c/L	mol/L	mol_c/L	mol/L	mol_c/L	mol/L	mol_c/L	mol/L	mol_c/L	mol/L	mol_c/L	mol/L	mol_c/L	mol/L	mol_c/L
Na	4.972	4.972	4.928	4.928	5.459	5.459	5.383	5.383	5.096	5.096	4.643	4.643	4.988	4.988	4.715	4.715	4.681	4.681	4.231	4.231	4.290	4.290
Mg	22.796	45.592	27.268	54.536	31.978	63.956	35.959	71.918	37.017	74.033	35.802	71.604	42.540	85.081	42.734	85.467	46.548	93.095	57.842	115.684	40.802	81.605
Al	2.166	6.498	5.737	17.210	2.935	8.804	0.428	1.283	0.076	0.227	0.085	0.254	0.091	0.274	0.040	0.120	0.024	0.072	0.013	0.040	0.006	0.018
K	ND		ND	0.000	1.946	1.946	ND	0.000	0.316	0.316	0.324	0.324	0.510	0.510	0.435	0.435	0.583	0.583	0.507	0.507	0.461	0.461
Ca	4.347	8.693	8.194	16.387	11.072	22.143	11.792	23.584	12.970	25.939	11.884	23.768	12.442	24.884	11.517	23.034	11.233	22.465	8.914	17.827	7.845	15.690
Mn	1.343	2.686	1.693	3.386	1.882	3.765	1.893	3.785	1.879	3.758	1.816	3.632	1.835	3.669	1.715	3.430	1.683	3.366	1.158	2.316	0.021	0.043
Fe3+	3.814	11.441	13.274	39.822	26.657	79.970	5.596	16.788	21.488	64.464	20.138	60.414	11.726	35.177	8.219	24.656	5.273	15.818	0.784	2.352	0.031	0.092
Ni	0.093	0.185	0.085	0.170	0.185	0.370	0.125	0.249	0.118	0.237	0.119	0.239	0.077	0.154	0.056	0.111	0.046	0.092	0.005	0.009	ND	0.000
Co	0.033	0.066	0.042	0.084	0.047	0.093	0.045	0.091	0.043	0.087	0.043	0.085	0.034	0.068	0.028	0.057	0.024	0.047	0.007	0.013	0.000	0.000
Cu	0.041	0.082	0.035	0.070	0.034	0.067	0.030	0.060	0.010	0.019	0.006	0.011	0.006	0.011	0.006	0.011	0.000	0.000	0.000	0.000	0.000	0.000
Zn	0.167	0.334	0.217	0.434	0.228	0.457	0.158	0.317	0.064	0.129	0.068	0.135	0.029	0.057	0.023	0.045	0.012	0.024	0.006	0.011	0.003	0.006
Fe2+	85.979	171.958	83.024	166.048	77.163	154.325	76.290	152.580	74.528	149.056	71.405	142.810	52.235	104.469	42.988	85.976	29.786	59.573	5.641	11.282	0.016	0.033
Ba	0.001	0.001	0.000	0.001	0.001	0.002	0.001	0.002	0.001	0.002	0.001	0.003	0.001	0.003	0.001	0.002	0.001	0.002	0.001	0.002	0.001	0.002
Pb	0.000	0.001	0.000	0.000	0.000	0.000	0.000	0.000	0.000	0.000	0.000	0.000	0.000	0.000	0.000	0.000	0.000	0.000	0.000	0.000	0.000	0.000
Sr	0.063	0.127	0.103	0.206	0.113	0.226	0.117	0.234	0.127	0.254	0.141	0.282	0.137	0.274	0.135	0.271	0.152	0.304	0.169	0.338	0.154	0.309
total		252.636		303.282		341.582		276.274		323.616		308.204		259.619		228.330		200.122		154.613		102.548
As*	0.000	0.001	0.000	0.001	0.000	0.000	0.000	0.000	0.000	0.000	0.000	0.000	0.000	0.000	0.000	0.000	0.000	0.000	0.000		0.000	0.000
Se	0.002	0.004	0.002	0.003	0.000	0.001	0.000	0.000	0.000	0.000	0.000	0.001	0.000	0.001	0.000	0.001	0.001	0.001	0.000	0.001	0.002	0.004
Mo	0.000	0.001	0.000	0.001	0.001	0.001	0.001	0.002	0.002	0.004	0.001	0.003	0.002	0.004	0.002	0.004	0.002	0.003	0.001	0.003	0.009	0.017
Cl	8.575	8.575	6.394	6.394	4.090	4.090	3.808	3.808	63.188	63.188	7.898	7.898	4.937	4.937	3.526	3.526	2.609	2.609	2.116	2.116	1.834	1.834
NO3	4.354	4.354	2.580	2.580	1.371	1.371	0.000	0.000	0.726	0.726	1.371	1.371	0.000	0.000	0.403	0.403	0.403	0.403	0.927	0.927	ND	0.000
SO4	160.212	320.425	232.644	465.288	202.426	404.851	202.894	405.788	180.148	360.296	182.542	365.084	176.348	352.696	149.906	299.813	114.902	229.804	68.343	136.685	55.851	111.701
Cr	ND	0.000	ND	0.000	0.012	0.012	ND	0.000	ND	0.000	ND	0.000	ND	0.000	ND	0.000	ND	0.000	ND		0.000	0.000
total		333.360		474.267		410.326		409.599		424.213		374.357		357.638		303.747		232.821		139.732		113.556
	% error	-13.8	% error	-22	% error	-9.14	% error	-19.44	% error	-13.45	% error	-9.69	% error	-15.9	% error	-14.2	% error	-7.55	% error	6.18	% error	-5.09

As, Se and Mo were assumed to be existing as oxyanions carrying a charge of -2 for As, -2 for Se and –2 for Mo over the pH range investigated (Eary *et al*.,1990)

Table B7: Concentration in mol/L and Mol_c/L for FA: AMD ratios of 1:1.5 for Matla fly ash and Navigation AMD**.**

	1 min		3mins		10 mins		30mins		60mins		90mins		150mins		210mins		360mins	
Elements	mol/L	molc/L	mol/L		mol/L	molc/L	mol/L		mol/L		mol/L		mol/L		mol/L		mol/L	
Na	5.835	5.835	6.816	6.816	6.842	6.842	6.461	6.461	5.502	5.502	5.659	5.659	5.150	5.150	4.724	4.724	4.709	4.709
Mg	30.026	60.052	38.691	77.381	40.588	81.176	39.822	79.643	43.777	87.554	49.401	98.802	34.404	68.808	14.381	28.761	17.584	35.168
Al	5.193	15.578	2.781	8.342	0.525	1.574	0.498	1.494	0.071	0.212	0.062	0.185	0.007	0.021	0.006	0.018	0.060	0.179
K	ND	ND	2.397	2.397	1.076	1.076	2.952	2.952	0.067	0.067	0.236	0.236	0.506	0.506	0.424	0.424	0.336	0.336
Ca	25.535	51.069	10.657	21.313	7.548	15.097	10.404	20.809	11.312	22.624	12.007	24.015	13.461	26.921	13.497	26.994	10.286	20.571
Mn	1.581	3.161	1.971	3.942	1.941	3.882	1.928	3.855	1.749	3.499	1.786	3.572	0.035	0.071	0.007	0.013	0.008	0.016
Fe3+	2.543	7.628	16.639	49.918	11.507	34.522	22.532	67.595	14.591	43.774	7.489	22.468	0.032	0.097	0.028	0.083	0.033	0.099
Ni	0.020	0.040	0.053	0.106	0.039	0.078	0.046	0.093	0.036	0.072	0.025	0.049	0.000	0.000	0.000	0.000	0.000	0.001
Co	0.041	0.081	0.050	0.101	0.050	0.101	0.047	0.093	0.030	0.060	0.023	0.046	0.000	0.000	0.000	0.000	0.000	0.000
Cu	0.141	0.282	0.123	0.245	0.124	0.248	0.119	0.238	0.011	0.023	0.012	0.025	0.000	0.000	0.000	0.001	0.000	0.000
Zn	0.210	0.421	0.239	0.478	0.173	0.345	0.154	0.308	0.021	0.042	0.025	0.049	0.003	0.006	0.002	0.003	0.002	0.004
Fe2+	78.877	157.755	85.536	171.073	72.175	144.350	69.400	138.800	41.665	83.330	32.229	64.458	0.001	0.002	0.001	0.002	0.001	0.003
Ba	0.003	0.005	0.004	0.008	0.000	0.001	0.008	0.017	0.001	0.002	0.001	0.002	0.000	0.000	0.000	0.000	0.000	0.000
Pb	0.001	0.001	0.001	0.002	0.001	0.002	0.001	0.002	0.000	0.000	0.000	0.000	0.116	0.232	0.120	0.241	0.157	0.314
Sr	0.166	0.332	0.138	0.277	0.124	0.248	0.130	0.261	0.133	0.266	0.136	0.272						
		302.241		342.398		289.540		322.620		247.025		219.838		101.814		61.266		61.400
As	0.000	0.001	0.001	0.002	0.001	0.002	0.001	0.002	0.000	0.001	0.000	0.000	0.000	0.000	0.000	0.000	0.000	0.000
Se	0.021	0.042	0.000	0.000	0.008	0.015	0.009	0.018	0.001	0.001	0.002	0.004	0.002	0.004	0.003	0.005	0.004	0.007
Mo	0.001	0.001	0.001	0.002	0.000	0.000	0.001	0.002	0.004	0.007	0.003	0.006	0.011	0.021	0.011	0.021	0.008	0.015
Cl	3.526	3.526	1.551	1.551	2.116	2.116	3.808	3.808	3.385	3.385	2.398	2.398	1.128	1.128	0.564	0.564	0.649	0.649
NO3	0.484	0.484	1.048	1.048	0.323	0.323	ND	0.000	6.209	6.209	3.548	3.548	1.572	1.572	0.629	0.629	2.387	2.387
PO4	1.369	4.107	ND	0.000	ND	0.000	ND	0.000	ND	0.000	1.000	3.001	0.000	0.000	0.168	0.505	0.000	0.000
SO4	227.358	454.716	216.323	432.646	198.157	396.315	188.372	376.744	171.976	343.952	139.080	278.159	55.382	110.764	33.083	66.167	39.517	79.034
Cr	ND	ND	ND	0.000	0.004	0.004	ND	0.000	ND	0.000	ND	0.000	ND	0.000	ND	0.000	ND	0.000
		462.876		435.251		398.773		380.574		353.555		287.117		113.490		67.892		82.092
	% error	20.99	% error	11.94	% error	15.87	% error	8.26	% error	17.60	% error	13.27	% error	5.42	% error	5.13	% error	14.42

UNIVERSITY of the WESTERN CAPE

Column leachate concentration for elements analyzed with drainage volume (mg/L) (n=4)

Table B8. Analytical results for fly ash solid core

FA core	drainage 1		drainage 2		drainage3		drainage4		drainage 5		drainage6		drainage7		drainage8	
element	ave	SD	ave	SD	ave	SD	ave	SD	ave	SD	ave	SD	ave	SD	ave	SD
B	7.0674	1.8557	0.8574	0.5558	0.7273	0.4591	1.6012	0.1714	2.7532	0.5029	3.9601	0.6362	5.6466	0.2170	5.8206	2.6734
Na	118.2698	9.7266	51.5786	1.2157	53.5169	0.3220	42.9099	1.3052	36.8938	0.9194	28.9214	0.8708	22.2097	0.2775	35.2795	13.0306
Mg	0.0494	0.0073	6.7123	6.6119	8.2259	1.9158	20.7984	11.2136	45.4523	25.9647	76.4975	43.1354	119.6805	36.6399	171.5821	35.1073
Al	0.0529	0.0210	0.1890		9.0892	0.0122	9.3289	0.0351	0.1851	0.0936	0.5992	0.3536	3.1191	2.9036	27.7867	27.2199
Si	0.3808	0.1141	2.7602	0.1090	4.5712	0.0049	3.6212	0.0217	2.4736	0.4284	2.3761	0.1310	2.6697	0.5362	1.5201	0.7229
K	33.8033	6.3454	22.3686	6.4599	24.6490	1.0385	29.3176	2.6001	35.0059	2.5130	32.5926	0.2978	29.8925	0.0032	34.3381	0.9028
Ca	791.0666	47.3456	461.9414	16.8327	450.6306	11.6440	454.0242	7.0622	560.3429	14.8058	611.2601	9.2169	578.2663	13.2110	561.4901	22.9370
V	0.0108	0.0017	0.0485	0.0196	0.1166	0.0119	0.1292	0.0005	0.0744	0.0662	0.0572	0.0559	0.0512	0.0501	0.1166	0.0593
Cr	1.5773	0.6567	2.6357	0.6507	2.1065	0.8260	1.5367	0.4767	0.5425	0.3227	0.5440		0.3750	0.0000	0.1740	
Mn	0.0017	0.0008	0.0370		0.0089	0.0075	0.0074	0.0046	2.2433	2.2330	7.6037	7.5584	15.8426	15.4205	19.7041	17.4608
Fe	1.9703	0.2235	1.2690	0.1387	1.7055	0.1020	2.0999	0.1580	1.3125	0.1451	13.9875	12.3649	55.5168	54.0827	27.3181	25.4650
Ni	0.0109	0.0003	0.0076	0.0006	0.0040		0.0092	0.0025	0.0318	0.0000	0.0241	0.0136	0.0712	0.0630	0.6700	0.0000
Co	0.0012	0.0001	0.0005	0.0000	0.0012	0.0003	0.0011	0.0002	0.0022	0.0008	0.0124	0.0109	0.0267	0.0252	0.0670	0.0641
Cu	0.0144	0.0005	0.0089	0.0055	0.0178	0.0066	0.0106	0.0035	0.0135	0.0010	0.0209	0.0021	0.0189	0.0041	1.4805	1.4450
Zn	0.0636	0.0044	0.0681	0.0022	0.0685	0.0052	0.0730	0.0049	0.0711	0.0073	0.0735	0.0171	0.1159	0.0450	1.1548	1.0644
As	0.0016	0.0005	0.0020		0.0014	0.0003	0.0026	0.0003	0.0021	0.0005	0.0020	0.0012	0.0017	0.0006	0.0215	0.0177
Se	0.7001	0.1726	0.4983	0.0273	0.5911	0.0298	0.5546	0.0051	0.4913	0.0357	0.4417	0.0316	0.3744	0.0770	0.4651	0.0920
Sr	38.4559	3.6289	34.3746	0.5153	35.6963	0.4203	34.7508	0.9017	34.9391	0.8984	33.8694	0.0101	30.9578	0.3562	28.7975	0.8088
Mo	1.7171	0.0945	1.9618	0.3797	1.8231	0.1795	1.3855	0.0386	0.8460	0.0305	0.4211	0.1695	0.2850	0.1543	0.3080	0.0659
Cd	0.0031	0.0002	0.0036	0.0006	0.0037	0.0001	0.0039	0.0013	0.0018	0.0002	0.0014	0.0004	0.0011	0.0000	0.0024	0.0007
Ba	0.1010	0.0546	0.0132	0.0042	0.0171	0.0022	0.0084	0.0047	0.0407	0.0364	0.0689	0.0206	0.1006	0.0258	0.0850	
Pb	0.0260	0.0156	0.0000	0.0000	0.0000		0.0010		0.0008	0.0001	0.0002	0.0000	0.0006	0.0002	0.2847	0.2787
SO4	2070.5000	226.0000	1478.7500	101.7500	1674.3900	10.9100	1446.0600	74.6400	1485.1150	132.4350	2042.8750	512.1250	2015.2400	102.2600	2610.1250	176.1250
Cl	33.2500	12.2500	12.2500	0.2500	19.3300	8.0200	138.3550	1.0450	239.5200	1.0100	331.2650	71.2350	268.6050	0.1450	256.5000	11.5000
NO3	271.0000	7.5000	ND	0.0000	74.5000	38.0000	113.5500	12.8500	75.1000	3.0000	63.6000	13.9000	28.1000	27.5000	70.6250	10.6250
PO4	ND		ND		ND		22.8500	1.3500	ND		ND		ND		14.3750	
alkalinity HCO3 (mg/L)	1479.6138	262.5000	297.4481	181.2500	137.2838	12.5000	75.5061	6.8750	50.3374	3.7500	38.1344	25.0000	74.7434		64.0658	
pH	12.0150	0.0150	10.0750	1.1950	9.1850	1.6150	9.1300	1.2200	8.6200	0.3600	6.6800	1.0800	6.2250	1.5150	6.5750	1.7550

UNIVERSITY of the WESTERN CAPE

Table B8 continued….

FA core	drainage9		drainage10		drainage11		drainage 12		drainage13		drainage 14		drainage 15		drainage 16	
element	ave	SD	ave	SD	ave	SD	ave	SD	ave	SD	ave	SD	ave	SD	ave	SD
B	12.860	1.131	17.735	2.090	15.411	12.527	18.664	3.300	24.175	0.996	26.194	0.479	15.387	0.867	12.048	9.996
Na	40.591	19.931	50.734	22.590	18.903	2.552	25.933	3.396	20.907	1.183	14.812	0.523	7.682	0.023	10.793	2.488
Mg	233.398	21.762	452.920	75.434	431.184	430.181	835.691	249.570	972.306	272.521	1222.741	191.172	993.974	80.504	1077.433	170.529
Al	5.943	5.595	5.172	4.953	0.091	0.057	18.109	15.968	34.012	22.227	77.968	46.807	83.347	52.136	290.826	
Si	3.587	1.797	1.038		1.249		2.979		2.570	0.518	6.231	1.128	6.718	1.247	5.051	4.489
K	30.257	3.363	20.523	10.037	22.463		11.505	1.138	22.487	0.012	21.308	0.902	4.300	2.849	BDL	
Ca	602.275	0.178	672.794	71.731	589.840		516.068	121.109	513.253	9.898	499.495	8.138	283.119	2.907	394.137	104.232
V	0.037	0.025	0.068	0.063	BDL		0.026	0.011	0.018	0.002	0.016		0.008	0.006	0.050	
Cr	0.130	0.050	0.000		BDL		BDL		BDL		BDL		BDL		BDL	
Mn	24.051	19.356	37.461	18.117	27.333	27.270	96.369	13.885	154.109	52.085	224.539	58.388	198.307	44.368	309.925	2.429
Fe	42.576	40.663	35.699	34.386	1.355	0.237	186.979	116.231	280.005	30.464	739.554	95.732	705.520	36.978	2378.258	909.831
Ni	2.095	2.016	0.277	0.250	0.088	0.048	0.382	0.112	0.384	0.088	0.727	0.180	0.654	0.149	1.717	0.151
Co	0.036	0.033	0.050	0.042	0.012	0.010	0.140	0.055	0.202	0.027	0.419	0.044	0.391	0.014	0.880	0.103
Cu	0.059	0.053	0.269	0.261	0.023	0.021	0.060	0.033	0.151	0.095	0.128	0.026	0.110	0.025	0.496	0.031
Zn	0.084	0.000	0.273	0.169	0.167	0.037	0.353	0.100	0.481	0.125	0.702	0.270	0.630	0.229	0.945	0.531
As	0.004	0.000	0.027	0.025	0.001	0.000	0.056	0.052	0.008	0.001	0.001	0.001	0.016	0.010	0.015	0.011
Se	0.254	0.073	0.234	0.081	0.190	0.076	0.145	0.008	0.294	0.012	0.098	0.015	0.181	0.007	0.241	0.203
Sr	27.584	2.437	26.118	2.376	10.687	10.557	23.246	2.148	20.966	0.446	20.286	1.221	12.515	0.727	21.434	2.021
Mo	0.299	0.029	0.303	0.013	0.107	0.101	0.061	0.040	0.023	0.013	0.065	0.040	0.030	0.015	0.082	0.027
Cd	0.002	0.001	0.003	0.001	0.001	0.000	0.003	0.000	0.003	0.001	0.007	0.002	0.011	0.000	0.011	0.007
Ba	0.089	0.054	0.101	0.007	0.154	0.058	0.354	0.280	0.101	0.004	BDL		BDL		BDL	
Pb		0.000	0.026	0.025	0.004	0.004	0.013	0.001	0.003	0.000	BDL		BDL		BDL	
SO4	2724.250	73.250	3113.125	161.875	5360.625	2569.375	4999.250	376.750	4194.500	189.500	9318.500	569.500	11357.500	57.500	15878.750	1103.750
Cl	343.000	37.000	173.750	7.500	119.375	25.625	85.750	18.250	ND		ND		ND		ND	
NO3	51.250	1.250	140.625	6.875	395.000	152.500	309.625	8.375	1328.500	332.500	410.000	0.000	368.000	31.000	453.750	21.250
PO4	ND		ND		ND		ND		ND		ND		ND		ND	
alkalinity HCO3 (mg/L)	91.523		112.878		45.761		ND		ND		ND		ND		ND	
pH	6.485	1.545	6.430	1.220	6.300	0.850	4.810	0.450	4.335	0.115	4.125	0.155	4.035	0.145	3.540	0.070

UNIVERSITY of the WESTERN CAPE

Table B9. Analytical results for solid residue core

SR core	drainage 1		drainage 2		drainage 3		drainage 4		drainage 5		drainage 6		drainage 7		drainage 8	
element	ave	SD	ave	SD	ave	SD	ave	SD	ave	SD	ave	SD	ave	SD	ave	SD
B	1.990	0.092	2.004	0.097	2.012	0.073	2.116	0.007	2.475	0.106	3.630	0.092	5.647	0.128	17.477	0.067
Na	271.717	6.743	61.336	4.272	25.015	0.934	19.054	0.439	16.116	0.263	13.843	0.264	22.210	0.253	12.210	0.273
Mg	4.590	1.202	3.993	1.315	5.059	0.278	4.356	0.123	4.692	0.069	9.644	0.920	119.680	5.203	291.843	6.408
Al	0.782	0.070	8.921	0.010	9.059	0.170	4.872	2.125	0.787	0.075	0.838	0.030	3.119	0.357	0.825	0.031
Si	1.667	0.232	1.249	0.110	1.092	0.098	1.192	0.085	1.190	0.050	1.153	0.015	2.670	0.031	1.662	0.035
K	107.688	0.502	85.317	2.267	55.475	2.961	42.639	1.420	36.355	0.931	31.174	1.229	29.892	0.203	28.530	2.085
Ca	381.444	5.340	449.615	3.411	458.928	7.553	483.103	24.251	544.198	3.046	565.381	17.668	578.266	16.711	542.301	13.801
V	0.029	0.007	0.027	0.005	0.025	0.000	0.027	0.001	0.028	0.001	0.031	0.002	0.051	0.001	0.021	0.000
Cr	0.805	0.020	0.593	0.018	0.397	0.029	0.217	0.009	0.074	0.028	0.038	0.007	0.375	0.004	0.029	0.008
Mn	0.031	0.017	0.020	0.008	0.010	0.001	0.008	0.000	0.009	0.001	0.008	0.003	15.843	0.000	0.031	0.005
Fe	1.145	0.018	1.590	0.072	1.727	0.015	1.355	0.083	1.216	0.102	1.605	0.039	55.517	0.046	1.480	0.122
Ni	0.012	0.000	0.019	0.013	0.002	0.000	0.019	0.005	0.026	0.001	0.005	0.000	0.071	0.000	0.929	0.145
Co	0.001	0.000	0.001	0.000	0.001	0.000	0.001	0.000	0.001	0.000	0.001	0.000	0.027	0.000	0.001	0.000
Cu	0.023	0.003	0.008	0.001	0.009	0.002	0.014	0.002	0.018	0.005	0.028	0.001	0.019	0.006	0.019	0.002
Zn	0.086	0.004	0.149	0.103	0.058	0.002	0.055	0.003	0.067	0.002	0.059	0.007	0.116	0.004	0.160	0.029
As	0.003	0.001	0.002	0.001	0.002	0.001	0.001	0.000	0.002	0.000	0.002	0.001	0.002	0.000	0.003	0.000
Se	0.139	0.004	0.084	0.009	0.068	0.009	0.053	0.006	0.028	0.006	0.007	0.006	0.374	0.004	0.020	0.001
Sr	20.148	0.218	26.794	0.301	28.329	0.081	29.167	0.100	30.429	0.186	31.501	0.548	30.958	0.093	31.350	0.312
Mo	1.346	0.015	0.441	0.012	0.300	0.012	0.248	0.003	0.230	0.004	0.227	0.001	0.285	0.002	0.235	0.001
Cd	0.003	0.000	0.001	0.000	0.001	0.000	0.001	0.000	0.001	0.000	0.001	0.000	0.001	0.000	0.001	0.000
Ba	0.108	0.012	0.116	0.003	0.130	0.002	0.138	0.003	0.135	0.003	0.143	0.009	0.101	0.001	0.113	0.007
Pb	0.009	0.006	0.004	0.004	0.002	0.002	0.002	0.001	0.002	0.001	0.002	0.000	0.001	0.001	0.007	0.000
SO4	2040.500	18.500	1504.250	6.750	1486.645	37.685	1292.800	38.880	1323.000	54.130	1372.250	15.160	1766.810	37.030	5714.375	550.625
Cl	27.250	4.750	8.750	0.750	5.270	0.270	88.220	2.310	249.710	9.390	263.705	6.945	272.305	9.075	635.625	256.875
NO3	235.000	5.500	BDL		379.000	3.500	426.450	8.050	16.500	5.500	BDL		0.900		189.375	171.875
PO4	BDL		3.000		BDL		10.500	1.600	BDL		6.500		2.300		BDL	
alkalinity HCO3 (mg/L)	56.250	18.750	50.000	12.500	43.750	18.750	33.750	1.250	34.375	1.875	35.000		50.625	0.625	71.875	8.125
pH	8.325	0.095	8.065	0.475	8.030	0.490	8.055	0.285	8.025	0.235	8.240	0.420	8.090	0.410	8.225	0.105

Table B9: continued….

SR core	drainage 9		drainage 10		drainage 11		drainage 12		drainage 13		drainage 14		drainage15		drainage 16	
	ave	SD	ave	SD	ave	SD	ave	SD	ave	SD	ave	SD	ave	SD	ave	SD
B	28.686	0.555	38.571	2.239	31.172	12.223	28.586	1.341	17.238	0.996	13.961	0.151	5.486	0.080	9.336	4.927
Na	11.353	0.185	12.115	0.565	18.552	6.869	15.177	0.121	12.920	1.183	9.467	0.233	5.822	0.389	10.066	0.139
Mg	527.324	24.277	1501.890	27.164	1466.064	505.891	1654.894	0.862	1150.077	272.521	1025.209	54.105	791.299	10.620	1098.584	141.107
Al	0.277	0.029	0.225	0.021	0.044	0.018	0.274	0.250	0.113	22.227	0.102	0.039	0.277	0.127	44.630	44.353
Si	1.889	0.090	2.353	0.138	2.341	0.601	1.264	0.416	4.724	0.518	9.821	1.566	4.479	0.059	2.469	0.621
K	19.565	0.840	16.589	1.591	41.027	19.803	12.929	0.898	9.715	0.012	13.728	1.267	BDL		BDL	
Ca	483.466	8.436	531.054	45.101	239.315	78.538	326.920	7.431	437.173	9.898	427.489	4.663	265.704	39.516	365.297	7.177
V	0.019	0.000	0.017	0.003	0.028	0.025	0.026	0.001	0.021	0.002	0.004	0.001	0.024		0.011	
Cr	0.028	0.014	0.002	0.002	0.531		BDL		BDL		BDL		BDL		BDL	
Mn	0.245	0.217	4.450	1.955	78.019	7.176	374.150	21.324	439.348	52.085	380.505	2.590	232.735	2.105	341.700	23.593
Fe	1.717	0.278	1.211	0.144	3.611	1.433	494.170	70.009	1201.318	30.464	2122.404	131.316	1888.943	148.626	2687.094	804.525
Ni	0.132	0.031	0.012	0.000	0.092	0.073	0.287	0.039	0.340	0.088	0.592	0.079	0.641	0.146	1.760	0.112
Co	0.001	0.000	0.001	0.001	0.018	0.001	0.169	0.029	0.350	0.027	0.628	0.000	0.542	0.003	0.953	0.016
Cu	0.004	0.000	0.008	0.002	0.066	0.058	0.088	0.028	0.091	0.095	0.161	0.095	0.113	0.034	0.550	0.234
Zn	0.118	0.003	0.166	0.008	0.223	0.008	0.341	0.020	0.399	0.125	0.472	0.081	0.363	0.021	0.658	0.036
As	0.004	0.000	0.005	0.000	0.006	0.003	0.008	0.005	0.008	0.001	0.010		0.028	0.024	0.025	
Se	0.011	0.001	0.015	0.009	0.051	0.047	0.110	0.023	0.153	0.012	0.088	0.014	0.103	0.012	BDL	
Sr	27.853	0.312	26.260	0.158	22.720	8.338	29.357	0.310	26.158	0.446	25.579	0.076	14.649	0.476	20.222	0.565
Mo	0.219	0.001	0.178	0.008	0.088	0.052	0.001	0.000	0.004	0.013	0.010	0.001	0.010	0.002	0.063	0.027
Cd	0.001	0.000	0.001	0.000	0.001	0.000	0.001	0.001	0.002	0.001	0.002	0.000	0.003	0.001	0.009	0.006
Ba	0.120	0.031	0.018		0.059	0.035	0.122	0.044	0.090	0.004	BDL		BDL		BDL	
Pb	BDL		0.001		0.005	0.004	0.008	0.002	0.001	0.000	0.000		BDL		BDL	
SO4	4084.500	118.500	5788.750	377.500	6929.375	166.875	9246.000	200.000	5711.000	156.000	12617.000	559.000	14549.000	120.000	14737.500	172.500
Cl	324.500	2.500	210.000	18.750	95.000	6.250	100.000	4.000	BDL		BDL		BDL		BDL	
NO3	5.000		55.000	1.250	210.000	3.750	292.000	24.000	1008.500	135.500	395.500	14.500	379.000	1.000	386.250	41.250
PO4	BDL		BDL		3.750		10.000	2.000	BDL		BDL		BDL		BDL	
alkalinity HCO3 (mg/L)	114.375	5.625	189.375	11.875	73.750	52.500	BDL		BDL		BDL		BDL		BDL	
pH	8.295	0.125	8.205	0.075	6.985	0.235	4.315	0.055	3.835	0.045	3.590	0.010	3.525	0.035	3.180	0.070

UNIVERSITY of the WESTERN CAPE

Table B10: Analytical results for solid residue (SR) + 5 % FA core

SR + 5 % FA	drainage 1		drainage 2		drainage 3		drainage 4		drainage 5		drainage 6		drainage 7		Drainage 8	
element	ave	SD	ave	SD	ave	SD	ave	SD	ave	SD	ave	SD	ave	SD	ave	SD
B	3.361	0.078	3.189	0.064	2.795	0.073	2.739	0.094	2.689	1.161	3.476	0.388	5.647	0.066	10.974	0.231
Na	304.161	3.179	79.426	3.975	27.982	0.934	21.256	0.843	16.484	74.182	15.670	1.406	22.210	0.017	12.850	0.161
Mg	15.393	1.058	7.179	0.846	6.969	0.278	6.600	1.258	6.143	5.259	7.076	2.064	119.680	0.649	144.393	0.351
Al	0.790	0.182	9.046	0.018	9.266	0.170	0.521	0.085	0.494		0.728	0.053	3.119	0.032	0.709	0.050
Si	0.812	0.295	0.991	0.011	0.755	0.098	1.018	0.141	0.789	2.008	1.054	0.024	2.670	0.121	1.125	0.156
K	107.138	1.749	96.203	0.948	58.469	2.961	47.554	2.667	34.665	69.301	30.952	1.602	29.892	1.129	26.076	0.264
Ca	388.810	3.378	464.349	5.160	439.634	7.553	540.829	17.984	464.683	171.838	591.299	36.215	578.266	6.816	635.995	26.392
V	0.017	0.013	0.017	0.006	0.026	0.000	0.028	0.002	0.026	0.049	0.029	0.003	0.051	0.002	0.022	0.002
Cr	1.464	0.035	0.994	0.095	0.815	0.029	0.518	0.016	0.236	0.938	0.139	0.022	0.375	0.026	0.053	0.019
Mn	0.058	0.032	0.046	0.015	0.019	0.001	0.009	0.005	0.011		0.007	0.005	15.843	0.002	0.014	0.007
Fe	2.305	1.131	1.823	0.008	1.713	0.015	1.236	0.025	1.116	0.562	1.680	0.308	55.517	0.297	1.215	0.038
Ni	0.011	0.003	0.004	0.001	0.009	0.000	0.025	0.003	0.026		0.006	0.000	0.071	0.000	0.528	0.008
Co	0.001	0.000	0.001	0.000	0.001	0.000	0.001	0.000	0.001	0.000	0.001	0.000	0.027	0.000	0.001	0.000
Cu	0.014	0.004	0.009	0.002	0.013	0.002	0.015	0.001	0.016	0.007	0.033	0.002	0.019	0.002	0.006	0.002
Zn	0.110	0.019	0.067	0.003	0.057	0.002	0.056	0.002	0.059	0.026	0.068	0.008	0.116	0.004	0.079	0.002
As	0.003	0.002	0.002	0.001	0.001	0.001	0.002	0.001	0.002		0.002	0.001	0.002	0.000	0.002	0.000
Se	0.169	0.008	0.132	0.006	0.128	0.009	0.123	0.010	0.082	0.160	0.039	0.003	0.374	0.000	0.030	0.002
Sr	18.017	0.377	26.111	0.086	27.997	0.081	29.569	0.968	27.903	12.210	31.614	1.054	30.958	0.362	32.661	0.153
Mo	1.500	0.021	0.625	0.009	0.386	0.012	0.298	0.001	0.227	0.564	0.241	0.000	0.285	0.007	0.241	0.002
Cd	0.003	0.000	0.002	0.000	0.001	0.000	0.001	0.000	0.001	0.001	0.001	0.000	0.001	0.000	0.001	0.000
Ba	0.111	0.011	0.127	0.010	0.129	0.002	0.134	0.005	0.124	0.056	0.153	0.016	0.101	0.007	0.129	0.005
Pb	0.001	0.001	0.001	0.000	BDL	0.002	0.001	0.000	0.001		0.004	0.001	0.001	0.000	0.003	0.001
SO4	2222.750	24.750	1550.500	12.000	1538.810	54.590	1378.190	10.190	1346.300	24.000	1301.890	20.880	1552.930	16.950	15857.500	6270.000
Cl	27.000	2.000	10.250	0.250	5.890	1.710	96.205	5.115	245.175	6.065	254.870	5.280	284.065	7.845	388.125	58.125
NO3	229.250	0.750	BDL		386.250	2.750	438.400	14.600	23.550	1.850	BDL		BDL		381.875	
PO4	BDL		BDL		BDL		BDL		3.350		BDL		69.750	58.950	BDL	
alkalinity HCO3 (mg/L)	50.000		56.250	6.250	43.750	6.250	35.625	0.625	30.625	3.125	30.625	0.625	43.750	1.250	53.125	5.625
pH	7.275	0.025	7.050	0.090	7.830	0.880	7.610	0.250	7.875	0.205	7.480	0.050	7.550	0.100	7.950	0.210

UNIVERSITY of the WESTERN CAPE

Table B10: continued…..

SR + 5 % FA	drainage 9		drainage 10		drainage 11		Drainage 12		Drainage 13		Drainage 14		Drainage 15		Drainage 16	
element	ave	SD	ave	SD	ave	SD	ave	SD	ave	SD	ave	SD	ave	SD	ave	SD
B	20.647	0.100	32.324	1.987	15.411	1.155	43.046	1.341	32.982	0.631	24.550	0.074	9.289	0.518	7.192	0.446
Na	12.826	0.644	15.002	0.579	18.903	0.451	13.979	0.121	15.804	0.745	10.712	0.596	5.825	0.181	9.974	0.340
Mg	313.999	11.119	924.756	135.504	431.184	6.300	1994.335	0.862	1762.116	53.468	1463.652	49.240	978.176	25.373	1137.902	56.550
Al	0.409	0.041	0.224	0.015	0.091	6.496	0.059	0.250	BDL		0.110		BDL		0.614	
Si	1.522	0.043	1.942	0.280	1.249	0.194	2.678	0.416	1.353	0.126	1.668	0.053	3.102	0.067	1.011	0.753
K	21.998	1.174	20.320	0.542	22.463	0.828	20.837	0.898	27.915	0.273	55.653	34.749	DBL		BDL	
Ca	510.931	15.778	627.034	56.918	589.840	8.283	334.336	7.431	473.059	25.363	448.258	4.053	259.013	5.545	336.750	22.808
V	0.019	0.001	0.019	0.001	BDL	0.000	0.005	0.001	0.023	0.004	0.034	0.025	0.007	0.001	0.046	
Cr	0.048	0.007	0.015	0.010	BDL		0.003		BDL		0.283		BDL		BDL	
Mn	0.017	0.002	0.179	0.124	27.333	1.393	45.809	21.324	172.512	50.756	288.603	58.868	253.880	9.391	376.629	15.440
Fe	1.899	0.145	1.116	0.230	1.355	0.100	2.086	70.009	97.122		485.790	260.041	686.660	94.167	1795.538	157.627
Ni	0.094	0.003	0.016	0.003	0.088	0.002	0.018	0.039	0.080	0.020	0.300	0.073	0.370	0.024	1.511	0.126
Co	0.001	0.000	0.001	0.000	0.012	0.000	0.012	0.029	0.058	0.028	0.229	0.084	0.330	0.005	0.896	0.027
Cu	0.003	0.002	0.017	0.003	0.023	0.001	0.014	0.028	0.060	0.001	0.070	0.002	0.058	0.009	0.429	0.078
Zn	0.098	0.005	0.154	0.003	0.167	0.004	0.255	0.020	0.309	0.047	0.227	0.022	0.197	0.016	0.438	0.104
As	0.003	0.000	0.005	0.001	0.001	0.000	0.005	0.005	0.007	0.001	0.007	0.004	0.010	0.004	0.017	0.006
Se	0.031	0.008	0.018	0.003	0.190	0.001	0.019	0.023	0.112	0.036	0.069	0.000	0.208	0.043	0.124	0.096
Sr	28.555	0.601	28.096	1.558	10.687	0.523	27.438	0.310	29.306	0.078	27.682	0.734	15.982	0.675	22.097	1.057
Mo	0.227	0.010	0.229	0.025	0.107	0.036	0.171	0.000	0.056	0.043	0.006	0.002	0.004	0.000	0.023	0.005
Cd	0.001	0.000	0.001	0.000	0.001	0.000	0.001	0.001	0.001	0.000	0.004	0.001	0.003	0.002	0.011	0.005
Ba	0.126	0.004	0.096	0.007	0.154	0.014	0.073	0.044	0.035	0.002	BDL		BDL		BDL	
Pb	0.001	BDL	0.003	0.001	0.004	0.001	0.001	0.002	0.003		BDL		BDL		BDL	
SO4	2878.000	66.000	3825.000	470.000	7966.875	809.375	7299.000	137.000	4876.000	349.000	10962.000	874.000	10974.000	0.000	14655.000	117.500
Cl	334.500	9.500	268.750	6.250	117.500	1.250	122.000	16.000	BDL		BDL		BDL		BDL	
NO3	BDL		26.875	14.375	220.000	160.000	203.000	83.000	960.500	319.500	365.000	38.000	257.000	0.000	338.750	58.750
PO4	BDL	3.750		4.375		15.000	3.000		BDL		BDL		BDL		BDL	
alkalinity HCO3 (mg/L)	76.875	4.375	144.375	25.625	250.000	41.250	221.250	48.750	91.250		BDL		BDL		BDL	
pH	8.250	0.210	8.060		8.230	0.020	7.745	0.295	6.170	0.690	4.655	0.255	4.185	0.085	3.560	0.170

UNIVERSITY of the WESTERN CAPE

Table B11: Analytical results for solid residue (SR) + 25 % FA core

SR + 25 % FA	drainage 1	drainge 2		drainage 3		drainage 4		drainage 5		drainage 6		drainage 7		drainage 8	
element	ave	ave	SD	ave	SD	ave	SD	ave	SD	ave	SD	ave	SD	ave	SD
B	2.773	2.694	0.181	1.645	0.000	1.488	0.028	1.703	0.166	2.490	0.144	4.414	0.235	8.000	0.015
Na	188.078	171.811	2.505	40.015	2.936	28.240	1.451	20.952	1.136	17.777	0.303	15.159	1.070	15.137	0.423
Mg	2.820	0.765	0.072	1.304	0.352	7.473	5.176	7.080	3.635	19.733	9.467	56.932	15.585	109.510	14.829
Al	0.225	8.962	0.020	9.211	0.015	0.638	0.001	0.646	0.045	0.634	0.079	0.452	0.057	0.397	0.146
Si	1.022	3.252	0.033	2.743	0.215	2.909	0.116	2.461	0.091	2.326	0.187	2.079	0.398	2.003	0.281
K	104.179	121.904	6.647	61.752	2.899	51.360	2.626	40.106	2.427	30.108	0.130	28.002	2.341	27.134	0.012
Ca	206.070	441.530	5.139	436.508	15.481	551.874	10.251	585.420	12.411	564.714	21.879	583.043	25.532	542.170	13.003
V	0.004	0.138	0.009	0.119	0.005	0.121	0.002	0.107	0.001	0.099	0.006	0.070	0.018	0.041	0.037
Cr	1.102	2.944	0.089	2.315	0.077	1.947	0.043	1.187	0.044	0.596	0.019	0.352	0.106	0.352	
Mn	0.209	0.011	0.002	0.003	0.000	0.002	0.000	0.002	0.001	0.007	0.004	1.671	1.668	3.758	3.711
Fe	0.455	1.769	0.159	1.730	0.330	1.357	0.174	1.388	0.537	1.477	0.071	1.612	0.171	1.350	0.061
Ni	0.010	0.003	0.000	0.010	0.000	0.027	0.001	0.019	0.010	0.005	0.001	0.003	0.001	0.560	0.049
Co	0.001	0.001	0.000	0.001	0.000	0.001	0.000	0.001	0.000	0.001	0.000	0.001	0.000	0.003	0.003
Cu	0.054	0.017	0.007	0.012	0.001	0.015	0.000	0.016	0.000	0.024	0.010	0.004	0.000	0.006	0.002
Zn	0.075	0.072	0.000	0.057	0.003	0.066	0.005	0.064	0.001	0.059	0.000	0.058	0.004	0.332	0.239
As	0.001	0.003	0.001	0.002	0.000	0.002	0.000	0.002	0.000	0.002	0.000	0.002	0.001	0.002	0.000
Se	0.131	0.314	0.014	0.347	0.001	0.341	0.003	0.241	0.005	0.140	0.002	0.090	0.001	0.084	0.024
Sr	8.528	30.098	0.016	35.313	1.580	37.716	1.132	36.397	0.886	33.544	1.077	33.555	1.079	32.231	0.672
Mo	0.992	1.404	0.034	0.794	0.021	0.557	0.014	0.421	0.001	0.339	0.007	0.318	0.019	0.282	0.024
Cd	0.002	0.003	0.000	0.002	0.000	0.001	0.000	0.001	0.000	0.001	0.000	0.001	0.000	0.001	0.000
Ba	0.074	0.176	0.039	0.161	0.005	0.173	0.000	0.157	0.017	0.183	0.016	0.166	0.033	0.143	0.040
Pb	BDL	0.000	0.000	0.000	0.000	0.000	0.000	0.000	0.000	0.001	0.000	0.001	0.000	0.002	0.000
SO4	2472.000	909.000	864.500	1536.905	25.895	1363.455	14.115	1320.205	7.185	1398.990	41.280	1596.175	18.805	5647.250	1794.250
Cl	51.500	8.750	5.250	15.225	7.055	102.205	3.845	249.135	12.345	272.855	3.445	273.790	4.300	444.750	90.250
NO3	47.500	BDL		320.500		419.000	2.400	49.200	3.800	1308.500	1296.500	7.550	1.850	2.000	
PO4	BDL	BDL		BDL		4.800		BDL		2.550		5.000		BDL	
alkalinity HCO3 (mg/L)	NA	112.500	12.500	62.500		55.000	1.250	53.125	6.875	48.125	3.125	55.000		48.125	18.125
pH	8.060	8.490	0.110	8.495	0.115	8.560	0.040	8.845	0.035	8.545	0.125	8.545	0.215	7.955	0.505

UNIVERSITY of the WESTERN CAPE

Table B11: continued…

SR + 25 % FA	drainage 9		drainage 10		drainage 11		Drainage 12		drainage 13		drainage 14		drainage 15		drainage 16	
element	ave	SD	ave	SD	ave	SD	ave	SD	ave	SD	ave	SD	ave	SD	ave	SD
B	14.507	0.927	26.110	3.401	29.214	8.638	39.840	1.581	32.420	0.365	31.296	2.082	12.147	1.184	10.910	2.341
Na	14.815	0.032	17.994	2.728	21.408	5.187	14.822	2.446	14.651	0.879	10.938	1.011	5.379	0.096	8.612	0.100
Mg	194.986	10.068	574.082	156.364	760.769	205.781	1401.220	134.799	1444.825	2.194	1548.809	110.759	1032.668	30.394	1186.640	22.290
Al	0.363	0.083	0.284	0.078	0.086	0.043	0.107	BDL	0.071	BDL	0.086	BDL	0.313	0.056	2.959	0.392
Si	1.836	0.069	1.415	0.161	1.473	0.489	1.379	1.111	9.700	8.124	3.316	0.423	1.329	0.105	1.538	
K	24.343	0.715	23.075	2.769	25.009	2.036	10.451	4.757	77.339	59.245	6.629	1.847	BDL	BDL	BDL	BDL
Ca	535.422	5.887	653.103	41.946	368.985	93.776	371.747	61.569	435.283	33.007	459.416	21.863	238.508	8.959	345.562	13.010
V	0.039	0.019	0.020	0.011	0.005	0.001	0.013	0.012	0.049	0.041	0.005	0.004	0.002	BDL	0.017	0.008
Cr	0.158	0.077	0.160	0.010	0.087		0.026	BDL	0.843	BDL	0.005	BDL	BDL	BDL	BDL	BDL
Mn	5.486	5.354	5.395	0.221	15.795	11.506	50.769	26.999	102.736	3.215	217.636	17.965	207.198	5.121	364.697	1.684
Fe	2.748	0.788	1.407	0.137	1.070	0.141	47.589	46.286	120.560	116.383	471.498	279.055	672.747	238.326	1888.486	208.529
Ni	0.048	0.014	0.014	0.000	0.024	0.006	0.052	0.037	0.146	0.044	0.382	0.094	0.437	0.049	1.447	0.018
Co	0.003	0.003	0.002	0.000	0.007	0.005	0.037	0.034	0.108	0.032	0.266	0.028	0.340	0.011	0.914	0.076
Cu	0.003	0.001	0.011	0.002	0.033	0.010	0.049	0.040	0.109	0.037	0.193	0.006	0.044	0.000	0.330	0.148
Zn	0.091	0.004	0.116	0.007	0.131	0.013	0.235	0.027	0.354	0.184	0.262	0.046	0.197	0.001	0.496	0.153
As	0.002	0.001	0.002	0.001	0.003	0.002	0.005	0.003	0.016	0.009	0.021	BDL	0.003	0.000	0.007	BDL
Se	0.093	0.017	0.099	0.012	0.077	0.034	0.163	0.068	0.100	0.003	0.059	0.028	0.131	0.026	0.177	0.082
Sr	28.907	0.215	29.475	0.681	22.397	2.119	23.387	1.677	23.144	2.238	26.473	1.045	14.883	0.722	22.409	1.302
Mo	0.251	0.015	0.264	0.021	0.207	0.054	0.096	0.073	0.083	0.051	0.060	0.053	0.003	0.001	0.011	0.004
Cd	0.001	0.000	0.001	0.000	0.001	0.000	0.001	0.000	0.002	0.002	0.001	0.000	0.002	0.000	0.008	0.002
Ba	0.134	0.012	0.126	0.009	0.091	0.012	0.074	0.007	BDL		BDL		BDL		BDL	
Pb	BDL		0.002	0.000	0.001	0.001	0.002	BDL	BDL		BDL		BDL		BDL	
SO4	2321.500	59.500	2871.250	510.000	3252.500	848.750	6223.000	177.000	4158.000	97.000	10793.500	272.500	12363.500	788.500	13815.000	82.500
Cl	324.500	14.500	274.375	30.625	113.750		98.000	2.000	BDL		BDL		BDL		BDL	
NO3	5.000		46.250	8.750	208.125	18.125	180.000	16.000	418.500	173.500	339.500	10.500	315.000	9.000	263.750	6.250
PO4	BDL		5.000		15.625	8.125	4.375		21.000	1.000	BDL		BDL		BDL	
alkalinity HCO3 (mg/L)	67.500	16.250	93.125	16.875	135.000	91.250	221.250		83.750		BDL		BDL		BDL	
pH	8.095	0.335	8.115	0.125	7.665	0.335	6.690	1.190	5.935	0.745	5.010	0.590	4.310	0.200	3.450	0.290

UNIVERSITY of the WESTERN CAPE

Table B12: Analytical results for solid residue (SR) + 40 % FA core

SR + 40 % FA	drainage 2		drainage 3		drainage 4		drainage 5		drainage 6		drainage 7		drainage 8		drainage 9	
element	ave	SD	ave	SD	ave	SD	ave	SD	ave	SD	ave	SD	ave	SD	ave	SD
B	0.909	0.050	0.681	0.015	0.684	0.026	0.861	0.008	1.301	0.003	2.190	0.006	4.481	0.193	9.385	0.680
Na	239.196	1.275	48.859	0.727	30.648	0.128	23.035	0.013	19.738	0.198	16.466	1.176	16.456	0.309	15.076	0.772
Mg	0.753	0.015	0.763	0.130	2.890	0.718	2.483	0.301	6.212	1.341	19.472	4.316	45.770	21.820	112.014	23.320
Al	8.865	0.035	9.241	0.026	0.582	0.093	0.671	0.022	0.782	0.027	0.627	0.123	0.670	0.063	0.476	0.014
Si	6.857	0.140	4.291	0.233	3.307	0.179	2.993	0.104	2.830	0.051	2.746	0.266	2.447	0.079	1.755	0.242
K	137.988	12.587	67.913	6.737	51.272	3.741	41.862	1.842	34.229	0.989	30.201	2.364	30.020	0.193	25.631	2.162
Ca	403.108	6.806	413.690	20.010	543.446	15.995	523.445	16.548	554.399	10.984	562.253	5.918	682.079	11.213	543.601	31.904
V	0.226	0.009	0.173	0.005	0.169	0.004	0.153	0.001	0.145	0.002	0.129	0.007	0.119	0.000	0.083	0.003
Cr	4.357	0.007	3.364	0.110	2.895	0.156	1.721	0.209	0.760	0.102	0.350	0.058	0.304	0.013	0.255	0.025
Mn	0.003	0.000	0.005		0.030	0.024	0.002	0.001	0.007	0.001	0.004	0.002	0.011	0.000	1.450	1.419
Fe	1.642	0.100	1.754	0.284	0.868	0.212	1.051	0.099	1.602	0.053	1.395	0.054	1.405	0.076	1.799	0.408
Ni	0.007		0.007	0.004	0.028	0.001	0.027	0.000	0.006	0.000	0.126	0.123	0.687	0.009	0.034	0.001
Co	0.001	0.000	0.001	0.000	0.001	0.000	0.001	0.000	0.001	0.000	0.001	0.000	0.001	0.000	0.001	0.000
Cu	0.013	0.004	0.011	0.001	0.008	0.000	0.014	0.001	0.028	0.003	0.006	0.001	0.010	0.002	0.002	0.001
Zn	0.077	0.002	0.057	0.004	0.052	0.005	0.060	0.006	0.060	0.004	0.048	0.000	0.077	0.005	0.065	0.009
As	0.006	0.001	0.003	0.000	0.002	0.000	0.003	0.000	0.002	0.000	0.002	0.000	0.003	0.000	0.003	0.000
Se	0.225	0.039	0.265	0.046	0.400	0.095	0.214	0.036	0.094	0.009	0.066	0.012	0.071	0.019	0.072	0.011
Sr	33.358	1.372	40.010	3.507	41.309	2.683	38.461	2.629	36.428	1.169	35.945	1.361	34.690	1.832	30.174	2.794
Mo	1.947	0.026	1.177	0.060	0.824	0.042	0.569	0.042	0.479	0.008	0.441	0.007	0.417	0.002	0.347	0.021
Cd	0.004	0.000	0.002	0.000	0.002	0.000	0.007	0.006	0.001	0.000	0.001	0.000	0.001	0.000	0.001	0.000
Ba	0.118	0.030	0.147	0.015	0.106	0.020	0.106	0.045	0.207	0.046	0.169	0.021	0.097	0.021	0.141	0.005
Pb	0.000	0.000	BDL		0.003	0.002	0.001	0.000	0.001	0.000	0.002	0.001	0.003	0.001	BDL	
SO4	1959.500	9.000	1546.915	32.665	1289.230	33.260	1264.270	47.180	1304.980	69.670	1487.520	14.570	1512.250	180.750	1931.000	99.000
Cl	22.000	2.500	8.425	2.845	98.560	9.450	253.230	5.260	258.925	3.925	294.340	9.810	108.750	0.750	307.500	11.500
NO3	BDL	158.500	22.500	333.850	5.050	45.600	17.100	6240.000	2212.500	24.000	12.200		BDL		25.000	15.000
PO4	BDL		BDL		3.800		3.800		BDL		22.350	6.150	2.500		BDL	
alkalinity HCO3 (mg/L)	256.250	43.750	75.000		46.875	1.875	56.250	2.500	51.875	0.625	51.875	1.875	56.250	2.500	66.875	3.125
pH	10.780	0.020	9.580	0.880	9.545	0.745	9.945	0.705	9.360	0.560	8.570	0.050	8.860	0.190	8.750	0.250

UNIVERSITY of the WESTERN CAPE

Table B12: continued…..

SR + 40 % FA	drainage 10		drainage 11		drainage 12		drainage 13		drainage 14		drainage 15		drainage 16	
element	ave	SD	ave	SD	ave	SD	ave	SD	ave	SD	ave	SD	ave	SD
B	22.1	1.7	26.1	0.9	30.5	3.7	34.9	1.0	36.4	0.9	21.3	1.8	21.7	2.6
Na	39.4	23.3	22.2	7.3	15.9	2.5	15.7	1.2	12.0	0.8	6.0	0.0	9.3	0.2
Mg	332.6	35.1	447.0	96.5	804.4	106.9	957.6	272.5	1154.0	193.6	1040.7	51.6	1253.5	28.8
Al	0.740	0.090	0.618	0.273	BDL		0.399	22.227	0.420		7.301	3.423	3.431	0.188
Si	1.21		1.34		1.43		4.19	0.52	2.68	0.61	5.56	0.81	1.89	
K	62.0	39.4	18.1	5.8	14.2	4.9	59.6	0.0	7.4	0.9	3.7		BDL	
Ca	535.2	62.9	475.4	35.4	444.5	60.9	502.7	9.9	440.9	0.2	264.8	5.1	349.1	27.5
V	0.061	0.004	0.026	0.004	0.002	0.001	0.046	0.002	BDL		0.009	0.004	0.008	
Cr	0.719	0.462	0.124		BDL		0.174		BDL		BDL		BDL	
Mn	19.3	13.0	37.2	26.5	76.8	15.4	97.8	52.1	135.6	17.0	137.7	23.9	291.2	26.0
Fe	17.2	15.8	45.7	44.4	109.6	106.4	206.5	30.5	487.5	190.4	430.8	58.3	1320.0	155.3
Ni	0.292	0.281	0.056	0.046	0.065	0.031	0.148	0.088	0.289	0.032	0.319	0.008	1.032	0.022
Co	0.006	0.005	0.023	0.020	0.059	0.033	0.126	0.027	0.212	0.023	0.245	0.014	0.627	0.087
Cu	0.098	0.091	0.075	0.063	0.020	0.015	0.170	0.095	0.093	0.060	0.070	0.011	0.725	0.369
Zn	0.427	0.349	0.147	0.050	0.176	0.039	0.154	0.125	0.191	0.004	0.210	0.003	0.313	0.022
As	0.023	0.020	0.009	0.006	0.005	0.005	0.014	0.001	0.008	0.001	0.014	0.007	0.009	
Se	0.257	0.132	0.082	0.043	0.122	0.023	0.096	0.012	0.170	0.061	0.021	0.006	0.170	0.105
Sr	30.151	0.828	27.887	1.798	25.335	1.234	24.027	0.446	23.461	0.629	14.821	0.571	22.476	1.098
Mo	0.225	0.081	0.154	0.120	0.083	0.071	0.025	0.013	0.031	0.004	0.044	0.013	0.006	0.004
Cd	0.002	0.001	0.001	0.000	0.001	0.001	0.002	0.001	0.001	0.000	0.004	0.000	0.009	0.000
Ba	0.121	0.004	0.180	0.076	0.082	0.011	BDL	0.004	BDL		BDL		BDL	
Pb	0.105	0.105	0.002	0.001	0.001		BDL	0.000	BDL		BDL		BDL	
SO4	2356.3		5570.0	3133.8	4108.8	347.5	3644.5	114.5	9819.5	121.5	10832.5	949.5	10370.0	7032.
Cl	232.5		125.0	16.3	56.9	0.6	BDL		BDL		24.0		BDL	
NO3	123.1	45.6	246.3	8.8	330.6	16.9	695.5	81.5	443.5	5.5	365.0	25.0	1211.3	743.8
PO4	BDL		3.125		BDL		BDL		BDL		BDL		BDL	
alkalinity HCO3 (mg/L)	80.00		77.50		57.50		72.50		BDL		BDL		BDL	
pH	7.52	0.98	6.80	1.40	5.63	0.96	5.03	0.58	4.68	0.62	3.78	0.74	3.90	0.04

UNIVERSITY of the WESTERN CAPE

Table B13: Analytical results for solid residue (SR) + 6 % FA core

SR + 6 % OPC	drainage 1		drainage 2		drainage 3		drainage 4		drainage 5		drainage 6		drainage 7		drainage 8	
element	ave	SD	ave	SD	ave	SD	ave	SD	ave	SD	ave	SD	ave	SD	ave	SD
B	0.336	0.091	0.091	0.058	0.140	0.097	0.170	0.121	2.770	2.770	2.384	0.367	67.153		NS	NS
Na	465.1	29.4	131.0	1.8	83.7	5.1	34.7	33.1	42.0	42.0	36.2	0.8	76.6	2.1	67.0	0.5
Mg	0.5	0.0	0.4	0.1	6.8	6.7	5.3	3.0	149.6	149.6	131.8	32.5	161.6	23.2	191.9	15.5
Al	0.91	0.06	9.01	0.02	9.33	0.05	0.08	0.03	0.72	0.72	10.30	10.17	82.88	32.57	129.41	35.90
Si	10.04	1.04	10.20	0.33	6.70	2.20	3.22	2.71	6.92	6.92	7.81	1.28	97.11	6.38	22.69	7.63
K	632.91	47.88	334.94	7.11	221.84	12.60	87.65	86.47	109.69	109.69	88.36	1.31	141.34		136.08	
Ca	360.00	0.02	392.31	1.27	409.47	9.71	248.85	240.98	411.28	411.28	495.88	61.66	401.49	28.84	619.99	32.97
V	0.06	0.01	0.04	0.00	0.03	0.01	0.01	0.01	0.00	0.00	0.00	0.00	0.17	0.03	0.12	0.06
Cr	1.46	0.13	0.35	0.03	0.23	0.01	0.08	0.03	0.04	0.04	BDL		0.57		0.44	
Mn	0.01	0.01	0.00	0.00	0.00	0.00	0.36	0.35	60.39	60.39	57.28	12.03	67.87	12.09	77.04	13.55
Fe	1.18	0.32	1.36	0.03	1.92	0.35	2.08	0.95	441.47	441.47	452.21	121.40	608.80	114.68	561.38	183.58
Ni	0.010	0.000	0.004	0.001	0.002	0.000	0.019	0.008	0.662	0.662	0.594	0.216	45.319	14.743	105.389	6.185
Co	0.001	0.000	0.001	0.000	0.001	0.000	0.001	0.000	0.123	0.123	0.117	0.035	0.162	0.010	0.214	0.030
Cu	0.015	0.002	0.013	0.008	0.012	0.001	0.052	0.043	0.023	0.023	0.042	0.007	14.490	6.715	5.400	0.316
Zn	0.125	0.010	0.079	0.005	0.080	0.001	0.059	0.011	0.370	0.370	0.438	0.282	8.255	3.258	2.621	0.205
As	0.002	0.001	0.001	0.001	0.001	0.001	0.001	0.000	0.001	0.001	0.002	0.001	0.063	0.013	0.031	0.006
Se	0.139	0.003	0.047	0.003	0.021	0.004	0.016	0.010	0.024	0.024	0.011	0.005	0.659	0.129	0.764	0.077
Sr	19.43	0.28	31.84	0.35	38.59	1.55	20.06	19.45	32.11	32.11	33.39	1.48	29.89	2.14	32.38	0.86
Mo	1.680	0.021	0.417	0.008	0.287	0.024	0.115	0.114	0.011	0.011	0.020	0.009	0.092	0.019	0.076	0.001
Cd	0.003	0.000	0.001	0.000	0.001	0.000	0.000	0.000	0.001	0.001	0.001	0.001	0.004	0.002	0.011	0.005
Ba	0.109	0.001	0.219	0.058	0.153	0.004	0.092	0.087	0.055	0.055	0.061	0.000	0.473		0.148	
Pb	0.001	0.000	0.001	0.000	0.001	0.000	0.001		0.000	0.000	0.004	0.000	0.545	0.149	0.596	0.018
SO4	2875.75	35.25	1906.00	2.00	1854.65	89.62	1767.48	135.02	7537.50	1530.00	2531.25	1.25	4002.50	31.25	4471.88	420.63
Cl	39.3	0.3	12.5	1.0	42.5	12.1	136.7	13.3	556.3	3.8	281.3	6.3	251.3	32.5	764.4	9.4
NO3	123.3	2.8	BDL		52.5	4.5	21.5	3.4	10.0		7.5		20.6	10.6	70.6	9.4
PO4	BDL		BDL		BDL		6.0		23.8	1.3	BDL		63.8	51.3	BDL	
alkalinity HCO3 (mg/L)	156.3	6.3	381.3	143.8	137.5	50.0	75.0									
pH	11.3	0.2	10.8	0.4	11.2	0.2	8.1	3.0	5.3	0.2	4.3	0.2	3.9	0.2	3.8	0.1

UNIVERSITY of the WESTERN CAPE

Table B13: continued

SR + 6 % OPC	drainage 9		drainage 11		drainage 12		drainage 13		drainage 14		drainage 15		drainage 16	
element	ave	SD	ave	SD	ave	SD	ave	SD	ave	SD	ave	SD	ave	SD
B	5.92	5.92	2.60	1.52	4.55	0.88	1.53	0.01	2.88	0.13	1.25	0.25	1.13	0.23
Na	65.22	65.22	46.61	3.37	32.29	0.02	25.31	1.47	21.39	0.12	10.87	1.12	17.23	1.74
Mg	161.96	161.96	134.48	0.50	140.53	12.36	136.19	1.84	177.14	9.78	126.62	11.45	206.68	29.17
Al	112.97	112.97	46.83	46.77	23.47	23.34	53.40	52.23	96.18	14.79	49.70	19.01	143.87	14.76
Si	5.27	5.27	4.89		3.92	3.05	8.35	3.09	7.02	1.69	3.79	1.32	31.49	19.60
K	17.60	17.60	16.62	3.73	25.37	0.84	85.15	80.17	16.08	1.79	1.55	0.12	129.32	
Ca	398.55	398.55	447.61	10.64	589.28	29.18	640.98	49.14	616.69	44.39	335.71	14.72	555.27	14.02
V	0.02	0.02	0.02	0.00	0.01		0.11	0.02	0.01	0.00	0.00	0.00	0.01	
Cr	0.17	0.17	BDL		BDL		0.70	0.21	BDL		BDL		2.32	
Mn	70.22	70.22	42.08	29.88	55.29	8.04	46.26	9.37	61.83	7.21	38.90	9.40	89.93	12.95
Fe	496.15	496.15	325.36	325.05	237.63	108.84	283.12	183.28	520.60	115.13	293.80	118.71	628.51	109.57
Ni	4.20	4.20	0.28	0.16	0.22	0.02	0.30	0.07	0.37	0.03	0.34	0.03	1.48	0.10
Co	0.15	0.15	0.06	0.05	0.08	0.01	0.08	0.02	0.13	0.02	0.09	0.02	0.18	0.02
Cu	0.47	0.47	0.10	0.07	0.09	0.02	0.21	0.04	0.10	0.03	0.10	0.01	0.35	0.10
Zn	0.91	0.91	0.37	0.29	0.42	0.11	0.34	0.13	0.61	0.10	0.58	0.10	0.91	0.12
As	0.01	0.01	0.01	0.00	0.01	0.00	0.03	0.01	0.01	0.00	0.01	0.00	0.04	0.03
Se	0.41	0.41	0.05	0.02	0.21	0.05	0.11	0.01	0.05	0.02	0.08	0.04	0.27	0.07
Sr	30.81	30.81	28.63	0.48	29.39	1.40	27.18	2.13	27.90	2.69	15.21	0.73	22.85	0.24
Mo	0.05	0.05	0.04	0.02	0.02	0.01	0.02	0.01	0.03	0.00	0.02	0.00	0.14	0.01
Cd	0.006	0.006	0.001	0.001	0.001	0.000	0.002	0.000	0.002	0.000	0.003	0.000	0.004	0.002
Ba	BDL		0.096	0.014	0.081	0.027	BDL		BDL		BDL		0.048	
Pb	1.01	1.01	0.04		0.03		0.02		BDL		BDL		0.02	0.00
SO4	4677.50		3333.75	1597.50	2712.50	533.75	2365.00	326.00	4726.50	526.50	5602.50	615.50	6862.50	865.00
Cl	367.50		215.63	1.88	117.50	8.75	BDL		23.00	4.00	83.50	62.50	BDL	
NO3			91.25	71.25	133.75	22.50	239.00	209.00	348.00	8.00	435.00	87.00	255.00	67.50
PO4														
alkalinity HCO3 (mg/L)														
pH	3.75		4.41	0.66	4.37	0.34	4.07	0.33	4.15	0.04	3.85	0.07	3.36	0.00

UNIVERSITY of the WESTERN CAPE

Saturation indices calculated using PHREEQC and WATEQ4 database for the column solid cores leachates are presented in Tables B14-C19 below

Table B14: Summary of saturation indices (SI) for mineral phases controlling element concentration in leachates for fly ash (FA) solid core.

Phase		drainage1	drainage2	drainage 3	drainage 4	drainage5	drainage6	drainage7	drainage8	drainage9	drainage10	drainage11	drainage12	drainage13	drainage 14	drainage 15	drainage 16
$Al(OH)_{3(a)}$	$Al(OH)_3$	-5.79	-3.26	-0.75	-0.75	-1.95	0.39	1.18	2.15	1.49	1.43	-0.38	-1.51	-2.22	-3.2	-3.63	-4.62
Alunite		-26.82	-13.6	-3.48	-3.55	-5.58	7.43	11.25	13.2	11.5	11.28	6.79	7.32	5.34	4.98	3.57	
Anhydrite	$CaSO_4$	-0.27	-0.39	-0.33	-0.36	-0.3	-0.2	-0.24	0.29	-0.18	-0.16	-0.07	-0.21	-0.9	-0.13	-0.31	-0.16
Aragonite		2.93	2.34	1.43	-248.03	0.98	-0.97			-1.04	-0.9	-1.47					
Basaluminite		-27.77	-13.95	-2.23	-2.69	-6.48	6.86	11.46	14.66	12	11.85	5.13	3.47	1.18	-1.55	-2.91	-5.86
Boehmite	AlOOH	-3.59	-1.05	1.46	1.46	0.26	2.6	3.38	4.36	3.7	3.64	1.82	0.7	-0.02	-1	-1.42	-2.42
Diaspore	AlOOH	-1.85	0.68	3.19	3.17	1.98	4.32	5.12	6.09	5.42	5.36	3.55	2.42	1.72	0.73	0.31	-0.68
Ettringite		3.66	-3.54	-3.24	-3.2	-8.18	-14.91	-16.6	-9.48	-14.16	-14.42	-19.16	-30.75	-36.94	-38.57	-41.47	-45.64
$Fe(OH)_{3(a)}$	$Fe(OH)_3$	2.36	4.08	4.85	4.84	4.86	3.84	3.05	3.76	3.67	3.42	1.49	-0.78	-4.78	-2.35	-2.72	-3.7
Ferrihydrite	FeOOH	0.47	2.19	2.96	2.95	2.97	1.95	1.16	1.87	1.78	1.53	-0.4	-2.67	-6.67	-4.24	-4.61	-5.59
Gibbsite	$Al(OH)_3$	-3.06	-0.54	1.97	1.95	0.76	3.09	3.9	4.87	4.2	4.14	2.33	1.2	0.51	-0.49	-0.91	-1.9
Goethite	FeOOH	3.82	5.56	6.33	6.39	6.41	5.39	4.53	5.24	5.19	4.93	3.01	0.74	-3.33	-0.86	-1.23	-2.21
Gypsum	$CaSO_4{:}2H_2O$	-0.04	-0.16	-0.1	-0.14	-0.07	0.02	0	0.52	0.05	0.07	0.16	0.02	-0.67	0.09	-0.09	0.07
Hematite	Fe_2O_3	14.42	17.92	19.46	19.58	19.62	17.57	15.85	17.27	17.17	16.66	12.81	8.27	0.13	5.07	4.34	2.38
Jarosite(ss)		-19.37	-8.13	-3.06	-3	-1.32	2.01	1.05	2.13	2.26	1.51	-3.31	-5.83	-17.81	-7.79	-8.86	
Jarosite-K		-18.57	-7.68	-2.77	-2.56	-0.97	1.97	0.76	1.91	2.1	1.29	-3.54	-6.43	-18.56	-8.52	-9.76	
Jarosite-Na		-21.77	-11.05	-6.16	-6.11	-4.65	-1.79	-3.1	-1.83	-1.49	-2.03	-7.32	-9.79	-22.33	-12.39	-13.21	-14.46
JarositeH		-31.46	-18.36	-12.66	-12.37	-10.34	-5.42	-6.26	-5.49	-5.11	-5.69	-10.4	-11.52	-23.59	-13.2	-13.64	-14.53
Jurbanite	$AlOHSO_4$	-17.68	-11.29	-7.08	-7.18	-7.38	-1.05	0.77	1.06	0.58	0.62	-0.66	1.05	0.55	0.98	0.88	0.91
Portlandite	$Ca(OH)_2$	-1.55	-5.51	-7.15	-7.08	-8.01	-11.9	-12.98	-11.78	-12.42	-12.49	-12.94	-15.92	-16.83		-17.98	-18.85
Rhodochrosite	$MnCO_3$	-1.47	0	-0.89	-250.14	1.14	-0.22			0.22	0.5	-0.13					
Siderite	$FeCO_3$	-13.62	-6.48	-4.16	-253.54	-3.07	-0.22			0.21	0.23	-1.69					
Sillimanite	Al_2SiO_5	-12.34	-4.69	0.87	0.52	-1.97	2.72	4.62	6.32	5.23	4.58	1.04	-0.84	-2.09	-3.8	-4.61	-6.71
SiO2(a)		-4.71	-2.02	-1.47	-1.58	-1.69	-1.67	-1.6	-1.85	-1.48	-2.02	-1.93	-1.55	-1.6	-1.22	-1.18	-1.29
Pyrolusite	MnO_2	4.34	-1.48	-4.75	-4.43	-4.1	-11.29	-13.09	-11.63	-11.77	-11.81	-12.58	-17.94		-20.53	-21.01	-22.82
Barite	$BaSO_4$	0.94	0.06	0.19		0.49	0.76		1.27		0.94	1.22		-0.99			
Brucite	$Mg(OH)_2$	0.32	-1.13	-2.69	-2.24	-2.92	-6.63	-7.46	-6.1	-6.64	-6.47	-6.89	-9.52	-10.32	-10.88	-11.24	-12.22
Magnetite	Fe_3O_4	8.94	16.17	19.32	19.54	20.09	18.97	16.87	18.64	18.58	17.87	12.22	6.9	-3.32			
Manganite	MnOOH	5.03	1.06	-1.37				-6.73			-5.81		-10.32				
Ni(OH)2		0.62	-1.15	-1.86	0.66	-1.61	-4.37	-4.55	-2.66	-2.78	-3.8		-6.86	-7.79	-8	-8.31	-8.9
Nsutite	MnO_2	3.83	-2.15	-5.41	-5.39	-5.06	-12.25	-13.72		-12.57	-12.61	-13.38	-18.73	-20.02	-21.21	-21.69	-23.5
Pyrochroite	$Mn(OH)_2$	-0.84	-2.81	-4.42	-4.29	-2.94	-6.24	-6.81	-6.05	-6.17	-6.1	-6.62	-8.99	-9.33	-10.09	-10.4	-11.22
Quartz		-3.42	-0.73	-0.18	-0.3	-0.41	-0.39	-0.31	-0.56	-0.2	-0.73	-0.65	-0.27	-0.31	0.07	0.11	-0.01
Sepiolite	$Mg_2Si_3O_{7.5}OH{:}3H_2O$	-3.37	1.74	0.27	0.67	-0.99	-8.37	-9.67	-7.69	-7.74	-9.01	-9.6	-13.72				
Calcite	$CaCO_3$	3.08	2.49	1.57	-247.88	1.13	-0.83		-250.7	-0.89	-0.75	-1.32					
Celestite	$SrSO_4$	0.47	0.47	0.52	0.46	0.44	0.48	0.44	0.94	0.42	0.37	0.13	0.39				
Cu(OH)2		-1.8	-1.93	-1.63					-0.32		-2.03						
CuCO3		-10.32	-7.05	-6.03	-255.64	-5.61	-4.6										
Smithsonite	$ZnCO_3$	-6.91	-2.88	-2.18		0.39	-1.62			-3.54	-2.93	-3.7					
Strontianite	$SrCO_3$	2.36	1.87	0.95						-1.76	-1.7	-2.6					
Pb(OH)2		0	-2.2		0.16	-1.66	-4.81	-5.12	-1.66		-3.31		-6.81				

UNIVERSITY of the WESTERN CAPE

Table B15: Summary of saturation indices (SI) for mineral phases controlling element concentration in leachates for solid residue (SR) core.

Phase		drainage1	drainage2	drainage 3	drainage 4	drainage5	drainage6	drainage7	drainage8	drainage9	drainage10	drainage11	drainage12	drainage13	drainage14	drainage15	drainage16
$Al(OH)_{3(a)}$	$Al(OH)_3$	-0.88	0.35	0.4	0.1	-0.65	-0.84	-0.12	-0.08	-1.4	-0.22	-0.49	-5.07	-6.64	-7.86	-7.77	-6.5
Alunite		-0.37	3.58	3.63	2.41	0.2	-1.06	1.63	-0.14	-2.46	-2.38	3.32	-1.44	-5.32	-7.33		
Aragonite		0.62	-248.37	-250.42	-0.73	0.35	0.55		0.53	0.87	0.97	-0.94					
Anhydrite	$CaSO_4$	-0.37	-0.34	-0.37	-0.4	-0.32	-0.3	-0.23	-0.35	-0.21	-2.72	1.72	-0.33	-0.35	-0.15	-0.31	-0.2
Basaluminite	$Al_4(OH)_{10}SO_4$	-0.37	4.21	4.6	3.3	0.35	-0.82	2.4	1.34	-2.82	0.79	1.27	-9.39	-14.97	-18.96	-18.35	-12.66
Boehmite	AlOOH	1.31	2.55	2.6	2.31	1.55	1.36	2.08	3.08	0.81	2.53	3	-2.87	-4.44	-5.66	-5.57	-4.3
Diaspore	AlOOH	3.07	4.28	4.33	4.04	3.28	3.1	3.81	5.1	2.54	5.01	3.93	-1.13	-2.71	-3.92	-3.83	-2.57
$Fe(OH)_{3(a)}$	$Fe(OH)_3$	5.11	5.1	5.16	5.06	5.01	5.13	6.67	3.21	5.15	3.12	2.04	-1.95	-2.92	-3.57	-3.88	-4.72
Ferrihydrite	FeOOH	3.22	3.21	3.27	3.17	3.12	3.24	4.78	1.86	3.26	1.31	1.78	-3.84	-4.81	-5.46	-5.77	-6.61
Gibbsite	$Al(OH)_3$	1.86	3.06	3.12	2.82	2.07	1.88	2.6	6.58	1.32	6.5	5.41	-2.35	-3.93	-5.14	-5.05	-3.78
Goethite	FeOOH	6.52	6.6	6.65	6.55	6.5	6.61	8.16	0.15	6.64	0.01	-0.26	-0.47	-1.44	-2.08	-2.39	-3.23
Gypsum	$CaSO_4{:}2H_2O$	-0.13	-0.11	-0.14	-0.17	-0.09	-0.07	0	19.96	0.02	19.79	17.62	-0.1	-0.12	0.08	-0.08	0.03
Hematite	Fe_2O_3	19.82	20	20.09	19.88	19.79	20.02	23.11	1.54	20.07	0.75	1.95	5.86	3.92	2.63	2.02	0.33
Jarosite(ss)		1.14	1.62	1.71	1.08	1	0.63	5.85	1.66	1.02	0.82	1.85	-7.41	-9.35	-9.64		
Jarosite-K		1.2	1.85	1.86	1.21	1.12	0.77	5.96	-2.42	1.12	-3.04	-2.21	-8.16	-10.22	-10.53		
Jarosite-Na		-2.15	-2.02	-2.22	-2.87	-2.97	-3.31	2.1	-7.27	-2.84	-7.87	-6	-11.8	-13.81	-14.39	-15.12	-16.51
JarositeH		-8.59	-7.44	-7.23	-7.79	-7.79	-8.28	-2.92	-4.87	-7.74	-5.6	-2.56	-12.82	-14.29	-14.47	-14.9	-16.2
Jurbanite	$AlOHSO_4$	-5.28	-3.83	-3.7	-4.12	-4.8	-5.41	-4.33	-9.22	-5.73	-9.19	-12.02	-1.29	-2.14	-2.48	-2.14	-0.26
Portlandite	$Ca(OH)_2$	-9.14	-9.31	-9.43	-9.33	-9.33	-8.89	-9.18	-1.07	-9.03	1.45	1.24	-17.27	-18.01	-18.69	-19.09	-19.6
Rhodochrosite	$MnCO_3$	-0.87	-249.93	-252.09	-2.87	-1.82	-1.68		-1.77	0.14	1.45	1.24					
Siderite	$FeCO_3$	-1.97	-250.39	-252.25	-2.78	-1.72	-2.07		0.3	-1.64	-0.64	0.31					
Sillimanite	Al_2SiO_5	0.55	2.51	2.63	2.08	0.57	0.17	1.97	-1.81	-0.72	-1.66	-1.65	-8.21	-10.79	-12.9	-13.05	-10.77
$SiO_{2(a)}$		-1.81	-1.95	-2	-1.96	-1.97	-1.98	-1.62		-1.77			-1.91	-1.34	-1.01	-1.35	-1.61
Pyrolusite	MnO_2	-7.81	-8.35	-8.69	-9.02	-9.1	-8.29	-5.36	-8.03	-6.81	-5.95	-9.52	-19.85	-21.32	-22.52	-23.05	-24.23
Brucite	$Mg(OH)_2$	-4.83	-5.18	-5.18	-5.18	-5.19	-4.46	-3.68	-3.3	-2.79	-2.53	-5.04	-10.37	-11.38	-12.11	-12.42	-12.93
Barite	$BaSO_4$	1.05	1.01	1.04	1.02	1.03	1.06	0.95	1.11	1.09	0.24	0.8	1.14	0.91			
Magnetite	Fe_3O_4	21.43	21.09	20.97		25.89	21.03	21.13	20.79	18.76		1.37	3.79	1.37	-0.33	-1.19	-3.37
Manganite	MnOOH	-3.22	-3.94	-4.17	-4.52	-4.57	-3.97	-0.89	-3.7	-2.55	-1.6	-3.95	-11.31	-12.59	-13.55	-14.02	-14.85
Ni(OH)2		-1.86	-1.62	-2.16	-2.64	-0.35	-0.67	-1.64	-2.96	-3.34		-8.8	-8.01	-8.8	-9.22	-9.38	-9.59
Nsutite	MnO_2	-9.36	-9.69	-9.77	-8.95	-6.02	-8.7	-7.48	-6.62	-10.19		-21.98	-20.22	-21.98	-23.18	-23.72	-24.89
Pb(OH)2		-0.52	-1.25	-1.86	-1.69	-0.74	-1.45		-2.67	-3.24		-9.83	-8.17	-9.83	-11.03		
Pyrochroite	$Mn(OH)_2$	-5.41	-5.86	-6.06	-6.43	-6.45	-6.07	-2.84	-5.78	-4.71	-3.66	-4.8	-9.48	-10.29	-11	-11.4	-11.89
Quartz		-0.5	-0.66	-0.71	-0.67	-0.68	-0.69	-0.33	-0.52	-0.48	-0.37	-0.36	-0.62	-0.05	0.28	-0.06	-0.32
Sepiolite	$Mg_2Si_3O_{7.5}OH{:}3H_2O$	-6.32	-6.2	-6.24	-4.81	-2.15	-1.99	-0.83	0.01	-4.97	-16.41	-16.72	-16.41	-16.72	-17.21	-18.85	-20.62
Calcite	$CaCO_3$	0.76	-248.23	-250.27	-0.58				0.68	1.01	1.12	-0.8					
Celestite	$SrSO_4$	0.3	0.38	0.36	0.32	0.37	0.39	0.43	0.63	0.49	0.42	0.43					
Cu(OH)2		-1.63	-1.94	-1.91	-1.74	-1.66	-1.44	-1.6	-1.62	-2.3	-2.03	-1.81	-6.78				
CuCO3		-4.92	-253.96	-255.88	-6.11	-4.94	-4.98		-4.84	-5.37	-4.84	-3.7					
Smithsonite	$ZnCO_3$	-252.56	-3.32	-2.27	-2.2	-252.85	-1.82	-1.7	-1.53	-2.66	-9.99	-21.62	-9.99				
Strontianite	$SrCO_3$	-251.01	-1.33	-0.28	-0.09	-251.31	-0.08	0.25	0.29	-1.35	-9.29	-10.74	-9.29				

UNIVERSITY of the WESTERN CAPE

Table B16: Summary of saturation indices (SI) for mineral phases controlling element concentration in leachates for SR + 5 % FA core.

phase		drainage1	drainage2	drainage 3	drainage 4	drainage5	drainage6	drainage7	drainage8	drainage9	drainage10	drainage11	drainage12	drainage13	drainage14	drainage15	drainage16
$Al(OH)_{3(a)}$	$Al(OH)_3$	0.16	1.34	0.6	-0.44	-0.75	-0.19	0.36	-0.71	-1.22	-1.31	-1.88	-1.58		-4.5		-7.22
Alunite	$KAl_3(SO_4)_2(OH)_6$	5.97	9.69	4.87	2.18	0.3	3	4.49	1.66	-2.05	-1.87	-3.2	-1.41		-0.02		
Anhydrite	$CaSO_4$	-0.35	-0.32	-0.37	-0.35	-0.37	-0.3	-0.3	0.12	-0.23	-0.2	0	-0.39	-0.39	-0.14	-0.35	-0.22
Basaluminite	$Al_4(OH)_{10}SO_4$	5.93	10.29	5.77	1.99	-0.04	2.93	5.04	0.83	-2.47	-2.47	-4.64	-2.76		-8.02		-16.49
Boehmite	AlOOH	2.36	3.55	2.8	1.77	1.46	2.01	2.57	1.49	0.99	0.9	0.33	0.62		-2.29		-5.02
Diaspore	AlOOH	4.11	5.28	4.53	3.5	3.18	3.74	4.29	3.22	2.71	2.62	2.05	2.35		-0.57		-3.29
Ettringite		-13.75	-11.67	-8.77	-11.76	-10.79	-11.51	-10.06	-10.04	-9.32	-10.3	-10.58	-14.49		-38.08		-51
$Fe(OH)_{3(a)}$	$Fe(OH)_3$	4.61	4.04	5.12	4.88	4.89	4.87	6.45	4.94	5.12	4.9	4.98	5.11	3.03	-0.97	-2.26	-3.76
Ferrihydrite	FeOOH	2.72	2.14	3.23	2.99	3	2.98	4.56	3.05	3.23	3.01	3.09	3.22	1.14	-2.86	-4.15	-5.65
Gibbsite	$Al(OH)_3$	2.9	4.06	3.32	2.28	1.96	2.51	3.07	1.99	1.49	1.4	0.83	1.12		-1.8		-4.51
Goethite	FeOOH	6.02	5.53	6.62	6.37	6.42	6.4	7.98	6.47	6.65	6.43	6.51	6.64	4.56	0.56	-0.73	-2.24
Gypsum	$CaSO_4{:}2H_2O$	-0.11	-0.09	-0.14	-0.12	-0.14	-0.07	-0.08	0.34	-0.01	0.03	0.23	-0.17	-0.17	0.08	-0.12	0.01
Hematite	Fe_2O_3	18.82	17.86	20.03	19.54	19.64	19.59	22.76	19.73	20.11	19.66	19.83	20.08	15.92	7.93	5.34	2.31
Jarosite(ss)		3.06	1.72	2.28	2.02	1.16	2.21	6.78	2.59	0.9	0.72	1.32	2.71	1.18	-4.85		
Jarosite-K		2.92	1.74	2.41	2.09	1.33	2.3	6.87	2.72	1.1	0.87	1.5	2.79	0.98	-5.29		
Jarosite-Na		-0.38	-2.07	-1.64	-1.99	-2.71	-1.71	3.02	-1.26	-2.84	-2.97	-2.27	-1.08	-2.97	-9.7	-12.3	-14.63
JarositeH		-5.82	-6.59	-6.49	-6.5	-7.33	-5.92	-1.4	-5.74	-7.71	-7.7	-7.24	-5.45	-5.82	-10.84	-12.7	-14.65
Jurbanite	$AlOHSO_4$	-2.1	-0.78	-3.09	-3.77	-4.65	-3.36	-2.91	-3.89	-5.66	-5.41	-5.87	-4.87		-1.37		-1.75
Portlandite	$Ca(OH)_2$	-11.26	-11.35	-9.84	-10.17	-9.61	-10.29	-10.17	-9.86	-8.94	-9.24	-9.15	-10.25	-13.18	-16.42	-17.63	-18.84
Rhodochrosite	$MnCO_3$	-1.61	-3.03	-251.71	-2.16	-1.84	-2.45		-1.97	-1.12			2.15	0.89			
Siderite	$FeCO_3$	-0.37	-1.75	-251.5	-0.96	-1.57	-0.82		-1.49	-1.76			-0.31	0.39			
Aragonite	$CaCO_3$	-0.46	-1.71	-250.25	-0.02	0.13	-0.16		0	0.76			0.41	-1.32			
Sillimanite	Al_2SiO_5	2.33	4.44	2.85	0.91	0.03	1.27	2.79	0.3	-0.63	-0.68	-2.01	-1.08		-7.12		-12.71
$SiO_{2(a)}$		-2.1	-2.04	-2.16	-2.03	-2.15	-2.02	-1.62	-1.96	-1.87	-1.76	-1.95	-1.6	-1.89	-1.8	-1.53	-2
Pyrolusite	MnO_2	-11.71	-12.21	-9.28	-10.73	-9.38	-11.16	-7.52	-9.47	-7.87	-7.55	-4.89	-6.57	-12.17	-18.16	-20.13	-22.56
Brucite	$Mg(OH)_2$	-6.43	-6.97	-5.44	-5.88	-5.31	-6.02	-4.67	-4.33	-2.97	-2.88	-3.11	-3.29	-6.41	-9.73	-10.88	-12.13
Barite	$BaSO_4$	1.07	1.05	1.04	1.01	0.99	1.05	0.88	1.24	1.06	0.91	1.25	0.84	0.42			
Magnetite	Fe_3O_4	20.3	19.05	21.53	21.02	20.88	21.21	25.89	20.95	21.21	20.73	20.81	21.68	17.01	6.54	3.13	-0.79
Manganite	MnOOH	-6.06	-6.75	-4.58	-5.81	-4.9	-6.28	-2.71	-5.06	-3.75	-3.25	-0.76	-1.95	-5.98	-10.46	-11.95	-13.69
$Ni(OH)_2$		-3.51	-4.16	-1.66	-2.75	-2.44	-3.59	-1.94	-1.28	-1.77	-1.72	-0.85	-3.46	-4.9	-7.46	-8.34	-8.98
Nsutite	MnO_2	-12.01	-12.92	-9.98	-11.43	-10.25	-12.02	-8.39	-10.34	-8.73	-8.41	-5.75	-7.43	-13.04	-19.02	-20.99	-23.35
$Pb(OH)_2$		-3.4	-3.31		-2.98	-2.4	-2.17	-2.38	-2.08	-2.24	-0.99	-0.78	-3.5	-4.76			
Pyrochroite	$Mn(OH)_2$	-7.2	-7.66	-6.27	-7.28	-6.63	-7.62	-4.12	-6.87	-5.86	-5.17	-2.85	-3.56	-6.01	-8.97	-10	-11.11
Quartz		-0.8	-0.75	-0.87	-0.74	-0.87	-0.74	-0.34	-0.68	-0.59	-0.47	-0.66	-0.32	-0.61	-0.51	-0.25	-0.72
Sepiolite	$Mg_2Si_3O_{7.5}OH{:}_{3H2O}$	-8.94	-10.04	-7.33	-7.82	-7.12	-8.17	-4.25	-4.6	-1.6	-1.09	-2.11	-1.43	-8.55	-14.89	-16.4	-20.28
Calcite	$CaCO_3$	-0.31	-1.56	-250.1	0.13	0.28	-0.02		0.14	0.9							
Celestite	$SrSO_4$	0.27	0.37	0.37	0.33	0.35	0.37	0.37	0.77	0.46	0.39	0.2	0.46	0.34	0.59	0.38	0.54
$Cu(OH)_2$		-2.13	-2.28	-1.75	-1.81	-1.69	-1.46	-1.62	-2.1	-2.33	-1.6	-1.46	-1.93	-3.17	-6.2	-7.26	-7.69
$CuCO_3$		-4.38	-5.6	-255.13	-4.62	-4.88	-4.27		-5.18	-5.57			-4.21				
Smithsonite	$ZnCO_3$	-2.68	-4.16	-252.48	-2.66	-2.44	-2.73		-2.78	-1.81			-1.51	-3.14			
Strontianite	$SrCO_3$	-1.16	-2.34	-250.82	-0.67	-0.48	-0.82		-0.68	0.12			-0.07	-1.92			

UNIVERSITY of the WESTERN CAPE

Table B17: Summary of saturation indices (SI) for mineral phases controlling element concentration in leachates for SR + 25 % FA core.

Phase		drainage1	drainage2	drainage 3	drainage 4	drainage5	drainage6	drainage7	drainage8	drainage9	drainage10	drainage11	drainage12	drainage 13	drainage 14	drainage 15	drainage16
$Al(OH)_{3(a)}$	$Al(OH)_3$	-1.15	0.04	-0.09	-1.36	-1.47	-1.2	-1.33	-0.82	-0.98	-1.28	-1.19	-0.26	-0.89	-3.69	-5.38	-6.95
Alunite		-0.12		0.8	-3.54	-4.54	-3.03	-3.24	1.03	-0.67	-2.05	0.02	5.71	6.43	0.61		
Anhydrite	$CaSO_4$	-0.55	-0.5	-0.37	-0.35	-0.31	-0.41	-0.27	-0.06	-0.24	-0.21	-0.43	-0.33	-0.41	-0.14	-0.37	-0.22
Basaluminite	$Al_4(OH)_{10}SO_4$	-0.78	2.63	1.53	-4.03	-3.98	-2.32	-2.75	0.99	-0.33	-2.68	-0.3	5.56	4.05	-4.84	-10.08	-14.66
Boehmite	AlOOH	1.05	2.23	2.12	0.86	0.73	1	0.87	1.38	1.21	0.93	1	1.93	1.31	-1.49	-3.18	-4.75
Diaspore	AlOOH	2.8	3.98	3.84	2.57	2.48	2.75	2.62	3.13	2.97	2.65	2.76	3.68	3.05	0.25	-1.44	-3.01
Fe(OH)3(a)	$Fe(OH)_3$	4.72	5.28	5.07	4.89	4.33	5.19	5.23	5.17	5.5	4.97	4.93	4.13	2.4	0.04	-1.97	-4.09
Ferrihydrite	FeOOH	2.83	3.39	3.18	3	3.19	3.3	3.34	3.28	3.61	3.08	3.04	2.24	0.51	-1.85	-3.86	-5.98
Gibbsite	$Al(OH)_3$	1.59	2.78	2.62	1.35	1.27	1.54	1.41	1.92	1.76	1.43	1.55	2.48	1.84	-0.96	-2.65	-4.22
Goethite	FeOOH	6.12	6.69	6.59	6.44	6.49	6.6	6.64	6.58	6.91	6.52	6.34	5.53	3.84	1.48	-0.53	-2.65
Gypsum	$CaSO_4{:}2H_2O$	-0.31	-0.26	-0.15	-0.12	-0.07	-0.17	-0.03	0.18	-0.01	0.01	-0.19	-0.1	-0.17	0.1	-0.13	0.01
Hematite	Fe_2O_3	19.03	20.16	19.97	19.68	19.75	19.98	20.05	19.94	20.6	19.83	19.46	17.85	14.47	9.76	5.73	1.5
Jarosite(ss)		1.07	-2.98	0.03	-1	-1.41	-0.28	0.01	2.7	2.46	0.66	2.16	2.94	0.36	-3.69		
Jarosite-K		1.08	-9.41	0.34	-0.61	-1.3	-0.27	0.02	2.59	2.37	0.88	1.98	2.48	0.03	-4.46		
Jarosite-Na		-2.42		-3.57	-4.58	-5.34	-4.25	-4	-1.41	-1.6	-2.93	-1.84	-1.12	-4.43	-7.96	-11.97	-15.59
JarositeH		-8.43		-9.21	-10.08	-11.2	-9.72	-9.42	-6.19	-6.54	-7.78	-6.5	-4.62	-7.14	-9.59	-12.57	-15.54
Jurbanite	$AlOHSO_4$	-4.88	-5.03	-5.15	-6.7	-7.12	-6.28	-6.31	-4.1	-4.94	-5.59	-4.27	-1.2	-0.62	-1.11	-1.28	-1.16
Portlandite	$Ca(OH)_2$	-10	-8.61	-8.46	-8.14	-7.83	-8.5	-8.46	-9.94	-9.46	-9.03	-10.52	-12.57	-13.84	-15.88	-17.63	-19.18
Rhodochrosite	$MnCO_3$		-1.07	-2.66	-1.9	-1.73	-1.46	1.02	0.63	1.23	1.34	1.54	1.21	0.42			
Siderite	$FeCO_3$		-2.11	-3.53	-2.77	-3.2	-2.47	-2.37	-1.24	-1.06	-1.58	-0.44	0.92	0.23			
Aragonite	$CaCO_3$		1.01	-0.22	1.06	1.25	0.89	1	0.12	0.59	0.83	0.29	-0.58	-1.61			
Sillimanite	Al_2SiO_5	-0.2	2.66	1.93	-0.71	-0.49	0.05	-0.26	0.77	0.4	-0.84	-0.11	1.73	1.18	-4.87	-8.65	-11.71
$SiO_{2(a)}$		-2.01	-1.52	-1.62	-1.61	-1.67	-1.67	-1.72	-1.71	-1.76	-1.9	-1.84	-1.86	-1.02	-1.48	-1.87	-1.8
Pyrolusite	MnO_2	-8.03	-7.55	-7.5	-7.48	-6.97	-7.62	-5.2	-7.37	-6.48	-5.8	-7.78	-11.25	-13.7	-17.24	-20.13	-23.31
Brucite	$Mg(OH)_2$	-5.64	-5.14	-4.8	-3.83	-3.52	-3.72	-3.24	-4.42	-3.67	-2.91	-3.97	-5.76	-7.09	-9.13	-10.79	-12.43
Barite	$BaSO_4$	0.94	1.13	1.13	1.09	1.13	1.14	1.18	1.27	1.13	1	0.95	0.92				
Magnetite	Fe_3O_4	19.83	21.09	20.77	20.24	20.13	20.77	20.88	21.3	22.15	20.93	20.87	19.43	15.1	8.96	3.62	-1.87
Manganite	MnOOH	-3.17	-3.12	-3.57	-3.77	-2.89	-3.24	-0.82	-2.4	-1.66	-1.65	-2.53	-5.02	-6.88	-9.5	-11.69	-14.01
$Ni(OH)_2$		-1.66	-2.64	-1.37	-1.9	-1.33	-2.21	-2.46	-0.92	-1.92	-2.85	-2.99	-4.09	-4.87	-6.45	-7.86	-9.04
Nsutite	MnO_2	-8.33	-7.86	-8.3		-7.27	-7.92	-5.5	-7.67	-6.79	-6.75	-8.09	-11.55	-14.16	-17.71	-20.6	-23.78
$Pb(OH)_2$			-2.51	-1.37	-2.85		-1.7	-2.13	-2.28		-2.19	-3.17	-4.39				
Pyrochroite	$Mn(OH)_2$	-5.09	-5.47	-5.92	-6.19	-5.59	-5.65	-3.22	-4.22	-3.61	-3.62	-4.05	-5.57	-6.67	-8.37	-9.86	-11.32
Quartz		-0.71	-0.22	-0.34	-0.33	-0.36	-0.36	-0.41	-0.41	-0.45	-0.62	-0.54	-0.56	0.27	-0.18	-0.58	-0.51
Sepiolite	$Mg_2Si_3O_{7.5}OH{:}3H_2O$	-2.01	-4.62	-4.49	-2.58	-1.81	-2.2	-1.4	-3.73	-2.37	-1.62	-3.24	-6.87	-7.11	-12.55	-17.04	-20.12
Calcite	$CaCO_3$	-6.1	1.15	-0.07	1.21	1.39	1.04	1.15	0.27		0.98	0.44	-0.43	-1.46			
Celestite	$SrSO_4$	0.01	0.28	0.48	0.43	0.43	0.31	0.43	0.67	0.44	0.38	0.3	0.41	0.26	0.57	0.38	0.54
$Cu(OH)_2$		-1.24	-1.76	-1.77	-1.65	-1.76	-1.59	-2.35	-2.22	-2.48	-1.82	-1.65	-2.65	-3.43	-5.14	-7.25	-8.08
Smithsonite			-1.84	-2.88	-1.9	-2.04	-2.07	-2.02	-1.86	-1.97	-1.74	-1.91	-2.49	-3.34			
Strontianite			0.47	-0.7	0.5	0.67	0.3	0.4	-0.47	-0.04	0.1	-0.29	-1.14	-2.26			

UNIVERSITY of the WESTERN CAPE

Table B18: Summary of saturation indices (SI) for mineral phases controlling element concentration in leachates for SR + 40 % FA core.

phase		drainage1	drainage2	drainage 3	drainage 4	drainage5	drainage6	drainage7	drainage8	drainage9	drainage10	drainage11	drainage12	drainage 13	drainage 14	drainage 15	drainage16
$Al(OH)_{3(a)}$	$Al(OH)_3$	N/A	-2.27	-1.08	-2.29	-2.66	-1.97	-1.32	-1.5	-1.58	-0.13	0.42		-2.52	-4.02	-5.57	-5.34
Alunite			-11.77	-5.15	-9.14	-11.59	-7.77	-3.48	-4.81	-4.65	3.84	7.84		4.18	0.7	-1.41	
Anhydrite	$CaSO_4$		-0.39	-0.38	-0.36	-0.36	-0.33	-0.29	-0.23	-0.26	-0.29	-0.15	-0.31	-0.34	-0.15	-0.34	-0.28
Basaluminite	$Al_4(OH)_{10}SO_4$		-10.83	-3.95	-9.12	-11.66	-7.47	-3.49	-4.3	-4.56	3.96	7.99		-0.57	-5.4	-9.73	-9.44
Boehmite	AlOOH		-0.07	1.12	-0.09	-0.45	0.23	0.89	0.7	0.62	2.06	2.62		-0.32	-1.82	-3.37	-3.14
Diaspore	AlOOH		1.68	2.87	1.65	1.28	1.97	2.62	2.45	2.36	3.81	4.36		1.42	-0.07	-1.62	-1.4
Ettringite			2.25	-2.05	-4.01	-2.15	-4.33	-7.46	-6.02	-7.21	-12.06	-15.61		-32.25	-37.55	-47.41	-45.35
$Fe(OH)_{3(a)}$	$Fe(OH)_3$		3.63	4.7	4.34	4.02	4.75	4.98	5.03	5.11	5.97	4.43		-0.11	-0.95	-3.75	-2.83
Ferrihydrite	FeOOH		1.74	2.81	2.45	2.13	2.86	3.09	3.14	3.22	4.08	2.54	1.43	-2	-2.84	-5.64	-4.72
Gibbsite	$Al(OH)_3$		0.47	1.66	0.44	0.06	0.76	1.4	1.24	1.14	2.6	3.15	-0.47	0.21	-1.29	-2.83	-2.62
Goethite	FeOOH		5.03	6.13	5.81	5.52	6.21	6.49	6.46	6.57	7.4	5.86		1.32	0.48	-2.31	-1.36
Gypsum	$CaSO_4{:}2H_2O$		-0.15	-0.14	-0.13	-0.13	-0.1	-0.06	0.01	-0.03	-0.05	0.08	2.89	-0.11	0.08	-0.11	-0.05
Hematite	Fe_2O_3		16.85	19.05	18.41	17.84	19.22	19.77	19.71	19.94	21.59	18.51	-0.08	9.44	7.74	2.16	4.07
Jarosite(ss)			-11.08	-4.48	-5.8	-8.1	-4.11	-0.82	-1.67	-0.91	5.92	3.92	12.58	-4.31	-5.56	-11.15	
Jarosite-K			-10.49	-4.13	-5.4	-7.56	-3.77	-0.58	-1.52	-0.73	5.85	3.59	-1.89	-4.88	-6.4	-12.25	
Jarosite-Na			-14.01	-8.02	-9.36	-11.54	-7.75	-4.56	-5.53	-4.7	1.91	-0.06	-2.4	-9.2	-9.92	-15.76	-13.32
JarositeH			-22.85	-14.94	-16	-18.42	-14.02	-9.91	-11.27	-10.23	-2.85	-3.81	-6.08	-11.04	-11.27	-15.9	-13.72
Jurbanite	$AlOHSO_4$		-11.57	-8.13	-9.47	-10.69	-8.76	-6.55	-7.21	-7.02	-3.04	-0.67	-8.48	-0.41	-0.75	-0.43	-0.62
Portlandite	$Ca(OH)_2$		-4.26	-6.49	-6.34	-5.47	-6.7	-8.21	-7.69	-7.98	-10.55	-12.23	-14.42	-15.62	-16.59	-18.65	-18.16
Rhodochrosite	$MnCO_3$		-1.09	-1.42	-0.37	-1.51	-1.03	-1.6		1.1	1.3	0.75	-0.14	-0.56			
Siderite	$FeCO_3$		-9.19	-5.92	-5.78	-7.17	-4.86	-2.72		-2.93	0.62	0.57	-0.25	-0.5			
Aragonite	$CaCO_3$		2.22	0.95	1.5	1.65	1.48	1.03	1.16	0.1	-0.82	-2.05	-2.51				
Sillimanite	Al_2SiO_5		-2.61	0.28	-2.38	-3.49	-1.75	-0.48	-0.65	-1.09	1.82	2.98		-2.4	-5.58	-8.36	-8.5
SiO2(a)			-2.18	-1.59	-1.7	-1.95	-1.71	-1.63	-1.68	-1.82	-1.94	-1.88	-1.87	-1.39	-1.57	-1.25	-1.72
Pyrolusite	MnO_2		0.14	-3.49	-2.82	-2.36	-4.18	-7.31	-5.87	-4.23	-8.09	-10.86	-14.97	-17.41	-18.84	-22.47	-21.45
Brucite	$Mg(OH)_2$		-0.76	-3.01	-2.41	-1.6	-2.44	-3.47	-2.64	-2.46	-4.53	-6.04	-7.96	-9.12	-9.95	-11.84	-11.4
Barite	$BaSO_4$		1.08	1.14	0.91	0.91	1.22	1.14	0.91	1.1	1.04	1.33	0.89				
Magnetite	Fe_3O_4		13.83	18.33	17.39	16.12	18.79	20.39	20.04	20.48	24.2	20.31	12.56	8.46	6.27	-1.2	1.53
Manganite	MnOOH		2.28	-0.27	0.27	0.17	-0.9	-3.41	-1.93	-0.34	-2.81	-4.85	-7.95	-9.63	-10.71	-13.44	-12.71
Ni(OH)2			0.46	-0.23	-0.22	0.32	-1.2	-1.08	1.84	-1.4	-1.9	-3.78	-5.9	-6.63	-7.22	-9.01	-8.29
Nsutite	MnO_2		-0.16	-3.91	-3.41	-3.11	-4.76	-8.06	-6.29	-4.82	-8.51	-11.28	-15.55	-17.83	-19.26	-22.89	-22.04
Pb(OH)2			-0.46		0.06	-0.15	-0.56	-1.47	0.12		-1.13	-4.03	-6.33				
Pyrochroite	$Mn(OH)_2$		-2.36	-3.71	-3.13	-3.63	-4.12	-5.84	-4.65	-2.95	-4.19	-5.5	-7.44	-8.51	-9.24	-11.07	-10.46
Quartz			-0.57	-0.09	-0.27	-0.66	-0.42	-0.34	-0.38	-0.53	-0.64	-0.58	-0.57	-0.09	-0.27	0.05	-0.43
Sepiolite	$Mg_2Si_3O_{7.5}OH{:}3H_2O$		2.17	-0.61	0.17	0.95	0.08	-1.82	-0.14	-0.29	-4.7	-7.56	-11.42	-12.21	-14.44	-17.26	-17.87
Calcite	$CaCO_3$		2.37	1.09	1.65	1.8	1.62	1.18	1.3	0.25	-0.68	-1.9	-2.37				
Celestite	$SrSO_4$		0.51	0.55	0.46	0.46	0.43	0.46	0.42	0.43	0.41	0.56	0.39	0.28	0.52	0.36	0.47
Cu(OH)2			-1.86	-1.89	-2.02	-1.72	-1.45	-2.09	-1.94	-2.63	-1.15	-2.12	-4.74	-5.04	-6.14	-8.1	-6.75
Smithsonite	$ZnCO_3$		-4.22	-3.27	-2.85	-3.4	-2.52	-2.07		-1.98	-1.69	-3.04	-4.1	-4.67			
Strontianite	$SrCO_3$		1.81	0.56	1.01	1.14	0.92	0.45		0.52	-0.52	-1.42	-2.67	-3.21			

UNIVERSITY of the WESTERN CAPE

Table B19: Summary of saturation indices (SI) for mineral phases controlling element concentration in leachates for SR + 6 % OPC core.

phase		drainage1	drainage2	drainage 3	drainage 4	drainage5	drainage6	drainage7	drainage8	drainage9	drainage11	drainage12	drainage13	drainage14	drainage15	drainage16
$Al(OH)_{3(a)}$	$Al(OH)_3$	-3.83	-2.35	-2.7	-1.77	-1.98	-1.57	-3.53	-3.69	-4	-1.56	-2.6	-3.12	-2.92	-4.3	-5.18
Alunite		-17.26	-11.8	-14.21	-2.59	6.19	7.75		4.9	3.43		5.56	5.29	5.47	1.52	2.1
Anhydrite	CaSO4	-0.36	-0.44	-0.35	-0.52	-0.15	-0.29	-0.3	-0.13	-0.27	-1.56	-0.2	-0.23	-0.1	-0.28	-0.08
Aragonite		1.73	2.44	1.14	0.44											
Basaluminite	$Al_4(OH)_{10}SO_4$	-18.08	-11.75	-13.94	-4.45	1.24	3.3	-2.57	-3.01	-4.05	2.79	0.13	-1.2	-0.26	-5.03	-8.1
Boehmite	AlOOH	-1.64	-0.15	-0.5	0.44	0.22	0.63	-1.32	-1.49	-1.8	0.64	-0.39	-0.93	-0.72	-2.1	-2.97
Diaspore	AlOOH	0.12	1.59	1.23	2.16	1.95	2.37	0.41	0.24	-0.07	2.38	1.34	0.82	1.02	-0.36	-1.24
Ettringite		2.27	2.2	4.38	-13.11	-29.79	-30.96	-40.83	-40.85	-42.86	-36.9	-35.28	-38.27	-37.4	-43.59	-46.61
Fe(OH)3(a)	$Fe(OH)_3$	2.92	3.37	3.15	5.14	0.79	-0.27	-2.92	-3.33	-3.57	-4.59	-1.93	-2.76	-2.36	-3.6	-4.7
Ferrihydrite	FeOOH	1.03	1.48	1.26	3.24	-1.1	-2.16	-4.81	-5.22	-5.46	-6.48	-3.82	-4.65	-4.25	-5.49	-6.59
Gibbsite	$Al(OH)_3$	-1.09	0.37	0.02	0.94	0.74	1.15	-0.81	-0.97	-1.28	1.16	0.12	-0.39	-0.19	-1.57	-2.47
Goethite	FeOOH	4.32	4.85	4.64	6.69	2.27	1.21	-1.44	-1.85	-2.09	-3.11	-0.45	-1.32	-0.92	-2.16	-3.19
Gypsum	$CaSO_4{:}2H_2O$	-0.13	-0.21	-0.12	-0.3	0.08	-0.06	-0.07	0.1	-0.03	-1.32	0.04	0	0.14	-0.05	0.15
Hematite	Fe_2O_3	15.43	16.5	16.07	20.17	11.33	9.2	3.91	3.1	2.61	0.56	5.89	4.15	4.94	2.47	0.43
Jarosite(ss)		-14.26	-11.57	-13.61	1.98	-1.22	-3.98		-9.46	-10.51		-7.85	-9.18	-8.27	-11.5	-11.77
Jarosite-K		-13.42	-10.72	-12.71	2.32	-1.59	-4.45		-10.1	-11.37		-8.54	-9.87	-9.12	-12.64	-12.42
Jarosite-Na		-17.31	-14.86	-16.86	-1.79	-5.73	-8.57	-13.17	-14.13	-14.52	-22.93	-12.16	-14.14	-12.73	-15.52	-17
JarositeH		-26.99	-23.33	-25.52	-6.89	-8.14	-10.53	-14.55	-15.32	-15.65	-24.59	-13.62	-15.24	-13.82	-16	-17.09
Jurbanite	$AlOHSO_4$	-14.13	-11.8	-12.93	-5.89	0.05	0.86	0.87	0.93	0.82	0.33	0.78	0.83	1.15	0.53	0.49
Portlandite	$Ca(OH)_2$	-3.24	-4.15	-3.28	-9.54	-15.35	-15.88	-17.85	-17.91	-18.24	-16.6	-16.73	-17.35	-17.33	-18.28	-18.89
Rhodochrosite	$MnCO_3$	-0.82	-0.89	-2.8	0.18											
Siderite	$FeCO_3$	-11.97	-9.22	-11.97	-1.25											
Sillimanite	Al_2SiO_5	-6.11	-2.93	-4.17	-1.47	-1.28	-0.42	-3.23	-4.19	-5.45	-0.6	-2.77	-3.36	-3.02	-6.05	-7.15
$SiO2_{(a)}$		-2.56	-2.06	-2.59	-1.55	-1.18	-1.14	-0.04	-0.67	-1.3	-1.34	-1.43	-1.1	-1.17	-1.43	-0.53
Pyrolusite	MnO_2	3.04	0.43	1.42	-7.17	-16.63	-18.17	-21.77	-22.21	-22.49	-18.95	-20.01	-21.44	-21.1	-22.59	-23.87
Brucite	$Mg(OH)_2$	0.09	-0.92	1.09	-5.05	-9.59	-7.49	-12.05	-12.22	-12.44	-10.9	-11.15	-11.8	-11.65	-12.49	-13.13
Barite	$BaSO_4$	1.08	1.3	1.16	0.93	0.83	0.74	1.68	1.17							0.72
Magnetite	Fe_3O_4	11.15	13.28	12.27	21.49		8.3					3.79	1.49	2.59	-0.81	-3.41
Manganite	MnOOH	4.62		2.83	-2.97	-9.31	-10.4					-11.79	-12.75	-12.5	-13.68	-14.8
$Ni(OH)_2$		1.23	-0.41	0.49	-2.83	-5.79	-6.46		-6.34			-7.81	-8.18	-8.05	-8.78	-9.27
Nsutite	MnO_2	2.74	-0.23	0.76	-8.13	-17.26	-18.8	-22.4	-22.84	-23.12		-20.65	-21.91	-21.57	-23.06	-24.67
$Pb(OH)_2$		-0.42	-0.33	-0.28	-2.54	-7.69	-7.21	-6.95	-7.18	-7.11		-7.18	-8.1			-9.6
Pyrochroite	$Mn(OH)_2$	-0.58	-2.43	-2.18		-8.43	-9.09	-10.89		-11.26		-10.02	-10.68	-10.51	-11.39	-12.01
Quartz		-1.26	-0.77	-1.3	-0.27	0.11	0.16	1.25	0.63	-0.01	-0.05	-0.14	0.2	0.13	-0.14	0.76
Sepiolite	$Mg_2Si_3O_{7.5}OH{:}3H_2O$	2.74	2.03	4.45	-4.84	-12.65	-13.85	-14.14	-16.37	-18.71	-15.74	-16.53	-16.74	-16.66	-19.14	-17.87
Calcite	$CaCO_3$	1.88	2.58	1.29	0.58											
Celestite	$SrSO_4$	0.33	0.47	0.57									0.34	0.51	0.32	0.48
$Cu(OH)_2$		-1.8	-1.76				-1.16				-30.96		-5.28			-7.21
Smithsonite	$ZnCO_3$	-5.72	-3.94													
Strontianite	$SrCO_3$	1.11														

UNIVERSITY of the WESTERN CAPE

XRD spectra of solid cores with depth compared to the fly ash are presented in figures B20-B23 below

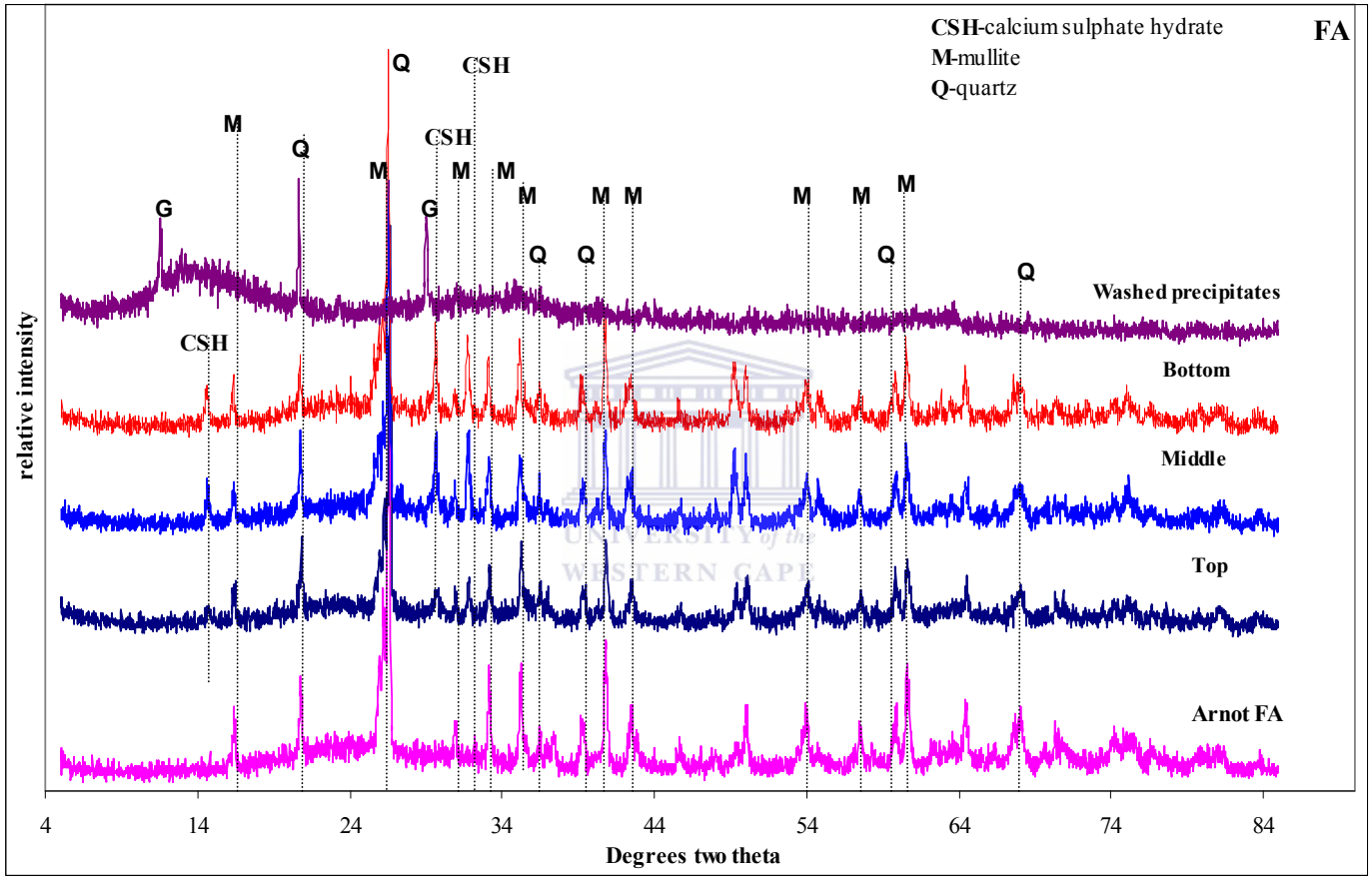

Figure B20: XRD spectra of FA solid core sections with spectra for precipitates washed down the solid core (G-gypsum).

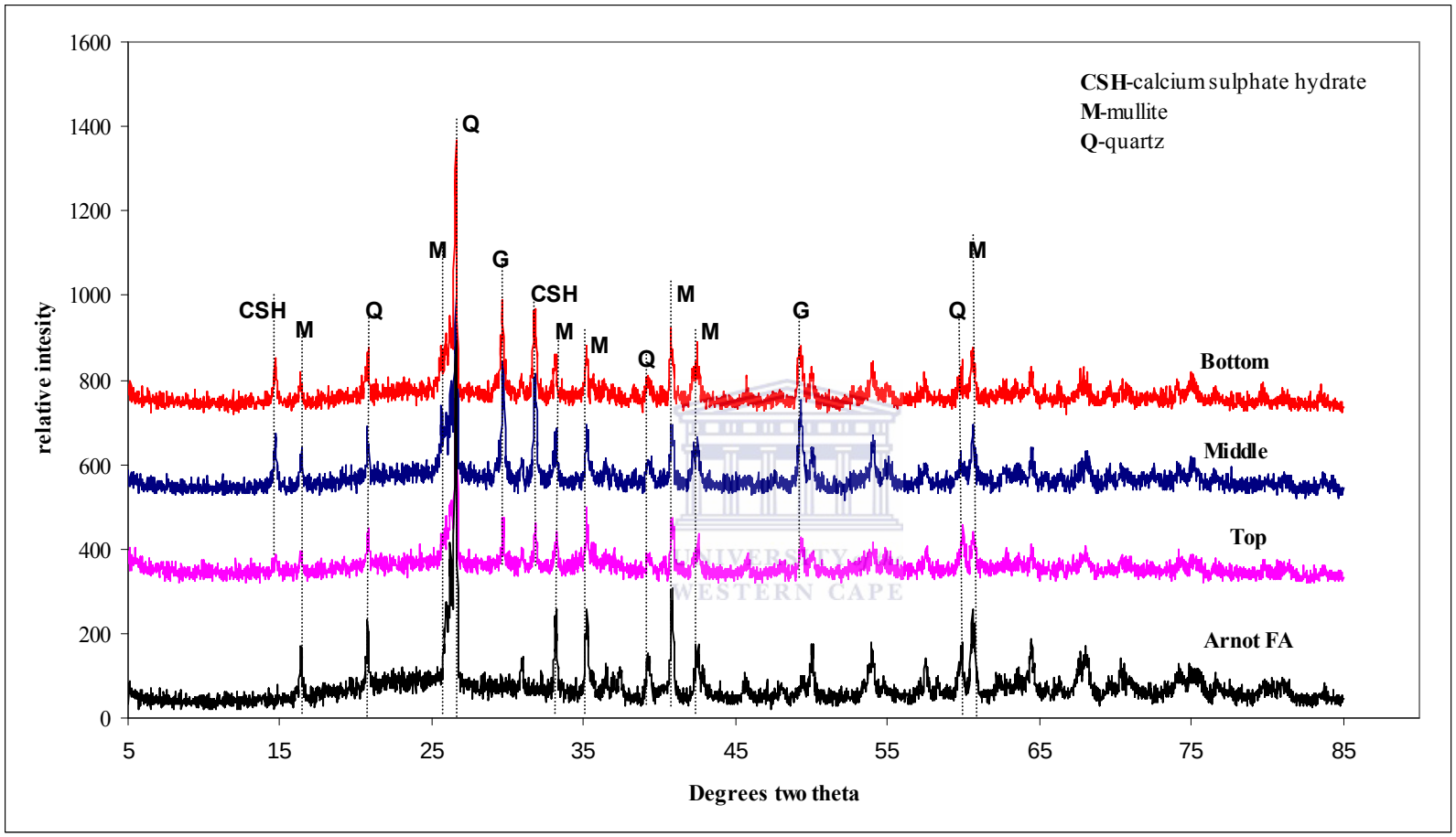

Figure B21: XRD spectra of solid residue core sections (G-gypsum)

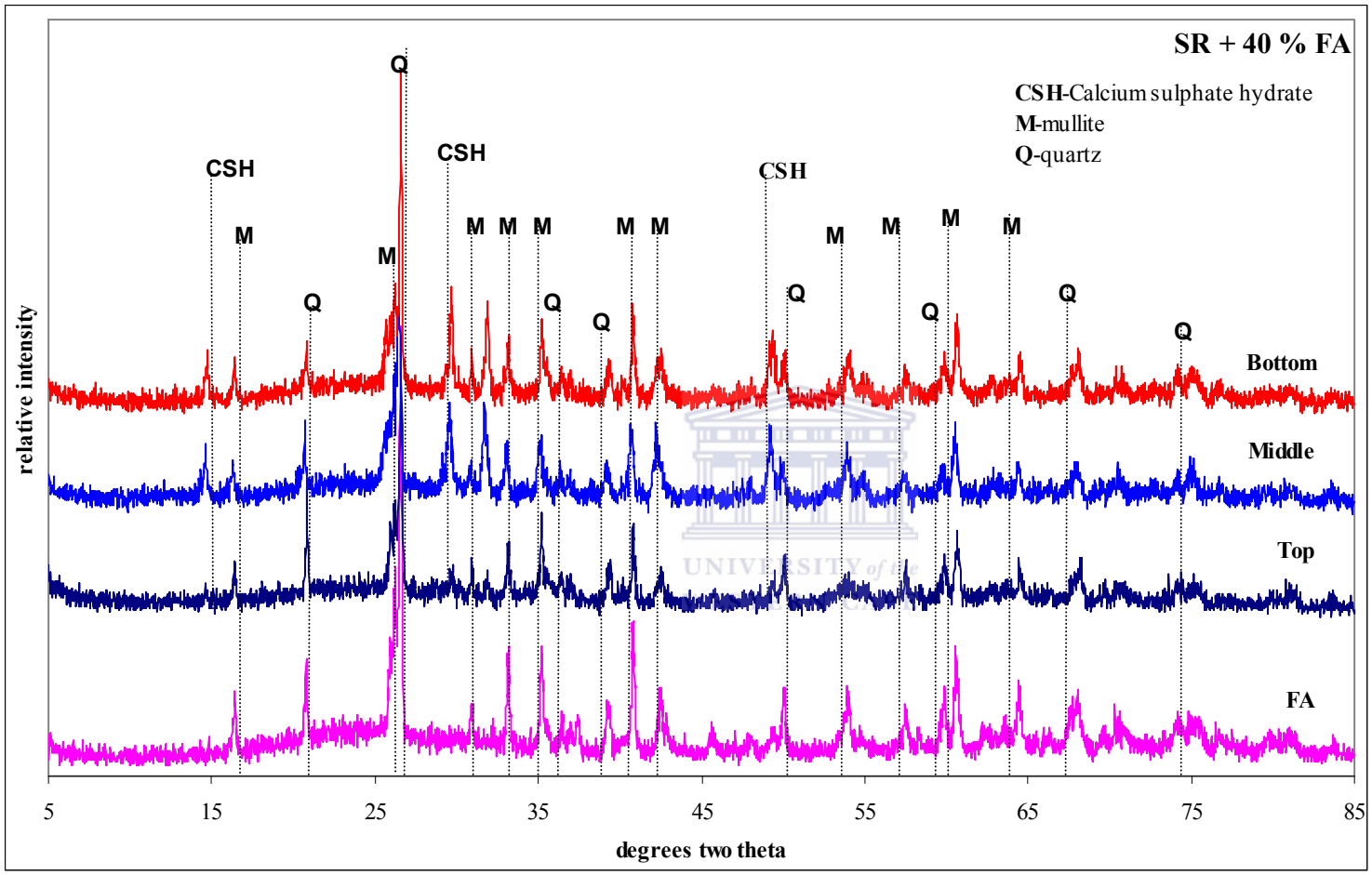

Figure B22: XRD spectra of solid residue (SR) + 40 % FA core sections (G-gypsum)

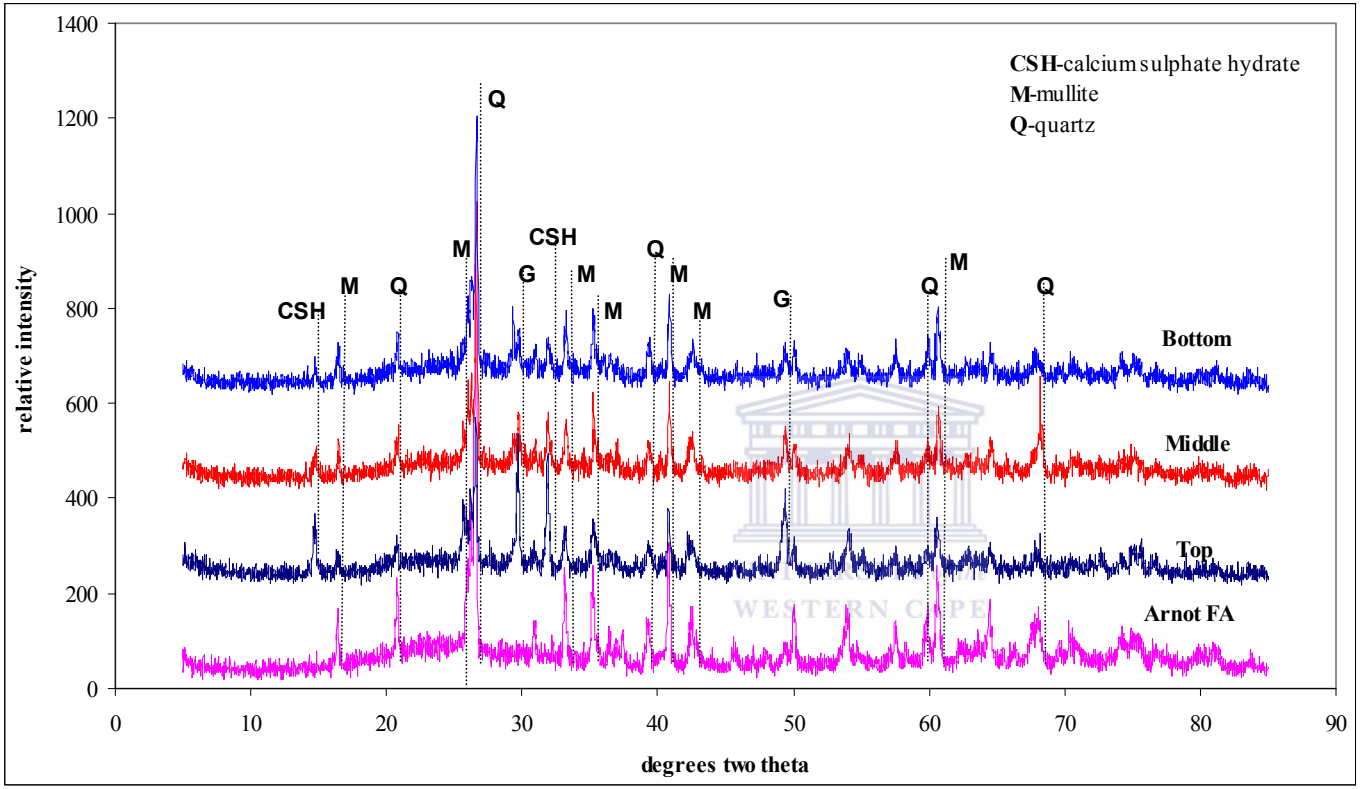

Figure B23: XRD spectra of solid residue (SR) + 6 % OPC core sections (G-gypsum)

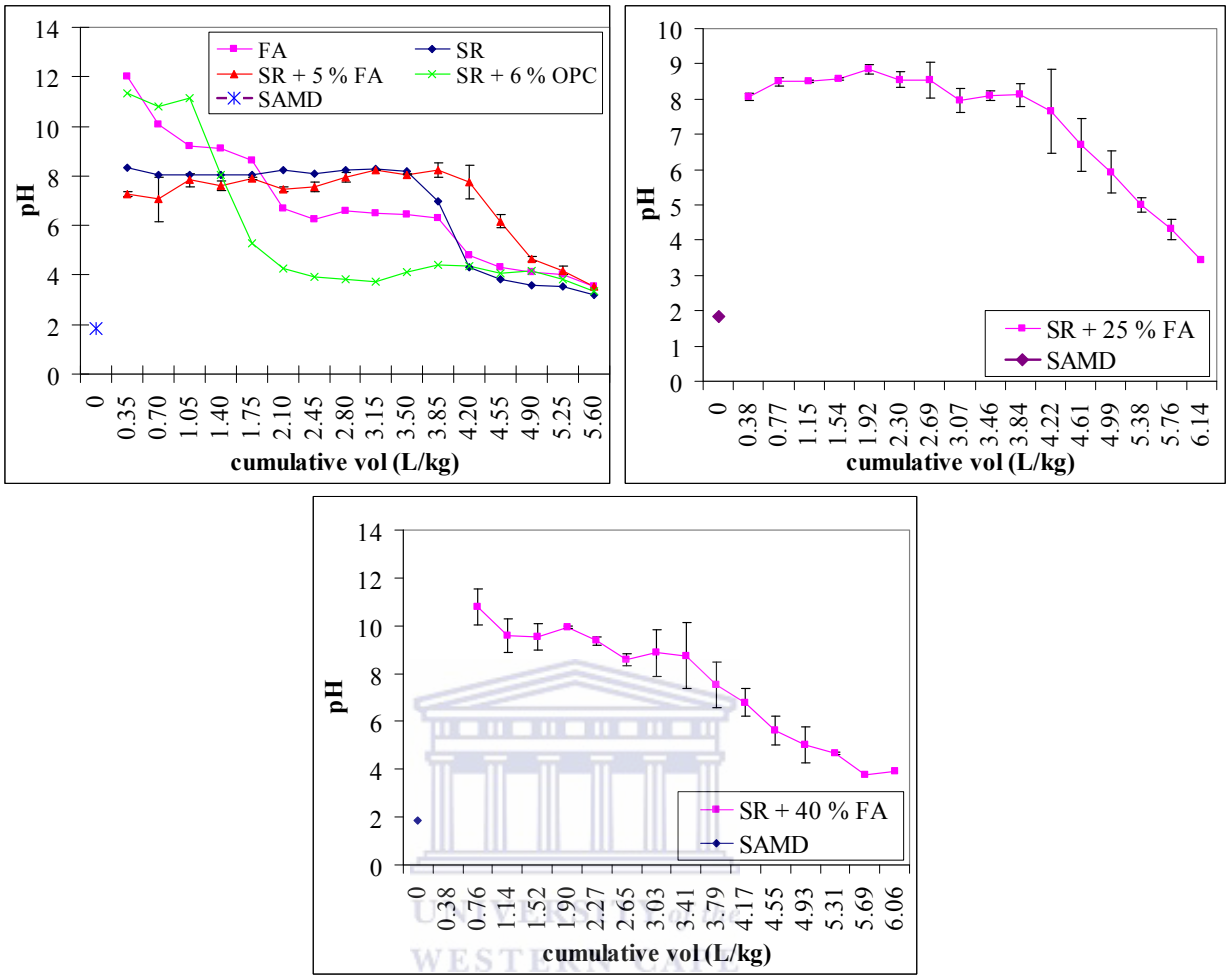

Figure B24: Summarized leachate pH trends versus evolving L/S ratios for FA, SR, SR + 5 % FA, SR + 25 % FA, SR + 40 % FA and SR + 6 % OPC solid cores (error bar represents one SD below and above the mean).